Runoff from Solar Panels at Lime Down

[1]Professor Richard Skeffington

Summary

1. This paper addresses the Applicant's claim that the construction of solar panels at Lime Down will not increase surface water runoff rates and hence flooding, and that no mitigation is required other than maintaining a grass sward under the panels. The peer-reviewed literature on this topic is evaluated. The Applicant bases their claim on an untested computer model from 2013. Since then, studies using a variety of models, including the only models tested against data, consistently show that the panels can increase runoff given certain conditions. The panels alter the distribution of rainwater, concentrating it on their lower edge, typically into drip points. Measured concentration factors averaged 5 to 10 times rainfall, though concentrations up to 23 times were measured in individual storms. To avoid enhancement of runoff and erosion, the soil under the drip line has to be able to adsorb this water and transmit it to areas where it can percolate into the groundwater or an engineered drainage system. If the soil infiltration capacity is exceeded, surface runoff can occur, leading to increased runoff volumes and higher flood peaks. Soils with a low infiltration capacity, low hydraulic conductivity and low storage capacity are particularly vulnerable to generating excess runoff, and it is suggested that solar developers should avoid these. Maintaining an adequate vegetation cover under the panels is essential, but may not be adequate with poor soil conditions.

2. At Lime Down it is proposed to use outsized tracking panels of which there is little experience in the UK. These are likely to generate more concentrated runoff than the panels typically used so far. For most of the time they will be held horizontally 2.5 m above ground level, which available measurements show can lead to concentration factors of around 16 times rainfall. Water falling from this height has more erosive power than a more typical panel where the lower edge is about 40 cm above ground level. Panels in horizontal configuration will cover about 60-66% of the ground area, shading and drying the underlying vegetation and making it difficult to maintain an adequate vegetation cover. The Applicant's soil survey and the National Soil Map show that the local soils are dominated by clays and shallow limestone soils with limited storage capacity. This provides an explanation for the existing flood-proneness of the area, and indicates a high risk that the presence of the solar farm will generate excess

runoff and flooding both on and off site. The Applicant addresses none of these issues in their Environmental Statement. They did, however, measure water infiltration rates at three locations in one of the commonest soil types. At all three locations, the infiltration rate was zero. It is hard to see how this is compatible with their assumption that the soils will absorb runoff from the panels without difficulty. There are no credible proposals for mitigation of excess runoff from the panel areas, which may not in fact be feasible. The applicant has therefore failed to demonstrate how these impacts could be minimised.

[1]Author

3. I am an Emeritus Professor of Geography and Environmental Science at the University of Reading. I have been involved in hydrological research since 1977, first as an environmental scientist in the electrical generation industry working on the effects of acid rain on freshwaters, and after I returned to academic life in 1999, working on modelling and monitoring freshwaters, and hydrology and climate change. I am a co-author of the standard paper on climate change and the water environment in England and Wales, and co-led the modelling workpackages of two large EU-funded projects, EUROLIMPACS and REFRESH, which investigated the predicted effects of climate change on waters across Europe. My publications on hydrological topics have been referenced more than 1000 times. I live adjacent to the Lime Down area. The evidence I have produced is based upon my professional expertise, and is my true and professional opinion.

Introduction

4. To justify building the Scheme in a flood-prone area, the Applicant has to apply the Exception Test. This has two criteria: this report is concerned with the second one which requires the Applicant to demonstrate that "the project will be safe for its lifetime taking into account the vulnerability of its users, without increasing flood risk elsewhere, and where possible will reduce flood risk overall". This paper will address the mechanisms whereby the Scheme will lead to an increase in flood risk both inside and outside the project limits. It will also be shown that the Applicant's proposed mitigation is ineffective in reducing flood risk.

5. The Applicant's Flood Risk Assessment ("FRA", Appendix 11-1 [APP-210], summarized in Environmental Statement Chapter 11, *Hydrology, Flood Risk and Drainage* [APP-063]), does

not consider the risk of surface water flooding arising from solar panel runoff. The only comment made on the risk in the FRA is at section 3.2.1

> "The Solar PV Panels have the potential to concentrate rainfall under the leeward edge of the panels themselves. Research in the United States by Cook and McCuen (Ref 11-27) suggested this increase would not be significant however, there is a potential increase in silt-laden runoff. With the implementation of suitable planting (such as a wildflower or grass mix) the underlying ground cover is strengthened and is unlikely to generate surface water runoff rates beyond the baseline scenario. This is detailed in the **Outline Landscape and Ecological Management Plan (LEMP); [EN010168/APP/7.18]**".

6. While reference is made to further detail to be provided in the Outline Landscape and Ecological Management Plan, no further information is given. No evidence is given to support the statement that a grass mix sown under the panels would totally alleviate any additional surface runoff, apart from the reference to Cook and McCuen.

7. In their response to the Relevant Representations [PDB-004] Table 2-8, the Applicant says "Regarding specific concerns that panels will increase flooding, the submitted assessment presented in ES Volume 3, Appendix 11-1 ES Volume 3, Appendix 11-1: Flood Risk Assessment and Drainage Strategy - Lime Down Covering Report [APP-210] reflects *established hydrological evidence* (my italics) that the addition of solar panels over a vegetated field does not materially increase runoff volumes, peak discharges or response times, and that changes in hydrologic response are primarily associated with alterations to ground cover beneath the panels rather than the panels themselves. Panelled areas are therefore designed so rainfall continues to drain to ground, with no creation of extensive impermeable surfaces and with controls in place to avoid any increase in discharge to watercourses".

8. However, it appears that the "established hydrological evidence" referred to is the Cook and McCuen model, which is outdated and has been undermined by subsequent studies, as this paper will show. On the contrary, there is ample evidence that in some circumstances solar panels can increase runoff, peak discharges and soil erosion, and shorten response times. The literature on this is reviewed in the next section.

Research on the Effects of Solar Panels on Runoff

9. The difficulty facing all models of the effects of solar panels on runoff is how to represent the fact that there is an impervious surface, the panels, raised above the ground surface. UK regulation seems to have started from the premise that the panels are therefore irrelevant, since there is the same amount of ground after the panels were built as there was before. [1] In contrast, the initial regulatory approach in the USA was to specifically regulate solar farm storm drainage and treating the panels as impervious surfaces on the ground [2], and mandated engineering measures to prevent the consequent excess runoff and erosion.

10. Both views are clearly wrong. The US view ignores the capacity of the ground under the panels to infiltrate water and mitigate runoff. The British view ignores the fact that the panels redistribute water. In particular, the panels concentrate water at the lower edge of the panel slope, often as discrete drip points, and that the ground under the panels is considerably drier. The question then arises as to whether the soil can assimilate the volume of water under the drip points, which is much greater than the natural rainfall rate. If the answer is “no”, then a surface water flow will develop. If it continues to flow over a saturated or impervious surface then there is the risk of soil erosion and a rill or small gully may develop. These transfer water much more quickly to drains and streams than percolation through the soil, leading to quicker runoff and higher flood peaks. If the surface water reaches the drier area under the panels, then it may return to the soil water or groundwater without causing flooding. On the other hand, drying some types of soil can cause an impervious surface crust to form, and the soil under the panels may no longer be able to assimilate much water. The soil under the drip line is likely to be saturated more frequently than it was before, and this may also increase runoff rates. Clearly the small-scale configuration of the panels, such as the orientation of the panels relative to the slope of the ground, and where any engineered mitigation is placed, will have a large effect on the outcomes. Modelling and measuring these effects is a considerable challenge as will be seen below.

11. The Applicant’s FRA makes reference to the paper prepared by *Cook and McCuen* (2013)[3], an early review of the hydrological effects of solar farms. The authors identify several potential problems, including increases in the volume of runoff, increased height of flow peaks, and increased kinetic energy of runoff from the panels leading to soil erosion. They built a

computer model on hydrological principles to test these issues, which concluded that "*the solar panels themselves did not have a significant effect on the runoff volumes, peaks, or times to peak*". This conclusion is often quoted by solar developers in the UK. In the paper itself, however, the conclusion was contingent on appropriate ground management, in the absence of which the model *could* show significant increases in peak discharge and potential for soil erosion:

> "The addition of solar panels over a grassy field does not have much of an effect on the volume of runoff, the peak discharge, nor the time to peak. With each analysis, the runoff volume increased slightly but not enough to require storm-water management facilities. However, when the land-cover type was changed under the panels, the hydrologic response changed significantly. When gravel or pavement was placed under the panels, with the spacer section left as patchy grass or bare ground, the volume of the runoff increased significantly and the peak discharge increased by approximately 100%. This was also the result when the entire cell was assumed to be bare ground."
>
> "The potential for erosion of the soil at the base of the solar panels was also studied. It was determined that the kinetic energy of the water draining from the solar panel could be as much as 10 times greater than that of rainfall. Thus, because the energy of the water draining from the panels is much higher, it is very possible that soil below the base of the solar panel could erode owing to the concentrated flow of water off the panel, especially if there is bare ground in the spacer section of the cell. If necessary, erosion control methods should be used."

12. Cook and McCuen suggested some management strategies to alleviate the risks identified:

> "Bare ground beneath the panels and in the spacer section is a realistic possibility (see Figs. 1 and 5). Thus, a good, well maintained grass cover beneath the panels and in the spacer section is highly recommended. If gravel, pavement, or bare ground is deemed unavoidable below the panels or in the spacer section, it may necessary to add a buffer section to control the excess runoff volume and ensure adequate losses. If these simple measures are taken, solar farms will not have an adverse hydrologic impact from excess runoff or contribute eroded soil particles to receiving streams and waterways."

13. However, Cook and McCuen did not model or assess proposed mitigation measures. There is no evidence that the Applicant's proposed "planting" would be effective. Additionally, as many subsequent authors have commented, Cook and McCuen's modelling was not validated by field measurements from real solar farms. Work over the last 15 years has somewhat clarified the range of factors which need consideration, and shown that many of Cook and McCuen's conclusions are flawed. These are reviewed below. The Applicant should not be quoting outdated work simply because it supports a pre-determined position.

14. Cook and McCuen were not the only authors to attempt to model runoff from solar panels. In a review of solar farm hydrology, *Yavari et al* (2022) [2] noted that, up to that time, evaluation of runoff generation was confined to model-based studies. They drew attention to several papers, some of which come to contrasting conclusions to Cook and McCuen:
    a. *Barnard et al* (2017) [4] used a combination of HEC-HMS hydrological models from the US Corps of Engineers and the Flo-2D routing model to design a drainage system for a large solar farm in West Texas. The system required both hard engineering (retention ponds) and SuDS-like features (swales and berms), as well as regrading of the site in places to prevent excess runoff and soil erosion. There was no suggestion that allowing water to infiltrate under the panels would be adequate on its own. The area has a similar annual rainfall to Lime Down, but rain typically comes in large convective storms so requires the ability to cope with heavier short-term rainfall than in the UK. The paper illustrates that it was felt necessary to use a connected set of models on a wide spatial scale, involving modelling of over 130,000 grid elements, to produce estimates of not only flood depths but velocities and off-site flows. These models were used to design flood mitigation works.
    b. *Pisinaras et al* (2014) [5] used the SWAT model to predict the effect of replacement of agriculture with solar farms in the Vosvozis river basin in NE Greece. The model demonstrated increased surface water runoff and percolation, although changes were not significant at the watershed scale. For small river basins (c. 10km^2), replacement of 1% or 5% of current agriculture with solar panels led to increases in surface runoff of up to 110 mm, according to the model. For the large river basins (c300 km^2) the effect was much smaller, about 6 mm, though not all the basin was modified. The area has a Mediterranean climate, with most rain falling in winter.

c. A non peer-reviewed study by *Edalat* (2017) which showed a modelled increase in runoff after solar panel installation. In this case, however, the model assumed the panels were flat impervious surfaces on the ground, which would exaggerate the effects.

15. A later model-only study by *Gullota et al* (2023) [6] used the US EPA Storm Water Management Model (SWMM). A variety of hydrological and soil conditions were simulated, with and without panels. In the short-term, the panels made little difference. However, when the model was parameterised to incorporate the redistribution of soil moisture by the panel structures over time, peak flows increased by 6-35%, and total runoff by 1-5%. These would be significant values for a project meant to last 60 years.

16. *Nair et al* (2024) [6] also used the SWMM, set up somewhat differently, to model a range of conditions in a model solar farm. In this case both peak runoff and total runoff volume were increased by the solar panels. The magnitude of the results depended on how the panels were oriented relative to the slope. These model-only studies show that different but credible models, with varying model parameterisations, applied in different climates, yield a wide range of results, including increases in peak runoff and runoff volume. There is no basis for assuming that the presence of solar panels will have no effects on runoff.

17. Genuine experiments where the experimenter is in control of artificial rainfall on an experimental solar setup are difficult to perform. *Baiamonte et al* (2023) [7] studied the effects of a pair of solar panels on runoff in a bare soil in Sicily. The panels increased runoff rates by a factor of about 11, and shortened the time to peak by a factor of about 4. These would be huge effects in the real environment. In contrast, *Wang and Gao* (2023) [8] worked with a similar plot-scale setup in a soil from the Loess Plateau in China, and found that the panels made little difference to runoff, but perhaps not surprisingly, reduced soil erosion. In practice these studies, which have bare soil, relatively steep slopes, and high rainfall rates are not very relevant to typical British conditions.

18. Modelling predictions which are tested against real data offer the most reliable way to predict the effects of solar panels on runoff. *Mulla et al* (2024) [9] measured soil hydrological values at 5 contrasting solar sites across the USA, with annual rainfall rates varying from 406 mm to

1245 mm. They built a hydrological model based on the observed facts: that solar panels collect and concentrate runoff along a drip edge; that this water percolates into the soil and migrates both downwards and laterally; that the open area between panel rows is available for water infiltration; and that the dry area under the rows of panels is also available for infiltration. They applied an established soil hydrology model, Hydrus-3D, to this framework, and calibrated it to each of the five sites. Their model gave good simulations of the observed soil moisture parameters during subsequent storm events. They used the model to predict the effects on runoff of the 100-year design storm for each site.

19. One of the aims of the *Mulla et al* (2024) paper was to demonstrate to US regulators that simply treating the solar panels as an impervious surface would lead to an exaggerated effect on runoff, and their model succeeded in this. The study yielded other insights, however, which are not mentioned in the paper Summary. One was that, averaged over the 5 sites, stormwater runoff was 14% higher in the presence of panels than it would have been in their absence. Another was the importance of soil type. The soil at the Minnesota site was a deep, coarse-textured soil with a high saturated hydraulic conductivity, and produced no excess runoff even in the 100-year storm. The other 4 sites all produced excess runoff in the 100-year storm in the presence of panels. The site in Georgia also produced excess runoff in the 10-year storm, and the sites in Oregon and New York in the 10-year and 2-year storms. The soil at the New York State site was shallow with limited storage capacity, and generated about 125 mm of runoff in 24 hours, from a rainfall input of 150 mm. The authors note ([9] Section 3.7) that:

> "one of the primary strategies solar developers should use for mitigating runoff is to select sites for development that have good potential for infiltration, avoiding development on sites with low permeability or shallow soils."

20. The Lime Down soils are mostly shallow with low permeability (see Section 6 below). The *Mulla et a*l (2024) paper, which is one of only two which have tested a hydrological model of a solar farm against real data, thus demonstrates that: (1) solar panels can increase water runoff in a range of soils, even in short return period storm conditions; and (2) that soil infiltration and storage capacity are vital attributes that need to be assessed. The authors used their data to generate an assessment model [10] which could be used for assessment in UK sites.

21. The other study which developed and tested a hydrological model of a solar farm against data is *Liu et al (*2023) [11]. Liu and co-workers developed a complex hydrological model (SOFAR) which takes into account the concentration of rainfall by the panels into driplines; soil moisture dynamics; vegetation growth; landform evolution; and hydrological connectivity, defined as "*the internal physical linkages between runoff/sediment generation in the upper parts of a catchment and the water/sediment received through the fluvial system*". They calibrated the model in a solar farm in the Loess Plateau of China, with an arid continental climate (annual rainfall, 186 mm). They then used the model to predict runoff and soil erosion under a range of conditions. Runoff due to the panels was considerably increased in all situations (99% to 150%), as was soil erosion (25% to 76% during operation). This is in a very different climatic environment to the UK, but it does show that the same physical processes that apply in the UK can produce large increases in runoff. It is also the only model which attempts to model the larger scale effects, through its hydrological connectivity parameters.

Conclusions on Research

22. It is clear from the above that it cannot be assumed that the existing ground surface will absorb all the water running from the panels as the Applicant claims, such that there will be no effects on runoff or soil erosion. Credible models, including the only ones tested against data, consistently show that the panels can increase runoff given certain conditions. The *Mulla et al* (2024) paper [9] highlights soils with a low infiltration capacity, low hydraulic conductivity and low storage capacity as particularly vulnerable. To assess the risks at Lime Down, it is thus necessary to know the condition of the soils, and also the characteristics of the panels which are to be used. These are discussed in the following sections.

Characteristics of the Solar Panels at Lime Down

23. Chapter 3 of the Environmental Statement (ES) [APP-055] states that where possible the site will use bifacial single-axis tracking panels which are considerably larger than those normally used in the UK, with a maximum height of 4.5 m. The panels will be aligned in north-south rows, and will rotate to the east and west daily, following the sun, and tilt up to a maximum inclination of 60° from horizontal. Some information about panel sizes is given in Table 3-1, ES

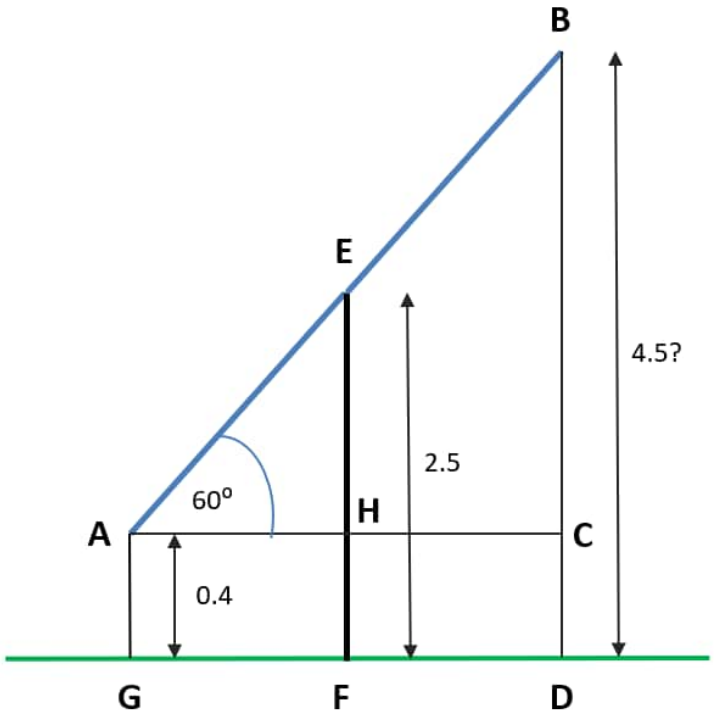

Ch3, p.7 [APP-055]. Only some dimensions are given, but there is enough information to work out the rest. The dimensions given are shown in Figure 1.

Figure 1: Tracking Panel Dimensions (m). The diagram shows a fully-tilted panel seen from the side.

24. The green horizontal line is the ground surface. The panels (blue) are mounted on posts (EF), 2.5 m high, pivoting around E. The maximum angle of tilt <BAC is 60° to the horizontal. The edge of the panel is then 0.4 m from the ground (AG). The maximum height above the ground (BD) is stated to be 4.5 m. These dimensions are not internally consistent. In these calculations, the assumption is made that the height of the lower edge above the ground (AG) and the height of the pivot post (EF) are correct. EH is thus 2.1 m, and the length of the panel from pivot to edge (AE) is 2.1/sin (60°) = 2.425 m. The full panel length (AB) is twice that = 4.85 m. BC is then 4.85 * sin (60°) = 4.2 m and the maximum panel height BD is 4.2 + 0.4 = 4.6 m rather than 4.5 m. The length of ground always covered by the panel (GD = AC) is 4.2/tan

(60°) = 2.425 m. When the panels are horizontal, the ground covered will be equal to AB = 4.85 m.

25. More information about panel sizes is given in the Climate Change chapter of the ES (Chapter 7 [APP-059].

26. IGP's reply to my query of 18 November 2025 (Appendix 1) states that the panel size is 2.4 x 1.3 m (these figures do not appear in either Chapter 3 or Chapter 7 of the ES), giving an area of 3.12 m^2, which is confirmed in Section 7.10.15. This is consistent with the tracking panel structure having two of these panels, one on each side of the pivot. Chapter 7 also states that there will be approximately 598,260 "modules" (7.10.11) and IGP states that the term "module" is used interchangeably with "panel" (Appendix 1) so the total area of panel in the scheme is 598,260 * 3.12 = 1,866,571 m^2.

27. Foundations for the panels would be piles driven into the ground up to 4 m deep. However, where it is necessary to protect archaeological remains, concrete blocks will be used for support (ES, 3.3.16). Concrete block would not be large enough to support the full-size tracker panels and in these cases there would only be half-size (1P) tracker panels (ES, 3.3.12) with a single panel spread over the tracker (ES, Appendix 3-3 [APP-184]).

28. In some places, fixed panels would be used, smaller than the tracking panels but still larger than normal. Dimensions are also given in Table 3-1, ES Ch3, p.7 [APP-055]. The maximum height is 3.5 m, the angle to the horizontal between 10° and 35°, and the minimum ground clearance 0.4 m. The applicant has also committed to using smaller 2.5 m high fixed panels in Field B11 to avoid glint and glare effects to residential properties (ES 3.3.17). However, it is clearly intended that the majority of panels will be tracking panels, and as these will be the worst-case scenario, subsequent analysis will concentrate on these.

29. The length of a single (2P) panel according to Fig. 1 is 4.85 m, which includes a small allowance for the frame. When water runs down the sloping panel, it will concentrate and drip from the bottom edge. The degree of concentration will in theory depend on the upright length of the panel divided by the width of the bottom edge. For the tracking panels at Lime Down this ratio is 4.85 / 1.3 = 3.73 and they will thus generate more concentrated runoff than a standard 2.3

x 1.1 m panel, where the ratio is 2.09. However, in practice the drips will be concentrated in certain locations, typically the edges of the panels, as illustrated in a presentation to the British Hydrological Society by *Burch et al* (2014) [12]. This makes the length of the lower edge less relevant, because a large volume of water will thus be concentrated on a small area, and in [12] erosive rills can be seen developing in these locations.

30. Two papers have tried to quantify the concentration factors under the drip edge relative to incoming rainfall. *Mulla et al* (2024) [9] report average 24-hour concentration factors of 10.6 times rainfall with a range of 2X to 23X at their Minnesota site. The high values were associated with wind directions driving rain onto the surface of the panels, while the low values were from wind directions behind the panels. At their New York State site, concentration factors were smaller with a mean of 3X and a range of 1X to 5X. They attribute the difference to the prevailing winds in New York running parallel to the panel arrays, whereas in Minnesota they are at right angles. At Lime Down, the N-S orientation of the tracking panels is roughly at right angles to the prevailing W to SW winds. At both sites, the arrangement used fixed 3 x 1 m panels in a double portrait arrangement, so concentrations probably a little greater than at Lime Down.

31. *Elamri et al* (2018) [13] reported an extensive investigation of rain redistribution by solar panels in an agrivoltaics scheme in France. Single axis tracking panels 2m long x 1 m wide were used. The concentration factors were about 5X when facing the wind and 2X when back to the wind, both at 50° tilt (Fig. 6). The concentration factor was much higher when the panel was held horizontal – about 16X. This has important implications for Lime Down (see below).

Arrangement of the Panels at Lime Down

32. Because the tracking panels will tilt by up to 60° in either direction, the position of the drip points will vary, unlike with fixed panels. This spreads the concentrated runoff over a wider area over time: however, the position of the drip point in an individual storm is not likely to move, so the risk of soil erosion and runoff generation will be unaltered. To work out the area which will be affected by the concentrated runoff it is necessary to know how the panels will be arranged. Table 3-1 of the ES [APP-055] states that the minimum separation between rows of panels when horizontal will be 2.5 m. The minimum width of a row of panels will thus be

2.5 + 4.85 = 7.35 m. Dimensions on the ground with panels at maximum density are shown in Fig. 2.

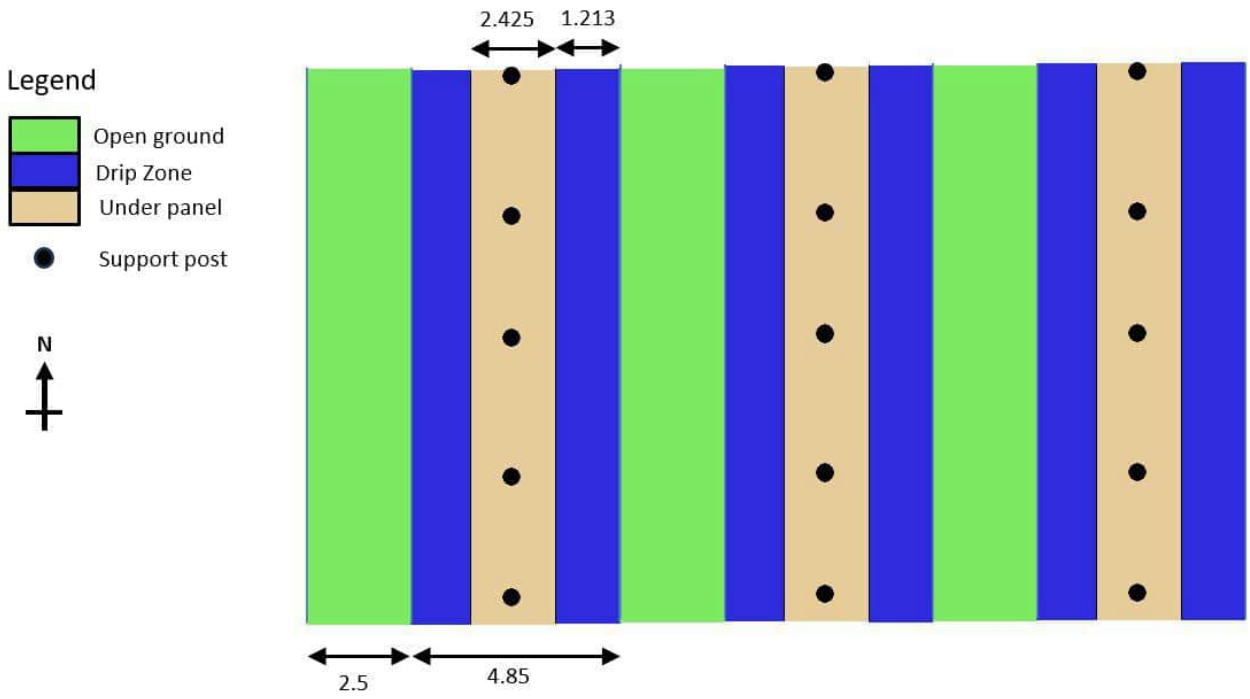

Fig. 2. Plan view of part of three rows of panels at maximum density. Measurements in metres.

33. Figure 2 shows part of an array of tracking panels seen from above. The panels are supported on the marked posts: post spacing is schematic as this is unknown. The green zones are open ground between the panels. The beige and blue zones together represent ground under the panels when they are being held horizontally. The beige zones are always under the panels; the blue zones mark the position of the drip edges depending on the degree of tilt. The blue zones represent the area of ground potentially subject to drip from the panels. This is (2*1.213)/7.35 or 33% of the ground area. The panel density at minimum separation with the panels horizontal is 4.85/7.35 = 66%. This is a high density. The panel separation in what appears to be a scale diagram in the Outline Ecological Protection and Mitigation Strategy [APP-284] is only slightly less dense at about 8.48 m separation between the rows. A substantial area of ground will thus be needed for absorption of concentrated runoff from the panels.

34. Table 3-1 of the ES [APP-055] states that the panels will be returned to the horizontal position at night. The panels will therefore be horizontal at least half the time. It is likely to be more

than that. The report by Pager Power on glint and glare (ES, Appendix 20-4 [APP-261] Section 2.2.4) is based on premise that the panels will revert to horizontal whenever the sun is not high enough to prevent self-shading by the panels, which at Lime Down is when the sun is less than 30° above the horizon. Below that, the energy loss from shading may exceed the energy gain from tilting the panels, and the glint and glare assessment is made on this basis. At the latitude of Hullavington (51.5°N), the sun never rises above 30° between 12 October and 28 February. The panels are thus likely to be horizontal through the wettest part of the year. It is unlikely that it will be possible to hold the panels exactly horizontal, and water will run off at the same discrete points throughout this period. *Elamri et al* (2018) measured a 16-fold concentration of water below their experimental horizontal panels, as noted above. Moreover, instead of dripping from the bottom edge of a panel typically about 40 cm above the ground surface, water from the Lime Down tracking panels will be falling from 2.5 m above the ground. This water will have more than 6 times the kinetic energy of water falling from 40 cm. The potential for erosion and runoff generation due to large volumes of water falling from a height is obvious, yet there is no assessment of this by the Applicant. Even when the panels are tilted and the lower edge is closer to the ground, the kinetic energy of water falling down a 60° slope is considerable. The Applicant has suggested that there will be small holes in the panels to reduce the volume of water that drips from the edge. These will be difficult to engineer given that surface tension and accumulated debris is likely to inhibit water from running down a small gap, and that the flows can go in either direction down the panel.

35. The Applicant's ES contains no analysis whatever of the hydrological issues relating to the outsize tracking panels. As shown above, the panels are likely to concentrate water in drip zones, and the height of the drip origins above the surface will give this water considerable erosive and runoff-generating potential.

Soils and Infiltration

36. The final issue that needs to be assessed is whether the soils in the Lime Down area are capable of absorbing the enhanced runoff from the solar panels. As with other issues, the Applicant has failed to evaluate this, but there is some evidence in the ES and in public information. An ideal soil to resist runoff would have a good capacity to absorb water (infiltration); a good capacity to transmit water elsewhere (hydraulic conductivity) and enough depth to temporarily store water. These properties can to some extent be inferred from the

soil texture – clay soils are poor at absorbing and transmitting water but have good storage capacity; sandy soils are good at infiltration but poor at storage; loamy soils have good all-round properties.

37. Appendix 17-1 of the ES: Agricultural Land Classification and Soil Survey Report [APP-243], though principally concerned with agricultural land classification, has some useful data. Of the 23 soil profiles with measurements of soil texture (Annex A), only one was not a clay or a soil with properties influenced by clay. There were 12 clays; 4 heavy clay loams; 4 medium clay loams; one silty clay; one medium silty clay loam and one silty loam. The presence of clay suggests low infiltration rates. The written descriptions of the sites [APP-243], Section 1.3.8 to 1.3.32) reinforce this picture. Lime Down A, C and E are said to be dominated by the slowly permeable clay soil type. Lime Down B has a mixture of clays and more permeable shallow limestone soils, and Lime Down D has limestone in the west and slowly permeable clays in the east.

38. This picture is borne out by the National Soil Map [14]. There are four soil associations in the area. On the west side, comprising most of areas A and C, is the Evesham 1 association, described as "*slowly permeable calcareous clayey soils*." In a band running through Areas B and D there is the somewhat better drained Sherbourne Association described as "s*hallow well drained brashy calcareous clayey soils over limestone*." Area E and parts of Areas B and D are underlain by the Wickham 3 association described as "*Slowly permeable seasonally waterlogged fine loamy over clayey and coarse loamy over clayey soils and similar more permeable soils with slight waterlogging."* And the area subject to flooding upstream of Corston is the Fladbury 1 association, described as "s*toneless clayey soils, in places calcareous variably affected by groundwater."* Soil associations are not uniform, but the preponderance of clay soils with impeded drainage is clear. The clay soils and the shallow limestone soils with little water holding capacity are what give the area its propensity to flooding.

39. Finally, the Applicant has measured soil infiltration rates at 3 sites in Field D1 of Lime Down D as described in Appendix 11-6, Section 3.2.5 [APP-215]. The soils in Field D1 are on the boundary between the Evesham 1 and Sherbourne series as described above. In all 3 cases there was *no* infiltration in the 3-hour observation time. It is hard to see how the Applicant

can claim that the soil under the panels can absorb excess runoff water when the only available measurements show that infiltration is in fact zero.

40. Soil compaction is another issue recognised to increase flood risk (e.g. [15]), especially where soil compaction coincides with soils characterized by a fine texture and a low infiltration capacity. This applies to some of the soils at Lime Down, and the National Soil Map [14] has ratings for susceptibility to compaction and potential for natural recovery from compaction. The soils of Area E and most of Area D are rated as highly susceptible to compaction with little potential for recovery, those of Areas A and C moderately susceptible but with potential for recovery and even the limestone soils of Area B are slightly susceptible to compaction. Construction of solar farms inevitably produces soil compaction. A survey of 32 solar farms by *Carvalho et al (2025)* [16] showed that even after years of operation, the soil under solar panels was consistently about 14% compacted compared to outside. The Applicant recognises compaction as an issue in the Outline Soil Resources Management Plan [APP-280], but has not assessed the location of sensitive soils or provided a detailed plan for avoidance or mitigation.

Mitigation

41. The Applicant does recognise that some of the additional hard surfaces introduced into the catchment will increase flood risk and proposes some minimal mitigation to address this, such as gravel-filled trenches round conversion units (ES, Chapter 11, 11.9). The remaining mitigation measures are concerned solely with protecting their own assets. The only mitigation proposed for panel runoff is to maintain a vegetation cover under the panels. The high density of panels proposed, and the proposal to keep them level most of the time and thus shading the ground, will make maintaining a vegetation cover difficult, as it will be under considerable stress because of reduced light intensity and shortage of water. Even under conventional panels, plant growth is reduced, as demonstrated by *Carvalho et al (2025)* [16] who found significant reductions in plant cover and above-ground biomass under panels relative to the outside in their study of 32 UK solar farms.

42. As this paper has demonstrated, the large panels, their height above the ground surface and the soils at Lime Down which have typically low infiltration rates are likely to generate considerable excess runoff and flooding both on and off site, contrary to the requirements of planning legislation, specifically Overarching National Policy on Energy EN-1. The application

must be refused unless the Applicant can demonstrate enough mitigation for these effects. Mitigation will not however be easy, as it would involve surface water management on a very large scale. This would require a considerable land take, and the obvious places for SuDS schemes or hard engineering structures like retention ponds would be in the fluvial or surface water flood zones where they would largely be ineffective. The Applicant should demonstrate that they have a credible and detailed plan to mitigate flooding before the Scheme is consented, as there is considerable doubt that such a thing is possible.

Conclusion

43. The Applicant's assertion that that the construction of solar panels at Lime Down will not increase surface water runoff rates and hence flooding is shown to be very questionable. The scientific literature shows that merely preserving vegetation cover under the panels will not automatically allow water to percolate into the soil. Consideration of the characteristics of the soils on site, the oversized solar panels, the way they concentrate water and their height above the ground shows that an increase in runoff rates and hence flooding is very likely. The Applicant provides no credible plan to mitigate this excess runoff.

References

1. *National Policy Statement for renewable energy infrastructure (EN-3)*. 2023, UK Government, Department of Energy Security and Net Zero London.
2. Yavari, R., et al., *Minimizing environmental impacts of solar farms: a review of current science on landscape hydrology and guidance on stormwater management.* Environmental Research: Infrastructure and Sustainability, 2022. **2**(3): p. 032002.
3. Cook, L.M. and R.H. McCuen, *Hydrologic response of solar farms.* Journal of Hydrologic Engineering, 2013. **18**(5): p. 536-541.
4. Barnard, T., M. Agnaou, and J. Barbis, *Two dimensional modeling to simulate stormwater flows at photovoltaic solar energy sites.* Journal of Water Management Modeling, 2017. **25**: p. C428.
5. Pisinaras, V., et al., *Conceptualizing and assessing the effects of installation and operation of photovoltaic power plants on major hydrologic budget constituents.* Science of The Total Environment, 2014. **493**: p. 239-250.

6. Gullotta, A., et al., *Modelling stormwater runoff changes induced by ground-mounted photovoltaic solar parks: a conceptualization in EPA-SWMM.* Water Resources Management, 2023. **37**(11): p. 4507-4520.
7. Baiamonte, G., L. Gristina, and S. Palermo, *Impact of solar panels on runoff generation process.* Hydrological Processes, 2023. **37**(12): p. e15053.
8. Wang, F. and J. Gao, *How a photovoltaic panel impacts rainfall-runoff and soil erosion processes on slopes at the plot scale.* Journal of Hydrology, 2023. **620**: p. 129522.
9. Mulla, D., et al., *Measuring and modeling soil moisture and runoff at solar farms using a disconnected impervious surface approach.* Vadose Zone Journal, 2024: p. e20335.
10. Galzki, J. and D. Mulla, *Stormwater runoff calculator for evaluation of low impact development practices at ground-mounted solar photovoltaic farms.* Discover Water, 2024. **4**(1): p. 35.
11. Liu, H., et al., *Effect of solar farms on soil erosion in hilly environments: A modeling study from the perspective of hydrological connectivity.* Water Resources Research, 2023. **59**(12): p. e2023WR035067.
12. Burch, T., et al., *Impact of solar parks on runoff generation and associated land drainage/flood risk consequences*, in *Hydrological impacts of energy projects*. 2014, British Hydrological Society: CIWEM, 106-109 Saffron Hill, Faringdon, London EC1N 8QS
13. Elamri, Y., et al., *Rain concentration and sheltering effect of solar panels on cultivated plots.* Hydrology and Earth System Sciences, 2018. **22**(2): p. 1285-1298.
14. *Soil site report, Extended Soil Report for location 390661E, 184683N, 5km x 5km.* 2025, Cranfield University.
15. Alaoui, A., et al., *Does soil compaction increase floods? A review.* Journal of Hydrology, 2018. **557**: p. 631-642.
16. Carvalho, F., et al., *Plant and soil responses to ground-mounted solar panels in temperate agricultural systems.* Environmental Research Letters, 2025. **20**(2): p. 024003.

Appendix 1 Query and Response to IGP about solar panel sizes

[Query to IGP, 18.11.2025]

To: [redacted], Senior Project Manager, Lime Down Solar Park

Dear [redacted]

In order to submit Relevant Representations to the Planning Inspectorate, it would be useful to know the size of the solar panels used, and how many of them are on the site.

There is not enough information in Chapter 3 [APP-055] to specify the size of the panels. There is more information in Chapter 7 [APP-059] which states (7.10.11) "A Solar PV Panel is composed of multiple modules. It is estimated the total number of modules for Lime Down will be 598,260".

A "module" is not defined anywhere, but in 7.10.13 it states that a module is composed of 156 individual solar cells. In 7.10.14 it is stated that a solar cell contains 11g of silicon, and a panel contains
1.584 kg of silicon. A panel therefore consists of 1584/11 = 144 solar cells, which is credible.

But this means that contrary to the first sentence which says that a panel consists of multiple modules, a panel (144 cells) is actually smaller than a module (156 cells). A panel also has a surface area of 3.10m2 (7.10.15).
Could you please clarify this and explain:
1. What are the typical dimensions of the panels you intend to use?
2. What is a module and what is its relationship to a panel?
3. How many panels or modules will there be on site?
4. Do any of the values in Chapter 7 need correction?
5. If the dimensions of the panels are not quite finalised, what values should we assume for Rochdale Envelope purposes?
Thank you
Richard Skeffington

[Reply 4.12.2025]

Dear Richard Skeffington,

Thank you for getting in touch and for your patience while we prepared this reply. In terms of panel dimensions, the figures used in the climate chapter carbon calculations (2.4m x 1.3m) are assumptions applied for the purposes of undertaking the climate assessment. The actual dimensions of the panels to be used have not yet been confirmed. These will require flexibility and will vary depending on the type of panel arrangement (fixed or tracker) selected, and well as the technology available at the time. Further detail on this is provided in ES Chapter 3: Scheme Description [APP-055] paragraph 3.2.21, with feasibility and optionality explained in Section 3.3 to S.6.

To clarify terminology, the solar PV panel is also referred to as a module, and each module is composed of multiple cells. For the purposes of assessment, it is estimated that Lime Down would require approximately 598,260.

There are no changes required to Chapter 7: Climate Change [APP-059] based on the above in terms of the dimensions and the assumptions used for the purposes of assessment. Two configurations were assessed, 144 cells per panel and 156 cells per panel. In line with the Rochdale Envelope approach, the 156-cell option represents the worse-case scenario, and as such is the one taken forward for assessment. The total embodied silicon from the solar PV panels is estimated at 6,160 tCO_2e under this worst-case scenario.

Kind regards,

[redacted]

Community Relations Team

Lime Down Solar Park

Table of Contents

SLD_Appendix F2 Runoff from Solar Panels at Lime Down 1
2.SLD_Article Yavari_2022_Solar Farm Hydrology 22
3.SLD_Article Cook McCuen 2013 Hydrologic-Response-of-Solar-Farms (1) 38
4.SLD_Article Barnard_2017 Solar 2D modelling 44
5.SLD_Article Pisinaras_2014_Hydrologic budget 52
6.SLD_Article Gullotta_2023_Solar_Runoff_EPA Model 64
7.SLD_Article Baiamonte_et_al.23_Solar hydrology 78
8.SLD_Article Wang_2023 Solar Rainfall Runoff erosion 94
9.SLD_Article Mulla_2024 - Measuring and modeling soil moisture and runoff at solar farms using a disconnected 105
10.SLD_Article Galski_2024 Solar runoff calculator 118
11.SLD_Article Liu_ 2023 - Effect of Solar Farms on Soil Erosion in Hilly Environments A Modeling Study 131
12.SLD_Article Burch 2014---Impact-of-solar-parks-on-runoff-generation 161
13.SLD_Article Elamri_2018 Solar rain redistribution 204
15. SLD_Article Alaoui 18 Soil Compaction floods 218
16.SLD_Article Carvalho_2025_Soil props UK solar farms 230

ENVIRONMENTAL RESEARCH
INFRASTRUCTURE AND SUSTAINABILITY

TOPICAL REVIEW • OPEN ACCESS

Minimizing environmental impacts of solar farms: a review of current science on landscape hydrology and guidance on stormwater management

ENVIRONMENTAL RESEARCH
INFRASTRUCTURE AND SUSTAINABILITY

OPEN ACCESS

RECEIVED
7 April 2022

REVISED
25 May 2022

ACCEPTED FOR PUBLICATION
8 June 2022

PUBLISHED
8 August 2022

TOPICAL REVIEW

Minimizing environmental impacts of solar farms: a review of current science on landscape hydrology and guidance on stormwater management

[redacted]

[1] Civil and Environmental Engineering, Penn State University, University Park PA 16802, USA
[2] Agricultural and Biological Engineering, Penn State University, University Park PA 16802, USA
[3] Agricultural and Biological Engineering/Civil and Environmental Engineering, Penn State University, University Park PA 16802, USA
[4] Civil and Environmental Engineering/Agricultural and Biological Engineering, Penn State University, University Park PA 16802, USA
* Author to whom any correspondence should be addressed.

E-mail: [redacted]

Keywords: utility-scale solar, stormwater management, ground-mounted solar, renewable energy, sustainable solar development

Abstract

As solar energy becomes an increasingly cheap source of renewable energy, major utility-scale ground solar panel installations, often called 'solar farms', are rapidly growing. With these solar farms often covering hundreds of acres, there is the potential for impacts on natural hydrologic processes, including runoff generation and erosion. Here we review the current state of scientific research on the hydrology and water quality impacts of solar farms, as well as management recommendations for minimizing any impacts. The limited field measurements indicate the redistribution of soil moisture around solar farms, but the net impacts on runoff and erosion are less clear. Research focused on coupling solar farms with agriculture as 'agrivoltaics' demonstrates reduced evaporative water losses and associated crop stress, particularly in more arid regions. With regards to land and the stormwater management associated with solar farms, most US states currently do not have solar farm-specific recommendations and instead defer to standard stormwater management permits and guidance. In states with solar farm-specific guidance, typical recommendations include minimizing construction-related compaction, ensuring a high cover of perennial vegetation with minimal maintenance, and designing with pervious space between solar panel rows to promote infiltration of any runoff; in some cases, structural stormwater management like infiltration basins may be required. In general, solar farms can be designed to minimize the impact on landscape ecohydrological processes, but more research is needed to determine whether current recommendations are adequate. In particular, there is a need for more field research on less ideal sites such as those with higher slopes.

1. Introduction

The advancement of human civilization depends on energy. Societies are growing, and the standard of living is rising, resulting in a growing demand for energy. The use of fossil fuels as a major energy source has led to environmental pollution and global warming. In addition, fossil fuels are not renewable. In recent decades, there has been a search for cheaper, affordable and more environmentally friendly and sustainable energy sources (Gunerhan *et al* 2008, Shorabeh *et al* 2019).

Amongst sustainable energy sources, solar energy is favored, owing to its plenitude and increasing affordability. It is more abundantly distributed in nature than any other renewable energy source. Solar energy has widely and exponentially grown in the last couple of decades (US Energy Information Administration (EIA) 2020). Solar photovoltaic (PV) technology converts the Sun's energy to environment-friendly electricity (Solangi *et al* 2011). This has been one of the most booming forms of renewable energy in recent years, due to technological advancements and favorable government policies that have made it increasingly affordable and accessible (Gunerhan *et al* 2008, Hassanpour Adeh *et al* 2018, Shorabeh *et al* 2019). PV development can also

be beneficial in terms of potentially supporting the reclamation of degraded land, economic opportunities, and rural electricity access. (Ravi *et al* 2016). It also avoids the greenhouse gas impacts, air quality concerns, and other sources of pollution caused by fossil fuels (Aman *et al* 2015, Hernandez *et al* 2014, Grigorescu *et al* 2019, Lambert *et al* 2021, Shorabeh *et al* 2019, Taha 2013, Vrînceanu *et al* 2019).

PV technology is deployed in various ways. One popular approach leverages the rooftops of residential or commercial buildings for solar panel installation, where solar panels are impervious panels of PV cells. Solar panel arrays mounted on the ground are another way of harvesting solar energy, particularly at a larger scale compared to residential rooftop solar. Utility-scale ground solar panel installations used for electricity generation of 1 MW or greater are commonly referred to as 'solar farms' (US Energy Information Administration (EIA) 2020). On solar farms, solar panels are mounted on metal supports, with panels arranged in long rows. The area under and between the panels could be paved, covered with gravel, bare soil, or vegetated. The interspace between the rows, as well as access paths or roads between clusters of rows, allows for maintenance as well as possible infiltration of water (Barnard *et al* 2017a, Gunerhan *et al* 2008, Zhu *et al* 2019).

Utility-scale solar energy development needs a lot of space, and its large-scale installation could potentially have some negative impacts on the environment, but this depends on the way that the solar farm is built and maintained (Hernandez *et al* 2019, 2014, Moore-O'Leary *et al* 2017). The area covered by solar farms can vary between 1 acre (0.40 ha) to several hundred acres, depending on the power generation capacity. The construction process of solar farms can require extensive landscape modification that could result in the modification of soil properties and vegetation (Aman *et al* 2015, Jacobson and Delucchi 2011). The addition of an impervious surface, as solar panels, could alter the site's hydrology and impact erosion. Changes in vegetation and ongoing maintenance of the site can also impact soil carbon dynamics and habitat provision (Barnard *et al* 2017a, Choi *et al* 2020a, Gunerhan *et al* 2008, Moore-O'Leary *et al* 2017, Walston *et al* 2021). There is increasing interest in leveraging solar farms for the provision of additional ecosystem services or benefits beyond solar power generation. This could include planting of certain vegetation to create pollinator habitats (Blaydes *et al* 2021, Graham *et al* 2021, Walston *et al* 2021, 2018). The concept of 'agrivoltaics' involves leveraging the solar farm for agriculture, such as sheep grazing or crop cultivation (Weselek *et al* 2019).

As solar energy becomes an increasingly cheap source of renewable energy, the number of solar farms is rapidly growing. As of 2022, there are approximately 5500 major solar projects across the US, with existing installations generating 55 GW, and projects under construction or in development generating 110 GW (Solar Energy Industries Association 2020). Thus, it is critical to ensure that these projects are implemented in the most sustainable way.

There is a small but growing body of scientific research seeking to understand the impacts of solar farms, specifically on landscape ecohydrology in a range of environmental and land conditions. Similarly, there are rapidly evolving guidance and/or regulations on best land development practices related to solar farm implementation. Thus, we seek to synthesize the current state of scientific knowledge and management recommendations, as well as to identify gaps. We review the current science on how solar farms impact landscape hydrology and related soil and vegetation characteristics, as well as review the current state of land and stormwater management guidance in US states with respect to solar farms.

2. Methods

In order to review the current science on solar farm hydrology, in mid-2022 we sought relevant scientific literature using Google Scholar and Web of Science to perform searches with the following key words: (solar farm, PV, or agrivoltaic) and (hydrology, stormwater management, soil moisture, runoff, or evapotranspiration). We have also followed references cited in these articles to identify additional relevant articles. This yielded 18 usable articles which are reviewed.

In addition, we reviewed available information on land and stormwater management recommendations from US states. In the US, most states have authority delegated from the US Environmental Protection Agency to oversee permitting processes related to land development under the National Pollutant Discharge Elimination System (NPDES). States may also choose to enact their own regulations relating to solar farm development and/or stormwater management. We searched the websites of US state agencies with jurisdiction over stormwater management regulations, in order to summarize the available rules and guidelines specific to stormwater management on solar farms. If we could not find stormwater management information specific to solar farms for a given state, we also attempted to contact the agency directly for information.

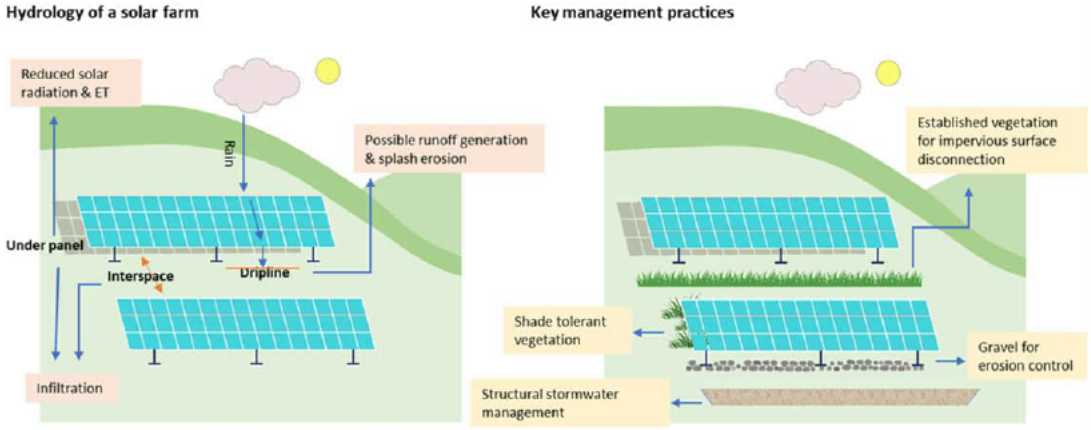

Figure 1. Key hydrological phenomena on a solar farm (left) and some example management practices for addressing stormwater management (right).

3. Review of scientific research on solar farm hydrology

Research on the landscape hydrology of solar farms is comprised of field-based and computational modeling studies. Field-based studies primarily address hydrologic components and landscape biophysical attributes, including soil moisture patterns, evapotranspiration, soil properties, and vegetation characteristics (table 1). Field studies span multiple continents and climatic zones, including Asia, North America and Europe. Modeling studies focus on simulating soil moisture, runoff generation, and erosion (table 2).

3.1. Solar farms and soil properties

Given that solar farms involve major construction activities during the site development process, there is potential for them to have impacts on soil properties and vegetation. Soil physical and chemical properties directly impact hydrologic processes, and thus we begin our review with understanding these impacts.

Some physical, chemical, and biological soil indicators can be lower on solar farms compared to semi-natural land cover types, depending on solar farm management strategies. Research on a solar farm in southern France with silty clay soils did not find differences in soil bulk density on solar farms as compared to semi-natural pinelands and shrublands, but did find a reduced water holding capacity (Lambert *et al* 2021). Research on a solar farm in Colorado, USA observed a greater coarse particle fraction on the solar farm as compared to an adjacent native grassland reference. The reason for the difference in particle size is likely the soil disturbance and vegetation removal during the construction phase of the solar farm, which causes erosion of the fine particles (Choi *et al* 2020a).

Some studies have found the carbon and nitrogen content to be lower in the soil on solar farms than in reference soils (Choi *et al* 2020a, Lambert *et al* 2021). Basal respiration and microbial biomass have also been measured at lower quantities on solar farms compared to reference land covers (Lambert *et al* 2021). However, at a solar farm on reclaimed cropland with meadow grasses, there were no significant differences in soil physical and chemical properties, as compared to a reference site (Armstrong *et al* 2016). There were some differences in soil biological indicators such as respiration, but the differences were not consistent throughout the year.

Some soil properties may also vary within the solar farm. Unsaturated hydraulic conductivity was found to be higher beneath solar panels on a solar farm in Colorado than at the edge or interspace area between panels (see the schematic of example solar farm in figure 1). The reason for this difference may be the reduced exposure to maintenance activities beneath the panel, which could induce compaction and reduce hydraulic conductivity (Choi *et al* 2020a). This in turn can impact patterns of soil moisture distribution, which is discussed later in section 3.4.

3.2. Solar farms, micrometeorology, and evapotranspiration

The presence of solar panels has the potential to alter multiple meteorological properties. They may change the balance of incoming solar radiation and emitted radiation, in turn altering soil temperature and evapotranspiration. The fact that they are typically mounted some distance above the ground and inclined may also affect wind dynamics. Additionally, the type and health of vegetation affects actual evapotranspiration (AET) rates, where vegetation may be influenced by the solar panels as well as by human management decisions.

Reduced solar radiation from shading has been documented beneath solar panels on solar farms in France, the United Kingdom, and Oregon and Nevada, USA. This results in lower mean daily soil and air temperatures

Table 1. Summary of the reviewed field-based studies on solar farm hydrologic phenomena, highlighting the basic study location and types of measurements made on hydrologic and related variables. An 'x' indicates that measurements were made for variables in the given category.

Source	Site characteristics			Types of measurements				
	Location	Climate zone	Solar farm info	Micro-meteorology	Soil Phys/Chem/ Bio properties	Veg-etation	Soil moisture	Runoff
AL-agele *et al* 2021	Corvallis, Oregon USA	Mediterranean warm, cool summer climates	0.8 ha agrivoltaic vegetable farm with 18 degree panel tilt. Silty clay loam soil	x	—	x	x	—
Armstrong *et al* 2016	Swindon, United Kingdom	Oceanic climate	Land cover prior to construction: the field site was arable cropland and was sown with a species-rich After construction: the control and interspace of the solar farm were re-seeded with species-rich meadow mixture meadow mixture	x	x	x		
Barron-Gafford *et al* 2019	Tucson, Arizona, USA	Arid climate, hot desert	Agrivoltaic site with crops (tomatoes, jalapenos, and chiltepin plants). Native soil was replaced with an organic garden blend (organic compost and an organic garden blend (organic compost and sandy soil) Age of the solar site: less than one year	x	—	x	x	—
Choi *et al* 2020a	Northern Jefferson County, Colorado, USA	Cold semi arid	The treatment site is revegetated with native grasses similar to the undisturbed condition (control point) Surficial soils at the solar site are paleosols with clay-enriched subsoil Age of the solar site: 8 years	x	x	—	x	—
Elamri *et al* 2018a, 2018b	Montpellier, France	Mediterranean hot summer	Agrivoltaic system (lettuce) with varying panel density and tilt. oil type is loamy clay deep alluvial soil (same site as Marrou et al. with updated ability for variable panel tilt)	x	—	—	x	—
Hassanpour Adeh *et al* 2018	Corvallis, Oregon USA	Mediterranean warm, Oregon USA	Agrivoltaic site with pasture. The soil classification for both the control and agrivoltaic systems is Woodburn silt clay Age of the solar site: 2 years	x	—	x	x	—
Lambert *et al* 2021	Southern France	Mediterranean hot summer climates	Soil type of solar farms are carbonatic pedofeatures Different control points with a land cover of pinewood, shrubland and abandoned vineyards were selected	—	x	x	x	—

(*continued on next page*)

Table 1. Continued Summary of the reviewed field-based studies on solar farm hydrologic phenomena, highlighting the basic study location and types of measurements made on hydrologic and related variables. An 'x' indicates that measurements were made for variables in the given category.

Source	Site characteristics			Types of measurements				
	Location	Climate zone	Solar farm info	Micro-meteorology	Soil Phys/Chem/ Bio properties	Veg-etation	Soil moisture	Runoff
Marrou 2013b *et al* 2013a,	Montpellier, France	Mediterranean hot summer climates	Agrivoltaic system (lettuce and cucumber) with varying panel density and a fixed 25 degree tilt. The soil type is loamy clay deep alluvial soil (same site as Elamri *et al* 2018a)	x	—	x	x	—
Uldrijan *et al* 2021	South Moravian Region, Czech Republic	Oceanic climate	The soil has textures of loamy-sand to clay-loam, vegetated with perennial grass mixture Age of the solar site: 7 years	—	—	x	—	—
Wu *et al* 2022	Northwestern China	Arid climate, cold desert	Solar farm with a panel tilt of 37.5 degrees, where a panel row is comprised of two adjoining sub panels with a 3 cm gap. Mixed gravel and sand soil substrate	—	—	—	x	—
Yue *et al* 2021	Western China	Arid climate, cold desert	The soil material is loess or gravel, soil texture is mainly sandy loam and light silt loam The main plant species are shallow-rooted plants Some of panels are fixed and some are rotating	x	—	—	x	—

Table 2. Summary of reviewed studies performing hydrological modeling of solar farms.

Source	Solar farm info	Modeling approach	Target variable(s)
Barnard *et al* 2017a	Three solar farm sites in west Texas and one solar site in Georgia USA (humid subtropical climate)	Flo-2D/HEC-HMS maps of maximum flow depth and velocity	The final products are
Cook and McCuen 2013	No specific geographic location Different scenarios: • Slope 1%–5% • Soil type B and C • Panel angle 30, 45 and 70 • Vegetation type: bare ground	Custom model in MATLAB (Water balance, Manning's Eqn)	Runoff depth, peak flow, erosion potential
Edalat 2017	Two solar farms in Nevada USA (arid climate) • Urban • Outside urban area	HEC-HMS	Runoff depth/peak flow
Elamri *et al* 2018b	Agrivoltaic solar farm in Montpellier, France (mediterranean hot summer	Hydrus 2D with custom AVrain module to simulate rain redistribution of panels	Solar panel rain redistribution /runoff, soil moisture
Pisinaras *et al* 2014	Low, medium, and high intensity solar the farm scenarios for sub-basins in 1%–5% of Vosvozis River watershed in northern Greece (Mediterranean hot summer climate) Solar farm scenarios replaced existing agricultural land use	SWAT	Surface runoff, infiltration, evapotranspiration
Walston *et al* 2021	Midwest United States (hot summer, continental climate) land use scenarios: • Agriculture scenario • Solar-turfgrass scenario • Solar-native grassland scenario	InVEST ecosystem services model	Sediment retention, water retention
Wu *et al* 2022	Solar farm in northwestern China (arid, cold desert climate)	Custom model using energy balance, AVrain and single bucket water balance	Soil moisture and temperature

below the panels in comparison to full sun reference sites during the spring and summer (AL-agele *et al* 2021, Armstrong *et al* 2016, Hassanpour Adeh *et al* 2018, Marrou *et al* 2013b, Yue *et al* 2021). Remote sensing of land surface temperature at a solar farm has also indicated overall reductions in soil temperature across the site as compared to pre-development data, though this approach could not explicitly evaluate changes below the panels (Edalat 2017). Wind and humidity changes were not as consistent. Wind speed and vapor pressure deficit did not change relative to solar panels at a solar farm in France (Marrou *et al* 2013b). However, wind speed, direction, and relative humidity were all altered around solar panels, as compared to the reference site at a solar farm in Oregon (Hassanpour Adeh *et al* 2018), and vapor pressure deficit decreased under solar panels on solar farms located in the United Kingdom and Arizona USA (Armstrong *et al* 2016, Barron-Gafford *et al* 2019).

There can be temporal variability in how solar farms affect meteorological properties and resulting soil dynamics. For example, solar panels decreased the soil temperature beneath the panels compared to reference sites, but these differences were more substantial in spring versus summer (Lambert *et al* 2021). Increases in soil temperature beneath solar panels relative to reference sites have also been observed during autumn and winter periods at solar farms located in the United Kingdom and western China, when solar panels may help prevent loss of longwave radiation (Armstrong *et al* 2016, Yue *et al* 2021). Remote sensing observations of the land surface temperature in Nevada found temperature differences to be greatest in winter when the Sun was lower and the shadows from solar panels were larger (Edalat 2017).

Reductions in solar radiation generally translate into reduced potential evapotranspiration (PET) under solar panels (Elamri *et al* 2018a, Hassanpour Adeh *et al* 2018). Solar farm impacts on evapotranspiration dynamics have been investigated in depth on prototypes of agrivoltaic systems in France, testing two crops (cucumber and lettuce) and two solar panel configurations (full panel density vs half density (Marrou *et al* 2013a). Results show that PET and AET were higher in the full Sun reference locations compared to the solar farm agrivoltaic sites. The reduction in AET was slightly more at the full density solar farm as opposed to the half density site, and differences also varied by crop type. For the lettuce agrivoltaics site, AET over the measured growing period was 103 mm at the full Sun reference, but reduced to 81 and 79 mm for the half density and full

density solar farm sites, respectively. Similarly, at the cucumber agrivoltaics site, AET was 178 mm at the full Sun reference, but reduced to 153 and 145 mm at the half density and full density solar farm sites, respectively. In general, ET fluxes were more affected in spring than in summer, indicating temporal variability in the solar panel influence (Marrou *et al* 2013a). The ratio of transpiration to evaporation also changed, increasing 3 – 4 times in the shaded area of the solar farm sites.

Additional research at this same agrivoltaic site explored the impact of variable panel tilting/tracking on solar radiation and ET (Elamri *et al* 2018a). While there was still a net reduction in solar radiation and ET under panels with panel tracking, it led to much less heterogeneity than at the sites with a fixed panel orientation.

3.3. Solar farms and vegetation

As with soil properties, vegetation on solar farms is a function of both initial human management decisions regarding the initial solar farm development, and ongoing operations and maintenance decisions on the solar farm. It is also affected by interactions with site soil properties and hydrology. Vegetation is explicitly leveraged as a stormwater management practice, as described later in this review, and is a critical managed element of agrivoltaics operations where solar farms are leveraged for the additional co-benefits of crop production. Thus we feel it is important to review what is known about changes in vegetation on solar farms.

Existing field research has focused on the assessment of vegetation coverage, biomass, and diversity, as well as on interactions with hydrologic processes via water use efficiency or water productivity. Findings are quite variable in these limited studies. Surveys of a solar farm (non-agrivoltaic site) in France largely found no major differences in plant community composition and coverage, relative to nearby reference shrubland and pineland sites. There was a slight increase in the relative abundance of shadow-tolerant plant types under solar panels (Lambert *et al* 2021). At a reclaimed brownfield site in the Czech Republic, where the land was sown with a meadow grass mixture during solar farm development, differences in plant composition within the solar farm were observed in a survey eight years after the initial development (Uldrijan *et al* 2021). A greater abundance of taller native perennial grasses was documented in the interspace between panel rows, where more shade-tolerant species and sometimes invasive grasses were observed beneath panels. At a solar farm in the United Kingdom, reduced plant species diversity was observed under solar panels, with reference and panel interspace areas dominated by forbs and legumes (Armstrong *et al* 2016).

Both increases and decreases in vegetation biomass have been documented under solar panels, depending on the climatic zone. In the areas with lower solar radiation (solar farms in the United Kingdom and the Czech Republic), reduced vegetation coverage and reduced biomass (up to four times lower) have been documented beneath solar panels, relative to panel interspace or reference areas (Armstrong *et al* 2016, Uldrijan *et al* 2021). However, the results of research in the solar farm located in Oregon show 126% more dry biomass beneath solar panels relative to the interspace zone and 90% more dry biomass relative to the reference site (Hassanpour Adeh *et al* 2018). This site is less energy-limited. Thus, the shading of solar panels helps to reduce ET losses and in turn to maximize the water use efficiency of plants, as well as to increase biomass. At crop agrivoltaic sites in Oregon and France, some reduction in crop yield and biomass has been observed under panels relative to nearby reference sites (AL-agele *et al* 2021, Elamri *et al* 2018a). At sites with solar panel tracking, biomass was only 16% less than the reference, compared to 30% or greater reductions at fixed panel sites (Elamri *et al* 2018a).

More efficient water use has been observed under solar panels in multiple cases, mainly because of the shading and reduced solar radiation and PET under the panels. This is particularly evident in locations abundant in solar radiation. In an agrivoltaics solar farm in Arizona, USA, the shade of the solar panels reduced plant drought stress and led to greater crop and food production (Barron-Gafford *et al* 2019). More efficient water use was also observed for lettuce crops in an agrivoltaics solar farm in France. Coverage of soil by crops was found to be important in reducing soil evaporation and maximizing the availability of water for transpiration and biomass production (Marrou *et al* 2013a). Water productivity also improved in the shade of panels at a tomato agrivoltaic site located in Oregon (AL-agele *et al* 2021). Modeling of water and vegetation dynamics at agrivoltaic sites in France successfully reproduced field data on rain and soil water redistribution, and allowed for the additional scenario exploration of plant-water interactions and optimization. The modeled scenarios indicated that the tilting of solar panels could help to minimize water interception and the associated redistribution of water. The scenarios also indicated that agrivoltaics could improve water productivity relative to more traditional agriculture, with only small reductions in crop yield (Elamri *et al* 2018a, 2018b).

3.4. Impact of solar panels on soil moisture distribution

On solar farms, the impervious surface of solar panels intercepts precipitation and drains the water into the interspace between panels. Previously discussed changes in evapotranspiration and soil physical and chemical properties can interact with this altered surface hydrology to cause some heterogeneity in the soil moisture content on solar farms.

Field measurements of the soil moisture on solar farms have often been focused on key locations relative to the solar panels. These have included the interspace area fully open to the sun between panels, under the lower front edge of the panel or 'dripline', underneath the center of the panels, and at the back (higher) edge of the panels where there is partial Sun (figure 1). Sometimes measurements may also be made at a control or reference area outside the main array of panels. At a solar farm in western Oregon, USA on silt clay soils, the soil beneath the center of solar panels was consistently wettest, followed by soil under the back edge of solar panels, and nearby reference soils, with the interspace soils being driest. At a 0.6 m depth, soil under the center of the panels remained near saturation (∼30% volumetric water content (VWC)), whereas the interspace area depleted from ∼30% to ∼20% VWC by the end of the growing season (Hassanpour Adeh *et al* 2018). Similar patterns have been observed at solar farms in China (Wu *et al* 2022, Yue *et al* 2021). Soil moisture at a northwest China site was wettest (10%–20% VWC) at the main dripline at the front of panels as well as under the center of the panel row where a small gap in panels was located; soils at the back edge of panels and nearby reference soils were driest (5%–10% VWC; Wu *et al* 2022). At an arid western China solar farm, soil moisture was consistently higher under panels—14.7% higher under fixed tilt panels compared to 11% higher under variable tilt panels (Yue *et al* 2021). Soil moisture was also consistently higher under solar panels at an agrivoltaics site located at Arizona, USA, as compared to an agricultural control site (Barron-Gafford *et al* 2019). At a solar farm in Colorado, USA (cold semi-arid climate) with paleosols and clay subsoil, some soil moisture variability was observed. Dripline soils were consistently higher (up to 20% – 30% VWC), especially following rain events (Choi *et al* 2020a). However, substantial variability in soil moisture at all locations relative to solar panels led to a lack of statistically significant differences. The reference site at nearby native grassland was consistently lower in moisture (∼5%). At an agrivoltaic site in France, higher soil moisture was observed at panel driplines, while soil moisture was lower under the panels and in the interspace (Elamri *et al* 2018b). Another solar farm in France did not demonstrate differences in soil moisture under solar panels compared to the interspace, but did observe overall reduced soil moisture at the solar farm sites as compared to a shrubland reference (Lambert *et al* 2021). Overall, the main panel dripline at the front of solar panel rows is consistently wetter, and interspace zones tend to be drier. However, under panel soil moisture may vary depending on the balance of evapotranspiration and runoff contributions, due to the climate and panel design.

There have also been some efforts to model soil moisture dynamics on solar farms. These studies have created or leveraged models of rain redistribution from solar panels, and then combined this with various approaches of water and energy balance representation to simulate soil moisture (Elamri *et al* 2018b, Wu *et al* 2022). In both cases, there was reasonable agreement between observed and simulated soil moisture. Suspected causes of inaccuracy included challenges in representing the complex energy dynamics under solar panels that influence evapotranspiration (Wu *et al* 2022) as well as challenges in the accurate representation of water redistribution (Elamri *et al* 2018b).

3.5. Solar farms and runoff

To our knowledge, at the time of the writing of this review, the evaluation of runoff generation has occurred only in published modeling-based studies. Many of these studies leverage existing modeling programs, with certain modifications used to represent the unique land cover type of the solar panels. None of these published studies, to our knowledge, have validated their models with field data specific to solar farms.

HEC-HMS (US Army Corps of Engineers 2021) has been leveraged in multiple studies. In one study, the runoff on a solar farm was simulated using a linked model which used a combination of Flo-2D and HEC-HMS (which uses a one-dimensional approach). To simulate the flow from upgradient catchments to the solar farm catchment, HEC-HMS was used. USDA Natural Resource Conservation Service Curve Number methods and shallow water equations were used to predict and route stormwater runoff across FLO-2D grids. The results were reported as maps of maximum flow depths and velocities (Barnard *et al* 2017a). HEC-HMS has also been used to study hydrologic dynamics in a Nevada, USA (arid climate) solar farm (Edalat 2017). It is shown that regardless of the orientation and tilt angles, runoff volume increases after solar panel installation. Impacts on peak flow are more variable, with the orientation of panels either increasing or decreasing peak flow rates. The results indicate that the panels also noticeably change the rain distribution onto the land surface. Therefore, panel orientation and tilt angles are important factors that need to be considered in stormwater channel design to carry runoff peak flow. One major limitation of this study was that solar panels were represented as an impervious surface on the ground, and infiltration could not be permitted under the panels, as would occur at an actual site; thus this approach likely overestimates runoff (Edalat 2017).

SWAT has also been leveraged for assessing the impact of solar farms on watershed hydrology (Pisinaras *et al* 2014). For a watershed in northern Greece, scenarios were implemented that induced land use change from agriculture to solar farms in 1 or 5% of the watershed area. Solar farm implementation was represented using soil physical property changes, curve number increase associated with imperviousness, ground cover change from cultivated to bare soil, and reduced solar radiation. The model demonstrated increased surface runoff

and percolation, and decreased ET due to solar panel implementation, but these changes were not significant at the watershed scale. However, there is the potential for local-scale impacts. For example, there were increases of ~100 mm in surface runoff for a given sub-basin, even for a low impact scenario of solar farm implementation (Pisinaras *et al* 2014).

Other research has relied on custom-built models for representing solar farms (Cook and McCuen 2013). A model written in MATLAB was based on the creation of NRCS type II storms for precipitation (hyetograph) inputs. A simple water balance for each land surface cell was used to allocate precipitation to storage or loss (runoff). Manning's equation was used to estimate runoff velocity and the associated kinetic energy relating to splash erosion. Model scenarios were constructed for a 30 cell grid solar farm, where each cell could have a portion allocated as wet, dry, or interspace. A variety of characteristics were manipulated to simulate changes in soil types, solar panel spacing, vegetation roughness, etc. The results indicated that the addition of solar panels over a grassy field does not change the volume of runoff, the peak discharge, nor time to peak. In general, it was not anticipated that structural stormwater management would be required to prevent adverse impacts (Cook and McCuen 2013).

Some US states, such as Minnesota, have recommended a simple modification to the calculation of impervious surface used in typical runoff modeling approaches for stormwater management planning. Minnesota's recommendation for the modification of runoff calculations leverages the ratio of impervious to pervious surface, where the pervious surface considers both the interspace area as well as the area directly below the panels. Runoff depth associated with this impervious to pervious ratio, as well as soil type, is determined using an Excel tool that leverages the output of an extensive series of models generated in XP-SWMM (Minnesota Pollution Control Agency 2019).

3.6. Solar farms and erosion

Research on the impacts of solar farms on erosion is quite limited. Some modeling results suggest solar panels can increase erosion. The energy and velocity of water draining from the panels is higher, which could cause erosion in soil below the base of the panels, especially if the interspace is bare. Increases (up to 10 times) of kinetic energy were simulated, which could lead to erosion and the need for erosion control measures, but this modeling effort was not validated by field measurements (Cook and McCuen and 2013).

A larger-scale modeling assessment has quantified changes in erosion and associated sediment loss, along with multiple other ecosystem services for hypothetical solar farms in the Midwestern US. These solar farm scenarios focused on vegetation, comparing hypothetical solar farms with native grassland or turfgrass with baseline agricultural land use. Modeling with InVEST, which leverages the revised universal soil loss equation, estimated sediment export under the solar-native grassland scenario to be 0.007 tons/ha/year, which was a reduction of over 95% and 77% compared to the agriculture and solar-turfgrass scenarios, respectively (Walston *et al* 2021). However, erosion estimates were based largely on landscape characteristics such as vegetated cover or slope and did not explicitly represent the fact that solar panels are elevated off the ground.

This existing work largely focuses on the potential for erosion on solar farms after initial construction. However, construction of solar farms can require substantial land manipulation. Thus, it is also important to consider this in erosion estimates, and manage this impact appropriately (see discussion in section 4). In addition to erosion associated with runoff, aeolian erosion is a concern in more arid environments, particularly when presence of vegetation is limited (Ravi *et al* 2016).

4. Review of guidance from US states on solar farm development and stormwater management

In our review of the guidelines and rules of different US states regarding stormwater management on solar farms, a major finding was that most states (close to 30) do not have any guidance for stormwater management specific to solar farms. For ten states, no definitive information was found online and no answer was received to email inquiries, and it is assumed that there is no solar farm specific guidance. In general, these states without specific guidelines defer to their standard rules regarding construction and stormwater management. This typically means that for construction that disturbs a certain area of land (often specified as 1 acre), the solar farm developer would need to follow requirements under the construction general permit for stormwater management. There also may be post-construction stormwater management requirements. The management of construction-related stormwater impacts is required to be managed by states or the US Environmental Protection Agency (US EPA) under the EPA's National Pollution Discharge Elimination System (NPDES) (US EPA 2015).

Twelve US states currently have solar farm-specific guidance relating to managing stormwater (table 3). These states are largely located in the north-central, eastern, and northwestern US. Guidelines from these states rely heavily on 'low impact development' practices (Davis 2005). This involves minimizing initial impacts on

the site during the construction process, as well as strategically planned development and site operations that maintain the natural characteristics of the land to mitigate stormwater. The stormwater management functions desired involve runoff volume reduction via infiltration and, to a lesser degree, evapotranspiration; these processes are in turn dependent on soil properties and vegetation. The reduction of erosion and/or retention of sediment relies on reducing the velocity of runoff through infiltration and enhanced surface roughness, particularly from vegetation (Davis *et al* 2012).

Some guidance relates to the initial site selection process for the solar farm. It is recommended to avoid soils with a slip potential, and well-draining soil types are ideal. Lesser sloped sites are ideal, though there is substantial variability in the recommended slope thresholds (e.g. Maryland recommends 5% or less, while other states recommend less than 10%). With considerations such as the slope or soil hydrologic class, certain categories (e.g. poorly draining soils or higher slopes) are generally permissible for solar farms, but would require additional structural stormwater management to be added (discussed further below).

During the construction process, it is recommended that soil compaction and disturbance be minimized, in order to maintain the soil's natural ability to infiltrate runoff. It is also critical to implement temporary erosion and sediment controls to prevent any impacts during the construction process. This may include erosion control socks, temporary sedimentation basins, or mulching the bare soil surface.

Another group of recommendations relates to how the solar farm site is designed. A key stormwater management practice mentioned by most states with specific guidance is to maintain a certain interspace distance between rows of solar panels. This leverages the 'low impact development' principle of disconnecting impervious surfaces. The pervious interspace between solar panel rows serves to promote infiltration of any runoff and the retention of eroded sediment. In this interspace, as well as under the panels, it is often recommended to maintain a certain proportion of vegetation cover on the site, at least 85% – 90%. A deep-rooted perennial vegetation cover, typically grasses, forbs, or legumes is recommended to facilitate infiltration and assist with erosion control. This may be satisfied by minimizing the impact to existing vegetation, or may be facilitated by seeding. Crop production may also occur, but additional considerations may be needed to ensure that harvesting does not facilitate increased runoff or erosion. It is also important to promote the establishment of more shade-tolerant vegetation under the panels. Minimal mowing, pesticide, or herbicide application is recommended.

The additional practice recommended in some cases is structural stormwater management. As noted above, these sorts of structural practices may be required for specific cases where a site has a high slope or poorly draining soils. Some structural practices are focused on runoff volume reduction via enhanced infiltration, and include features like infiltration basins or infiltration trenches. Other structural practices may be focused on erosion prevention and sediment control and involve stone drip or splash pads near the dripline area under solar panel rows.

5. Discussion and conclusions

5.1. Insights from ecohydrologic research on solar farms

There is a small but growing body of work characterizing how solar farm development changes soil properties, vegetation, and hydrologic processes. Most existing work focuses on soil properties, vegetation, soil water, and micrometeorological characteristics or evapotranspiration; there is no published work yet in the academic literature, to our knowledge, documenting the direct measurement of runoff on solar farms.

The results of scientific research vary from findings of no net impact of solar farms on these ecohydrological properties to detection of some impacts. Field soil moisture measurements often demonstrated variability with respect to the solar panels. These changes in soil moisture relative to panels demonstrate the impact of panels on solar radiation, runoff redistribution, and the corresponding evapotranspiration. Particularly in regions where evapotranspiration is not energy-limited (e.g. warm arid regions), there is a climatic sweet spot where the shading of solar panels can help reduce evapotranspiration and maximize water efficiency and facilitate enhanced crop production in association with solar farms (Barron-Gafford *et al* 2019, Hassanpour Adeh *et al* 2018). Results from agrivoltaic systems indicate that crops can still achieve high yield under the fluctuating shade of these systems (Marrou *et al* 2013a). However, more extensive research is merited in agrivoltaic systems across a range of climate settings and crop types.

In wetter climates, there is an interest in keeping soils from reaching sustained levels of saturation and the associated runoff generation. Solar panels introduce heterogeneity in the soil moisture distribution, with precipitation accumulating along the dripline at the lower edge of the panels. It is essential that appropriate management practices are implemented to prevent this heterogeneity from manifesting in increased runoff and erosion generation. Variable panel tilting may also be considered to reduce the redistribution of water.

Table 3. Example guidelines from US states regarding stormwater management on solar farms. The table is not comprehensive of every guideline for all listed states, but provides examples of the range of guidelines currently available.

Category	Recommendation	Source of example
	Site conditions	
Site slope	Ideally <5%; >5% requires various additional management considerations. For slopes >8%, additional management needed to maintain sheet flow and prevent erosion.	Maryland (MA DOE 2021) North Carolina (NC DEQ 2018), Rhode Island (RI DEM 2021)
	<10% is favorable; additional management considerations if >10%.	Pennsylvania (PA DEP, 2019)
Soils	For soils with a depth to bedrock of 12″ or less, plans must show that soil will be enhanced by the addition of at least 4″ of top soil.	New Hampshire (NH DES 2020)
	Sites with soils having a slip potential should be more closely evaluated for any geotechnical issues—especially in areas with moderate to steep slopes. 2. Soil compaction should be avoided.	Pennsylvania
	Considerations during construction	
Considerations during construction	To minimize disturbance and compaction, construction vehicles and equipment should avoid interspace areas during installation of the solar panels to effectively use interspace later for impervious disconnection/infiltration.	Maryland
	Erosion and sediment control practices are needed. Temporary erosion control, such as mulch, must be put on exposed soil at the site to prevent erosion during rain events until vegetation is established.	Massachusetts (Mass DEP 2017), Minnesota (MN PCA, 2021), New Hampshire
	Avoid soil compaction and/or topsoil removal. Ifthe soil is compacted or removed, it should be amended to return to its pre-development condition.	Massachusetts, New Hampshire, North Carolina
	Post-construction stormwater management	
Modeling runoff from impervious area	The calculation of water quality volume depends on the slope (if >15%, then panels are an effective impervious area, if not then the evaluation of vegetated areas is emphasized).	Connecticut (CT DEEP 2020)
	For water quality and water quantity calculations, solar panels are considered disconnected impervious surfaces.	Minnesota, Virginia (VA DEQ 2022)
	Curve number adjustment is permitted to account for infiltration under impervious panels. With certain steeper slope + soil drainage classes, there cannot be the assumption that infiltration will occur under panels.	New Hampshire
	Solar panels are not considered impervious surfaces, so they do not need to be considered in the calculation of impervious cover at a site.	New Jersey (New Jersey Legislature 2021)
Panel orientation	Parallel orientation of the solar panels is recommended with respect to slope, in order to prevent flow concentration. If not, runoff should be directed to infiltration practices.	Rhode Island
	The orientation of panels should be considered with respect to drainage pattern, flow concentration, drainage area, and velocity.	Connecticut
Vertical clearance of panels	< 10 feet in order to minimize erosion at the dripline.	Connecticut, Massachusetts, North Carolina, Ohio (OH EPA 2019), Pennsylvania
Impervious disconnection	In general, all states with solar-specific stormwater guidance leverage the disconnection of the impervious surface (i.e., solar panel rows) with well-established vegetation as a key stormwater management strategy, under certain site conditions. More details are noted in the examples below.	
	The vegetated interspace area receiving runoff must be equal to or greater in length than the disconnected surface (e.g., the width of the row of solar panels). Runoff must sheet flow onto and across vegetated areas to maintain the disconnection.	Maryland, North Carolina, Pennsylvania, Rhode Island
	Solar panel rows are spaced in a manner to allow sunlight penetration sufficient to support vegetation between the solar panel rows.	Massachusetts, Rhode Island
	Pervious space is required between rows of panels. This allows for the use of the 'disconnected impervious credit method', which often results in a reduction in the water treatment volume required.	Minnesota
	Under some conditions such as the existence of an uncompacted soil profile, dense and healthy vegetation maintenance, it is possible to easily manage the runoff from panels by disconnection. The disconnection length depends on the soil type, where well-draining soils require a shorter interspace (e.g. 1:1 solar panel to interspace distance along the slope) compared to more poorly draining soils.	Ohio

(*continued on next page*)

Table 3. Continued Example guidelines from US states regarding stormwater management on solar farms. The table is not comprehensive of every guideline for all listed states, but provides examples of the range of guidelines currently available.

Category	Recommendation	Source of example
	Site conditions	
Vegetation	In areas receiving disconnected runoff, groundcover vegetation must be maintained in good condition and should be protected from future compaction (e.g., by planting shrubs or trees along the perimeter).	Maryland
	Include cool-season, warm-season, shade-resistant, and legumes as necessary to develop a dense, year-round groundcover that accounts for differences in the temperature and shading from panels.	North Carolina, Ohio, Rhode Island
	Utilize low- and slow-growing grass varieties to reduce compaction and damage from frequent mowing. Low maintenance grass mixture recommended. The use of fertilizers, pesticides, and herbicides should be minimized.	North Carolina, Ohio, Rhode Island
	>90% deep-rooted perennial vegetative cover with a density capable of resisting accelerated erosion and sedimentation is required. If mowed, do not cut to < 4 in. In agrivoltaic applications, this may include hand-harvested or small machine-harvested crops.	Pennsylvania
	There should be at least 85% coverage. Maintain the vegetation height that maximizes sheet flow - no shorter than 4″ and not taller than 12″ (grass) or 18″ (meadow).	Rhode Island
Post-construction structural stormwater management	When the slope >5%, spreaders, terraces, or berms may be used to prevent concentrated flow and promote infiltration. When the slope >10%, more extensive stormwater management is required.	Maryland
	If the disconnected interspace is not adequate for the volume reduction of runoff or other site conditions merit it, other types of permanent stormwater management for non-erosive conveyance of runoff must be constructed, such as infiltration trenches or berms, wet sedimentation basins, or sand filters.	Connecticut, Massachusetts, Minnesota, Pennsylvania
	A stone drip pad to prevent erosion at the dripline, if panels have a fixed inclination.	Ohio
	Where panels are not oriented generally parallel with the slope and/or where slopes are >8%, runoff needs to be either intercepted by stone trenches for infiltration and/or directed non-erosively to an infiltration practice. Add scour control if instances of erosion/scour develop. Regular inspection and maintenance of infiltration practices is required, and to look for erosion	Rhode Island
	For a solar array in an open field, it is expected that the designer will show compliance with flow control related requirements by using infiltration and/or dispersion type management practices	Washington (Washington State Department of Ecology 2021)

At the time of this review, we were unable to find any study that directly evaluated runoff generation on solar farms through field measurement. Thus, we are still lacking critical insight into whether solar farms change runoff generation, and whether existing site and stormwater management practices are adequate to prevent adverse impacts. As a result, existing hydrologic models of solar farms are largely uncalibrated. There is also a bias in the sort of sites being evaluated. In general, existing environmental research on solar farms has focused on more ideal sites, i.e. those on sites with lower slopes and well-draining soils. Thus, we are neglecting sites that could be more vulnerable to changes in hydrologic processes with solar farm development.

In general, there is still also a need for simultaneous evaluation of multiple environmental co-benefits from solar farm land management, considering how certain vegetation or crop choices could help manage runoff, but also provide habitat or food.

5.2. Connecting observed phenomena to management decisions

While there are some environmental conditions that are linked to the inherent characteristics of ground-mounted solar panels (e.g. that there will be at least some level of shading and interception of water from an inclined panel above the ground), many phenomena can be influenced strongly by specific decisions in how the solar farm is constructed and managed.

Changes in certain soil properties (e.g. the reduction in soil organic matter) between solar farms and reference sites indicate the impacts of initial solar farm development, such as some removal of soil and/or vegetation and regrading of soil. This is something that can be changed by a more careful development process. Other soil property changes in different parts of the solar farm (under panel versus interspace) indicate the impacts of continued maintenance between the panels, such as mowing, that may induce some compaction. Thus, these observed detrimental impacts should be addressed as solar farm development guidance is developed. There are opportunities to select management practices that minimize adverse impacts (e.g. soil compaction) and maximize additional benefits- for example, leveraging sheep grazing for vegetation management in lieu of frequent mowing.

5.3. Key gaps in regulatory/management approaches and scientific knowledge

Most states in the US currently rely on construction general permits for guiding solar farm development, which may not be adequate for the unique design of solar farms (Great Plains Institute 2021). Only 12 of 50 US states had solar-specific stormwater management guidance, as of the writing of this review. The management practices currently recommended largely leverage low impact development practices of disconnection of the solar panel impervious surface, well-developed shade-tolerant vegetation, and minimal impact of construction practices on soil properties. Where necessary, given site conditions or solar panel configuration, structural stormwater practices such as infiltration practices are recommended. These recommendations are an important start, but validation is needed to confirm that these current practices are adequate, and appropriately tailored to the site conditions. There is a particular lack of guidance relating to appropriate stormwater management practices for solar farms in arid environments (table 3).

Given that runoff volume and quality are key metrics in the stormwater regulatory realm, it is a major gap that there is a lack of field research studying runoff on solar farms. It is also critical that hydrologic modeling approaches be improved to appropriately represent the unique design of solar panels, in that there is an impervious surface with the ability to infiltrate water underneath. In particular, approaches are needed that are simple enough to be widely implemented by those personnel preparing runoff calculations and associated permits for proposed solar farm development.

Though this review focused on hydrology and stormwater management, it is critical that future research and management consider simultaneous evaluation of some of the many other ecosystem services (or disservices) that could be provided by solar farms (Moore-O'Leary *et al* 2017). The role of solar farms (and how precisely they are developed) can also be explored further within the food-energy-water nexus (Lee *et al* 2021). Hernandez *et al* recently proposed a framework of 'techno-ecological synergy' which pushes us to think more broadly about how to implement renewable energy technologies where they will minimize ecological impact and maximize additional co-benefits (Hernandez *et al* 2019). Thus, instead of simply considering how to minimize the environmental impacts for an already proposed solar farm, we need to also think more broadly about what are the most optimal sites for this type of development. This includes considering how to leverage existing impervious surface for the implementation of utility-scale solar energy, such as parking lots or warehouses. With these multi-criteria and system frameworks, we can ensure that solar farms are developed in the most sustainable manner.

Acknowledgments

We thank anonymous reviewers for their constructive comments that improved the manuscript. This project was supported by the U.S. Geological Survey via the Pennsylvania Water Resources Research Center, under award #G21AP10576-PA and project #E04.

Data availability statement

No new data were created or analysed in this study.

ORCID iDs

Rouhangiz Yavari https://orcid.org/0000-0002-1088-6197
Raj Cibin https://orcid.org/0000-0001-5374-8504
Lauren McPhillips https://orcid.org/0000-0002-4990-7979

References

AL-agele H A, Proctor K, Murthy G and Higgins C 2021 A case study of tomato (*Solanum lycopersicon* var. Legend) production and water productivity in agrivoltaic systems *Sustainability* **13** 2850

Aman M M, Solangi K H, Hossain M S, Badarudin A, Jasmon G B, Mokhlis H, Bakar A H A and Kazi S N 2015 A review of safety, health and environmental (SHE) issues of solar energy system *Renew. Sustain. Energy Rev.* **41** 1190–204

Armstrong A, Ostle N J and Whitaker J 2016 Solar park microclimate and vegetation management effects on grassland carbon cycling *Environ. Res. Lett.* **11** 074016

Barnard T, Agnaou M and Barbis J 2017 Two dimensional modeling to simulate stormwater flows at photovoltaic solar energy sites *J. Water Manage. Model.* **25**

Barron-Gafford G A *et al* 2019 Agrivoltaics provide mutual benefits across the food-energy-water nexus in drylands *Nat. Sustain.* **2** 848–55

Blaydes H, Potts S G, Whyatt J D and Armstrong A 2021 Opportunities to enhance pollinator biodiversity in solar parks *Renew. Sustain. Energy Rev.* **145** 111065

Choi C S, Cagle A E, Macknick J, Bloom D E, Caplan J S and Ravi S 2020a Effects of revegetation on soil physical and chemical properties in solar photovoltaic infrastructure *Front. Environ. Sci.* **8** 140

Connecticut Department of Energy and Environmental Protection (CT DEEP) 2020 *Guidance regarding solar arrays and the general permit for the discharge of stormwater and dewatering wastewaters from construction activities* Connecticut guidance for construction of solar array projects https://portal.ct.gov/-/media/DEEP/water_regulating_and_discharges/stormwater/construction/200108GuidanceforConstructionofSolarArrayProjects.pdf

Cook L M and McCuen R H 2013 Hydrologic response of solar farms *J. Hydrol. Eng.* **18** 536–41

Davis A P 2005 Green engineering principles promote low-impact development *Environ. Sci. Technol.* **39** 338A–44A

Davis A P, Stagge J H, Jamil E and Kim H 2012 Hydraulic performance of grass swales for managing highway runoff *Water Res.* **46** 6775–86

Edalat M M 2017 *Remote Sensing of the Environmental Impacts of Utility-Scale Solar Energy Plants* (Las Vegas: University of Nevada)

Elamri Y, Cheviron B, Lopez J-M, Dejean C and Belaud G 2018a Water budget and crop modelling for agrivoltaic systems: application to irrigated lettuces *Agric. Water Manag.* **208** 440–53

Elamri Y, Cheviron B, Mange A, Dejean C, Liron F and Belaud G 2018b Rain concentration and sheltering effect of solar panels on cultivated plots *Hydrol. Earth Syst. Sci.* **22** 1285–98

Graham M, Ates S, Melathopoulos A P, Moldenke A R, DeBano S J, Best L R and Higgins C W 2021 Partial shading by solar panels delays bloom, increases floral abundance during the late-season for pollinators in a dryland, agrivoltaic ecosystem *Sci. Rep.* **11** 7452

Great Plains Institute 2021 *Photovoltaic Stormwater Management Research and Testing (PV-SMaRT) Potential Stormwater Barriers and Opportunities* (Great Plains Institute) https://betterenergy.org/wp-content/uploads/2021/10/PV-SMaRT-Potential-Stormwater-Barriers-and-Opportunities.pdf

Gunerhan H, Hepbasli A and Giresunlu U 2008 Environmental impacts from the solar energy systems *Energy Sources* A **31** 131–8

Hassanpour Adeh E, Selker J S and Higgins C W 2018 Remarkable agrivoltaic influence on soil moisture, micrometeorology and water-use efficiency *PLoS One* **13** e0203256

Hernandez R R *et al* 2019 Techno-ecological synergies of solar energy for global sustainability *Nat. Sustain.* **2** 560–8

Hernandez R R *et al* 2014 Environmental impacts of utility-scale solar energy *Renew. Sustain. Energy Rev.* **29** 766–79

Grigorescu I, Vrînceanu A, Vrînceanu A, Dumitrașcu M, Mocanu I, Dumitrică C, Mitrică B, Kuscicsa G and Șerban P 2019 Regional differences in the spatial distribution and environmental consequences of PV farms in southern Romania *Ukrainian Geogr. J.* **3** 60–9

Jacobson M Z and Delucchi M A 2011 Providing all global energy with wind, water, and solar power: I. Technologies, energy resources, quantities and areas of infrastructure, and materials *Energy Pol.* **39** 1154–69

Lambert Q, Bischoff A, Cluchier A, Cueff S and Gros R 2021 Effects of solar park construction and solar panels on soil quality, microclimate, CO_2 effluxes and vegetation under a Mediterranean climate *Land Degradation and Development* **32** 5190–5202

Lee K, Khanal S and Bakshi B R 2021 Techno-ecologically synergistic food-energy-water systems can meet human and ecosystem needs *Energy Environ. Sci.* **14** 3700–16

Marrou H, Dufour L and Wery J 2013a How does a shelter of solar panels influence water flows in a soil-crop system? *Eur. J. Agron.* **50** 38–51

Marrou H, Guilioni L, Dufour L, Dupraz C and Wery J 2013b Microclimate under agrivoltaic systems: is crop growth rate affected in the partial shade of solar panels? *Agric. For. Meteorol.* **177** 117–32

Maryland Department of the Environment (MA DOE) 2021 *Maryland Stormwater Design Guidance—Solar Panel Installations* (Maryland Department of the Environment) https://mde.maryland.gov/programs/Water/StormwaterManagementProgram/Documents/ESDMEP%20Design%20Guidance%20Solar%20Panels.pdf

Massachusetts Department of Environmental Protection (Mass DEP) 2017 *MassDEP Wetlands Program Policy 17-1: Photovoltaic System Solar Array Review|Mass.gov* (Massachusetts Department of Environmental Protection) https://mass.gov/guides/massdep-wetlands-program-policy-17-1-photovoltaic-system-solar-array-review

Minnesota Pollution Control Agency 2019 *Stormwater Management for Solar Projects and Determining Compliance with the NPDES Construction Stormwater Permit (Minnesota Stormwater Manual)* (Minnesota Pollution Control Agency) https://stormwater.pca.state.mn.us/index.php/Stormwater_management_for_solar_projects_and_determining_compliance_with_the_NPDES_construction_stormwater_permit

Moore-O'Leary K A, Hernandez R R, Johnston D S, Abella S R, Tanner K E, Swanson A C, Kreitler J and Lovich J E 2017 Sustainability of utility-scale solar energy—critical ecological concepts *Front. Ecol. Environ.* **15** 385–94

New Hampshire Department of Environmental Services (NH DES) 2020 *New Hampshire Guidance for Large Solar Arrays* (New Hampshire Department of Environmental Services) https://sulloway.com/wp-content/uploads/2020/09/NHDES-Solar-Stormwater-Guidance_2.28.20.pdf

New Jersey Legislature 2021 *Bill S291: Exempts Solar Panels from Impervious Surface or Impervious Cover Designation* (New Jersey Legislature) https://njleg.state.nj.us/bill-search/2010/S921

North Carolina Department of Environmental Quality (NC DEQ) 2018 *NCDEQ Stormwater Design Manual: Solar Farms* (North Carolina: North Carolina Department of Environmental Quality) https://deq.nc.gov/about/divisions/energy-mineral-and-land-resources/stormwater/stormwater-program/stormwater-design

Ohio Environmental Protection Agency (OH EPA) 2019 Ohio guidance on post-construction storm water controls for solar panel arrays https://epa.ohio.gov/static/Portals/35/storm/Guidance+on+Post-Construction+Storm+Water+Controls+for+Solar+Panel+Arrays.pdf

Pennsylvania Department of Environmental Protection (PA DEP) 2019 Pennsylvania Department of Environmental Protection (PA DEP) 2021 Chapter 102 Permitting for Solar Farms: Frequently Asked Questions (FAQ) https://files.dep.state.pa.us/Water/BPNPSM/StormwaterManagement/ConstructionStormwater/Solar_Panel_Farms_FAQ.pdf

Pisinaras V, Wei Y, Bärring L and Gemitzi A 2014 Conceptualizing and assessing the effects of installation and operation of photovoltaic power plants on major hydrologic budget constituents *Sci. Total Environ.* **493** 239–50

Ravi S, Macknick J, Lobell D, Field C, Ganesan K, Jain R, Elchinger M and Stoltenberg B 2016 Colocation opportunities for large solar infrastructures and agriculture in drylands *Appl. Energy* **165** 383–92

Rhode Island Department of Environmental Management (RI DEM) 2021 *Rhode Island Freshwater Wetlands Program and Stormwater Construction Permitting Ground-Mounted Solar Array Guidance* (Rhode Island Department of Environmental Management) http://dem.ri.gov/programs/benviron/water/permits/ripdes/stwater/pdfs/solar-guidance.pdf

Shorabeh S N, Firozjaei M K, Nematollahi O, Firozjaei H K and Jelokhani-Niaraki M 2019 A risk-based multi-criteria spatial decision analysis for solar power plant site selection in different climates: a case study in Iran *Renew. Energy* **143** 958–73

Solangi K H, Islam M R, Saidur R, Rahim N A and Fayaz H 2011 A review on global solar energy policy *Renew. Sustain. Energy Rev.* **15** 2149–63

Solar Energy Industries Association 2020 Major solar projects list https://seia.org/research-resources/major-solar-projects-list

Taha H 2013 The potential for air-temperature impact from large-scale deployment of solar photovoltaic arrays in urban areas *Sol. Energy* **91** 358–67

Uldrijan D, Kováčiková M, Jakimiuk A, Vaverková M D and Winkler J 2021 Ecological effects of preferential vegetation composition developed on sites with photovoltaic power plants *Ecol. Eng.* **168** 106274

US Army Corps of Engineers 2021 HEC-HMS https://hec.oce.army.mil/software/hec-hms/

US Energy Information Administration (EIA) 2020 *U.S. Energy Information Administration (EIA)—Data. Monthly Energy Review* (US Energy Information Administration) https://eia.gov/totalenergy/data/browser/index.php?tbl=T10.06#/?f=M%start=200001

US EPA 2015 *Stormwater Discharges from Construction Activities [Overviews and Factsheets]* (US EPA) https://epa.gov/npdes/stormwater-discharges-construction-activities

Virginia Department of Environmental Quality (VA DEQ) 2022 *Virginia Guidance for Solar Farms* (Virginia Department of Environmental Quality) https://deq.virginia.gov/home/showpublisheddocument/13985/637842474433400000

Vrînceanu A, Grigorescu I, Dumitraşcu M, Mocanu I, Dumitrică C, Micu D, Kucsicsa G and Mitrică B 2019 Impacts of photovoltaic farms on the environment in the Romanian plain *Energies* **12** 2533

Walston L J, Li Y, Hartmann H M, Macknick J, Hanson A, Nootenboom C, Lonsdorf E and Hellmann J 2021 Modeling the ecosystem services of native vegetation management practices at solar energy facilities in the Midwestern United States *Ecosyst. Serv.* **47** 101227

Walston L J, Mishra S K, Hartmann H M, Hlohowskyj I, McCall J and Macknick J 2018 Examining the potential for agricultural benefits from pollinator habitat at solar facilities in the United States *Environ. Sci. Technol.* **52** 7566–76

Washington State Department of Ecology 2021 *Washington Stormwater Requirements for Solar Farms* (Washington State Department of Ecology) https://ecology.wa.gov/

Weselek A, Ehmann A, Zikeli S, Lewandowski I, Schindele S and Högy P 2019 Agrophotovoltaic systems: applications, challenges, and opportunities. A review *Agron. Sustain. Dev.* **39** 35

Wu C, Liu H, Yu Y, Zhao W, Liu J, Yu H and Yetemen O 2022 Ecohydrological effects of photovoltaic solar farms on soil microclimates and moisture regimes in arid northwest China: a modeling study *Sci. Total Environ.* **802** 149946

Yue S, Guo M, Zou P, Wu W and Zhou X 2021 Effects of photovoltaic panels on soil temperature and moisture in desert areas *Environ. Sci. Pollut. Res.* **28** 17506–18

Zhu Z, Chen Z, Chen X and Yu G 2019 An assessment of the hydrologic effectiveness of low impact development (LID) practices for managing runoff with different objectives *J. Environ. Manage.* **231** 504–14

Minnesota Pollution Control Agency (MN PCA) 2021 *Stormwater management for solar projects and determining compliance with the NPDES construction stormwater permit* Minnesota Pollution Control Agency https://stormwater.pca.state.mn.us/index.php?title=Stormwater_management_for_solar_projects_and_determining_compliance_with_the_NPDES_construction_stormwater_permit

Hydrologic Response of Solar Farms

Lauren M. Cook, S.M.ASCE[1]; and Richard H. McCuen, M.ASCE[2]

Abstract: Because of the benefits of solar energy, the number of solar farms is increasing; however, their hydrologic impacts have not been studied. The goal of this study was to determine the hydrologic effects of solar farms and examine whether or not storm-water management is needed to control runoff volumes and rates. A model of a solar farm was used to simulate runoff for two conditions: the pre- and postpaneled conditions. Using sensitivity analyses, modeling showed that the solar panels themselves did not have a significant effect on the runoff volumes, peaks, or times to peak. However, if the ground cover under the panels is gravel or bare ground, owing to design decisions or lack of maintenance, the peak discharge may increase significantly with storm-water management needed. In addition, the kinetic energy of the flow that drains from the panels was found to be greater than that of the rainfall, which could cause erosion at the base of the panels. Thus, it is recommended that the grass beneath the panels be well maintained or that a buffer strip be placed after the most downgradient row of panels. This study, along with design recommendations, can be used as a guide for the future design of solar farms. **DOI: 10.1061/(ASCE)HE.1943-5584.0000530.**

CE Database subject headings: Hydrology; Land use; Solar power; Floods; Surface water; Runoff; Stormwater management.

Author keywords: Hydrology; Land use change; Solar energy; Flooding; Surface water runoff; Storm-water management.

Introduction

Storm-water management practices are generally implemented to reverse the effects of land-cover changes that cause increases in volumes and rates of runoff. This is a concern posed for new types of land-cover change such as the solar farm. Solar energy is a renewable energy source that is expected to increase in importance in the near future. Because solar farms require considerable land, it is necessary to understand the design of solar farms and their potential effect on erosion rates and storm runoff, especially the impact on offsite properties and receiving streams. These farms can vary in size from 8 ha (20 acres) in residential areas to 250 ha (600 acres) in areas where land is abundant.

The solar panels are impervious to rain water; however, they are mounted on metal rods and placed over pervious land. In some cases, the area below the panel is paved or covered with gravel. Service roads are generally located between rows of panels. Although some panels are stationary, others are designed to move so that the angle of the panel varies with the angle of the sun. The angle can range, depending on the latitude, from 22° during the summer months to 74° during the winter months. In addition, the angle and direction can also change throughout the day. The issue posed is whether or not these rows of impervious panels will change the runoff characteristics of the site, specifically increase runoff volumes or peak discharge rates. If the increases are hydrologically significant, storm-water management facilities may be needed. Additionally, it is possible that the velocity of water draining from the edge of the panels is sufficient to cause erosion of the soil below the panels, especially where the maintenance roadways are bare ground.

The outcome of this study provides guidance for assessing the hydrologic effects of solar farms, which is important to those who plan, design, and install arrays of solar panels. Those who design solar farms may need to provide for storm-water management. This study investigated the hydrologic effects of solar farms, assessed whether or not storm-water management might be needed, and if the velocity of the runoff from the panels could be sufficient to cause erosion of the soil below the panels.

Model Development

Solar farms are generally designed to maximize the amount of energy produced per unit of land area, while still allowing space for maintenance. The hydrologic response of solar farms is not usually considered in design. Typically, the panels will be arrayed in long rows with separations between the rows to allow for maintenance vehicles. To model a typical layout, a unit width of one panel was assumed, with the length of the downgradient strip depending on the size of the farm. For example, a solar farm with 30 rows of 200 panels each could be modeled as a strip of 30 panels with space between the panels for maintenance vehicles. Rainwater that drains from the upper panel onto the ground will flow over the land under the 29 panels on the downgradient strip. Depending on the land cover, infiltration losses would be expected as the runoff flows to the bottom of the slope.

To determine the effects that the solar panels have on runoff characteristics, a model of a solar farm was developed. Runoff in the form of sheet flow without the addition of the solar panels served as the prepaneled condition. The paneled condition assumed a downgradient series of cells with one solar panel per ground cell. Each cell was separated into three sections: wet, dry, and spacer.

The dry section is that portion directly underneath the solar panel, unexposed directly to the rainfall. As the angle of the panel from the horizontal increases, more of the rain will fall directly onto

[1]Research Assistant, Dept. of Civil and Environmental Engineering, Univ. of Maryland, College Park, MD 20742-3021.

[2]The Ben Dyer Professor, Dept. of Civil and Environmental Engineering, Univ. of Maryland, College Park, MD 20742-3021 (corresponding author). E-mail: [redacted]@eng.umd.edu

Note. This manuscript was submitted on August 12, 2010; approved on October 20, 2011; published online on October 24, 2011. Discussion period open until October 1, 2013; separate discussions must be submitted for individual papers. This paper is part of the ***Journal of Hydrologic Engineering***, Vol. 18, No. 5, May 1, 2013. © ASCE, ISSN 1084-0699/2013/5-536-541/$25.00.

the ground; this section of the cell is referred to as the wet section. The spacer section is the area between the rows of panels used by maintenance vehicles. Fig. 1 is an image of two solar panels and the spacer section allotted for maintenance vehicles. Fig. 2 is a schematic of the wet, dry, and spacer sections with their respective dimensions. In Fig. 1, tracks from the vehicles are visible on what is modeled within as the spacer section. When the solar panel is horizontal, then the length longitudinal to the direction that runoff will occur is the length of the dry and wet sections combined. Runoff from a dry section drains onto the downgradient spacer section. Runoff from the spacer section flows to the wet section of the next downgradient cell. Water that drains from a solar panel falls directly onto the spacer section of that cell.

The length of the spacer section is constant. During a storm event, the loss rate was assumed constant for the 24-h storm because a wet antecedent condition was assumed. The lengths of the wet and dry sections changed depending on the angle of the solar panel. The total length of the wet and dry sections was set equal to the length of one horizontal solar panel, which was assumed to be 3.5 m. When a solar panel is horizontal, the dry section length would equal 3.5 m and the wet section length would be zero. In the paneled condition, the dry section does not receive direct rainfall because the rain first falls onto the solar panel then drains onto the spacer section. However, the dry section does infiltrate some of the runoff that comes from the upgradient wet section. The wet section was modeled similar to the spacer section with rain falling directly onto the section and assuming a constant loss rate.

For the presolar panel condition, the spacer and wet sections are modeled the same as in the paneled condition; however, the cell does not include a dry section. In the prepaneled condition, rain falls directly onto the entire cell. When modeling the prepaneled condition, all cells receive rainfall at the same rate and are subject to losses. All other conditions were assumed to remain the same such that the prepaneled and paneled conditions can be compared.

Rainfall was modeled after an natural resources conservation service (NRCS) Type II Storm (McCuen 2005) because it is an accurate representation of actual storms of varying characteristics that are imbedded in intensity-duration-frequency (IDF) curves. For each duration of interest, a dimensionless hyetograph was developed using a time increment of 12 s over the duration of the storm (see Fig. 3). The depth of rainfall that corresponds to each storm magnitude was then multiplied by the dimensionless hyetograph. For a 2-h storm duration, depths of 40.6, 76.2, and 101.6 mm were used for the 2-, 25-, and 100-year events. The 2- and 6-h duration hyetographs were developed using the center portion of the 24-h storm, with the rainfall depths established with the Baltimore IDF curve. The corresponding depths for a 6-h duration were 53.3, 106.7, and 132.1 mm, respectively. These magnitudes were chosen to give a range of storm conditions.

During each time increment, the depth of rain is multiplied by the cell area to determine the volume of rain added to each section of each cell. This volume becomes the storage in each cell. Depending on the soil group, a constant volume of losses was subtracted from the storage. The runoff velocity from a solar panel was calculated using Manning's equation, with the hydraulic radius for sheet flow assumed to equal the depth of the storage on the panel (Bedient and Huber 2002). Similar assumptions were made to compute the velocities in each section of the surface sections.

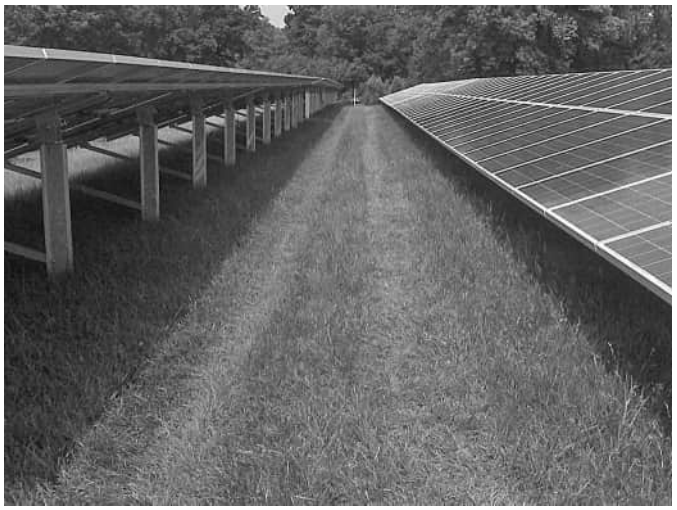

Fig. 1. Maintenance or "spacer" section between two rows of solar panels (photo by John E. Showler, reprinted with permission)

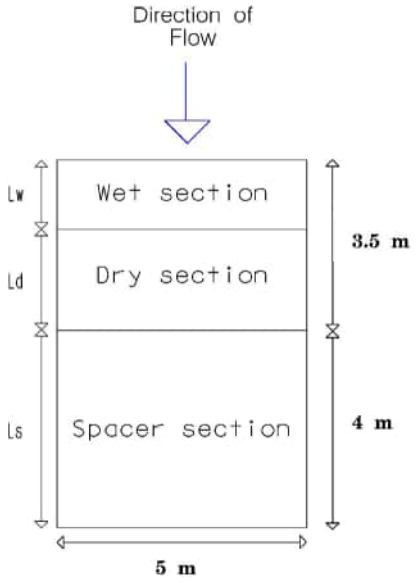

Fig. 2. Wet, dry, and spacer sections of a single cell with lengths *Lw*, *Ls*, and *Ld* with the solar panel covering the dry section

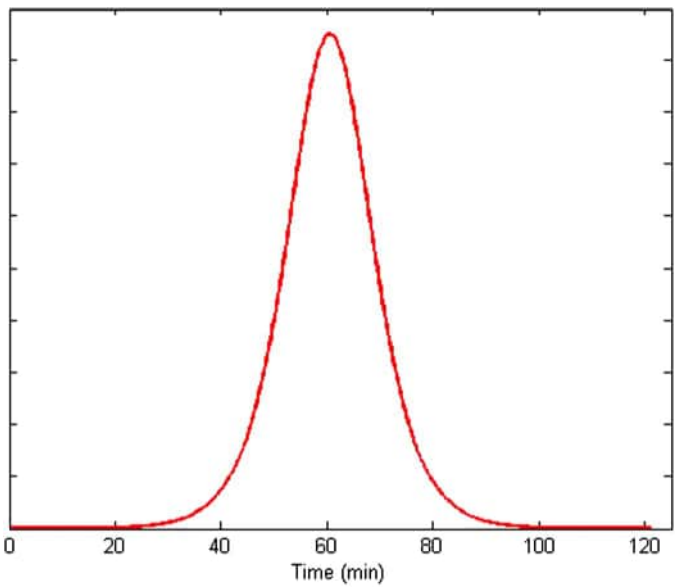

Fig. 3. Dimensionless hyetograph of 2-h Type II storm

Runoff from one section to the next and then to the next downgradient cell was routed using the continuity of mass. The routing coefficient depended on the depth of flow in storage and the velocity of runoff. Flow was routed from the wet section to the dry section to the spacer section, with flow from the spacer section draining to the wet section of the next cell. Flow from the most downgradient cell was assumed to be the outflow. Discharge rates and volumes from the most downgradient cell were used for comparisons between the prepaneled and paneled conditions.

Alternative Model Scenarios

To assess the effects of the different variables, a section of 30 cells, each with a solar panel, was assumed for the base model. Each cell was separated individually into wet, dry, and spacer sections. The area had a total ground length of 225 m with a ground slope of 1% and width of 5 m, which was the width of an average solar panel. The roughness coefficient (Engman 1986) for the silicon solar panel was assumed to be that of glass, 0.01. Roughness coefficients of 0.15 for grass and 0.02 for bare ground were also assumed. Loss rates of 0.5715 cm/h (0.225 in./h) and 0.254 cm/h (0.1 in./h) for B and C soils, respectively, were assumed.

The prepaneled condition using the 2-h, 25-year rainfall was assumed for the base condition, with each cell assumed to have a good grass cover condition. All other analyses were made assuming a paneled condition. For most scenarios, the runoff volumes and peak discharge rates from the paneled model were not significantly greater than those for the prepaneled condition. Over a total length of 225 m with 30 solar panels, the runoff increased by 0.26 m^3, which was a difference of only 0.35%. The slight increase in runoff volume reflects the slightly higher velocities for the paneled condition. The peak discharge increased by 0.0013 m^3, a change of only 0.31%. The time to peak was delayed by one time increment, i.e., 12 s. Inclusion of the panels did not have a significant hydrologic impact.

Storm Magnitude

The effect of storm magnitude was investigated by changing the magnitude from a 25-year storm to a 2-year storm. For the 2-year storm, the rainfall and runoff volumes decreased by approximately 50%. However, the runoff from the paneled watershed condition increased compared to the prepaneled condition by approximately the same volume as for the 25-year analysis, 0.26 m^3. This increase represents only a 0.78% increase in volume. The peak discharge and the time to peak did not change significantly. These results reflect runoff from a good grass cover condition and indicated that the general conclusion of very minimal impacts was the same for different storm magnitudes.

Ground Slope

The effect of the downgradient ground slope of the solar farm was also examined. The angle of the solar panels would influence the velocity of flows from the panels. As the ground slope was increased, the velocity of flow over the ground surface would be closer to that on the panels. This could cause an overall increase in discharge rates. The ground slope was changed from 1 to 5%, with all other conditions remaining the same as the base conditions.

With the steeper incline, the volume of losses decreased from that for the 1% slope, which is to be expected because the faster velocity of the runoff would provide less opportunity for infiltration. However, between the prepaneled and paneled conditions, the increase in runoff volume was less than 1%. The peak discharge and the time to peak did not change. Therefore, the greater ground slope did not significantly influence the response of the solar farm.

Soil Type

The effect of soil type on the runoff was also examined. The soil group was changed from B soil to C soil by varying the loss rate. As expected, owing to the higher loss rate for the C soil, the depths of runoff increased by approximately 7.5% with the C soil when compared with the volume for B soils. However, the runoff volume for the C soil condition only increased by 0.17% from the prepaneled condition to the paneled condition. In comparison with the B soil, a difference of 0.35% in volume resulted between the two conditions. Therefore, the soil group influenced the actual volumes and rates, but not the relative effect of the paneled condition when compared to the prepaneled condition.

Panel Angle

Because runoff velocities increase with slope, the effect of the angle of the solar panel on the hydrologic response was examined. Analyses were made for angles of 30° and 70° to test an average range from winter to summer. The hydrologic response for these angles was compared to that of the base condition angle of 45°. The other site conditions remained the same. The analyses showed that the angle of the panel had only a slight effect on runoff volumes and discharge rates. The lower angle of 30° was associated with an increased runoff volume, whereas the runoff volume decreased for the steeper angle of 70° when compared with the base condition of 45°. However, the differences (~0.5%) were very slight. Nevertheless, these results indicate that, when the solar panel was closer to horizontal, i.e., at a lower angle, a larger difference in runoff volume occurred between the prepaneled and paneled conditions. These differences in the response result are from differences in loss rates.

The peak discharge was also lower at the lower angle. At an angle of 30°, the peak discharge was slightly lower than at the higher angle of 70°. For the 2-h storm duration, the time to peak of the 30° angle was 2 min delayed from the time to peak of when the panel was positioned at a 70° angle, which reflects the longer travel times across the solar panels.

Storm Duration

To assess the effect of storm duration, analyses were made for 6-h storms, testing magnitudes for 2-, 25-, and 100-year return periods, with the results compared with those for the 2-h rainfall events. The longer storm duration was tested to determine whether a longer duration storm would produce a different ratio of increase in runoff between the prepaneled and paneled conditions. When compared to runoff volumes from the 2-h storm, those for the 6-h storm were 34% greater in both the paneled and prepaneled cases. However, when comparing the prepaneled to the paneled condition, the increase in the runoff volume with the 6-h storm was less than 1% regardless of the return period. The peak discharge and the time-to-peak did not differ significantly between the two conditions. The trends in the hydrologic response of the solar farm did not vary with storm duration.

Ground Cover

The ground cover under the panels was assumed to be a native grass that received little maintenance. For some solar farms, the area beneath the panel is covered in gravel or partially paved because the panels prevent the grass from receiving sunlight. Depending on the

volume of traffic, the spacer cell could be grass, patches of grass, or bare ground. Thus, it was necessary to determine whether or not these alternative ground-cover conditions would affect the runoff characteristics. This was accomplished by changing the Manning's n for the ground beneath the panels. The value of n under the panels, i.e., the dry section, was set to 0.015 for gravel, with the value for the spacer or maintenance section set to 0.02, i.e., bare ground. These can be compared to the base condition of a native grass ($n = 0.15$). A good cover should promote losses and delay the runoff.

For the smoother surfaces, the velocity of the runoff increased and the losses decreased, which resulted in increasing runoff volumes. This occurred both when the ground cover under the panels was changed to gravel and when the cover in the spacer section was changed to bare ground. Owing to the higher velocities of the flow, runoff rates from the cells increased significantly such that it was necessary to reduce the computational time increment. Fig. 4(a) shows the hydrograph from a 30-panel area with a time increment of 12 s. With a time increment of 12 s, the water in each cell is discharged at the end of every time increment, which results in no attenuation of the flow; thus, the undulations shown in Fig. 4(a) result. The time increment was reduced to 3 s for the 2-h storm, which resulted in watershed smoothing and a rational hydrograph shape [Fig. 4(b)]. The results showed that the storm runoff

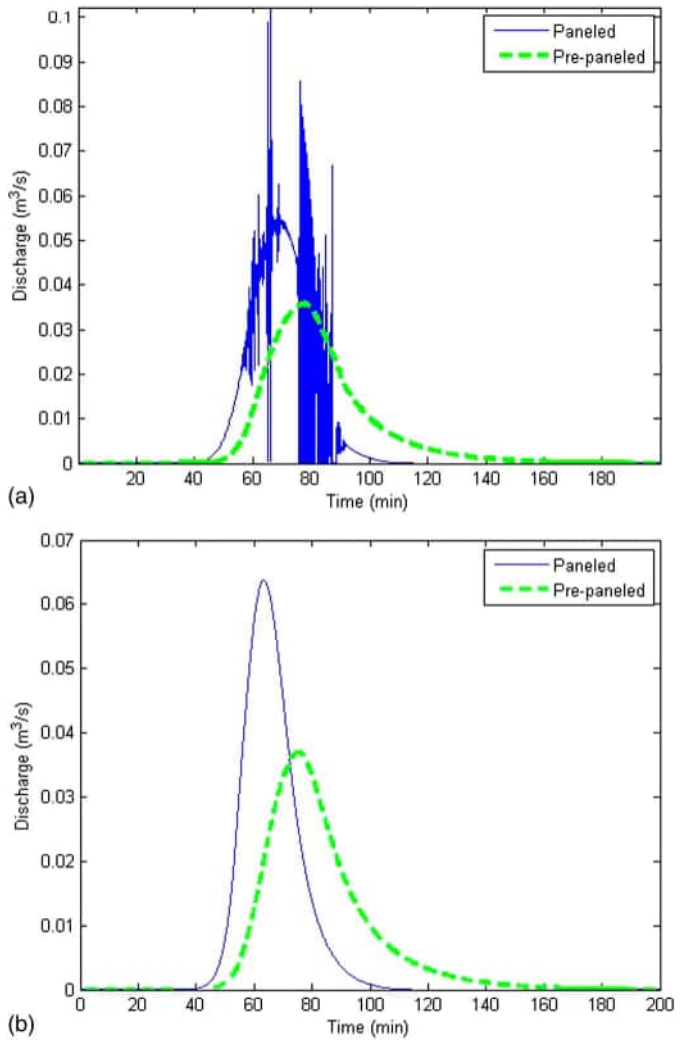

Fig. 4. Hydrograph with time increment of (a) 12 s; (b) 3 s with Manning's n for bare ground

increased by 7% from the grass-covered scenario to the scenario with gravel under the panel. The peak discharge increased by 73% for the gravel ground cover when compared with the grass cover without the panels. The time to peak was 10 min less with the gravel than with the grass, which reflects the effect of differences in surface roughness and the resulting velocities.

If maintenance vehicles used the spacer section regularly and the grass cover was not adequately maintained, the soil in the spacer section would be compacted and potentially the runoff volumes and rates would increase. Grass that is not maintained has the potential to become patchy and turn to bare ground. The grass under the panel may not get enough sunlight and die. Fig. 1 shows the result of the maintenance trucks frequently driving in the spacer section, which diminished the grass cover.

The effect of the lack of solar farm maintenance on runoff characteristics was modeled by changing the Manning's n to a value of 0.02 for bare ground. In this scenario, the roughness coefficient for the ground under the panels, i.e., the dry section, as well as in the spacer cell was changed from grass covered to bare ground ($n = 0.02$).The effects were nearly identical to that of the gravel. The runoff volume increased by 7% from the grass-covered to the bare-ground condition. The peak discharge increased by 72% when compared with the grass-covered condition. The runoff for the bare-ground condition also resulted in an earlier time to peak by approximately 10 min. Two other conditions were also modeled, showing similar results. In the first scenario, gravel was placed directly under the panel, and healthy grass was placed in the spacer section, which mimics a possible design decision. Under these conditions, the peak discharge increased by 42%, and the volume of runoff increased by 4%, which suggests that storm-water management would be necessary if gravel is placed anywhere.

Fig. 5 shows two solar panels from a solar farm in New Jersey. The bare ground between the panels can cause increased runoff rates and reductions in time of concentration, both of which could necessitate storm-water management. The final condition modeled involved the assumption of healthy grass beneath the panels and bare ground in the spacer section, which would simulate the condition of unmaintained grass resulting from vehicles that drive over the spacer section. Because the spacer section is 53% of the cell, the change in land cover to bare ground would reduce losses and decrease runoff travel times, which would cause runoff to amass as it

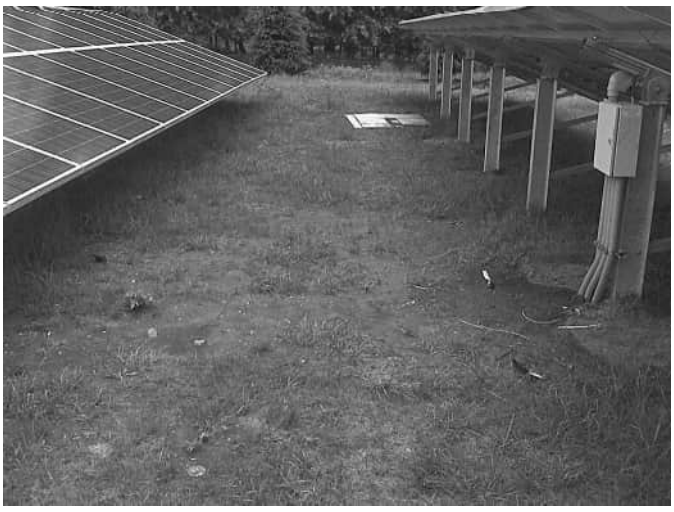

Fig. 5. Site showing the initiation of bare ground below the panels, which increases the potential for erosion (photo by John Showler, reprinted with permission)

moves downgradient. With the spacer section as bare ground, the peak discharge increased by 100%, which reflected the increases in volume and decrease in timing. These results illustrate the need for maintenance of the grass below and between the panels.

Design Suggestions

With well-maintained grass underneath the panels, the solar panels themselves do not have much effect on total volumes of the runoff or peak discharge rates. Although the panels are impervious, the rainwater that drains from the panels appears as runoff over the downgradient cells. Some of the runoff infiltrates. If the grass cover of a solar farm is not maintained, it can deteriorate either because of a lack of sunlight or maintenance vehicle traffic. In this case, the runoff characteristics can change significantly with both runoff rates and volumes increasing by significant amounts. In addition, if gravel or pavement is placed underneath the panels, this can also contribute to a significant increase in the hydrologic response.

If bare ground is foreseen to be a problem or gravel is to be placed under the panels to prevent erosion, it is necessary to counteract the excess runoff using some form of storm-water management. A simple practice that can be implemented is a buffer strip (Dabney et al. 2006) at the downgradient end of the solar farm. The buffer strip length must be sufficient to return the runoff characteristics with the panels to those of runoff experienced before the gravel and panels were installed. Alternatively, a detention basin can be installed.

A buffer strip was modeled along with the panels. For approximately every 200 m of panels, or 29 cells, the buffer must be 5 cells long (or 35 m) to reduce the runoff volume to that which occurred before the panels were added. Even if a gravel base is not placed under the panels, the inclusion of a buffer strip may be a good practice when grass maintenance is not a top funding priority. Fig. 6 shows the peak discharge from the graveled surface versus the length of the buffer needed to keep the discharge to prepaneled peak rate.

Water draining from a solar panel can increase the potential for erosion of the spacer section. If the spacer section is bare ground, the high kinetic energy of water draining from the panel can cause soil detachment and transport (Garde and Raju 1977; Beuselinck et al. 2002). The amount and risk of erosion was modeled using the velocity of water coming off a solar panel compared with the velocity and intensity of the rainwater. The velocity of panel runoff was calculated using Manning's equation, and the velocity of falling rainwater was calculated using the following:

$$V_t = 120\, d_r^{0.35} \tag{1}$$

where d_r = diameter of a raindrop, assumed to be 1 mm. The relationship between kinetic energy and rainfall intensity is

$$K_e = 916 + 330 \log_{10} i \tag{2}$$

where i = rainfall intensity (in./h) and K_e = kinetic energy (ft-tons per ac-in. of rain) of rain falling onto the wet section and the panel, as well as the water flowing off of the end of the panel (Wischmeier and Smith 1978). The kinetic energy (Salles et al. 2002) of the rainfall was greater than that coming off the panel, but the area under the panel (i.e., the product of the length, width, and cosine of the panel angle) is greater than the area under the edge of the panel where the water drains from the panel onto the ground. Thus, dividing the kinetic energy by the respective areas gives a more accurate representation of the kinetic energy experienced by the soil. The energy of the water draining from the panel onto the ground can be nearly 10 times greater than the rain itself falling onto the ground area. If the solar panel runoff falls onto an unsealed soil, considerable detachment can result (Motha et al. 2004). Thus, because of the increased kinetic energy, it is possible that the soil is much more prone to erosion with the panels than without. Where panels are installed, methods of erosion control should be included in the design.

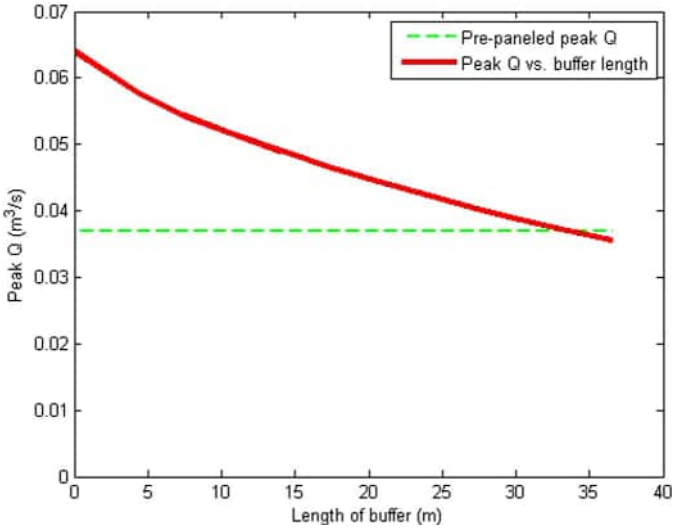

Fig. 6. Peak discharge over gravel compared with buffer length

Conclusions

Solar farms are the energy generators of the future; thus, it is important to determine the environmental and hydrologic effects of these farms, both existing and proposed. A model was created to simulate storm-water runoff over a land surface without panels and then with solar panels added. Various sensitivity analyses were conducted including changing the storm duration and volume, soil type, ground slope, panel angle, and ground cover to determine the effect that each of these factors would have on the volumes and peak discharge rates of the runoff.

The addition of solar panels over a grassy field does not have much of an effect on the volume of runoff, the peak discharge, nor the time to peak. With each analysis, the runoff volume increased slightly but not enough to require storm-water management facilities. However, when the land-cover type was changed under the panels, the hydrologic response changed significantly. When gravel or pavement was placed under the panels, with the spacer section left as patchy grass or bare ground, the volume of the runoff increased significantly and the peak discharge increased by approximately 100%. This was also the result when the entire cell was assumed to be bare ground.

The potential for erosion of the soil at the base of the solar panels was also studied. It was determined that the kinetic energy of the water draining from the solar panel could be as much as 10 times greater than that of rainfall. Thus, because the energy of the water draining from the panels is much higher, it is very possible that soil below the base of the solar panel could erode owing to the concentrated flow of water off the panel, especially if there is bare ground in the spacer section of the cell. If necessary, erosion control methods should be used.

Bare ground beneath the panels and in the spacer section is a realistic possibility (see Figs. 1 and 5). Thus, a good, well-maintained grass cover beneath the panels and in the spacer section is highly recommended. If gravel, pavement, or bare ground is

J. Hydrol. Eng., 2013, 18(5): 536-541

deemed unavoidable below the panels or in the spacer section, it may necessary to add a buffer section to control the excess runoff volume and ensure adequate losses. If these simple measures are taken, solar farms will not have an adverse hydrologic impact from excess runoff or contribute eroded soil particles to receiving streams and waterways.

Acknowledgments

The authors appreciate the photographs (Figs. 1 and 5) of Ortho Clinical Diagnostics, 1001 Route 202, North Raritan, New Jersey, 08869, provided by John E. Showler, Environmental Scientist, New Jersey Department of Agriculture. The extensive comments of reviewers resulted in an improved paper.

References

Bedient, P. B., and Huber, W. C. (2002). *Hydrology and floodplain analysis*, Prentice-Hall, Upper Saddle River, NJ.

Beuselinck, L., Govers, G., Hairsince, P. B., Sander, G. C., and Breynaert, M. (2002). "The influence of rainfall on sediment transport by overland flow over areas of net deposition." *J. Hydrol.*, 257(1–4), 145–163.

Dabney, S. M., Moore, M. T., and Locke, M. A. (2006). "Integrated management of in-field, edge-of-field, and after-field buffers." *J. Amer. Water Resour. Assoc.*, 42(1), 15–24.

Engman, E. T. (1986). "Roughness coefficients for routing surface runoff." *J. Irrig. Drain. Eng.*, 112(1), 39–53.

Garde, R. J., and Raju, K. G. (1977). *Mechanics of sediment transportation and alluvial stream problems*, Wiley, New York.

McCuen, R. H. (2005). *Hydrologic analysis and design*, 3rd Ed., Pearson/Prentice-Hall, Upper Saddle River, NJ.

Motha, J. A., Wallbrink, P. J., Hairsine, P. B., and Grayson, R. B. (2004). "Unsealed roads as suspended sediment sources in agricultural catchment in south-eastern Australia." *J. Hydrol.*, 286(1–4), 1–18.

Salles, C., Poesen, J., and Sempere-Torres, D. (2002). "Kinetic energy of rain and its functional relationship with intensity." *J. Hydrol.*, 257(1–4), 256–270.

Wischmeier, W. H., and Smith, D. D. (1978). *Predicting rainfall erosion losses: A guide to conservation planning, USDA Handbook 537*, U.S. Government Printing Office, Washington, DC.

Two Dimensional Modeling to Simulate Stormwater Flows at Photovoltaic Solar Energy Sites

Thomas E. Barnard,[1] Mohamed Agnaou[2] and James Barbis[1]

[1]Amec Foster Wheeler, Blue Bell, Pennsylvania; [2]Atkins, Tampa, Florida.

Abstract

Solar farms (sometimes known as solar parks or solar fields) are the large scale use of photovoltaic (PV) solar panels to generate green, clean electricity at scale, usually to feed into the grid. Solar farms can cover anything between 1 acre (0.40 ha) and several hundred acres (120+ ha), and are usually developed in rural areas. Solar farms consist of arrays of ground mounted rectangular panels that are sloped toward the sun at either fixed or adjustable angles. Amec Foster Wheeler assessed several candidate solar farm sites in Texas for stormwater flooding hazard and designed the stormwater management system for a site in Georgia using two-dimensional (2D) hydrologic and hydraulic (H&H) models to simulate the infiltration and overland flow. The FLO-2D software package was used to develop a rectangular grid for runoff calculation. The Soil Conservation Service (SCS) method and the shallow water equations were used to route stormwater runoff across FLO-2D grids. Results were exported to ArcGIS for the creation of maps that displayed maximum velocities and flow depths for different storm events. Input data required for the development of the models was obtained from publicly available sources including U.S. Geological Survey (USGS) 1/3 arc-second digital elevation models (DEM), National Land Cover Database (NLCD), U.S. Department of Agriculture (USDA) soil data and National Hydrography Dataset (NHD) data. These data inputs were supplemented with site field survey data. ESRI ArcGIS software and other tools were used to process the data for the assignment of curve numbers (CN) and ground roughness coefficients (Manning's *n* value) to the model grid cells. HEC–HMS modeling software was used to develop runoff hydrographs from offsite drainage areas which were then added to the FLO-2D model as an inflow boundary condition. Models were created to identify the flooding risks on a conceptual level, to evaluate the final grading design, and to develop a stormwater permitting plan. Model results were also used to estimate the scour potential at the piles that supported the panels. This work demonstrates the use of spatially varied 2D H&H models in assessing potential sites and in designing stormwater control measures for solar farms.

1 Background

This paper describes the use of two-dimensional (2D) numerical hydrologic and hydraulic models to assess the impact of stormwater on proposed solar farm sites and to assess the design of a stormwater management system at a recently constructed solar farm. Where appropriate, 2D models are linked to an upstream watershed hydrologic and one dimensional (1D) hydraulic model.

1.1 Solar Farms

Solar farms (sometimes known as solar parks or solar fields) are the large scale application of solar photovoltaic (PV) panels to generate green, clean electricity at scale, usually to feed into the supply and distribution grid. Solar farms can cover between 1 acre and several hundred acres (from 0.4 ha to a few hundred hectares), and are usually developed in rural areas. Some may be located on completed landfills. Solar farms consist of arrays of ground mounted rectangular solar panels that are sloped to face the sun at either fixed or adjustable angles. Ancillary equipment includes access roads and electronic switching equipment.

1.2 Stormwater Management Issues

Solar panels are impervious. They are generally installed in a manner that allows stormwater to fall directly to the ground. In order to encourage infiltration and discourage erosion, the site is graded to encourage sheet flow of runoff across the site, including areas under the panels. Slopes are generally <5% but may be as high as 10%.

After panel installation, the ground is seeded with grass or other native cover. The grass is mowed once or twice a year.

Cook and McCuen (2013) analysed runoff from solar panel sites under pre- and post-development conditions with numerical models. They concluded that the panels themselves did not have a significant effect on runoff volumes, peak flows, or time to peak flow. However, these findings have not been verified by field measurements.

Barnard, Thomas E., Mohamed Agnaou and James Barbis. 2017. Two Dimensional Modeling to Simulate Stormwater Flows at Photovoltaic Solar Energy Sites. Journal of Water Management Modeling 25:C428. https://doi.org/10.14796/JWMM.C428 © CHI 2017. www.chijournal.org ISSN 2292-6062.

The approach generally taken in the design of stormwater management at solar farms is to consider the runoff characteristics of the soil to be identical to those of the soil in the absence of the panels. There may be an adjustment in the impervious area calculation to account for the presence of foundations, access roads and supporting structures. This impervious area is typically <5% of the total site area.

1.3 Regulatory Considerations

A few states have developed guidance or specific requirements for stormwater management at solar farm sites. For example guidance from the Maryland Department of the Environment refers to the gas strip between panels as disconnections (see Figure 1). The disconnections should be located on gradual slopes (≤5%) to maintain sheet flow. Level spreaders, terraces or berms may be used to maintain sheet flow conditions if the average slope is >5% (MDE 2013).

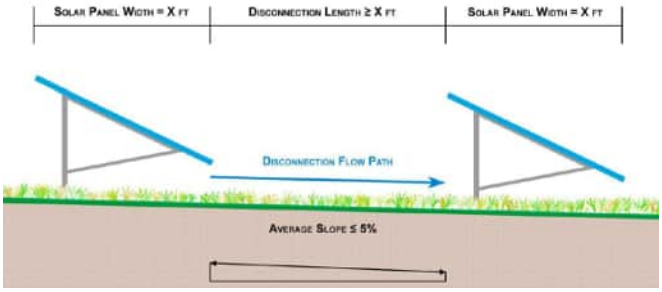

Figure 1 Typical installation for slope ≤5% (MDE 2013).

The Pennsylvania Department of Environmental Protection guidance includes (PA DEP 2011):

1. Vegetal cover has 90% or better uniform coverage since in a previous cover scenario, the vegetation will typically be the primary (and sometimes the sole) BMP:
   - a meadow condition is preferable, particularly for slopes between 5% and 10%;
   - mowed areas, where approvable, should be kept to 4 in., 10.6 cm (min); and
   - vegetated areas will not be subject to chemical fertilization or herbicides or pesticides.
2. Individual PV panels within an array are arranged in a fashion that:
   - allows the passage of runoff between each module thereby minimizing the creation of concentrated runoff; and
   - allows the growth of vegetation beneath and between arrays.
3. Ground mounted solar panels are supported with structures or foundations occupying minimal space (maximum 5% of the total project area).
4. Solar panels are situated on mild slopes (10% maximum).
5. The lowest vertical clearance of the solar array is at an elevation of 10 ft (3.05 m) or less from the ground, but is also at an adequate height to promote vegetative growth below the array.

Under New Jersey law S-921 solar panels are now exempt from zoning limitations on impervious cover—a planning term for hard surfaces such as buildings and driveways that prevent water from absorbing into the ground (DeGrezia 2010). In regards to solar panels, municipalities had been inconsistent in their impervious cover requirements, with some treating solar panels as impervious. S-921 addresses this inconsistency—solar panels cannot be restricted through impervious coverage limitations. Other agencies have similar exemptions.

2 Stormwater Modeling for Solar Farms

2.1 1D and 2D Modeling Approaches

There two approaches to modeling stormwater flows at solar farm sites. The traditional approach (subcatchment 1D) is based on a network of subcatchments linked with 1D conveyance and flow control structures. In the 2D approach, a model domain is extended beyond the site boundary to include local runoff flowing onto the site. It is delineated into rectangular grid cells or triangular mesh nodes. The shallow water equations (Vreugdenhil 1994) are used to quantify flow between cells at each model time step. The two methods are compared in Table 1.

Table 1 Comparison of subcatchment 1D and 2D runoff methods.

Component	Subcatchment 1D Approach	2D Approach
Precipitation	Time series	Time series
Runoff	Various hydrologic methods	Mass balance
Flow Paths	Predefined by user	Model determines, may vary over simulation
Hydraulic Routing	Sub catchment → 1D conveyance structure	Cell → Cell
Input	Geometery, travel time, *n*-value, infiltration rates	Elevation, *n*-value, infiltration rates, boundary flows and water elevations
Output	Hydrograph, velocity and depth in conveyance structures	Hydrograph, velocity and depth time series across entire site

Both approaches begin with a time series of precipitation. The rainfall event may vary or be constant with respect to space. The precipitation may represent a hypothetical design storm or an actual recorded event.

In the subcatchment 1D approach, the runoff rate from each subcatchment is calculated at each time step using any appropriate hydrologic method. For the 2D approach, the volume of runoff at each cell is calculated from a mass balance analysis of precipitation, net inflow, infiltration and the change in volume (depth × cell area).

The flow paths in the subcatchment 1D approach are pre-defined by the modeler. The discharge from any subcatchment is directed to another subcatchment, a 1D conveyance, or a flow control structure. 1D hydraulics are used to model flow

through conveyance structures. The flow paths are constant throughout the simulation period. In the 2D approach water may flow between any two neighbouring cells in either direction over every time step. The rate of flow is determined from considerations of the hydraulic gradient, energy and momentum. This scheme allows flow to change direction, altering overall flow patterns during the simulation. At locations where the flow is one-dimensional in nature (flow paths are parallel), a 1D channel may be included within a 2D model.

The data required for subcatchment 1D models includes the delineation of subcatchments, travel time along each subcatchment's longest flow path and infiltration properties. For the 2D approach, the models require the elevation, ground surface roughness coefficients (Manning's *n* values) and soil infiltration properties of each cell. Inflow hydrographs and initial surface water elevations at the boundaries may also be included.

The output from a subcatchment 1D model provides an outflow hydrograph from each subcatchment. The discharge, depth and velocity along the 1D conveyance segments are also generated. The 2D model will produce time series results for depth and velocity at all cells. Discharge hydrographs can be generated for any user defined cross section in the 2D model.

In general, 2D models are recommended for sites where the flow paths are unknown, two dimensional in nature or change during the storm event, or where information regarding the flow depths and velocities throughout the PV site are required.

2.2 Linked Models

Solar farm sites may be subject to runoff from upgradient sources. In such instances there are two options:

1. A single 2D model extended to the top of all catchments; and
2. Linked models that utilize a subcatchment 1D model for regional offsite runoff and a 2D model for the stormwater flows onsite and any local offsite runoff.

A single 2D model is simple in structure. When a site is near the top of a catchment, it is an appropriate option. However, if there is a large area contributing runoff to a site and the 2D regime is extended over the complete drainage area, the computation may require excessive time and computer power. Since the information of interest concerns the flows and velocities in the vicinity of the panels and the discharges from the site, it is not necessary to compute flows and velocities throughout the complete drainage area.

Figure 2 shows the configuration a site where the linked model option is appropriate. Subcatchments 1, 2 and 3 discharge to the stream that flows near the edge of the panel array. High flows from this stream may encroach on the site. Subcatchment 4 flows directly on to the site.

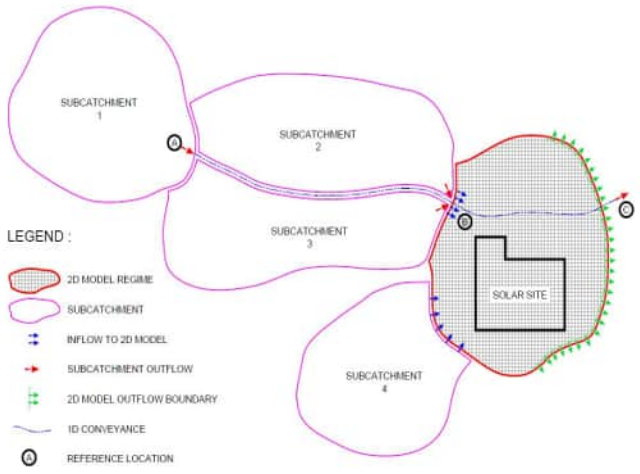

Figure 2 Schematic layout of linked model to simulate stormwater flow at solar site.

A subcatchment 1D model is constructed to simulate upgradient stormwater flows. Outflow hydrographs for subcatchments 1 through 4 are calculated using hydrologic methods. The subcatchment 1 hydrograph is routed from point A to point B using an appropriate routing procedure. At location B the hydrographs for subcatchments 2 and 3 are added to discharge from stream A–B.

The 2D model domain is extended over the solar panels and includes the portion of the stream the flows near the site. Note that it includes the stream between locations B and C. The subcatchment 4 outflow is defined as an inflow boundary along the intersection of subcatchment 4 and the 2D regime. At location B, the combined flows from subcatchments 2 and 3 and stream A–B are defined as an inflow boundary. On the downslope edge of the 2D regime, an outflow boundary is defined.

3 Case Studies

3.1 Preliminary Site Assessment

Amec Foster Wheeler was tasked to evaluate potential flooding at three proposed solar farm sites in west Texas. The project sizes and flooding issues are shown in Table 2. All three sites had significant upstream catchments that were the sources of flows near the boundary and potentially onto the sites. The details of the analysis varied from site to site. This section describes the general modeling approach.

Table 2 Proposed sites in west Texas.

Site	Size (ha)	Flooding Issues
1	1 055	142 km^2 upstream catchment, a draw along the site boundary
2	502	Major river, controlled dam upstream, 1 479 km^2 additional catchment
3	1 147	1 786 km^2 upstream catchment, private dam, diversions to irrigation canals

For each site a linked model set was developed. HEC–HMS software was used to produce hydrographs from regional

upstream sources and to route the flow to the upstream boundary of the 2D domain. The FLO-2D software package was used to develop a 2D model extending over each site. A rectangular grid (typically 50 ft × 50 ft, 15.24 m × 15.24 m) was defined. The domain of the model was expanded beyond the site boundary in order to include local upgradient flows that might impact the site. The HEC–HMS hydrographs were assigned as offsite inflows at appropriate locations along the boundary.

Figure 3 shows a typical configuration of the linked model set. The proposed site is indicated with the diagonal hatching. The 2D model regime is extended to the top of the local catchment. Flow from the regional catchment enters the 2D regime at two locations. DA-15 discharges into a branch of Leon Creek. The main stem of Leon Creek carries flow for DA-14 and other upstream subcatchments. Boundary cells located where the slope is away from the 2D regime are designated as outflow cells. The input parameters for the linked model are shown in Table 3.

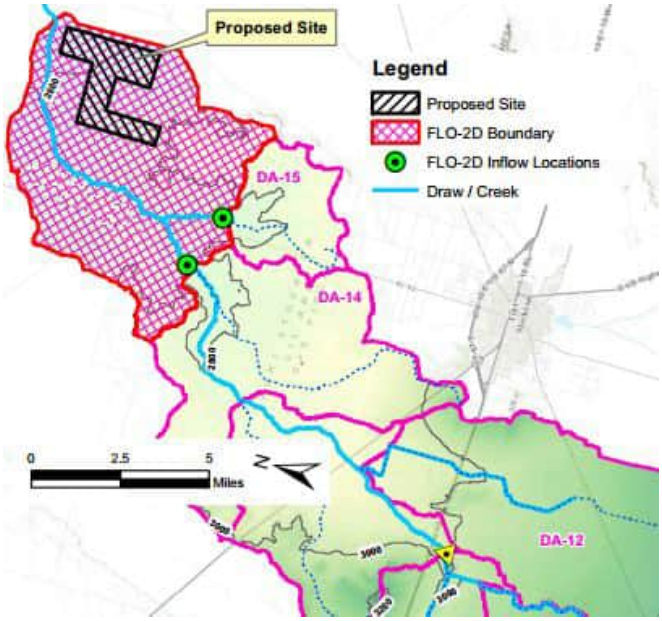

Figure 3 Layout of subcatchment 1D and 2D components for analysis of runoff.

Table 3 Input parameters for models.

	Subcatchment	1D Routing	2D
Software	HEC–HMS	HEC–HMS	FLO-2D
Input Parameters	Precipitation	Channel Length	Preciptiation
	Time of Concentration	Channel Slope	Elevation
	Curve Number	Cross Section	*n*-value
			Curve Number

The sources of data are given in Table 4. The 24 h precipitation values were obtained from Asquith and Roussel (2004). The 24 h precipitation depths for the west Texas sites are shown in Table 5. These total rain amounts were used with the SCS Type II curve to generate hyetographs for the model runs.

Table 4 Data sources for west Texas sites.

Data	Source	Comments
Precipitation	Asquith and Roussel (2004)	Varied by site
Site elevation	Lidar	High quality
Vicinity elevation	USGS	1/3 arc second
Land use/land cover	National Land Cover Database	2006 data, 30 m × 30 m pixel size
Soils	USDA Web soil survey	Infiltration rates, particle size, depth to water table
Base maps	ESRI online	

Table 5 Typical 24 h rainfall depths for west Texas sites.

Return Interval, y	Total Depth, mm
5	76
10	89
25	102
50	114
100	152

The topographic data that was used in the hydrologic analysis model, was developed by blending the following data sources using ESRI Spatial Analyst and 3D Analyst extensions:

- publicly available lidar data;
- USGS 1/3 arc second data for areas that are not covered by the lidar data; and
- supplemental field survey data for specific ground features (ditches, levees, …) that are not captured by USGS DEM or lidar data.

The multiple topographic sources were blended together to achieve a surface that provides the appropriate level of hydrologic and hydraulic detail for a suitable grid spacing in the FLO-2D model. Ground surface elevations within the blended surface were in the NAVD88 vertical datum.

The USDA Web Soil Survey tool was used to query the Soil Survey Geographic Database (SSURGO), and to develop soil maps and reports for each project site. The tables were queried to obtain information on particle size, hydrologic soil group and infiltration rates.

Land cover data for each site was developed from the National Land Cover Database (Fry et al. 2011). This dataset is based on 16 land cover classifications and has a 30 m × 30 m resolution.

The FLO-2D model for each site was developed according to the following procedure:

1. Elevations of the grid elements were assigned by building a point file from a DEM;
2. The curve numbers (CNs) used to calculate runoff were developed by combining the soil and the land cover data. The values were adjusted to Antecedent Runoff Condition I (ARC I) in consideration of the normally dry weather in the region; and
3. Manning's *n* values were assigned according to the land cover following guidance in the FLO-2D reference manual as shown in Table 6.

Table 6 Manning's n values for land cover classifications.

NLCD ID	Description	n value
11	Open Water	0.018
21	Developed, Open Space	0.040
22	Developed, Low Intensity	0.068
23	Developed, Medium Intensity	0.068
31	Barren Land	0.011
41	Deciduous Forest	0.360
42	Evergreen Forest	0.320
43	Mixed Forest	0.400
52	Shrub/Scrub	0.100
71	Herbaceous	0.368
82	Cultivated Crops	0.170
90	Woody Wetlands	0.086
95	Emergent Herbaceous Wetlands	0.183

HEC–HMS Model

The subcatchments were delineated using the DEM and ArcHydro tools

The lag time t_{lag} for each subbasin, for use in the SCS unit hydrograph method, was computed according to the formula

$$t_{lag} = 0.6\, t_c \quad (1)$$

where the time of concentration, t_c, is given by

$$t_c = t_{sheet} + t_{shallow} + t_{channel} \quad (2)$$

Curve numbers were developed according to the same procedure used for the 2D cells.

Hydraulic Routing

Flow was routed through the 1D channels using the Muskingum–Cunge method. Channel lengths, slopes and cross sections were derived from the USGS elevation data. Routing parameters used for the natural (earthen) and irrigation (concrete) channel types are shown in Table 7.

Table 7 Routing parameters used for 1D conveyance structures.

Channel Type	Manning's n	Cross Section Type
Natural	0.055	Eight point
Irrigation channel	0.02	Trapezoid

The HEC–HMS model was run for 5 d. The outflow hydrographs were added to the FLO-2D model as inflow boundary conditions. The flows were spread across cells that represented channels. Figure 4 shows an example of inflow hydrographs. Note that the Node1 hydrograph peaked at approximately 2 500 cfs (71 m³/s) at 16 h into the simulation period while the Node 2 hydrograph peaked at 43 500 cfs (1 203 m³/s) at 30 h after the start of the storm.

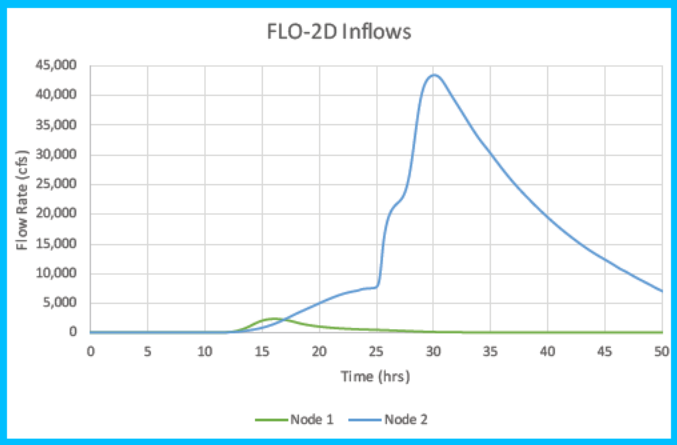

Figure 4 Inflow hydrographs at proposed solar site in west Texas.

The FLO-2D model was run for 48 h. The software generated a time series of velocity and depth at each cell. This data was imported into ArcMap to produce maps of maximum depth and velocity such as those presented for site 3 in Figures 5 and 6. For this site the figures indicate that flood depths were in the 0.5 ft to 1.0 ft (15.24 cm to 30.5 cm) range in the small area in the northeast section of the site but remained <0.5 ft (15.24 cm) throughout the remainder of the site. Maximum velocities were in the 0.5 ft/s to 1.0 ft/s (15.24 cm/s to 30.5 cm/s) range in the western section of the site and a portion of the eastern section while remaining <0.5 ft/s (15.24 cm/s) throughout the remainder of the site. The flow in Leon Creek reached a depth of 8 ft (2.44 m) and a velocity 6 ft/s (1.83 m/s) at a location along the centreline and northern end of the site. However, the Leon Creek flows did not encroach on the site.

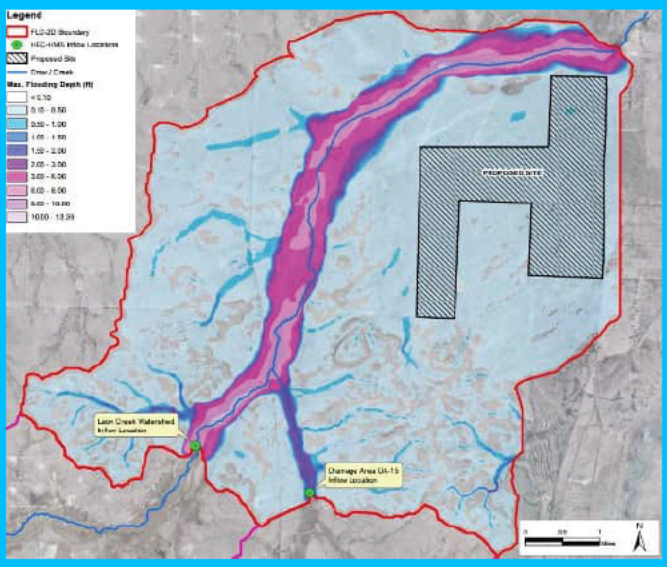

Figure 5 Maximum flow depths.

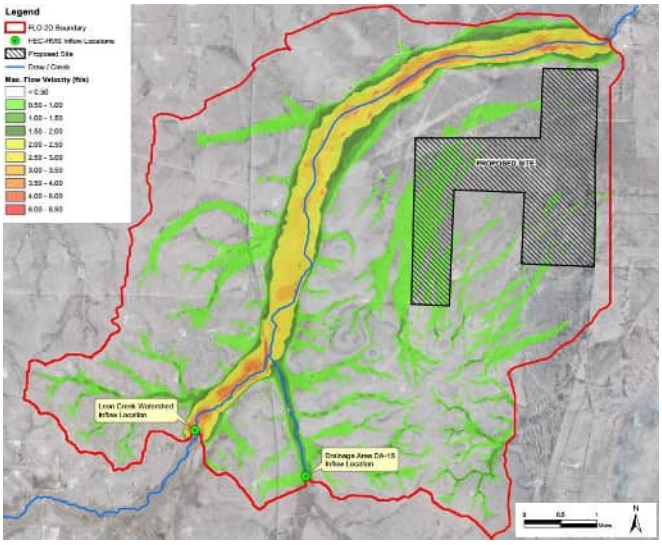

Figure 6 Maximum flow velocities.

3.2 Design of Stormwater Controls

Amec Foster Wheeler was tasked to develop a stormwater management plan for a proposed 1 000 MW PV project at a 1 060 acre (429 ha) site in Georgia (see Figure 7). The site straddles the topographic divide of three drainages. There is no flow of stormwater on to the site from offsite sources.

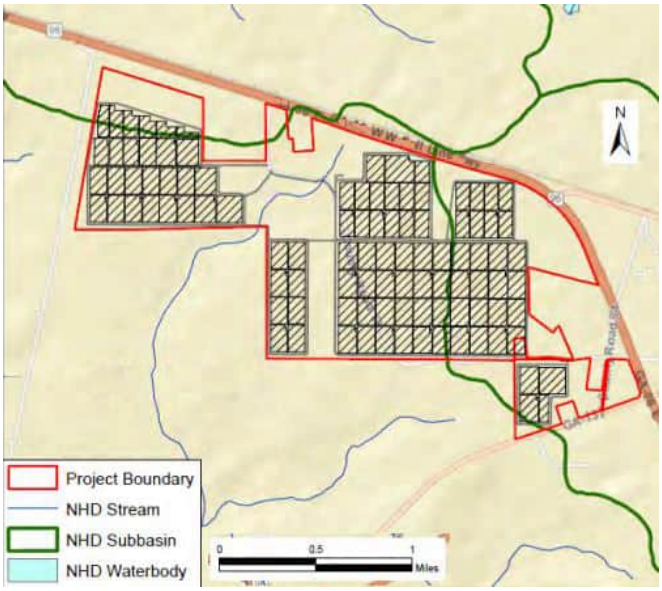

Figure 7 Site layout; hatching indicates the locations of solar panels.

Stormwater management was subject to the eleven minimum standards in the *Georgia Stormwater Management Manual* (Atlanta Regional Commission 2001). The focus of this analysis is to demonstrate that post development flows did not exceed pre-development flows for 24 h storms with 1 y, 25 y and 100 y return intervals.

The site was graded by removing higher areas and constructing swales and detention ponds. Design criteria included:

- maximum depth for 100 y storm: 1 ft (30.5 cm);
- maximum slopes: south to north 2%, east to west and north to south 5%;
- material balance of cut and fill; and
- general maintenance of predevelopment flow paths.

The 2D model approach was selected for the project. FLO-2D software was used to develop 133 881 grid elements each 25 ft × 25 ft (7.62 m × 7.62 m). The model domain included the site and was extended ~300 ft (91.4 m) beyond the property boundaries (Figure 8 below). Additional model features included a levee to represent the berming action of a highway located at the northern site boundary and seven culverts were included to simulate 1D flow within the 2D domain.

Elevations of the grid elements were developed from three data sources: field survey, photogrammetric survey and USGS 1/3 arc second DEM data. The 24 h rainfall depth was obtained from the *Georgia Stormwater Management Manual* (CSMM) (Atlanta Regional Commission 2001). The SCS Type II rainfall distribution was used to derive the hyetographs. Soil data was obtained from the U.S. Department of Agriculture web based soil survey and land use data were obtained from the 2011 U.S. Land Cover dataset. The curve numbers and Manning's *n* values were assigned to grid cells based on land use using the ESRI ArcGIS Spatial Analyst tool. Initial abstraction was set to 0.05.

In order to account for runoff leaving the site it was delineated into 13 subcatchment areas. Each area represents the catchment contributing to a discharge at the site boundary. The drainage area boundaries and the longest flow paths were determined using the ESRI ArcHydro tool. In the FLO-2D model, a cross section was defined where each subcatchment crossed the site boundary. This enabled FLO-2D to calculate a hydrograph for each subcatchment.

The final grading of the site was obtained by using an iterative process. Preliminary grading plans were produced and used to define the grid element elevations for the post development 2D model. The model was run and locations that did not meet the maximum depth and subcatchments that exceeded the no increase in runoff were identified. The grading was revised and in some cases berms and detention ponds were added. The peak runoff rate and total volume for each drainage area for pre and post-development conditions were compared. The process was repeated until the design criteria were met.

When the final grading was completed, results from the FLO-2D model were used to produce maps of maximum depth and velocity for each model run. Figures 8 and 9 present maps of maximum flood depth and velocity for the 100 y storm. The dark red areas of Figure 8 indicate the locations of detention ponds.

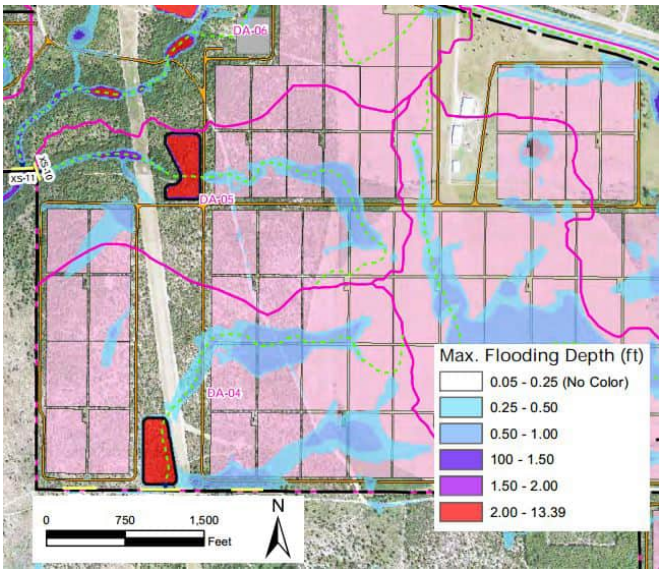

Figure 8 Maximum flood depths from 100 y storm.

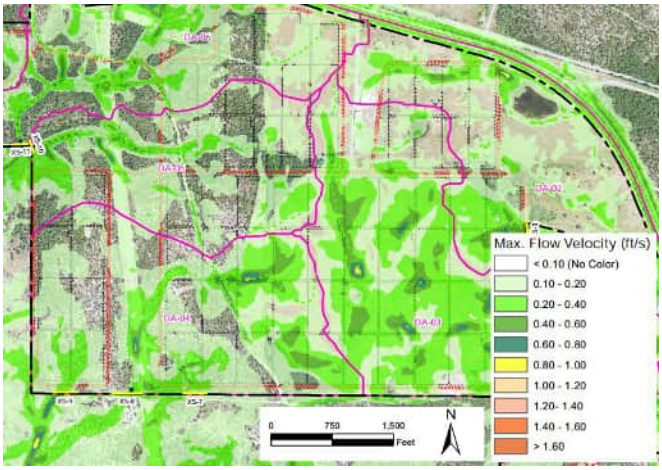

Figure 9 Maximum velocities for 100 y storm.

The *Georgia Stormwater Management Manual* (Atlanta Regional Commission 2001) requires that all stormwater runoff generated from a site should be adequately treated before discharge. Site features are to be developed to capture and treat the water quality volume resulting from the first 1.2 in. (30.5 mm) rainfall from the site. The water quality volume is calculated by the following equation and Table 8 shows the calculated quantities for the project site.

$$WQ_v = \frac{1.2 R_v A}{12} \quad (3)$$

where:

WQ_v = water quality volume (acre-ft),
A = drainage area (acre), and

$$R_v = 0.05 + 0.009\,(I) \quad (4)$$

where:

I = percent impervious cover (%).

Table 8 Partial list water quality capture volume by drainage basin.

Basin	Drainage Area (ha)	Impervious Area (ha)	Percent Impervious	WQ_v (ha-m)
DA-01	27.3	0.80	2.97%	0.064
DA-02	72.8	0.36	0.49%	0.12
DA-03	93.2	1.06	1.14%	0.17
DA-04	65.4	0.00	0.00%	0.10
DA-05	52.5	0.00	0.00%	0.08

The potential for scour at the supporting driven piles was analysed using the methods described in *Hydraulic Engineering Circular 18* (Arneson et al. 2012). The maximum depth and velocities occurring during the 100 y storm event were considered. The foundation piles at the site consisted of standard structural steel wide flange shapes. In the HEC-18 calculation the parameters for a square nose section were used. The angle of attack was varied from 0° to 90°. The angle of attack used was 45° as it resulted in the greatest scour depth. The calculated scour depth ranged from 0.6 ft to 0.7 ft (18.3 cm to 21.3 cm). This value represents the worst case for the site. The scour depth will be lower over the majority of the site. Figure 10 shows how scour depth varies over the range of depths and velocities predicted to occur at the site for the 100 y storm.

Figure 10 Scour analysis at solar farm site.

4 Conclusions

This paper presents procedures modeling the runoff from PV sites under pre- and post-development conditions. The traditional subcatchment 1D approach is compared with the 2D approach. In general, 2D models are recommended for sites where the flow paths are unknown, are two-dimensional in nature or change during the storm event, or where information regarding the flow depths and velocities throughout the PV site is required. 2D models produce information regarding flow depths and velocities that is not available from subcatchment runoff models.

For sites that are subject to runoff originating from large upgradient areas a linked model set is recommended. Such a

configuration is computationally efficient and produces the results required for the design of the facility.

References

Arneson, L. A, L. W. Zevenbergen, P. F. Lagasse and P.E. Clopper. 2012. *Evaluating Scour at Bridges*, 5th ed. Washington, DC: U.S. Department of Transportation Federal Highway Administration. Hydraulic Engineering Circular No. 18. https://www.fhwa.dot.gov/engineering/hydraulics/pubs/hif12003.pdf

Asquith, W. H. and M. C. Roussel. 2004. *Atlas of Depth–Duration of Precipitation Annual Maxima for Texas*. Austin, TX: U.S. Geological Survey Water Resources Division. FHWA/TX–04/5–1301–01–1. https://pubs.usgs.gov/sir/2004/5041/pdf/sir2004-5041.pdf

Atlanta Regional Commission. 2001. *Georgia Stormwater Management Manual*. Vol 2: Technical Handbook. Atlanta, GA.: Atlanta Regional Commission. http://documents.atlantaregional.com/gastormwater/GSMMVol2.pdf

Cook, L. M. and R. H. McCuen. 2013. "Hydrologic Response of Solar Farms." *Journal of Hydrologic Engineering* 18:536–41. https://doi.org/10.1061/(ASCE)HE.1943-5584.0000530.

DeGrezia, C. 2010 "New Legislation Promotes Solar Panel Development." *New Jersey Zoning and Land Use Law*. www.njlandlaw.com/archives/815#more-815

FLO-2D. 2015. FLO-2D Reference Manuals. Nutrioso, AZ: FLO-2D Software. https://www.flo-2d.com/download/

Fry, J., G. Xian, S. Jin, J. Dewitz, C. Homer, L. Yang, C. Barnes, N. Herold and J. Wickham. 2011. "Completion of the 2006 National Land Cover Database for the Conterminous United States." *Photogrammetric Engineering and Remote Sensing* 77 (9): 858–64.

MDE (Maryland Department of the Environment). 2013. *Stormwater Design Guidance—Solar Panel Installation*. Baltimore, MD: Maryland Department of the Environment. http://mde.maryland.gov/programs/water/StormwaterManagementProgram/Documents/ESDMEP%20Design%20Guidance%20Solar%20Panels.pdf

PA DEP. 2011 *Information to Use in the Determination of Stormwater Management (SWM) Impacts for Solar Projects*. http://www.chesco.org/DocumentCenter/View/7375

Vreugdenhil, C. B. 1994. *Numerical Methods for Shallow Water Flow*. Boston, MA: Kluwer Academic Publishers.

Science of the Total Environment 493 (2014) 239–250

Contents lists available at ScienceDirect

Science of the Total Environment

journal homepage: www.elsevier.com/locate/scitotenv

Conceptualizing and assessing the effects of installation and operation of photovoltaic power plants on major hydrologic budget constituents

Vassilios Pisinaras [a], Yang Wei [b], Lars Bärring [b], Alexandra Gemitzi [a,*]

[a] Department of Environmental Engineering, School of Engineering, Democritus University of Thrace, 67100 Xanthi, Greece
[b] Rossby Centre, Swedish Meteorological and Hydrological Institute, 60176 Norrköping, Sweden

HIGHLIGHTS

- Photovoltaic power plants effects on major hydrologic budget constituents are identified, conceptualized and simulated with SWAT model.
- Spatially, the effects are analyzed in basin and local (sub-basin) scale.
- The long-term effects of land use change from agricultural to photovoltaic power plants were investigated by applying downscaled climate projection data from a Regional Climate Model driven by 5 different General Circulation Models.

GRAPHICAL ABSTRACT

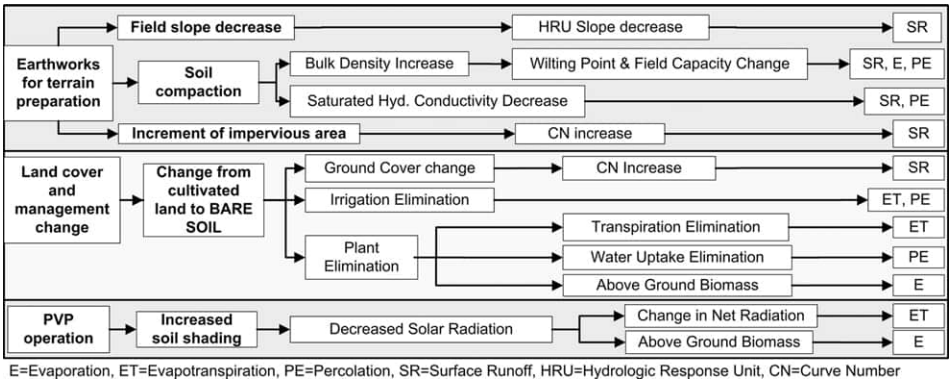

E=Evaporation, ET=Evapotranspiration, PE=Percolation, SR=Surface Runoff, HRU=Hydrologic Response Unit, CN=Curve Number

ARTICLE INFO

Article history:
Received 18 March 2014
Received in revised form 28 May 2014
Accepted 28 May 2014
Available online 18 June 2014

Editor: D. Barcelo

Keywords:
Climate change
SWAT model
Land use change
Hydrology
Photovoltaic parks

ABSTRACT

This study addresses the effects of land use change from agricultural to photovoltaic parks (PVPs) on the hydrology of an area. Although many environmental effects have been identified and analyzed, only minor attention has been given to the hydrologic effects of the installation and operation of PVPs. The effects of current PVP installation and operation practices on major hydrologic budget constituents (surface runoff, evapotranspiration and percolation) were identified, conceptualized, quantified and simulated using SWAT model. Vosvozis river basin located in north Greece was selected as a test site. Additionally, long-term effects were simulated using dynamically downscaled climate projections by a Regional Climate Model (RCM) driven by 5 different General Circulation Models (GCMs) for the period 2011–2100. Results indicate that surface runoff and percolation potential are significantly increased at the local scale and have to be considered during PVP siting, especially when sensitive and protected ecosystems are involved.

1. Introduction

As global greenhouse gas emissions cause an increasing concern on human community regarding climate change, alternative energy sources are substituting for the use of fossil fuel. Solar power plants are among those energy sources which are considered to be environmentally friendly, in terms of emission reduction of greenhouse gases

* Corresponding author. Tel./fax [redacted].
E-mail address: [redacted]@env.duth.gr (A. Gemitzi).

http://dx.doi.org/10.1016/j.scitotenv.2014.05.132
0048-9697/

(Pehnt, 2006) and other hazardous substances, such as mercury, cadmium or even particulates. However, there are other environmental impacts which have not yet been investigated. Turney and Fthenakis (2011) conducted a thorough review on the environmental effects related to the large scale solar power plants and pointed out that hydrology is one of the fields in which impact study is needed. Photovoltaic parks (PVPs) require large land portions to be covered with solar panels, ranging between 20 and 40 m^2/kW_{peak}, which absorb a high amount of the incoming solar radiation; therefore, they reduce the earth's albedo. Nemet (2009) conducted a study on the radiative forcing due to the installation of widespread PVPs. He concluded that the overall radiative forcing from substitution of PV for fossil fuels is much larger than the one caused by the local reduction of earth's albedo. Moreover, the installation of a PVP causes changes to the physical nature of soil, by changing the preexisting vegetation and by converting to impervious a significant portion of the land occupied for this purpose in order to construct concrete footings for the solar panels to be mounted onto. Turney and Fthenakis (2011) list many interventions related to the installation and operation of PVPs that alter the hydrology of an area, such as: alteration of ground slopes if necessary to less than 5%, periodical mowing of vegetation, installation of inverters, transformers and collector boxes, trenching for electrical and communications cables, construction of access roads, maintenance vehicles moving in the area, and water consumption for washing the panels. Nevertheless, their effects on the hydrology of an area occupied by photovoltaic installations have not yet been investigated.

Climate change is expected to significantly affect hydrological processes, especially in semi-arid and arid regions (IPCC, 2007) and Mediterranean region (Erol and Randhir, 2012). De Paola et al. (2014) analyzed the Intensity–Duration–Frequency rainfall curves for three cities in Africa and concluded that a rise of frequency of extreme events is expected and therefore flood risk is increasing. Luo et al. (2013) simulated climate change impacts on hydrology and water quality in northern Coastal Ranges and western Sierra Nevada, USA using SWAT model and concluded that the sensitivity of both hydrologic cycle and water quality to the projected climate change is high.

Within the present work, it is attempted to identify and analyze the effects of installation and operation of PVPs in the major hydrologic components. Furthermore, a generalized conceptualization of those effects is proposed with a view to a wider application in other climate and land uses change studies. Finally, the hydrologic effects are quantified and simulated in a medium sized basin in northern Greece, i.e., Vosvozis river basin (Fig. 1). For this purpose the widely applied hydrologic model SWAT (Neitsch et al., 2011) was calibrated and verified for the period 2008–2012 and various scenarios of impacts extent and land occupation by PVPs were tested. Moreover, dynamically downscaled projected climate data driven by 5 GCMs under SRES-A1B scenario were used as input to the developed model in order to assess the

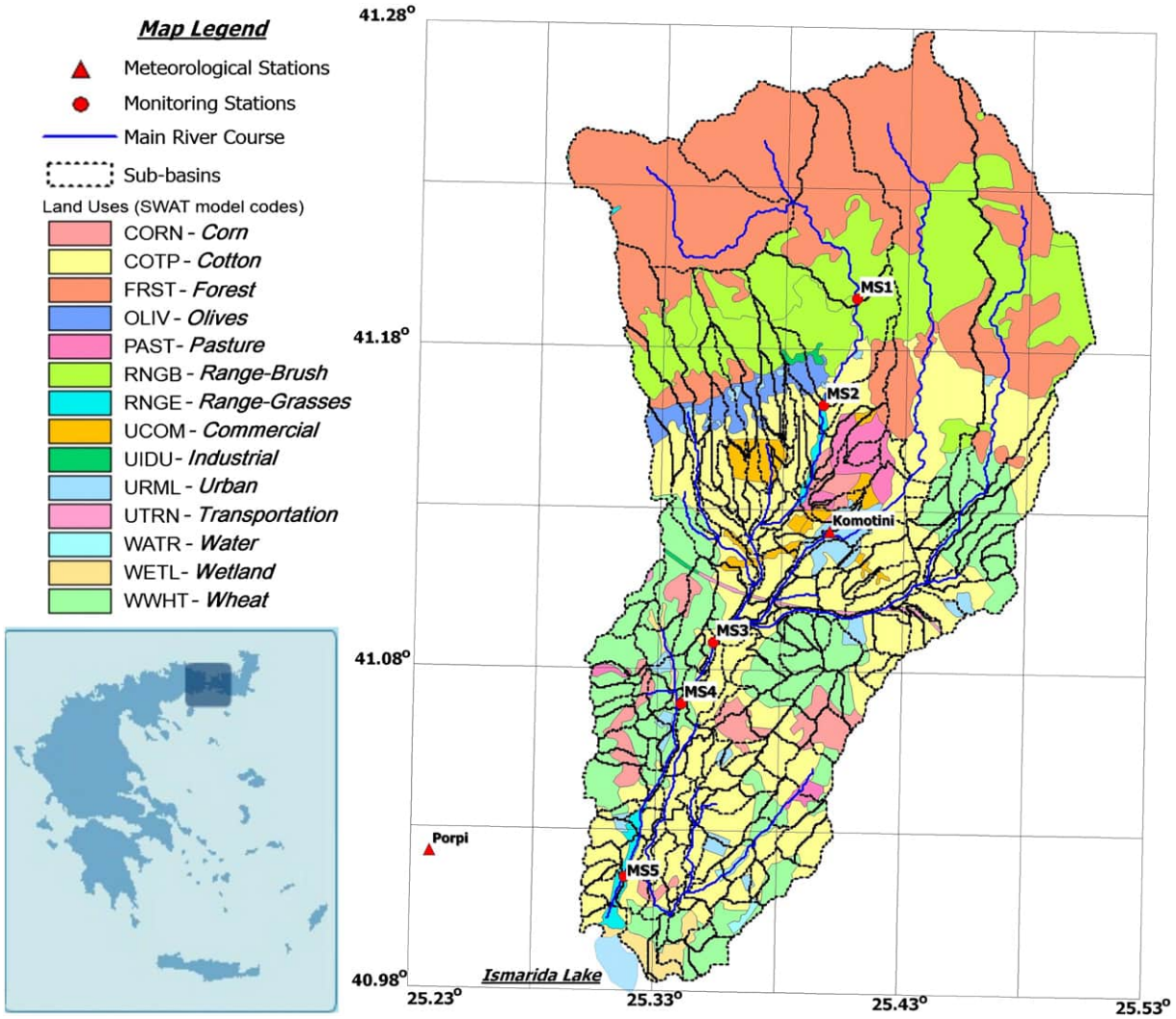

Fig. 1. Location and land use map of the study area.

long-term effects of PVPs on the hydrology of the test site for the period 2011–2100.

2. Materials and methods

2.1. Study area description

Vosvozis river basin in Thrace (Northern Greece) (Fig. 1) constitutes a typical Mediterranean watershed, especially suitable for the installation of PV systems due to the abundance of sunlight, its rural character and the presence of a large proportion of plain land. The catchment size is 340 km^2, extending from the Greek–Bulgarian borders down to the Thracian sea. Vosvozis river discharges into Ismarida Lake, which is an important ecosystem, protected by the Ramsar Treaty, it is designated as Natura 2000 area and it is part of the National Park of Eastern Macedonia and Thrace. Ismarida Lake is an ecosystem where complex interactions among surface waters, groundwaters and sea waters are taking place. Previous research in the area has proved the hydraulic connection of Ismarida Lake and Vosvozis river with the groundwater system. Gemitzi and Stefanopoulos (2011) and Gemitzi et al. (2013) have shown that Ismarida Lake recharges the groundwater system and therefore it should be considered as a groundwater dependent ecosystem. Therefore, any changes on land uses in Vosvozis catchment area are expected to affect Ismarida Lake and the associated aquifer system.

The climate of the area is characterized as Mediterranean with dry hot summers and mild winters. The average annual precipitation is 628 mm and the average annual temperature is 15 °C. The area is characterized by intense agriculture, cattle breeding and urban land uses. The main cultivations are corn, cotton and wheat, as illustrated in Fig. 1. Water is used mainly for irrigation and urban supply. During the last years, several legislative frameworks have been established in Greece which aims to promote the development of renewable energy sources, including photovoltaic power systems. One of the most recent legislative regulations with regard to renewable energy sources is the Law 3851/10 (Official Government Gazette of Greece, 2010), which motivates farmers to install small scale PVPs in agricultural areas, thus promoting land use change and activity modification from agricultural to energy production.

2.2. Model development

2.2.1. Data set and model parameterization

The SWAT model (SWAT2009 version) (Neitsch et al., 2011) was used for the purposes of this study. SWAT model has been widely used for the assessment of climate and land use change effects at the catchment hydrologic regime (Wu et al., 2012; Kim et al., 2013; Luo et al., 2013). SWAT model basic data requirements include topography, land use, soil and weather data. It is calibrated and validated using simulated against observed river discharge data. Thus, five monitoring stations were established in Vosvozis river basin (Fig. 1), in which river flow measurements were performed on a weekly or biweekly basis for the period October 2008 to April 2012. River flow was determined by in-stream wading measurements using a Hydrological Services Pty OSS-B1 current meter. The monitoring process resulted in 580 river flow measurements in total for the five monitoring stations.

Land use distribution for the study basin was defined using a hybrid approach of CORINE data and general crop pattern data derived from Apostolakis (2009). The appropriate SWAT land cover/plant codes were assigned to each land use and a reclassified land use map was produced (Fig. 1), which was used as input to SWAT model. Soil data were obtained by the local authorities and were enriched with recent soil data from Misopolinos (2009), which were incorporated into SWAT soil database.

Digital Elevation Model (DEM) quality can strongly influence the hydrologic simulation results (Defourny et al., 1999). For the mountainous area, DEM was constructed by digitization of the 1:50,000 scale topographic map of the Hellenic Military Geographical Service. For the lowland area, where low slopes are observed, that were not sufficiently represented by the 1:50,000 scale topographic map, 1:5000 topographic maps of the Hellenic Military Geographical Service were digitized. The resolution of the final DEM was 50 × 50 m. Due to the fact that some parameters included in land use change scenarios, such as solar radiation, are assigned at the sub-basin level and not at the Hydrologic Response Unit (HRU) level, the agricultural part of Vosvozis river basin was densely subdivided into small sub-basins in order to be able to develop low PVP coverage scenarios. This does not affect the validity of model performance, as indicated by the results provided by Cho et al. (2010), showing that watershed subdivision did not affect streamflow prediction stability. Vosvozis river basin was subdivided into 211 sub-basins and 265 Hydrologic Response Units (HRUs). Weather data were collected from two meteorological stations shown in Fig. 1, including daily values of precipitation, maximum/minimum temperature, wind speed, solar radiation and relative humidity for the period October 2008 to April 2012.

Two methods are available within SWAT model for surface runoff simulation: the SCS runoff method (USDA-SCS, 1972) and the Green & Ampt infiltration method (Green and Ampt, 1911). Despite the fact that infiltration is directly simulated in Green & Ampt method, it requires sub-daily meteorological data. Hydrologic simulation in a sub-daily time step is not the case for the current study and therefore the widely applied SCS method was used for the purposes of this study. The parameter that controls surface runoff potential in SCS method is the curve number (CN) which ranges between 30 and 100. Lower CN values indicate low runoff potential, while higher values correspond to increasing runoff potential.

SWAT model interface offers several methods for the calculation of potential evapotranspiration. As solar radiation changes are crucial for the purposes of this study, a method which incorporates solar radiation in evapotranspiration calculations should be used. Between Penman–Monteith (Monteith, 1965) and Priestley and Taylor (1972) methods, the former was chosen, as the latter tends to underestimate potential evapotranspiration in semi-arid and arid areas (Neitsch et al., 2011).

2.2.2. Model calibration/verification

Calibration and validation processes are critical for model reliability, as there are parameters, which are difficult to be measured or estimated, thus increasing the degree of uncertainty in simulation. Model calibration could be either manual or automatic. As there are no continuous streamflow time series available, manual calibration was used for the purposes of this study.

Model calibration was based on daily streamflow data for the period October 2008 to October 2010. Several statistical methods and indices have been proposed and assessed for hydrological model evaluation. Legates and McCabe (1999) indicate that, not only correlation-based criteria, but also summary statistics and absolute error criteria have to be used in order to maintain a sufficient hydrological model evaluation. Krause et al. (2005) investigated the performance of several criteria used for the assessment of hydrological models and concluded that, unlike R^2, weighted R^2 (wR^2) is capable to reveal systematic model errors. They also found that the most sensitive criteria to low flow conditions area the logarithmic Nash–Sutcliffe Efficiency (Nash and Sutcliffe, 1970) (lnNSE) and the modified NSE. Moriasi et al. (2007) reviewed several model performance evaluation criteria used in a wide range of watershed models applications. They concluded that NSE, percent bias (PBIAS) and the ratio of the root mean square error to the standard deviation of measured data (RSR), in combination with graphical methods, should be used for model performance evaluation.

According to the above, the SWAT model application within this study was initially evaluated through a visual inspection of calibration results in the form of scattergrams, in which simulated streamflows are plotted versus observed ones and a linear regression line is fitted

to (regression line gradient b and coefficient of determination R^2 are also calculated). Then wR^2, NSE, lnNSE, PBIAS, RSR and mean absolute error (MAE) were calculated. The same evaluation criteria were used for model validation assessment with streamflow data for the period November 2010 to April 2012.

2.3. PVP installation and operation effect identification and conceptualization

Based on the current practices applied in PVP siting, installation and operation, three interventions performed in a PVP terrain, which can potentially affect the local hydrology, were recognized. Hydrologic cycle components within a watershed are interacting in a complex way. Therefore, within the present work it is attempted to conceptualize the assessment process by identifying and assigning the PVP installation and operation effects that directly affect the fundamental hydrologic budget components. Indirectly, almost every hydrological component will be affected, as they are in constant interaction. Moreover, SWAT model parameters that describe the specific impact of the affected hydrological process were identified and properly adjusted in order to develop short-term and long-term impact scenarios. The three interventions identified and the subsequent conceptualization of their effects in the major hydrologic budget components are presented in Fig. 2 and described in detail below, while the corresponding equation relating the affected hydrologic budget components to SWAT model parameters is presented in Section A1 of Supplementary Material.

2.3.1. Earthworks for terrain preparation and PV mounting

The first intervention includes the earthworks for field flattening and related equipment installation (PV mounting systems, cables, inverters etc.). In general, low slope areas (<5%) are preferable for the construction of PVPs due to the fact that they are easier approached and the optimum orientation of photovoltaic panels is easier to be obtained, while less earthworks are required. Nevertheless, PVPs can be constructed in relatively high slope terrains. Any changes made in the slope of the PVP terrain will directly affect surface runoff potential. When applying SCS method for surface runoff simulation within SWAT model, CN is properly adjusted according to the slope of the corresponding HRU. Therefore, any changes in the slope of the HRU in which PVP is constructed will affect CN and subsequently surface runoff.

Depending on the case, earthworks may be required in order to eliminate the geomorphological anomalies of the installation terrain. Due to the fact that earthworks and related equipment installation are conducted using heavy machinery, soil compaction is likely to be observed, which refers to the packing effect of mechanical forces on soils (Ozgoz et al., 2006). Alaoui et al. (2011), in their review article, indicated that in most studies investigating the effects of soil compaction, bulk density (BD) was found to be increased in the upper soil layer, while the decrement in pore volumes of compacted upper soil layer, resulted in significantly lower saturated hydraulic conductivity (KSAT) values. The degree to which those soil hydraulic properties are affected by soil compaction depends on several factors, including soil type, moisture content and mechanical force amount load. Despite the fact that during the cultivation process, tractors and harvesting machines contribute to soil compaction, soil compaction effects are relieved by processes such as freezing/thawing, wetting/drying and tillage (Hakansson, 2005). Thus, the extent of recovering for PVP compacted soils is expected to be lower, since these soils are not tilled. Any change in BD affects wilting point and subsequently field capacity of the soil layer. Field capacity is related to retention parameter used in daily CN

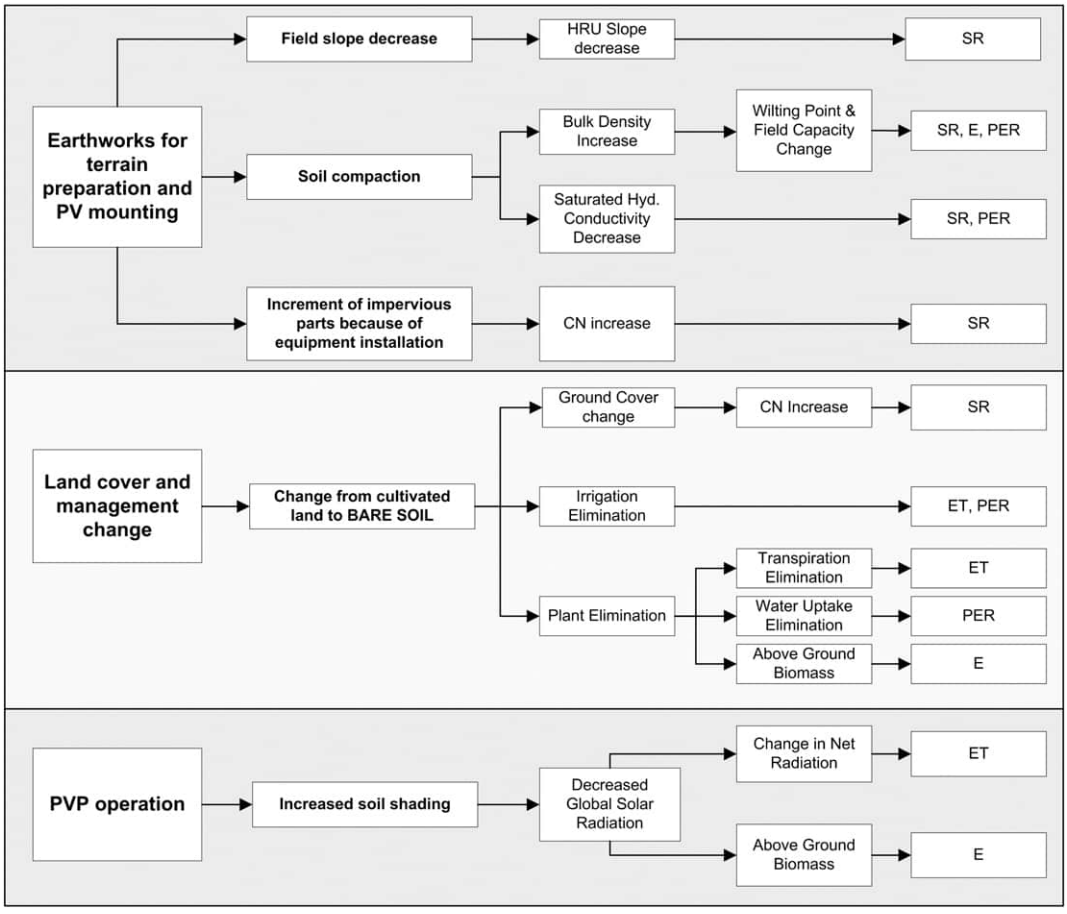

Fig. 2. Conceptualization scheme of PVP installation and operation impacts on major hydrologic components. (E = evaporation, ET = evapotranspiration, PER = percolation, SR = surface runoff, HRU = hydrologic response unit, CN = curve number).

calculation, when the daily CN is calculated as a function of water content and therefore surface runoff is affected. Moreover, soil water evaporation is affected, as field capacity constitutes the threshold water content value below which the evaporative demand of a soil layer decreases. Finally, percolation is affected by soil compaction, as field capacity and KSAT are related to travel time for percolation.

When concrete footings are constructed for PV panel mounting purposes and little prefab buildings are installed, a part of the PVP terrain is substituted by impervious areas. This will directly increase the potential of surface runoff, which is reflected in the modeling process by CN increment in SWAT model.

2.3.2. Land cover and management operations change from agricultural to PVP

The second significant intervention expecting to affect the hydrologic regime of an area is the land use change from agricultural to energy production. Cultivation includes several processes that directly affect the hydrologic regime of the agricultural field, such as plant growth and irrigation, which are eliminated when agricultural land is converted to PVP. Surface runoff is directly related to land cover. Peng and Wang (2012) measured surface runoff for six different land use covers, including forestland, cropland and pastureland using the large runoff field method. Their results indicated that the annual surface runoff can vary significantly with regard to land use type. The effects of land cover change from agricultural to energy production in surface runoff are reflected by changes in CN values, which are higher for bare soil when compared to CN values for the dominant crops of the study area (cotton, wheat and corn). These variations of CN values indicate a significant potential of land use change to affect surface runoff.

Depending on climate conditions and crop type, irrigation could constitute a significant component of the hydrologic budget. When agricultural irrigated land is substituted by PVPs, changes are expected for all the components of the hydrologic budget as irrigation ceases. The most significant change however, is expected to be observed in evapotranspiration due to changes in both transpiration and evaporation processes.

2.3.3. PVP operation

One of the fundamental principles concerning PVP construction is the orientation of photovoltaic panels in the way that they provide the maximum absorption of solar radiation. Within a PVP, several factors have to be taken into account for the definition of energy budget, as there are shaded surfaces of PVP terrain located under the PV panels and unshaded surfaces existing between the PV arrays, which serve to avoid PV panels shading from each other. Concerning the shaded surfaces of a PVP, from the total short-wave radiation, only short-wave diffuse radiation received from the ground should be taken into account. Therefore, significant changes are expected to be observed in ground's energy budget, which will affect evapotranspiration, as according to Penman–Monteith equation, evapotranspiration is directly related to solar radiation.

Studies investigating the energy budget and heat fluxes within a PVP are absent. Therefore, the ground energy balance was simulated with Autodesk Ecotect Analysis software for a typical PVP in order to estimate the shading effects of fixed mounting systems in solar radiation amounts reaching the ground. Despite the fact that Autodesk Ecotect software is mainly used for building energy analysis, for the purposes of this study, it was used in order to identify the extent of decrease in incident (direct and diffuse) solar radiation approaching the ground surface of a PVP. The incident solar radiation was simulated for a hypothetical PVP of 100 kWp, which is constructed in a zero slope terrain. Fixed mounting systems were assumed, whose characteristics are similar to those used in the study of Bakos (2009). South orientation of PV arrays was assumed with an inclination of 25° in order to maintain maximum electricity production during the year, while the appropriate row-to-row PV panel spacing was estimated to 6 m according to Macomber et al. (1981), in order to avoid shading effects of adjacent rows. More details can be found in Section A2 of Supplementary Material.

2.4. PVP installation and operation impact scenarios development

The conceptualization of PVP installation and operation impacts on the hydrologic regime revealed a large amount of parameters influenced, while the degree of influence for some parameters, such as BD, KSAT and solar radiation (SLR) is highly uncertain. For this reason, three scenarios were developed based on intensity and extent of interventions. The first scenario, referred as low impact scenario, incorporates mild interventions, both during PVP construction and operation. According to low impact scenario, earthworks are limited as there is no need for field flattening and mounting systems are installed through pile driving and consequently, there is no need for concrete footing. Therefore, no changes in field slope are anticipated, while soil compaction is expected to be recovered because of drying/wetting and freezing/thawing processes; thus, bulk density and saturated hydraulic conductivity do not change. Agricultural land is substituted with bare soil, while the mounting system type and installation height are expected to cause a low decrease (20%) in solar radiation amount reaching the ground.

The second scenario, referred as medium impact scenario, involves medium interventions during the construction and operation of a PVP. Despite the fact that there is no need for concrete footing for PV mounting, earthworks are more intensive for field flattening, resulting in soil compaction that cannot be recovered by the drying/wetting and freezing/thawing processes. So, bulk density increases by 15%, while saturated hydraulic conductivity decreases by 50%. Similar to the previous scenario, agricultural land is substituted with bare soil, but mounting system setting and installation height cause higher reduction in solar radiation (40%).

The last scenario, referred as high impact scenario, incorporates serious interventions during PVP installation, as well as, during operation. Extensive earthworks are required for field flattening and mounting systems are installed in concrete footing. The extensive earthworks resulted in substitution of agricultural land with bare soil, significant increase in bulk density (30%) and decrease in saturated hydraulic conductivity (the original values were multiplied by 0.1). Moreover, PV mounting systems are closely installed to each other and the installation height is low, resulting in significant decrease in solar radiation reaching the ground (60%). Those three scenarios were tested for 1% and 5% coverage of the study basin. Each coverage, either 1% or 5%, was spatially distributed in five different ways in the catchment site, with PVP replacing different parts of the agricultural area, as illustrated in Fig. 3.

In order to predict the long-term impacts of the above mentioned land-use change scenarios, climate scenarios for the future have to be used as climate input to the SWAT model. For the purposes of the present study, data from the Rossby Centre regional climate model, RCA3 (Samuelsson et al., 2011) were used, which were driven by the following 5 Global Circulation Models (GCMs): a) CCSM3, b) CNRM, c) ECHAM5-r3, d) HADCM3-Q0 and e) IPSL. Nikulin et al. (2011) provided technical details and an evaluation of these regional scenarios and the driving GCMs. Despite the fact that the application of Regional Climate Models (RCMs) offers a much higher spatial resolution in meteorological variables simulation when compared to GCMs, a systematic bias is typically noticed in the hydro-meteorological variables produced by the RCM. This bias originates from either the driving GCM or parameterizations in RCMs (Kotlarski et al., 2005; Kay et al., 2006; Graham et al., 2007). Therefore, the primary hydrological variables such as precipitation and temperature need to be adjusted to get realistic time series for use in local impact studies (Graham et al., 2007; Yang et al., 2010).

In this work, Distribution-Based Scaling (DBS) approach was used in order to further correct RCM precipitation and minimum and maximum temperature for impact model applications. Details about DBS can be found in Yang et al. (2010). The DBS approach aims to maximize

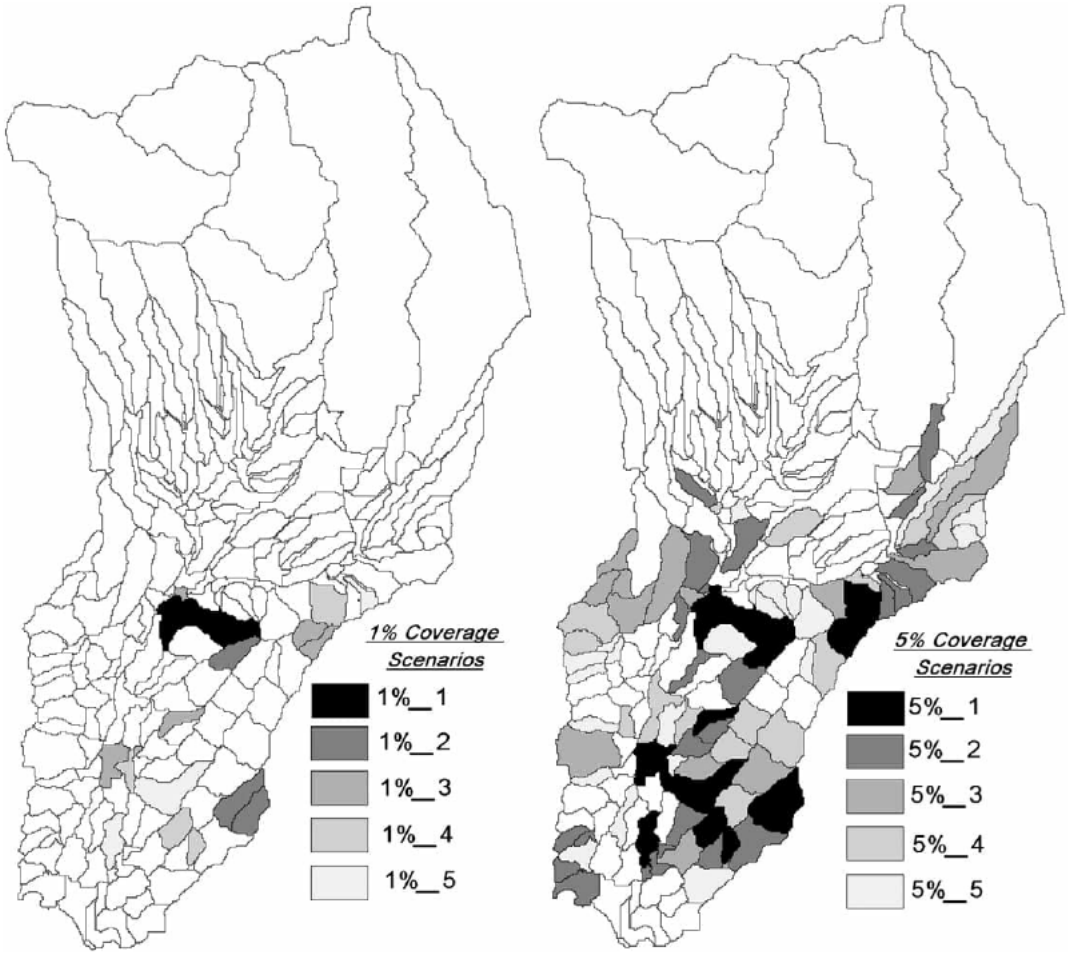

Fig. 3. Spatial distribution of scenarios with 1% and 5% coverage of agricultural land with PVPs.

utilization of RCM outputs to get more realistic input data for hydrological studies. With the DBS approach, statistical properties such as daily mean, standard deviation of temperature as well as distribution and frequency of precipitation days are much improved compared to direct RCM output. Relative humidity, solar radiation and wind speed RCM data were corrected using the widely used linear scaling approach, according to which daily RCM data are corrected by calculating a monthly correction factor for each parameter.

3. Results and discussion

3.1. Global radiation simulation results

The simulation results indicated a significant decrease of incident solar radiation reaching the ground surface of the hypothetical PVP, in relation to the incident solar radiation reaching the ground surface of the same terrain, when it is not covered by PVs. The decrease of average daily radiation in monthly basis ranges between 40% and 47.6% for panel inclination 25°, row-to-row spacing distance of 6 m (Fig. 4, line 25°, 6 m), while on the annual basis the decrease is 43.4%. Lower decreases were observed during summer months, while higher insolation decreases were observed during winter months, which depend mainly on differences of the sun path.

In order to test the influence of PV panel arrays density in insolation, the row-to-row spacing was decreased to 4 m. Moreover, the influence of PV panel inclination on insolation was tested by increasing inclination from 25° to 30° for both row-to-row spacing distances of 4 and 6 m. Thus, three more insolation simulations were performed and their results are presented in Fig. 4. Row-to-row spacing strongly influences the insolation reaching ground surface of a PVP, as decreasing row-to-row spacing from 6 m to 4 m was found to further decrease insolation by 7.3 to 13.5% for 25° inclination and by 6.3 to 13.1% for 30° inclination. With regard to PV panel inclination, the increment from 25° to 30° presented lower insolation decrease during the whole year when row-to-row spacing is 6 m, while insolation was decreased during May and summer months when row-to-row spacing is 4 m and remained almost stable for the other months of the year. Significant changes in energy budget have also been reported in studies investigating the effects of PV panel installation on roofs. Scherba et al. (2011), concluded that adding PV panels to a black roof reduced the daily sensible heat flux by 11%, while for PV-covered white and green roofs the daily sensible heat flux reduction was up to about 50%.

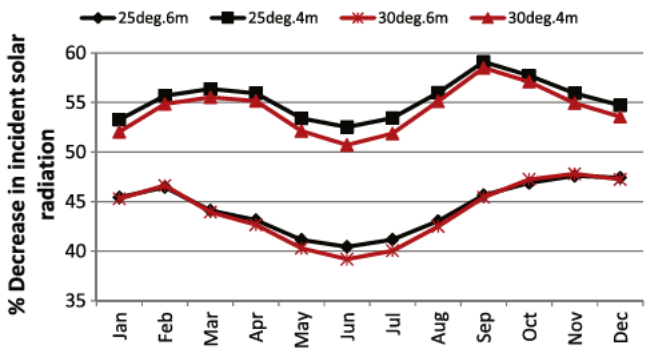

Fig. 4. Monthly decrease of ground surface incident solar radiation for several combinations of PV panels inclination and row-to-row spacing.

3.2. SWAT model calibration and validation

The statistical assessment results of SWAT model calibration and validation in Vosvozis river watershed are presented in Table 1, while the corresponding scattergrams of observed versus simulated streamflow are presented in Section A3 of Supplementary Material. Moriasi et al. (2007) indicate that SWAT model calibration for streamflow is satisfactory when NSE > 0.50, RSR < 0.70 and −25% < PBIAS < 25%. Based on this, both calibration and validation results were satisfactory, as indicated in Table 1, according to which NSE ranged from 0.86 to 0.97 for calibration and from 0.82 to 0.90 for validation, while the corresponding ranges for RSR was 0.19–0.38 for calibration and 0.04–0.387 for validation and for PBIAS is −6.12%–3.14% for calibration and −2.68%–9.13% for validation. The most widely used model performance assessment index (R^2) ranged between 0.87 and 0.98, thus indicating satisfactory model performance. lnNSE variation range was much lower than NSE variation range. Due to the fact that lnNSE is sensitive to low flow conditions, it is indicated that model response in low river flows observed during summer (less than 0.1 m^3/s) was worse than the overall model response. This does not significantly affect model performance, as those low river flows are not contributing significantly to the water budget. Except from MS1, the regression line gradient *b* in all monitoring stations is higher than 1, indicating that the model overestimated river flows. This overestimation (or underestimation for MS1) does not significantly affect model performance as wR^2 values in which *b* is incorporated, were satisfactory. As expected, calibration results are better than validation results, but validation results were also satisfactory.

3.3. Short-term land use change scenarios results

The short-term (2008–2012) effects of land use change from agricultural to PVP as described in the scenarios presented above were investigated at the basin scale, in order to assess the effects of 1% and 5% coverage of agricultural areas with PVP, and also at the sub-basin scale, in order to assess the local effects of land use change. The results for basin scale are presented in Fig. 5, while the corresponding results for sub-basin scale are presented in Fig. 6. The general trend observed both in basin and sub-basin scale is that surface runoff and percolation increase, while evapotranspiration decreases. These trends became more intense, as land use change impact increases from low to medium and high impact scenarios. Also, as impact intensity increased, a small increment in surface runoff was observed, while further decrement of evapotranspiration mostly contributed to increment of percolation. This fact indicates that after the allocation of precipitation water in surface runoff, more water is available to enter and remain in the soil profile, as evaporation decreases because of the shadowing effects.

The highest impact of land use change at the basin scale was presented for evapotranspiration, while the lowest impact was presented for percolation, both for 1% and 5% coverage. The decrement of soil permeability, as well as transpiration elimination, is a key process affecting the major hydrologic budget constituents, as illustrated by the significant increase in surface runoff and the significant decrease in evapotranspiration, even from the low impact scenario.

The coverage of 1% basin area with PVPs does not significantly affect the hydrologic budget of the basin, as surface runoff changes ranged between 0.9 and 1.27 mm, while the corresponding ranges for evapotranspiration and percolation were −2.3 to −5.2 mm and 0.17 to 0.52 mm, respectively (Fig. 5). Significantly higher, but not important at the basin scale was the impact for 5% basin coverage with PVPs (Fig. 5). The wide range of variation of the major hydrologic constituents change illustrated both at the basin and sub-basin scale indicates that the spatial distribution of PVP coverage and the corresponding spatial variability in soil profile composition and properties are key parameters for the assessment of land use change from agricultural to PVPs. This is more obvious in the box-plots presenting the variation of change at the sub-basin scale for 5% coverage (Fig. 6). Especially for evapotranspiration and percolation, the variation range exceeded 100 mm and 300 mm, respectively.

At the sub-basin scale, the results illustrated a significant potential for surface runoff to be locally increased, even in low impact scenario, by more than 100 mm on the median, which subsequently increases the local flood risk. One could expect that surface runoff should not be increased due to the fact that the major part of the study area is cultivated with summer crops (cotton and corn), which are not active during winter, while during summer, their water needs are satisfied by irrigation. However, the fact that crop water requirements during the summer cultivation period are satisfied not only from irrigation but also from soil water implies that water in the soil profile at the end of the cultivation period is significantly decreased and has to be replenished before surface runoff is generated. For the same reason, an increasing trend was presented for percolation and subsequently for groundwater recharge (Fig. 6). Especially for the Mediterranean region, this is a favorable impact, as groundwater constitutes the most significant resource for the satisfaction of water needs and its role is important for the regional and local economies (Aureli et al., 2008). Furthermore, due to the fact that agrochemicals used for crop cultivation purposes will no longer be applied when land use changes from agricultural to PVPs, lower groundwater pollution risk is expected.

When irrigation of an agricultural field is made from groundwater, the groundwater availability in the aquifer is expected to be increased due to irrigation elimination. However, some amounts of water are required during PVP operation for PV panels washing. The water consumption for PV panel washing is highly uncertain, as it varies by site and developer and washing rates are not well documented. Based on Aspen Environmental Group studies (2011a, 2011b) and industry knowledge an estimate of 0–18.93×10^{-3} m^3/MWh is reported by US-DOE (2012). Even when considering the highest consumption rate of 18.93×10^{-3} m^3/MWh, it is negligible when compared to water consumption for irrigation in semi-arid areas. For a PVP like the one presented by Bakos (2009) of 60 kWp, which is estimated to produce 74 MWh/y and covers an area ranging between 1200 and 2400 m^2, the

Table 1
Statistical assessment results of SWAT model calibration and validation using river discharge data from the 5 monitoring stations located in Vosvozis river basin. (NSE = Nash–Sutcliffe efficiency, lnNSE = logarithmic NSE, b = regression line gradient, R^2 = coefficient of determination, wR^2 = weighted R^2, PBIAS = percent bias, RMSE = root mean squared error, RSR = RMSE–observations standard deviation ratio).

	Calibration					Validation				
	MS1	MS2	MS3	MS4	MS5	MS1	MS2	MS3	MS4	MS5
NSE	0.86	0.90	0.94	0.96	0.97	0.86	0.90	0.83	0.88	0.82
lnNSE	0.70	0.66	0.57	0.81	0.74	0.62	0.67	0.64	0.63	0.78
b	0.96	1.03	1.00	1.05	1.06	0.94	0.99	1.00	0.99	1.03
R^2	0.87	0.91	0.95	0.97	0.98	0.88	0.91	0.86	0.90	0.86
wR^2	0.83	0.89	0.95	0.93	0.92	0.83	0.90	0.86	0.89	0.83
PBIAS (%)	3.14	6.15	0.97	0.53	3.88	9.31	0.40	2.45	1.23	2.68
RMSE (m^3/s)	0.13	0.14	0.22	0.17	0.18	0.07	0.07	0.20	0.17	0.19
RSR	0.38	0.32	0.24	0.19	0.19	0.33	0.29	0.04	0.04	0.39

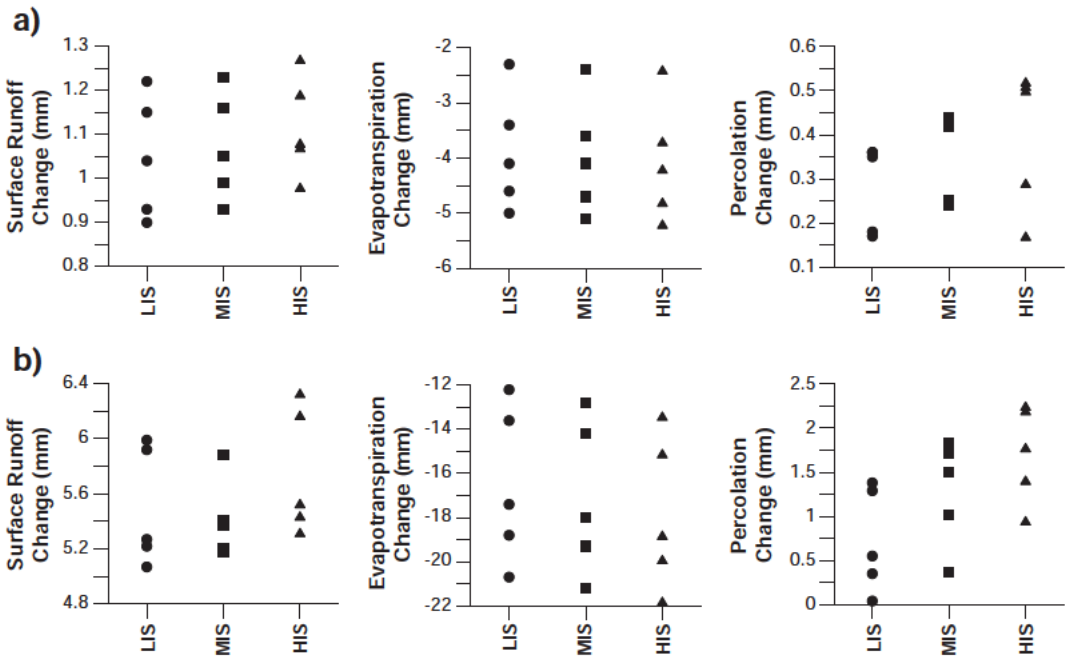

Fig. 5. Basin scale effects of land use change from agricultural to PVP on annual surface runoff, evapotranspiration and percolation for a) 1% PVP coverage and b) 5% basin coverage with PVPs for the period 2008–2012. LIS, MIS and HIS correspond to low, medium and high impact scenarios, respectively.

maximum water consumption is 1.4 m^3 or 0.58–1.16 mm per year. This water amount is low compared to water needs of crops like corn and cotton, which require more than 500 mm H_2O per growing season, mostly provided by irrigation in the Mediterranean region.

3.4. Long-term land use change scenarios results

Before the presentation and assessment of long-term effects of land use change from agricultural to PVP, future trends of precipitation and temperature resulted from the bias-correction process are analyzed and compared to historical data for the period 1954–2010 from Porpi meteorological station (Fig. 1) and are representative of the lowland climate conditions. In terms of precipitation projection, except from downscaled IPSL and downscaled HADCM3 projected data which demonstrate increased average annual precipitation (5% and 13%, respectively) for the period 2011–2100 compared to period 1954–2010, all other projections indicated a decrease of average annual precipitation, ranging between 4 and 10%. IPSL projection indicated periods in which precipitation is well above the historical annual average, while there was no significant drought period signal observed. According to

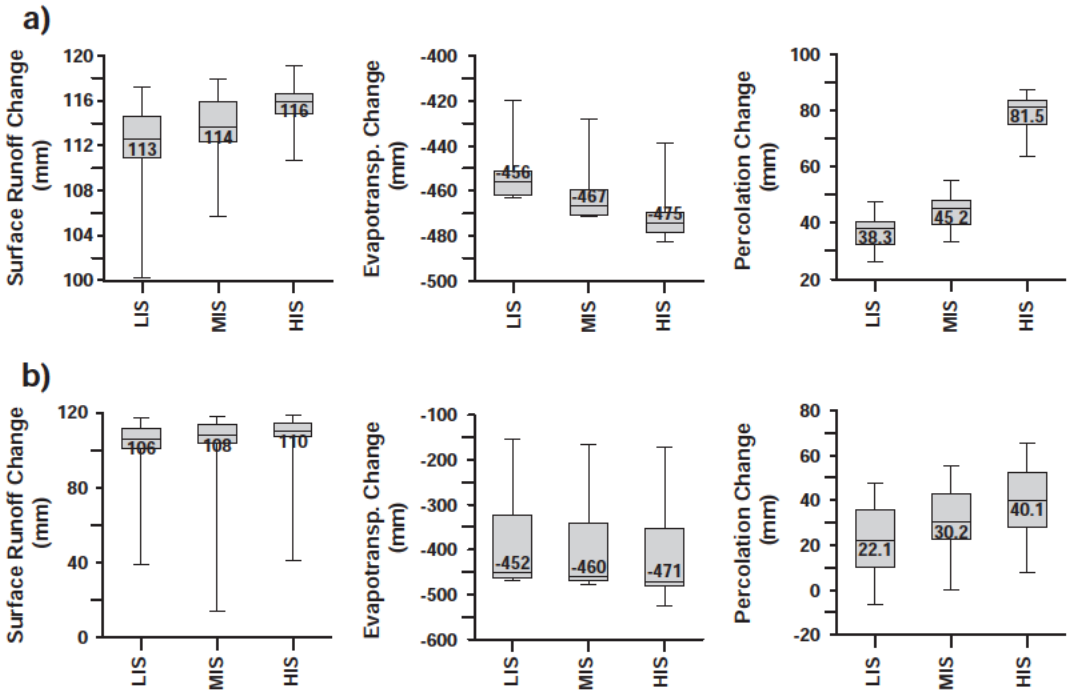

Fig. 6. Sub-basin scale effects of land use change from agricultural to PVP on annual surface runoff, evapotranspiration and percolation for a) 1% PVP coverage and b) 5% basin coverage with PVPs for the period 2008–2012. LIS, MIS and HIS correspond to low, medium and high impact scenarios, respectively.

downscaled CCSM3 data, annual precipitation demonstrated small variation for the period 2011–2070, while for the period 2070–2100, it was significantly decreased. For the same periods, annual precipitation according to downscaled HADCM3 projection was presented increasing and decreasing, respectively. Downscaled ECHAM5 projected precipitation data indicate two significant drought periods, the intensity and duration of which are similar or higher to the drought period observed during 1981–1994. In the same way, downscaled CNRM precipitation data indicated 3 significant drought periods and the strongest decreasing precipitation trend of all projections. Precipitation projection from downscaled CNRM, CCSM and ECHAM data are presented to be more realistic when compared to precipitation data variation for the period 1954–2010. Both annual maximum dry and wet spells demonstrate an increasing trend for all projections, compared to historical period. This fact indicates that after the extended dry spells, extended wet spells are expected to be observed. Also, extreme precipitation event frequency is expected to be increased. Concerning temperature, all projections demonstrated increasing trend, as illustrated in Fig. 7, and average temperature for the study area is presented to be increased from 3.5 °C (downscaled CCSM3 projection) to more than 5 °C (downscaled HADCM3 projection). In terms of solar radiation, it was found to be almost stable, while relative humidity indicated a decreasing trend which is more intense for downscaled HADCM3 projection. Finally, wind speed indicated increasing trend for all downscaled climate projections, except from IPSL, which indicated decreasing trend.

PVP coverage combinations 1_5 and 5_2 presented in Fig. 3 were chosen in order to assess the long-term effects of 1% and 5% land use change from agricultural to PVP, respectively. Those PVP coverage combinations were found to have the highest overall impact among the several PVP coverage distributions tested in short-term scenarios. At the basin scale, long- term impacts of land use change from agricultural to PVP presented in Fig. 8 are comparable to the corresponding results of short-term impacts both for 1% and 5% coverage, except from percolation, whose change was found to be negative under the low impact scenario, both for 1% and 5% coverage. In terms of surface runoff, the strongest increasing trend was observed for IPSL climate projection, thus reflecting the effects of higher precipitation simulated by this model, compared to the other four models. In contrast, the weakest increasing trend was observed for CNRM climate projection, which is consistent to the lowest average precipitation simulated by this model for the period 2011–2100. Concerning evapotranspiration, the strongest decreasing trend was observed for CCSM climate projection, whereas the weakest decreasing trend was observed for IPSL and HADCM climate projections. CCSM climate projection indicates the lowest temperature increase among the 5 climate projections and therefore the lowest temperature stress for the cultivated crops in the basin. This fact results in higher transpiration amounts and consequently higher evapotranspiration values simulated with CCSM climate projection data, which further produced higher change in evapotranspiration (Fig. 8), when transpiration was eliminated. Taking into account the findings of Nemet (2009), according to which PVPs may cover up to 0.39% of land by 2100 in case of high-diffusion of PVPs, the effects of PVP installation and operation are expected to be insignificant at the basin scale.

The results of long-term assessment land use change from agricultural to PVP at the sub-basin scale are illustrated in Fig. 9. The effects of temperature stress in evapotranspiration mentioned above are reflected in evapotranspiration change at the sub-basin scale, indicating higher evapotranspiration change for CCSM projection compared to evapotranspiration change simulated with the other climate projections, while the most wide inter-quartile range is presented for IPSL projection, reflecting the significantly different precipitation variation pattern compared to the other climate projections. The evapotranspiration change simulated for 1% coverage was about 15 to 20 mm higher than evapotranspiration change simulated for 5% coverage, thus indicating the importance of local soil profile properties and composition.

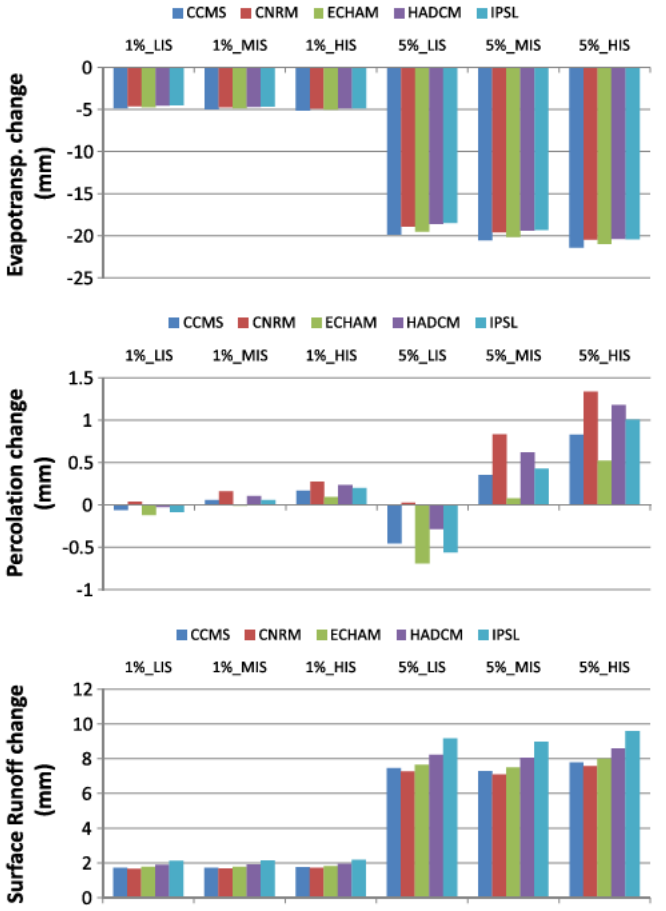

Fig. 8. Basin scale effects of land use change from agricultural to PVP on annual surface runoff, evapotranspiration and percolation for 1% and 5% PVP coverage during the period 2011–2100. LIS, MIS and HIS correspond to low, medium and high impact scenarios, respectively.

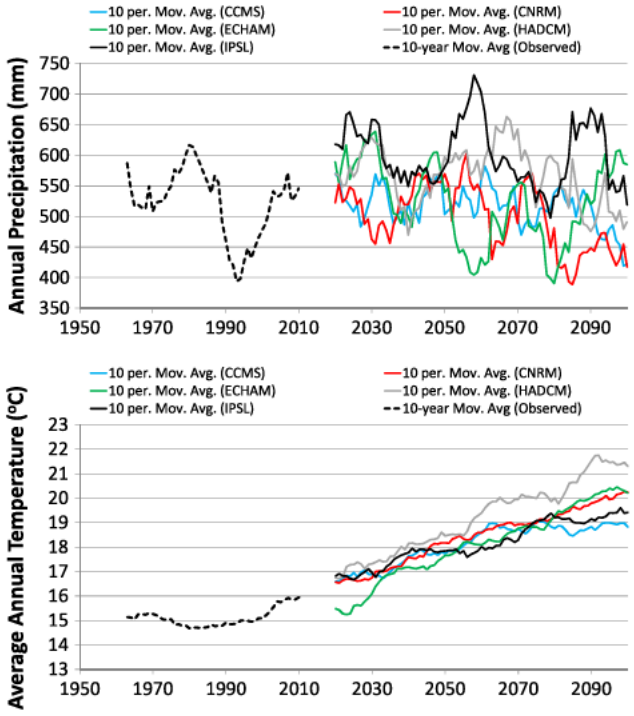

Fig. 7. 10-year moving average of historical (1954–2010) and projected (2011–2100) annual total precipitation and annual average temperature in Porpi (Fig. 1).

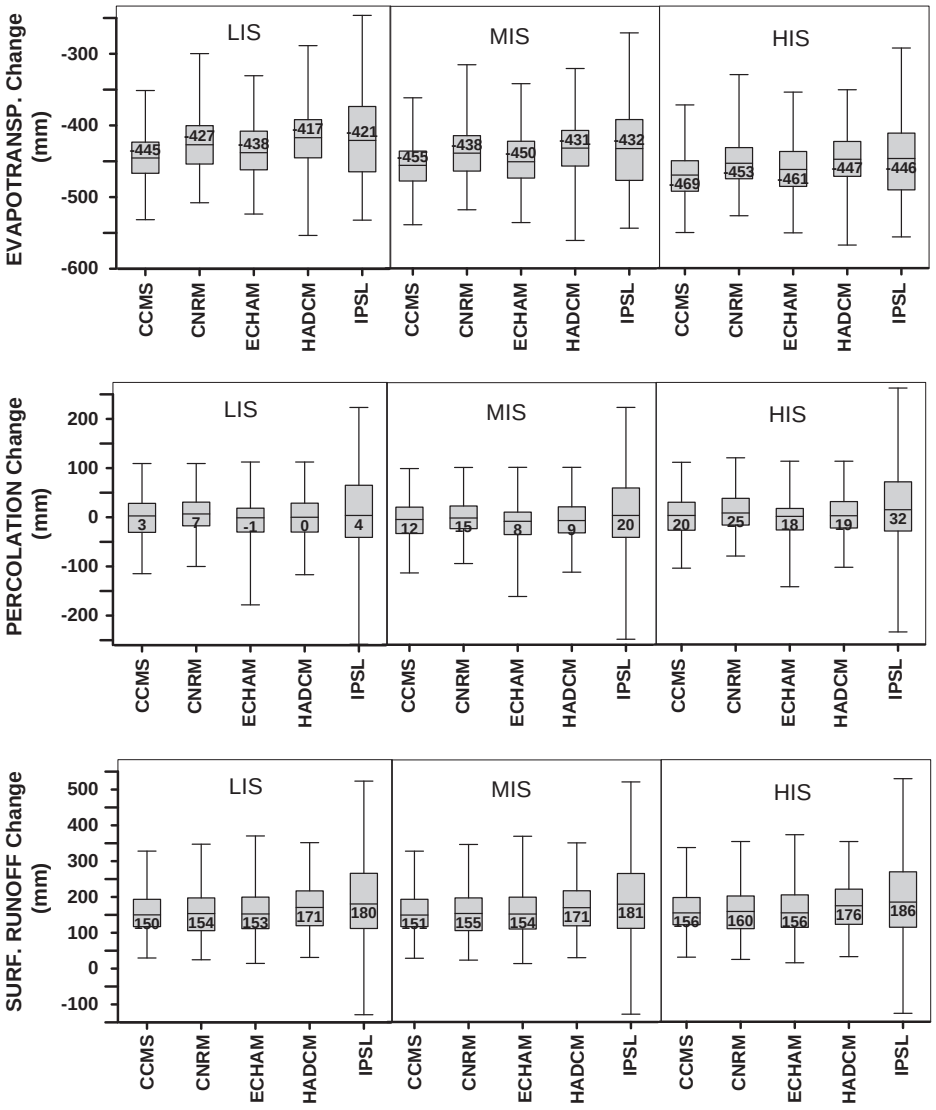

Fig. 9. Sub-basin scale effects of land use change from agricultural to PVP in annual surface runoff, evapotranspiration and percolation for 1% PVP coverage during the period 2011–2100. LIS, MIS and HIS correspond to low, medium and high impact scenarios, respectively.

Evapotranspiration was found to be further decreased from low to high impact scenarios, both for 1% and 5% coverage and all climate projections. For 5% coverage the decrement of evapotranspiration between the impact scenarios was found to be higher, demonstrating once again the effects of local conditions.

The clear increasing trend observed for percolation in the short-term assessment results for both 1% and 5% coverage presented in Fig. 6 was not observed in long-term assessment of land use change from agricultural to PVP, especially under low impact scenario. Median percolation change for ECHAM and HADCM climate projections under low impact scenario and both 1% and 5% coverage was negative, while interquartile range for all projections included both negative and positive percolation change values. The variation trend of percolation became clearer for medium and high impact scenarios, as interquartile range of percolation change included almost only positive values, but median percolation change increase was significantly smaller when compared to the corresponding results from short-term assessment. It is indicated that local soil water balance, part of which is percolation, may vary significantly according to local soil profile composition and properties and therefore resulted in high variation of percolation. Higher percolation increase was observed for IPSL climate projection, while lowest percolation increase was observed for ECHAM climate projection results.

Runoff potential presented a significant increasing trend at the sub-basin scale, as indicated by the significant increase in surface runoff for all climate projections (Figs. 9, 10). Higher runoff increase was indicated for IPSL projection, reflecting the higher projected precipitation amounts compared to the other four projections. Also, a wider interquartile range was presented for surface runoff change under this climate projection, indicating higher precipitation variability and extremes. Overall, surface runoff increase at the sub-basin level was significantly higher for the long-term assessment compared to the results of short-term assessment presented in Fig. 6. When comparing medium and high impact scenarios to low impact scenario, surface runoff was not significantly increased, indicating that further decrease of soil permeability by further increasing the corresponding CN did not significantly affect surface runoff.

4. Conclusions

Taking into account the anticipated climate change effects, the present work demonstrated that the effects of land use change from agricultural to PVPs do not significantly affect surface runoff, evapotranspiration and percolation at the basin scale, even for large coverage of the basin with PVPs. However, the effects of land use change from agricultural to

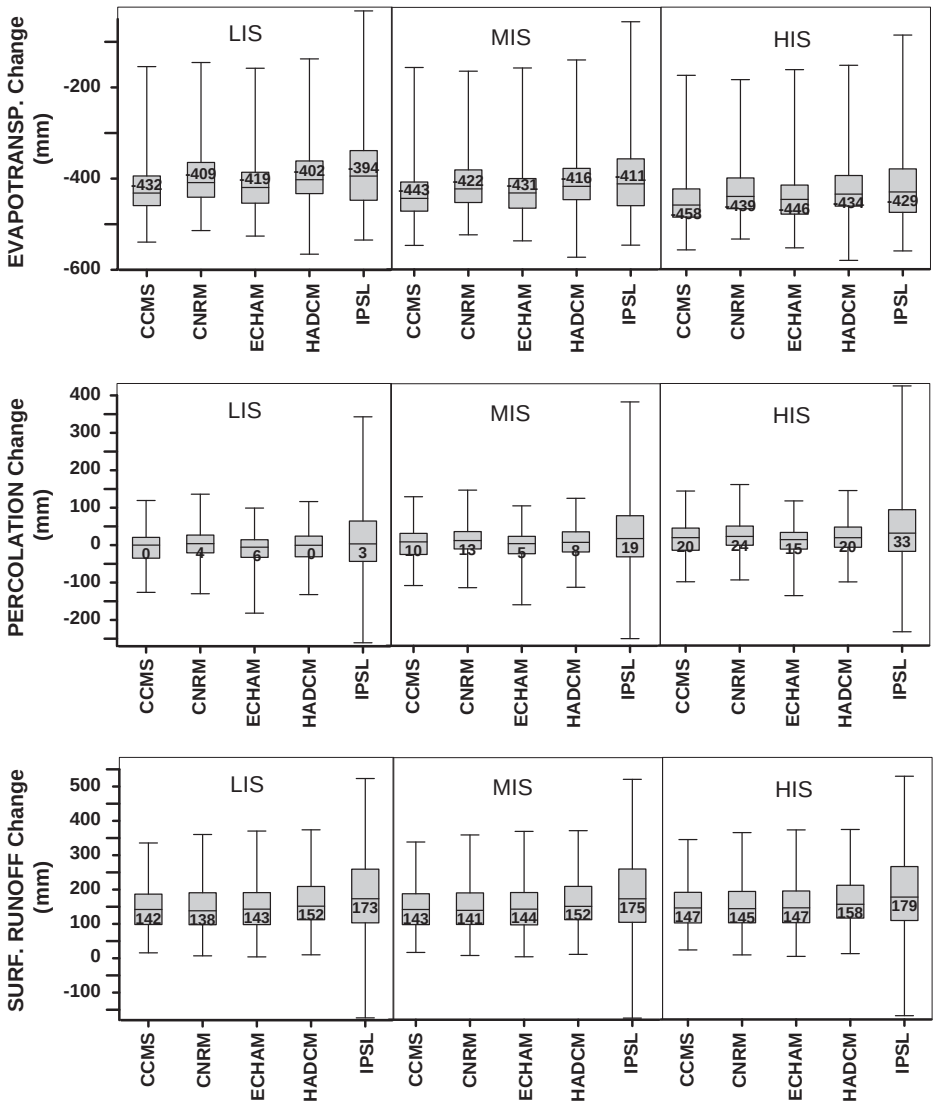

Fig. 10. Sub-basin scale effects of land use change from agricultural to PVP on annual surface runoff, evapotranspiration and percolation for 5% PVP coverage during the period 2011–2100. LIS, MIS and HIS correspond to low, medium and high impact scenarios, respectively.

PVPs were presented to be potentially significant at the local (sub-basin) scale, depending on the local hydrological conditions, which have to be addressed by the decision makers when allocating land for such uses. PVPs installation and operation may have both favorable and unfavorable impacts on the local hydrology of an area. A significant potential for surface runoff to be increased was indicated which has to be taken into account when siting PVPs. Therefore, special attention should be paid when allocating land for PVPs in flood prone areas and policy makers should be aware of the fact that increasing PVPs coverage in such areas may result in increased flood risk. On the other hand, the increasing trend of percolation and subsequently of groundwater recharge may be favorable for areas such as Mediterranean region. Moreover, taking into account the fact that PVP installation and operation minimize the use of fertilizers and pesticides involved in agricultural land uses, it may be assessed that a positive effect is to be anticipated both for surface water and groundwater quality.

Acknowledgments

The presented herein work was developed within the frames of the European FP7 project GENESIS (Groundwater and Dependent Ecosystems: New Scientific and Technical Basis for Assessing Climate Change and Land-use Impacts on Groundwater Systems), grant agreement no.: 226536—GENESIS CP-IP.

Authors acknowledge Thomas Sant for English corrections as well as the anonymous reviewers for their constructive comments and suggestions.

Appendix A. Supplementary information

Supplementary information to this article can be found online at http://dx.doi.org/10.1016/j.scitotenv.2014.05.132.

References

Alaoui A, Lipiec J, Gerke HH. A review of the changes in the soil pore system due to soil deformation: a hydrodynamic perspective. Soil Tillage Res 2011(115–116):1–15. http://dx.doi.org/10.1016/j.still.2011.06.002.

Apostolakis ADB1.1. Technical Report—Volume I: "Crop pattern of the year 2009 in the Prefecture of Rodopi". Athens, Greece: Greek Biotope-Wetland Centre; 2009.

Aspen Environmental Group. California valley solar ranch conditional use permit, and Twisselman reclamation plan and conditional use permit. Final Environmental Impact Report (DRC2008-00097, DRC2009-00004); 2011a [San Francisco, USA].

Aspen Environmental Group. Topaz solar farm conditional use permit. Final Environmental Impact Report (DRC2008-00009); 2011b [San Francisco, USA].

Aureli A, Ganoulis J, Margat J. Groundwater resources in the Mediterranean region: importance, uses and sharing. Paris: UNESCO International Hydrological Programme (IHP); 2008. p. 96–105.
Bakos GC. Distributed power generation: a case study of small scale PV power plant in Greece. Appl Energy 2009;86:1757–66. http://dx.doi.org/10.1016/j.apenergy.2008.12.021.
Cho J, Lowrance RR, Bosch DD, Strickland TC, Her Y, Vellidis G. Effect of watershed subdivision and filter width on SWAT simulation of a coastal plain watershed. J Am Water Resour Assoc 2010;46(3):586–602. http://dx.doi.org/10.1111/j.1752-1688.2010.00436.x.
De Paola F, Giugni M, Topa MA, Bucchignani E. Intensity–duration–frequency (IDF) rainfall curves, for data series and climate projection in African cities. SpringerPlus 2014;3:133. http://dx.doi.org/10.1186/2193-1801-3-133.
Defourny P, Hecquet G, Philippart T. Digital terrain modeling: accuracy assessment and hydrological simulation sensitivity. In: Lowell K, Jaton A, editors. Spatial accuracy assessment: land information uncertainty in natural resources. Michigan: Ann Arbor Press; 1999. p. 61–70.
Erol A, Randhir TO.. Climatic change impacts on the ecohydrology of Mediterranean watersheds. Clim Chang 2012;114:319–41. http://dx.doi.org/10.1007/s10584-012-0406-8.
Gemitzi A, Stefanopoulos K. Evaluation of the effects of climate and man intervention on ground waters and their dependent ecosystems using time series analysis. J Hydrol 2011;403(1–2):130–40. http://dx.doi.org/10.1016/j.jhydrol.2011.04.002.
Gemitzi A, Stefanopoulos K, Schmidt M, Richnow HH. Seawater intrusion into groundwater aquifer through a coastal lake—complex interaction characterised by water isotopes ^{2}H and ^{18}O. Isot Environ Health Stud 2013;50(1):74–87. http://dx.doi.org/10.1080/10256016.2013.823960.
Graham LP, Hagemann S, Jaun S, Beniston M. On interpreting hydrological change from regional climate models. Clim Chang 2007;81:97–122. http://dx.doi.org/10.1007/s10584-006-9217-0.
Green WH, Ampt GA. Studies on soil physics, 1. The flow of air and water through soils. J Agric Sci 1911;4:11–24. http://dx.doi.org/10.1017/S0021859600001441.
Hakansson I. Machinery-induced compaction of arable soils. Incidence–consequences–counter-measures. Sweden: Department of Soil Sciences, Division of Soil Management, Swedish University of Agricultural Sciences; 2005.
IPCC. The physical science basis. Contribution of working group I to the fourth assessment report of the intergovernmental panel on climate change. In: Solomon S, Qin D, Manning M, Chen Z, Marquis M, Averyt KB, Tignor M, Miller HL, editors. Climate change 2007: the physical science basis. Cambridge, United Kingdom and New York, NY, USA: Cambridge University Press; 2007. p. 996.
Kay AL, Jones RG, Reynard NS. RCM rainfall for UK flood frequency estimation. I. Method and validation. J Hydro 2006;318(1–4):151–62.
Kim J, Choi J, Choi C, Park S. Impacts of changes in climate and land use/land cover under IPCC RCP scenarios on streamflow in the Hoeya River Basin, Korea. Sci Total Environ 2013;452–453:181–95. http://dx.doi.org/10.1016/j.scitotenv.2013.02.005.
Kotlarski S, Block A, Böhm U, Jacob D, Keuler K, Knoche R, et al. Regional climate model simulations as input for hydrological applications: evaluation of uncertainties. Adv Geosci 2005;5:119–25. http://dx.doi.org/10.5194/adgeo-5-119-2005.
Krause P, Boyle DP, Bäse F. Comparison of different efficiency criteria for hydrological model assessment. Adv Geosci 2005;5:89–97. http://dx.doi.org/10.5194/adgeo-5-89-2005.
Legates DR, McCabe GJ. Evaluating the use of "goodness-of-fit" measures in hydrologic and hydroclimatic model validation. Water Resour Res 1999;35(1):233–41. http://dx.doi.org/10.1029/1998WR900018.
Luo Y, Ficklin D, Liu X, Zhang M. Assessment of climate change impacts on hydrology and water quality with a watershed modeling approach. Sci Total Environ 2013;450–451:72–82. http://dx.doi.org/10.1016/j.scitotenv.2013.02.004.
Macomber HL, Ruzek JB, Costello FA. Photovoltaic stand-alone systems. DOE/NASA/0195–1; 1981.
Misopolinos N. The soil map of Eastern Macedonia-Thrace Region. Greece: Aristotle University of Thessaloniki, School of Agriculture, Lab of Applied Soil Sciences; 2009.
Monteith JL. Evaporation and Environment, 19th Symposia of the Society for Experimental Biology. Cambridge: University Press; 1965 [p. 205–234].
Moriasi DN, Arnold JG, Van Liew MW, Bingner RL, Harmel RD, Veith TL, et al. Model evaluation guidelines for systematic quantification of accuracy in watershed simulations. Trans ASABE 2007;50(3):885–900. http://dx.doi.org/10.13031/2013.23153.
Nash JE, Sutcliffe JV. River flow forecasting through conceptual models. Part I. A discussion of principles. J Hydrol 1970;10(3):282–90. http://dx.doi.org/10.1016/0022-1694(70)90255-6.
Neitsch SL, Arnold JG, Kiniry JR, Williams JR. Soil and water assessment tool, theoretical documentation. Version 2009. Texas Water Resources Institute Technical Report No. 406. Texas, USA: Texas A&M University System College Station; 2011.
Nemet GF. Net radiative forcing from widespread deployment of photovoltaics. Environ Sci Technol 2009;43(6):2173–8. http://dx.doi.org/10.1021/es801747c.
Nikulin G, Kjellström E, Hansson U, Jones C, Strandberg G, Ullerstig A. Evaluation and future projections of temperature, precipitation and wind extremes over europe in an ensemble of regional climate simulations. Tellus A 2011;63(1):41–55. http://dx.doi.org/10.1111/j.1600-0870.2010.00466.x.
Official Government Gazette of Greece. Law 3851, Volume 85, Issue A, 1753 – 1780, 4/6/2010.
Ozgoz E, Oztekin T, Günal H. Assessment of wheel traffic effect on soil compaction using a soil core sampler. N Z J Agric Res 2006;49(3):299–306. http://dx.doi.org/10.1080/00288233.2006.9513720.
Pehnt M. Dynamic life cycle assessment (LCA) of renewable energy technologies. Renew Energy 2006;31(1):55–71. http://dx.doi.org/10.1016/j.renene.2005.03.002.
Peng T, Wang SJ. Effects of land use, land cover and rainfall regimes on the surface runoff and soil loss on karst slopes in southwest China. Catena 2012;90:53–62. http://dx.doi.org/10.1016/j. catena .2011.11.001.
Priestley CHB, Taylor RJ. On the assessment of surface heat flux and evaporation using large-scale parameters. Mon Weather Rev 1972;100:81–92. http://dx.doi.org/10.1175/1520-0493(1972)100<0081:OTAOSH>2.3.CO;2.
Samuelsson P, Jones CG, Willén U, Ullerstig A, Gollvik S, Hansson U, et al. The Rossby Centre Regional Climate model RCA3: model description and performance. Tellus A 2011;63(1):4–23. http://dx.doi.org/10.1111/j.1600-0870.2010.00478.x.
Scherba A, Sailor DJ, Rosenstiel TN, Wamser CC. Modeling impacts of roof reflectivity, integrated photovoltaic panels and green roof systems on sensible heat flux into the urban environment. Build Environ 2011;46(12):2542–51. http://dx.doi.org/10.1016/j.buildenv.2011.06.012.
Turney D, Fthenakis V. Environmental impacts from the installation and operation of large-scale solar power plants. Renew Sust Energ Rev 2011;15(6):3261–70. http://dx.doi.org/10.1016/j.rser.2011.04.023.
USDA-SCS. National engineering handbook. Hydrology section 4, chap. 4–10. Washington, DC, USA: US Dept. of Agriculture, Soil Conservation Service; 1972.
US-DOE. SunShot vision study. Chapter 7: solar power environmental impacts and siting challenges. Washington D.C., USA: United States Department of Energy; 2012.
Wu Y, Liu S, Gallant AL. Predicting impacts of increased CO_2 and climate change on the water cycle and water quality in the semiarid James River Basin of the Midwestern USA. Sci Total Environ 2012;430:150–60. http://dx.doi.org/10.1016/j.scitotenv.2012.04.058.
Yang W, Andréasson J, Graham PL, Olsson J, Rosberg J, Wetterhall F. Distribution-based scaling to improve usability of regional climate model projections for hydrological climate change impacts studies. Hydrol Res 2010;41:211–29. http://dx.doi.org/10.2166/nh.2010.004.

Water Resources Management (2023) 37:4507–4520
https://doi.org/10.1007/s11269-023-03572-3

Modelling Stormwater Runoff Changes Induced by Ground-Mounted Photovoltaic Solar Parks: A Conceptualization in EPA-SWMM

Aurora Gullotta[1] · Tagele Mossie Aschale[1,2] · David J. Peres[1] · Guido Sciuto[3] · Antonino Cancelliere[1]

Received: 14 June 2023 / Accepted: 25 July 2023 / Published online: 9 August 2023

Abstract

A modelling framework for the simulation of stormwater runoff in ground-mounted photovoltaic solar parks is proposed. Elements in the solar park and their mutual interactions during precipitation events are conceptualized in EPA-SWMM. We demonstrate the potential of the framework by exploring how different factors influence runoff formation. Specifically, we carry out simulations for different sizes of the installation, soil types and input hyetographs. We also show the effect of ground cover, by changing the surface roughness. Outflow discharge from the park is compared to that from a reference catchment to evaluate variations of peak flow and runoff volume. Results highlight no practical changes in runoff in the short term after installation. However, in the long term, modifications in soil cover may lead to some potential increase of runoff. For instance, increments of the peak flow from the solar park up to 21% and 35% are obtained for roughness coefficient reductions of 10% and 20%, respectively. The proposed modelling approach can be beneficial for studying hydrological impacts of solar parks and thus for planning measures for their mitigation.

Keywords Environmental impacts · Renewable energy · Sustainable water resources management · Peak flow · EPA-SWMM

✉ Aurora Gullotta
[redacted]@unict.it

[1] Department of Civil Engineering and Architecture, University of Catania, Via A. Doria 6, Catania 95125, Italy

[2] Department of Geography and Environmental Studies, Debre Markos University, Debre MarkosP.O. Box 269, Ethiopia

[3] Ambiens Srl, Via Roma, 44, Valguarnera Caropepe, Enna 94019, Italy

1 Introduction

The continuous growth of global population causes increasing concerns on food, water, and energy sectors (Sarkodie and Owusu 2020; Makaronidou 2020). The energy generation processes are facing major challenges such as sustainability, cost, security, and market price fluctuations (Almomani 2020; Ebhota and Jen 2020). In addition, the increase in environmental awareness and the application of more stringent discharge regulations has directed the scientific community to work on developing alternative, sustainable, and renewable energy sources (Ahmad et al. 2020; Tawalbeh et al. 2021; Yavari et al. 2022; Bertsiou and Baltas 2022; Loucks 2023).

Among all the renewable energy sources, solar photovoltaic (PV) is one of the most widespread in the word (Ravi et al. 2014; Armstrong et al. 2016; Barron-Gafford et al. 2016; Hassanpour Adeh et al. 2018). Although solar energy is universally recognised as environmentally friendly energy source, impacts on surface hydrology of large parks have not been comprehensively addressed in literature (Turney and Fthenakis 2011; Pisinaras et al. 2014; Yavari et al. 2022). With growing concern over the impact of land use changes on stormwater runoff, the construction of large-scale solar power plants may face obstacles in the future unless appropriate quantification of this impact is addressed and proper measures are taken to mitigate potential increment of flow peak and volume discharge (Turney and Fthenakis 2011).

Assessment of runoff generation in PV solar parks can be carried out by modelling-based approaches, that have the advantage, with respect to purely experimental studies, to allow the investigation of the influence of different hydrological conditions (Yavari et al. 2022). For instance, among the studies based on such approach, Barnard et al. (2017) set up a 1D/2D model by coupling Flo-2D and HEC-HMS to simulate stormwater runoff at three selected solar PV installations in west Texas. However, no comparison with the pre-installation scenario has been carried out thus preventing the possibility to evaluate the impacts on stormwater runoff induced by the presence of solar panels. HEC-HMS was also used to study hydrologic dynamics in a Nevada solar farm (Edalat 2017). The simulations showed that runoff volume always increases after solar panels installation. However, one major limitation of this study was that solar panels were represented as an impervious surface on the ground, and simulation of the infiltration process could not be permitted under the panels, as it would indeed occur at an actual site. Thus, this approach likely overestimates runoff volume. The Soil & Water Assessment Tool (SWAT) was used for assessing the impact of PV solar parks on watershed hydrology by Pisinaras et al. (2014). Solar parks installation was represented by implementing in the model soil physical properties/ground cover changes, curve number increases associated with imperviousness, and reduced solar radiation. In this case, model limitations consist in the fact that the dynamics of the runoff formation in the solar park are not explicitly taken into account. Other researchers developed a custom-built model for representing runoff in solar parks (Cook and McCuen 2013). The results indicated that the addition of solar panels over a grassy field does not change the volume of runoff, the peak discharge, nor time to peak. More recently, Wang and Gao (2023) conducted experiments at the plot-scale to investigate impacts of PV panels on rainfall-runoff and soil erosion processes. Results showed that runoff volume, peak flow discharge rate and overland flow velocity are not remarkably impacted by the presence of PV panels. However, further investigations are needed to transfer the obtained results at the plot scale to a real scale solar park.

Analysis of the literature on the topic highlights a research gap consisting in the lack of a comprehensive tool for the assessment of the impacts of real-scale solar parks on stormwater runoff, by taking into account the hydrological processes occurring within the park and all the variables affecting the park response to precipitation events. In this paper, with the aim of overcoming many of the mentioned limitations within previous studies, we propose a novel conceptualization of PV power parks response to precipitation events capitalizing on the use of the free and open-source Storm Water Management Model (SWMM) (Rossman 2015). The conceptualization allows to take into account the complex hydrological process occurring in the solar parks during precipitation events and to assess how the process of runoff in the park is affected by the extension of the PV installation, soil properties and the characteristics of the rainfall events. Moreover, effects of long term changes in roughness surface induced by the presence of the panels can be taken into account in the analysis. We demonstrate the potentialities of the proposed approach considering a layout of the PV installation (panels size and inclination) as well as characteristics of the precipitation events that are encountered in Sicily (south Italy).

2 Conceptual Model

2.1 Water Paths in Ground-Mounted PV Solar Parks

Panels in ground-mounted PV solar parks are usually placed on a metal frame that is mounted on the ground to hold the panels at a fixed angle. The frame usually can hold more than one panel rows (usually from 2 to 4) in the vertical direction (Fig. 1a). Panels on the metal frame are then arranged in rows of different length (Fig. 1b). Panels rows are separated by corridors to allow for maintenance operations as well as the movement of vehicles.

The presence of the panels rows in the solar park induces a redistribution of the rainfall approaching the ground as compared to the pre-installation scenario. Based on the input/output during precipitation events, three different parts of the PV installation can be distinguished: the panel area, the under-panel area and the corridor (Fig. 2a). The water fallen on the impervious panels surface is rapidly drained towards the corridor immediately downstream the panels row. In this way, each corridor receives both the direct rainfall and the runoff from the impervious surface of the panel. The under-panel area, instead, is not directly reached by the rainfall but it can receive the runoff from the upstream corridor and let the

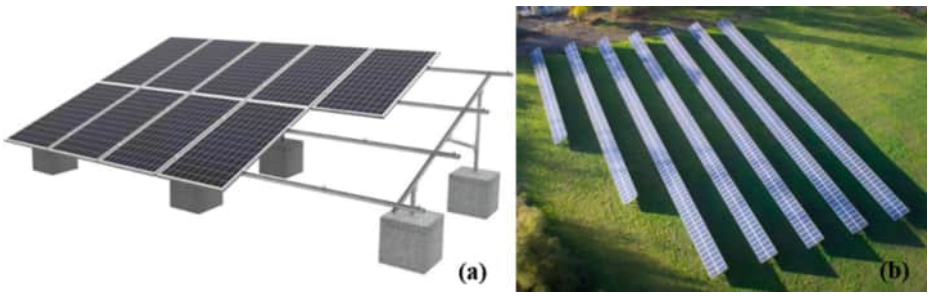

Fig. 1 (**a**) metal frame to hold panels and (**b**) panels arranged in rows in typical ground-mounted solar PV parks

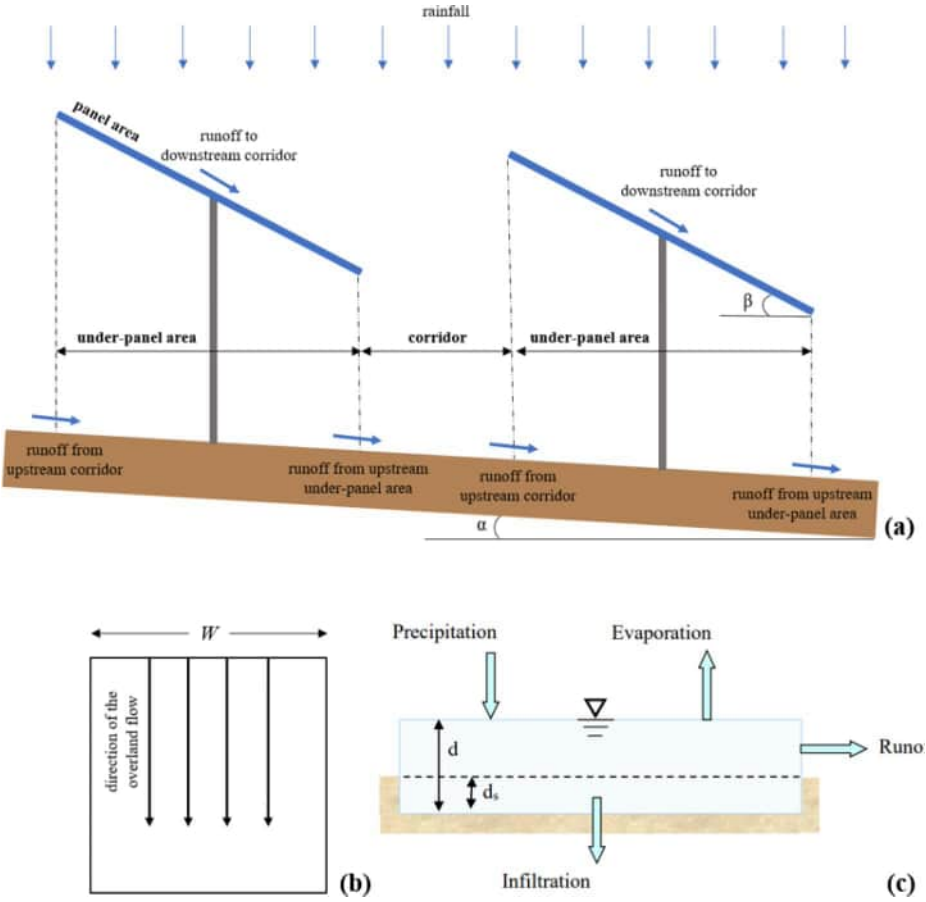

Fig. 2 (**a**) water paths in typical ground-mounted solar PV parks, (**b**) subcatchment conceptualization and (**c**) scheme of the nonlinear reservoir model in EPA-SWMM.

water infiltrate. Runoff from the under-panel area is collected by the corridor immediately downstream the panels row.

Water infiltration occurs both in the under-panel area and in the corridor. However, the corridor is likely to reach saturated conditions earlier as compared to the under-panel area because of the concentration of three different contributions (rainfall, runoff from panel area, runoff from the upstream under-panel area).

It is worth noting that in the adopted scheme for water paths showed in Fig. 2a, the same flow direction is assumed for the ground and for the panels rows. Actually, direction of the PV panels is generally set with the aim to maximize the exposure of the panels to solar radiation, regardless of the ground slope direction. In case of different flow directions for the ground and for the panels rows, water paths within the PV installation are not the same of those described in this section and have to be investigated case by case. As an example, if

panels rows and are placed along the main ground flow direction, runoff from the corridors would not be routed to the under-panel areas, thus, practically, reducing the available areas for infiltration within the park.

2.2 Modelling Ground Mounted PV Solar Parks with EPA-SWMM

The Storm Water Management Model (SWMM) is a free and open-source software developed by the United States Environmental Protection Agency (US-EPA). The release n. 5.1 of the software was used in this study (Rossman 2015).

SWMM is a dynamic rainfall-runoff model used for single event or continuous simulation. The software is widely used in literature and was recently applied for estimation of runoff from urban areas also in presence of low impact development (Ferrans and Temprano 2022; Hashemi and Mahjouri 2022; Nazari et al. 2023; Zhuang and Lu, 2023) and for optimization problems in water distribution systems (Gullotta et al. 2021a, b). The runoff component of SWMM operates on a collection of subcatchment areas that receive precipitation and generate runoff, after computation of water losses. The software conceptualizes subcatchments as rectangular surfaces with uniform slope S and width W [m] (Fig. 2b). Overland flow is generated by modelling the subcatchment as a nonlinear reservoir (Chen and Shubinski 1971), as sketched in Fig. 2c.

In particular, the subcatchment experiences inflow from precipitation and losses from evaporation and infiltration. The net difference ponds on the subcatchment surface with a depth d [m] (Fig. 2c). A part of the ponded depth, d_s [m], can fill the depression storage, while the remaining part (d-d_s) become runoff outflow q. From conservation of mass, the net change in depth d per unit of time t can be expressed as (Rossman 2016):

$$\frac{\partial d}{\partial t} = i - e - f - q \tag{1}$$

where i, e, f and q are the flow rates per unit of area [$m^3/s/m^2$] for precipitation, evaporation, infiltration and runoff, respectively.

Flow rate is calculated by using the Manning equation for an open rectangular channel of width W, slope S and a given roughness coefficient n [$s/m^{1/3}$]. Infiltration losses can be computed within the software by using different infiltration models. For the conceptualization proposed in this paper, Green Ampt method is used to model infiltration in pervious subcatchments (Green and Ampt 1911). Water losses for evaporation are not taken into account in this work since only simulations of single events have been carried out so that evaporation process can be neglected.

In order to reproduce water paths described at Sect. 2.1, panel areas, under-panel areas and corridors are modelled in EPA-SWMM as rectangular subcatchments (placed in series) with different input/output settings. In particular, precipitation input is set up for subcatchments representing panel areas and corridors but not for those representing under-panel areas. Moreover, runoff from each subcatchment is discharged to downstream subcatchments according to the flow paths showed in Fig. 2 (i.e., panel area to corridor, corridor to under-panel area and under-panel area to corridor). Runoff from the most downstream subcatchment is assumed to be the outflow from the solar park. Finally, infiltration is allowed for all the subcatchments except for those representing panel areas.

3 Modelling Scheme

3.1 PV Power Plant Hydrological Characteristics

For the demonstration carried out in this study, we have considered the following characteristics of the subcatchments. Panel areas in the PV park are modelled as totally impervious subcatchments with inclination $\beta = 30°$ to the horizontal (Fig. 2a). This inclination is common for PV installations at the latitude of south Italy. A metal frame holding 2 panels in the vertical direction is supposed, with single panel having a length of 2.38 m and a width of 1.3 m, which are within typical dimensions for industrial panels used in solar parks. Panels' surface is usually made of very smooth glass; therefore, $n = 0.007$ is associated to subcatchments representing panel areas. Corridors and under-panel areas are modelled as totally pervious subcatchments. Length of corridors is usually optimized to minimize shadows effects between two panels rows. However, a minimum distance (range 2.5-3 m) between two panels rows has to be guaranteed to allow for the safe moving of maintenance vehicles. In the model, a length of 2.7 m is associated to the corridors, while the length of the under-panel areas can be derived projecting the length of 2 panels to the horizontal (i.e., 4.12 m). Ground slope in the solar park is set equal to 1% (Palmer et al. 2019).

Besides, a reference catchment with the same extension of the park is modelled. In order to maintain the same modelling scale and enable comparison, the reference catchment is divided in subcatchments equivalent to the corridors and the under-panel areas (same area and ground slope). In this case, all the subcatchments in the reference have the precipitation input and allow for infiltration. Moreover, each of these subcatchments discharges its runoff to the subcatchment immediately downstream. Runoff from the most downstream subcatchment is assumed to be the outflow from the reference catchment and used for comparison with runoff from the solar park. Ground cover for the reference catchment is assumed to be grass, by setting a roughness Manning coefficient $n = 0.15$ (McCuen et al. 1996).

Since, as already stated, we are assuming that direction of flow coincides with the slope of the panels, all terms in Eq. (1) are linear functions of the subcatchment width W and therefore all simulations are carried out by setting $W = 1$ m for all the subcatchments in the PV solar park and in the reference catchment. Results obtained (in terms of runoff per unit of width) can then be scaled for any size of the solar park by simply multiplying for the actual width of the installation.

Single events simulations are run in EPA-SWMM setting a time step of 1 s. In the following sections, variables and parameters potentially affecting the runoff from the PV solar park are discussed.

3.1.1 PV configurations

Simulations have been carried out considering three different configurations of the solar park. In particular, sequences of 10, 20 and 40 panels rows are modelled to represent small, medium and large PV installations, respectively. The three selected extensions (extension 1, 2 and 3 in the following of the paper) correspond to total areas per unit of width of the installation of about 70, 135 and 270 square meters.

3.1.2 Soil type

To test the impacts of soil texture on runoff from solar parks, simulations have been performed for three different soil types. In particular, Green Ampt infiltration parameters for loamy sand, clay loam and silty clay soil type (soil type A, B and C in the following of the paper) have been associated to subcatchments in the software, thus going from more pervious to less pervious soil (Rawls et al. 1983). In each simulation, the same soil type is assumed for the solar park and the reference catchment.

Fraction of soil porosity that is initially dry (i.e., initial deficit) has to be specified in the software. Initial deficit equal to zero is representative of saturated conditions. An initial deficit equal to the difference between the soil porosity (saturated soil) and the field capacity has been set up. The chosen initial condition for soil moisture is typical of soils in the winter season at the beginning of a precipitation event with a sufficient antecedent dry weather period.

3.1.3 Storm characteristics

Precipitation events given as input for the simulations are derived from the Depth-Duration-Frequency (DDF) curves of the rain gage of Agira in Sicily (south Italy). Values of parameters of the DDF curves, in the power law form $h = at^n$, of the selected rain gage correspond to the median of 139 stations in Sicily (Failla 2022). Events of 5, 20 and 50-years return period (RP) are simulated. Parameters a of the DDF curves are equal to 34.72, 49.02 and 58.09 for RP of 5, 20 and 50 years, respectively, while corresponding exponents n are equal to 0.339, 0.354 and 0.360.

Besides magnitude, influence of duration and temporal distribution of the precipitation event is investigated. First, constant intensity rainfall events with duration of 10 min, 1 and 3 h and rainfall intensity derived from the DDF curves are given as input to the model. Then, hyetographs of 1 and 3 h durations derived from the Chicago method (Keifer and Chu, 1957) are considered. For the construction of the Chicago hyetographs, a time step of 10 min is adopted and the highest peak of precipitation height is placed almost in the middle (3rd time step for the 1-hour hyetograph and 9th time step for the 3-hour hyetograph). When deriving precipitation heights for sub-hourly durations, exponent of the DDF curve is changed in 0.5 (Engman and Hershfield 1981).

3.1.4 Ground Cover

Different ground covers have been assumed, related to short and long term conditions after PV installation. In the short term after installation of the PV park, no significant changes in ground cover are expected with the respect to the pre-installation scenario. In the long term, operation of the PV solar parks involves the use of maintenance vehicles that could affect the soil properties in the area between panel rows - in terms of compaction and reduced hydraulic conductivity (Pisinaras et al. 2014; Choi et al. 2020). Moreover, the area under the panel rows may experience, in time, a lower vegetation growth rate as compared to the space between rows because of the reduced amount of photosynthetic active radiation (Armstrong et al. 2016; Jahanfar et al. 2019). Hence, changes in surface roughness are taken into account here. In particular, the presence of the panels rows together with the mainte-

nance activities of the park usually lead to a reduction of the surface roughness. Therefore, simulations have been run by assuming the same roughness coefficient of the reference catchment for corridors and under-panel areas, thus allowing evaluation of the runoff from the park in the short term after installation (short-term condition). Secondly, progressive reduction (by 10% and 20%) of the original roughness coefficient is supposed for corridors and under-panel areas in order to evaluate the impacts on runoff of long term changes in surface roughness induced by the presence of the solar park (long-term condition).

4 Results and Discussion

A total of 135 simulations have been run for the short-term condition by combining all the model parameters and precipitation inputs described in the methodological section.

Figures from 3 to 5 compares the outflows from the PV solar park and from the reference catchment as resulting from 9 simulations.

In order to assess the impact on runoff of the park extension, Figs. 3a, 3b and 3c show outflows from parks of extension 1, 2 and 3, respectively, and soil type C. In the 3 simulations, the precipitation input is a Chicago hyetograph of 1 hour duration and 20-years RP.

For fixed soil type and precipitation input, increments of the park extension result in increments of the peak flow and of the total runoff volume (Fig. 3a, b and c). In particular, peak flow per unit of width increases by 33% each time the area of the solar park is doubled (from extension 1 to 2 and from extension 2 to 3), due to the non-linearity of the processes involved in the runoff formation. The outflow curve from the solar park follows the corresponding curve from the reference catchment both in the rising and in the recession limb of the hydrograph, regardless of the park extension. Minimal differences between the two outflow curves can be observed at the beginning of the precipitation event (first 20 min), with values of the outflow from the solar park slightly higher than those from the reference catchment. Analysis of the simulations output allows to ascribe this behaviour to the most downstream part of the solar park. Indeed, the generic corridor in the solar park receives in input the direct rainfall and the runoff from the panel area. The two contributions are practically simultaneous as the time of concentration of the panel area is in the order of a few seconds. Therefore, for a given soil infiltration capacity, the corridor generates excess of runoff with the respect to the portion of the reference catchment placed at an equal distance from the outlet. This excess of runoff can be later infiltrated in downstream under-panel areas and

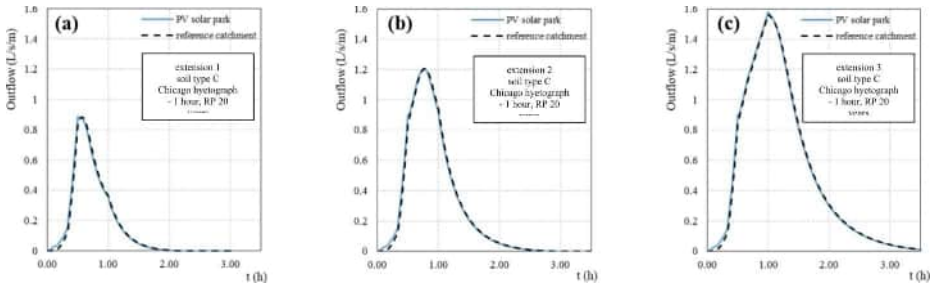

Fig. 3 Outflows from the PV solar park and from the reference catchment for different park extensions (short-term condition)

corridors. However, the most downstream corridor delivers the runoff directly to the outlet thus anticipating the time for the beginning of the runoff as observed in Fig. 3a, b and c.

Influence of the soil type on the runoff from the solar park is shown in Figs. 4a, 4b and 4c, referring to simulations run for solar park of same extension (3) and precipitation input (Chicago hyetograph 3-hours duration, 50-years RP) but different soil type (A, B and C, respectively).

For fixed solar park extension and precipitation input, changing from sandy to clay soils results in increased peaks flow and total runoff volumes, due to the reduction in infiltration capacity (Fig. 4a, b and c). In particular, peaks flow from solar park results equal to 0.2, 2.5 and 2.8 L/s per unit of width for soil type A, B and C, respectively. Peak flow and total runoff volume from the solar park are greater than the corresponding values from the reference catchment only for soil type A (Fig. 4a). Indeed, in soil with high infiltration capacity, almost all the precipitation is infiltrated. In this case, excess of runoff from the corridor immediately upstream the outlet (with no other downstream under-panel areas and corridors available for infiltration) assumes a greater relative weight. However, the increment of peak flow and total runoff showed in Fig. 4a is not significant in absolute terms (peak flow for unit of width less than 0.25 L/s). The same conclusion can be drawn for other simulations with soil type A in which differences in the outflows from the solar park and from the reference catchment are observed.

Finally, Figs. 5a, 5b and 5c show outflows from solar parks of extension 2 and soil type C for constant precipitation input of durations 10 minutes, 1 hour and 3 hours, respectively, and 20-years RP.

For fixed solar park extension and soil type, outflow from the solar park is equal to that from the reference catchment (in terms of peak flow and total runoff volume) regardless of the duration of the precipitation event as shown in Fig. 5a, b and c.

Temporal distribution of the rainfall does not influence the aggravation of outflow from the solar park as compared to the reference catchment. Indeed, Figs. 3b and 7b report results of simulations carried out for parks of same extension and soil type, in which the 1-hour, 20-years RP precipitation event is given as input in the form of a Chicago hyetograph (Fig. 3b) or constant rainfall (Fig. 5b). In both cases, outflow curves from the solar park follow the corresponding curves from the reference catchment during the whole simulation.

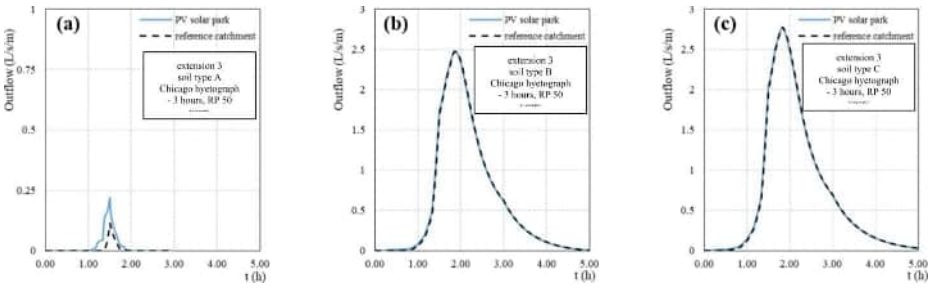

Fig. 4 Outflows from the PV solar park and from the reference catchment for different soil types (short-term condition)

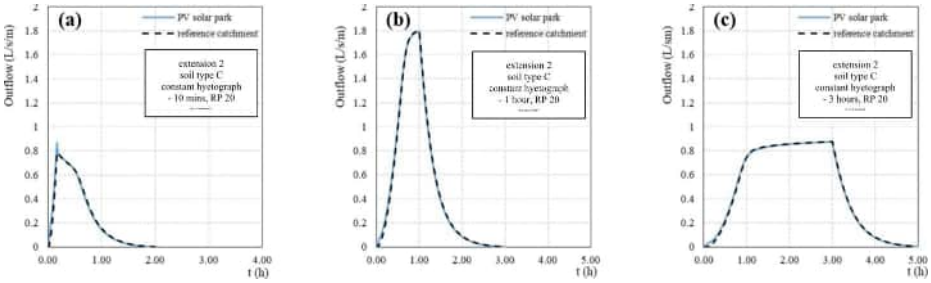

Fig. 5 Outflows from the PV solar park and from the reference catchment for different duration of the precipitation event (short-term condition)

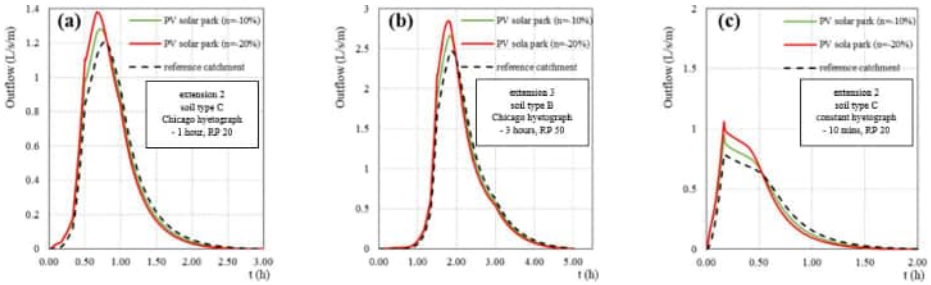

Fig. 6 Outflows from the PV solar park and from the reference catchment for different combinations of model parameters and precipitation inputs (long-term analysis)

Finally, simulations that differ only for the RP of the precipitation event also led to outflow curves from the solar park practically equal to those from the reference catchment, regardless of the magnitude of the event.

Globally, no significant increments of the peak flow and of the total runoff volume from the solar park as compared to the reference catchment were observed in all the 135 simulations for short-term condition. This result is in line with modelling and experimental findings of previous studies (Cook and McCuen 2013; Wang and Gao 2023).

To evaluate the effects of possible long-term changes in land cover induced by the presence of the PV installation, a reduction of the roughness surface is supposed for subcatchments representing corridors and under-panel areas in the model. In particular, the original Manning coefficient for those subcatchments is progressively reduced by 10% and 20% (i.e., $n=0.135$ and $n=0.12$, respectively). Figure 6 shows comparison between outflows from the PV solar park and from the reference catchment for 3 long-term condition simulations. Model parameters and precipitation inputs of the simulations related to Fig. 6a, b and c are the same of those discussed for Figs. 3b, 4b and 5a, respectively.

In all the simulations, the reduction of the surface roughness surface in corridors and under-panel areas leads to increased peaks flow as compared to the short-term analysis. For the events analysed in Fig. 6, a 10% reduction of the Manning coefficient results in peak flow increases of about 6% (Fig. 6a), 8% (Fig. 6b) and 21% (Fig. 6c). The percentage of peak flow increase is even greater if the Manning coefficient is reduced by 20% (15% increase for events in Figs. 6a and b and 35% for event in Fig. 6c).

The reduced roughness surface allows for a faster surface runoff from the upstream part of the solar park towards the outlet. Indeed, both the rising and the recession limb of the hydrograph from the solar park are anticipated with respect to those of the hydrograph from the reference catchment. Runoff velocity increases passing from a 10% to a 20% reduction of the Manning coefficient for all the events showed in Fig. 6. Also this result is in agreement with simulation studies carried out by Cook and McCuen 2013).

As a consequence of the increased runoff velocity, total runoff volumes from the solar park are greater than those from the reference catchment for all analysed events. Indeed, the potential of water infiltration is related to the ponding time above the subcatchment surface, which decreases as runoff velocity increases. For the events showed in Fig. 6, runoff volumes from the solar park increase with respect to the reference catchment in the order of 1–3% for a 10% Manning coefficient reduction and in the order of 2–5% if the Manning coefficient is reduced by 20%.

5 Conclusion

In this paper a modelling framework for the simulation of stormwater runoff in ground-mounted photovoltaic solar parks is proposed. EPA-SWMM software is used in a novel way to model all the elements in the solar park and their mutual interactions during precipitation events.

The modelling exercise showed the potentialities of the proposed conceptualization. Specifically, by comparing outflow discharges from the park and from a reference catchment (pre-installation condition), the proposed approach was successful in simulating some of the main impacts of PV power plant realization on peak flow and total runoff volume. In particular, simulations were run considering 3 different sizes of the PV installation (small, medium, large), 3 different soil types and input hyetographs of different return periods, shapes and durations. A first set of simulations have been run by assuming the same roughness surface for the solar park and the reference catchment (short-term condition). Then, the impacts of the presence of the panels rows (as well as of the maintenance activities) on the roughness surface have been considered. The proposed conceptualization allows to successfully simulate the spatial redistribution of the rainfall and infiltration fluxes due to the presence of the panel rows. The modelling exercise shows that when the surface roughness of the solar park is decreased, peak flow increases in the order of 6–35% as compared to the pre-installation scenario. Increased values (1–5%) of the total runoff volume are obtained as well.

The proposed modelling framework may be useful for operators in the field of photovoltaic for the evaluations of the outflow discharge from the solar park for different configurations of the installation, soil type and ground cover. The use of a free and open-source software adds value to the research and could represent a boost for the development and the improvement of the modelling framework as well as for a simple and wide diffusion of the results. Future availability of experimental data on runoff from solar park would help increasing the reliability of the obtained results; further investigations will also attempt to extend model applications at the watershed scale.

Future steps of the work may include the evaluation of other impacts on the ground cover induced by presence of the PV installation as well as the investigation of the solar park

behaviour in long period simulations. Finally, other layouts of the PV installation should be considered in future works, especially those implying a reduction of the available area for infiltration within the park.

Author Contribution Aurora Gullotta: Conceptualization, Methodology, Software and Writing – Original draft. Tagele Mossie Aschale: Conceptualization, Methodology, Software. David J. Peres: Supervision, Funding acquisition, Writing – Review & Editing. Guido Sciuto: Supervision. Antonino Cancelliere: Supervision, Funding acquisition, Project administration.

Funding The research presented in this paper is being carried out in collaboration with the company Ambiens S.r.l. The company has funded the 3-years (2021–2023) doctoral course of the PhD student Tagele Mossie Aschale at University of Catania. Research of Aurora Gullotta is being conducted for the the 3-years (2022–2024) research project "Sustainable and smart strategies for the mitigation of the impacts of renewable energy production plants on the soil and the microclimate" funded by the PON Research and Innovation 2014–2020 "Education and research for recovery - REACT-EU" – Action IV.6 Research contracts on green topics – in partnership with Ambiens S.r.l.
Open access funding provided by Università degli Studi di Catania within the CRUI-CARE Agreement.

Data Availability The data presented in this study are available on request from the corresponding author.

Declarations

Ethical Approval Not applicable.

Consent to Participate Not applicable.

Consent to Publish Not applicable.

Competing Interests The authors have no relevant financial or non-financial interests to disclose.

References

Ahmad L, Khordehgah N, Malinauskaite J, Jouhara H (2020) Recent advances and applications of solar photovoltaics and thermal technologies. Energy, 207

Almomani F (2020) Prediction of biogas production from chemically treated co-digested agricultural waste using artificial neural network. Fuel 280:118573

Armstrong A, Ostle NJ, Whitaker J (2016) Solar Park Microclimate and Vegetation Management Effects on Grassland Carbon Cycling. Environ Res Lett 11(7):12

Barnard T, Agnaou M, Barbis J (2017) Two dimensional modeling to simulate stormwater flows at photovoltaic solar energy sites. J Water Manage Model 25:C428

Barron-Gafford GA, Minor RL, Allen NA, Cronin AD, Brooks AE, Pavao-Zuckerman MA (2016) The photovoltaic Heat Island Effect: larger solar power plants increase local temperatures. Sci Rep 6:35070

Bertsiou MM, Baltas E (2022) Energy, Economic and Environmental Analysis of a Hybrid Power Plant for Electrification, and drinking and Irrigation Water Supply. Environ Process 9:22

Chen CW, Shubinski RP (1971) Computer simulation of urban storm water runoff. J Hydraulics Div 97(2):289–301
Choi CS, Cagle AE, Macknick J, Bloom DE, Caplan JS, Ravi S (2020) Effects of Revegetation on Soil Physical and Chemical Properties in Solar Photovoltaic infrastructure. Front Environ Sci 8:140
Cook LM, McCuen RH (2013) Hydrologic response of solar farms. J Hydrol Eng 18(5):536–541
Ebhota WS, Jen T-C (2020) Fossil fuels environmental challenges and the role of solar photovoltaic technology advances in fast tracking hybrid renewable energy system. Int J Precis Eng Manuf 7(1):97–117
Edalat MM (2017) Remote Sensing of the Environmental Impacts of Utility-Scale Solar Energy Plants. Ph.D. dissertation, University of Nevada
Engman ET, Hershfield DM (1981) Characterizing short duration rainfall intensities for runoff calculation. Trans ASAE 24SW:347352
Failla N (2022) Analisi delle piogge intense in Sicilia e cambiamenti climatici: aggiornamento e proiezioni future. Master's Thesis. University of Catania – Department of Civil Engineering and Architecture
Ferrans P, Temprano J (2022) Continuous quantity and quality modeling for assessing the Effect of SUDS: application on a conceptual Urban Drainage Basin. Environ Processes, 9(4)
Green WH, Ampt GA (1911) Studies on soil physics. J Agric Sci 4(1):1–24
Gullotta A, Butler D, Campisano A, Creaco E, Farmani R, Modica C (2021a) Optimal location of valves to improve equity in intermittent water distribution Systems. J Water Resour Plan Manag 147(5):04021016
Gullotta A, Campisano A, Creaco E, Modica C (2021b) A simplified methodology for optimal location and setting of valves to improve equity in intermittent water distribution Systems. Water Resour Manage 35(13):4477–4494
Hashemi M, Mahjouri N (2022) Global sensitivity analysis-based design of low Impact Development Practices for Urban Runoff Management under uncertainty. Water Resour Manage 36(9):2953–2972
Hassanpour Adeh E, Selker JS, Higgins CW (2018) Remarkable agrivoltaic influence on Soil Moisture, Micrometeorology and Water-Use Efficiency. PLoS ONE, 13(11), e0203256
Jahanfar A, Drake J, Sleep B (2019) Margolis L Evaluating the shading effect of photovoltaic panels on green roof discharge reduction and plant growth. Journal of Hydrology, 568, 919–928.
Keifer CJ, Chu HH (1957) Synthetic storm pattern for drainage design. Journal of the Hydraulics Division, v. 83, p. 1–25
Loucks DP (2023) Meeting Climate Change Challenges: searching for more adaptive and innovative decisions. Water Resour Manage 37:2235–2245
Makaronidou M (2020) Assessment on the Local Climate Effects of Solar Photovoltaic Parks. Ph.D. dissertation, Lancaster University
McCuen R, Johnson P, Ragan R (1996) Hydrology, FHWA-SA-96-067, Federal Highway Administration, Washington, DC
Nazari A, Roozbahani A, Hashemy Shahdany SM (2023) Integrated SUSTAIN-SWMM-MCDM Approach for Optimal Selection of LID Practices in Urban Stormwater Systems. Water Resources Management
Palmer D, Gottschalg R, Betts T (2019) The future scope of large-scale solar in the UK: site suitability and target analysis. Renewable Energy 133:1136–1146
Pisinaras V, Yang W, Bärring L, Gemitzi A (2014) Conceptualizing and assessing the effects of installation and operation of photovoltaic power plants on major hydrologic budget constituents. Sci Total Environ 493 C:239–250
Ravi S, Lobell DB, Field CB (2014) Tradeoffs and synergies between Biofuel Production and large solar infrastructure in deserts. Environ Sci Technol 48(5):3021–3030
Rawls WJ, Brakensiek DL, Miller NL (1983) Green-ampt infiltration parameters from Soils Data. J Hydraul Eng 109:62–70
Rossman LA (2015) Storm Water Management Model user's Manual Version 5.1. U.S. Environmental Protection Agency
Rossman LA (2016) Storm Water Management Model Reference Manual volume I – hydrology. U.S. Environmental Protection Agency
Sarkodie SA, Owusu PA (2020) Bibliometric analysis of water–energy–food nexus: sustainability assessment of renewable energy. Curr Opin Environ Sci Health 13:29–34
Tawalbeh M, Al-Othman A, Kafiah F, Abdelsalam E, Almomani F, Alkasrawi M (2021) Environmental impacts of solar photovoltaic systems: a critical review of recent progress and future outlook. Sci Total Environ 759:143528
Turney D, Fthenakis V (2011) Environmental impacts from the installation and operation of large-scale solar power plants. Renew sustainable energy reviews 15(6):3261–3270
Wang F, Gao J (2023) How a photovoltaic panel impacts rainfall-runoff and soil erosion processes on slopes at the plot scale. J Hydrol, 620

Yavari R, Zaliwciw D, Cibin R, McPhillips L (2022) Minimizing environmental impacts of solar farms: a review of current science on landscape hydrology and guidance on stormwater management. Environ Research: Infrastructure Sustain 2(3):032002

Zhuang Q, Li M, Lu Z (2023) Assessing runoff control of low impact development in Hong Kong's dense community with reliable SWMM setup and calibration. J Environ Manage, 345

Impact of solar panels on runoff generation process

Article *in* Hydrological Processes · November 2023

DOI: 10.1002/HYP.15053

CITATIONS
0

READS
214

3 authors:

[redacted] Giorgio Baiamonte
Università degli Studi di Palermo
96 PUBLICATIONS **1,419** CITATIONS
SEE PROFILE

[redacted] uciano Gristina
niversità degli Studi di Palermo
114 PUBLICATIONS **2,966** CITATIONS
SEE PROFILE

Salvatore Samuel Palermo
Università degli Studi di Palermo
9 PUBLICATIONS **6** CITATIONS
SEE PROFILE

Received: 28 July 2023 | Revised: 28 November 2023 | Accepted: 29 November 2023

DOI: 10.1002/hyp.15053

RESEARCH ARTICLE

WILEY

Impact of solar panels on runoff generation process

Giorgio Baiamonte | Luciano Gristina | Samuel Palermo

Department of Agricultural, Food and Forest Sciences, University of Palermo, Palermo, Italy

Correspondence
Giorgio Baiamonte, Department of Agricultural, Food and Forest Sciences, University of Palermo, viale delle Scienze 13, 90128 Palermo, Italy.
Email: [redacted]@unipa.it

Abstract

Because of the benefits of solar energy, solar photovoltaic (PV) technology is being deployed at an unprecedented rate and the number of photovoltaic panels is sharply increasing. Agrophotovoltaic systems (solar farms) seem to be the most sustainable tools to create renewable energy without compromising agricultural production. However, utility-scale solar energy development is land intensive and its large-scale installation can have negative impacts on the environment. Moreover, its impacts on soil and on relative hydrological processes have been poorly studied. This article aims to evaluate the impact of solar panels on the runoff generation process, which is directly linked to the soil erosion process. Using a rainfall simulator, runoff measurements for a rainfall intensity equal to 56 mm/h were carried out by assuming different panel arrangements with respect to the maximum slope direction of the field (cross slope and aligned slope). Results were compared to a control reference of the same plot, with no panels (bare soil). Physical models found in the literature were then applied and calibrated, to upscale the models to a much higher hillslope length. Results showed that solar panels increase the peak discharge by about 11 times compared to the reference hillslope. A moderate effect of PV panel arrangement was observed on the peak discharges (11.7 and 11.5 times higher, for cross slope and aligned slope panels, respectively), whereas the time to runoff was the lowest for aligned slope panels (0.3 h), higher for cross slope panels (0.62 h), and the highest (1.2 h), for the bare soil hillslope. As it would be expected, upscaling the models to longer hillslopes resulted in increases in outlet discharges, and in the time to runoff, with an exception for aligned slope panels.

KEYWORDS
border irrigation, experimental measurement, infiltration model, kinematic wave model, rainfall simulator, runoff generation, solar panels

1 | INTRODUCTION

The need for climate change mitigation, energy security improvement, and sustainable human activities is driving a rapid transition from carbon fuels to renewable energy (IPCC, 2014). Solar energy is one of the renewable energy systems with the greatest climate change mitigation potentials with life cycle emissions as low as 14 g CO_2-eq·kW·h^{-1}, compared to 608 g CO_2-eq·kW·h^{-1} for natural gas (Hernandez et al., 2014).

At the global level, several analyses have shown that photovoltaic (PV) power systems could grow almost sixfold over the next 10 years, reaching a cumulative capacity of 2840 GW globally by 2030 and

rising to 8519 GW by 2050, resulting in a total expected installed capacity almost 18 times higher than that of 2018. Around 60% of the total PV capacity in 2050 would be produced by solar farms at the utility-scale, while the remaining 40% would be distributed individually (rooftop system) (IRENA, 2019). In Italy, the creation of photovoltaic fields installed on the ground are one cause of reversible soil consumption currently covering more than 17 500 hectares of land.

The Integrated National Energy and Climate Plan (PNIEC, 2023) aims to instal 52 GW of PV systems by 2030, However, considering the 22 GW installed by 2020, an additional 30 GW are necessary. Thus, over additional 50 000 ha of land will be necessary to reach the national plan's target.

Such a large land use change due to the expected increase in PV systems in the next future must be weighed against the strong trade-off made with agricultural land (Dupraz et al., 2011), and the subsequent landscape impact caused by the installation of the panels. In fact, it seems necessary to investigate approaches aimed at making the spread of the PV panels compatible with the natural landscape as well as with agricultural production. Specifically, the visual impact of photovoltaic parks, caused by the large area covered by the panels, and the consequences of their installation on soil fertility and, in the long term, land value (Bignami, 2010) must be considered.

These considerations are confirmed by important changes regarding the application of photovoltaics in agriculture contained in the legislative decree transposing directive 2009/28/EC, approved by the Council of Ministers on 3 March 2011. Article 8 of this decree contains specific provisions aiming to place a limit on the subtraction of agricultural land, an issue brought up on several occasions by trade associations.

Low income from farming has encouraged agricultural entrepreneurs to replace agricultural activity with photovoltaic systems, leading to large-scale land-use changes and subsequent trade-offs. Recently economic incentives have aimed to combine renewable energy production needs with agricultural activity to improve environmental safeguards. This policy direction suggests further development, expansion, and opportunities for PV systems.

Several studies have been conducted on the technology of PV systems, and on the effect that they have on-farm productivity and ecosystem modification (Wu et al., 2022; Zainol Abidin et al., 2021), often due to non-uniform water distribution on the ground and changes in soil quality. The latter because the solar panels located above the cultivated soil have an unexplored effect on rain redistribution, protecting large parts of the soil but also concentrating flows on a limited part of it (Elamri et al., 2018).

From the soil quality point of view, physical, chemical, and overall soil quality indexes are more altered under solar panels than in open fields (Lambert et al., 2021) mainly due to solar park construction altering soil structure and as well as soil physical characteristics.

On the contrary, few studies have been carried out on the impact that PV systems have on the runoff generation process and on soil erosion (Choi et al., 2020; Elamri et al., 2018). These studies have only focused on the spatial patterns of rain redistribution on the ground, between panels and bare soil. They have also shown the strong differences in rain drop size distribution and consequently in rain kinetic energy and have investigated and modelled runoff velocity (Cook & McCuen, 2013).

Cook and McCuen (2013) also studied the potential soil erosion at the base of solar panels, identifying evident high detachment processes caused by the high intensity and kinetic energy of the discharge flowing off the panels as well as high transport processes and rill erosion phenomena. However, no quantitative information was given about the impact of solar panels on the runoff generation process causing soil erosion.

In consideration of the above, the objective of this article is to investigate the impact of solar panels on the runoff generation process from both an experimental and theoretical point of view. The effect of the different orientations of solar panels with respect to the maximum slope direction of the PV system site is also analysed. Finally, physical models provided by the literature that help explain the impact of solar panels on runoff generation have been calibrated for the experimental layouts, so that the same models could be upscaled to different hillslope length values.

2 | MATERIALS AND METHODS

2.1 | Description of the experimental layout

The experimental measurements were carried out at Santa Margherita Belice (Agrigento, Sicily), at the coordinates 37°41′43.04″ N, 13°02′49.14″ E. To investigate the influence of solar panels on runoff generation, a 'bare soil' hillslope (layout A) was considered as a useful control reference (Figure 1a). The solar panels were installed on the same hillslope later. To also investigate the effect of solar panels' orientation with respect to the maximum slope direction, two different panel arrangements were selected (Figure 1b,c). In particular, layout B) (cross slope) regards the case in which the panels' slopes cross that of the hillslope, thus their slope is perpendicular to the maximum slope direction of the hillslope (Figure 1b). In layout C (aligned slope), the slope of two panels is along that of the hillslope, and the discharge flowing off from the upstream (US) panel provides an additional contribution to the downstream (DS) panel (Figure 1c). The cross slope panel case accounts for east–west exposition, whereas the aligned slope case accounts for north–south exposition.

The experimental plot was wide $B = 1$ m and long $L = 3$ m with a slope $S_0 = 14\%$. it was hydraulically separated along the plot boundary and a Gerlach apparatus was installed at the outlet for runoff measurements. Figure 2a illustrates the experimental layout corresponding to layout B (cross slope panels, Figure 1b), including the rainfall simulator and Gerlach apparatus, while Figure 2b shows layout C (aligned slope, Figure 1c).

Generally, solar panels can come in several sizes. In the present investigation, the selected panel size was $L_p = 0.8$ m (length) and $B_p = 1$ m (width B equal to that of the plot, Figure 1c). Their were spaced 0.3 m apart for cross slope panels, and 0.7 m apart for aligned slope panels.

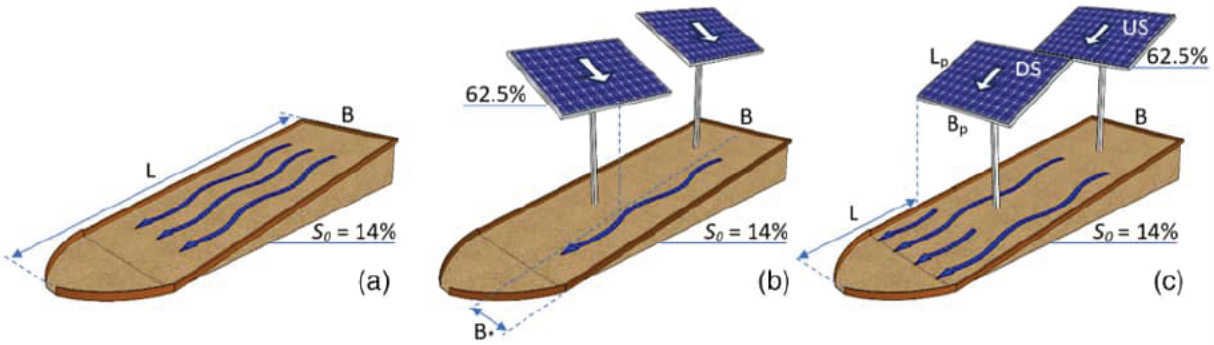

FIGURE 1 Schematic representation of the experimental setup: (a) bare soil (a), (b) cross slope panels (b), and (c) aligned slope panels (c).

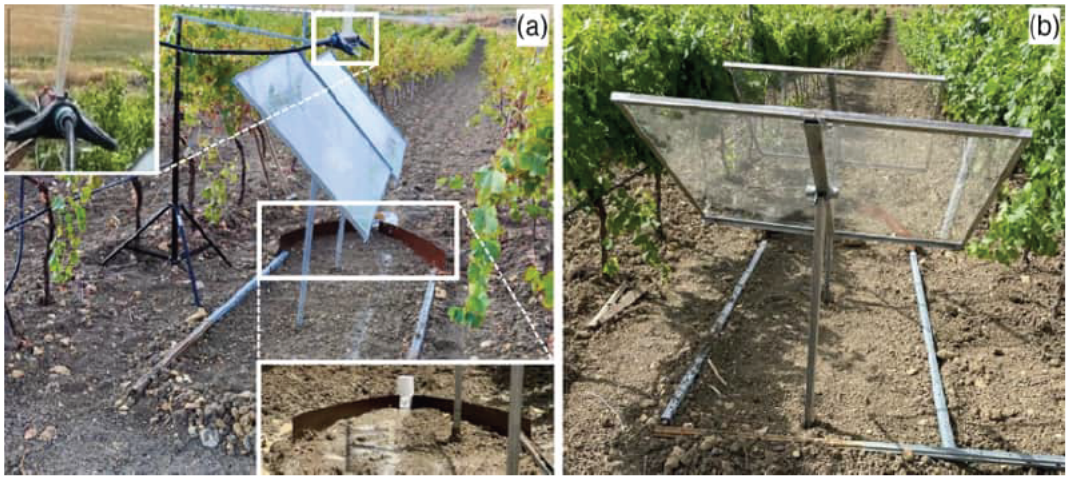

FIGURE 2 Images illustrating (a) the layout B (cross slope panels, Figure 1b), and (b) the layout C (aligned slope panels, Figure 1c). In Figure 2a), the rainfall simulator and the Gerlach apparatus are also zoomed in.

Panels were built by using glass plates on a tilting metal support that can be adjusted according to the correct angle with respect to the sun (Figure 2b). The angle was set to 62.5% for both cross and aligned slope panels in correspondence with the commonly applied angle over the horizon (32°). The height from the ground was the same as in reality (1 m).

An automated sprinkler (Figure 2a) that runs in cycles was used to simulate rainfall. One cycle takes 11 s and consists of the sprinkler boom moving back and forth once. During cycles, the rainfall simulator applied rainfall over the entire the area of interest.

The average applied rainfall during one cycle (cycle rainfall load) was determined by calibration with rain gauges. Thus, before performing runoff measurements, the spatial distribution of rainfall intensity simulated by the rainfall simulator illustrated in Figure 2a was analysed.

A grid of 7 × 24 (168) catch cans were arranged on the bare plot (Figure 1a) to collect the rainfall depth during a simulated rainfall of 240 min and the rainfall intensity was calculated in each point. Figure 3 shows the empirical distribution of rainfall intensity together with the fitted normal distribution corresponding to the mean, $\mu = 56.04$ mm/h, and to the standard deviation, $\sigma = 7.93$ mm/h. The coefficient of variation was CV = 14.1%. The corresponding Christiansen uniformity coefficient was equal to UC = 89%, making the simulated rainfall uniform enough for the purpose of this study. Also, due to the satisfactory goodness of fit of the normal distribution, the mean value $i = 56$ mm/h (Figure 3) was considered as a representative value of the simulated rainfall for the entire plot, and it was imposed as a constant during experimental runs for the three layouts.

Of course, for layouts B and C the solar panels strongly altered the water application uniformity on the plot due to the concentration of runoff off from the panels at their outlets. To have an idea of how much the applied water volume characteristics changed when hitting the soil without and with panels, Figure 4 shows a comparison of the water granulometry patterns. The different patterns were detected by using the flour pellet method (Kincaid et al., 1996; Kohl, 1974), without panels (Figure 4a) and at the outlet of the panels (Figure 4b). As expected the drop size distribution of the simulated rainfall was significantly altered when the water hitting the soil was concentrated at the panels' outlet (Cook & McCuen, 2013).

This issue may be important for the overland flow process analysed in this study, but it would be much more relevant in the context of soil erosion, since the energy associated with the water application

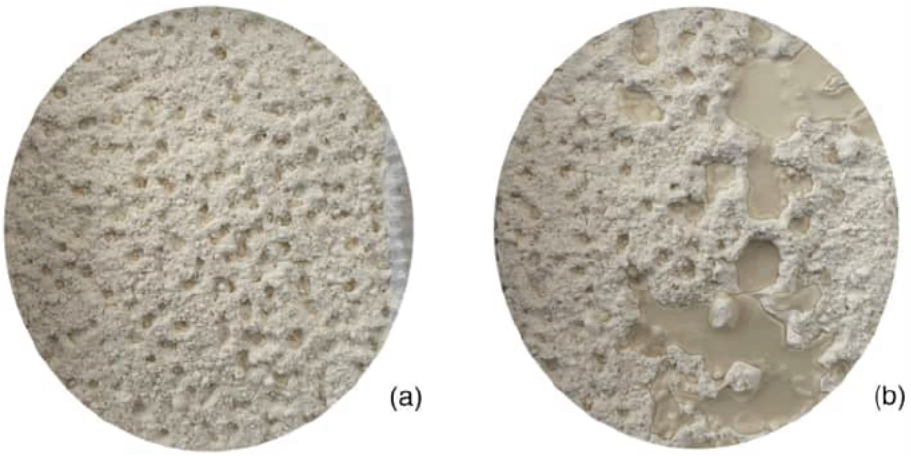

FIGURE 3 Empirical distribution of rainfall intensity measured by 7 × 24 (168) catch cans arranged on the bare plot (Figure 1a). The red line indicates the fitted normal distribution ($\mu = 56.04$ mm/h, blue dot; $\sigma = 7.93$ mm/h; CV = 14.1%).

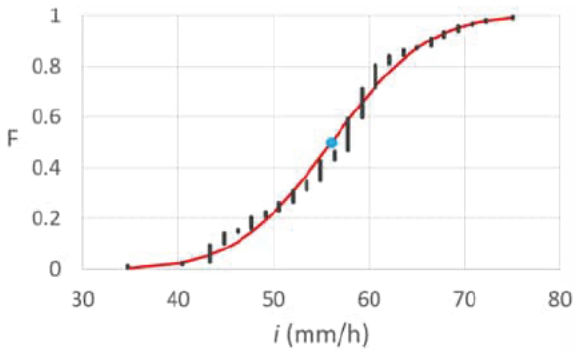

FIGURE 4 Flour cup exposed to a rainfall with intensity $i = 56$ mm/h (a) under open ground, and (b) under the solar panel outlet.

rate when there are no panels would be expected to be much less than that when the panels are present.

The runoff samples were collected in 1-L bottles every 5 min. The time to fill the runoff bottle was recorded. After each run, the sample bottles were immediately weighed to determine the runoff volume. The bottles were subsequently incubated in an oven at 105°C for at least 24 h or until the sediments were dried. The dry weights were then recorded to calculate the sediment delivery, and thus to correct the surface runoff calculation.

2.2 | Applying simplified overland flow models

For layout A (bare soil), an already available simplified overland flow model (GA-KW model, Baiamonte & Agnese, 2010) was applied that combines the Green and Ampt model (Green & Ampt, 1911), to account for infiltration, and the 1D kinematic wave model (Woolhiser & Liggett, 1967), to account for the transportation process along the hillslope.

The GA-KW model is shortly summarized in Appendix A and can be directly applied to layout A (bare hillslope), under the assumption that the plot is perfectly planar, and thus the flow is rigorously downslope and the unsteady and spatially varied overland generation occurs as a sheet flow that entirely covers the hillslope. Rainfall (minus infiltration losses) constitutes the lateral inflow to the plane.

Under a constant rainfall intensity of i (mm/h), Baiamonte and Agnese (2010) derived the characteristic curves corresponding to three domains of the kinematic plane (the first two for the rising limb of the hydrograph, and the third for the falling limb), depending on parameters related to rainfall, hillslope geometry, and soil. The singularity of such a solution is its ability to account for the decreasing of the infiltration capacity, f (mm/h), during the runoff generation process, that in turn determines an increase in the rainfall excess intensity, $r = i \quad f$. For the case of an impervious hillslope, Baiamonte and Agnese (2010) also showed that their solution agrees with the kinematic wave model originally introduced by Woolhiser and Liggett (1967).

In the following, only the parameters referring to the soils and to the hillslope which were calculated for the experimental layouts, and minor model description, are reported. For model details, the reader can refer to Baiamonte and Agnese (2010) or to Appendix A.

According to Green and Ampt (1911), overland flow generation starts when rainfall intensity exceeds the soil infiltration capacity and the time to ponding, t_p, is reached (Baiamonte, 2016). The time to ponding, τ_p, normalized with respect the sorptivity time scale, t_c, is written here:

$$\tau_p = \frac{t_p}{t_c} = \frac{1}{\rho(\rho \quad 1)}, \tag{1}$$

where ρ is the ratio between the rainfall intensity, i (mm/h), and saturated hydraulic conductivity, K_s (mm/h), whereas the sorptivity time scale t_c (h) reads:

$$t_c = \frac{(\theta_s \quad \theta_0)\,\psi_m}{K_s} = \frac{\omega}{K_s}, \tag{2}$$

where θ_s (cm^3 cm^{-3}) and θ_0 (cm^3 cm^{-3}) are the volumetric water contents corresponding to the saturated and antecedent soil moisture conditions, respectively, and ψ_m (mm) is the matric potential at the

wetting front. In Equation (2), the temporal scale t_c, was also written by consolidating the soil hydrological characteristics θ_s, θ_0 and ψ_m in the ω (h) parameter, which will be calibrated later.

Regarding the hillslope geometry, the following hillslope 'geometry' parameter, k_*, needs to be determined (see Appendix A):

$$k_* = \frac{3.6\sqrt{S_0}}{n_{Mann}\, L}, \tag{3}$$

where S_0 is the slope, and 3.6 is a conversion factor that lets the length of the hillslope, L, be expressed in (m), the Manning friction factor, n_{Mann}, be expressed in ($m^{-1/3}$ s), and the specific discharge, q, be expressed in (mm/h).

In the GA-KW model, a dimensionless parameter, $\tau_{eq,i}$, introduced later (Baiamonte & Singh, 2016), synthesizes both the hillslope geometry and the soil hydrological characteristics, that is, the ratio between $t_{eq,i}/t_c$, with $t_{eq,i} = 1/\sqrt{k_*}\, i$ that only depends on the rainfall intensity and on the hillslope geometry:

$$\tau_{eq,i} = \frac{1}{t_c\sqrt{k_* i}} = \frac{K_s}{\omega}\sqrt{\frac{n_{Mann}\, L}{i\sqrt{S_0}}}. \tag{4}$$

This parameter denotes the time to equilibrium corresponding to an impervious hillslope, $t_{eq,i}$, normalized with respect to the sorptivity temporal scale, t_c. The soil (t_c) is the scale factor and plays an important role in simulating the overland flow process on an infiltrating hillslope.

The separation of the 1st and 2nd domain ($t < t_k$ or $t > t_k$, respectively) of the kinematic plane depends on the normalized kinematic wave arrival time, t_k, associated with the corresponding infiltration capacity, f_k (Baiamonte & Singh, 2016). The time t_k represents the time that an observer (the runoff), starting from the top of the hillslope, takes to reach the bottom (during the infiltration process). If the duration of rainfall, t_r, is less than t_k, the recession starts before the observer has achieved the bottom of the hillslope, whereas if $t_r > t_k$, the raising limb of the hillslope continues because of the decreasing infiltration capacity as described by the Green-Ampt model. Of course, the falling limb occurs for $t > t_r$ (3rd domain).

The relationships of t_k and f_k are reported here, respectively, in a more compacted dimensionless form that was derived in Baiamonte and Singh (2016):

$$\tau_k = \frac{t_k}{t_c} = \tau_p + \frac{\rho^{1}}{(f_{*k}\ \ \rho^{1})}\ \ \frac{\rho^{1}}{(1\ \ \rho^{1})} + \psi_k \text{ with } \psi_k = ln\left(\frac{f_{*k}\ \ \rho^{1}}{f_{*k}(1\ \ \rho^{1})}\right), \tag{5a}$$

$$f_{*k} = \frac{f_k}{i} = 1\ \ \frac{(1\ \ \rho^{1})(f_{*k}\ \ \rho^{1})^2}{(f_{*k}+1\ \ 2\rho^{1})\rho^{2}}\left(\tau_{eq,i}^2\ \ \frac{2\rho^{1}\psi_k}{f_{*k}\ \ \rho^{1}}\ \ \psi_k^2\right), \tag{5b}$$

where $\tau_{eq,i}$ is expressed by Equation (4).

For the layout B (cross slope panels), the overland flow model considered for the layout A can also be applied. Indeed, for cross slope panels, a uniform water application rate, flowing out from the panels, is assumed to be uniformly applied over the hillslope characterized by a width B_* less than that of the layout A (see Figure 1b). Thus, the reduced hillslope is also assumed to be perfectly planar for layout B, and the flow is rigorously downslope, whereas the lateral in flow is represented by the discharge flowing off from the panels along the perpendicular direction with respect to the slope of the hillslope. In such a condition, all the runoff water particles move linearly downslope, so that no water passes under the solar panel (see Figure 1b).

One more assumption is introduced: that the equilibrium between the rainfall intensity, i(mm/h), and the outlet panel specific discharge, q(mm/h), is instantaneous ($q = i$), which is not far from the actual conditions since the length of the panels is usually very small, compared to the length of the hillslope characterized by a slope S_0 that is much less than that of the solar panels (62.5%).

For layouts C (aligned slope), the overland flow model considered for layouts A and B cannot be applied, since the assumption of a uniform water application rate, which is at the base of the GA-KW model, is far from being appropriate. This is because the water application rate generated over the upstream panel (US) concentrates at the panel bottom, and later interacts with that of the downstream panel (DS) where, similarly to the US panel, the discharge outflowing from the panel is generated. Thus, contrarily to the situation in cross slope panels, where it is assumed that no water passes under the solar panels, on aligned slope panels, all the runoff water particles move linearly downslope, so that their outflows interact. Therefore, for this layout the area right under the DS solar panel is subject to infiltration (Figure 1c).

Layout C can also be addressed by likening it to border irrigation, where a similar runoff generation process can be recognized. Indeed, in border irrigation, water is introduced at the upstream end of the hillslope (at the bottom of each panel in our case) and is allowed to move as a sheet flow which covers the entire width of the border in the downstream direction (Singh & Su, 2022). It should be noted that if we have a matrix of aligned slope panels on a hillslope, there would be a contribution from the space between panels flowing downward, which in this study did not occur (with panel width being equal to the hillslope width).

A simplified mathematical model for border irrigation was introduced by Singh and Yu (1987). The model is described in two companion articles. In the first article (Singh & Yu, 1987), the advance and storage phases are developed, while the second article accounts for the vertical and horizontal recession phases. For the purpose of this work, which aims to investigate the impact of solar panels on the alteration of peak discharge, only the advance and storage phases leading to the rising limb of the hydrograph were considered.

Singh and Yu (1987) used the volume balance approach and calibrated their model by experimental data from vegetated and nonvegetated borders (Atchison, 1973; Roth, 1971). Average errors were found very limited, making their approach suitable to be applied. In the following, only a brief description of the border irrigation model

and of its parameters will be given, and for further details the reader may refer to Singh and Yu (1987).

For the advance and storage phases, the model parameters are (i) Kostyakov's empirical infiltration parameter, K (m/min^A) (Kostyakov, 1932), (ii) Kostyakov's time exponent, A, (iii) Manning's roughness factor, n_{Mann} (min m$^{1/3}$), iv) distance, L_{av}, at which the average surface water depth, h_{av}, between $x = 0$ and advance front $x = S$, reaches 95% of the normal water depth h_0, and v) the entrance normal flow depth coefficient, α.

Although the parameters L_{av} and α are related to many factors such as infiltration rate, slope and surface roughness, Singh and Yu (1987) verified that L_{av} and α are slightly related to these factors, compared to the other parameters of the model, thus they were assumed to be constant, as suggested by Singh and Yu (1987). In particular, $L_{av} = 75$ m for a nonvegetated border, $L_{av} = 225$ m for a vegetated border, and $\alpha = 0.620$ for both a vegetated and nonvegetated border.

The advance front reaches the end of the border ($x = L$) at $t = T_a$ (min), and the inflow continues until the cut off time, t_r. After the time T_a, the storage phase begins to develop, where the water depth variation from upstream (normal water depth, h_0, corresponding to the Manning equation) to downstream (h_e) is assumed to be linear. Singh and Yu (1987) derived the temporal variation of water depth at the downstream end, h_e:

$$h_e = \left[\frac{n_{Mann}}{60\sqrt{S_0}}\left(q_0 \quad \frac{KL}{T_a}\left(t^A \quad (t \quad T_a)^A\right)\right)\right]^{0.6}, \tag{6}$$

where the factor 60 makes it possible to express n_{Mann} in (m$^{-1/3}$ s), S_0 is the slope, and q_0 (m^3/m/min) is the unit width inflow rate that, maintaining the assumption of instantaneous equilibrium at the bottom of each panel, can be related to the rainfall intensity i and to the panel length L_p, with surface area $S = B_p \times L_p$ (Figure 1c):

$$q_0 = \frac{i L_p}{60 \times 1000}, \tag{7}$$

where 60×1000 lets q_0 be expressed in (L/h/m), and i in mm/h. In Equation (6), the term in round brackets is the net outflow discharge, Q, of interest, which accounts for the infiltration during the storage phase, and it is rewritten here to express Q and i in (L/h/m), L in (m), K in (mm/h^A), n_{Mann} in (m$^{-1/3}$ s) and t and T_a in hours:

$$Q = i L_p \quad \frac{KL}{60^{1\ A} T_a}\left(t^A \quad (t \quad T_a)^A\right). \tag{8}$$

Equation (8) can be applied to determine the outlet discharge that depends on the distance L from the edge of the panel to the outlet (Figure 1c), from the time that the advance front reaches the outlet, T_a (h), and of course from Kostyakov's infiltration parameters, K and A.

Equation (8) can also be rewritten to express the specific outflow discharge, q (mm/h), that is, the discharge Q per unit surface area $(L_p + L)\,B$, which is useful to consider to obtain the quasi-equilibrium condition (i.e., when $q \cong i \quad K_s$):

$$q = \frac{i B L_p T_a \quad 60^{A\ 1} KL\left(t^A \quad (t \quad T_a)^A\right)}{B(L_p + L)\,T_a}. \tag{9}$$

Of course, for $t = T_a$, when the advance front reaches the end of the border, the outflow matches the inflow rate i minus the infiltration rate according to Kostyakov's equation:

$$q = \frac{i B L_p \quad 60^{A\ 1} KL}{B(L_p + L)}. \tag{10}$$

where q is in mm/h.

3 | RESULTS

3.1 | Experimental measurements

For layouts A–C, Figure 5 plots the output's specific discharge, q (mm/h), versus the time, for the two replications performed for each layout. Figure 5 shows that runoff measurements were carried out mostly for the rising limb of the hydrograph. This is because the purpose of this work is to investigate the impact of solar panels on the alteration of peak discharge at the end of the rising limb. Thus, measurements for the recession of the hydrograph, after the rainfall ceased, were only carried out for a few cases of the second replication (run #2, Figure 5a,b).

Although the hillslope was regularized before performing the measurements, and the latter were carried out after a long dry period with neither rainfall nor irrigation, two replications exhibited quite dispersed measurements. This can be ascribed to the following reasons: (i) the antecedent moisture conditions, (ii) the spatial variability of the soil's hydrological characteristics and of the field microtopography, (iii) the rainfall uniformity and (iv) the experimental error. In particular, microtopography can govern runoff dynamics as a net result of local heterogeneities in the flow paths and ponding (Baiamonte et al., 2014). This in turn controls the development of the surface water layer that connects and flows downslope (Caviedes-Voullième et al., 2021; McDonnell et al., 2021).

However, considering the complexity of the studied process, measurements were judged to be accurate enough to be analysed, especially for layouts A and B. The highest peak discharge of Figure 5a, occurring for the first replication (run #1) could be caused by occasional soil bumps that disturbed the overland flow, which were not contemplated in the physical model. On the other hand, Figure 5c clearly shows a drop in discharge in both replications determined by the aligned slope panels, making evident the time in which the contribution of the US panel reaches the outlet, quickly increasing the discharge flowing out the DS panel. The maximum specific discharge can be observed for layout B) (cross slope panels, Figure 5b).

It is important to note that for the three layouts, the rainfall duration was enough to achieve the equilibrium condition, which is useful for the models' calibration. Moreover, a comparison of Figure 5a–c

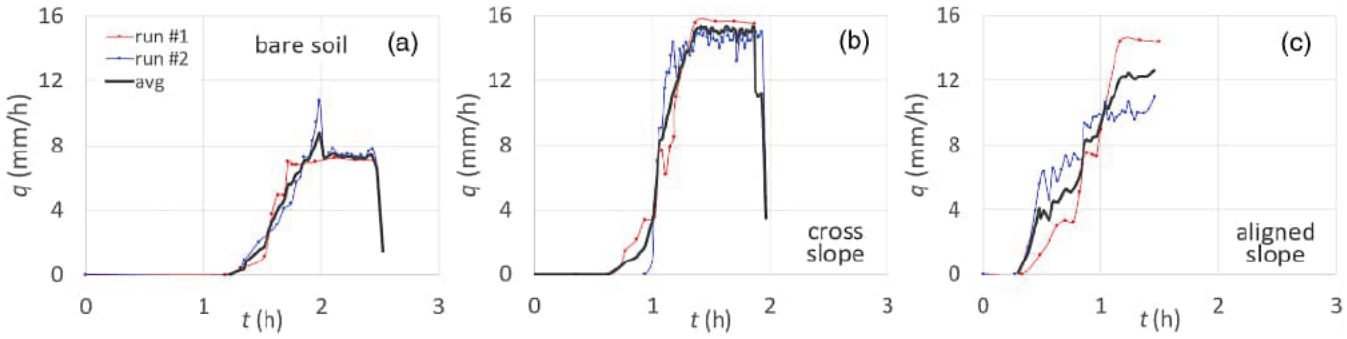

FIGURE 5 Temporal variations of specific discharge measurements performed with two replicates and their average (avg), corresponding to (a) layout A (bare soil), (b) layout B (cross slope panels) and (c) layout C (aligned slope panels) (Figure 1).

TABLE 1 Input parameters corresponding to Layouts A and B.

Layout	Model	i (mm/h)	K_s (mm/h)	ρ	t_c (h)	t_r (h)	L (m)	n_{Mann} (s m$^{-1/3}$)	S_0 (%)	k_* (equation (3))
(A) bare soil	GA-KW	56	**39.2**	1.38	**0.484**	2.47	3	**0.909**	0.14	0.4939
(B) cross slope panels		**62.1***		1.58		1.87				

Note: *Indicates that the amplified rainfall intensity. Bold values indicate calibrated parameters.

shows that runoff generation is quicker when panels are arranged aligned with the hillslope (0.3 h) (Wang & Gao, 2023) (Figure 5c) rather than arranged cross slope (0.62 h) (Figure 5b), and that the lowest and the most delayed response occurred for bare soil (1.2) (Figure 5a). The latter is probably due to the delay effect induced by the infiltration process being much more pronounced than when panels lay on the hillslope. The times to runoff generated by the calibrated models were very close to those observed.

For the three layouts, Figure 5 also plots the average value of the two replications (avg, black lines) that will be considered for the models' calibration, as discussed in the next section.

3.2 | Calibrating the overland flow models

For layout A (bare soil), Table 1 reports the input parameters required by the overland flow GA-KW model (Baiamonte & Agnese, 2010). Note that only the rainfall intensity, i (mm/h), the slope, S_0, and the length of the hillslope, L (m), were strictly considered as input parameters, while the saturated hydraulic conductivity, K_s (mm/h), the sorptivity time scale, t_c (h), and the Manning coefficient, n_{Mann} (s m$^{-1/3}$), are parameters that need to be calibrated according to the runoff measurements. Indeed, for layout A, by combining Equation (1) and Equation (2), the observed time to ponding, t_p, and the specific discharge at the equilibrium (i K_s) makes it possible to derive both the saturated hydraulic conductivity, K_s, and the ω (h) parameter, which is related to the sorptivity time scale, t_c, and consolidates the role of ψ_m, θ_s and θ_0 (Equation (2)). The n_{Mann} parameter was calibrated by minimizing the mean square errors between the measured and estimated specific discharges. In Table 1, the values of the calibrated parameters are indicated in bold. Note that the calibration of n_{Mann} provides a high value equal to 0.909 s m$^{-1/3}$. This occurrence could be ascribed to the marginally/partially inundated flow regime (Lawrence, 1997) characterizing the experimental conditions. Indeed, for the low water depths provided by the model (2–4 mm), the macroscale surface roughness may determine high frictional resistance in overland flow. Experimental measurements of Abrahams and Parsons (1994) and of Roels (1984) showed that in such a particular condition, where the inundation ratio (i.e., the ratio of the mean flow depth to the average roughness height) is close to the unity, the Darcy–Weisbach friction factor may reach 20–30, and for water depths 2–4 mm, these values correspond to Manning coefficients equal to 0.803–1.192 s m$^{-1/3}$, and to 0.819–1.196 s m$^{-1/3}$, respectively, justifying our finding.

As previously observed, for layout B, the GA-KW model was also applied since it was assumed that the discharge outflowing from the panels was uniformly applied to the hillslope (Figure 1b). The parameters calibrated for layout A were also imposed for layout B), since it was assumed that the soil's hydrological characteristics and the hillslope roughness did not significantly differ from those of layout A (bare soil). However, because of the different panels' orientation, the hillslope width was reduced by replacing B by B_* (Figure 1b). Since the GA-KW model was applied in terms of the specific discharge, q (mm/h), it was enough to amplify the rainfall intensity by considering the reduced width B_*. The B_* value, and the associated amplified rainfall intensity, was calibrated by once again minimizing the mean square errors between the measured and estimated specific discharges. Thus, an amplified rainfall intensity of 62.1 mm/h was obtained (Table 1).

For layouts A and B, the results obtained by the calibrated GA-KW model are illustrated in Figure 6a,b. Note that for layout B, which was calibrated by imposing the K_s, t_c and n_{Mann} values obtained in layout A, the difference between the observed and calculated discharge is worse than that of layout A, as would be expected, because these parameters were not recalibrated. Furthermore, Figure 6a shows that contrarily to the experimental runs that achieved the

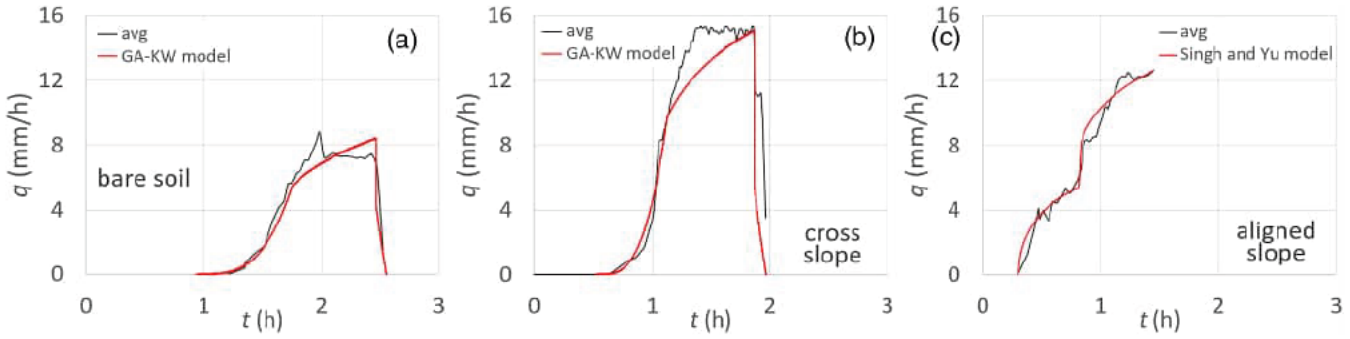

FIGURE 6 Comparison between the temporal variations of the average specific discharge measurements (avg) with those obtained by models' calibration corresponding to (a) layout A (bare soil), (b) layout B (cross slope panels), and (c) layout C (aligned slope panels) (Figure 1).

TABLE 2 Output parameters corresponding to Layouts A and B.

Layout	Model	t_p (h)	ω (h)	t_k (h)	f_k (mm/h)	h_k (mm)	q_k (mm/h)	$f(t_r)$ (mm/h)	$h(t_r)$ (mm)	$q(t_r)$ (mm/h)
(A) bare soil	GA-KW	0.932	19.0	1.754	47.35	3.33	5.48	45.19	4.13	8.41
(B) cross slope panels		0.524		1.130	50.53	4.43	9.70	46.55	5.53	15.09

TABLE 3 Input parameters corresponding to Layout C.

Layout	Model	Panel	i (mm/h)	T_a (h)	t_r (h)	K (mm/h^A)	A	L (m)	n_{Mann} (s m$^{-1/3}$)	S_0 (%)
(C) aligned slope panels	Singh and Yu (1987)	DS	56	**0.300**	1.442	**124.21**	**0.758**	0.7	0.909	0.14
		US		**0.817**		**41.21**		2.2		

Note: Bold values indicate calibrated parameters.

equilibrium condition, for the GA-KW model the outlet discharge increases in the 2nd kinematic domain, and the equilibrium is not reached. The latter could be ascribed to the formation of a soil seal that actually reduces the soil permeability providing the equilibrium and to the fact that the physical model does not account for such a process. It is expected that the seal formation could be more relevant when panels are applied (see Figure 6b), since the greater energy of the water application rate concentrated at the panel outlet could favour splash erosion (van Dijk et al., 2002). The latter mobilizes more soil particles than the direct impact of rainfall. Once deposited later because of overland flow, these may also contribute to decreasing permeability along the path (Slattery & Bryan, 1994).

For layouts A and B, the output parameters corresponding to the application of GA-KW model t_p (Equation (1)), ω (Equation (2)), t_k (Equation (5a)), f_k (Equation (5b)), the water depth at the kinematic arrival time h_k, (Baiamonte & Agnese, 2010) and the corresponding specific discharge q_k, the infiltration capacity at the rainfall duration $f(t_r)$, and the corresponding water depth and discharge, $h(t_r)$ and $q(t_r)$, are all reported in Table 2.

For layout C and for the two aligned slope panels (DS and US), Table 3 reports the input parameters required by the border irrigation model (Singh & Yu, 1987). In particular, for each panel, Table 3 reports the rainfall intensity i, Kostyakov's infiltration parameters, K and A, the time of the advance phase T_a, the duration of the rain, t_r, the length L of each aligned slope panel (Figure 1c), Manning's roughness factor, n_{Mann} and the slope of the plot, S_0.

Note that i, n_{Mann} and S_0 are the same values established for layouts A and B. In other words, the remaining time T_a, K, and A were considered as calibrated parameters. This is because the Singh and Yu model accounts for the Kostiakov infiltration model, rather than the GA model, with new parameters to be calibrated. By fitting the Singh and Yu model to the experimental measurements, only the advance phase, T_a, was expected to be changed for the US and DS panels, because of the different distance from the outlet. Contrarily, fit also became necessary to diversify the scale parameter K associated with the US and DS panels, to obtain reasonable results.

Specifically, minimizing the mean square errors between the measured and estimated specific discharges, $A = 0.758$, for both panels, and K_{DS} and K_{US} resulted in values of 124.21 and 41.21 mm/h^A for DS and US panels, respectively (Table 3).

This issue might appear meaningless because the initial soil characteristics are the same downstream of the two panels. However, it could be justified, by considering that, contrary to layouts A and B where a uniform water application rate was applied, for layout C, the runoff generated by the US panel overflows on the soil that was already wetted by the DS panel. It is reasonable to suppose that this occurrence determines a reduction in soil permeability to be associated with the US panel, which is in line with the calibrated K values. These considerations are supported by the work of Zimmermann et al. (2013), who studied two sampling approaches so as to adequately characterize K_s spatial variability along flowlines. These authors found that in the lower parts of flowlines, soil permeability

TABLE 4 Output parameters corresponding to Layouts C).

Layout	Model	Panel	h_e (mm)	$q(t_r)$ (mm/h)	$Q(t_r)$ (L/h)	$\Sigma Q(t_r)$ (L/h)
(C) aligned slope panels	Singh and Yu (1987)	DS	1.204	13.46	20.19	37.75
		US	1.107	5.85	17.56	

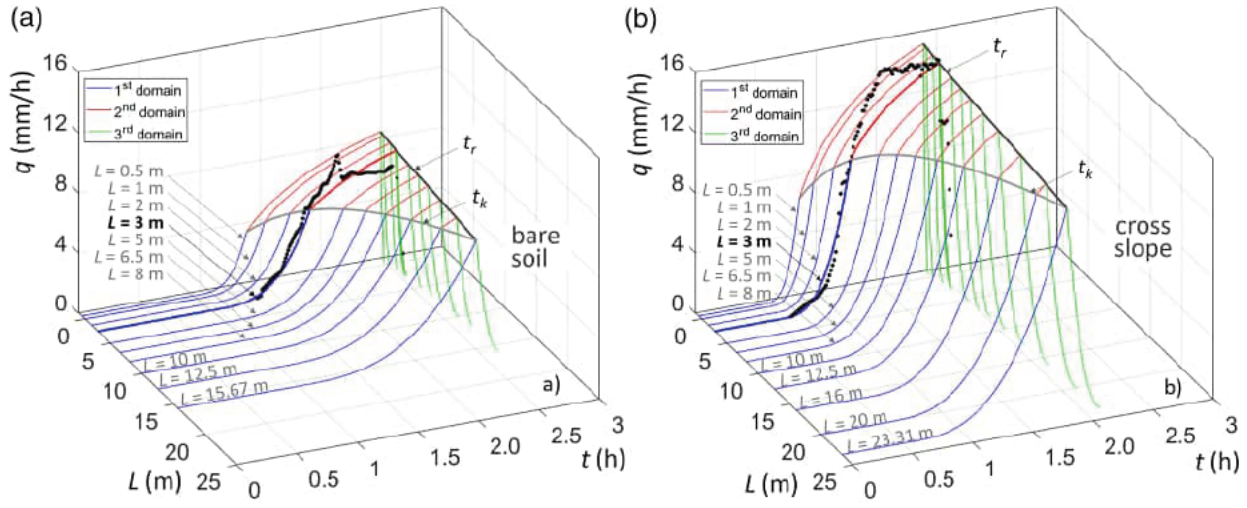

FIGURE 7 Temporal variation of the specific discharge, q (mm/h), obtained by upscaling the Green-Ampt Kinematic-Wave model (GA-KW, Baiamonte & Agnese, 2010) calibrated for $L = 3$ m to different L, (a) for layout A, and (b) for layout B.

decreased, since flowlines had been subject to topsoil removal due to steady erosion by overland flow.

Moreover, it is not farfetched to suppose that the overland flow generated by the DS panel, determines the development of compaction and sealing that also contribute to a decrease in surface permeability (Römkens et al., 1985; Yair & Lavee, 1985). Indeed, sedimentational seals developed during overland flow, and afterflow seals consisting of deposited fine clay particles, may also contribute to decreasing permeability along the path (Slattery & Bryan, 1994).

For layout C, the calibration of the Singh and Yu model provided an excellent fitting of the experimental measurements, as depicted in Figure 6c. In the same figure, as for the experimental discharges, a drop in discharge determined by aligned slope panels can be observed, showing the time in which the contribution of the US panel reaches the outlet, adding to that of the DS panel.

For both DS and US panels, the output parameters corresponding to the application of the Singh and Yu model, the water depth at the end of the plot h_e, the specific discharge at the end of the rainfall, $q(t_r)$, and the volumetric discharge of each panel, $Q(t_r)$, and the cumulated one $\Sigma Q(t_r)$, are reported in Table 4.

4 | UPSCALING AND DISCUSSION

The results obtained through the calibration of both the GA-KW model (layouts A and B) and the Singh and Yu model (layouts C) allows these same models, calibrated for the hillslope 3 m length, to be upscaled to different Ls. This issue is of interest since the actual impact of solar farms or PV systems involves a multitude of panels that could exasperate the increase of the peak discharge that this present work has analysed at a small scale (3 m × 1 m, Figure 1).

For layouts A and B, Figure 7a,b illustrate the 3D plots, respectively, where the rising limb of the hydrograph is represented for different L. The rainfall intensity and the duration of rainfall was set equal to that considered in the experimental runs, $i = 56$ mm/h and, $t_r = 2.47$ and 1.87 h, for layouts A and B, respectively. Of course, the kinematic arrival time, t_k, increased as the hillslope length increased, which was varied until the duration of rainfall ($t_k = t_r$) was achieved, resulting in $L = 15.67$ m for layout A, and $L = 23.31$ m for layout B.

As expected, increasing the length of the hillslope determined a slower response in terms of specific discharge. A comparison between Figure 7a,b also shows that for a fixed upscaled length, the specific discharges when panels are cross slope with respect to the hillslope is greater than those of bare soil, clearly demonstrating their impact on surface runoff.

It is also important to consider that the effect of the length, L, on the hillslope response, for fixed slope, reflects the effect of the slope, S_0, for fixed hillslope length, because the effect of both L and S_0 is lumped (consolidated) in the k_* parameter (Equation 3). For the calibrated n_{Mann} value (0.909 s m$^{-1/3}$), Table 5 reports the k_* values calculated by Equation (3), for fixed slope ($S_0 = 14\%$) by varying the length L (Figure 7a,b), and for fixed length ($L = 3$ m) by varying the slope S_0. Table 5 shows that to any pair (L, S_0) corresponds the same k_* value, indicating that for fixed $L = 3$ m, Figure 7a,b also show the effect of the S_0 values reported in Table 5.

TABLE 5 For the calibrated $n_{Mann} = 0.909$ s m$^{-1/3}$, values of k_* (Equation (3)) corresponding to the upscaled L, for fixed $S_0 = 14$ %, and corresponding to the upscaled S_0, for fixed $L = 3$ m.

L (m)	k_*	S_0
($S_0 = 14$ %)	Equation (3)	($L = 3$ m)
0.5	2.964	5.0400
1	1.482	1.2600
2	0.741	0.3150
3	0.494	0.1400
5	0.296	0.0504
6.5	0.228	0.0298
8	0.185	0.0197
10	0.148	0.0126
12.5	0.119	0.0081
16	0.093	0.0049
20	0.074	0.0031
23.31	0.064	0.0023

The results of upscaling obtained for layouts A and B are reported in Table 6, which shows that as L increases, values of the kinematic arrival time, t_k, and of the corresponding specific discharge, also increase. Contrarily, for layouts A and B, the specific discharge at the end of the rainfall, $q(t_r)$ decreases, but it results in higher outlet discharges, that is, when expressing Q in (L/h).

For layout C, upscaling the Singh and Yu model to different L, required extrapolating the empirical Kostyakov's infiltration parameter, K, based on the calibration results (Table 3), whereas the shape factor A was assumed as a constant for any L.

In the hydrologic literature, the temporal and spatial variation of the saturated hydraulic conductivity, K_s, which is related to the K parameter (Su et al., 2016), has often been described by a power-law. Beven (1982) used the simple piston displacement model to simulate flow in the unsaturated zone, adopting a power-law to describe K_s decreasing as soil depth increases (Baiamonte & Agnese, 2016). Akgün (2010) studied the compaction permeameter tests on mixtures ranging from 15% to 30% bentonite content and showed that the hydraulic conductivity decreased with increased bentonite content, also obeying a power-law. Contrarily, a decaying exponential-law was employed for K_s by Baiamonte et al. (2019) to describe how K_s decreases due to the subsidence phenomena of *Posidonia oceanica* (L.) Delile residues, exposed to a constant rainfall intensity.

The most widely used approach of interest for this work relates saturated permeability to porosity via a power-law (Guarracino et al., 2014), which can also be derived from the Kozeny (1927) and Carman (1937) infiltration models. Since the reduction of Kostyakov's infiltration parameter K was ascribed to sedimentational seals developed during overland flow, and thus is also related to a reduction in soil porosity, the simple decaying power-law was also applied in the context of this work, to extrapolate the decreasing K parameter. The model's calibration provided only two K values, since only two aligned slope panels were installed to perform the experimental runs. A decreasing potential power-law was assumed for extrapolating K to more than two panels, that is, at increasing L (Figure 1c).

Figure 8 plots the power-law applied to Kostyakov's empirical parameters, K (mm/h^A), which were obtained by the calibration of the Singh and Yu model, versus the length L (m). Figure 8 also shows the K values extrapolated by the power-law for three and four panels (red dots), under the assumption of the same interspace panels adopted in the experimental runs (0.7 m). The resulting K values are also reported in Table 6, together with the T_a and h_e parameters, and the output discharges were obtained by upscaling the Singh and Yu model to different L values (Figure 1c).

The corresponding hydrographs are plotted in Figure 9, in terms of specific discharge, q (mm/h) (Figure 9a) and outlet discharge (Figure 9b). Figure 9b also graphs the cumulated discharge, ΣQ, which results from the combined contributions flowing out from the panels, under the assumption of validity of the superposition principle.

Results clearly show that for the aligned slope panels, the outlet discharge is greater than that of the bare soil (no panels), demonstrating the impact of solar panels on overland flow generation. This is also true for layout C.

Finally, for a homogeneous comparison of discharge, by fixing the hillslope length at 3 m and the duration of rainfall at $t_r = 1.44$ h, which corresponds to the rainfall's duration for layout C, the generated outlet discharge was analysed for the case with no panels and the cases with panels. In particular, the ratio between the resulting outlet discharge for layouts A–C, Q_A, Q_B and ΣQ_C, respectively, were estimated by the models. The outlet discharge of layouts B and C compared to layout A (no panels) were found to be 11.7 and 11.5 times greater than that obtained for bare soils, clearly indicating (i) the important effect of the panels providing discharges that are much greater than that corresponding to bare soil, and (ii) that the panels' orientation slightly affects the outlet discharge, since for both of the studied orientation, the discharge ratios are similar to each other.

According to the results obtained by upscaling the models, longer hillslopes further increased outlet discharges, as well as time to runoff, with the exception of aligned slope panels where the same parameters did not vary with the hillslope length.

These results, although predictable and based on simplified assumptions, quantify the effect of solar panels on runoff generation and suggest that erosion control methods should be used to mitigate soil detachment and transportation. Thus, a grass cover beneath the panels and in the interspace between panels (for aligned slope panels) is highly recommended, because the soil appears much more prone to erosion generated by the higher discharges produced when solar panel systems are adopted.

5 | CONCLUSIONS

Solar farms are the energy generators of the future; thus, it is important to determine the environmental and hydrologic effects of both existing and planned farms. This is even more true because

TABLE 6 Results obtained by upscaling the models calibrated for $L = 3$ m to different L.

Layout	Model	L (m)	t_k (h)	t_r (h)	K_s (mm/h)	t_c (h)	$q(t_k)$ (mm/h)	$q(t_k)$ (L/h)	$q(t_r)$ (mm/h)	$q(t_r)$ (L/h)
(A) bare soil	Green Ampt and Kinematic Wave (Baiamonte & Agnese, 2010)	0.5	1.361	2.467	39.2	0.484	3.603	1.80	8.659	4.33
		1	1.483				4.275	4.27	8.592	8.59
		2	1.640				5.019	10.04	8.491	16.98
		3	**1.754**				**5.483**	**16.45**	**8.408**	**25.22**
		5	1.926				6.095	30.48	8.264	41.32
		6.5	2.029				6.418	41.71	8.166	53.08
		8	2.119				6.676	53.41	8.070	64.56
		10	2.224				6.959	69.59	7.943	79.43
		12.5	2.339				7.241	90.51	7.779	97.24
		15.67	2.467				7.531	118.00	7.532	118.02

Layout	Model	L (m)	t_k (h)	t_r (h)	K_s (mm/h)	t_r (h)	$q(t_k)$ (mm/h)	$q(t_k)$ (L/h)	$q(t_r)$ (mm/h)	$q(t_r)$ (L/h)
(B) cross panels	Green Ampt and Kinematic Wave (Baiamonte & Agnese, 2010)	0.5	0.837	1.867	39.2	0.484	6.588	3.29	15.374	7.69
		1	0.927				7.717	7.72	15.297	15.30
		2	1.044				8.945	17.89	15.182	30.36
		3	**1.130**				**9.696**	**29.09**	**15.089**	**45.27**
		5	1.259				10.664	53.32	14.929	74.65
		6.5	1.337				11.171	72.61	14.823	96.35
		8	1.405				11.576	92.61	14.721	117.77
		10	1.485				12.008	120.08	14.591	145.91
		12.5	1.573				12.442	155.53	14.432	180.40
		16	1.680				12.920	206.72	14.206	227.30
		20	1.787				13.349	266.98	13.928	278.56
		23.306	1.866				13.642	317.94	13.645	318.01

Layout	Model	L (m)	T_a (h)	t_r (h)	K (mm/h^A)	A	h_e (mm)	q (t_r) (mm/h)	Q (t_r) (L/h)	$\Sigma Q(t_r)$ (L/h)
(C) aligned slope panels	Singh and Yu (1987)	0.7	0.300	2.694	124.21	0.758	1.325	15.79	23.69	23.69
		2.2	**0.817**		**41.21**		**1.276**	**15.32**	**22.25**	**45.95**
		3.7	1.333		24.97		1.238	14.91	21.14	67.09
		5.2	1.850		17.99		1.194	14.50	19.90	86.99

Note: Bold values refer to the hillslope lengths for which the models were calibrated.

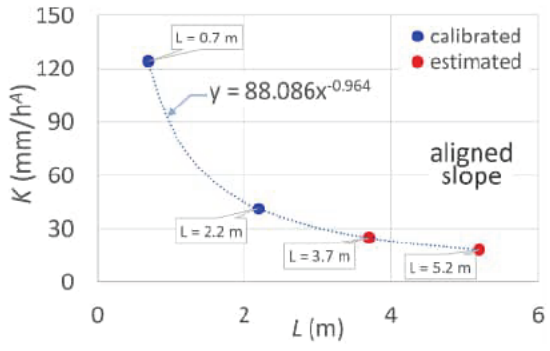

FIGURE 8 For layout C (aligned slope panels), Kostyakov's infiltration empirical parameter, K (mm/h^A), versus the length L (m) (Figure 1c). Red dots indicate the K values estimated by the power law relationship, also indicated.

agrophotovoltaic systems (solar farms) seem to be the most sustainable tool to create renewable energy without compromising agricultural production. In this context, a multidisciplinary approach to study the impact of these kinds of systems becomes more and more important, especially regarding the identification of the most suitable areas for their construction.

In this article, the impact of solar panels on the runoff generation process was investigated from both an experimental and theoretical point of view. The different arrangement of solar panels with respect to the maximum slope direction of the hillslope where the panels are placed was also analysed. Physical models introduced in the literature helped explain the impact of solar panels on runoff generation. The models were calibrated for the experimental layouts and were then upscaled to different hillslope length values.

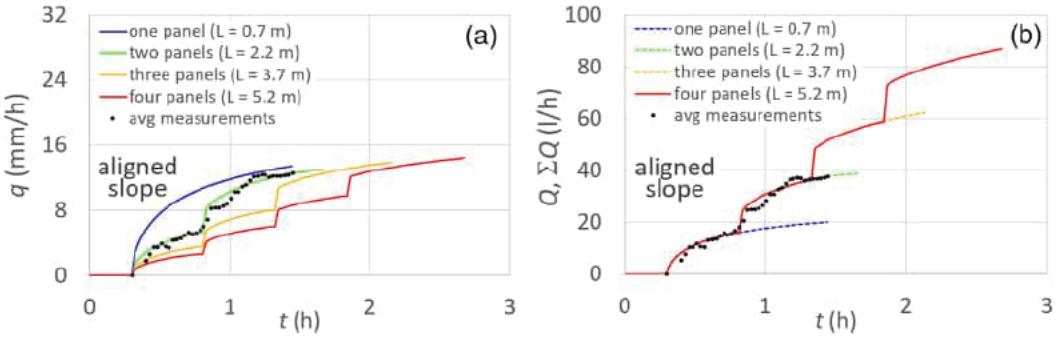

FIGURE 9 For layout C (aligned slope panels), temporal variation (a) of the specific discharge, q (mm/h), and (b) of the outlet discharge for 1–4 panels, Q (L/h) and cumulated, ΣQ (L/h), obtained by upscaling to different L the Singh and Yu model (Singh & Yu, 1987) that was calibrated for $L = 2.2$ m.

Results showed that solar panels increased the outlet discharge when panels were arranged in a cross slope (layout B) and aligned slope (layout C), by 11.7 and 11.5 times, respectively, compared to bare soil (layout A—no panels). This clearly indicates (i) the important effect of the panels on discharges that are much greater than those occurring on bare soil, and (ii) that the panels' orientation slightly affects the outlet discharge, since for both of the studied orientations, the discharge ratios were similar to each other.

Furthermore, solar panels also affected the time to runoff, which was observed to be the lowest for aligned slope panels (0.3 h), higher for cross slope panels (0.62 h), and the highest for the bare soil hillslope (1.2 h). The calibrated theoretical models estimated times to runoff that were very close to those observed.

As it would be expected, upscaling the models to longer hillslope further increased the simulated outlet discharge values, as well as the time to runoff, with an exception for aligned slope panels where time to runoff did not vary with the hillslope length.

The evidence provided by this research suggests that agricultural soils should preferentially not be left bare under solar panel structures, because of an increased risk of runoff and of the relative soil erosion process.

DATA AVAILABILITY STATEMENT

The data that support the findings of this study are available from the corresponding author upon reasonable request.

ORCID

Giorgio Baiamonte https://orcid.org/0000-0002-7092-1177

REFERENCES

Abrahams, A. D., & Parsons, A. J. (1994). Hydraulics of interrill overland flow on stone-covered desert surfaces. *Catena*, *23*, 111–140.

Akgün, H. (2010). Geotechnical characterization and performance assessment of bentonite/sand mixtures for underground waste repository sealing. *Applied Clay Science*, *49*(4), 394–399. Conference Paper.

Atchison, K. T. (1973). Retardance coefficient and other data for a vegetated irrigation border. Unpublished M.S. Thesis, University of Arizona, Tucson, AZ, USA.

Baiamonte, G. (2016). Simplified model to predict runoff generation time for well-drained and vegetated soils. *Journal of Irrigation and Drainage Engineering-ASCE*, *142*(11), 04016047. https://doi.org/10.1061/(ASCE)IR.1943-4774.0001072

Baiamonte, G., & Agnese, C. (2010). An analytical solution of kinematic wave equations for overland flow under Green-Ampt infiltration. *Journal of Agricultural Engineering*, *1*, 41–49. http://agroengineering.org/index.php/jae/article/view/jae.2010.1.41

Baiamonte, G., & Agnese, C. (2016). Quick and slow components of the hydrologic response at the hillslope scale. *Journal of Irrigation and Drainage Engineering-ASCE*, *142*(10), 4016038. https://doi.org/10.1061/(ASCE)IR.1943-4774.0001053

Baiamonte, G., D'Asaro, F., & Calvo, R. (2019). Gravity-driven infiltration and subsidence phenomena in *Posidonia oceanica* residues. *Journal of Hydrologic Engineering ASCE*, *24*(6), 4019016. doi:10.1061/(ASCE)HE.1943-5584.0001791

Baiamonte, G., D'Asaro, F., & Grillone, G. (2014). Simplified probabilistic-topologic model for reproducing hillslope rill network surface runoff. *Journal of Irrigation and Drainage Engineering-ASCE*, *141*(7), 4014080. https://doi.org/10.1061/(ASCE)IR.1943-4774.0000854

Baiamonte, G., & Singh, V. P. (2016). Analytical solutions of kinematic wave time of concentration for overland flow under Green-Ampt infiltration. *Journal of Hydrologic Engineering ASCE*, *21*(3), 4015072. https://doi.org/10.1061/(ASCE)HE.1943-5584.0001266

Beven, K. J. (1982). On subsurface stormflow: Predictions with simple kinematic theory for saturated and unsaturated flows. *Water Resources Research*, *18*(6), 1627–1633.

Bignami, D. (2010). E i pannelli colonizzano i campi. *Terra e Vita*, *43*, 16 (in italian).

Brutsaert, W. (2005). *Hydrology: An introduction*. Cambridge University Press.

Carman, P. C. (1937). Fluid flow through granular beds. *Transactions. Institute of Chemical Engineers*, *15*, 150–166.

Caviedes-Voullième, D., Ahmadinia, E., & Hinz, C. (2021). Interactions of microtopography, slope and infiltration cause complex rainfall-runoff behavior at the hillslope scale for single rainfall events. *Water Resources Research*, *57*, e2020WR028127. https://doi.org/10.1029/2020WR028127

Choi, C. S., Cagle, A. E., Macknick, J., Bloom, D. E., Caplan, J. S., & Ravi, S. (2020). Effects of revegetation on soil physical and chemical properties in solar photovoltaic infrastructure. *Frontiers in Environmental Science*, *8*, 1–9. https://doi.org/10.3389/fenvs.2020.00140

Cook, L. M., & McCuen, R. H. (2013). Hydrologic response of solar farms. *Journal of Hydrologic Engineering*, *ASCE*, *18*(5), 536–541. https://doi.org/10.1061/(ASCE)HE.1943-5584.0000530

Courant, R., & Hilbert, D. (1962). *Methods of Mathematical Physics*, vol. 2, Wiley-Interscience.

Dupraz, C., Marrou, H., Talbot, G., Dufour, L., Nogier, A., & Ferard, Y. (2011). Combining solar photovoltaic panels and food crops for optimising land use: Towards new agrivoltaic schemes. *Renewable energy*, *36*, 2725–2732.

Elamri, Y., Cheviron, B., Mange, A., Dejean, C., Liron, F., & Belaud, G. (2018). Rain concentration and sheltering effect of solar panels on cultivated plots. *Hydrology and Earth System Sciences*, *22*, 1285–1298. https://doi.org/10.5194/hess-22-1285-2018

Giráldez, J. V., & Woolhiser, D. A. (1996). Analytical integration of the kinematic equation for runoff on a plane under constant rainfall rate and smith and Parlange infiltration. *Water Resources Research*, *32*(11), 3385–3389.

Green, W. H., & Ampt, G. A. (1911). Studies of soil physics, I, flow of air and water through soils. *The Journal of Agricultural Science*, *4*, 1–24.

Guarracino, L., Rötting, T., & Carrera, J. (2014). A fractal model to describe the evolution of multiphase flow properties during mineral dissolution. *Advances in Water Resources*, *67*, 78–86. https://doi.org/10.1016/j.advwatres.2014.02.011

Hernandez, R. R., Easter, S. B., Murphy-Mariscal, M. L., Maestre, F. T., Tavassoli, M., Allen, E. B., Barrows, C. W., Belnap, J., Ochoa-Hueso, R., Ravi, S., & Allen, M. F. (2014). Environmental impacts of utility-scale solar energy. *Renewable and Sustainable Energy Reviews*, *29*, 766–779. https://doi.org/10.1016/j.rser.2013.08.041

IPCC, Intergovernmental Panel on Climate Change. (2014). Climate change: Impacts, adaptation, and vulnerability. Part A: Global and sectoral aspects. In C. B. Field, et al. (Eds.), *Contribution of Working Group II to the Fifth Assessment Report of the Intergovernmental Panel on Climate Change*. Cambridge Univ Press.

IRENA. (2019). Future of solar photovoltaic: Deployment, investment, technology, grid integration and socio-economic aspects (A global energy transformation: paper), International Renewable Energy Agency, Abu Dhabi.

Kincaid, D. C., Solomon, K. H., & Oliphant, J. C. (1996). Dropsize distribution for irrigation sprinklers. *Transactions of the American Society of Agricultural Engineers*, *39*(3), 839–845.

Kohl, R. A. (1974). Drop size distribution from a medium sized agricultural sprinkler. *Transactions of the American Society of Agricultural Engineers*, *17*(5), 690–693.

Kostyakov, A. N. (1932). On the dynamics of the coefficient of water percolation in soils and on the necessity of studying it from a dynamic point of view for purpose of amelioration. Trans Sixth Committee International Soc Soil Sci, Part A, Russian, pp. 17–21.

Kozeny, J. (1927). Über kapillare leitung des wassers im boden. *Sitzungsber Akad Wiss*, *136*, 271–306.

Lambert, Q., Bischoff, A., Cueff, S., Cluchier, A., & Gros, R. (2021). Effects of solar park construction and solar panels on soil quality, microclimate, CO_2 effluxes, and vegetation under a Mediterranean climate. *Land Degradation Development*, *32*(18), 5190–5202. https://doi.org/10.1002/ldr.4101

Lawrence, D. S. L. (1997). Macroscale surface roughness and frictional resistance in overland flow. *Earth Surface Processes and Landforms*, *22*, 365–382.

McDonnell, J. J., Spence, C., Karran, D. J., van Meerveld, H. J., & Harman, C. J. (2021). Fill-and-spill: A process description of runoff generation at the scale of the beholder. *Water Resources Research*, *57*, e2020WR027514. https://doi.org/10.1029/2020WR027514

PNIEC. (2023). Integrated National Energy and Climate Plan. https://commission.europa.eu/energy-climate-change-environment/implementation-eu-countries/energy-and-climate-governance-and-reporting/national-energy-and-climate-plans_en

Roels, J. M. (1984). Flow resistance in concentrated overland flow on rough slope surfaces. *Earth Surface Processes and Landforms*, *9*, 541–551.

Römkens, M. J. M., Baumhardt, R. L., Parlange, M. B., Parlange, J.-Y., Whisler, F. D., & Prasad, S. N. (1985). Effect of rainfall characteristics on seal hydraulic conductance. In F. Callebaur, D. Grabriels, & M. DeBoodt (Eds.), *Proceedings of International Symposium on the Assessment of Soil Surface and Crusting* (pp. 228–235). Flanders Research Center for Soil Erosion and Soil Conservation.

Roth, R. L. (1971). Roughness during border irrigation. [Masters dissertation, Univ. of Arizona, Tucson, AZ, USA].

Singh, V. P., & Su, Q. (2022). Irrigation engineering. In *Principles, processes, procedures, design, and management*. University Press.

Singh, V. P., & Yu, F. X. (1987). A mathematical model for border irrigation I. Advance and storage phases. *Irrigation Science*, *8*, 151–174.

Slattery, M. C., & Bryan, R. B. (1994). Surface seal development under simulated rainfall on an actively eroding surface. *Catena*, *22*(1), 17–34. https://doi.org/10.1016/0341-8162(94)90063-9

Su, L., Wang, Q., Shan, Y., & Zhou, B. (2016). Estimating soil saturated hydraulic conductivity using the Kostiakov and Philip infiltration equations. *Soil Science Society of America Journal*, *80*, 1463–1475. https://doi.org/10.2136/sssaj2016.04.0125

van Dijk, A. I. J. M., Bruijnzeel, L. A., & Rosewell, C. J. (2002). Rainfall intensity–kinetic energy relationships: A critical literature appraisal. *Journal of Hydrology*, *261*, 1–23.

Wang, F., & Gao, J. (2023). How a photovoltaic panel impacts rainfall-runoff and soil erosion processes on slopes at the plot scale. *Journal of Hydrology*, *620*, 129522.

Woolhiser, D. A., & Liggett, J. V. (1967). Unsteady, one-dimensional flow over a plane—The rising hydrograph. *Water Resources Research*, *3*(3), 753–771.

Wu, C., Liu, H., Yu, Y., Zhao, W., Liu, J., Yu, H., & Yetemen, O. (2022). Eco-hydrological effects of photovoltaic solar farms on soil microclimates and moisture regimes in arid Northwest China: A modeling study. *Science of the Total Environment*, *802*, 149946. https://doi.org/10.1016/j.scitotenv.2021.149946

Yair, A., & Lavee, H. (1985). Runoff generation in arid and semi-arid zones. In M. G. Anderson & T. P. Burt (Eds.), *Hydrological forecasting* (pp. 183–220). Wiley.

Zainol Abidin, M. A., Mahyuddin, M. N., & Mohd Zainuri, M. A. A. (2021). Solar photovoltaic architecture and agronomic management in agrivoltaic system: A review. *Sustainability*, *13*(14), 7846. https://doi.org/10.3390/su13147846

Zimmermann, A., Schinn, D. S., Francke, T., Elsenbeer, H., & Zimmermann, B. (2013). Uncovering patterns of near-surface saturated hydraulic conductivity in an overland flow-controlled landscape. *Geoderma*, *195–196*, 1–11.

How to cite this article: Baiamonte, G., Gristina, L., & Palermo, S. (2023). Impact of solar panels on runoff generation process. *Hydrological Processes*, *37*(12), e15053. https://doi.org/10.1002/hyp.15053

APPENDIX A: The GA-KW model

The Green-Ampt Kinematic wave model (GA-KW) model deals with the analytical solution of kinematic wave equations for overland flow occurring in a hillslope where the infiltration process is governed by the Green-Ampt model (Baiamonte & Agnese, 2010). The kinematic wave equations can be derived by the so-called shallow water equations (Brutsaert, 2005), expressing the conservation of mass and momentum, respectively:

$$\frac{\partial h}{\partial t}+L\frac{\partial q}{\partial x}=(i \quad f), \tag{A1}$$

$$\frac{\partial u}{\partial t}+u\frac{\partial u}{\partial x}+g\frac{\partial h}{\partial x}=g(S_0 \quad S_f) \quad \frac{u}{h}(i \quad f), \tag{A2}$$

where h is the mean depth of flow, t is the time, L is the hillslope length, q is the specific discharge, x is the downslope distance from the top of the hillslope, i is the rainfall intensity, f is the infiltration capacity, u is the flow velocity, g is the acceleration due to gravity, S_0 is the bed slope, and S_f is the friction slope. Under the assumption that the inertia and diffusion effects are negligible with respect to that of gravity and of friction, Equation (A2) simply reduces to $S_f = S_0$. Physically, this equivalence states that the friction slope is assumed to be equal to the bed slope, therefore the Manning equation can be written as a function of S_0:

$$q=\left(\frac{\sqrt{S_0}}{n_{\text{Mann}}L}\right)h^m=k_*h^m, \tag{A3}$$

where n_{Mann} is the Manning friction factor, m accounts for the flow regime (m is usually taken to be equal to 5/3 for turbulent flow, to 2 for transitional flow and to 3 for laminar flow) and the k_* parameter (in brackets) consolidates the hillslope 'geometry' (length, slope and roughness).

By assuming the common initial and boundary conditions of null water depth $h(0, t) = h(x, 0) = 0$, Equations (A1) and (A3) lead to:

$$\frac{\partial h}{\partial t}+m\,k_*L\,h^{m\ 1}\frac{\partial h}{\partial x}=(i \quad f). \tag{A4}$$

Equation (A4) describes the kinematic wave approximation and can be solved by the method of characteristics (Courant & Hilbert, 1962), which converts Equation (A4) to a pair of ordinary differential equations, expressing the time variation of water depth:

$$\frac{dh}{dt}=r(t)=i \quad f(t), \tag{A5}$$

and the characteristic curve:

$$\frac{dx}{dt}=L\frac{dq}{dh}=m\,k_*\,L\,h^{m\ 1}=m\,u. \tag{A6}$$

The unique relationship between q and h, expressed by (A3), together with (A5) and (A6) allows to state that an imaginary observer moving in x t plane at a speed equal to the kinematic wave celerity would see the flow rate increases at a rate equal to the lateral inflow (i f). The characteristic curves may be grouped in several domains, recognizable in a x t plane, depending on their origin: the distance axis at the time to ponding for the first domain, the part of the time axis from t_p up to the duration of rain, t_r, for the second domain, and the rest of x t plane for the third domain (falling limb).

According to the Green and Ampt model, the infiltration rate $f(t)$ in Equation (A5) is given by:

$$t \quad t_p=t_c\left(\frac{K_s}{(f \quad K_s)} \quad \frac{K_s}{(i \quad K_s)}+\Psi\right), \tag{A7}$$

where t_p is the time to ponding, t_c is the sorptivity time scale (Equation (2)), K_s is the saturated hydraulic conductivity, and the dimensionless function Ψ is equal to:

$$\Psi=ln\left(\frac{i(f \quad K_s)}{f(i \quad K_s)}\right). \tag{A8}$$

By using Equation (A7), the cumulative depth of rainfall excess at any instant t, $h(t)$, was derived (Baiamonte & Agnese, 2010):

$$h(t)=\int_{t_p}^{t}r(t)dt=\int_{t_p}^{t}(i \quad f(t))dt=t_c\left(\frac{i \quad f}{f \quad K_s}K_s+i\,\Psi\right), \tag{A9}$$

where $r(t)$ is the instantaneous rainfall excess. Under the assumption of transitional flow regime ($m = 2$), in the following only the solutions provided by the integration of the kinematic equations in the first two domains (Baiamonte & Agnese, 2010; Giráldez & Woolhiser, 1996) are reported.

Domain 1: Characteristic originating at **($0 < x < L, t = t_p$)**

For the first domain, at the time to ponding, characteristics, originating at any section distant x_0 from the top of the hillslope, are defined as:

$$\int_{x_0}^{x}dx=m\,k_*L\int_{t_p}^{t}h^{m\ 1}dt=m\,k_*L\int_0^h\frac{h^{m\ 1}}{i \quad f}dh. \tag{A10}$$

Integration of Equation (A10) provided (Baiamonte & Agnese, 2010):

$$\frac{x}{L}=\frac{t_c^2\,k_*}{(f \quad K_s)^2(i \quad K_s)}\cdot\Big[(i \quad f)(f+i \quad 2K_s)K_s^2 +i(i \quad K_s)(f \quad K_s)\Psi(2K_s+(f \quad K_s)\Psi)\Big]. \tag{A11}$$

Domain 2: Characteristic originating at **($x = 0, t_p < t < t_r$)**

To analytically derive the characteristic curves of the second domain, originating at any time $t_0 > t_p$, it is first necessary to express the water depth h as a function of t_0 (through f_0):

$$h=\int_{t_0}^{t}(i \quad f)dt=(i \quad f)(t \quad t_0) \quad \int_f^{f_0}(t \quad t_0)df, \tag{A12}$$

where f_0 is the infiltration capacity at the time t_0. To integrate Equation (A10), Equation (A3) was applied by replacing the pair (t_p, i) with the pair (t_0, f_0), obtaining:

$$h = t_c\left(\frac{K_s(f_0 - f)(i - K_s)}{(f - K_s)(f_0 - K_s)} + i\Psi_0\right), \tag{A13}$$

where Ψ_0 function is defined by:

$$\Psi_0 = ln\left(\frac{f_0(f - K_s)}{f(f_0 - K_s)}\right), \tag{A14}$$

Finally, to derive characteristics in the second domain, Equation (A13) can be used for the integration of Equation (A6), which for $m = 2$, yielded (Baiamonte & Agnese, 2010):

$$\frac{x}{L} = \frac{t_c^2 k_*}{(f - K_s)^2(f_0 - K_s)^2}\left((f_0 - f)K_s^2\right)\left[2ff_0 - fi + f_0 i - (f + 3f_0)K_s + 2K_s^2\right] + 2[f(f_0 - i) + f_0(i - K_s)](f - K_s)(f_0 - K_s)K_s\Psi_0 + i(f - K_s)^2(f_0 - K_s)^2\Psi_0^2. \tag{A15}$$

Solutions in Equations (A11) and (A15), together with Equation (-A3) allow deriving the rising limbs of the hydrographs displayed in Figure 6a,b and in Figure 7a,b, in terms of specific discharges, q (mm/h). The kinematic arrival time t_k, and the corresponding infiltration capacity, f_k, separating the 1st and 2nd domains (Figure 7a,b) are given in dimensionless terms by Equations (5a) and (5b).

Journal of Hydrology 620 (2023) 129522

Contents lists available at ScienceDirect

Journal of Hydrology

journal homepage: www.elsevier.com/locate/jhydrol

Research papers

How a photovoltaic panel impacts rainfall-runoff and soil erosion processes on slopes at the plot scale

Feng Wang [a,c], Jihui Gao [b,*]

[a] School of Water and Environment, Chang'an Univeristy, Xi'an 710054, China
[b] State Key Laboratory of Hydraulics and Mountain River Engineering, Sichuan University, Chengdu 610065, China
[c] Key Laboratory of Subsurface Hydrology and Ecological Effect in Arid Region of Ministry of Education, Xi'an 710054, China

ARTICLE INFO

This manuscript was handled by Marco Borga, Editor-in-Chief, with the assistance of Kelly Kibler, Associate Editor

Keywords:
Photovoltaic panel
Hillslope
Rainfall-runoff
Soil erosion
Rainfall simulation

ABSTRACT

Photovoltaic (PV) power plants are fast growing worldwide due to the environmental benefit of solar power generation and the development of photovoltaic technology. However, the impacts of PV panels on rainfall-runoff and soil erosion processes in hillslope are not well understood. This study quantitatively investigated these impacts on a plot-scale slope through rainfall simulation experiments. A bare plot with in-situ loess soil in the Chinese Loess Plateau was divided to two 4 m × 1 m slopes (i.e., a test slope with a PV panel above its middle and a control slope without cover) as the study site in which 1-hr artificial rainfall with varying intensities (30 mm hr^{-1} to 100 mm hr^{-1}) were conducted. The result showed that runoff volume, peak flow discharge rate and overland flow velocity were not remarkably different between the panel slope and the control slope, although the soil surface under the PV panel was rougher than the surface of the control slope. However, the slope with the PV panel produced 27 %–63 % less sediment flux at the outlet than the control slope, especially under heavy rainfall. This was attributed to the weakened splash erosion on the slope section under the PV panel due to the rainfall interception by the panel, which indicated that the key impact of the PV panel was preventing soil detachment by raindrop impacts. The PV panel delayed runoff start time under rainfall with heavy rainfall intensities (80 and 100 mm hr^{-1}) due to the overland flow attenuation of the depression beneath the lower edge of the PV panel. These findings implied that PV panels on hillslopes may have the potential to retain soil organic matter in top soil layers and to improve soil structure (e.g., soil sealing control and soil aggregate protection), which may benefit to hillslope soil conservation and vegetation restoration in long term.

1. Introduction

Hillslope hydrology including rainfall-runoff and soil erosion processes is a major concern in many areas such as soil and water conservation, flood forecasting and agricultural sustainability development (Jia et al., 2013; Li and Pan, 2018; Morbidelli et al., 2018). Land use plays an important role in hillslope hydrological processes (Birch et al., 2021; Gao et al., 2018b). Recently, there is a new type of land use, the photovoltaic (PV) power plants (Hernandez et al., 2015), which may largely affect the hillslope rainfall-runoff and soil erosion processes, but has not been fully understood in hillslope hydrology (Shobe, 2022).

Among renewable energy recourses, the facility of solar energy usually possesses long lifespan and low life-circle carbon emission, and it has a great potential to meet the future energy demand and to mitigate the anthropogenic impact on climate change (Creutzig et al., 2017; Martinopoulos and Tsalikis, 2018). In recent years, solar PV technologies, which convert light directly to electricity, have been one of the fastest growing energy technologies because of technological advancements and policy supports (Dinesh and Pearce, 2016; Hu et al., 2016; Tawalbeh et al., 2021). The global cumulative solar PV capacity reached 602 GW in 2019, which had doubled in three years (IEA, 2021). In China, the PV markets are expending very fast, and the cumulative installed PV capacity had a triple growth from 77.4 GW in 2016 to 205.2 GW in 2019 (IEA, 2021) and will reach 600 GW before 2030 (Wang et al., 2021b). Some researchers estimate that around 250000 km^2 of land will be transformed in the next 30 years if all PV panel arrays are ground-mounted, under an optimistic scenario for global solar energy deployment by 2050 (8500 GW) (Choi et al., 2020). Particularly, the PV power plants in the Chinese Loess Plateau are growing fast since 2013. For instance, the total area of the PV power plants in Ningxia province

* Corresponding author.
E-mail address: [redacted]@outlook.com (J. Gao).

https://doi.org/10.1016/j.jhydrol.2023.129522
Received 10 October 2022; Received in revised form 28 March 2023; Accepted 11 April 2023
Available online 14 April 2023

which mostly located in the Loess Plateau was estimated at 134.6 km^2 by the year of 2019, nearly tripled compared to 2013, from remote sensing data (Xia et al., 2022). Most of these power plants are over 10 km^2 and located in sparse grasslands and aridlands (Kruitwagen et al., 2021; Xia et al., 2022).

However, PV power plants require large areas due to the low density of solar energy (Wang et al., 2021a). Hillslope areas contain a large portion of land which is suitable for large-scale PV installations (Fig. 1) (Kim and Park, 2021; Yang et al., 2019), and there is a wide range of acceptable slopes for PV power plant installation (from 5 to 11.3°) (Anwarzai and Nagasaka, 2017; Charabi and Gastli, 2011; IRENA, 2013; Yushchenko et al., 2018). Furthermore, Yang et al. (2019) estimated the large-scale PV power generation potential in China using a GIS-based model, and indicated that the large-scale PV power plants should be planned in areas with slope lower than 20°.

Due to the structure of PV arrays, solar radiation and rainfall can be intercepted to a great extent by PV panels (Elamri et al., 2018; Yue et al., 2021). Many studies focused on the solar radiation reduction of PV panels which has direct impacts on evaporation, wind speed, air temperature, and soil temperature (Armstrong et al., 2016; Barron-Gafford et al., 2019; Lambert et al., 2021; Liu et al., 2019). On the other hand, rainfall interception due to PV panels, which can be vital to rainfall-runoff and soil erosion processes in hillslopes, is not comprehensively investigated by now. The raindrops intercepted by PV panels during rainfall will concentrate along the lower edges of PV panels and fall onto ground surface, causing heterogeneous spatial distribution of rainfall (Barron-Gafford et al., 2019; Jahanfar et al., 2019). Some researches indicated that runoff in slopes or hillslopes can be increased by PV panels. Jahanfar et al. (2019) conducted a long-term study comparing the discharge between the green roofs with or without PV panels, and the results indicated that the PV panels increased the cumulative discharge about 30% and the peak discharge over 50% in rainfall events. Pisinaras et al. (2014) quantified the hydrological budget constituents of PV power plants using SWAT model. They found that annual surface runoff was increased at the catchment scale as the land use changed from agriculture to PV power plants. However, from another perspective, the interception of raindrops by the PV panels could dramatically reduce the areas where rain splash erosion occurs (Elamri et al., 2018). The reduction of splash erosion may not only decrease hillslope soil erosion (Darvishan et al., 2014), but also reduce soil surface sealing which may lead to higher surface hydraulic conductivity (infiltration) and less runoff (Armenise et al., 2018; Assouline, 2004). Besides, Cook and McCuen (2013) adapted numerical models to analyze runoff from solar panel sites under pre- and post-development conditions. They found that the PV panels did not have a significant effect on runoff volumes, peak discharges, or time to peak discharge. The influence of PV panels on hillslope runoff is complicated and unclear, as some researchers think PV panels increase hillslope runoff while others believe PV panels have negative or negligible effect on hillslope runoff. Also, it can be inferred that the impact of PV panels on hillslope soil erosion process, which may cause large environmental and economic consequences such as soil loss and land degradation (Alewell et al., 2019; Prosdocimi et al., 2016), is complicated because it is susceptible to hillslope runoff process. Generally, there is a lack of comprehensive researches focusing on the mechanisms of PV panel impacts on hydrological and sediment processes, especially on hillslope soil erosion process which have not been studied yet (to the authors' knowledge) by field experiments. As PV power plants have been widely installed in hillslopes in arid and semi-arid regions, there is a concern that hillslope erosion might be enhanced due to the rainfall redistribution of PV panels.

Rainfall simulation is extensively used as a research tool in studies on overland flow and soil erosion (e.g., Di Prima et al., 2018; Shi et al., 2012), as well as studies on their responses to the changes of land use

Fig. 1. Photovoltaic power plants in hillslopes in the Loess Plateau of China. (The top two figures were from sohu.com; the bottom two figures were from Shanxi Economic Daily.).

and soil property (e.g., Fang et al., 2015; Keesstra et al., 2019). By controlling variables or conditions strictly, rainfall simulation is able to produce detailed experiment data of runoff and soil erosion focusing on the effect of a specific factor (Cuomo et al., 2016). Plot scale rainfall simulation experiments allow the accurate measurements of overland flow rate, soil sediment flux, microtopography change, etc., which usually help to find principal mechanisms in rainfall-runoff and soil erosion processes (e.g., runoff generation, dynamics of erosion and deposition) (Han et al., 2021; Martínez-Murillo et al., 2013; Ran et al., 2018; Zhang et al., 2018).

With the fast growth of PV power industry, the knowledge of the hydrological effects of PV panels in hillslopes is essential for the plans of PV power plant construction especially in arid and semi-arid regions. In this study, rainfall simulation experiments on slopes were conducted to investigate how a PV panel impacts rainfall-runoff and soil erosion processes in a slope, which may provide guidance for siting PV plants and evaluating the hydrological effects of PV power plants.

2. Methodology

2.1. Slope experiment set-up

This experimental study was conducted at a study plot located near the Hancheng city, Shannxi, China (35.31°N, 110.39°E), and the plot had a natural land surface which had very sparse grass on it. Two 4 m × 1 m slopes (i.e., a test slope with a PV panel coving the middle of the slope and a control slope with no covering) in the plot were set up, and the two slopes were divided by 0.7 m-high plastic plates (Fig. 2). The plastic plates which were to delimit the experimental slopes were vertically and carefully inserted into the soil with minimized disturbance to the soil. The slope gradient of the experiment slopes is about 8.7%, which is within the range of normal slope for PV power plants (Anwarzai and Nagasaka, 2017; IRENA, 2013; Yushchenko et al., 2018). The soil of the experimental plot was silt loam (with 14% clay, 67% silt, and 19% sand), and the porosity and bulk density of the soil were 0.48 and 1.24 g cm ^{3}, respectively. The sparse grass cover of the two slopes was carefully pulled out and removed one week before the rainfall experiment in order to minimize the ground surface difference between the test slope and control slope. The study plot was surrounded by 0.2 m-high plastic plates to prevent possible water loss due to splashing-out. Two runoff collectors were set at the outlets of the test and control slopes, which directed overland flow into containers for measurement.

A downslope-facing PV panel was placed in the middle of the test slope (Fig. 2c). It has a size of 1650 mm (length) × 950 mm (width) × 40 mm (thickness), which is commonly adopted in PV power plants. The fixed mounting PV system was chosen, and the lower edge of the PV panel was 0.5 m above the ground with the panel having a 30° angle with the ground surface. These setups of the PV panel were according to typical PV power plants in the north of China (please note that these PV panel settings are not representative of many modern PV arrays which tilt dynamically to track the sun)..

The rainfall simulator consisted of a water tank, a pressure-

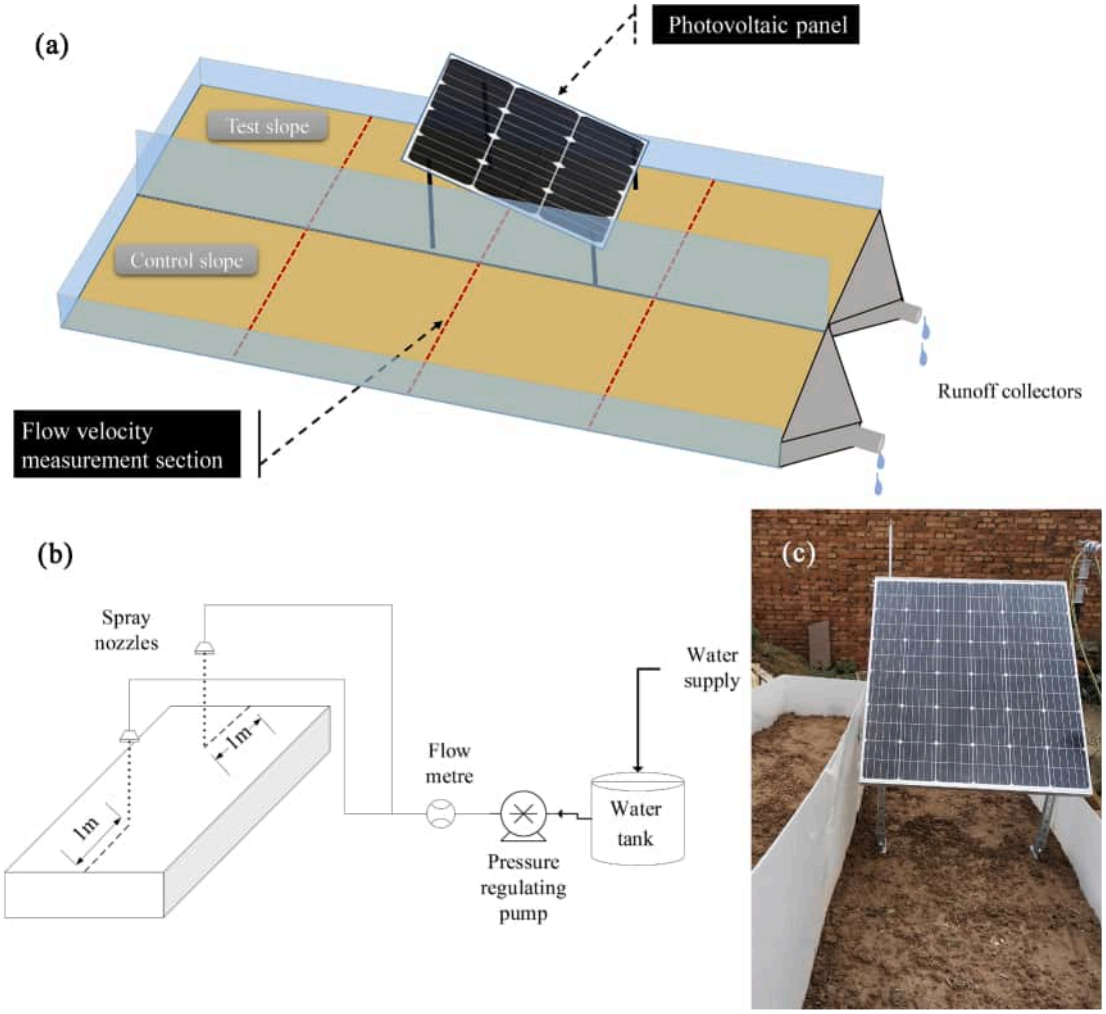

Fig. 2. The instrument set-up: (a) the schematic representation of the study plots, (b) the rainfall simulator set-up, and (c) the PV panel placed on the test slope.

096

regulating pump, two spray nozzles, a flow meter, a steel bracket, and pipelines (Fig. 2b). The spray nozzles that generated raindrops in experiment were 1/4 HH Fulljet model from Spraying Systems Co., which had a spray angle of 60°. The nozzles of the Fulljet model have been applied for rainfall simulation in many experimental studies (e.g., Abrantes et al., 2018; Loiola et al., 2019) and it well simulated natural rainfall in these studies. The position and direction of the spray nozzles are shown in Fig. 2b. The height of the nozzle was 3.5 m above the slope, allowing the water drops to reach their settling velocity before hitting the panel and ground. The mean size of the simulated raindrops was 1.7 mm diameter (having a range of 0.5–3.5 mm) which was measured in rainfall experiment with the filter paper method (Best, 1950). This indicated that the simulated rainfall was similar to the natural one in mean raindrop size (Best, 1950).

The rainfall intensity was precisely controlled by the pressure regulating pump, and the rainfall intensity and spatial uniformity was calibrated and tested before the experiment. After using a large plastic sheet to cover the two slopes, the rainfall intensity was determined with 10 rain gauges (each with 15 cm inner diameter and 20 cm height), which were distributed uniformly above the two slopes. The rainfall spatial uniformity is calculated using the coefficient of uniformity (CuC) defined by Christiansen (1941):

$$CuC = 1 \quad \frac{\sum_1^N |x_i \quad \bar{x}|}{N\bar{x}} \tag{1}$$

in which x_i is the rainfall amount in each rain gauge, $\bar{x}$ is the average amount of rainfall and N is the total number of the rain gauges placed over the plot to collect rainfall. After the test, the simulated rainfall had the CuCs higher than 0.8 for all the rainfall intensities used in the experiment, indicating that the simulated rainfall can be considered spatially uniform (Aksoy et al., 2012).

2.2. Experiment design

In this study, four rainfall scenarios were considered in the rainfall experiment, which fell into two rainfall intensity ranges (Table 1). According to the rainfall frequencies in the south of the Chinese Loess Plateau (Ran et al., 2020), the scenarios with 30 mm hr^{-1} and 50 mm hr^{-1} rainfall intensities represented moderate rainfall, and the scenarios with 80 mm hr^{-1} and 100 mm hr^{-1} rainfall intensities represented typical storms (Table 1). Under all these rainfall intensities, infiltration-excess overland flow dominated during the rainfall experiments. The rainfall duration of each scenario run is 1 h. There was an around-10-day interval between each two successive rainfall scenarios, achieving similar initial soil water content from 25 % to 27 % (in the 0–5 cm top soil layer) before each rainfall simulation run. The daily rainfall and air temperature of the study site was shown in Fig. 3.

Four days before the first experiment, a rainfall run with 20 mm hr^{-1} intensity and 10 min duration were conducted on the study plot. The reasons of this pretreatment rainfall were: firstly, make the surface soil reach a high moisture level which is close to that during rainy season at the Loess Plateau, as most rainfall and soil erosion occurs in rainy season in this semi-arid region; secondly, as the soil surface was a little bit disturbed due to the removal of the very sparse grass, the water penetration during the short and light artificial rainfall can help smooth the soil surface and diminish the small impact of the grass removal.

In this study, no extra replication of each rainfall scenario was conducted. This was because this experimental study was conducted in a field study site with natural land surface. The microtopography of the slopes was changed after each rainfall experiment due to soil erosion (e.g., the development of rill and gully) which may considerably influence surface flow process. Due to these alterations, replication under identical rainfall intensity is not possible because there is no way to restore the pre-existing surface microtopography. At the same time, the runoff and soil-erosion differences between the PV panel slope and the control one was the key observable in this study. Hence, the comparisons of the runoff and soil erosion results of the two slopes and whether these comparison results were consistent under varying rainfall intensities were important in this study.

In each scenario run, overland flow and sediment samples were taken in every minute at the two outlets of the slopes during the first 15 min after runoff generated, then the sampling interval was extended to 3–5 min as overland flow became stable. The sediment samples from the collector were dried at 110 °C for more than 24 hr and then weighed and recorded. Each slope was divided into 4 sections with equal spacing, with each section measuring 1 m × 1 m (Fig. 2a). The mean overland flow velocity in each section was determined by using the $KMnO_4$ dye tracer method (Abrahams et al., 1986; Zhang et al., 2010).

Table 1
Rainfall simulation runs.

No.	Intensity (mm hr^{-1})	Date
1	30	10/24/2021
2	50	11/04/2021
3	100	11/15/2021
4	80	11/25/2021

3. Results

3.1. Runoff

In the rainfall experiments, the runoff started 16.6 % and 4.0 % earlier in PV panel slope than that in the control slope under the 30 mm hr^{-1} and 50 mm hr^{-1} rainfall intensities, respectively. But, the start times were delayed 88.7 % and 178.8 % by the PV panel under the 80 mm hr^{-1} and 100 mm hr^{-1} rainfall intensities (Fig. 4 and Table 2), respectively.

Under different rainfall intensities, the total runoff of the PV panel slope was 0.7–4.0 % lower than that of the control slope (Table 2). The hydrographs of the two slopes were also quite close (see Fig. 5). The differences in peak discharge rates between the two slopes were lower than 3.5% (Table 2). For the runs under the 30 mm hr^{-1} and 50 mm hr^{-1} rainfall intensities, the runoff rate kept increasing until the rainfall stopped; while for the runs under the 80 mm hr^{-1} and 100 mm hr^{-1} rainfall intensities, the runoff rate quickly increased with time, approaching steady state about 5–8 min after rainfall started.

3.2. Soil erosion

Contrary to the runoff results, there were large differences between the soil erosion results of the two slopes. The soil erosion mass and average sediment concentration of the PV panel slope were 27 %–63 % lower than those of the control slope (Table 2). For instance, under the 80 mm hr^{-1} rainfall, the PV panel slope only produced 37 % soil erosion mass and 38 % average sediment concentration of the control slope.

For an individual event, the soil erosion rate increased quickly in the first 10–15 min, and then fluctuated in a range between 65 % and 100 % of the peak erosion rate (Fig. 5). As rainfall continued, the differences between the soil erosion rates of the PV panel slope and the control slope became greater. For example, under the 50 mm h^{-1} rainfall, differences between the soil erosion rates of the PV panel slope and the control slope increased from 23 % on average in the first 15 min to 45 % on average in the last 20 min.

3.3. Slope micro relief and overland flow velocity

The PV panel on the slope resisted a part of the raindrops and created concentrated water drops at its lower edge, which had an influence on the slope micro relief. A depression had been created under the lower edge of the PV panel by water drops since the first rainfall experiment run (Fig. 6b).

Compared with the relative smooth soil surface of the control slope

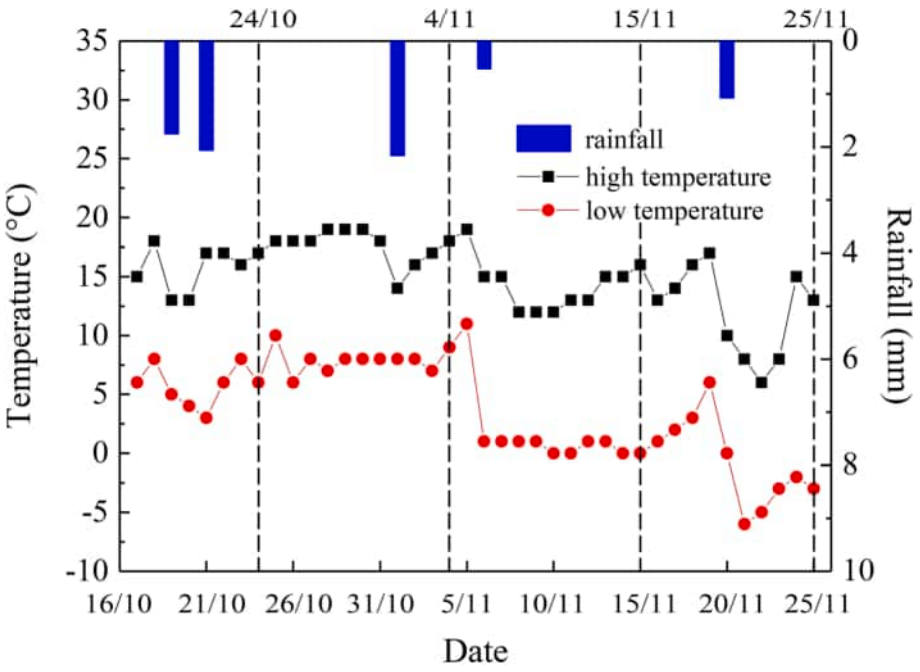

Fig. 3. The daily rainfall and the highest and lowest air temperature of the site between 16/10/2021 and 25/11/2021 (the dotted lines marking the date of each experiment).

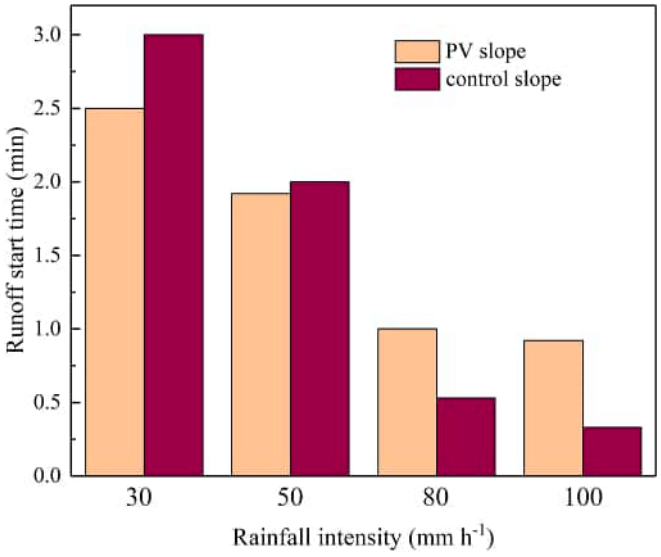

Fig. 4. The runoff start time under different rainfall intensities.

(Fig. 6a), the soil surface under the PV panel was rougher. For example, under the 80 mm hr^{-1} rainfall, a big part of the ground surface under the PV panel did not have soil surface seal (see the red square in Fig. 6b). Although there was obvious difference in micro relief between the two slopes, the mean overland flow velocities of the two slopes only have 1.5–4.0% difference (Fig. 7).

4. Discussion

4.1. The effect of PV panel on overland flow

The rainfall experiment results showed that the PV panel did not have remarkable influence on runoff volume and peak discharge rate at the slope outlet, although the PV panel on the slope blocked part of the raindrops during rainfall and created concentrated water drops at the lower edge of the panel. Previously, a modelling study conducted by Cook and McCuen (2013) also indicated that the installation of PV panels over a grassy field did not have considerable effect on the volume of runoff, the peak discharge, and the time to peak. In this study, the probable reasons were: on one hand, the interception of raindrops by the PV panel reduced the land surface area of infiltration, leading to the increase of runoff; on the other hand, the interception of raindrops also greatly reduced the soil surface sealing under the PV panel (Fig. 6b) so that more surface water infiltrate into area under the panel compared with the control slope due to the higher hydraulic conductivity of

Table 2
The runoff and sediment flux at the outlet in the rainfall experiments.

No.	Intensity (mm hr^{-1})	Slope condition	Runoff start time (min)	Total runoff (m^3)	Peak discharge rate (ml s^{1})	Total sediment flux (kg)	Average sediment concentration (kg m^{3})
1	30	With panel	2.5	0.078	24.8	0.48	6.15
		Control	3.00	0.080	25.2	0.67	8.38
2	50	With panel	1.92	0.142	47.2	0.94	6.62
		Control	2.00	0.144	47.8	1.23	8.54
3	80	With panel	1.0	0.252	84.0	1.93	7.66
		Control	0.53	0.254	81.2	3.15	12.40
4	100	With panel	0.92	0.324	102.2	1.54	4.75
		Control	0.33	0.338	103.0	2.46	7.28

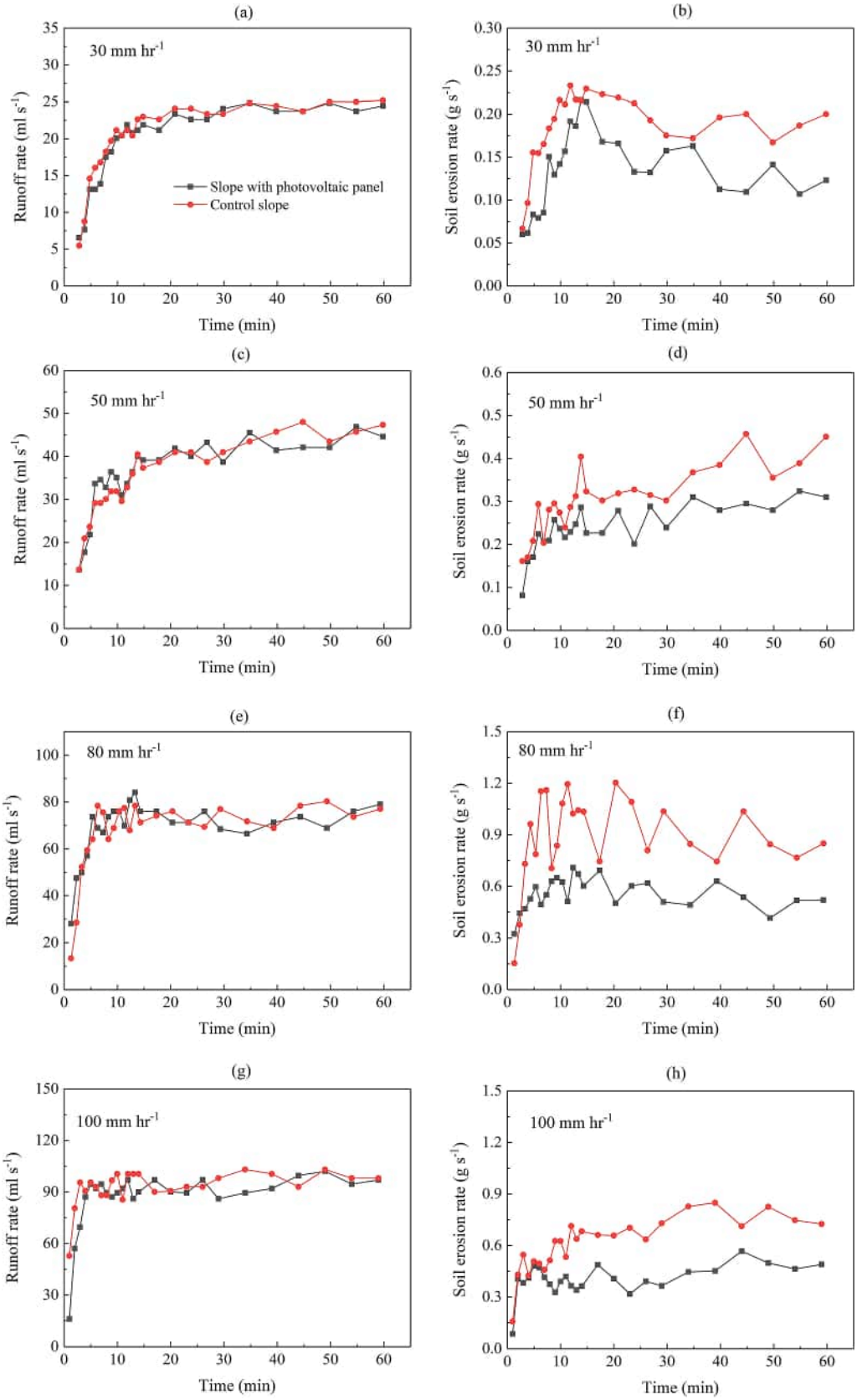

Fig. 5. Runoff rates (a, c, e, and f) and soil erosion rates (b, d, f, and h) during rainfall experiments.

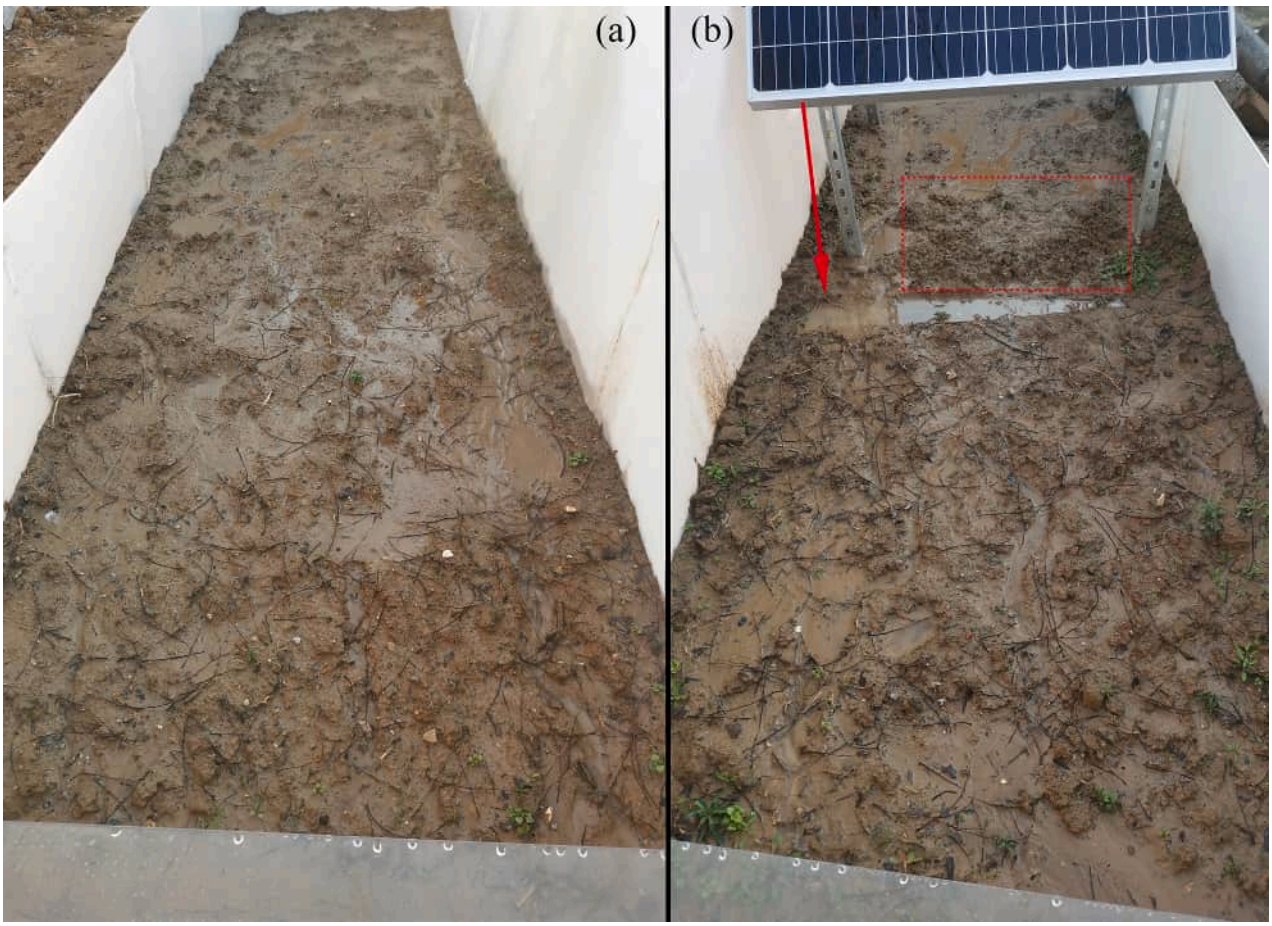

Fig. 6. The slope micro relief after the 80 mm hr^{-1} rainfall run on 25th Nov. 2021: (a) the control slope and (b) the PV panel slope. (The red arrow pointed to the depression created by the water drops at the lower edge of the PV panel, and the red square pointed out the rough soil surface under the PV panel.). (For interpretation of the references to colour in this figure legend, the reader is referred to the web version of this article.)

unsealed top soil layer. In consequence, the combined effect of the PV panel on infiltration may result in no large difference in runoff between the two slopes.

This finding was inconsistent with some previous studies, which indicated that the runoff volume and peak discharge rate of the PV panel hillslope may largely increase (Jahanfar et al., 2019). The experimental plots (with around 3% slope gradient) used in Jahanfar et al. (2019) were quite permeable on green roofs, in which saturation-excess overland flow seemed to be the dominate runoff generation mechanism and soil sealing should be highly limited. For their one-year experiment, the shading effect of PV panels can reduce evapotranspiration rate and largely increase the soil moisture content of the plots compared with the control plot, probably resulting in increase of runoff volume and peak discharge rate. Thus, unlike our study plot which dominated by infiltration-excess overland flow, changing in infiltration process did not affect runoff volume and peak too much in their study. This comparison implied that different runoff generation mechanisms may lead to different impacts of PV panels on rainfall-runoff process, which may need further investigation. Using SWAT model, Pisinaras et al. (2014) found that the land use change from agriculture to PV power plants can lead to increase in annual surface runoff and percolation potential, which seemed to be not parallel with the result of this study. This may be because that their modelling study area was over 100 km^2 and the time scale was many years (5 to 90 years) so their research scales were very different from those of this study which focused on plot-scale rainfall-runoff events. Under their much larger time and spatial scales, the impact of land use change from agriculture to PV power plants on land surface hydrology was the decrease of annual evaporation and the increase of soil water content of their study catchment. However, in this plot-scale study, the result above indicated that there was no large impact of the PV panel on infiltration in the short-time rainfall experiments, in which the evaporation difference of the two slopes can be ignored.

Under the moderate rainfall with the 30 mm hr^{-1} or 50 mm hr^{-1} intensity, the runoff start time of the PV panel slope was shorter than the control one. Because the PV panel quickly concentrated rain water at downslope area, the runoff started faster on the PV panel slope; while the runoff generated slowly on the control slope due to the moderate rainfall intensity. On the contrary, under heavy rainfall with 80 mm hr^{-1} or 100 mm hr^{-1} intensity, the runoff start time of the PV panel slope was later than the control slope. The rain water quickly filled the depressions and converged into overland flow on the control slope. However, in the PV panel slope, the small depression beneath the lower edge of the panel partly intercepted rain water at the beginning of rainfall, so it took longer to generate overland flow at the outlet than the control slope.

In general, the mean overland flow velocity was not affected by the PV panel (Fig. 7). It seemed that the rough soil surface beneath the PV panel did not considerably influence the mean overland flow velocity. This may be because, even though the soil surface under the PV panel was rougher than the control slope (Fig. 6), the most surface water from upslope flowed in the rills so the mean flow velocity was close to that on the control slope.

4.2. *The effect of PV panel on slope soil erosion process*

The PV panel slope produced much less soil erosion than the control

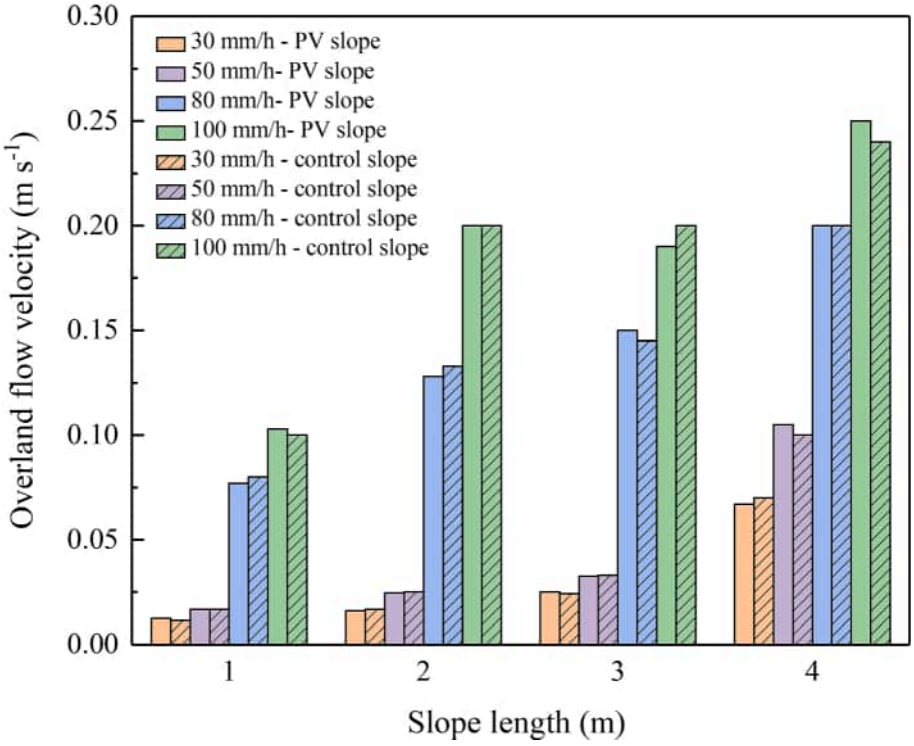

Fig. 7. The mean overland flow velocities at different slope sections after 30 min rainfall.

slope, especially under heavy rainfall. As there were restricted differences in the mean overland flow velocities on the two slopes and the discharge rates at the two outlets, it could be inferred that, for the two slopes, the sediment transport capacities of the slope section downslope from the position under the PV panel are close to the sediment transport capacities of the corresponding slope section of the control slope. Thus, the main reason for the decrease in soil erosion beneath the PV panel was most likely attributed to the fact that PV protected the soil surface from direct exposure to rainfall.

For the PV panel slope, the splash erosion on the slope section under the PV panel was effectively prevented due to the rainfall interception of the PV panel. Raindrop splash is important in the detachment and transport of soil particles during soil erosion process on slope (Chaplot and Poesen, 2012). Many previous studies focusing on hillslope erosion pointed out that attenuating raindrop impact can decrease soil erosion on slopes. By adapting metal or nylon meshes above the test slopes to minimize splash erosion, researchers found that soil erosion on slope decreased 10.0 %–86.8 % (Lu et al., 2016; Vaezi et al., 2017; Zhang et al., 2020). Thus, the interception of raindrops by the PV panel largely reduced the splash erosion in the slope.

On the other hand, although the PV panel also limited the formation of soil surface seal, which normally reduces soil surface erodibility and controls soil erosion (e.g., Lu et al., 2017; Luk et al., 1993), under the PV panel because of the absence of raindrops (Armenise et al., 2018; Assouline, 2004), the lack of this soil surface seal did not increase soil erosion in the experiments. This is because the soil erosion process in the slope section under the PV panel was mainly rill erosion and the interrill erosion was restricted (see Fig. 6) as sheet flow was mitigated due to raindrops blocking. Note that the surface area which rill erosion can directly impact is much smaller than that of interrill erosion which is driven by sheet flow. Hence, the lack of soil surface seal resulted in limited impact on soil erosion in the PV panel slope during the rainfall experiments. At the same time, overland flow from upslope area (which was the upstream area of the depression) in the PV panel slope was much less than that of the control slope because of the PV panel's rainfall interception. Less overland flow of the PV panel slope can only transport less sediment from the upslope area than the control slope, although the overland flow velocities were similar for both the slopes (see Fig. 7). Besides, the erosivity of water drops from the lower edge of the PV panel was greatly attenuated, during the most time of each rainfall, by the water pond which was created by the water drops from the PV panel in the early stage of each rainfall event. Even with their terminal velocities, the waterdrops normally lose their impact on the soil surface when they drop into depressions that deeper than 3 times of their diameters (Engel, 1967; Hartley and Alonso, 1991; Kinnell, 2012). In this experiment, the diameters of water drops running off PV panels were shorter than 10 mm and their terminal velocities would not be arrived with 0.5 m height to the ground. The water pond which reached a depth over 15 mm less than 3 min after rainfall started and absorbed most of the kinetic energy of the water drops.

Therefore, the PV panel reduced the splash erosion under it, and the absence of structural soil seal under the panel did not considerably affect the erosion process. The energy of the concentrated water drops (or falls) from the panel during rainfall did not did not have a meaningful impact on erosion and sediment transportation.

It should be noted that the 80 mm hr^{-1} scenario had much larger soil erosion rate than the 100 mm hr^{-1} one. This may be because that the 80 mm hr^{-1} scenario was conducted on 25th Nov. 2021 (Table 1and Fig. 3), when the air temperature was below 0 ℃ at night and above 0 ℃ during the daytime, so the freeze–thaw action may make the top-layer soil easier to be eroded (Sun et al., 2021a; Wang et al., 2017).

4.3. Limitations of the experiment

As a preliminary experimental study at the plot scale, the spatial scale of the result has not yet matched the larger scales of PV applications (e.g., big PV panel arrays or solar farms). With multiple PV panels (or arrays) above larger land surface, the impact of them on the runoff and soil erosion processes would be more complicated at these larger scales. Taking a hillslope with a PV panel array in the Chinese Loess Plateau as an example here, the experiment result above indicated that a single PV panel reduced soil erosion and did not meaningfully change

the total runoff amount during rainfalls, but there are many land surface patches without the cover of PV panels among covered patches in the hillslope. Hence, there would be concerns that whether these uncovered patches would be vulnerable to soil erosion and, on the other side, whether the covered patches lacking soil surface seal would be vulnerable to soil erosion, given that our study shows that PV panels do not inhibit runoff generation. If these are true, the positive effect of single PV panels on soil erosion reduction, which was found in this study, would be offset. However, in our opinion, these two offset effects would not be large. First, for the uncovered patches, given the topography and soil erosion features of hillslopes in arid and semi-arid regions such as the Chinese Loess Plateau, the development of widespread and complex rill and gully system in hillslope is fast and effective during rainfall-runoff processes (Hofer et al., 2012; Poesen et al., 2003) and thus the path length of sheet flow is usually not very long. This normally induces that sheet flow concentration may not large enough to transport much sediment in these uncovered patches. In fact, over 60% total erosion are derived to rill and gully erosion in the Loess Plateau (Shen et al., 2016; Sun et al., 2021b). Then for the covered patches, precipitation is intercepted by the PV panels during rainfall, which further mitigates sheet flow and its erodibility in the hillslope. Thus, the concerns of soil erosion reduction offset would not be fully realized. Definitely, this issue depends on the topography of the hillslope with the PV panel array and needs further field experiments to be dealt with.

However, the results of this pilot study may have a potential of being upscaled to help these investigations at larger scales. Based on the results, experiments with a PV panel block (consists of 2 or more panels) and further with large PV panel arrays can be purposefully designed and conducted in the next steps (e.g., to deal with the example raised above). The findings of these next-step works and this study would then improve the modelling of solar farm impact on runoff and erosion at the catchment scale, which will help to build new modules representing the mechanisms of PV panel impacts (found in the experiments) in catchment hydrological models. Meanwhile, the observations of runoff and sediment variations before and after a solar farm construction can be analyzed from the perspective provided by this experimental study to support the development and management of the solar farm.

The settings of the PV panel in the experiment, including the specific height and angle of panel, was according to the typical PV panel installations in Northern China (also similar to some installations in other arid and semi-arid regions), but this may be not representative of some modern PV panel setups which allow the panels to dynamically track the sun. At the same time, a water pond (15 mm depth) under the lower edge of the PV panel was created after the rainfall experiments in this study. It is worried about that, if a PV panel is higher and steeper than the one in this study, this type of 'plunge pool' would be much larger and bring additional risk of severe soil erosion. Although, in some real cases, higher or steeper PV panels can enlarge the dropping velocity of the water running off the panels (which may lead to deeper and larger depressions on the ground), this will cause larger water depth in the depressions which can effectively attenuate the erodibility of the dropping water. Normally, waterdrops with their terminal velocities can have meaningful impact within the range of 3 times of their diameters when they drop into water surface (Engel, 1967; Hartley and Alonso, 1991; Kinnell, 2012). The diameters of water drops running off PV panels have little chance to be longer than 10 mm and their terminal velocities would not be reached with small heights from ground (the heights of most PV panels in application are less than 3 m), which means that the depressions may not be deeper than 30 mm. Thus, this depression formation is a self-limited process and would not bring large additional soil erosion.

Finally, it should be noted that, in this study, the land surface of the pair slopes was bare and the PV panel was not set to be very high and steep, which may be favorable to the soil erosion difference between the two slopes. This mitigation effect of real-case application of a single PV panel may be changed depending on the conditions of it.

4.4. The potential benefits of PV panels for vegetation restoration and flood delay

The experiment results indicated that the PV panel can greatly reduce soil erosion in the slope (especially under heavy rainfall), which implied that, in natural hillslope in arid or semi-arid regions, PV panels may lead to retain organic matter (from plant litter) in the top soil layer under the PV panels. This organic matter retaining may be favorable to vegetation restoration under the PV panels in arid and semi-arid regions. As PV panels nowadays normally have long lifespans over 25 years (Xu et al., 2018), their long-term positive effect on soil conservation and vegetation restoration may be considerable and worthy further studies. For instance, in the Chinese Loess Plateau which suffered from the severe loss of soil and organic matter (Xin et al., 2011; Zhao et al., 2015) and the lack of precipitation (Gao et al., 2018a), PV panels, which have been generally considered to reduce evapotranspiration rate and increase soil moisture in hillslopes due to sunlight blocking (Jahanfar et al., 2020; Jiang et al., 2022), may help the vegetation restoration on the land surface under the panels in hillslopes due to this organic matter retaining effect. Meanwhile, as soil structure is important for soil functions (Rabot et al., 2018), rain drop interception of PV panels, which can lead to prevention of soil surface sealing and preservation of surface soil aggregates under PV panels, may attenuate soil function deterioration under the PV panels and promoted vegetation restoration. Certainly, all these benefits to vegetation restoration are contingent on PV panels aiding, or at least not reducing, the health of vegetation under PV panels, which needs more investigations to be fully verified.

Furthermore, as the overland flow generated more slowly on the PV panel slope under heavy rainfall than the control slope, it may be inferred that PV power plants, which can cover large area of a catchment, may delay the catchment flood start time or even the time to flood peak. This might bring potential benefit of flood delay in arid and semi-arid regions. Hence, the impacts of PV power plants on hydrological processes need to be explored at larger scales in the future.

5. Conclusions

In this study, a series of rainfall simulation experiments were conducted at a bare loess soil plot to investigate the impact of a PV panel on runoff and soil erosion processes in a plot-scale slope. The rainfall-runoff and soil erosion processes of a slope with a PV panel above the middle of it and a control slope with no cover were observed and compared.

The result indicated that the PV panel did not have considerable effect on runoff volume, peak flow discharge, and overland flow velocity. It may be due to the absence of structural soil seal under the PV panel causing more infiltration there, which offset the reduction of infiltration due to the interception of raindrops by the PV panel. However, the PV panel largely reduced slope soil erosion by 27 %–63 %. This is because of the weakened splash erosion on the slope section under the PV panel due to the rainfall interception by the panel. This finding indicated that the key impact of the PV panel is preventing soil detachment by raindrop impacts. Under heavy rainfall, a delay of overland flow generation was observed, which plausibly suggested that PV panels in hillslopes may have the potential to delay flood start time.

In this experimental study, it should be noted that the PV panel was set not very high and steep and the study slopes were bare, which may be favorable to the soil erosion difference between the two slopes. In real-case application of a single PV panel, the soil-erosion mitigation effect of the panel may be changed under varying conditions.

In arid and semi-arid regions, hillslopes with sparse vegetation, which suffer severe soil erosion, are quite common. Our findings implied that PV power plants in these hillslopes may lead to retaining of soil organic matter and improving of soil structure, which may benefit to hillslope soil conservation and vegetation restoration in long term. In the future studies, the advantage of PV panels on water and soil conservation and catchment ecology will be worthy of investigations.

CRediT authorship contribution statement

Feng Wang: Conceptualization, Methodology, Validation, Formal analysis, Investigation, Resources, Writing – original draft, Writing – review & editing, Funding acquisition. **Jihui Gao:** Conceptualization, Methodology, Validation, Formal analysis, Resources, Writing – original draft, Writing – review & editing, Supervision, Funding acquisition.

Declaration of Competing Interest

The authors declare that they have no known competing financial interests or personal relationships that could have appeared to influence the work reported in this paper.

Data availability

Data will be made available on request.

Acknowledgements

This research was financially supported by the National Key Research and Development Program of China (Grant No. 2019YFC1510603), the National Natural Science Foundation of China (Grant No. 42271038), and the Natural Science Basic Research Program of Shannxi (Grant No. 2021JQ-247).

References

Abrahams, A.D., Parsons, A.J., Luk, S.H., 1986. Field measurement of the velocity of overland flow using dye tracing. Earth Surface Processes Landforms 11 (6), 653–657. https://doi.org/10.1002/esp.3290110608.

Abrantes, J., Prats, S.A., Keizer, J.J., de Lima, J., 2018. Effectiveness of the application of rice straw mulching strips in reducing runoff and soil loss: Laboratory soil flume experiments under simulated rainfall. Soil Tillage Res. 180, 238–249. https://doi.org/10.1016/j.still.2018.03.015.

Aksoy, H., Unal, N.E., Cokgor, S., Gedikli, A., Yoon, J., Koca, K., Inci, S.B., Eris, E., 2012. A rainfall simulator for laboratory-scale assessment of rainfall-runoff-sediment transport processes over a two-dimensional flume. Catena 98, 63–72.

Alewell, C., Borrelli, P., Meusburger, K., Panagos, P., 2019. Using the USLE: Chances, challenges and limitations of soil erosion modelling. Int. Soil Water Conservation Res. 7 (3), 203–225. https://doi.org/10.1016/j.iswcr.2019.05.004.

Anwarzai, M.A., Nagasaka, K., 2017. Utility-scale implementable potential of wind and solar energies for Afghanistan using GIS multi-criteria decision analysis. Renew. Sustain. Energy Rev. 71, 150–160. https://doi.org/10.1016/j.rser.2016.12.048.

Armenise, E., Simmons, R.W., Ahn, S., Garbout, A., Doerr, S.H., Mooney, S.J., Sturrock, C.J., Ritz, K., 2018. Soil seal development under simulated rainfall: Structural, physical and hydrological dynamics. J. Hydrol. 556, 211–219.

Armstrong, A., Ostle, N.J., Whitaker, J., 2016. Solar park microclimate and vegetation management effects on grassland carbon cycling. Environ. Res. Lett. 11 (7), 074016 https://doi.org/10.1088/1748-9326/11/7/074016.

Assouline, S., 2004. Rainfall-induced soil surface sealing: a critical review of observations, conceptual models, and solutions. Vadose Zone J. 3, 570–591. https://doi.org/10.2136/vzj2004.0570.

Barron-Gafford, G.A., Pavao-Zuckerman, M.A., Minor, R.L., Sutter, L.F., Barnett-Moreno, I., Blackett, D.T., Thompson, M., Dimond, K., Gerlak, A.K., Nabhan, G.P., Macknick, J.E., 2019. Agrivoltaics provide mutual benefits across the food-energy-water nexus in drylands. Nat. Sustainability 2 (9), 848–855.

Best, A.C., 1950. The size distribution of raindrops. Q. J. R. Meteorolog. Soc. 76 (327), 16–36. https://doi.org/10.1002/qj.49707632704.

Birch, A.L., Stallard, R.F., Bush, S.A., Barnard, H.R., 2021. The influence of land cover and storm magnitude on hydrologic flowpath activation and runoff generation in steep tropical catchments of central Panama. J. Hydrol. 596, 126138.

Chaplot, V., Poesen, J., 2012. Sediment, soil organic carbon and runoff delivery at various spatial scales. Catena 88 (1), 46–56. https://doi.org/10.1016/j.catena.2011.09.004.

Charabi, Y., Gastli, A., 2011. PV site suitability analysis using GIS-based spatial fuzzy multi-criteria evaluation. Renew. Energy 36 (9), 2554–2561. https://doi.org/10.1016/j.renene.2010.10.037.

Choi, C.S., Cagle, A.E., Macknick, J., Bloom, D.E., Caplan, J.S., Ravi, S., 2020. Effects of Revegetation on Soil Physical and Chemical Properties in Solar Photovoltaic Infrastructure. Front. Environ. Sci. 8 https://doi.org/10.3389/fenvs.2020.00140.

Christiansen, J.E., 1941. The uniformity of application of water by sprinkler systems. Agri. Eng. 22 (3), 89–92.

Cook, L.M., McCuen, R.H., 2013. Hydrologic Response of Solar Farms. J. Hydrol. Eng. 18 (5), 536–541. https://doi.org/10.1061/(ASCE)HE.1943-5584.0000530.

Creutzig, F., Agoston, P., Goldschmidt, J.C., Luderer, G., Pietzcker, R.C., 2017. The underestimated potential of solar energy to mitigate climate change. Nat. Energy 2 (9), 17140. https://doi.org/10.1038/nenergy.2017.140.

Cuomo, S., Della Sala, M., Pierri, M., 2016. Experimental evidences and numerical modelling of runoff and soil erosion in flume tests. Catena 147, 61–70. https://doi.org/10.1016/j.catena.2016.06.044.

Darvishan, A.K., Sadeghi, S.H., Homaee, M., Arabkhedri, M., 2014. Measuring sheet erosion using synthetic color-contrast aggregates. Hydrol. Process. 28 (15), 4463–4471. https://doi.org/10.1002/hyp.9956.

Di Prima, S., Concialdi, P., Lassabatere, L., Angulo-Jaramillo, R., Pirastru, M., Cerdà, A., Keesstra, S., 2018. Laboratory testing of Beerkan infiltration experiments for assessing the role of soil sealing on water infiltration. Catena 167, 373–384.

Dinesh, H., Pearce, J.M., 2016. The potential of agrivoltaic systems. Renew. Sustain. Energy Rev. 54, 299–308. https://doi.org/10.1016/j.rser.2015.10.024.

Elamri, Y., Cheviron, B., Mange, A., Dejean, C., Liron, F., Belaud, G., 2018. Rain concentration and sheltering effect of solar panels on cultivated plots. Hydrol. Earth Syst. Sci. 22 (2), 1285–1298.

Engel, O.G., 1967. Initial Pressure, Initial Flow Velocity, and the Time Dependence of Crater Depth in Fluid Impacts. J. Appl. Phys. 38 (10), 3935–3940.

Fang, H., Sun, L., Tang, Z., 2015. Effects of rainfall and slope on runoff, soil erosion and rill development: an experimental study using two loess soils. Hydrol. Process. 29 (11), 2649–2658. https://doi.org/10.1002/hyp.10392.

Gao, G.Y., Fu, B.J., Zhang, J.J., Ma, Y., Sivapalan, M., 2018a. Multiscale temporal variability of flow-sediment relationships during the 1950s–2014 in the Loess Plateau, China. J. Hydrol. 563, 609–619. https://doi.org/10.1016/j.jhydrol.2018.06.044.

Gao, J., Kirkby, M., Holden, J., 2018b. The effect of interactions between rainfall patterns and land-cover change on flood peaks in upland peatlands. J. Hydrol. 567 (12), 546–559. https://doi.org/10.1016/j.jhydrol.2018.10.039.

Han, D., Deng, J., Gu, C., Mu, X., Gao, P., Gao, J., 2021. Effect of shrub-grass vegetation coverage and slope gradient on runoff and sediment yield under simulated rainfall. Int. J. Sedim. Res. 36 (1), 29–37.

Hartley, D.M., Alonso, C.V., 1991. Numerical study of the maximum boundary shear stress induced by raindrop impact. Water Resour. Res. 27 (8), 1819–1826. https://doi.org/10.1029/91wr01219.

Hernandez, R.R., Hoffacker, M.K., Murphy-Mariscal, M.L., Wu, G.C., Allen, M.F., 2015. Solar energy development impacts on land cover change and protected areas. Proc. Natl. Acad. Sci. 112 (44), 13579–13584. https://doi.org/10.1073/pnas.1517656112.

Hofer, M., Lehmann, P., Stahli, M., Seifert, S., Krafczyk, M., 2012. Two approaches to modeling the initiation and development of rills in a man-made catchment. Water Resour. Res. 48 https://doi.org/10.1029/2011wr010719.

Hu, A., Levis, S., Meehl, G., Han, W., Washington, W., Oleson, K., van Ruijven, B., He, M., Strand, W., 2016. Impact of solar panels on global climate. Nat. Clim. Chang. 6 (3), 290–294.

IEA, 2021. Key World Energy Statistics 2021, IEA, https://www.iea.org/reports/key-world-energy-statistics-2021.

IRENA, 2013. Unleashing the solar potential in ECOWAS: seeking areas of opportunity for grid-connected and decentralised PV applications. An opportunity-based approach. International Renewable Energy Agency.

Jahanfar, A., Drake, J., Sleep, B., Margolis, L., 2019. Evaluating the Shading Effect of Photovoltaic Panels on Green Roof Discharge Reduction and Plant Growth. J. Hydrol. 568, 919–928. https://doi.org/10.1016/j.jhydrol.2018.11.019.

Jahanfar, A., Drake, J., Gharabaghi, B., Sleep, B., 2020. An experimental and modeling study of evapotranspiration from integrated green roof photovoltaic systems. Ecol. Eng. 152, 105767 https://doi.org/10.1016/j.ecoleng.2020.105767.

Jia, X.X., Shao, M.A., Wei, X.R., Wang, Y.Q., 2013. Hillslope scale temporal stability of soil water storage in diverse soil layers. J. Hydrol. 498, 254–264. https://doi.org/10.1016/j.jhydrol.2013.05.042.

Jiang, S., Tang, D., Zhao, L.u., Liang, C., Cui, N., Gong, D., Wang, Y., Feng, Y.u., Hu, X., Peng, Y., 2022. Effects of different photovoltaic shading levels on kiwifruit growth, yield and water productivity under "agrivoltaic" system in Southwest China. Agric Water Manag 269, 107675.

Keesstra, S.D., Rodrigo-Comino, J., Novara, A., Giménez-Morera, A., Pulido, M., Di Prima, S., Cerdà, A., 2019. Straw mulch as a sustainable solution to decrease runoff and erosion in glyphosate-treated clementine plantations in Eastern Spain. An assessment using rainfall simulation experiments. Catena 174, 95–103.

Kim, H.G., Park, C.Y., 2021. Landslide susceptibility analysis of photovoltaic power stations in Gangwon-do, Republic of Korea. Geomat. Nat. Haz. Risk 12 (1), 2328–2351. https://doi.org/10.1080/19475705.2021.1950219.

Kinnell, P.I.A., 2012. Raindrop-induced saltation and the enrichment of sediment discharged from sheet and interrill erosion areas. Hydrol. Process. 26 (10), 1449–1456. https://doi.org/10.1002/hyp.8270.

Kruitwagen, L., Story, K.T., Friedrich, J., Byers, L., Skillman, S., Hepburn, C., 2021. A global inventory of photovoltaic solar energy generating units. Nature 598 (7882), 604–610.

Lambert, Q., Bischoff, A., Cueff, S., Cluchier, A., Gros, R., 2021. Effects of solar park construction and solar panels on soil quality, microclimate, CO2 effluxes, and vegetation under a Mediterranean climate. Land Degrad. Dev. 32 (18), 5190–5202. https://doi.org/10.1002/ldr.4101.

Li, C.J., Pan, C.Z., 2018. The relative importance of different grass components in controlling runoff and erosion on a hillslope under simulated rainfall. J. Hydrol. 558, 90–103. https://doi.org/10.1016/j.jhydrol.2018.01.007.

Liu, Y.u., Zhang, R.-Q., Huang, Z.e., Cheng, Z., López-Vicente, M., Ma, X.-R., Wu, G.-L., 2019. Solar photovoltaic panels significantly promote vegetation recovery by

modifying the soil surface microhabitats in an arid sandy ecosystem. Land Degrad. Dev. 30 (18), 2177–2186.
Loiola, C., Mary, W., da Silva, L.P., 2019. Hydrological performance of modular-tray green roof systems for increasing the resilience of mega-cities to climate change. J. Hydrol. 573, 1057–1066. https://doi.org/10.1016/j.jhydrol.2018.01.004.
Lu, P., Xie, X.L., Wang, L.H., Wu, F.Q., 2017. Effects of different spatial distributions of physical soil crusts on runoff and erosion on the Loess Plateau in China. Earth Surface Processes And Landforms 42 (13), 2082–2089. https://doi.org/10.1002/esp.4175.
Lu, J., Zheng, F.L., Li, G.F., Bian, F., An, J., 2016. The effects of raindrop impact and runoff detachment on hillslope soil erosion and soil aggregate loss in the Mollisol region of Northeast China. Soil Tillage Res. 161, 79–85. https://doi.org/10.1016/j.still.2016.04.002.
Luk, S., Cai, Q., Wang, G., 1993. Effects of surface crusting and slope gradient on soil and water losses in the hilly loess region, North China. Catena Supplement, 24: 29-29.
Martínez-Murillo, J.F., Nadal-Romero, E., Regüés, D., Cerdà, A., Poesen, J., 2013. Soil erosion and hydrology of the western Mediterranean badlands throughout rainfall simulation experiments: A review. Catena 106, 101–112. https://doi.org/10.1016/j.catena.2012.06.001.
Martinopoulos, G., Tsalikis, G., 2018. Diffusion and adoption of solar energy conversion systems – The case of Greece. Energy 144, 800–807. https://doi.org/10.1016/j.energy.2017.12.093.
Morbidelli, R., Saltalippi, C., Flammini, A., Govindaraju, R.S., 2018. Role of slope on infiltration: A review. J. Hydrol. 557, 878–886. https://doi.org/10.1016/j.jhydrol.2018.01.019.
Pisinaras, V., Wei, Y., Bärring, L., Gemitzi, A., 2014. Conceptualizing and assessing the effects of installation and operation of photovoltaic power plants on major hydrologic budget constituents. Sci. Total Environ. 493, 239–250. https://doi.org/10.1016/j.scitotenv.2014.05.132.
Poesen, J., Nachtergaele, J., Verstraeten, G., Valentin, C., 2003. Gully erosion and environmental change: importance and research needs. Catena 50 (2–4), 91–133. https://doi.org/10.1016/s0341-8162(02)00143-1.
Prosdocimi, M., Cerdà, A., Tarolli, P., 2016. Soil water erosion on Mediterranean vineyards: A review. Catena 141, 1–21. https://doi.org/10.1016/j.catena.2016.02.010.
Rabot, E., Wiesmeier, M., Schlüter, S., Vogel, H.J., 2018. Soil structure as an indicator of soil functions: A review. Geoderma 314, 122–137. https://doi.org/10.1016/j.geoderma.2017.11.009.
Ran, Q., Wang, F., Li, P., Ye, S., Tang, H., Gao, J., 2018. Effect of rainfall moving direction on surface flow and soil erosion processes on slopes with sealing. J. Hydrol. 567, 478–488.
Ran, Q.H., Wang, F., Gao, J.H., 2020. The effect of storm movement on infiltration, runoff and soil erosion in a semi-arid catchment. Hydrol. Process. 34 (23), 4526–4540. https://doi.org/10.1002/hyp.13897.
Shen, H.O., Zheng, F.L., Wen, L.L., Han, Y., Hu, W., 2016. Impacts of rainfall intensity and slope gradient on rill erosion processes at loessial hillslope. Soil Tillage Res. 155, 429–436. https://doi.org/10.1016/j.still.2015.09.011.
Shi, Z.H., Fang, N.F., Wu, F.Z., Wang, L., Yue, B.J., Wu, G.L., 2012. Soil erosion processes and sediment sorting associated with transport mechanisms on steep slopes. J. Hydrol. 454-455, 123–130.
Shobe, C.M., 2022. How impervious are solar arrays? On the need for geomorphic assessment of energy transition technologies. Earth Surface Processes Landforms 47 (14), 3219–3223. https://doi.org/10.1002/esp.5489.
Sun, L., Guo, H., Liu, B., Wu, S., Weckler, P.R., Yang, J., 2021b. Characterizing erosion processes on a convex slope based on 3D reconstruction method. Geoderma 402, 115364.
Sun, B., Ren, F., Ding, W., Zhang, G., Huang, J., Li, J., Zhang, L., 2021a. Effects of freeze-thaw on soil properties and water erosion. Soil and Water Research 16 (4), 205–216.
Tawalbeh, M., Al-Othman, A., Kafiah, F., Abdelsalam, E., Almomani, F., Alkasrawi, M., 2021. Environmental impacts of solar photovoltaic systems: A critical review of recent progress and future outlook. Sci. Total Environ. 759, 143528.
Vaezi, A.R., Ahmadi, M., Cerda, A., 2017. Contribution of raindrop impact to the change of soil physical properties and water erosion under semi-arid rainfalls. Sci. Total Environ. 583, 382–392. https://doi.org/10.1016/j.scitotenv.2017.01.078.
Wang, Y., He, J., Chen, W., 2021b. Distributed solar photovoltaic development potential and a roadmap at the city level in China. Renew. Sustain. Energy Rev. 141, 110772 https://doi.org/10.1016/j.rser.2021.110772.
Wang, T., Li, P., Ren, Z., Xu, G., Li, Z., Yang, Y., Tang, S., Yao, J., 2017. Effects of freeze-thaw on soil erosion processes and sediment selectivity under simulated rainfall. J. Arid. Land 9 (2), 234–243.
Wang, P., Zhang, S., Pu, Y., Cao, S., Zhang, Y., 2021a. Estimation of photovoltaic power generation potential in 2020 and 2030 using land resource changes: An empirical study from China. Energy 219, 119611. https://doi.org/10.1016/j.energy.2020.119611.
Xia, Z., Li, Y., Chen, R., Sengupta, D., Guo, X., Xiong, B.o., Niu, Y., 2022. Mapping the rapid development of photovoltaic power stations in northwestern China using remote sensing. Energy Rep. 8, 4117–4127.
Xin, Z., Yu, X., Li, Q., Lu, X.X., 2011. Spatiotemporal variation in rainfall erosivity on the Chinese Loess Plateau during the period 1956–2008. Reg. Environ. Chang. 11 (1), 149–159. https://doi.org/10.1007/s10113-010-0127-3.
Xu, L., Zhang, S., Yang, M., Li, W., Xu, J., 2018. Environmental effects of China's solar photovoltaic industry during 2011–2016: A life cycle assessment approach. J. Clean. Prod. 170, 310–329. https://doi.org/10.1016/j.jclepro.2017.09.129.
Yang, Q., Huang, T., Wang, S., Li, J., Dai, S., Wright, S., Wang, Y., Peng, H., 2019. A GIS-based high spatial resolution assessment of large-scale PV generation potential in China. Appl. Energy 247, 254–269.
Yue, S., Guo, M., Zou, P., Wu, W., Zhou, X., 2021. Effects of photovoltaic panels on soil temperature and moisture in desert areas. Environ. Sci. Pollut. Res. 28, 17506–17518. https://doi.org/10.1007/s11356-020-11742-8.
Yushchenko, A., de Bono, A., Chatenoux, B., Kumar Patel, M., Ray, N., 2018. GIS-based assessment of photovoltaic (PV) and concentrated solar power (CSP) generation potential in West Africa. Renew. Sustain. Energy Rev. 81, 2088–2103. https://doi.org/10.1016/j.rser.2017.06.021.
Zhang, X., Li, P., Li, Z.B., Yu, G.Q., Li, C., 2018. Effects of precipitation and different distributions of grass strips on runoff and sediment in the loess convex hillslope. Catena 162, 130–140. https://doi.org/10.1016/j.catena.2017.12.002.
Zhang, G.-H., Luo, R.-T., Cao, Y., Shen, R.-C., Zhang, X.C., 2010. Correction factor to dye-measured flow velocity under varying water and sediment discharges. J. Hydrol. 389 (1), 205–213. https://doi.org/10.1016/j.jhydrol.2010.05.050.
Zhang, X.C.(., Zheng, F.L., Chen, J., Garbrecht, J.D., 2020. Characterizing detachment and transport processes of interrill soil erosion. Geoderma 376, 114549.
Zhao, X., Wu, P., Gao, X., Persaud, N., 2015. Soil Quality Indicators in Relation to Land Use and Topography in a Small Catchment on the Loess Plateau of China. Land Degrad. Dev. 26 (1), 54–61. https://doi.org/10.1002/ldr.2199.

Received: 23 January 2024 | Accepted: 10 March 2024

DOI: 10.1002/vzj2.20335

Vadose Zone Journal

ORIGINAL ARTICLE

Special Section: Tribute to Rien van Genuchten, Recipient of the 2023 Wolf Prize for Agriculture

Measuring and modeling soil moisture and runoff at solar farms using a disconnected impervious surface approach

David Mulla[1] | Jake Galzki[1] | Aaron Hanson[2] | Jirka Simunek[3]

[1]Department of Soil, Water, and Climate, University of Minnesota, Saint Paul, Minnesota, USA

[2]Institute on Environment, University of Minnesota, Saint Paul, Minnesota, USA

[3]Department of Environmental Sciences, University of California, Riverside, Riverside, California, USA

Correspondence
David Mulla, Department of Soil, Water, and Climate, 1991 Upper Buford Circle, University of Minnesota, Saint Paul, MN 55108, USA.
Email: [redacted]@umn.edu

Assigned to Associate Editor Jan Hopmans

Funding information
Solar Energy Technologies Office, Grant/Award Number: DE-AC36-08GO28308

Abstract

Ground-mounted photovoltaic sites are often treated as impervious surfaces in stormwater permits. This ignores the pervious soils beneath and between solar arrays and leads to an overestimation of runoff. Our objective was to improve solar farm stormwater hydrology models by explicitly considering the disconnected impervious nature of solar design and site characteristics. Experimental sites established on utility scale solar farms in Colorado, Georgia, Minnesota, New York, and Oregon had perennial vegetative plantings with mean precipitation ranging from 40.6 to 124.5 cm, and soil texture ranging from loamy sand to clay. Soil moisture measurements were collected beneath arrays, under drip edges, and in the vegetated area between arrays at each site. Hydrus-3D models for soil moisture and stormwater hydrology were developed that accounted for precipitation falling on solar panels, drip edge redistribution of rainfall, infiltration, and runoff in the pervious areas between solar arrays and beneath panels. Drip edge runoff averaged 3- to 10-times incident precipitation at the New York and Minnesota sites, respectively. Root mean square error values between measured sub-hourly soil moisture and predicted moisture for large measured single storm events averaged 0.029 across all five sites. Predicted runoff depths were strongly affected by precipitation depth, soil texture, soil profile depth, and soil bulk density. Runoff depths across the five experimental sites averaged 13%, 25%, and 45% of the 2-, 10-, and 100-year design storm depths, clearly showing that these solar farms do not behave like impervious surfaces, but rather as disconnected impervious surfaces with substantial infiltration of runoff in the vegetated areas between and beneath solar arrays.

1 | INTRODUCTION

Climate change poses an existential threat to ecosystems and their human, animal, insect, and plant life as a result of increasing temperatures and changes in precipitation patterns. As a result, there is a significant shift away from nonrenewable to renewable energy. At the end of 2021, over 120 or 670 GW in utility-scale ground-mounted solar photovoltaic

Abbreviations: NOAA, National Oceanic and Atmospheric Administration; NRCS, Natural Resource Conservation Services; PV, photovoltaic; PV-SMaRT, photovoltaic stormwater management research and testing; RCN, runoff curve number; RMSE, root mean square error; SWMM, storm water management model.

(PV) capacity were either installed or in the "interconnection queue" across the United States, respectively (Rand et al., 2022). If developed, approximately 2 million ha of land would be needed (based on 2.4–3.2 ha/MW produced) to construct the solar capacity in the interconnection queue. By the end of 2050, the U.S. Department of Energy projects that roughly 4.2 million ha could be needed to deploy solar energy to meet U.S. climate and electrification goals (Heath et al., 2022).

Utility scale ground-mounted solar farms typically focus on maximizing production of renewable energy, rather than on reducing runoff and erosion or providing pollinator habitat (Hernandez et al., 2014). Government jurisdictions having permitting authority accordingly often treat ground-mounted PV facilities as predominantly impervious surfaces in local stormwater and water quality permitting (GPI, 2021; Yavari et al., 2022). Most hydrologic models used to estimate stormwater runoff do not explicitly assess the impacts on hydrology of the disconnected impervious arrays at solar farms, including an inability to account for arrays that intercept precipitation and reroute it to the drip edges of solar panels, or to account for areas directly beneath solar panels that can infiltrate runoff. Inaccurate estimates of stormwater runoff at solar farms result in the need to install costly structural practices such as on-site infiltration basins, and a resulting decrease in the area on the project site available for production of solar energy.

Only a handful of studies have been conducted on the hydrology of utility-scale ground-mounted solar PV sites (Yavari et al., 2022). A simple hydrologic model for the impact of disconnected impervious solar PV sites on stormwater runoff was developed by Cook and McCuen (2013). They used soil hydrologic group to estimate runoff curve numbers (RCNs) and Manning's n values to estimate velocity of runoff in response to rainfall hyetographs representing 2-, 25-, and 100-year return frequencies. The most important factors affecting runoff were (in decreasing order) storm characteristic (return frequency and duration), ground cover (gravel vs. turf grass), and soil hydrologic group (C vs. B). Factors that had little impact on runoff included the landscape slope and panel tilt angle. Surprisingly, Cook and McCuen (2013) concluded that there were no differences in stormwater runoff between simulations in the presence or absence of solar panels. This was perhaps due to the presence of grass plantings beneath and between the solar arrays that enhanced infiltration. However, no experimental measurements were collected to verify model performance in the Cook and McCuen (2013) study, and the impacts of concentrated drip edge runoff on stormwater runoff were not considered.

A majority of runoff modeling efforts at ground-mounted solar sites make no attempt to directly consider either their disconnected impervious nature or how detailed combinations of soil factors affect infiltration (e.g., texture, depth, bulk density, saturated hydraulic conductivity, etc.). An example is the application of the widely used FLO-2D hydrologic model to simulate infiltration and runoff and route surface flows across utility-scale solar PV sites (Barnard et al., 2017). Model inputs include precipitation, elevation, land cover, and soil hydrologic group, which are used to estimate RCN and Manning's n roughness coefficients. Model outputs are generated by assuming an absence of solar array surfaces, and these outputs are subsequently empirically adjusted for the percent impervious cover.

Recently, there have been attempts to simulate infiltration under varying rainfall inputs with consideration for solar panel orientation and angle impacts on drip edge runoff and on sheltering of soil from rain using sophisticated soil hydrologic models such as Hydrus-3D (Elamri et al., 2018). Drip edge runoff in Elamri et al. (2018) varied from five times incident rainfall when panels were oriented facing the wind to two times incident rainfall when panels were oriented away from the wind. These differences caused large increases in near-surface soil moisture content in areas directly beneath the drip edge as compared with areas directly beneath panels, which were much drier, or in the area between panels, which had intermediate soil moisture levels. Simulated soil moisture contents were apparently in reasonable agreement with moisture contents measured using neutron probes installed beneath panels, under the drip edge, or between arrays (though detailed accuracy statistics were not provided). No estimates of stormwater runoff were provided by Elamri et al. (2018).

Urban stormwater management has long been plagued by the relentless expansion of impervious surfaces such as roads, parking lots, and building roof tops. To counter the adverse impacts of these surfaces on stormwater runoff, there has been an increasing interest in urban green infrastructure, including vegetated roof tops (Hilten et al., 2008; Vergroesen & Joshi, 2010) Similarly, in the solar industry, it is standard

Core Ideas

- Hydrus-3D accurately estimated soil moisture and infiltration beneath and between solar arrays.
- Solar panel drip edge runoff averaged from 3X to 10X precipitation depth falling on panels.
- Design storm depth, soil texture and depth, and soil bulk density had a large impact on solar farm runoff.
- Solar farm runoff on coarse-textured, deep soils was much less than runoff from fine-textured, shallow soils.
- Solar farm hydrology is accurately represented with a disconnected impervious modeling framework.

practice to cover pervious ground surfaces at solar farms with gravel or to plant low-growing turf grass (Walston et al., 2021). More recently, many states have been promoting the establishment of native prairie or pollinator habitat at solar farms (Moore-O'Leary et al., 2017) in order to enhance pollinator habitat, improve soil moisture retention (Hassanpour Adeh et al., 2018), and reduce stormwater runoff and soil loss (Walston et al., 2021). Yet, the impact of native prairie or pollinator habitat vegetation on soil moisture, infiltration, and stormwater runoff at solar farms is rarely studied.

Given this background information, there is a critical need to develop better approaches for modeling impacts of perennial vegetation practices such as native prairie or pollinator habitat at solar farms. Furthermore, there is a critical need to develop models that can comprehensively evaluate impacts on soil moisture and stormwater runoff of factors such as climate, soil type, soil depth, soil bulk density, drip edge runoff, and solar array design factors. The Photovoltaic Stormwater Management Research and Testing (PV-SMaRT; https://www.nrel.gov/solar/market-research-analysis/pv-smart.html) experimental and modeling study described here was designed to estimate soil moisture and stormwater runoff at large-scale solar farms having perennial vegetation plantings in five states across the conterminous United States. In addition, soil moisture and stormwater runoff were modeled using Hydrus-1D and Hydrus-3D (Šimůnek et al., 2008) as affected by soil characteristics (texture, bulk density, and saturated hydraulic conductivity), perennial vegetative cover, solar panel drip edge runoff, and solar array design factors (array spacing and orientation). To the authors knowledge, this is the first effort ever attempted to collect experimental data to calibrate and validate a sophisticated numerical soil hydrology model that simulates both soil moisture and stormwater runoff across a wide range of ground-mounted solar PV sites having perennial vegetated cover.

2 | MATERIALS AND METHODS

2.1 | Experimental sites

Experimental sites consisted of five ground-mounted solar PV installations, generating a combined nameplate and facility capacity between 1 and 18 MW, located in Colorado, Georgia, Minnesota, New York, and Oregon (Table 1). To protect confidentiality of project partners, the exact locations of each experimental site are not provided. Installations in Minnesota and New York had south-facing fixed arrays, whereas tracking arrays facing east (morning) or west (afternoon) were at sites in Colorado, Georgia, and Oregon. Array spacing varied between 5.6 m at the Colorado site and 7.6 m at the Minnesota site. Individual solar panel dimensions were 3 m × 1 m. Lines of arrays were generally oriented along flat (Georgia) to moderate (Colorado) slope topographic contours and consisted of either single (1 portrait in Table 1) or double (2 portrait in Table 1) panels in portrait orientation. Mean annual precipitation ranged from a high of 124.5 cm in Georgia and New York to a low of 40.6 cm in Colorado and Oregon. Perennial ground cover between and beneath solar arrays was well established and dense at all sites, ranging from mowed cover crops at Georgia to native pollinator, grass, or prairie vegetation at the other sites.

Soils varied considerably across the five experimental sites. Colorado was a Renohill clay (US Taxonomic classification: Fine, smectitic, mesic Ustic Haplargids), while Georgia was a deep Greenville sandy clay (Fine, kaolinitic, thermic Rhodic Kandiudults), Minnesota was a deep Hubbard sandy loam (Sandy, mixed, frigid Entic Hapludolls). New York was a shallow Erie channery silty clay loam (Fine-loamy, mixed, active, mesic Aeric Fragiaquepts), while Oregon was a Phoenix clay (Very fine, smectitic, mesic Xeric Epiaquerts).

2.2 | Site sampling and monitoring

All soil samples and infiltrometer measurements described below were taken underneath the panel, at the drip edge, and in the full sun area between panels in order to provide ground truth data for model results beneath the panels, at the drip edge, or in the full sun area. Soil samples were collected from two different solar array row locations at each site to a depth of 30 cm to estimate soil textural class based on percent sand, silt, and clay (Bouyoucos, 1962). At the same two array locations, surface soil samples were collected to a depth of 20 cm using an Uhland sampler to estimate soil bulk density (Doran & Mielke, 1984). Field saturated soil hydraulic conductivity was estimated in surface soils at the same six locations for each site using a Cornell sprinkle infiltrometer, with corrections for soil textural class (van Es & Schindelbeck, 2006). All samples correspond to locations for soil moisture monitoring described below.

Figure 1 illustrates the in situ precipitation and soil moisture monitoring strategy at each experimental site. Incident daily precipitation was measured from July 2020 to October 2022 using the Meter ECRN rain gauges in the full sun area. Another rain gauge was installed beneath the drip edge of fixed orientation panels at Minnesota and New York. TEROS 10 soil moisture sensors (Meter Group, Inc.) were installed at each site in July 2020 at two depths (15 and 30 cm) in the full sun area and beneath the drip edge, and at one depth (15 cm) beneath the array. Soil moisture measurements were recorded at 15 min intervals using a Meter ZL6 datalogger and averaged over hourly intervals for analysis. Replicate measurements using this monitoring setup were taken at each site in a different solar panel row.

TABLE 1 Solar installation design specifications and site characteristics.

Site	Capacity (MW)	Area (ha)	Landscape slope (%)	Array type	Panel No. and arrangement	Array spacing (m)	Mean annual precipitation (cm)	Ground cover
CO	1.0	2.4	5	Tracking	1 portrait	5.6	40.6	Native mix
GA	1.3	3.2	1.5	Tracking	1 portrait	6.2	124.5	Mowed cover crops
MN	4.5	11.7	2.5	Fixed	2 portrait	7.6	94.0	Prairie mix
NY	18.0	43.7	3	Fixed	2 portrait	7.0	124.5	Tall grass
OR	13.0	18.6	3	Tracking	2 portrait	6.4	40.6	Native pollinators

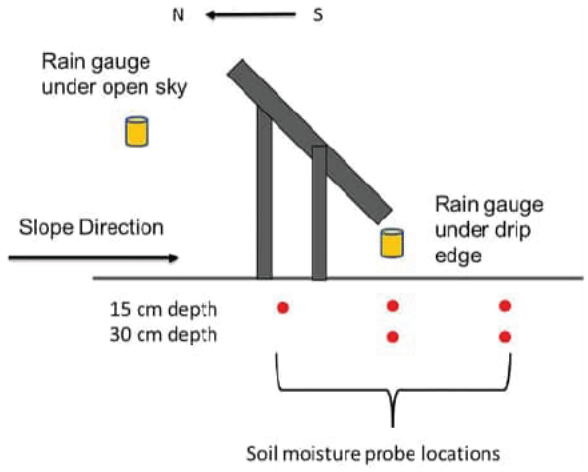

FIGURE 1 Monitoring layout for fixed array photovoltaic sites at Minnesota and New York. At Colorado, New York, and Oregon, the same layout was used without a rain gauge under drip edge.

2.3 | Soil moisture and stormwater runoff modeling

Hydrus numerical soil hydrologic models were used to simulate infiltration, redistribution, evapotranspiration, soil moisture, and surface runoff at each of the five experimental sites (Simunek et al., 2008). Hydrus-1D was used to simulate one-dimensional vertical variably saturated soil water flow in the area between solar panels using measured precipitation, while Hydrus-3D, driven either by the largest storm in the precipitation monitoring data or by 2-, 10-, and 100-year design storms, was used to simulate two-dimensional water flow in the cross-sectional area extending across three successive continuous solar array segments composed of solar panels, panel drip edges, and a full sun vegetated area (Figure S1). This cross-section represents the complex hydrologic characteristic of the disconnected impervious solar farms studied in this project.

Hydrus models numerically solve the nonlinear Richards partial differential equation for variably-saturated water flow in the vadose zone, representing soil hydraulic functions using van Genuchten models for the soil moisture characteristic and hydraulic conductivity curves (van Genuchten & Nielsen, 1985). Stormwater runoff is generated when incoming intensity of rainfall (plus solar panel drip edge runoff) exceeds soil infiltration rate. Runoff occurs primarily when soils are saturated, rainfall intensity is high, and soils are relatively low in permeability.

Initially, a standard Hydrus-1D model (v4.xx) was used for the purposes of calibrating van Genuchten model parameters in Hydrus-1D using at least 3 months of continuously monitored precipitation and 1-h soil moisture measurements versus predicted soil moisture contents for vertical soil profiles in the full sun area between solar arrays (Figure 1, Table S1). Outputs of Hydrus-1D included volumetric soil moisture contents at various depths and surface runoff. Initial estimates for saturated and field capacity moisture contents were based on histograms of longer term soil moisture content measurements (generally 1 year of data), following the method of Chandler et al. (2017). Initial estimates for van Genuchten soil hydraulic properties were based on neural network interpolators embedded in Hydrus (Schaap et al., 2001) using measured soil texture, saturated moisture content, bulk density, and saturated hydraulic conductivity. Certain Hydrus model parameters applied at the upper boundary condition were left at default values. These include parameters that control model convergence (HCrit = 10,000 cm) and initiation of runoff (h0 = 0 cm). However, because Hydrus-1D simulations could not account for horizontal hydrologic connections between the shaded area beneath panels, the area beneath the panel drip edge, and the full sun area, the upper boundary condition for Hydrus-1D simulations in the full sun area during rainy days was estimated by adding incident daily precipitation to the effective normalized drip edge runoff factor. This normalized runoff factor was estimated based on the ratio of impervious width (based on panel dimensions) to total spacing width between arrays. Normalized drip panel runoff is treated as an additional source of water input spread out across the entire vegetated area between arrays in Hydrus-1D simulations. This increases the runoff potential because drip edge runoff is added to incoming precipitation in the full sun areas between arrays. Calibrated estimates of soil hydraulic properties were set based on minimizing the root mean square

error (RMSE) between predicted Hydrus-1D soil moisture and measured soil moisture contents from data at sensors located only in the full sun area between arrays.

Following calibration of the vertical Hydrus-1D model in the full sun area, a Hydrus-3D model (v3.x) with an overland flow module was used for short-term (2-day) simulations of soil moisture and runoff in response to measured storms (generally the largest measured storms with a duration of <1 day) at 15 min time steps for each site. The Hydrus-3D domain considered was a 2-D cross-section extending across and beneath three successive continuous areas with solar panels, below the panel drip edge, and in the full sun vegetated area (Figure S1). Following slight calibration of Hydrus-3D with 2-day simulations based on the largest measured storm events, additional Hydrus-3D simulations were generated involving 24-h design storms at 2-, 10-, and 100-year return frequencies determined from National Oceanic and Atmospheric Administration (NOAA) Atlas 14 tables appropriate for each of the five experimental sites. These simulations were motivated by an interest in representing runoff from 24-h design storms of varying return frequency that are of interest to regulatory agencies that issue solar farm construction permits that consider storm event impacts on stormwater runoff.

Hydrus-3D software code was modified to represent upper boundary conditions for disconnected impervious surfaces typical of solar farms (Figure S1) having three successive lines of solar arrays that accounted for (a) interception of rainfall by impervious solar panels with subsequent drip edge runoff, (b) incident precipitation in the full sun pervious area downslope of arrays, (c) surface runoff and sub-surface lateral soil moisture migration from the full sun area to the pervious area beneath the next downslope panel, and (d) resulting overland runoff from the three impervious upslope solar arrays and their three downslope pervious areas. Simulation of soil moisture contents during 2-day periods experiencing large magnitude measured storm events was initiated with an antecedent moisture content of field capacity (Table S1) estimated using long-term experimental data from each site using the method of Chandler et al. (2017). A no flux lower boundary condition was imposed to accurately estimate temporal variations in soil moisture beneath and between solar arrays. Directly beneath solar arrays, an upper boundary condition involving no precipitation was imposed. Beneath the solar panel drip edge, an experimentally measured upper boundary condition involving a drip edge multiplier for incident rainfall was imposed across a ground surface width ranging from 22.5 to 35.5 cm below the actual drip edge; the width relates to the drip edge multiplier used at each site to maintain water balance within the system. In the full sun area, an upper boundary condition was imposed for ambient daily precipitation. Spacing of numerical finite difference grids in the Hydrus model was approximately 5 cm vertically and between 5 and 50 cm for horizontal nodes. Higher nodal densities were used around the transitions between the three segments with differing upper boundary conditions (no precipitation beneath the panel, increased incident precipitation beneath panel drip edge, and incident precipitation in area between the arrays). Runoff from the uppermost drip edge and full sun area was routed by the Hydrus-3D model downslope, where it could infiltrate under the panel in the next downslope array. This process was repeated for the second and third lines of arrays. Cumulative runoff was predicted from the full sun area downslope of the third line of arrays.

Root water uptake in daily Hydrus modeling was simulated using the Feddes' et al. (2001) algorithm without considering compensation. Root distribution with depth was assumed constant with a rooting depth of 50 cm. Feddes' parameters represented perennial vegetation at each experimental site using "pasture" in the Hydrus default database. Hourly solar radiation, temperature, and humidity data were taken from the nearest solar radiation database location in the National Solar Radiation Database (https://nsrdb.nrel.gov/), and evapotranspiration rates were estimated by Hydrus based on these measurements using a Penman–Monteith energy balance approach accounting for vapor pressure deficit recorded at the site. Evapotranspiration plays a small role during the time when larger experimentally measured storms are occurring when compared to evapotranspiration over long-term seasonal data that includes long, dry periods between storms. A daily average evapotranspiration rate of 3 mm/day was imposed in the full sun area between arrays, corresponding well to the average observed drawdown of soil moisture in the full sun moisture probe in 48-h simulations. No evapotranspiration was assumed in areas beneath panels due to minimal solar radiation reaching these areas during storm events. In addition, different soil hydraulic properties were applied in the full sun area and the area beneath panels during model calibration to reflect differences in soil moisture arising from differences in infiltration, soil bulk density, and impacts of surface crusting.

Initial parameters for the Hydrus-3D modeling were based on calibrated Hydrus-1D parameters. Hydrus-3D parameters were adjusted slightly to account for soil crusts observed in shaded areas beneath arrays, to account for soil horizonation at the Georgia and New York sites, and to account for focused runoff directly beneath the drip edges that had not been accounted for in Hydrus-1D modeling. Final Hydrus-3D model parameters were set based on minimizing the RMSE during 48-h simulations between predicted and measured soil moisture contents from soil moisture sensors installed in the full sun, under panel, and beneath drip edge locations shown in Figure 1. RMSE was minimized primarily by varying van Genuchten parameters α symbol and n and to a much lesser extent, saturated soil hydraulic conductivity and soil bulk density during model calibration.

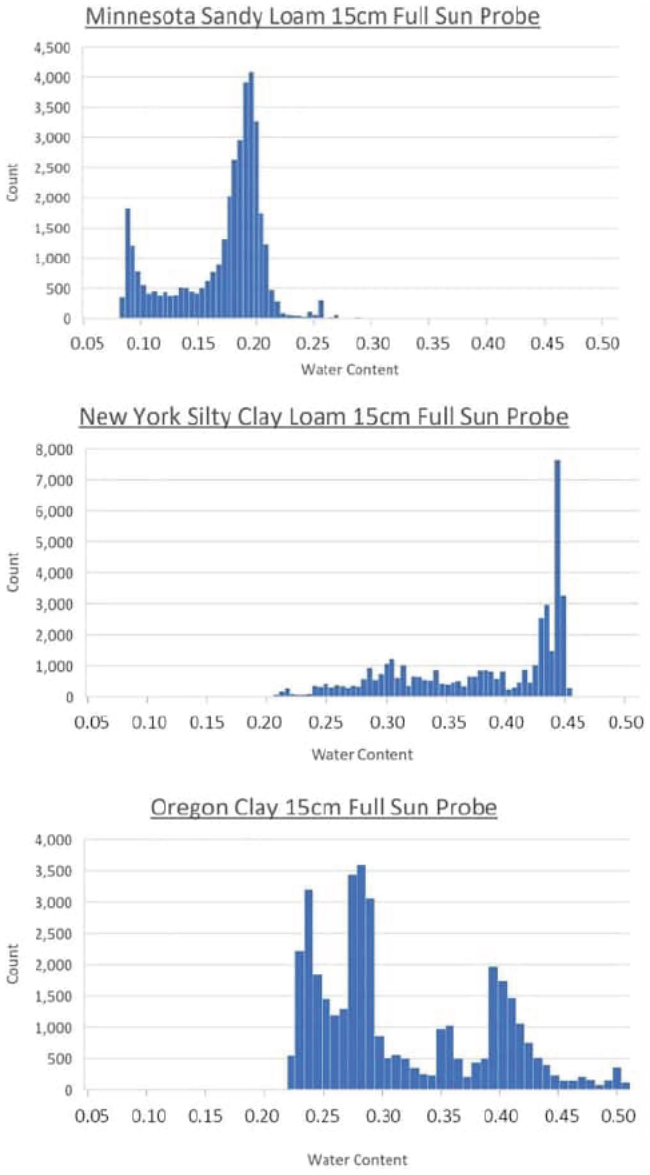

FIGURE 2 Minnesota (MN) (top), New York (NY) (middle), and Oregon (OR) (bottom) histograms for volumetric soil moisture (*x*-axis) versus count of observed soil moisture occurrences in each soil moisture bin (*y*-axis) for full sun sensors at a depth of 15 cm. Based on the Chandler et al. (2017) method, field capacity water content is 0.19, 0.43, and 0.4 for the MN, NY, and OR sites, respectively.

3 | RESULTS AND DISCUSSION

3.1 | Soil characteristics

Soils at the five experimental sites (Table S1) ranged in texture from sandy loam (Minnesota) to clay (Colorado and Oregon). Soil depths varied from shallow (0–46 cm) at New York to deep (0–150 cm) at Georgia and Minnesota. Distinct A and B horizons were present at Georgia and New York, while soils at the other three sites had relatively homogeneous sub-soils. Histograms of long-term soil moisture content measurements (e.g., Figure 2 and Figure S2, following the method of Chandler et al., 2017) indicated that field capacity ranged from 0.19 at the sandy loam site in Minnesota to 0.43 at the silty clay loam site in New York (Table S1). Saturated hydraulic conductivity measurements ranged from a low of 2.9 cm/h at the silty clay loam site in New York to a high of 25.3 cm/h at the sandy loam site in Minnesota.

3.2 | Measured drip edge runoff

Daily drip edge runoff values (mm/day) from fixed orientation arrays in Minnesota and New York (Figure S3) were divided by incident daily precipitation depth (X) to estimate the drip edge runoff multiplier factor. At the Minnesota site, drip edge multiplier values averaged 10.6X and ranged between 2X and 23X, but had no significant relationship with daily precipitation. The low values in Minnesota were associated with situations where wind was blowing from the north, driving much of the precipitation under solar arrays. The highest values were likely associated with situations where wind was blowing from the south, driving most of the precipitation directly against solar arrays. At the New York site, drip edge multiplier values averaged 3X and ranged between 1X and 5X. This narrower range of scatter at the New York site relative to the Minnesota site is likely due to prevailing winds that generally blew parallel to array orientation (E–W). Drip edge multiplier used in Hydrus modeling represents an average over dozens of storm events, primarily during the dominant rainy season.

3.3 | Hydrus-1D Predictions of Soil Moisture Content

Hydrus-1D predictions of soil moisture content were calibrated against 3–4 months of measured soil moisture at depths of 15–30 cm from full sun areas between arrays (Table 2). Because Hydrus-1D simulations could not simultaneously represent infiltration in the full sun area as well as beneath the panel drip edges, the upper boundary condition for the full sun area during rainy days was estimated by adding an effective drip edge runoff factor to incident daily precipitation. This was determined based on the ratio of impervious panel width to the total spacing from panel to panel.

3.4 | Hydrus-1D saturated hydraulic conductivity values

Construction of solar facilities occurred in 2019, 2020, 2019, 2019, and 2018, respectively, for the Colorado, Georgia, Minnesota, New York, and Oregon sites. Saturated hydraulic conductivity measurements were estimated after 2–3 years of vegetation establishment. Measured Saturated hydraulic

TABLE 2 Hydrus-1D calibrated van Genuchten hydraulic properties and root mean square error (RMSE) between measured and Hydrus-1D predicted soil moisture values in full sun area.

Site	Soil moisture sensor location/ depth(s) (cm)	Precipitation measurement period for Hydrus-1D simulations	Saturated volumetric water content	Residual volumetric water content	α	n	Saturated hydraulic conductivity (cm/h)	RMSE
CO	Full sun/15, 30	Mar. 20–July 21, 2021	0.49	0.11	0.02	1.4	5.0	0.041
GA	Full sun/15, 30	Sept. 10–Dec. 31, 2020	0.44	0.09	0.024	1.4	2.0	0.027
MN	Full sun/15, 30	July 16–Oct. 31, 2020	0.44	0.06	0.027	1.6	20.0	0.017
NY	Full sun/15, 30	July 4–Oct. 31, 2020	0.48	0.09	0.005	1.3	2.5	0.027
OR	Full sun/15, 30	Jan. 1–Mar. 31, 2021	0.50	0.11	0.04	1.3	0.5	0.021

conductivity values reflect impacts of solar farm construction activities as well as mitigating impacts from growth of perennial vegetation. Hydrus-1D calibrated van Genuchten saturated hydraulic conductivity values (Table 2) matched experimentally measured values (Table S1) reasonably well for all sites except Georgia and Oregon. At Georgia, Hydrus-1D calibrated saturated hydraulic conductivity (2.0 cm/h) was smaller than the measured value (7.9 cm/h). The calibrated value for Hydrus-1D is likely influenced by the need to account for impacts of a change to finer texture in the Georgia sub-soil below a depth of 20 cm. At Oregon, Hydrus-1D calibrated saturated hydraulic conductivity (0.5 cm/h) was smaller than the measured value (3.8 cm/h), which was obtained during summer when the clay soil exhibited large desiccation cracks. The calibrated value for Hydrus-1D likely better represents the slower soil infiltration processes that occur during rainfall events in the early spring, when antecedent moisture content is relatively large, and desiccation cracks are absent. Calibrated saturated volumetric water content values (Table 2) were not estimated using measured soil bulk density results at Colorado, New York, or Oregon because of the impacts of desiccation cracks in very dry soil at Colorado and Oregon, or dense rooting masses in soil at New York.

3.5 | Hydrus-3D modeling of storm-event based drip edge runoff

Measured average drip edge multipliers of 10.6X and 3X were used at the fixed-panel Minnesota and New York sites, respectively (Table 3). The tracking array sites of Georgia and Colorado had panel widths that were half that at the Minnesota site. At these sites, a multiplier of 5X (half of the Minnesota multiplier) was used to simulate a worst-case scenario where wind did not redirect any rainfall around the panel. In addition, because the Georgia measured storm event occurred at night when panels were held parallel to the ground, the 5X multiplier for the Georgia site was split and applied to each edge of the panel. Oregon panel width was the same as Minnesota, however during the measured storm event used for Hydrus-3D modeling, winds drove precipitation under the panel from the west; therefore, a 5X multiplier was used to simulate Oregon's panel interception rate. In addition, half the precipitation was applied underneath half of the wind-blown side of the Oregon panel. For all Hydrus-3D simulations, drip edge multipliers were applied to the upper boundary condition at the panel edge; the width of ground surface area where the multiplier was applied was calculated to preserve water balance in the system. This ground surface area where panel runoff was infiltrated varied between 22.5 and 35.5 cm, which was based on observations of soil scour (rather than assuming a very narrow scour band directly beneath the drip edge).

3.6 | Hydrus model accuracy at predicting soil moisture content

3.6.1 | Hydrus-1D model accuracy

RMSE values (Table 2) for calibrated Hydrus-1D simulations of soil moisture content at the five experimental sites ranged from 0.017 to 0.041, indicating very good accuracy. RMSE values were lowest in the coarsest textured soil (Minnesota) and highest in one of the finest textured soils (Colorado).

Example comparisons between daily measured and Hydrus-1D predicted soil moisture at the 15-cm depth in the full sun region between arrays are shown for the New York site in Figure 3 (top). Soil moisture values were accurately predicted at the fixed solar arrays in New York (RMSE of 0.027), but there was a tendency to slightly underpredict peak values of soil moisture following the onset of individual storms at the tracking arrays in Oregon and Georgia. The steep decreases in modeled water content in July and August correspond to dry periods without significant rainfall. The underprediction is reasonable, given that Hydrus-1D is unable to explicitly account for concentrated runoff at panel drip edges that would travel downslope into the full sun

TABLE 3 Hydrus-3D van Genuchten model parameters and root mean square error (RMSE) for predicted versus measured soil moisture driven by selected measured storm events.

Site	Soil moisture sensor location/ depth(s) (cm)	Measured storm event depth/drip edge multiplier (cm)	Saturated volumetric water content	Residual volumetric water content	α	n	Saturated/crust hydraulic conductivity (cm/h)	RMSE
CO	Full sun/15 Under panel/15 East and west drip edges/15	3.0/5X	0.49	0.10	0.01	1.3	7.5/0.75	0.019
GA A Horizon	Full sun/15 Under panel/15 East and west drip edges/15	2.0/5X	0.38	0.09	0.03	1.4	8.0/0.1	0.023
GA B Horizon			0.40	0.08	0.025	1.25	3.0/NA	
MN	Full sun/15, 30 Under panel/15 South drip edge/30	9.0/10.6X	0.42	0.06	0.10	2.0	25.0/2.0	0.033
NY A Horizon	Full sun/15,30 Under panel/15 South drip edge/30	4.3/3X	0.50	0.09	0.005	1.3	0.5/NA	0.028
NY B Horizon			0.50	0.09	0.01	1.5	3.0/NA	
OR	Full sun/15 Under panel/15 East and west drip edges/15	4.1/5X	0.50	0.11	0.04	1.4	2.0/0.2	0.038

Note: NA indicates no soil crust.

area during a given storm. In Hydrus-1D, the drip edge runoff is averaged over the entire full sun area and then added to incident rainfall for the location in the middle of the full sun area. In general, the timing of increases in soil moisture is closely tied with, but lags slightly, the onset of a precipitation event. The slight lag is due to the way drip edge runoff is redistributed into the full sun area with Hydrus-1D modeling. In Hydrus-3D modeling (Figure 3, bottom), the lag increases because of the distance between the drip edge and the full sun area sensors. Predicted soil drying curves at the end of a precipitation event follow experimental drying curves reasonably well at Oregon (RMSE of 0.021), but are somewhat faster to decline than experimental drying curves at the wetter Georgia (RMSE of 0.027) site (results not shown).

3.6.2 | Hydrus-3D model accuracy

Two-day simulations with Hydrus-3D of soil moisture content for selected measured storm events (exemplified by Figure 3, bottom) required slight modifications in Hydrus-1D calibrated surface layer saturated hydraulic conductivity values (Table 3) to account for soil crusting beneath solar arrays at the Colorado, Georgia, Minnesota, and Oregon sites where vegetation tended to be less dense than in the full sun area. Crust hydraulic conductivity values ranged between 0.1 and 2.0 cm/h at the latter sites for the ground surface node in the Hydrus-3D domain. No crusting was observed at the New York site. In addition, Hydrus-3D sub-soil hydraulic conductivity values at Georgia and New York were modified to account for sub-soils with markedly different texture than surface soils, bringing modeled (Table 3) and measured (Table S1) saturated hydraulic conductivity values at Georgia and Oregon into close agreement.

Comparison between Hydrus-3D predicted and measured soil moisture contents at the New York site (Figure 3 [bottom], Figure S4) showed that the magnitude of increases in soil moisture from beginning to end of the storm events agreed closely with each other. The timing of predicted soil moisture content increases lagged measured increases somewhat at Oregon, but was relatively well-timed at all other sites. RMSE values (Table 3) for 2-day simulations of soil moisture content with Hydrus-3D at the five experimental sites averaged over all sensor locations within a site ranged from 0.019 to 0.038, indicating very good accuracy.

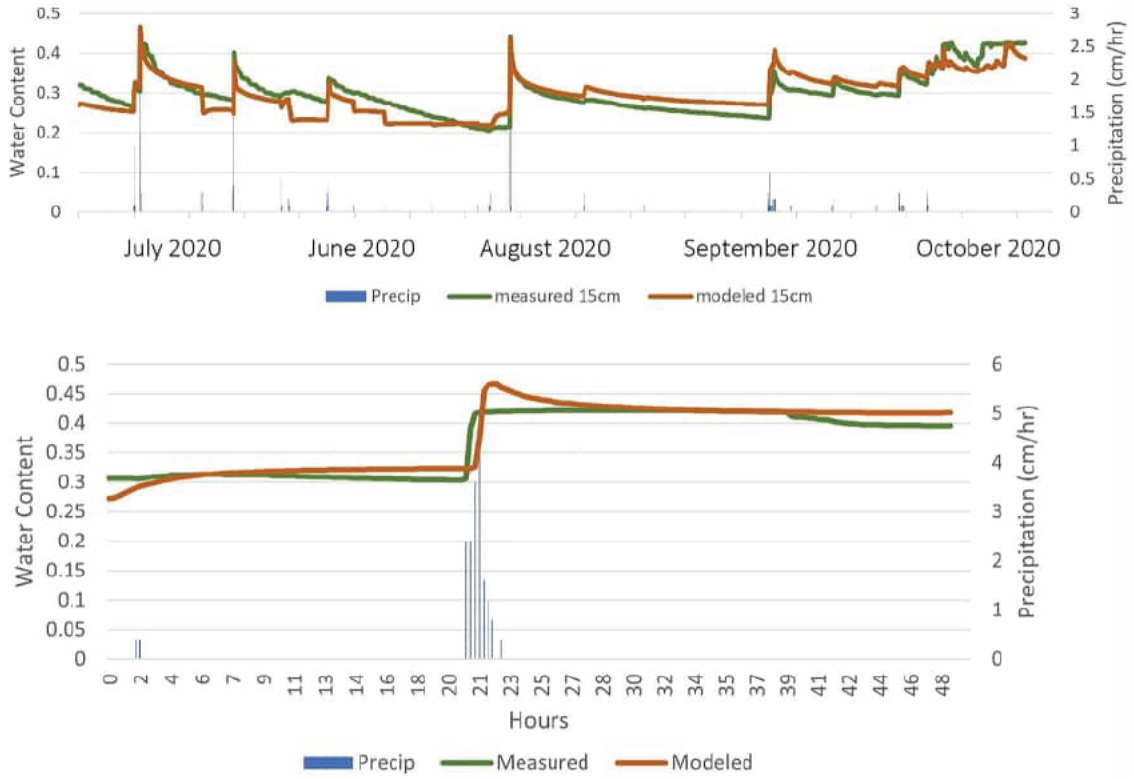

FIGURE 3 (Top) Measured versus predicted soil moisture over a 3.5-month monitoring period using full sun 15-cm depth sensors at New York with Hydrus-1D modeling and (bottom) with Hydrus-3D modeling over a 2-day period that includes a large measured storm event.

3.7 | Hydrus-3D estimates of stormwater runoff across a range of design storms

The calibrated and validated Hydrus-3D model was subsequently used to simulate soil moisture contents and runoff from soils using 24-h 2-, 10-, and 100-year return frequency design storms from NOAA Atlas 14 tables appropriate for each of the five experimental sites. We did not directly monitor runoff at any of the sites. However, we noted clear signs of runoff at all sites except Minnesota based on soil erosion and scour. Figure S5 illustrates the evolution of soil moisture content for the sandy loam and silty clay loam soils at Minnesota and New York. The wetting front reaches the bottom of soil profile after an extended period of infiltration, as shown in Figure S5. The no flux lower boundary condition promotes soil saturation at shallower depths in fine-textured soils, leading to runoff. No runoff was generated in the coarse-textured Minnesota soil with the 24-h 100-year return frequency design storm, whereas there was significant runoff generated in the fine-textured, shallow New York soil. The Minnesota soil exhibited pronounced vertical infiltration patterns, particularly directly underneath the array drip edges. Surface soils in the full sun area and beneath the solar arrays of the Minnesota soil remained unsaturated throughout the duration of the design storm, allowing for enhanced infiltration that prevented runoff. In contrast, the New York soil exhibited rapid onset of saturated soil starting beneath the array drip edges, leading to runoff after only 6 h of rainfall. After 18 h of rainfall, the New York soil was uniformly saturated in the near surface region. This comparison illustrates the large impact that soil texture has on stormwater runoff at solar farms. One of the primary strategies solar developers should use for mitigating runoff is to select sites for development that have good potential for infiltration, avoiding development on sites with low permeability or shallow soils.

Figure 4 illustrates the magnitudes of 24-h 2-, 10-, and 100-year return frequency design storms and associated Hydrus-3D simulated stormwater runoff depths at the five experimental sites. 100-year design storms varied from about 23.8 cm at Georgia to 14.2 cm at Colorado. Despite a 24-h, 100-year return frequency design storm depth of 18 cm at the sandy Minnesota site, this site generated no runoff due to coarse textured deep soil profile with a large saturated hydraulic conductivity value. The 100-year design storms generated 6.1, 13.3, 0, 12.5, and 6.5 cm of runoff during a 24-h period at Colorado, Georgia, Minnesota, New York, and Oregon, respectively. High runoff at Georgia was due primarily to high intensity precipitation, while high runoff at New York (81.9% of the 100-year design storm depth) was primarily due to very shallow soil depth and limited capacity for storage of infiltrated water. Moderate runoff on the low-permeability clay soils in Colorado and Oregon was due to a combination

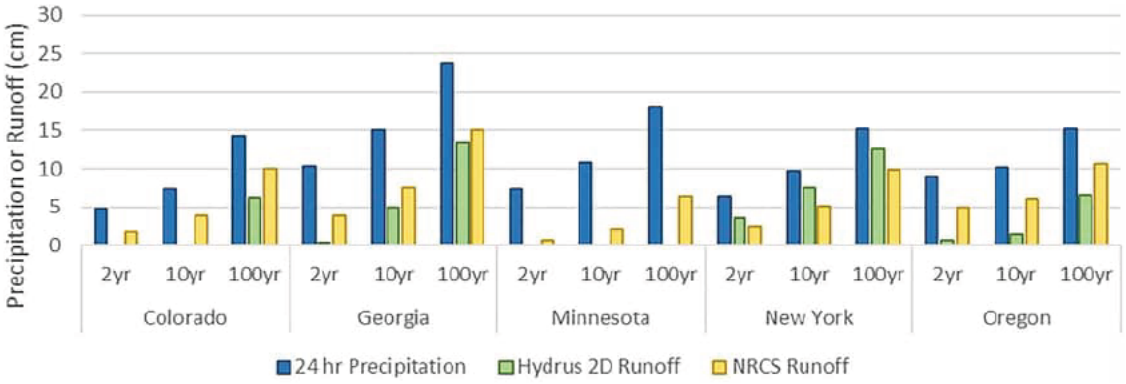

FIGURE 4 Two-, 10-, and 100-year design storms (cm) at the five experimental study sites and corresponding Hydrus-3D stormwater runoff (cm) in comparison with corresponding Natural Resources Conservation Service (NRCS) runoff curve number stormwater runoff (cm).

of relatively low-intensity rainfall combined with low soil bulk densities associated with deep-rooted native and pollinator vegetation. Hydrus-3D runoff averaged 12.9%, 24.8%, and 44.8% of design storm depth for the 2-, 10-, and 100-year 24-h design storms, respectively, for the Colorado, Georgia, Minnesota, New York, and Oregon sites. Clearly, runoff from these sites is much less than runoff that would be generated from completely impervious surfaces, which would have runoff depths that are equal to (100% of) design storm depths.

3.8 | Comparisons of stormwater runoff for Hydrus versus NRCS runoff curve number methods

Most engineers attempting to predict solar farm runoff rely on Natural Resource Conservation Service (NRCS) RCN tied to specific soil types at each site. Post-construction NRCS RCN values based on soil hydrologic group and perennial ground cover of pasture were estimated to be 85, 72, 58, 81, and 85 at Colorado, Georgia, Minnesota, New York, and Oregon, respectively. These RCN values generated stormwater runoff depths for the 24-h 100-year design storm of 10.0, 15.1, 6.3, 9.9, and 4.2 cm at Colorado, Georgia, Minnesota, New York, and Oregon, respectively (Figure 4). These depths are 3.9, 1.8, 6.3, 13.6, and 4.3 cm larger than the corresponding runoff depths generated by Hydrus-3D for the 100-year storm at Colorado, Georgia, Minnesota, and Oregon, respectively. The RCN runoff depth for the 100-year storm at New York generated 2.6 cm less runoff than Hydrus-3D, this difference was a result of increases in runoff caused by shallow soil depth at the New York site that were properly accounted for in Hydrus-3D simulations, but not in RCN-based estimates. Averaged across the 2-, 10-, and 100-year design storms at all sites, NRCS RCN runoff estimates were 58% larger than Hydrus-3D runoff estimates, even though the NRCS RCN method did not explicitly consider presence of the solar arrays. NRCS RCN runoff estimates were considerably larger than Hydrus-3D runoff estimates at the Minnesota site, where Hydrus-3D predicted no runoff for any of the design storms. Runoff depths with the Hydrus-3D approach are not surprisingly more accurate than depths generated using the RCN-based runoff approach because Hydrus-3D was explicitly calibrated for site-specific characteristics such as soil depth, saturated hydraulic conductivity, and vegetative cover that are only dealt with in an average sense using the RCN method. Stormwater runoff predictions with Hydrus-3D across the five experimental sites in the presence of solar arrays were on average 14% larger than runoff in the absence of solar panels. Thus, the disconnected impervious nature of solar arrays, along with the presence of perennial vegetation, can mitigate much of the runoff that would otherwise be expected by installing impervious solar arrays.

3.9 | Comparisons between Hydrus-3D modeling of solar farm runoff and conventional modeling

Recently, two other studies have conceptually explored modeling of stormwater runoff from solar farms using the concept of disconnected impervious surfaces (Gullotta et al., 2023; Nair et al., 2023). Both studies conducted runoff modeling with US Environmental Protection Agency's storm water management model (SWMM). Neither study evaluated model accuracy, because experimental data on soil moisture, infiltration, and runoff were not measured in either study. SWMM is a one-dimensional rainfall excess runoff model that simulates infiltration using a Green–Ampt approach that depends on soil texture and simulates runoff using a Manning's n roughness coefficient that is sensitive to vegetative cover. In contrast, the present study used experimental data to evaluate accuracy of the Hydrus-3D model, which is explicitly capable of considering impacts of soil texture, soil depth, and bulk density, along with vegetative cover impacts on soil moisture content, infiltration, and runoff.

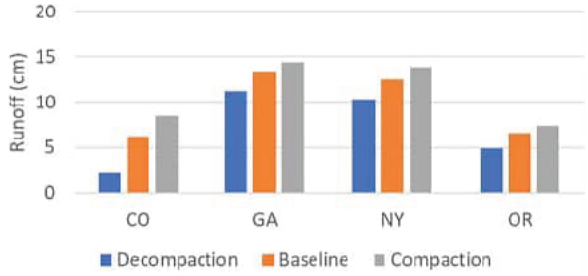

FIGURE 5 Runoff (cm) from 100-year design storms at Colorado (CO), Georgia (GA), New York (NY), and Oregon (OR) experimental sites in response to 25% increases or decreases in soil bulk density relative to runoff under baseline soil bulk density values.

Hydrus-3D uses a Manning's roughness coefficient (n), which was kept at the minimum default value of 0.01. Generally, all sites studied had relatively smooth surfaces, as soils were never tilled. Surface roughness was controlled largely by vegetation effects. In this respect, the impacts of surface roughness and vegetation on infiltration and runoff in the present study were experimentally accounted for by incorporating the sprinkler infiltrometer measurements of field saturated hydraulic conductivity into Hydrus models. Initiation of runoff is controlled by a parameter h0 setting the maximum pressure head for surface ponding before onset of runoff, which was set at the default value of 0 cm.

Hydrus-3D results with and without solar arrays at each of the five experimental sites showed that runoff increased by 14% with arrays present. While a similar result was obtained by Nair et al. (2023) for solar arrays installed on a site with a 23% slope, Gullotta et al. (2023) stated that there were no differences in runoff between sites with or without solar arrays. Their SWMM modeling indicated that changes in soil texture had a larger impact on runoff than changes in vegetative cover (as controlled by the Manning's n factor). The latter results are consistent with those from the present study, though they arise from completely different modeling approaches. Neither the Nair et al. (2023) nor the Gullotta et al. (2023) modeling studies were able to account for impacts of changes in soil depth or soil bulk density on runoff. In the present study, a comparison of runoff from 100-year storms of similar magnitude at New York and Oregon (Figure 4) showed that the shallow silty clay loam soils at New York had roughly double the runoff of the clay soils at Oregon, indicating that soil depth has a large impact on solar farm runoff. This difference is critical, since the simple act of selecting sites with deeper soils for solar farm development can greatly reduce the potential for stormwater runoff, just as managing sites with post-construction tillage to avoid soil compaction and/or perennial vegetation to promote infiltration can greatly reduce stormwater runoff.

The present study also indicates that soil bulk density has a significant impact on runoff (Figure 5). Hydrus-3D simulations were conducted to estimate runoff with 100-year storms at the four sites (Colorado, Georgia, New York, and Oregon) that generated runoff by varying soil bulk density by plus or minus 25% of baseline bulk density values. Increasing bulk density by 25% caused increases in runoff averaging 17% across the four sites, while decreasing bulk density by 25% caused an average 2.5-fold decrease in runoff across the four sites. These results show that management practices that prevent soil compaction and promote low soil bulk density during and after construction of solar facilities can result in significant reductions in solar farm runoff. These practices to reduce soil bulk density could include avoiding heavy machinery traffic during construction when soils are wet, ripping soils after construction ends (if soils have become compacted), and planting deep-rooted vegetation after solar panels have been installed.

The SWMM model explicitly allows for consideration of runoff routing across large areas with many rows of solar arrays, whereas the finite difference algorithms used in Hydrus-3D have run-time limitations that only allow consideration of relatively small areas with homogeneous soil extending across no more than three rows of solar arrays. Nevertheless, the Hydrus-3D model is very useful at illustrating (within these small areas) the relative importance on runoff of factors such as design storm depth, soil texture, soil depth, soil bulk density, vegetation, slope steepness, and presence or absence of solar arrays and their spacing, if present. Nair et al. (2023) pointed out that concentrated runoff is likely to occur when more than three or four rows of solar arrays are considered. They addressed this issue by routing SWMM-generated runoff for sub-areas having four rows of arrays to specified channels, diversion areas, and structural holding basins. Such routing of concentrated runoff was not used in the present study, which seems reasonable based on simulation of only three rows of solar arrays, which Nair et al. (2023) also treated as having sheet flow.

4 | CONCLUSIONS

Ground-mounted PV sites are often treated as impervious surfaces (GPI, 2021), which our research results show is not correct. Ignoring the disconnected pervious soils beneath and between solar arrays leads to an overestimation of runoff. Based on experimental measurements of precipitation and soil hydrology at ground-mounted PV sites in Colorado, Georgia, Minnesota, New York, and Oregon with vegetative plantings of perennial vegetation, we adapted a numerical Hydrus-3D model for infiltration, soil moisture, and runoff at each site. The model was very accurate at representing soil moisture for large storms occurring within a 2-day period at all sites. This study improves on estimation of stormwater runoff at solar farms by considering experimentally measured factors such

as rainfall hitting solar panels, generating concentrated runoff at a drip edge, and the subsequent infiltration of this water downslope in a pervious sunlit area having a wide range of surface conditions, as well as in a pervious area beneath the adjacent downslope row of solar arrays that are themselves impervious to rainfall. Many of these factors are currently ignored by other stormwater models used at ground mounted solar facilities. Runoff across the five experimental sites estimated using Hydrus-3D was, on average, considerably lower than runoff estimated using the standard NRCS RCN method, primarily because of increased capacity for infiltration of runoff beneath solar panels that are shielded from rainfall as well as infiltration in the vegetated areas between solar arrays. These improved runoff estimates using Hydrus-3D for solar PV sites with perennial vegetation could significantly reduce the need to install expensive stormwater mitigation practices at ground-mounted solar PV sites. Further, the model provides useful insight into variations in runoff at solar farms due to the complex interplay between disconnected impervious surfaces, drip edge runoff, and variations in soil texture, soil depth, soil bulk density, and vegetative cover.

AUTHOR CONTRIBUTIONS

David Mulla: Conceptualization; funding acquisition; methodology; project administration; supervision; writing—original draft. **Jake Galzki**: Data curation; formal analysis; methodology; validation; visualization; writing—review and editing. **Aaron Hanson**: Data curation; investigation. **Jirka Simunek**: Software.

ACKNOWLEDGMENTS

This research was supported by the US Department of Energy Office of Energy Efficiency and Renewable Energy under the Solar Energy Technologies Office Award Number DE-AC36- 08GO28308. We acknowledge helpful suggestions on research direction by the PV-SMaRT Water Quality Task Force Advisory Board members. Assistance with installation of monitoring equipment at research sites during the COVID pandemic is acknowledged for Dr. Tim Green (CO), Dr. Craig Kvien (GA), Dr. Scott McArt (NY), and Maggie Graham (OR).

CONFLICT OF INTEREST STATEMENT

The authors declare no conflicts of interest.

ORCID

David Mulla https://orcid.org/0000-0001-7040-5888
Jirka Simunek https://orcid.org/0000-0002-0166-6563

REFERENCES

Barnard, T., Agnaou, M., & Barbis, J. (2017). Two-dimensional modeling to simulate stormwater flows at photovoltaic solar energy sites. *Journal of Water Management Modeling*, *25*, C428. https://doi.org/10.14796/JWMM.C428

Bouyoucos, G. J. (1962). Hydrometer method improved for making particle size analyses of soils. *Agronomy Journal*, *54*, 464–465. https://doi.org/10.2134/agronj1962.00021962005400050028x

Chandler, D. G., Seyfried, M. S., Mcnamara, J. P., & Hwang, K. (2017). Inference of soil hydrologic parameters from electronic soil moisture records. *Frontiers in Earth Science*, *5*, Article 25.

Cook, L. M., & Mccuen, R. H. (2013). Hydrologic response of solar farms. *Journal of Hydrologic Engineering*, *18*, 536–541.

Doran, J. W., & Mielke, L. N. (1984). A rapid, low-cost method for determination of soil bulk density. *Soil Science Society of America Journal*, *48*, 717–719. https://doi.org/10.2136/sssaj1984.03615995004800040004x

Elamri, Y., Cheviron, B., Mange, A., Dejean, C., Liron, F., & Belaud, G. (2018). Rain concentration and sheltering effect of solar panels on cultivated plots. *Hydrology and Earth System Sciences*, *22*, 1285–1298.

Feddes, R. A., Hoff, H., Bruen, M., Dawson, T., De Rosnay, P., Dirmeyer, P., Jackson, R. B., Kabat, P., Kleidon, A., Lilly, A., & Pitman, A. J. (2001). Modeling root water uptake in hydrological and climate models. *Bulletin of the American Meteorological Society*, *82*, 2797–2810.

Great Plains Institute. (2021). *Photovoltaic stormwater management research and testing (PV-SMaRT): Potential stormwater barriers and opportunities*. Great Plains Institute. https://betterenergy.org/wp-content/uploads/2021/10/PV-SMaRT-Potential-Stormwater-Barriers-and-Opportunities.pdf

Gullotta, A., Aschale, T. M., Peres, D. J., Sciuto, G., & Cancelliere, A. (2023). Modelling stormwater runoff changes induced by ground-mounted photovoltaic solar parks: A conceptualization in EPA-SWMM. *Water Resources Management*, *37*, 4507–4520.

Hassanpour Adeh, E., Selker, J. S., & Higgins, C. W. (2018). Remarkable agrivoltaic influence on soil moisture, micrometeorology and water-use efficiency. *PLoS ONE*, *13*, e0203256.

Heath, G., Ravikumar, D., Ovaitt, S., Walston, L., Curtis, T., Millstein, D., Mirletz, H., Hartmann, H., & McCall, J. (2022). *Environmental and circular economy implications of solar energy in a decarbonized U.S. grid* (NREL/TP-6A20-80818). National Renewable Energy Laboratory. https://www.nrel.gov/docs/fy22osti/80818.pdf

Hernandez, R. R., Easter, S. B., Murphy-Mariscal, M. L., Maestre, F. T., Tavassoli, M., Allen, E. B., Barrows, C. W., Belnap, J., Ochoa-Hueso, R., Ravi, S., & Allen, M. F. (2014). Environmental impacts of utility-scale solar energy. *Renewable and Sustainable Energy Reviews*, *29*, 766–779. https://doi.org/10.1016/j.rser.2013.08.041

Hilten, R. N., Lawrence, T. M., & Tollner, E. W. (2008). Modeling stormwater runoff from green roofs with HYDRUS-1D. *Journal of Hydrology*, *358*, 288–293.

Moore-O'leary, K. A., Hernandez, R. R., Johnston, D. S., Abella, S. R., Tanner, K. E., Swanson, A. C., Kreitler, J., & Lovich, J. E. (2017). Sustainability of utility-scale solar energy—Critical ecological concepts. *Frontiers in Ecology and the Environment*, *15*, 385–394.

Nair, A. A., Rohith, A. N., Cibin, R., & McPhillips, L. E. (2023). A framework to model the hydrology of solar farms using EPA SWMM. *Environmental Modeling & Assessment*, *29*, 91–100. https://doi.org/10.1007/s10666-023-09922-0

Rand, J., Wiser, R. H., Gorman, W., Millstein, D., Seel, J., Jeong, S., & Robson, D. (2022). *Queued up: Characteristics of power plants*

seeking transmission interconnection as of the end of 2021. Lawrence Berkeley National Lab.

Schaap, M. G., Leij, F. J., & Van Genuchten, M. T. (2001). Rosetta: A computer program for estimating soil hydraulic parameters with hierarchical pedotransfer functions. *Journal of Hydrology*, *251*, 163–176.

Šimůnek, J., Van Genuchten, M. T., & Šejna, M. (2008). Development and applications of the HYDRUS and STANMOD software packages and related codes. *Vadose Zone Journal*, *7*, 587–600. https://doi.org/10.2136/vzj2007.0077

van Es, H., & Schindelbeck, R. (2006). *Field procedures and data analysis for the Cornell sprinkle infiltrometer*. Cornell University.

Van Genuchten, M. T., & Nielsen, D. R. (1985). On describing and predicting the hydraulic properties. *Annales Geophysicae*, *3*, 615–628.

Vergroesen, T., & Joshi, U. M. (2010). Green roof runoff experiments in Singapore. In *Novatech 2010–7ème Conférence Internationale sur les Techniques et Stratégies Durables pour la Gestion des Eaux Urbaines par Temps de Pluie [7th International conference on sustainable techniques and strategies for urban water management]* (pp. 1–10). GRAIE.

Walston, L. J., Li, Y., Hartmann, H. M., Macknick, J., Hanson, A., Nootenboom, C., Lonsdorf, E., & Hellmann, J. (2021). Modeling the ecosystem services of native vegetation management practices at solar energy facilities in the Midwestern United States. *Ecosystem Services*, *47*, 101227.

Yavari, R., Zaliwciw, D., Cibin, R., & McPhillips, L. (2022). Minimizing environmental impacts of solar farms: A review of current science on landscape hydrology and guidance on stormwater management. *Environmental Research: Infrastructure and Sustainability*, *2*, 032002.

SUPPORTING INFORMATION

Additional supporting information can be found online in the Supporting Information section at the end of this article.

How to cite this article: Mulla, D., Galzki, J., Hanson, A., & Simunek, J. (2024). Measuring and modeling soil moisture and runoff at solar farms using a disconnected impervious surface approach. *Vadose Zone Journal*, *23*, e20335. https://doi.org/10.1002/vzj2.20335

Discover Water

Research

Stormwater runoff calculator for evaluation of low impact development practices at ground-mounted solar photovoltaic farms

Jake Galzki[1] · David Mulla[1]

Received: 1 April 2024 / Accepted: 6 June 2024
Published online: 11 June 2024

Abstract
Estimating runoff at ground-mounted solar photovoltaic (PV) installations is challenging because of the disconnected nature of impervious solar panels and the pervious ground surface underneath and between panel rows. There is a need for improved tools to estimate how low impact development practices at these solar installations affect stormwater runoff. The objective of this study was to develop an innovative spreadsheet-based runoff calculator that rapidly estimates stormwater runoff from ground-mounted solar PV sites. The calculator is built on a 2-D hydrologic model (Hydrus-2D/3D) calibrated and validated using experimental data from five commercial solar farms in Colorado, Georgia, Minnesota, New York, and Oregon. The Hydrus-2D/3D hydrologic model was then used to generate nomographs for stormwater runoff that were incorporated into an easy-to-use Excel-based solar farm runoff calculator. This calculator allows for rapid estimation of NRCS stormwater runoff curve number (CN) values at solar farms by considering several complex factors unique to PV installations including: soil and topographic characteristics, surface cover, disconnected impervious surface factors associated with various solar panel designs, and climatic factors. The solar farm runoff calculator quickly estimates runoff CN for pre- and post-construction scenarios, and can estimate actual depth of runoff based on a user-specified 24-h design storm depth. Factors that have the most significant impact on stormwater runoff include design storm return frequency, soil texture, soil bulk density, and soil depth. Ground surface cover has a moderate impact on stormwater runoff, and factors that have a lesser impact on stormwater runoff include slope and array size, spacing and orientation on the landscape. The runoff calculator allows for accurate estimates of runoff generated by disconnected impervious surfaces and low impact development practices at solar farms as affected by a wide range of site-specific conditions.

Keywords Solar farm · Stormwater runoff · Soil texture · Soil depth · Soil bulk density · Perennial vegetation · Hydrus-2D/3D

1 Core ideas

- Hydrus-2D/3D was used to generate nomographs for solar farm stormwater runoff
- Nomographs were built into an easy-to-use Excel spreadsheet-based solar farm runoff model
- Design storm depth, soil texture, depth and bulk density had a large impact on solar farm runoff
- Low impact vegetative surface cover had a moderate impact on solar farm runoff
- Solar array size, spacing and orientation on the landscape had a small impact on runoff

✉ Jake Galzki, [redacted]@umn.edu; David Mulla[redacted]@umn.edu | [1]Department Soil, Water & Climate, University of Minnesota, Twin Cities, 1991 Upper Buford Circle, St. Paul, MN 55108, USA.

2 Introduction

Solar energy has recently become the most economical form of electricity generation in the US [1]. Due to a push for increased reliance on renewable energy sources combined with the cost-efficiency of solar energy, photovoltaic (PV) electricity generating installations have had an increasing role in the US electrical grid and are expected to expand drastically in the years to come [2]. Empirical data regarding the impact of PV installations on stormwater runoff is limited [3], and approaches for estimating their hydrologic impact vary widely across the country. In the worst case, ground mounted solar facilities are often mis-represented as completely impervious surfaces, which implies runoff responses like those from rooftops or paved surfaces. This ignores the disconnected impervious nature of these facilities, in which runoff from solar arrays enters pervious areas between arrays where infiltration can occur.

Low impact development (LID) strategies attempt to utilize natural and engineered infiltration techniques to control stormwater [4]. LID approaches in relation to PV systems are often associated with rooftop solar installations, such as reduction of impervious surfaces and implementation of native or site-appropriate vegetation [4]. Studies on green roofs, where vegetation is introduced to impervious building rooftops, show both modeled [5] and measured [6] reductions in stormwater generation. Several recent studies shift focus from rooftop solar and explore the impact of ground-mounted PV installations on local hydrology and stormwater [7–10]. Walston et al. (2021) looked specifically at native vegetation management practices at ground-mounted PV installations and their impact on ecosystem services. They found that native vegetation at solar installations increase pollinator supply, carbon storage potential, and sediment and water retention [11].

The Photovoltaic Stormwater Management Research and Testing (PV-SMaRT) project provided funding to the University of Minnesota by DOE-SETO to develop research-based, PV-specific tools to estimate how low impact management practices at ground-mounted PV sites impact stormwater runoff. A previously published PV-SMaRT funded paper [12] described how a numerical hydrologic model (Hydrus-2D/3D) was field-calibrated and validated against soil moisture measurements at five commercial PV solar farms with perennial vegetation located in Colorado, Georgia, Minnesota, New York and Oregon. These sites were chosen to represent a wide variety of soil factors and climatic regimes to determine their impacts on stormwater runoff. Complex factors unique to PV installations were considered in this hydrologic modeling such as rainfall interception by solar panels, generation of concentrated runoff at a drip-edge, and the subsequent infiltration of drip-edge runoff downslope in a pervious area having a wide range of surface conditions, as well as in a pervious area beneath the adjacent downslope row of solar arrays that are themselves impervious to rainfall. These factors are currently ignored by other stormwater models commonly applied at solar farms, which either assume that the entire facility is either pervious or impervious, or that it has a level of imperviousness that is calculated by averaging the area of arrays and the area of pervious surfaces between arrays [13, 14].

The objective of the current paper was to extend the previously developed PV-SMaRT Hydrus-2D/3D stormwater runoff model [12] for ground-mounted PV installations by developing a user-friendly spreadsheet-based calculator that can rapidly evaluate pre- and post-construction site conditions at ground-mounted PV installations and their impacts on stormwater runoff. This objective is achieved by using results from nearly 1,000 simulations of the numerical Hydrus-2D/3D model to develop exponential regression equations relating soil texture, soil bulk density, and soil depth to a runoff CN. This regression is further supplemented with results from field test sites in the PV-SMaRT project to account for panel width and spacing (ground-to-cover ratio) as well as orientation along the slope of the landscape. Finally, slope and ground cover (bare soil, row crop, perennial vegetation, etc.) are incorporated into the calculator using extensively studied relationships from the literature [15–17].

3 Methods

A numerical hydrologic model was developed from the PV-SMaRT study [12] simulating stormwater runoff at ground mounted solar PV facilities using Hydrus-2D/3D software [18]. This model simulates water flow in variably saturated soils based on the van Genuchten hydraulic conductivity equation [19] and can calculate infiltration through a soil profile as well as expected overland runoff. The Hydrus-2D/3D model was chosen to simulate soil moisture and stormwater runoff at PV facilities because of its ability to accurately represent soil hydrologic processes and account for multiple upper boundary conditions. These boundary conditions include incident precipitation that occurs in the area between solar panels, an area with potentially zero precipitation that impacts the ground underneath a panel in the absence of wind, and an area of

concentrated precipitation that represents panel runoff accumulating and falling on the ground at the downslope panel edge. The model can also route overland runoff underneath subsequent downslope arrays and account for infiltration under the panel (Fig. 1). Nodal spacing of model domains was approximately 5 cm vertically and between 5 and 50 cm for horizontal nodes. Higher nodal densities were used where the upper boundary condition transitioned from no precipitation (under panel) to concentrated precipitation (drip edge runoff) to incident precipitation between panels in attempt to accurately quantify this transition. A three-panel domain created originally for the five PV-SMaRT field-test sites produced satisfactory results (RMSE values for soil moisture content ranging from 0.023 to 0.038), while preserving the likelihood of convergence for the Hydrus model [12].

Initial analysis of the PV-SMaRT study modeling results determined that design storm size, soil bulk density, and soil profile depth had the largest impact on resultant runoff amounts [12]; therefore, these were the initial variables that received focus in model simulations used to develop the user-friendly spreadsheet-based PV runoff calculator. Twelve soil textures were simulated with associated default van Genuchten soil hydraulic properties. For each of the twelve major soil textures, simulations included 5 design storms, variable soil profile depths of 50, 100, and 150 cm, and bulk density values of 1.0, 1.2, 1.35, 1.5, and 1.7 g/cm^3. 24-h design storms were initially chosen based on common hydrologic design considerations and consisted of 2-year (8.9 cm), 10-year (10.2 cm), and 100-year (15.2 cm) return frequencies obtained from the NOAA Precipitation Data Server [20]. These specific values represented the most common intensities among the five PV-SMaRT sites, and 24-h storms were simulated based on NOAA Atlas 14 synthetic rainfall distributions [21]. Some soils with high infiltration rates (coarse textures, low bulk densities, deep profiles, etc.) occasionally yielded zero runoff for these design storms, thus storms of 20 and 25 cm were added to ensure runoff would be initiated for most simulations in order to inform subsequent curve number regressions.

Runoff values were recorded for each of the combinations of twelve soil textures, five bulk densities, three profile depths, and five design storms yielding a database of nearly 1,000 combinations of rainfall and runoff. Elhakeem and Papanicolaou (2009) used exponential regression to translate rainfall and runoff measurements from small rainfall simulator plots in six Iowa counties into a runoff CN [22]. A similar approach was used here; rainfall and runoff combinations for simulated solar farms were translated into curve numbers for every combination of texture, bulk density and profile depth based on the NRCS curve number method standard equation [23]:

$$Q = \frac{\left(P - I_a\right)^2}{\left(P - I_a + S\right)} \text{for } P > I_a$$

Q = Runoff (mm)P = Precipitation (mm)S = Soil moisture retention after runoff begins (mm)I_a= Initial abstraction (mm) where I_a= 0.2 SCurve Number (CN) is then determined as:

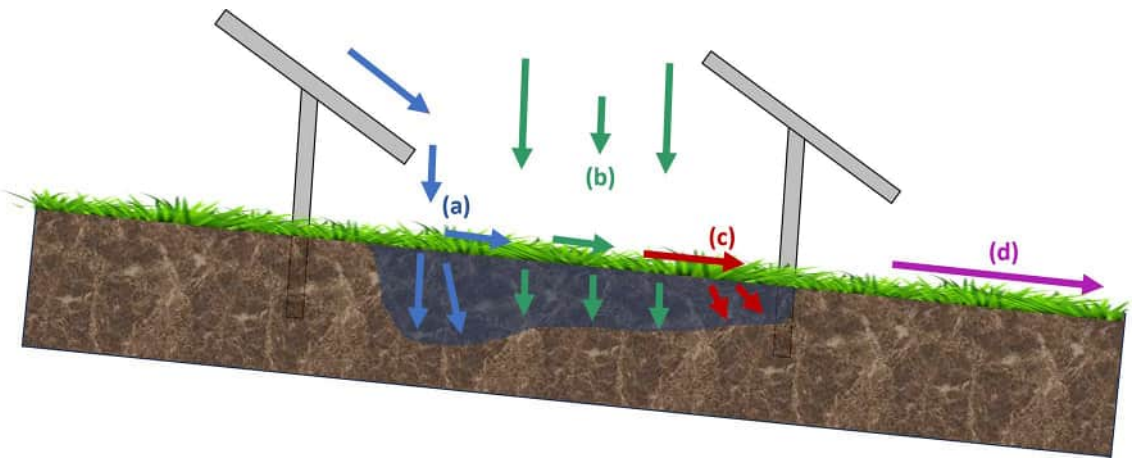

Fig. 1 Hydrus-2D/3D representation of **a** drip edge runoff, **b** incident precipitation, **c** surface and lateral soil moisture migration under downslope panel, and **d** overland runoff

$$CN = \frac{25{,}400}{S + 254}$$

3.1 Soil texture and bulk density

The resultant database included a CN value for every soil texture, bulk density, and profile depth combination. For a given soil texture, variations in bulk density produced the largest changes in predicted runoff, relative to variations in other site-specific factors. A relationship between CN and bulk density was determined for each soil texture using exponential regression:

$$CN = a * b^{x}$$

CN = Curve Number$x$ = Bulk Density (g/cm^3)

An excel spreadsheet was utilized to store the resultant database of regression coefficients, which was then used as a lookup table to calculate a baseline CN for any user-defined soil texture and bulk density combination. The allowable range of bulk density values within the calculator is between 1 and 1.8 g/cm^3.

3.2 Soil profile depth

Depth to an impermeable layer, or soil profile depth, was the next most important variable identified in driving expected runoff rates and CN values in the original PV-SMaRT publication [12]. As depth to an impermeable layer increased in simulations, CN values and runoff decreased in Hydrus simulations. For most soil textures, changes in runoff became negligible at depths greater than approximately 100 to 150 cm. Soil profile depth had a larger impact on runoff CN for coarser-textured soils with higher infiltration rates; heavier-textured soils were limited more by surface infiltration rates, and depths greater than 100 cm yielded little change in runoff CN. The CN regression relationship with bulk density described in the previous section was thus developed for each soil texture at two different depths: 50 cm and either 100 or 150 cm (depending on which depth limited CN). CN value for a user-specified profile depth is then determined by linear interpolation between the shallower and deeper bulk density regression. CN interpolations were constrained by the deeper profile curve for each soil texture, so CN values would not change when profile depth exceeded the CN-limited depth. The allowable range of profile depth values within the calculator ranges between 30 and 150 cm.

3.3 Ground cover

Soil texture, soil bulk density, and soil depth create a baseline CN value in the calculator for any user-defined combination within the allowable input range. Other data input parameters are then accounted for by modifying this baseline CN. Abundant research has been completed on the impact of ground cover on runoff CN [15]. NRCS lookup tables, commonly known as TR-55 tables, were utilized to account for ground cover effects other than the perennial vegetation studied at PV-SMaRT solar farm sites. Pasture/grassland in fair condition (50–75% ground cover, not heavily grazed) was chosen from the TR-55 tables as the baseline ground cover to approximate these plantings. Deviation of TR-55 CN values from this condition were then used to calculate a CN modifier for different ground cover conditions. TR-55 lookup tables also rely on hydrologic soil group to provide accurate CN estimates. Each soil texture was simulated within the calculator for low, medium, and high bulk density values as determined from chapter 3 of the NRCS Soil Survey Manual relating texture and bulk density classes [24]. This yielded a relation for each texture and bulk density combination to an expected value of saturated hydraulic conductivity. Resultant values of saturated hydraulic conductivity were then used to infer soil hydrologic group from chapter 7 of the National Engineering Handbook [25], so a relationship between CN and soil hydrologic group could be estimated (Table 1). Baseline CN is then used within the calculator to approximate hydrologic soil group and provide a modifier unique to a given hydrologic soil group and ground cover combination.

3.4 Panel presence, width and spacing

As determined in the first PV-SMaRT publication [12], changes in panel size and spacing had a smaller impact on runoff than changes in bulk density and soil depth; to explore this factor in detail would compound the number of simulations already approaching 1,000 and would require far more data processing than the scope of this research requires. These

Table 1 Baseline Curve Number (CN) translation to a Hydrologic soil group for determining ground cover CN modifier

Baseline CN Range	Hydrologic Soil Group
0–40	A
41–60	B
61–80	C
81–100	D

factors are instead accounted for by modifying the baseline CN based on existing PV-SMaRT Hydrus-2D/3D simulation results. All Hydrus simulations in the calculator were run with 3 m (10 foot) panels spaced at 7.6 m (25 feet) on center. This was used as the baseline condition within the calculator, and CN modifiers change baseline CNs according to their deviation from these conditions. Panels were assumed to be at a 45-degree angle in simulations, a common condition observed in the original PV-SMaRT study sites, to simulate high precipitation interception and subsequent panel runoff. Multiple angles are not directly accommodated within the calculator, but panel width and panel spacing were accommodated by converting to a ground-to-cover ratio. This ratio is calculated by dividing the horizontal ground distance with no panel covering by the horizontal distance covered by a panel at a 45-degree tilt. It is analogous to a permeable-to-impermeable ratio as viewed from above. Ground-to-cover ratios for the PV-SMaRT sites ranged from as low as 1:1 (equal amounts of permeable to impermeable area) to 4.5:1. Panel spacings with a ground-to-cover ratio less than 1:1 would cause shading on adjacent panel rows and would theoretically be avoided except for extreme slope conditions; spacings with very high ratios would also be theoretically avoided since they would start to diminish potential electricity generation at a PV site. Ground to cover ratios were simulated at PV-SMaRT solar farm sites ranging from 1:1 to 7:1 to obtain a relationship between runoff and panel spacing.

Additional Hydrus simulations were run for each soil texture with all panels removed from the model domain and the upper boundary condition set to incident precipitation. Resultant runoff CN values from these simulations were then compared to simulations in the presence of solar panels to create a CN modifier to account for panel presence within the calculator.

3.5 Panel orientation

Baseline Hydrus simulations were run for solar arrays installed either along the contours of the landscape or parallel to the local slope. This allowed for panel runoff to be routed and infiltrated both between solar panels and beneath the subsequent downslope panels. It is possible to have panel installations that are perpendicular to local slope, or positioned up and down slope, where runoff accumulates in a concentrated area at the drip edge and flows downslope between panels (no infiltration underneath panels). Additional Hydrus simulations were conducted to capture this condition for each soil texture. Simulations were created using drip edge runoff amounts that accumulate in a concentrated area as opposed to infiltrating beneath downslope panels. Data from measurements of drip edge runoff relative to incident precipitation at the PV-SMaRT solar study sites determined that runoff from a 3 m (10 foot) fixed panel was approximately 10 times the incident precipitation rate on average [12], so this value was used in Hydrus simulations with panels oriented up and down slope.

3.6 Slope

Slope at PV-SMaRT solar farm study sites varied between 1.5 and 5%. A recent publication [26] outlines two common methods of slope adjustment on CN, namely the Sharpley-Williams method and the Huang method, both allowing for consideration of a greater range in slopes than those occurring at the relatively flat PV-SMaRT study sites. Both methods are used within the spreadsheet runoff calculator tool, and the greater slope-adjusted CN of the two is used when slopes are more than 10% to provide the most conservative slope-modified runoff estimate.

3.7 Final calculator considerations

Certain combinations of the baseline variables for soil texture, bulk density, and depth can combine with other CN modifiers to produce CN values slightly outside the theoretical range of possible CN values. In these uncommon instances,

the calculator restricts the final CN value to be within the theoretical bounds of the curve number method, namely 30 for the lower threshold and 100 for the upper threshold.

The steps used in the present paper for the Hydrus-2D/3D pre-processing simulations that were used to generate nomographs, and the subsequent steps used in the easily used solar farm Excel-based runoff calculator are depicted in Fig. 2. Baseline CN nomographs are generated using Hydrus-2D/3D simulations based on a wide range in values for soil characteristics such as soil texture, soil depth and bulk density. The baseline Hydrus-2D/3D generated CN value nomographs are then modified by taking into account adjustments for ground cover, slope, and solar array characteristics to generate a set of final runoff CN nomographs. These nomographs are then incorporated into an easy to use Excel-based solar farm runoff calculator. The user then inputs site-specific data (soil texture, soil depth, soil bulk density, ground cover condition, slope, solar array characteristics and desired 24-h storm depth for a desired return frequency storm) for the solar farm of interest into the solar farm calculator. Nomographs within the solar farm calculator use these inputs to generate a site-specific runoff CN value and stormwater depth runoff estimate.

4 Results

4.1 Soil texture and bulk density

Soil texture and bulk density have a very large influence on CN and expected runoff (Fig. 3). When soil profile depth and bulk density is held at a constant (50 cm and 1.4 g/cm^3), CNs range from a low of 43 (Loamy Sands) to a high of 85 (Clay Loam). For a 25.4 cm (10 in) 24-h precipitation event, these CNs translate into expected runoff values of 6.76 cm for Loamy Sands (2.66 in) to 20.60 cm for Clay Loams (8.11 in), an increase of 13.84 cm (5.45 in) in runoff. Bulk density was found to be a significant driver of CN and runoff amongst the variables analyzed in the first PV-SMaRT publication [12]. For a medium textured soil (Sandy Clay) held at a constant 50 cm profile depth, bulk density yields a CN of 58 at its lowest (1.0 g/cm^3) and 89 at its highest end of the bulk density range (1.8 g/cm^3). These CN values would yield a range of expected runoff from the above storm of 11.61 cm (4.57 in) for an uncompacted loose soil to 22.12 cm (8.71 in) for a

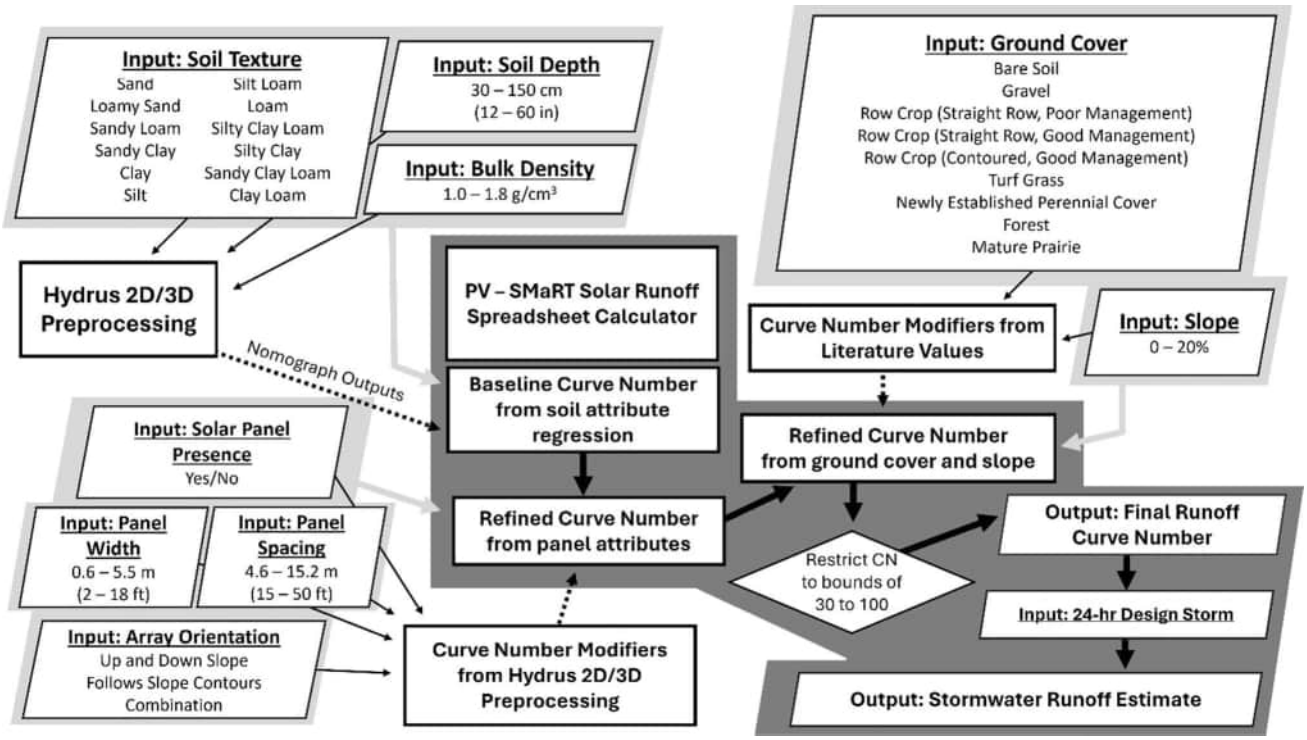

Fig. 2 Workflow diagram describing the Hydrus-2D/3D pre-processing steps to generate runoff curve number nomographs that are incorporated into an easy-to-use solar farm Excel-based stormwater calculator (shaded portion of diagram) with all inputs and the allowable data input ranges for numerical factors as well as variable options if they are categorical factors

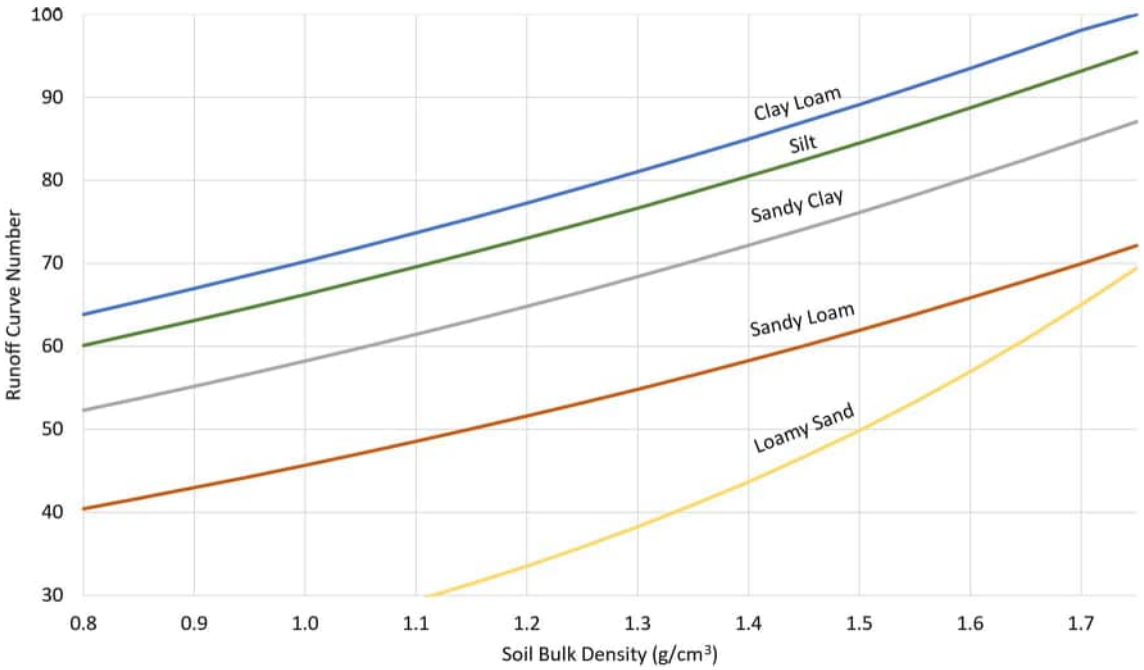

Fig. 3 Relationship of bulk density and Curve Number (CN) for selected soil textures held at a constant 50 cm profile depth

compacted dense soil, an increase in 10.52 cm (4.14 in). Preventing or mitigating soil compaction during and after solar facility construction through traffic/vegetation management practices as well as decompacting soil after construction could be highly effective practices to reduce runoff. Native bulk densities should also be considered during the siting phase of potential PV projects to determine runoff implications of different site selections.

4.2 Soil profile depth

Depth to an impermeable layer was found to be the next most sensitive parameter affecting solar farm runoff. When soil texture and bulk density are held constant (Clay Loam and 1.4 g/cm^3), soil depth differences yield CN values ranging from 62 for depths greater than 100 cm, and as high as 94 for depths shallower than 30 cm. For a 25.4 cm (10 in) 24-h precipitation event, these CN values translate into expected runoff values of 13.2 cm (5.2 in) for the deeper profile and 23.6 cm (9.3 in) for the shallower profile, an increase of 10.4 cm (4.1 in). When evaluating a very coarse textured soil such as a Sand, these CN values range from 30 (soil depth > 150 cm) to 74 (soil depth < 30 cm). For the above precipitation event, this translates to a range of 2.5 cm (1.0 in) of runoff for the deep profile to 17.3 cm (6.8 in) of runoff for the shallow profile, an increase of 14.8 cm (5.8 in). Figure 4 illustrates the relationship between profile depth and bulk density changes for selected soil textures. Cut and fill construction techniques that remove topsoil would typically increase expected runoff and should be minimized. Soil profile depth should also be considered during the site selection phase of a project to identify sites with deeper soils that could reduce potential runoff.

4.3 Baseline curve number values

The runoff calculator computes a baseline CN with user-input of soil texture, bulk density, and soil depth. This allows for a wide range of site-specific soil characteristics to be represented within the calculator which were directly informed by HYDRUS-2D/3D model results. Figure 5 displays good agreement between actual HYDRUS-2D/3D model results and the exponential regression nomographs in the solar farm runoff calculator for a silt loam soil across a range of bulk densities and multiple soil profile depths. Once the baseline CN is established with soil characteristics, the calculator then allows for further adjustment to baseline CN values by accommodating specific choices for ground cover, ground surface slope, and panel size, spacing and orientation.

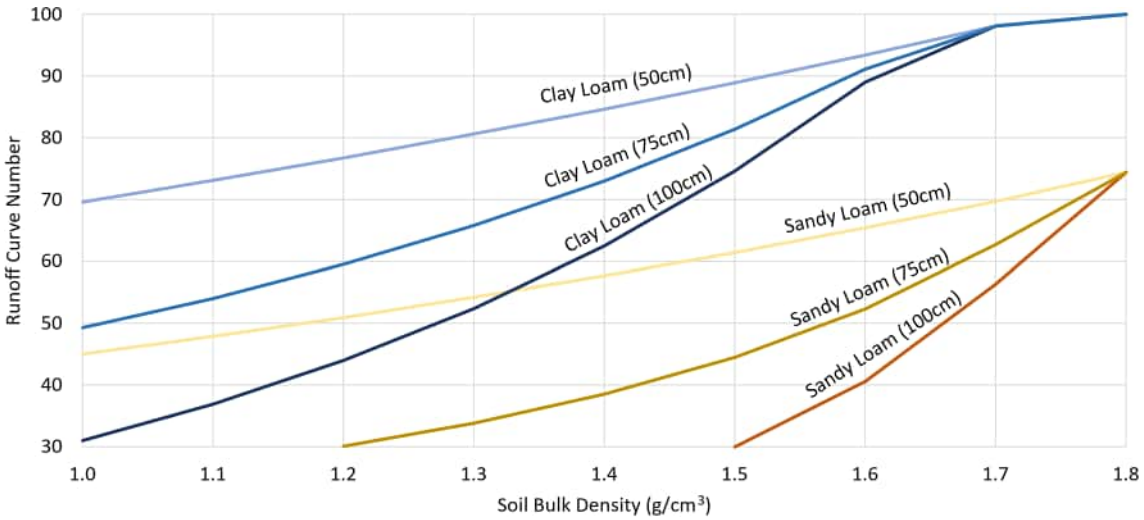

Fig. 4 Relationship between bulk density, soil profile depth, and Curve Number (CN) value for selected soil textures and depths in parentheses

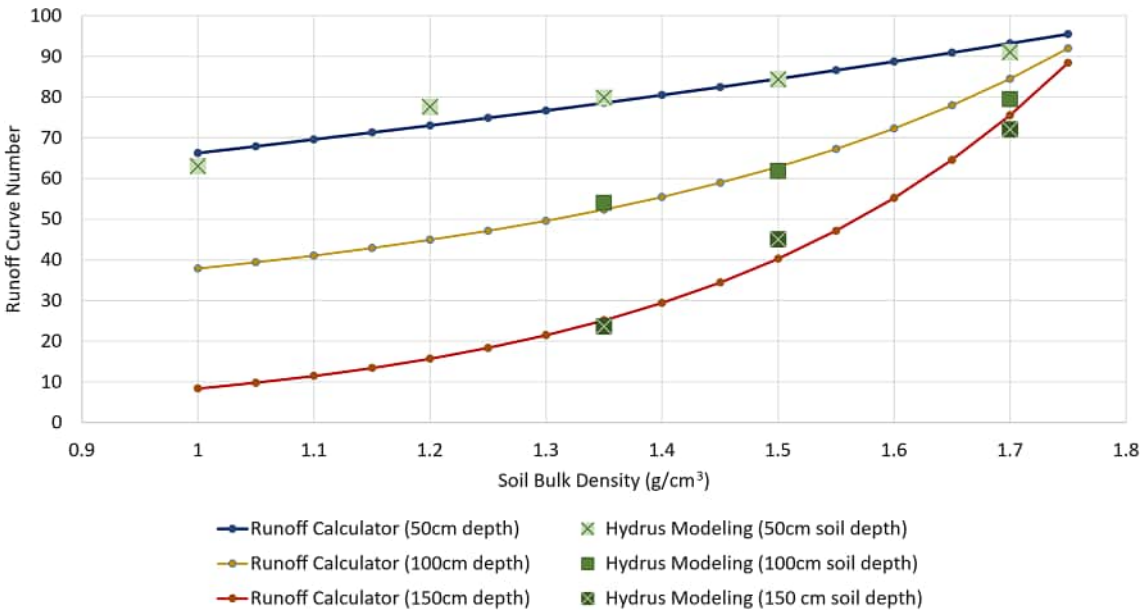

Fig. 5 Comparison of runoff Curve Number (CN) values generated by HYDRUS-2D/3D modeling results and the PV-SMaRT solar farm runoff calculator CN values and resulting regression curves for a silt soil texture as affected by soil bulk density at multiple soil profile depths

4.4 Ground cover

Ground covers considered in the calculator include bare soil, gravel, row crops (with multiple management considerations), turf grass, newly established pollinator, forest, and mature prairie. Table 2 provides the percent change in CN for each ground cover condition and soil hydrologic group with respect to the baseline ground cover of newly established perennials. CN values increase from baseline values by as much as 57% if low impact practices such as perennial cover are converted to bare soil for hydrologic group A soils, implying a much larger expected runoff amount without low impact cover. Ground cover should be an important consideration of PV installations both during site selection and post-construction management of a site. Conversion of low impact ground cover (forest/mature prairie) to high impact ground cover (gravel/bare soil) should be avoided. Establishment of moderately low

Table 2 Percent change in Curve Number (CN) values for multiple ground cover types relative to the baseline ground cover of "Newly Established Perennial Cover"

Ground Cover Type	Soil Hydrologic Group			
	A (%)	B (%)	C (%)	D (%)
Bare Soil	57	25	15	12
Gravel	55	23	13	8
Row Crop (Straight Row, Poor Management)	47	17	11	8
Row Crop (Straight Row, Good Management)	37	13	8	6
Turf Grass	39	14	9	6
Row Crop (Contoured, Good Management)	31	7	3	1
Newly Established Perennial Cover	0	0	0	0
Forest	− 27	− 13	− 8	− 6
Mature Prairie	− 39	− 16	− 10	− 7

impact ground covers, such as newly established perennial cover, could reduce stormwater runoff in comparison with a higher impact ground cover (row crop/turf grass).

4.5 Panel presence, width and spacing

The addition of panels and their respective size and spacing had less of an impact on resultant curve numbers (Fig. 6) than the baseline CN inputs of soil texture, bulk density, and soil depth. When adding solar panels to a landscape with typical bulk density and profile depth values (1.4 g/cm^3 and 50 cm), average CN values for all soil textures increase. This increase ranges from an average across all soil textures of 3.7 points for widely set panels (ground-to-cover ratio of 4:1) to 7.7 points for narrowly spaced panels (ground-to-cover ratio of 1:1). For example, simulating a 25.4 cm (10 in) 24-h storm over a medium textured Sandy Clay with no panels present yields an expected runoff value of 13.9 cm (5.5 in). When adding solar panels for a Sandy Clay soil with a range in ground-to-cover ratios, predicted runoff increases from 15.7 cm (6.2 in) with wide panel spacing to 17.0 cm (6.7 in) with narrow panel spacing. This translates to a 14% increase in runoff for widely spaced panels and a 23% increase in runoff for narrowly spaced panels. Wider panel spacings allow for a larger area between arrays where low impact vegetative plantings can mitigate runoff. The runoff calculator can quickly be used to indicate how runoff from a baseline condition having no solar panels compares with runoff from a post-construction condition with solar panels installed with various panel widths and array spacings.

4.6 Panel orientation

The orientation of panel arrays with respect to the local slope of the landscape had a moderate impact on CNs. When converting panel arrays that follow the landscape contours (parallel to slope) to panel arrays that are installed up and

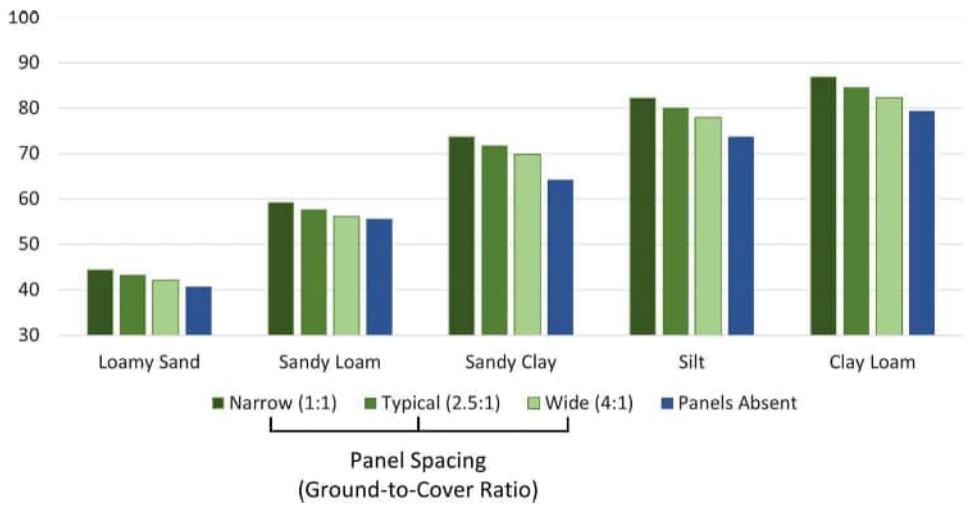

Fig. 6 Relationship of panel presence and absence as well as multiple panel spacings with resultant Curve Number (CN) values

down the slope (perpendicular to slope), resultant CN values increase for every soil texture. The average increase in CN value from a baseline condition of a 50 cm soil depth and a bulk density of 1.4 g/cm^3 is 8.2 points. For example, a Clay soil with the above baseline soil conditions and panels parallel to slope has a CN of 72.1 with expected runoff from a 25.4 cm (10 in) 24-h storm of 16.5 cm (6.5 in). When panel arrays are oriented up and down the landscape slope, CN increases to 78.9 and expected runoff increases to 18.7 cm (7.4 in), an increase of 2.2 cm (0.9 in). Orienting panel arrays along topographic contours results in lower runoff than arrays installed perpendicular to slope, because concentrated flow is reduced and vegetation between arrays is able to more efficiently infiltrate runoff.

4.7 Slope

Slope did not make a significant difference in CN and runoff values for the relatively flat PV-SMaRT study sites; however, research suggests CN modification for steeper slopes. When comparing relatively flat slopes of 5% (baseline condition in the calculator) to a steeper landscape of 20%, CN value increases for every soil texture in the calculator. When comparing all soil textures with the baseline condition of 50 cm profile depth and 1.4 g/cm^3 bulk density, the average CN increase is 3.6 points when slope increases from 5 to 20%. For example, a Clay soil with the above baseline soil conditions and a 5% slope has a CN of 72.1 with expected runoff from a 25.4 cm (10 in) 24-h storm of 16.51 cm (6.5 in). When slope is increased to 20%, CN increases to 76.0 and expected runoff increases to 18.0 cm (7.0 in) an increase of 1.5 cm (0.5 in).

4.8 Discussion

The runoff calculator is intended to accurately reflect the impacts of varying several site characteristics by providing nearly instantaneous estimates of associated runoff given the disconnected impervious nature of solar facilities. It summarizes a multitude of research findings on complex design considerations into a very straightforward tool that can be used by even novice users. The runoff calculator can be used for both assessing site suitability in the pre-construction stage of a proposed project and for evaluating potential runoff impacts in the post-construction period with and without low impact development practices. By providing rapid estimates of expected runoff change for numerous site characteristic combinations, users can evaluate different management considerations to select site design and management practices that minimize runoff using green design principles. This approach can help avoid elevated costs to mitigate stormwater runoff associated with installation of expensive water retention structures. For sites with heterogenous characteristics (multiple slope classes, two unique soil types, etc.), runoff CN values can be generated for each sub-region of a solar farm and area-weighted to provide better runoff estimates. CN values generated in the PV-SMaRT runoff calculator can also be used as inputs for conventional stormwater modeling approaches with models such as the US EPA's Stormwater Management Model (SWMM) or HydroCAD.

4.9 Case study

The PV-SMaRT solar farm runoff calculator described above is a spreadsheet-based approach for estimating the impact of soil texture, soil depth, soil bulk density, slope, ground cover characteristics, and solar array design characteristics on stormwater curve number values and stormwater runoff for a specified 24-h design storm depth. A case study based on comparing a coarse soil (Sandy Loam) and a fine soil (Clay) illustrates how each variable within the runoff calculator can affect resultant CN values for both soil textures. Figures 7 and 8 display a set of typical baseline site condition input variables (blue fields) for these two soil textures. For baseline conditions, CN for the coarse soil is 42.0; while CN increases to 71.2 when changing only soil texture to a fine-textured Clay soil. For a 25.4 cm (10 in) 24-h storm, these CN values generate runoff depths of 6.3 cm (2.5 in) and 16.2 cm (6.4 in), respectively, on the Sandy Loam and Clay soils.

Table 3 represents the above baseline conditions shown in Figs. 7 and 8 for both soil textures in the "Mid CN Condition" columns. The impact of changes in each individual variable are also evaluated for their effect on CN values in the columns labeled lower and higher CN condition. For example, when the Sandy Loam is changed from a typical bulk density of 1.4 g/cm^3 to a compacted bulk density of 1.8 g/cm^3, CN value increases drastically by 39.2 points from the baseline CN value to 81.2. Preventing and mitigating soil compaction is key to reducing runoff from solar farms. When soil depth decreases to 30 cm for the Sandy Loam, CN value increases dramatically by 37.8 points to 79.8. When baseline vegetation condition of "Newly Established Pollinator" is changed to a "Bare Soil" condition, the Sandy Loam CN value increases by 24.1 points to 66.1, showing the benefits of perennial vegetation between arrays on runoff mitigation. When panel spacing is decreased from 7.6 m to 4.6 m, CN shows a smaller increase of only 1.2 points to 43.2. The magnitude of CN value

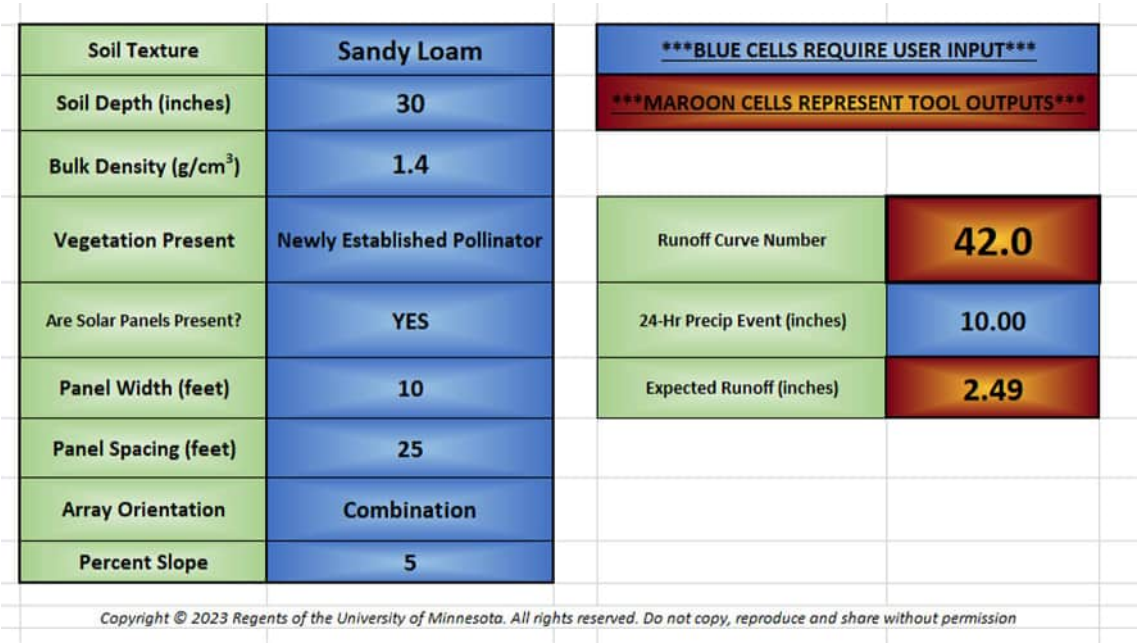

Soil Texture	Sandy Loam
Soil Depth (inches)	30
Bulk Density (g/cm^3)	1.4
Vegetation Present	Newly Established Pollinator
Are Solar Panels Present?	YES
Panel Width (feet)	10
Panel Spacing (feet)	25
Array Orientation	Combination
Percent Slope	5

BLUE CELLS REQUIRE USER INPUT

MAROON CELLS REPRESENT TOOL OUTPUTS

Runoff Curve Number	42.0
24-Hr Precip Event (inches)	10.00
Expected Runoff (inches)	2.49

Fig. 7 Case study example of baseline runoff calculator inputs (blue fields) and runoff curve number and runoff outputs (maroon fields) for a coarse-textured soil

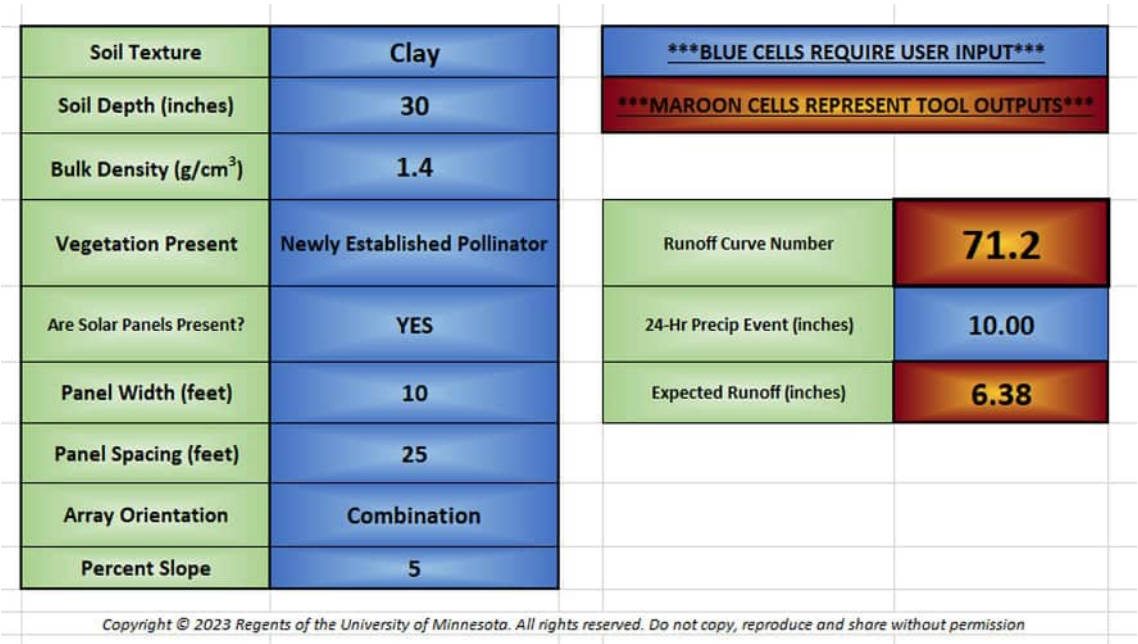

Soil Texture	Clay
Soil Depth (inches)	30
Bulk Density (g/cm^3)	1.4
Vegetation Present	Newly Established Pollinator
Are Solar Panels Present?	YES
Panel Width (feet)	10
Panel Spacing (feet)	25
Array Orientation	Combination
Percent Slope	5

BLUE CELLS REQUIRE USER INPUT

MAROON CELLS REPRESENT TOOL OUTPUTS

Runoff Curve Number	71.2
24-Hr Precip Event (inches)	10.00
Expected Runoff (inches)	6.38

Fig. 8 Case study example of baseline runoff calculator inputs (blue fields) and runoff curve number and runoff outputs (maroon fields) for a fine-textured soil

changes from baseline (mid CN condition) for the lower and higher CN condition scenarios are smaller with the Clay soil texture than the Sandy Loam texture (Table 3). This is particularly true for changes in soil depth and vegetative cover.

The case study with two soil textures illustrates how widely runoff CN values can vary depending on specific combinations of site-characteristics. Runoff is affected most by soil texture, soil bulk density, and soil profile depth. Soil compaction can be avoided by controlling vehicle traffic on wet soils and by minimizing landscape grading during construction activities. Runoff mitigation is enhanced if site selection focuses on avoiding locations with fine-textured, shallow soils. Ground cover has a moderate impact on runoff, and low impact perennial vegetation plantings are particularly beneficial

Table 3 Effect of input variables within the runoff calculator with low, typical, and high values on resultant Curve Number (CN) values as simulated on a coarse- (Sandy Loam) and a fine-textured soil (Clay)

	Variable Input Values			Sandy Loam Curve Numbers			Clay Curve Numbers		
Input Variable	*Lower CN Condition*	*Mid CN Condition*	*Higher CN Condition*	*Lower CN Condition*	*Mid CN Condition*	*Higher CN Condition*	*Lower CN Condition*	*Mid CN Condition*	*Higher CN Condition*
Bulk Density	1 g/cm^3	1.4 g/cm^3	1.8 g/cm^3	30.0	42.0	81.2	45.4	71.2	100.0
Soil Depth	150 cm	75 cm	30 cm	30.0	42.0	79.8	67.2	71.2	78.9
Vegetation	Mature Prairie	Newly Established Pollinator	Bare Soil	30.0	42.0	66.1	64.0	71.2	82.0
Panel Prescence and Spacing	No Panels	7.6 m Spacing	4.6 m Spacing	40.5	42.0	43.2	66.4	71.2	73.1
Panel Width	1.5 m	3 m	4.6 m	37.1	42.0	43.2	66.4	71.2	72.8
Array Orientation	Follows Slope Contours	Combination	Up and Down Slope	38.5	42.0	45.6	68.0	71.2	74.4
Slope	1%	5%	15%	42.0	42.0	47.2	71.2	71.2	74.7

for runoff mitigation and reductions in soil bulk density. Panel presence, spacing, width and orientation have an impact on runoff, but play a smaller role than soil bulk density and vegetation characteristics.

5 Conclusions

A user-friendly spreadsheet-based runoff CN calculator for ground mounted solar PV facilities was developed based on regression curves representing nearly 1,000 Hydrus 2D/3D simulations run for different soil textures, soil depths, soil bulk densities and design storms. User inputs include soil texture, soil depth, soil bulk density, vegetative cover, presence or absence of solar arrays, panel spacing, panel width and orientation, and slope. The runoff calculator quickly estimates CN values for pre- and post-construction scenarios, including low impact development practices such as avoidance of compacted soils, perennial vegetation plantings, and wider array spacings. Users can input a 24-h design storm depth of interest and the calculator will estimate expected depth of runoff. Solar farm stormwater depths can range from values typical of completely impervious surfaces to no runoff, depending on the specific combination of soil texture, soil depth, bulk density, vegetation type, array spacing and orientation.

This runoff calculator can provide accurate and nearly instantaneous runoff estimates to novice users to inform both site-suitability decisions as well as construction management and installation choices. This tool can provide financial savings by promoting low impact development practices that reduce the need for costly runoff mitigation structures. If applied with thoughtful consideration, it also has the potential to encourage low impact development principles on the ever-increasing area of utility scale ground-mounted PV installations that will be installed in the years to come; this will minimize the impact of this landuse change on overland runoff and associated surface water quantity and quality issues. If low impact design considerations are prioritized during installation of ground-mounted PV operations, this tool could significantly reduce runoff volume from commercial solar PV sites and provide a net benefit in water quality when converting from certain high impact pre-existing landuse conditions.

Author contributions David Mulla: Conceptualization, Funding acquisition, Methodology, Project administration, Supervision, review and editing; Jake Galzki: Experimental data collection, Software initial and boundary conditions, processing, original draft, review and editing.

Funding This research was supported by the US Department of Energy (DOE) Office of Energy Efficiency and Renewable Energy under the Solar Energy Technologies Office (SETO) Award Number DE-AC36- 08GO28308. We acknowledge helpful suggestions on research direction by the PV-SMaRT Water Quality Task Force Advisory Board members.

Data availability Data cannot be shared openly but are available on request from authors: selected data sets generated during the current study are available from the corresponding author on reasonable request, but restrictions apply to the availability of these data, which were based on privacy agreements with cooperating solar farm operators, and so are not publicly available.

Code availability The https://license.umn.edu/product/pv-smart-solar-runoff-calculator-version-30.

Declarations

Competing interests The authors declare no competing interests.

References

1. Kannan N, Vakeesan D. Solar energy for future world: a review. Renew Sustain Energy Rev. 2016;62:1092–105.
2. Victoria M, Haegel N, Peters IM, Sinton R, Jäger-Waldau A, del Canizo C, Breyer C, Stocks M, Blakers A, Kaizuka I, Komoto K. Solar photovoltaics is ready to power a sustainable future. Joule. 2021;5(5):1041–56.
3. Yavari R, Zaliwciw D, Cibin R, McPhillips L. Minimizing environmental impacts of solar farms: a review of current science on landscape hydrology and guidance on stormwater management. Environ Res. 2022;2:032002.
4. Guillette A. Low impact development technologies. Updated 3 November, 2016. Whole Building Design Guide (WBDG)—National Institute of Building Sciences. 2004. https://www.wbdg.org/resources/low-impact-development-technologies
5. Hilten RN, Lawrence TM, Tollner EW. Modeling stormwater runoff from green roofs with HYDRUS-1D. J Hydrol. 2008;358:288–93.
6. Vergroesen T, Joshi UM. Green roof runoff experiments in Singapore. In Novatech 2010–7ème Conférence Internationale sur les Techniques et Stratégies Durables pour la Gestion des Eaux Urbaines par Temps de Pluie. 7th International Conference on sustainable techniques and strategies for Urban Water Management. GRAIE, Lyon, France, 2010, pp. 1–10
7. Elamri Y, Cheviron B, Mange A, Dejean C, Liron F, Belaud G. Rain concentration and sheltering effect of solar panels on cultivated plots. Hydrology Earth Sys Sci. 2018;22:1285–98.
8. Gullotta A, Aschale TM, Peres DJ, Sciuto G, Cancelliere A. Modelling stormwater runoff changes induced by ground-mounted photovoltaic solar parks: a conceptualization in EPA-SWMM. Water Resour Manage. 2023;37:4507–20.
9. Hassanpour Adeh E, Selker JS, Higgins CW. Remarkable agrivoltaic influence on soil moisture, micrometeorology and water-use efficiency. PLoS ONE. 2018;13: e0203256.
10. Nair AA, Rohith AN, Cibin R, McPhillips LE. A framework to model the hydrology of solar farms using EPA SWMM. Environ Model Assess. 2023. https://doi.org/10.1007/s10666-023-09922-0.
11. Walston LJ, Li Y, Hartmann HM, Macknick J, Hanson A, Nootenboom C, Lonsdorf E, Hellmann J. Modeling the ecosystem services of native vegetation management practices at solar energy facilities in the Midwestern United States. Ecosys Serv. 2021;47: 101227.
12. Mulla DJ, Galzki J, Hanson A, Šimůnek J. Measuring and modeling soil moisture and runoff at solar farms using a disconnected impervious surface approach. Vadose Zone J. 2024. https://doi.org/10.1002/vzj2.20335.
13. Barnard T, Agnaou M, Barbis J. Two-dimensional modeling to simulate stormwater flows at photovoltaic solar energy sites. J Water Manag Model. 2017;25:C428. https://doi.org/10.14796/JWMM.C428.
14. Cook LM, McCuen RH. Hydrologic response of solar farms. J Hydrol Engin. 2013;18:536–41.
15. Cronshey, R., 1986. Urban hydrology for small watersheds (No. 55). US Department of Agriculture, Soil Conservation Service, Engineering Division.
16. Sharpley A, Williams J. Epic—erosion/productivity impact calculator: i. model documentation. II: User Manual; Technical Bulletin, No. 1768 1990; United State Department of Agriculture: Washington, DC, USA, 1990
17. Huang M, Gallichand J, Wang Z, Goulet M. A modification to the soil conservation service curve number method for steep slopes in the Loess Plateau of China. Hydrol Process. 2006;20:579–89.
18. Šimůnek J, van Genuchten MTh, Šejna M. Development and applications of the HYDRUS and STANMOD software pack-ages and related codes. Vadose Zone J. 2008;7:587–600. https://doi.org/10.2136/vzj2007.0077.
19. Van Genuchten MT. A closed-form equation for predicting the hydraulic conductivity of unsaturated soils. Soil Sci Soc Am J. 1980;44(5):892–8.
20. National Oceanic and Atmospheric Administration (NOAA) Atlas 14. 2013. Volume 8. Precipitation-Frequency Atlas of the United States. National Weather Service, Silver Spring, MD.
21. United States Department of Agriculture (USDA) Natural Resources Conservation Service (NRCS). 2019. 210-National Engineering Handbook, Part 630 Hydrology, Chapter 4, Storm Rainfall Depth and Distribution. USDA-NRCS, Washington, D.C.
22. Elhakeem M, Papanicolaou A. Estimation of the runoff curve number via direct rainfall simulator measurements in the state of Iowa, USA. Water Resour Manage. 2009;23:2455–73. https://doi.org/10.1007/s11269-008-9390-1.
23. Hawkins RH, Ward TJ, Woodward DE, Van Mullem JA, editors. Curve number hydrology: State of the practice. Reston: American Society of Civil Engineers; 2008.
24. United States Department of Agriculture (USDA) Soil Science Division Staff. Soil survey manual. C. Ditzler, K. Scheffe, and H.C. Monger (eds.). USDA Handbook 18. Government Printing Office, Washington, D.C. 2017
25. United States Department of Agriculture (USDA) Natural Resources Conservation Service (NRCS). 2009. 210-National Engineering Handbook, Part 630 Hydrology, Chapter 7, Hydrologic Soil Groups. USDA-NRCS, Washington, D.C. 2009
26. Akbari A, Samah AA, Daryabor F. Raster-based derivation of a flood runoff susceptibility map using the revised runoff curve number (CN) for the Kuantan watershed, Malaysia. Environ Earth Sci. 2016;75:1–8.

AGU ADVANCING EARTH AND SPACE SCIENCES

Water Resources Research

RESEARCH ARTICLE
10.1029/2023WR035067

Effect of Solar Farms on Soil Erosion in Hilly Environments: A Modeling Study From the Perspective of Hydrological Connectivity

Hu Liu[1,2,3], Chuandong Wu[1,2,3], Yang Yu[4], Wenzhi Zhao[1,2], Jintao Liu[5], Hailong Yu[6], Yanli Zhuang[1,2], and Omer Yetemen[7]

[1]Northwest Institute of Eco-Environment and Resources, Chinese Academy of Sciences, Lanzhou, China, [2]Linze Inland River Basin Research Station, Chinese Ecosystem Research Network, Lanzhou, China, [3]University of Chinese Academy of Sciences, Beijing, China, [4]School of Soil and Water Conservation, Beijing Forestry University, Beijing, China, [5]State Key Laboratory of Hydrology-Water Resources and Hydraulic Engineering, Hohai University, Nanjing, China, [6]School of Geography and Planning, Ningxia University, Yinchuan, China, [7]Eurasia Institute of Earth Sciences, Istanbul Technical University, Istanbul, Turkey

Abstract Hydrological connectivity (HC) is a useful framework for understanding hydrological responses to landscape changes. We present herein a novel model (SOFAR) for utility-scale solar farms (USFs), combining modules of soil moisture dynamics, roof effects of photovoltaic panels (PVs), vegetation growth and landform evolution. By augmenting the model with a DEM-based HC index, we investigate hydrological behaviors following the construction of a USF in China's Loess Hilly Region. Nine scenarios are designed, to explore the effects of co-evolving ecohydrology and landscape on soil erosion and HC in USFs deployed in different climates and terrains, by altering the annual precipitation, rainfall frequency, and ground slope. Our results show that the USF considerably increased runoff (99.18%–154.26%) during its operational period, and soil erosion rate (21.4%–74.84% and 25.35%–76.18%) and HC (0.08%–0.26% and 0.47%–0.91%) throughout construction and operational periods, respectively. The highest erosion rates were detected in the PV installation zones and in the areas close to the river channel. We prove the hypothesis that HC is a critical indicator for sediment yield in a USF, and thus the long-term responses of soil erosion to USF installation and development can be explained in terms of HC. We conclude that USFs may increase soil erosion, mainly by increasing local HC and runoff, and higher background HC may in turn further aggravate the effects of USFs on soil erosion. Our results underscore the importance of including landscape ecohydrologic and geomorphic feedbacks, to improve the environmental impact assessment of USFs.

Hu Liu and Chuandong Wu contributed equally to this work.

Key Points:

- Precipitation and relief amplitude are major controlling factors for soil erosion in utility-scale solar farms in hilly areas
- Utility-scale solar farms may increase soil erosion, mainly by increasing runoff and local hydrological connectivity
- Higher background hydrological connectivity could aggravate the effects of utility-scale solar farms on soil erosion

Supporting Information:

Supporting Information may be found in the online version of this article.

Correspondence to:

H. Liu,
[redacted]@lzb.ac.cn

Citation:

Liu, H., Wu, C., Yu, Y., Zhao, W., Liu, J., Yu, H., et al. (2023). Effect of solar farms on soil erosion in hilly environments: A modeling study from the perspective of hydrological connectivity. *Water Resources Research*, *59*, e2023WR035067. https://doi.org/10.1029/2023WR035067

Received 23 APR 2023
Accepted 15 NOV 2023

Author Contributions:

Conceptualization: Hu Liu, Chuandong Wu
Data curation: Yang Yu, Yanli Zhuang
Funding acquisition: Hu Liu, Wenzhi Zhao, Yanli Zhuang, Omer Yetemen
Investigation: Hu Liu, Chuandong Wu, Hailong Yu
Methodology: Hu Liu, Chuandong Wu
Resources: Hu Liu, Hailong Yu
Software: Chuandong Wu

1. Introduction

As an alternative to conventional fossil fuels, renewable energy (e.g., solar, wind, hydropower, etc.) is becoming the primary means of meeting energy demand (Dhonde et al., 2022; Makaronidou, 2020). Comparing all the renewable types, based on environmental, economic, and safety criteria, solar energy appears to be the most promising and attractive one (Bórawski et al., 2019). However, solar farms have a large land footprint (Rahman et al., 2022), and the unprecedented growth of utility-scale solar farms (USFs, defined as solar farms with nameplate-generating capacity larger than 5 MW (Kruitwagen et al., 2021)) creates potential conflicts with other land uses (e.g., agriculture, pasture, industry or settlements) (Dhonde et al., 2022), and thus raises the issue of land cost (Lee, 2019; Randle-Boggis et al., 2020). Accordingly, an ever-growing number of USFs need to find homes on cheaper land such as hilly terrain and lower mountain slopes (Chiabrando et al., 2009; Makaronidou, 2020). However, mounting USFs in these environments also incurs disadvantages, including increased storm-water runoff, soil erosion (Figure S1 in Supporting Information S1), and sediment transport (L. M. Cook & McCuen, 2013), which in turn pose considerable threats to the local and surrounding environments (Bolinger & Seel, 2018). This is even more likely to be the case in regions where storms occur frequently, vegetation cover is low, or soil is easily lost (e.g., Loess Plateau in China) (Yu et al., 2020). Thus it is of extreme importance to understand the potential effects of USFs (both existing and proposed) on hydrological behavior in hilly regions (Phalane, 2021), for better designing and managing USFs, with the goal of sustainable development (L. M. Cook & McCuen, 2013; Makaronidou, 2020).

Supervision: Hu Liu, Wenzhi Zhao
Validation: Hu Liu, Chuandong Wu, Yang Yu
Visualization: Chuandong Wu, Jintao Liu, Omer Yetemen
Writing – original draft: Hu Liu, Chuandong Wu
Writing – review & editing: Hu Liu, Chuandong Wu, Yang Yu, Wenzhi Zhao, Jintao Liu, Omer Yetemen

Given the rare in situ and long-term field observations available at most USFs around the world, modeling is currently the only practical option for achieving this end (Baartman et al., 2018; Cabal et al., 2021). PV-affected hydrological behaviors in USFs have been investigated in a few previous studies (Chiabrando et al., 2009). For example, Walston et al. (2021) reported significantly increased sediment and water retention at USFs across the midwestern USA; L. M. Cook and McCuen (2013) concluded that whether the addition of photovoltaic panels (PVs) affects hydrological processes depends largely on whether there are changes in the land-cover type under the PVs; Edalat (2017) reported that an increase in the tilt angle of PVs results in decreases in peak flow, peak flow time, and runoff. These works, however, were limited in the sense that they did not consider the co-evolution of landscape and vegetation under the impact of PVs over the life span of a USF. Indeed, besides the significant changes in land use and ground cover during installation, PVs may also significantly change microclimates (i.e., solar radiation and rainfall), so that soil and vegetation in USFs could more intensely evolve to adapt to the altered environments, over the course of their long operational periods (Hernandez et al., 2014; Makaronidou, 2020). Overlooking the long-term co-evolution effects might lead to unexpected bias in the predictions of hydrological responses to the shift in land uses, especially when USFs are installed in hilly environments. However, how to evaluate hydrological behaviors in response to the installation of USFs during their long operational periods remains a challenge (Hernandez et al., 2015; Murphy-Mariscal et al., 2018).

Addressing the above-noted issues requires solutions that can intelligibly and quantitatively describe the interface between ecohydrological processes and landscape development: for example, the extent and distribution of the expected effects of PVs on the processes of rainfall runoff and erosion deposition as they occur over the life span of USFs in hilly environments (Wacha et al., 2018). The concept of hydrological connectivity (HC) depicts "water-mediated transport of matter, energy and/or organisms within or between elements of the hydrologic cycle" (Pringle, 2001), and thus appears to be a likely candidate (Souza & Hooke, 2021). Using this concept, previous works have evaluated the potential ecological and hydrological impacts of altered ground surface conditions from the aspects of vegetation dynamics (Foerster et al., 2014; Souza & Hooke, 2021), biological conservation (Pringle, 2001), land use changes (Boix-Fayos et al., 2007), and so on (Freeman et al., 2007; Kompanizare et al., 2018). Indeed, HC is the dynamic representation of internal linkages between runoff and sediment generation in upper parts of catchments and in receiving waters, and thus it is both a cause and a consequence of landscape evolution (Bracken & Croke, 2007). Given the potential of HC for increasing the understanding of the interface between ecohydrology and landscape evolution, combining the index of HC with a model that could coordinate biotic and abiotic effects caused by PVs on vegetation dynamics may allow us to better evaluate the long-term hydrological behaviors in USFs in hilly environments. We present herein a novel model with this property (the Solar-Farm model, SOFAR), and the long-term effects of PVs on hydrologic response in USFs are estimated and analyzed from the perspective of HC through this model, with the help of an additional tool for HC calculation.

The SOFAR model is based on but considerably extended from our earlier model, which was developed for a single PV (Wu et al., 2022). Besides keeping the basic modules of the earlier design for soil moisture dynamics and roof effects of PVs, SOFAR is also made spatially explicit and dynamic by coupling a module for vegetation growth [modified from Nouvellon et al. (2000)] and a module for landform evolution [modified from Saco et al. (2007)]. The SedInConnect tool developed by Cavalli et al. (2013) is adopted in this work as the means to calculate the value of HC, with the iterated DEM (digital elevation model) from the SOFAR model as the input. As previous researches reported that PVs could variably increase soil erosion rates, depending on the sitings of the USFs (e.g., Barnard et al., 2017; L. M. Cook & McCuen, 2013), and that there is a known positive relationship between HC and soil erosion (Cavalli et al., 2013), we hypothesize that HC could be a critical indicator for sediment yield in a USF, and thus the long-term responses of soil erosion to USF installation and development could be explained and understood in terms of HC: that is, USFs enhance soil erosion and sediment yield by increasing HC. This work tests the hypothesis through modeling efforts, with the aims of analyzing the potential erosion that can come from the long-term deployment of USFs, and revealing how a solar farm affects soil erosion, by highlighting the co-evolving nature of ecohydrology and landscape (Jahanfar et al., 2019). Based on the results, this work also discusses storm-water management strategies that can prevent potential erosion in USFs deployed in hilly environments, from the perspective of HC (Souza & Hooke, 2021).

The modeling scheme reported in this work provides a possible method of predicting soil erosion affected by USFs in hilly regions, and a potential tool to identify the erosion-risk areas in such USFs as well. The findings from this work will also contribute to an improved understanding of the hydrological responses to USF

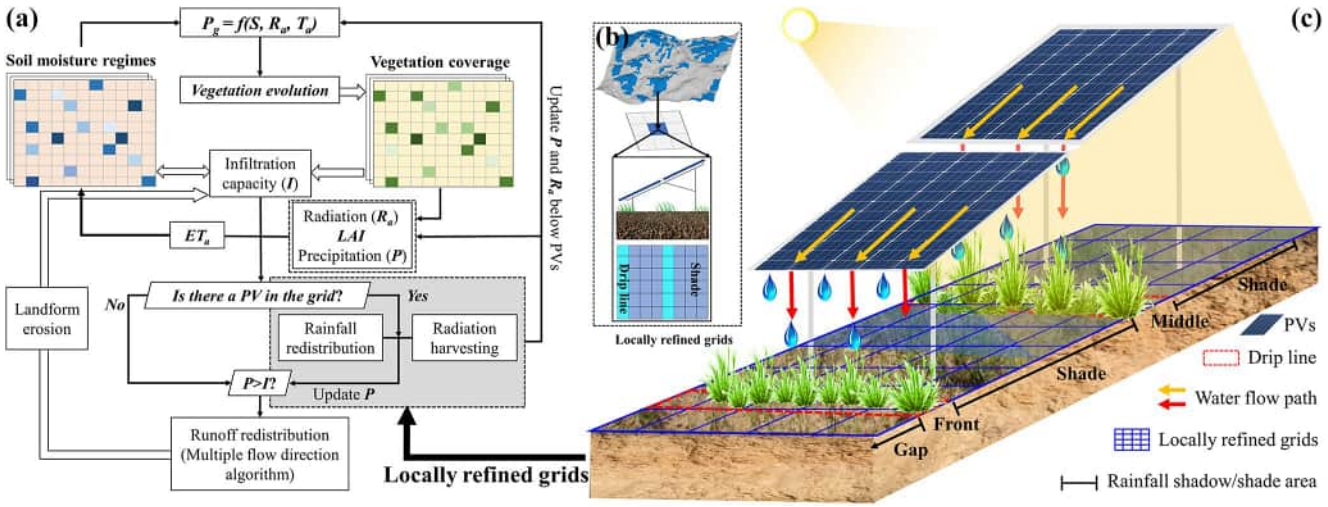

Figure 1. Schematic diagrams of the SOFAR model and the locally refined grid structure, and the runoff flow path on an individual photovoltaic panel (PV). Structure and feedbacks among the sub-models of the SOFAR model (a). Locally refined grids used in the SOFAR model, where the blue coarse grid indicates a photovoltaic array (which in turn consists of 20 single PVs) (b). Schematic diagram of fine-grid structure applied to the underlying ground surface, the narrow gap between two adjacent PVs, and simplified schematic drawing of runoff path on a PV (c).

installation and development in hilly regions, and ultimately facilitate decisions on USF siting and management both in the Chinese Loess Plateau and elsewhere.

2. Materials and Methods

2.1. Model Structures and Simulation Method

2.1.1. The SOFAR Model

The Solar-Farm model (SOFAR) describes the fundamental physical and ecohydrological processes occurring in a solar farm at a daily time step, and includes four major modules: (1) soil moisture dynamics, (2) roof effects of PVs, (3) vegetation growth, and (4) landform evolution (Figure 1). Model parameter definitions are listed in Table 1. The model is driven by daily meteorological variables including precipitation, maximum temperature, minimum temperature, sunshine duration, and initial DEM. The SOFAR model combines these individual modules to describe the ecological, hydrological, and geomorphic processes in USFs. However, it is challenging to simulate the roof effects of PVs at the mesoscale (i.e., solar-farm scale), because of the huge number of individual data points that would need to be considered. For example, as shown in Figure 1c, when rainfall reaches a PV, it flows along the downslope direction (as indicated by yellow arrows), and then out of the narrow gap between the sub-panels (orange arrows) or off the downslope edge (red arrows). In other words, the PVs concentrate rainfall as downpour, resulting in an increase in runoff along the driplines (about 0.4-m width, including the 0.1-m width dripline itself, and the 0.15-m width areas on each side affected by splashing downpour) onto the underlying ground surface. Thus, a coarse-spatial resolution (e.g., 3 m × 3 m) is not capable of capturing the information about water receiving and discharging processes that occur at such a fine scale. On the other hand, if a uniform high spatial-resolution scheme were to be adopted, the calculations required would be prohibitively time-consuming.

Hence, in order to obtain a trade-off between accuracy and efficiency, two spatial resolutions are considered in the model: farm-level (3 m × 3 m) and panel-level (0.1 m × 0.1 m) (Figure 1c). Nested rectangular grids are applied to the ground surface for running the simulation: coarse-grid meshes (or farm-level grids) are first produced for the whole computational domain (i.e., the whole USF), and then the grids installed with PVs are identified and locally refined as panel-level grids. The grids of these differing resolutions are interactively connected through water transfer and storage processes: topography-driven runoff and infiltration are calculated in the coarse grids, while at the same time the PV-enhanced runoff and infiltration are estimated in the fine grids. However, in each calculation iteration, topography-driven runoff into a coarse grid with PV installation is set to be evenly distributed over the corresponding fine grids, and as additional water input, to calculate the routing infiltration.

Table 1
Model Parameter Definitions and Values Estimated for the Hongsibu Site

Definition	Parameter	Grass	Shrub
Soil parameters (units)			
Soil porosity (v v^{-1})	n	0.55	0.55
Active soil depth (mm)	Zr	600	600
Time step (d)	t	1	1
Saturated hydraulic conductivity (cm d^{-1})	K_S	50.8	50.8
Empirical constant	N	2	2
Empirical constant	b	1.62	1.62
Field capacity (v v^{-1})	S_{fc}	0.4	0.3
Bare soil infiltration capacity (mm d^{-1})	I_b	8[a]	5[a]
Vegetation infiltration capacity (mm d^{-1})	I_V	15[a]	10[a]
Incipient stomatal closure (v v^{-1})	S^*	0.14[b]	0.10[b]
Wilting point (v v^{-1})	S_w	0.06	0.042
Hygroscopic point (v v^{-1})	S_h	0.03[c]	0.03[c]
Critical soil evaporation (mm d^{-1})	E_{min}	0.1	0.1
Photovoltaic panel parameters (units)			
Inclination angle (°)	β	37.2	
PVs' re-radiation coefficient (%)	η	0.6[d]	
Rainfall interception coefficient (m^2 m^{-2})	K_p	0.3	
Vegetation parameters (units)			
Empirical constant (−)	k_1	0.384[e]	0.384[e]
Specific leaf area index for living biomass (m^2 g^{-1})	C_g	0.06[e]	0.09[e]
Specific leaf area index for dead biomass (m^2 g^{-1})	C_d	0.062[a]	0.094[a]
Minimum temperature for photosynthesis (°C)	T_{min}	7[e]	5[e]
Optimum temperature for photosynthesis (°C)	T_{opt}	25[e]	25[e]
Minimum root-to-shoot ratio (−)	r_x	0.15	1.05[e]
Maintenance respiration coefficient for aboveground parts (g DM g DM^{-1})	m_a	0.08[e]	0.008[e]
Growth respiration coefficient for aboveground parts (g DM g DM^{-1})	g_a	0.15[e]	0.18[e]
Maintenance respiration coefficient for belowground parts (g DM g DM^{-1})	m_r	0.03[e]	0.02[e]
Growth respiration coefficient for belowground parts (g DM g DM^{-1})	g_r	0.11[e]	0.08[e]
Erosive parameters (units)			
Density of the sediment (kg m^{-3})	ρ_s	1,200	
Porosity of the sediment (v v^{-1})	n_p	0.2[f]	
Empirical coefficient (−)	m_1	0.6[f]	
Empirical coefficient (−)	n_1	0.8[f]	
Maximum diffusion coefficient (m^2 s^{-1})	D_{max}	0.002[g]	
Minimum diffusion coefficient (m^2 s^{-1})	D_{min}	0.001[g]	
Maximum erodibility for bare soil (−)	β_b	0.04[f]	
Erodibility for covered soil (−)	β_v	0.02[f]	
Minimum erodibility for soil (−)	β_{min}	0[f]	

Note. The values labeled "a" through "f" are estimated through a genetic algorithm (GE) based on the initial values or ranges reported in the literature.
[a]Yetemen et al. (2015). [b]Istanbulluoglu et al. (2012). [c]Laio et al. (2001). [d]Hu et al. (2016). [e]Nouvellon et al. (2000). [f]Saco and Mariano (2013). [g]Sun et al. (2016).

Based on the updated soil moisture resulting from the routing infiltration, the PV-enhanced runoff and the local infiltration in the fine grids are determined, then averaged and assigned back to the corresponding coarse grid.

Besides runoff and infiltration, we also adopt a similar strategy to upscale the PV-induced changes—e.g., soil moisture content, leaf area index, vegetation coverage, etc.—from panel level to farm level (Figure 1). The method can be generally described as:

$$\mathrm{Val}_i^F = \frac{\left(\sum_{j=1}^{N} \mathrm{val}_j^P\right)}{N} \text{ for } i_{\mathrm{th}} \text{ grid installed PVs} \tag{1}$$

where Val_i^F is the value of the ith grid of the farm-level installed PVs; val_j^P represents the value of the jth grid of the panel-level; and N is the total number of grids divided at the panel-level.

To the best of our knowledge, this study is the first attempt to explicitly describe these processes across the life span of a USF within the framework of a PV-effect model at the mesoscale (i.e., solar-farm scale). Compared to the modeling studies at the PV-unit level—for example, Elamri et al. (2018) focused only on the rainfall interception of PVs, Jahanfar et al. (2020) only on radiation reduction—the salient aspect of SOFAR is the explicit treatment of both rainfall concentration and radiation harvesting in USFs. Compared to other modeling works at utility or larger scales—for example, Barnard et al. (2017) and Edalat and Stephen (2017) simply treated PVs as an impervious surface on the ground (infiltration could not be permitted under the panels, as would occur under real-world conditions); Walston et al. (2021) plainly represented erosion as a function of landscape characteristics (e.g., vegetation cover or slope), without considering the enhanced splash erosion along the driplines caused by PVs' being elevated above the ground—SOFAR not only overcomes the shortcomings of these previous models, but also benefits from elaborating the importance of landscape ecohydrologic and geomorphic feedbacks, to improve the environmental impact assessment of USFs by incorporating the modules of vegetation growth and landform evolution into the model.

(1) Soil Moisture Dynamics

In the SOFAR model, the soil moisture dynamics were simulated using a bucket concept, following the general scheme described in Rodriguez-Iturbe (2000). The root-zone average soil water balance equation is described as Equation 2, which is solved using the finite difference method.

$$nZ_r \frac{\partial S}{\partial t} = P_{\mathrm{in}} - I - R - \mathrm{ET}(S, \mathrm{LAI}_t, \mathrm{LAI}_g, \mathrm{Ra}_{\mathrm{in}}) + \frac{\partial K(S)}{\partial S} \tag{2}$$

where n represents the soil porosity; Z_r (mm) is the effective root depth; S is the average relative volumetric water content of the soil profile; t (d) is the time step; P_{in} (mm) is the daily precipitation amount (its value is equal to the intercepted rainfall (I_{PVs}) if a PV is present); I (mm) is the canopy interception loss; R (mm d^{-1}) represents the runoff; ET (mm d^{-1}) is the evapotranspiration, which is a function of soil moisture content (S), leaf area index (i.e., the total leaf area index LAI_t, and the index of the green leaf area LAI_g; both of them will be defined later in Equations 20–22), and available radiation ($\mathrm{Ra}_{\mathrm{in}}$), including actual evaporation from soil E (mm d^{-1}) and actual daily transpiration T (mm d^{-1}); and K (cm h^{-1}) is the hydraulic conductivity. Available radiation includes two types: the natural net radiation (estimated in Appendix A) and available radiation beneath the PVs.

The amount of infiltration (I_a)—the effective precipitation—is restricted by three factors: available water, infiltration capacity, and available pore space in the root zone (Yetemen et al., 2015).

$$I_a = \min\{P_{\mathrm{in}} - I + R_{\mathrm{in}}, I_c, nZ_r(1 - S)\} \tag{3}$$

where R_{in} (mm) is the runoff from upstream sources.

Vegetation enhances soil infiltration capacity through increasing pore structures, as has been verified by field experiments and modeling studies (Dunne et al., 1991). Therefore, infiltration capacity (I_C), accounting for the effects of both soil characteristics and plant dynamics, is expressed as the weighted average of the I_C of bare soil (I_b) and of a fully averaged surface (I_V). In Equation 5, the vegetation cover rate (V_t) is derived from total leaf area index (LAI_t) (Yetemen et al., 2015), which is affected by the PVs through altering rainfall distribution and available radiation.

$$I_c = I_b(1 - V_t) + I_V V_t \tag{4}$$

$$V_t = 1 - \exp(-0.75\mathrm{LAI}_t) \tag{5}$$

Surface runoff depth (mm) is expressed as a mass balance among precipitation, canopy interception, infiltration, and runoff from upstream sources.

$$R_{\mathrm{out}} = P_{\mathrm{in}} - I - I_a + R_{\mathrm{in}} \tag{6}$$

The total evapotranspiration from a fragmented landscape is calculated as the sum of the soil evaporation and canopy transpiration. The potential transpiration ($T_{\max}$, mm d^{-1}) and evaporation ($E_{\max}$, mm d^{-1}) are calculated through the Penman-Monteith equation, modified with the canopy coverage of green leaves (f_g) and percentage cover of bare soil (f_s) referring to the separation method described in Nouvellon et al. (2000), respectively.

$$T_{\max} = f_g \frac{\Delta(R_a - G) + \rho_a c_p (e_s - e_a)/r_{ac}}{\lambda\left[\Delta + \gamma(1 + r_{sc}/r_{ac})\right]} \tag{7}$$

$$E_{\max} = f_s \frac{\Delta(R_a - G) + \rho_a c_p (e_s - e_a)/r_{as}}{\lambda\left[\Delta + \gamma(1 + r_{ss}/r_{as})\right]} \tag{8}$$

where R_a (MJ m^{-2} d^{-1}) is the net radiation, which is replaced by I_s for a grid with PVs; G (MJ m^{-2} d^{-1}) represents the daily soil heat flux; $(e_s - e_a)$ represents the vapor pressure deficit of the air; ρ_a (kg m^{-3}) is the average air density measured at constant pressure; c_p (MJ kg^{-1}°C^{-1}) is the specific heat of air at a constant pressure; Δ is the slope of the saturated vapor pressure curve at air temperature T_a; r_{sc} and r_{ss} are the surface resistances for a full canopy and bare soil, respectively; and r_{ac} and r_{as} are the corresponding aerodynamic resistances for canopy and bare soil, respectively.

The dependence of daily transpiration loss (T_a, mm d^{-1}) on soil moisture is expressed as a piecewise function (Laio et al., 2001), wherein transpiration is equal to zero, because stomata are fully closed when the soil moisture content drops below the wilting point (S_w).

$$T_a = \begin{cases} T_{\max}, & S^* < S < 1 \\ T_{\max}\frac{S - S_w}{S^* - S_w}, & S_W < S < S^* \\ 0, & 0 < S < S_w \end{cases} \tag{9}$$

where S^* represents the soil moisture threshold level for a plant when it starts to reduce transpiration under water stress (Srivastava et al., 2021). Just as for transpiration loss, evaporation loss from the soil is given by:

$$E_a = \begin{cases} E_{\max}, & S^* < S \le 1 \\ E_{\min} + (E_{\max} - E_{\min})\frac{S - S_w}{S^* - S_w}, & S_w < S \le S^* \\ E_{\min}\frac{S - S_h}{S_w - S_h}, & S_h < S \le S_w \\ 0, & 0 < S \le S_h \end{cases} \tag{10}$$

where $E_{\min}$ (mm d^{-1}) is the soil evaporation when soil moisture content is equal to the wilting point, and S_h is the hygroscopic point.

Hydraulic conductivity K (cm h^{-1}) is a function of soil moisture content and saturated hydraulic conductivity (K_s, cm d^{-1}).

$$K(S) = K_s\left(\frac{S}{S_{fc}}\right)^{N+b+3} \tag{11}$$

where S_{fc} (v v^{-1}) is the field water content, and the constants N and b are empirical coefficients.

(2) Roof Effects of PVs

The roof effects of PVs are several. The PVs concentrate rainfall along their downslope edges, resulting in a downpour at those locations; the panels harvest radiation, causing a radiation reduction of about 67%–90% (Armstrong et al., 2016; Liu et al., 2019; Tanner et al., 2020); and the panels shade the subsurface soil. To

capture the roof effects of PVs, the AVrain model [Agrivoltaic Plot Rain Redistribution Model, proposed by Elamri et al. (2018)] was coupled into the SOFAR model to estimate the rainfall intercepted by the PVs and the related concentration of the rainfall process. The details of the method adopted in the SOFAR model to estimate the radiation harvested by the PVs are described in Wu et al. (2022), and are illustrated in Appendix A.

Rainfall concentration. In the model, the irregular flow of water above the PVs is simplified to a homogeneous downward flow, which is injected into the driplines. The incidence angle (α_{rain}) and the interception of rainfall are given by

$$\tan(\alpha_{\text{rain}}) = V_W / V_D \tag{12}$$

$$I_{\text{PVs}} = P_{\text{in}}[\cos(\beta) - \tan(\alpha_{\text{rain}})\sin(\beta)]K_p \tag{13}$$

where α_{rain} is the incidence angle of the rainfall with respect to the vertical direction; V_W (m s^{-1}) is the average velocity of the wind at the site; V_D (m s^{-1}) is the velocity of the raindrops; I_{PVs} (mm) is the amount of rainfall intercepted by the PVs; β represents the inclination angle of the PV; and parameter K_P is the area coefficient (the ratio of the area of the PV to the area of the narrow drip zone), which represents the process of the PVs' concentrating rainfall into a narrow area.

Radiation harvest. Different from natural surfaces, a part of the radiation absorbed by PVs is transformed into electricity. According to the energy balance equation, the available radiation of the area beneath a PV (I_s) is given by

$$I_s = I_{\text{PV}}(1 - \varepsilon - \alpha_{\text{PV}})\eta + I_{ds} \tag{14}$$

where I_{PV} represents direct radiation incident on the surface of the PV; ε is the energy transformation efficiency of the PV, which is 0.18; α_{PV} is the albedo of the PV's surface, equal to 0.1; η is the PV's re-radiation coefficient; and I_{ds} is the available diffuse radiation of the sheltered area.

(3) Vegetation Growth

For the sake of simplicity of the model, the biomass of the whole plant is divided into three biomass pools: living aboveground biomass (B_{ag}), standing dead biomass (B_{ad}) (e.g., withered leaves and dead branches), and living root biomass (B_r) (Nouvellon et al., 2000). The dynamics of the three biomass pools are described as the following differential equations with respect to daily time step:

$$\frac{dB_{ag}}{dt} = (1 - a_r)P_g + T_{ra} - R_{at} - S_a \tag{15}$$

$$\frac{dB_r}{dt} = a_r P_g - T_{ra} - R_{rt} - S_r \tag{16}$$

$$\frac{dB_{ad}}{dt} = S_a - L \tag{17}$$

where P_g (g DM d^{-1}) is the daily gross dry matter fixed through photosynthesis; a_r represents the dry matter allocation coefficient from aboveground parts to root tissues; T_{ra} (g DM d^{-1}) represents the carbohydrates transported from the roots to the living aboveground tissues; R_{at} (g DM d^{-1}) and R_{rt} (g DM d^{-1}) are total respiration from aboveground and root tissues, respectively; S_a (g DM d^{-1}) and S_r (g DM d^{-1}) represent the senescence rates of the living shoots and the roots, respectively; and L (g DM d^{-1}) is the litter fall, which is affected by the amount of precipitation.

Photosynthesis. Photosynthesis, the source of carbohydrates for the whole plant, is expressed as

$$P_g = \begin{cases} R_a \varepsilon_c \varepsilon_l \varepsilon_e f_1(S) f_2(T_{\text{air}}) & \text{for fully sky} - \text{exposed areas} \\ I_s \varepsilon_c \varepsilon_l \varepsilon_e f_1(S) f_2(T_{\text{air}}) & \text{for the areas under the PVs} \end{cases} \tag{18}$$

where the radiation term is equal to natural net radiation (R_a) for the natural case and the fully sky-exposed area (i.e., the gap area between two photovoltaic arrays; its value is equal to I_s) for the area beneath the PVs; ε_c is the ratio of photosynthetically active radiation to extraterrestrial radiation; ε_l represents the efficiency of

radiation absorption by green leaves; and ε_e is the energy efficiency. Functions f_1 and f_2 account for the stress incurred by soil moisture deficit and temperature, respectively.

$$\varepsilon_l = \left[1 - e^{(-k_l \mathrm{LAI}_t)} \frac{\mathrm{LAI}_g}{\mathrm{LAI}_t}\right] \tag{19}$$

where k_1 is an empiric constant; LAI_t is the index of the total leaf area, consisting of green and dead leaves; and LAI_g represents the index of the green leaf area.

$$\mathrm{LAI}_g = C_g B_g \tag{20}$$

$$\mathrm{LAI}_d = C_d B_d \tag{21}$$

$$\mathrm{LAI}_t = \mathrm{LAI}_g + \mathrm{LAI}_d \tag{22}$$

where LAI_d is the index of the dead leaf area, and c_g and c_d are empirical coefficients for living and dead biomass, respectively.

The effect of water stress on photosynthesis is estimated using the "static" water stress equation (Porporato et al., 2001) as a function of soil moisture condition and time.

$$f_1(S) = \begin{cases} 1, & S^* < S < 1 \\ 1 - \left[\frac{S^* - S}{S^* - S}\right]^{P_s}, & S_w < S \le S^* \\ 0, & 0 < S \le S_w \end{cases} \tag{23}$$

where P_s is an empiric parameter referring to Yetemen et al. (2015).

Air temperature (T_{air}, °C) affects photosynthesis through the moderating activity of enzymes, and those effects are expressed as a piecewise function.

$$f_2(T_{\mathrm{air}}) = \begin{cases} 1, & T_{\mathrm{opt}} < T_{\mathrm{air}} \\ 1 - \frac{T_{\mathrm{opt}} - T_a}{T_{\mathrm{opt}} - T_{\mathrm{min}}}, & T_{\mathrm{min}} \le T_{\mathrm{air}} \le T_{\mathrm{opt}} \\ 0, & T_{\mathrm{air}} < T_{\mathrm{min}} \end{cases} \tag{24}$$

where T_{min} and T_{opt} are the minimum and optimum temperatures, respectively, for photosynthesis.

Allocation. Dry matter allocation patterns are imperative for simulating the spatial patterns and temporal dynamics of plant biomass in terrestrial ecosystems. Herein, optimal partitioning theory (i.e., to maintain the homeostasis of the different nutrients or materials necessary for vegetation growth, biomass is allocated in priority to the construction of the organs responsible for capturing the most limiting resource) is adopted in the model. The allocation coefficient (a_r) is used to regulate the fractions of available carbohydrates allocated to aboveground and belowground parts. It is hypothesized that a balance must be maintained between shoots and roots such that the amount of aboveground phytomass does not exceed what the present root biomass can support (Nouvellon et al., 2000). This balance is described as:

$$B_{ax} = r_x B_{ag} - B_r \tag{25}$$

where r_x is the root-to-shoot ratio below which translocation occurs. If $B_{ax} > 0$, biomass is transported from the shoots to the roots. Otherwise, there is no biomass allocation. T_{ar} is calculated so that the root-to-shoot ratio is fixed to r_x at a daily time step:

$$r_x = \frac{B_r + T_{ar}}{B_{ag} - T_{ar}} \tag{26}$$

$$T_{ar} = \frac{B_{ax}}{1 + r_x} \tag{27}$$

$$a_r = \begin{cases} 1, T_{ar} > P_g \\ \frac{T_{ar}}{P_g}, T_{ar} \le P_g \end{cases} \quad (28)$$

However, a_r is given a value of 0.71 when the shoot senescence rate exceeds 0.012 (Nouvellon et al., 2000).

Root-to-shoot translocation. During early season regrowth, or later in the season under some circumstances (e.g., grazing has removed a critical amount of green biomass), carbohydrates will be transported from roots to shoots (T_{ra}). It is assumed that this translocation has occurred when (a) the 10-day average soil temperature is higher than 12.5°C; (b) the average 5-day soil water potential is higher than −1.2 MPa; and (c) $B_r > r_x B_{ag}$. If all three conditions are met, then:

$$T_{ra} = t_r B_r \quad (29)$$

where t_r is the proportion of dry matter of the roots translocated to the shoots (=0.005 at 25°C). It is assumed that translocation is a function of temperature, with a $Q_{10} = 3$ (herein, Q_{10} describes the change in respiration with a temperature rise of 10°C: e.g., a Q_{10} modeled to be 3 means the respiration triples per 10°C rise in temperature (Hans Lambers, 2019)).

Respiration. For both aboveground and root tissues, the rate of respiration is divided into two components: maintenance respiration and growth respiration. For the whole plant, total respiration (R_t) is the sum of aboveground respiration (R_{at}) and root respiration (R_{rt}).

$$R_{at} = m_a f_3(T_{\text{air}}) B_{ag} + g_a \left[(1 - a_r) P_g + T_{ra}\right] \quad (30)$$

$$R_{rt} = m_r f_3(T_{\text{air}}) B_r + g_r (a_r P_g) \quad (31)$$

where m_a and m_r represent the maintenance respiration rates for aboveground and root tissues, respectively; and g_a and g_r are the growth respiration rates for aboveground and root components, respectively. Function $f_3(T_{\text{air}})$ accounts for the effect of temperature on maintenance respiration rate with $Q_{10} = 2$.

(4) Landform Evolution

The topographic changes induced by the fluvial erosion and diffusive processes are simulated through the mass-transport continuity equation (Saco et al., 2007).

$$\frac{\partial z}{\partial t} = U - \frac{\nabla \cdot q_s}{\rho_s (1 - \eta_p)} - \nabla \cdot q_d \quad (32)$$

$$q_s = \beta_1 q^{m_1} S_p^{n_1} \quad (33)$$

$$q_d = D S_p \quad (34)$$

where z (m) is the topographic elevation; U (m d^{-1}) is the rate of tectonic uplift, which is ignored over a short time period; $\nabla\cdot$ is the divergence operator; q_s (kg d^{-1} m^{-1}) is the fluvial sediment transport per unit width; q_d (m^3 d^{-1} m^{-1}) is the diffusive mass transport per unit width; ρ_s (kg m^{-3}) is the density of the sediment; η_p is the porosity of the sediment; β_1 represents the rate of sediment delivery (m^2 g^{-1}); S_P is the topographic slope; and D (m^3 d^{-1} m^{-1}) is the diffusion coefficient, to simulate diffusive transport processes (e.g., rainfall splash, soil creep).

Because vegetation could interfere with the erosion response of the landscape by affecting the rate of sediment delivery, vegetation coverage was introduced into the parameter β_1 based on the work of Saco and Mariano (2013).

$$\beta_1 = \begin{cases} \beta_b (1 - V_t)(1 - \beta_v B V_t), & \beta_v B < 1 - \beta_{\min}/\beta_b \\ \beta_{\min}, & \beta_v B \ge 1 - \beta_{\min}/\beta_b \end{cases} \quad (35)$$

where β_b is the maximum erodibility for bare soil, which is assumed to decrease linearly with increasing biomass density at a rate given by β_v to a minimum value given by $\beta_{\min}$; and V_t (m^2 m^{-2}) is the vegetation coverage (Equation 5).

Field observations and modeling studies of rainfall splash erosion or rill erosion in arable land have reported a strong nexus between rainfall erosivity and rainfall intensity (Carollo et al., 2018; Mermut et al., 1997); however, this impact of rainfall intensity on rainfall splash erosion was not included in the work of Saco et al. (2007). In USFs, as PVs harvest rainfall and cause a concentrated downpour, the kinetic energy of the flow that drains from the panels was found to be greater than that of the rainfall alone (L. M. Cook & McCuen, 2013), resulting in an enhancement of rain splash erosion along the drip lines. Therefore, it could be problematic to assess the impact of USFs on landscape erosion without considering changes of rainfall intensity (or the kinetic energy of water flowing out from the edges of the PVs). Consequently, two modified diffusion coefficients, D_b and D_{PV}, for natural conditions and the land below the PVs, respectively, are introduced into the SOFAR model, and calculated as an exponential function of rainfall according to the results in Carollo et al. (2018):

$$D_b = \begin{cases} D_{b,\min}, & P_{\mathrm{in}} < P_{\min} \\ D_{b\,\max} \cdot \left[1 - \exp\left(\frac{P_{\max} - P_{\mathrm{in}}}{P_{\max} - P_{\min}} - 1\right)\right], & P_{\min} \le P_{\mathrm{in}} \le P_{\max} \\ D_{\max}, & P_{\mathrm{in}} > P_{\max} \end{cases} \tag{36}$$

$$D_{\mathrm{PV}} = \begin{cases} D_{b\,\min}, & I_{\mathrm{PVs}} < P_{\min} \\ [D_{b\,\max} K_{\mathrm{PV}} A_r + D_{b\,\max}(1 - A_r)] \cdot \\ \left[1 - \exp\left(\frac{P_{\max} - I_{\mathrm{PVs}}}{P_{\max} - P_{\min}} - 1\right)\right], & P_{\min} \le I_{\mathrm{PVs}} \le P_{\max} \\ D_{b\,\max} K_{\mathrm{PV}} A_r + D_{b\,\max}(1 - A_r), & I_{\mathrm{PVs}} > P_{\max} \end{cases} \tag{37}$$

where $P_{\max}$, 52.7 mm d^{-1} is the observed daily maximum precipitation from 1980 to 2017 at the Hongsibu site; and $P_{\min}$ (mm d^{-1}) is a threshold, and rainfall splash erosion does not occur when the daily precipitation falls below this threshold, because of canopy interception (Laio et al., 2001). However, the minimum diffusion coefficient, $D_{b\min}$, is not equal to zero when precipitation is lower than $P_{\min}$, because other diffusive erosion processes still occur. $D_{b\max}$ is the maximum diffusive erosion rate. The most widely used method for estimating the kinetic energy of rainfall (K_e, in/h) described in L. M. Cook and McCuen (2013) and Wischmeier and Smith (1978), is given by Equation 38. According to Equations 12 and 13, the amount of rainfall harvested by PVs is about five times that of natural rainfall, while the area of the drip line (A_r) is only one-six of the shaded area below the PVs (i.e., the projection area of PVs on the ground) (Figure 1c). Accordingly, the value of the kinetic energy parameter (K_{PV}), which was adopted to represent the changes of kinetic energy, was calculated from these three equations and is equal to 5.9.

$$K_e = 916 + 330 \log_{10} P_{\mathrm{in}} \tag{38}$$

2.1.2. The Hydrological Connectivity Index

Hydrological connectivity (HC) describes the internal physical linkages between runoff/sediment generation in the upper parts of a catchment and the water/sediment received through the fluvial system (Hooke, 2003; Van Nieuwenhuyse, 2012). Although the term HC is also used for subsurface flow (Buttle et al., 2004), we only consider Hortonian overland flow in this work, as it is the main runoff-generating mechanism in arid and semi-arid environments (Bryan & Yair, 1982). Since this study is concerned more with erosion behaviors than with other hydrological processes following the installation of USFs, we use a topography-based index of connectivity (HC) to understand hydrologic relationships among different parts of the catchment, and quantify the potential connections between hillslopes and features that act as targets or storage areas (sinks) for transported sediment. The index is defined as the ratio of the upslope component of connectivity (D_{up}) to the downslope component of connectivity (D_{dn}) (Borselli et al., 2008; Cavalli et al., 2013), which reflects the probability of sediment delivery from source to sink as described in Appendix B with details:

$$\mathrm{HC}_k = \log_{10}\left(\frac{D_{\mathrm{up},k}}{D_{\mathrm{dn},k}}\right) = \log_{10}\left(\frac{\overline{W_k} \cdot \overline{S_k}\sqrt{A_k}}{\sum_{i=k}^{k} d_i/(W_i \cdot S_i)}\right) \tag{39}$$

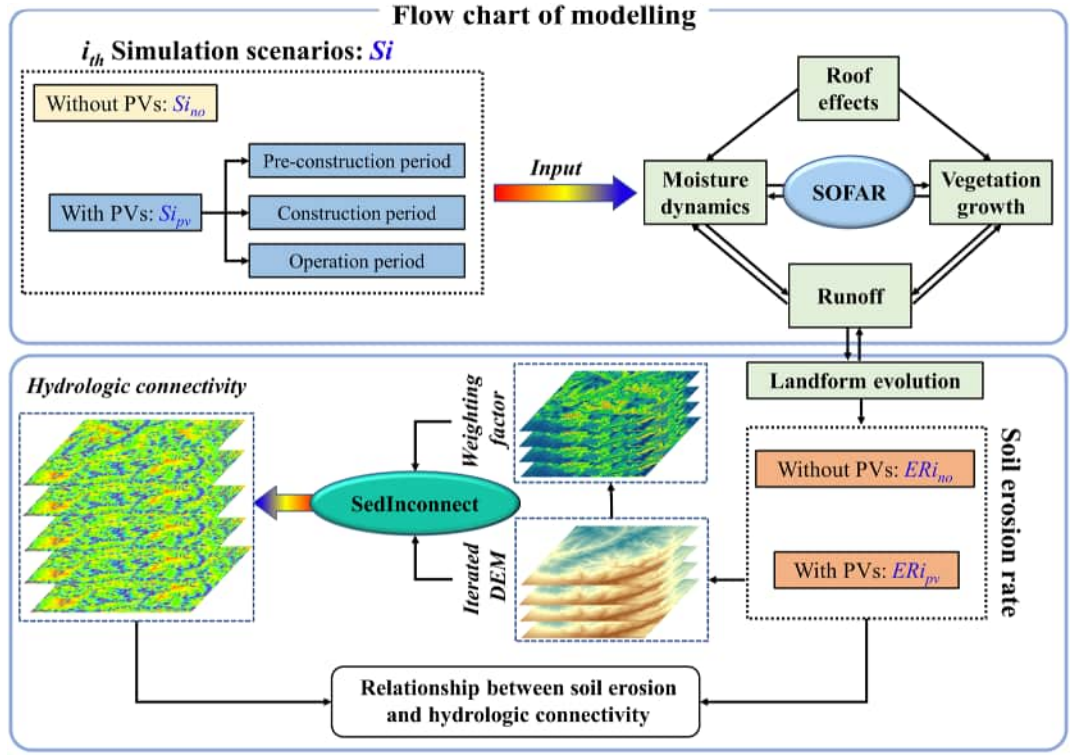

Figure 2. Pipeline of simulation of soil erosion and hydrologic connectivity in this study.

where HC_k is the HC of the k_{th} grid; $\overline{W}$ is the average weighting factor of the upslope contributing area (dimensionless); $\overline{S}$ is the average slope gradient of the upslope contributing area ($m \cdot m^{-1}$), which is the mean of all slopes in the upstream contributing area; A is the upslope contributing area (m^2); d_i is the length of the i_{th} cell of the k_{th} grid along the downslope path (m); W_k is the weight of the k_{th} cell (dimensionless, W_i ranges from 0 to 1); and S_i is the slope gradient of the i_{th} cell of the k_{th} downslope grid ($m \cdot m^{-1}$). More details of the methods used to calculate the upslope and downslope components of HC can be found in Appendix B. The DEM from the landscape evolution module in the SOFAR model, and raster maps of weighting factors with resolutions of 3×3 m based on the DEM (Appendix B), were applied as the main input data for calculating HC values. According to the definition in Appendix B, a higher value of HC means a higher hydrologic connectivity—in other words, a higher probability of sediment being transported from source to sink.

2.1.3. Pipeline of the Simulation Approach

In this work, the SOFAR model is combined with the HC Index to achieve a simulation of USF effects on soil erosion in hilly environments (Figure 2). SOFAR is the key to the simulation approach, in which the four modules were tightly bound to simulate both the above- (e.g., radiation harvest, rainfall redistribution, vegetation biomass yield, LAI dynamics, flood generation, soil erosion, et al.) and below-ground (e.g., soil moisture redistribution, soil biomass accumulation, et al.) dynamics of water, sediments, and vegetation, through ecohydrological processes such as infiltration, runon/runoff, and evapotranspiration. The module of soil moisture dynamics calculates the moisture balance of root-zone soil, with consideration of the processes of infiltration, run-off, drainage and evapotranspiration, and with the requirements of, as daily inputs, rainfall and radiation. The PV roof-effects module provides the estimation of PV-changed rainfall and radiation for the modules of soil moisture dynamics and vegetation growth. The vegetation growth module simulates the changes in vegetation and soil biomass, with consideration of both water- and energy-related changes caused by the roof effects of PVs in a USF. The landform evolution module is employed to determine the long-term erosion, and the model iteratively updates DEM at a daily timestep, with the inputs of calculated runoff and sediment from the upper slopes. The iterated DEM from the SOFAR model is then input into the SedInconnect tool to calculate the HC indexes, which in turn are used to analyze their relationship with the soil erosion occurring in the USF. A detailed flowchart of the simulation approach is illustrated in Figure 2.

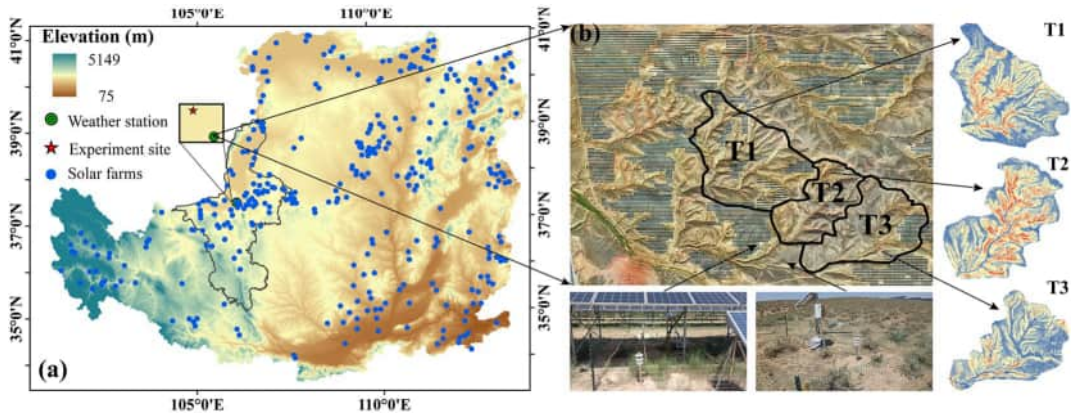

Figure 3. Map of Hongsibu site, and aerial view of the solar farm in the study site. Location of the experiment site, and meteorological variables and soil moisture monitoring instruments at the site (a); aerial view of the solar farm (shaded areas depict photovoltaic arrays) and the three sub-catchments selected within the solar farm (b).

2.2. Site Description

Instead of using a virtual environment, this study used a real-world USF site (Hongsibu solar farm) for conducting the model simulations. Data sets from this site—e.g., climate, soils, USF design and DEM—were adopted to parameterize the model, to validate the model performance, and to provide a basis for scenario design. The site (37°61′N, 106°12′E; 1,350 m a.s.l.) is located in a hilly landscape (part of the Yellow River Basin, administratively belonging to Wuzhong, China) at an elevation of 1,240–1,450 m, in the Loess Plateau of China (Figure 3a) (Zhang et al., 2021). This area has a typical temperate continental arid climate with an annual average temperature of 9.2°C (maximum daily temperature of 29.7°C and minimum daily temperature of −14.2°C). The average annual precipitation is approximately 186 mm, average annual potential evapotranspiration is about 2,387 mm, and average annual wind speed is about 2.9–3.7 m s^{-1} based on the last 38 years of available meteorological records (1980–2017 inclusive). The annual sunshine duration is up to 2,900–3,550 hr with total solar radiation of 4,936–6,119 MJ m^{-2} yr^{-1}. The rainfall scarcity combined with abundant sunlight implies that this region has extensive potential for solar energy production (Guan et al., 2020). A large number of USFs have been built in this region, and the cumulative installed capacity of solar power had reached 7.81 GW by the end of 2020 (Sun et al., 2021; Tang & Low, 2020). The terrain in this region is hilly but not mountainous, and the predominant vegetation is mixed-shrub communities including *Populus L.*, *Zygophyllaceae*, *Ulmusglaucescens*, *Leguminosae*, *Elaeagnaceae*, and so on (Zhang et al., 2022). After 6 years of operation, *Artemisia annua* (an annual herb) has become the dominant plant in the USF. However, *Reaumuria soongorica* (a perennial shrub) remains the dominant plant in natural conditions outside the USF (Figure S2 in Supporting Information S1). The soil in this region exhibits a sandy loam texture (50% clay, 30% silt, and 20% sand). The main land use of the region is rural and consists predominantly of grazing—i.e., dry farm land.

The USF where we conducted the study was built in 2016 with an installation capacity of 200 MW. Native shrublands were cleared and slightly leveled to the local terrain slope in order to build the solar farm. Solar modules were installed above the ground, and the disturbed ground was naturally recolonized by native grasses during the years following the installation. The PVs are arranged in east–west-orientated rows and inclined southward at a tilt angle of 36.2°, and the length and width of a single photovoltaic array (which consists of two sub-panels with a 3-cm gap between them) are 4 and 1 m, respectively (Figure 1c). Given the large area and rugged terrain, we selected only the northwest area of the solar farm (about 27 MW of generating capacity) with relatively uniform soil texture and significant topographical variation, for detailed study (Figure 3b). This section (hereinafter referred to as the "Hongsibu site") covers an area of 232 ha of land, and 33.87% of the total site area is covered by the impervious PVs (the land footprint is about 2.8 ha MW^{-1}). To comparatively analyze the effects of background HC on the hydrological responses in a USF, we further delineated three adjacent sub-catchments (T1–T3) within the Hongsibu site from the DEM (Figure 3b and Table 2). Onsite vegetation is maintained through sheep grazing or irregular mowing (less than once a year) as with many other solar farms in arid northwestern China (Wu et al., 2022).

Table 2
Characteristics of the Three Sub-Catchments Delineated in the Hongsibu Site

Sub-catchment	Length (m)	Width (m)	Relief amplitude (m)	Mean slope (°)
T1	800	548	51.4	17.61
T2	547	305	49.8	19.74
T3	700	476	53	13.81

2.3. Data Acquisition

The meteorological data from 1980 to 2016 (daily maximum and minimum air temperature, sunshine duration, and total precipitation, used to run the SOFAR model) (Ren et al., 2012), observed at the Wuzhong weather station—which is about 40 km away from the solar farm (Figure 3a)—were obtained from the National Meteorological Science Data Center, China. The Wuzhong weather station and the Hongsibu site are close enough to each other—especially when considering the open and uniform landscapes (topography, vegetation, etc.) in this region—that they experience very similar weather conditions and share almost the same surface conditions. Accordingly, historical records from the Wuzhong weather station represent reasonably well the weather conditions of the Hongsibu site. The 38 years of observations were input to a weather generation model (WeaGETS) (Chen et al., 2012), to stochastically generate a 50-year climate time series. Further, increased rainfall variability scenarios were produced by replacing local precipitation frequency (i.e., dry and wet periods in the WeaGETs) with the precipitation frequencies at other weather stations often experiencing torrential precipitation events and unpredictable droughts. Micrometeorological and soil-moisture data (from 04/27/2021 to 09/17/2022) at the site were collected using automatic weather stations and moisture sensors, and used to calibrate the SOFAR model. Three miniature weather stations were installed 50 cm above the ground at different positions beneath the PVs (i.e., Front, Middle, and Gap, according to water and light conditions, Figure 1c), and in the natural bare zone (set as Control) to measure the near-surface microclimates, including air temperature, relative humidity, precipitation, and wind velocity and direction. The volumetric soil moisture profiles (eight in total) were measured with a Time-Domain Transmissometer (TDT) (Acclima SDI-12, USA) at each zone (including the Control) and in-between positions (except for the Control); the probes were installed at four depths below the soil surface (10, 20, 40, and 60 cm) in each profile, and data were collected at 10-min scan intervals. The reference monitoring site (Control, with shrubs of short height, i.e., 0.2–0.5 m) was located in an open space approximately 100 m away from the PVs, so that it was assumed to not be affected by the PVs (Figure 3b). The VWC and meteorological observations were used to validate the model parameters. Furthermore, the fine landscape characteristics of the Hongsibu site (i.e., DEM) were obtained from unmanned aerial vehicle photogrammetry and ground surveys. The obtained DEM was then input into the SOFAR model for running the soil erosion processes.

2.4. Parameterization and Scenario Setting

Before calibrating the parameters of the model, the most common parameter ranges were determined based on lab results, field survey results, and the related literature (Laio et al., 2001; Nouvellon et al., 2000). Eight months of field observations were divided into calibration period and validation period: that is, observed volumetric water content (VWC) from 04/27/2021 to 09/07/2021 and collected vegetation samples in July 2021 were used to estimate parameters through the genetic algorithm (GE) by varying local soil and vegetation parameters within physically plausible ranges at the site, and field VWC from 09/10/2021 to 11/19/2021 were used to validate the simulation results of the SOFAR model. Furthermore, the MODIS products of LAI (MOD15A2) (an 8-day composite data set at 500 m resolution) from 04/27/2021 to 09/16/2021 was collected, to calibrate the parameters of vegetation growth module. The estimated set of parameter values that could lead to a best fit of the modeled soil moisture behavior with the measured data was used to run the scenario analysis. GE is a randomized search algorithm based on natural selection and genetic mechanisms in biology, and was employed to estimate the values of parameters based on observation results, with the Nash–Sutcliffe efficiency coefficient (NSE) as the fitness function (Appendix C). GE searches among a population of offered parameters, and works with a coding of the parameter set using probabilistic transition rules (Cheng et al., 2006). In this study, six settings (the initial values of input parameters of the GE procedure) were defined before running GE, including number of variables, population size, parent number, mutation rate, maximal generation, and minimal fitness value. Because the installation of runoff and sediment plots was not allowed at the Hongsibu site for safety reasons, the values of erosive parameters were set to empirical constants [for example, density (ρ_s) and porosity (n_p) of the sediment] as referred to in Saco et al. (2007), or to reported values (i.e., the diffusion coefficient, D) that were experimentally determined at a site with the same soil type and textural class on the Chinese Loess Plateau (Sun et al., 2016) (Table 1).

To estimate the effects of climate and terrain in controlling the effects of USFs on hydrological connectivity and soil erosion, nine scenarios were designed by altering the mean annual precipitation amount, the frequency

Table 3
Summaries of the Simulation Scenarios

Scenarios	Description	Relief amplitude (m)	Mean slope (slope range)	Precipitation (mm year^{-1})	Rainfall variability (%)	With/ Without PVs
Increased annual precipitation						
Scenario 1 (S1)	Baseline scenario with data from the Hongsibu site	88.43	12.96° (0.02°–55.56°)	186	465.87	$S1_{pv}/S1_{no}$
Scenario 2 (S2)	Same geomorphology as S1, but wetter meteorological conditions			377	355.46	$S2_{pv}/S2_{no}$
Scenario 3 (S3)	Same geomorphology as S1, but wettest meteorological conditions			506	381.60	$S3_{pv}/S3_{no}$
Increased rainfall variability						
Scenario 4 (S4)	Same annual precipitation amounts and geomorphology as S1, but longer duration of precipitation intermittency	88.43	12.96° (0.02°–55.56°)	188	593.39	$S4_{pv}/S4_{no}$
Scenario 5 (S5)	Same annual precipitation amounts and geomorphology as S2, but longer duration of precipitation intermittency			390	560.57	$S5_{pv}/S5_{no}$
Scenario 6 (S6)	Same annual precipitation amounts and geomorphology as S3, but longer duration of precipitation intermittency			588	533.57	$S6_{pv}/S6_{no}$
Increased relief amplitude						
Scenario 7 (S7)	Steeper hilly topography, but with meteorological conditions the same as S1	106.79	16.83° (0.04°–67.35°)	186	465.87	$S7_{pv}/S7_{no}$
Scenario 8 (S8)	Steeper hilly topography, but with meteorological conditions the same as S2			377	355.46	$S8_{pv}/S8_{no}$
Scenario 9 (S9)	Steeper hilly topography, but with meteorological conditions the same as S3			506	381.60	$S9_{pv}/S9_{no}$

Note. Annual rainfall variability (CV) was calculated as the ratio of the standard deviation (Std) of annual precipitation to annual average precipitation (Mean): CV = Std/Mean.

of precipitation events, and the ground slope (Table 3). Scenario 1 (S1) adopted the local climatic variables and landscape of the Hongsibu site to assess soil erosion following the installation of the solar farm. Because USFs are widely distributed across the climate gradient (150–800 mm year^{-1}) of the Chinese Loess Plateau (van Hateren et al., 2023), Scenarios S2 and S3 were designed to represent the cases where USFs were built at other sites with similar thick loess soil on the plateau (Zhu et al., 2018), but where annual precipitation is two-fold and three-fold that of the Hongsibu site, respectively. Additional numerical scenarios (S4–S6) with increased rainfall variability (or decreased rainfall frequency, but where the amounts of annual precipitation were set to be the same as scenarios S1–S3, Figures S3 and S4 in Supporting Information S1), were investigated, to highlight the impacts of varied rainfall patterns on hydrological behaviors in USFs in the context of climate change (Quijano-Baron et al., 2022).

Since terrain features (including slope, aspect, elevation, etc.) have been confirmed as among the major potential factors in controlling the hydrological behavior of any region (Baartman et al., 2013; Cavalli et al., 2013), we also included terrain variables in our scenario analyses. However, because PV arrangements are dominantly determined by aspect, for siting USFs in hilly environments (i.e., if the terrain aspect changed, PV arrangements would be changed considerably), we did not consider the aspect of terrain in these analyses. The influence of terrain in this study was evaluated via the scenarios S7–S9, in which a steeper terrain produced by 20% stretching of the DEM (DEM_s) of the Hongsibu site, described as Equation 40, was added to the scenarios 1–3 (S1–S3). Through this setting, about 1% of the PVs were distributed within areas where the slopes are steeper than 20°, which is the recommended slope limit for solar farm siting (Yang et al., 2019). To analyze the impact of catchment morphology, simulation results from the scenarios were also compared among the three delineated sub-catchments (T1–T3, Figure 3b, Table 2) at the Hongsibu site.

$$DEM_s = 1.2 \cdot (DEM_i - DEM_{min}) + DEM_{min} \quad (40)$$

where DEM_i represents the original value of the DEM of the ith grid, and DEM_{min} is the minimum value of DEM at the Hongsibu site.

In order to quantify the effects of the USF on soil erosion compared with the natural case, each scenario simulation included two numerical experiments (Figure 2): (a) the natural case (e.g., $S1_{no}$) and (b) the case with the PVs (e.g., $S1_{pv}$) (as shown in Table 3). The case without the PVs is the baseline for comparison in each of the scenarios. To comprehensively reflect the effects of the USF on soil erosion, the length of the simulation period was taken to be 50 years, which is longer than the usual life span of a USF (20–30 years) (Oudes & Stremke, 2021). The 50-year simulation period was further divided into three stages: pre-construction period (i.e., natural conditions, 8 years), construction period (i.e., site preparation, 2 years), and operational period (i.e., the PVs successfully produce electricity, 40 years). As a result, through testing the differences in the simulation results between different stages, the influences of PVs on hydrological behaviors in USFs can be further highlighted.

The pre-construction period was characterized by the natural land cover; vegetation in the areas with PVs installed was removed throughout the construction period, then native grasses filled in and grew there during the operational period of the USF. The scheme of removing vegetation throughout the construction period of the USF is parameterized by simply zeroing out the LAI. For the operation period, the SOFAR model uses functional plant types to represent the difference of vegetation type between solar farm and natural surface throughout the whole USF life span. Specifically, the vegetation parameters were divided into two groups: grass and shrubs (Table 1), and the parameters associated with grass were used for the grids when the case with the PVs installed was performed. Although slight land leveling was also applied at the Hongsibu site during its construction period, we did not consider this treatment in designing the scenarios, because we lacked details of this procedure and thus excessive uncertainties could have been introduced if incorrect information were included in the modeling.

3. Results

3.1. Model Performance and Parameter Calibration

Figure 4 shows the VWC response of the SOFAR model driven by the meteorological data observed at the Hongsibu site, with the parameter values presented in Table 1. The simulated soil moisture dynamics responding to rainfall and the intermittent droughts at the four different positions beneath the PVs were in overall good agreement with the field observations from 04/27/2021 to 11/18/2021 (NSE = 0.53–0.78). However, the SOFAR model slightly overestimated the soil moisture content of Gap and Front at the beginning of the growing season, and underestimated the soil moisture content of Front at the end of growing season (Figures 4a–4d). Slight underestimation also occurred in Middle at the beginning of the growing season. These inaccuracies may be attributed to the bias of input precipitation records, as evidenced by the differences in rainfall records from the miniature weather stations deployed in the USF even though they were located close to each other. To lower the uncertainties associated with the inputs (e.g., rainfall), we used the average time-series data from the weather stations as inputs to run the SOFAR model for later scenario analyses. Furthermore, the heterogeneity in soil compaction induced by different anthropogenic activity intensities is another likely reason for the modeling bias (Nawaz et al., 2013). For example, more frequent human disturbances (e.g., equipment maintenance and regular inspections) might lead to more soil compaction at the Gap and Front than at the Middle.

With respect to vegetation growth, the model captures well the dynamics of LAI in the whole USF (Figure 4e) as compared with the MODIS products of LAI (MOD15A2) (NSE = 0.91). However, there remains a slight divergence in the simulated results, which might be attributed to the rough spatial resolution (i.e., 500 m) and possible over-simplicity of the model. Moreover, the LAI for different areas beneath and beside a PV module during the 2022 growing season is plotted in Figure S5a in Supporting Information S1, and we found that the model-projected spatial gradient of LAI was in line with the observed vegetation pattern under the PVs (Figure S5b in Supporting Information S1). To validate the runoff projected by the SOFAR model, the reported runoff coefficients (defined as the surface runoff depth divided by rainfall) around the Hongsibu site (Zhang et al., 2004) were collected and compared with the model-predicted ones. Our results showed that the model-predicted runoff coefficients for the natural cases in Scenarios S1–S3 are well within the observed range. For example, the modeled runoff coefficients are between 0.001 and 0.03, and the reported runoff coefficients are between 0 and 0.08 (Figure S6a in Supporting Information S1). Furthermore, we also compared the modeled long-term mean values of soil erosion rate under natural conditions at the Hongsibu site (i.e., 0.07–0.33 mm yr^{-1}) against the reported values from nearby areas. Our results indicate that the parameterization of the land evolution module reproduces well the range of soil erosion rates in this region (Table S1 in Supporting Information S1).

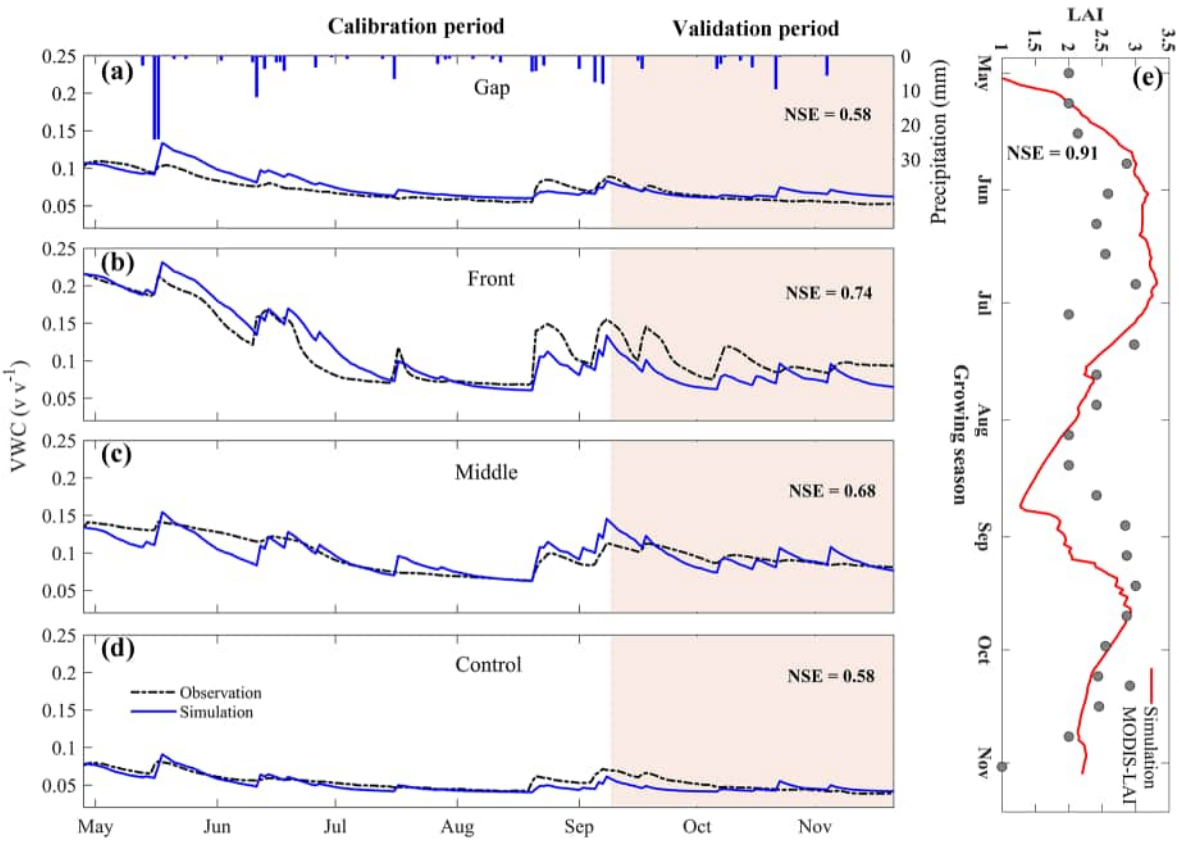

Figure 4. Parameter calibration and validation of the SOFAR model at the Hongsibu site. Blue solid line and dashed line represent simulated and observed daily soil volumetric water content (VWC), respectively. The leaf area index (LAI) was validated by the MODIS products of LAI (MOD15A2) with an 8-day composite, throughout the growing season of 2021.

Given that erosion and all the rest of the results are largely driven by runoff, a quick evaluation of before and after runoff with the USF installation is also needed. Although we did not have runoff or sediment measurements for the USF, nor were any such measurements available in any other similar sites in this region, we used some field observations to achieve a qualitative validation of before and after runoff (and erosion as well) associated with the USF installation. For example, regarding the model-predicated runoff enhancement by the USF, we collected a remotely sensed image (Gaofen-2, with the resolution of 0.8 m) taken on 10 October 2015 (before installation of the USF), and a UVA-image taken on 18 September 2022 (after installation of the USF) (Figures S6b and S6c in Supporting Information S1). An intermittent water pond formed by runoff from part of the USF was detected in both the images. We found that although very similar precipitation (i.e., 57.6 and 58 mm, respectively; Figures S6d and S6e in Supporting Information S1) was received during the 30 days before each of the image dates, a considerably larger area of the pond was recorded in the later one (134 m^2 vs. 3,075 m^2) (Figures S6b and S6c in Supporting Information S1). Based on the above efforts, we believe the simulations of the SOFAR model generally perform well, and provide a reasonably decent description of the dynamics of both the hydrological regimes and the vegetation cover in the USF.

3.2. Effects of a Solar Farm on Soil Erosion

Figure 5a plots the annual erosion rate during the construction period of the USF and the natural (undisturbed) case, under the nine simulation scenarios. The human activities involved in the USF construction (i.e., removing vegetation) incurred 21.4%–74.84% increases in the soil erosion rate compared to that of the natural case, at the Hongsibu site. Meanwhile, the accumulative soil erosion depth increased by 0.15–0.77 mm when the USF construction was begun (Table S2 in Supporting Information S1). Specifically, compared to the natural case, the PVs incurred average increases of 74.83% (0.2 mm $year^{-1}$), 43.47% (0.35 mm $year^{-1}$), and 39.44% (0.38 mm $year^{-1}$) in soil erosion rate for scenarios with different annual precipitation amounts (S1–S3, respec-

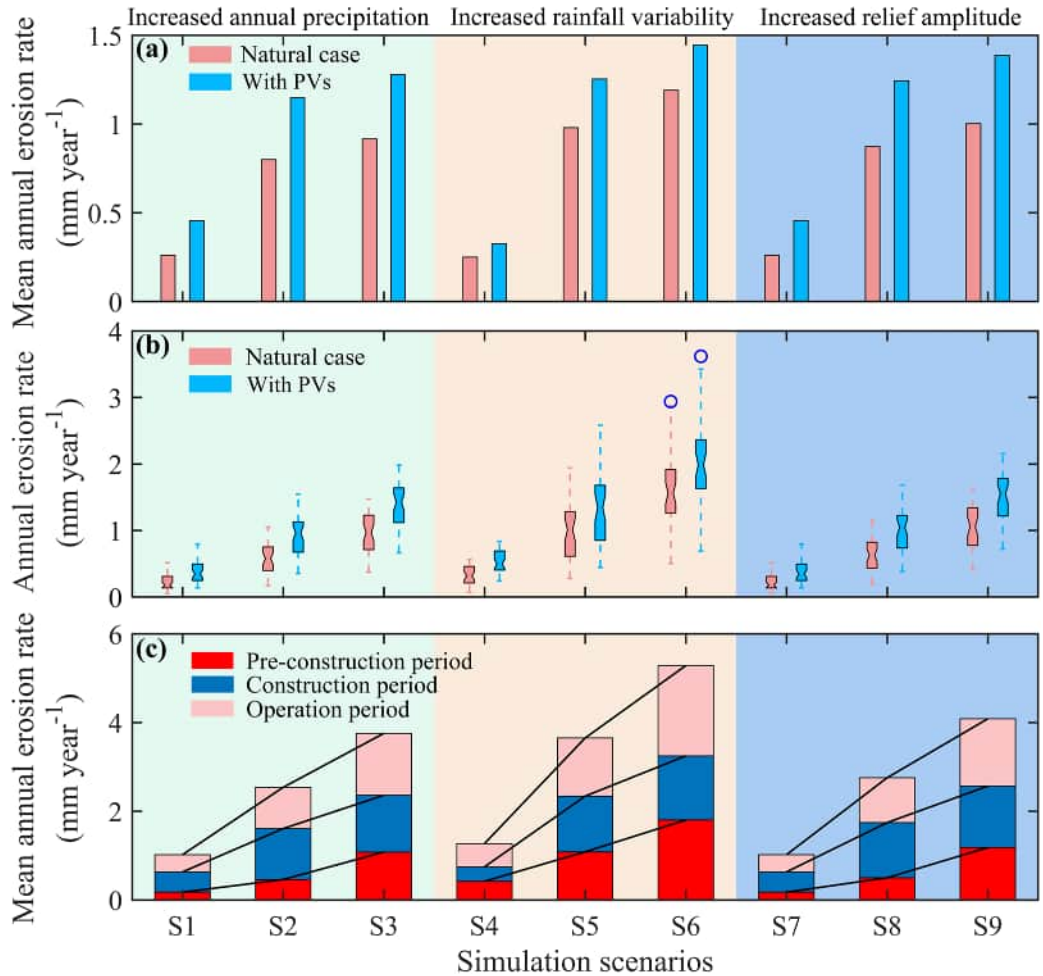

Figure 5. Effects of the USF on soil erosion rate. Soil erosion rate throughout the construction period of the USF (i.e., with PVs), and soil erosion rate of the natural case (i.e., without PVs) (a); soil erosion rate throughout the operational period of the USF (i.e., with PVs), and soil erosion rate of the natural case (i.e., without PVs) (b); mean annual soil erosion rates of the pre-construction period, construction period, and operational period, respectively (c). The upper and lower edges of the boxes (in Panel b) indicate the 75th and 25th percentiles, respectively; the upper and lower short lines extending from the box edges indicate 1.5-fold the interquartile range, and the notches within the boxes indicate median values.

tively) (Figure 5a; Figure S7a in Supporting Information S1). Under the scenarios with higher rainfall variability (S4–S6), the soil erosion rate in the USF increased by up to 30.08% (0.08 mm year^{-1}), 27.98% (0.28 mm year^{-1}), and 21.4% (0.26 mm year^{-1}), respectively, compared with the natural cases in these scenarios (Figure 5b; Figure S7b in Supporting Information S1). Soil erosion rate in the USF increased only slightly, by 74.84% (0.2 mm year^{-1}), 42.29% (0.37 mm year^{-1}), and 38.18% (0.39 mm year^{-1}), respectively, when relief amplitude increased by 20% (Scenarios S7–S9, Figure 5c; Figures S7c in Supporting Information S1).

As shown in Figure 5b; Figure S7 in Supporting Information S1, during the 40-year operating period of the USF, the soil erosion rate in the USF was significantly higher than that of the natural case for each of the nine simulation scenarios. Specifically, compared to the natural case, the soil erosion rates increased by 76.18% (0.17 mm year^{-1}), 60.34% (0.35 mm year^{-1}), and 44.29% (0.43 mm year^{-1}), respectively, for the scenarios with different annual precipitation amounts (S1–S3) (Table S3 in Supporting Information S1). When rainfall variability was enhanced, the differences in annual soil erosion rate (compared to the natural case) decreased, but the accumulative erosion depth increased: that is, the differences in annual soil erosion rates were 59.35% (0.19 mm year^{-1}), 34.46% (0.33 mm year^{-1}), and 25.35% (0.42 mm year^{-1}), respectively, for Scenarios S4–S6. Similar trends in the annual soil erosion rates were also found in the results of increasing relief-amplitude scenarios S7–S9: that is, 76.17% (0.17 mm year^{-1}), 59.96% (0.38 mm year^{-1}), and 43.42% (0.46 mm year^{-1}),

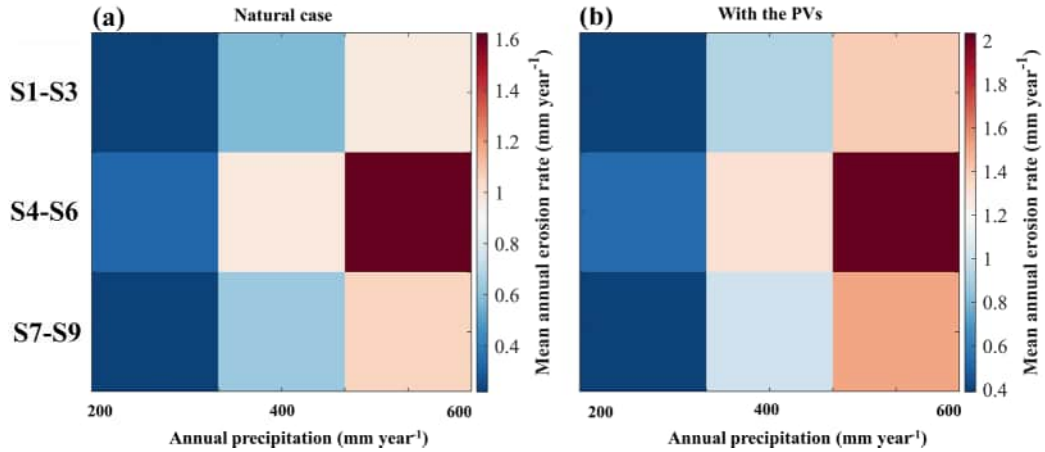

Figure 6. Changes in the mean soil erosion rate (ER) for the nine simulation scenarios. Changes in the mean soil erosion rate in the natural case (a); changes in the mean soil erosion rate in the utility-scale solar farm (b).

respectively. Overall, our results showed that construction activities for the USF incurred more intensive soil erosion than did the natural case, and this increase in soil erosion was continuous throughout the whole study period (Figure 5c). Figure 6 plots the mean soil erosion rate of the natural case and the cases with PVs under the nine simulation scenarios, and the results showed that: (a) the soil erosion rate considerably increases along with the mean annual amount of precipitation in both the natural case and the simulation scenarios with the PVs; (b) the soil erosion rate has higher sensitivity to rainfall variability than to either annual precipitation amount or terrain relief amplitude. Furthermore, as shown in the map of soil erosion occurring over the whole site (Figures S8 and S9 in Supporting Information S1), a more serious erosion was clearly observed in the installation zones of the PVs, followed by the areas close to the river channel which are characterized by higher HC (Figure S10 in Supporting Information S1).

3.3. Linking Hydrologic Connectivity to Soil Erosion in a Solar Farm

Figures 7a–7c plots the changes in runoff incurred by the USF compared with the natural case; the USF noticeably increased surface runoff. Specifically, during the installation period, construction activity for the USF incurred a 10.03%–72.87% increase of mean annual runoff, compared with the natural case; and during the long-term deployment of the USF, mean annual runoff was 99.18%–154.26% higher than that of the natural case (Table S4 in Supporting Information S1). Further, the hydrologic connectivity (HC) values throughout the construction period and the operational period were calculated. Figures 7d–7f shows that the USF incurred a 0.08%–0.26% increase ($p < 0.05$) in HC during the construction period, and a 0.47%–0.91% increase ($p < 0.05$) in HC during the operational period. The construction activity of the USF increased the HC by averages of 0.003, 0.004, and 0.002, respectively, for the scenarios with increased annual precipitation (S1–S3), increased rainfall variability (S4–S6), and increased relief amplitude (S7–S9), respectively, while after 40 years of operation of the USF, HC increased by up to 0.015, 0.014, and 0.013, respectively, for each group of scenarios (Figures 7d–7f).

We further compared the HC patterns of the delineated sub-catchments in the Hongsibu site (T1–T3). Overall, the areas close to the fluvial or basin outlets were usually associated with higher hydrologic connectivity (Figure 8a). The spatial-temporal patterns of background HC differed among the three sub-catchments, and the background HC values for the sub-catchments T1, T2, and T3 were −1.26, −1.99, and −2.18, respectively. Figures 8b and 8c plots the average HC values and the average erosion rates of three subbasins under the natural case. Our results show that the landscapes with higher hydrologic connectivity (i.e., higher HC value) were more likely to be exposed to the risks of soil erosion (Figures 8c and 8b; Table S5 in Supporting Information S1). Clearly the hypothesis "HC could be a critical indicator for sediment yield in a USF, and thus the long-term responses of soil erosion to USF installation and operation could be explained and understood in terms of HC" is true.

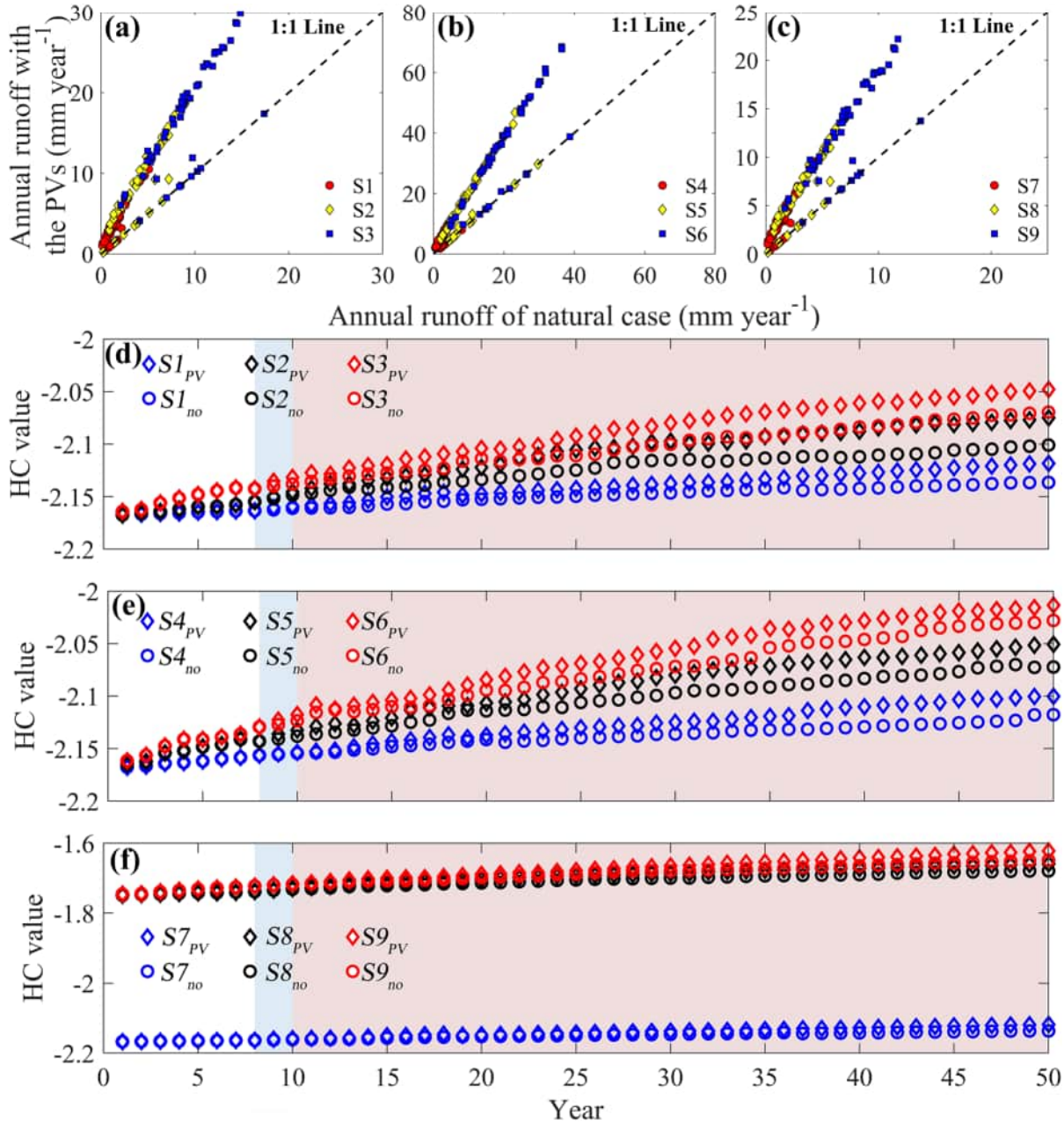

Figure 7. USF-enhanced annual runoff, and mean hydrological connectivity (HC) for the entire USF. Compared to the natural case, changes in annual runoff of the USF for the increased annual precipitation scenarios (a), the increased rainfall variability scenarios (b), and the increased relief amplitude scenarios (c); compared to the natural case, changes in hydrological connectivity of the USF for the increased annual precipitation scenarios (d), the increased rainfall variability scenarios (e), and the increased relief amplitude scenarios (f). The blue and pink backgrounds represent the construction period and operational period of the solar farm, respectively.

4. Discussion

4.1. Does a Solar Farm Increase Soil Erosion by Increasing HC?

In recent years, USFs with the potential to incur an increase in runoff or flood peak time have been reported (Nair et al., 2022). For example, L. M. Cook and McCuen (2013) reported that when compared to areas without a USF, PVs incurred 7% and 73% increases in storm runoff and peak discharge, respectively. Our predicted results also confirm that the USF incurred a 99.18%–154.26% increase in annual runoff (Figure 7a). As for soil erosion in the USF, previous researches have reported that PVs might be favorable for co-located vegetation (Adeh et al., 2018; Barron-Gafford et al., 2019; P. Cook, 2011; Marrou et al., 2013), which in turn might offset the erosion caused

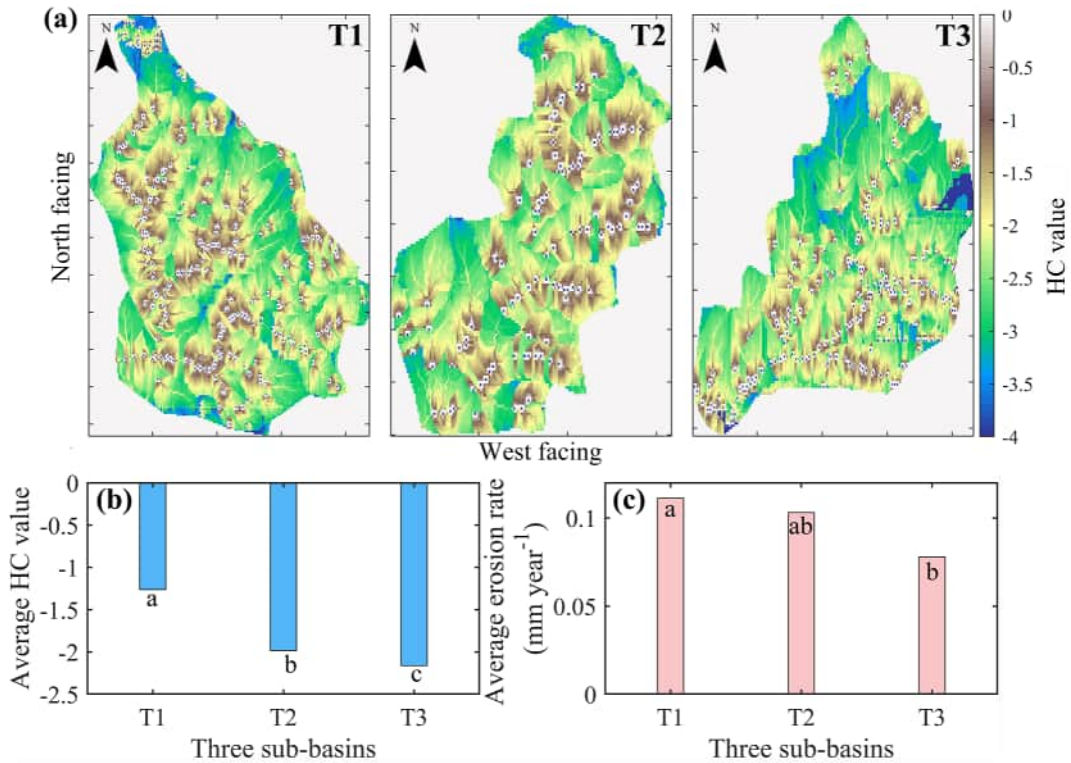

Figure 8. Map of hydrologic connectivity (HC), average HC values, and annual erosion rates of the three sub-basins. Hydrologic connectivity values for the three sub-basins under Scenario 1 (a); HC values of the three sub-basins (b); annual erosion rates of the three sub-basins. Different lowercase letters indicate significant differences among different sub-basins at a 0.05 threshold (c).

by concentrated flows caused by PVs. This effect, however, was not supported by our results. As shown in Figure 5b, our results showed that the soil erosion rate increased by 25.35%–76.18% after the installation of the USF. However, the vegetation recovery during the operational period could mitigate the erosion rate (Figure S11 in Supporting Information S1). For example, the erosion rate of the construction period averaged 0.15 mm year^{-1} higher than that of the operation period for Scenarios S1, S2, S7, and S8. Obviously, the positive effects from vegetation recovery are not sufficient to fully offset (although they still can mitigate) the negative effects of the PVs, especially when solar farms are built in areas characterized by high HC, where annual precipitation is higher, or where extreme precipitation events are frequent (as in the results of Scenarios S3, S4–S6, and S9, shown in Figure S11 of the Supporting Information S1). Furthermore, the variations in erosion rate between the construction period and the operation period also highlight the importance of considering dynamic vegetation in the study of the hydrologic response of USFs.

Soil erosion rate is a function of rain splash and runoff (Battany & Grismer, 2000). For a USF, rain splash is the dominant factor causing erosion because PVs redistribute rainfall and amplify its intensity along the driplines (~ five times higher than natural rainfall intensity, at the Hongsibu site). However, rain splash erosion does not redistribute large amounts of soil; rather, it serves to detach soil particles for transport by runoff (Battany & Grismer, 2000). Our results indicate that runoff explains most of the changes of soil erosion in a solar farm (Figures 9a and 9b). However, we argue that runoff is not the only dominative factor for soil erosion when up to 40 years of deployment of a USF are considered. Figure 7 shows that the USF enhanced HC throughout its whole life-span under different simulation scenarios, and Figure 9 further indicates that erosion rate is directly proportional to HC. Accordingly, both the results prove that a USF could change both HC and the feedback between erosion and HC. In other words, while the USF changed HC at the site, the changes in HC could also have affected soil erosion by changing the capacity of the transporting sediment, which also further consolidates our hypothesis that HC could be a critical indicator for sediment yield in a USF, and the long-term responses of soil erosion to USF installation and development could be explained and understood in terms of HC. It also means that the spatiotemporal patterns of HC could help us identify the potential erosion risk in a USF.

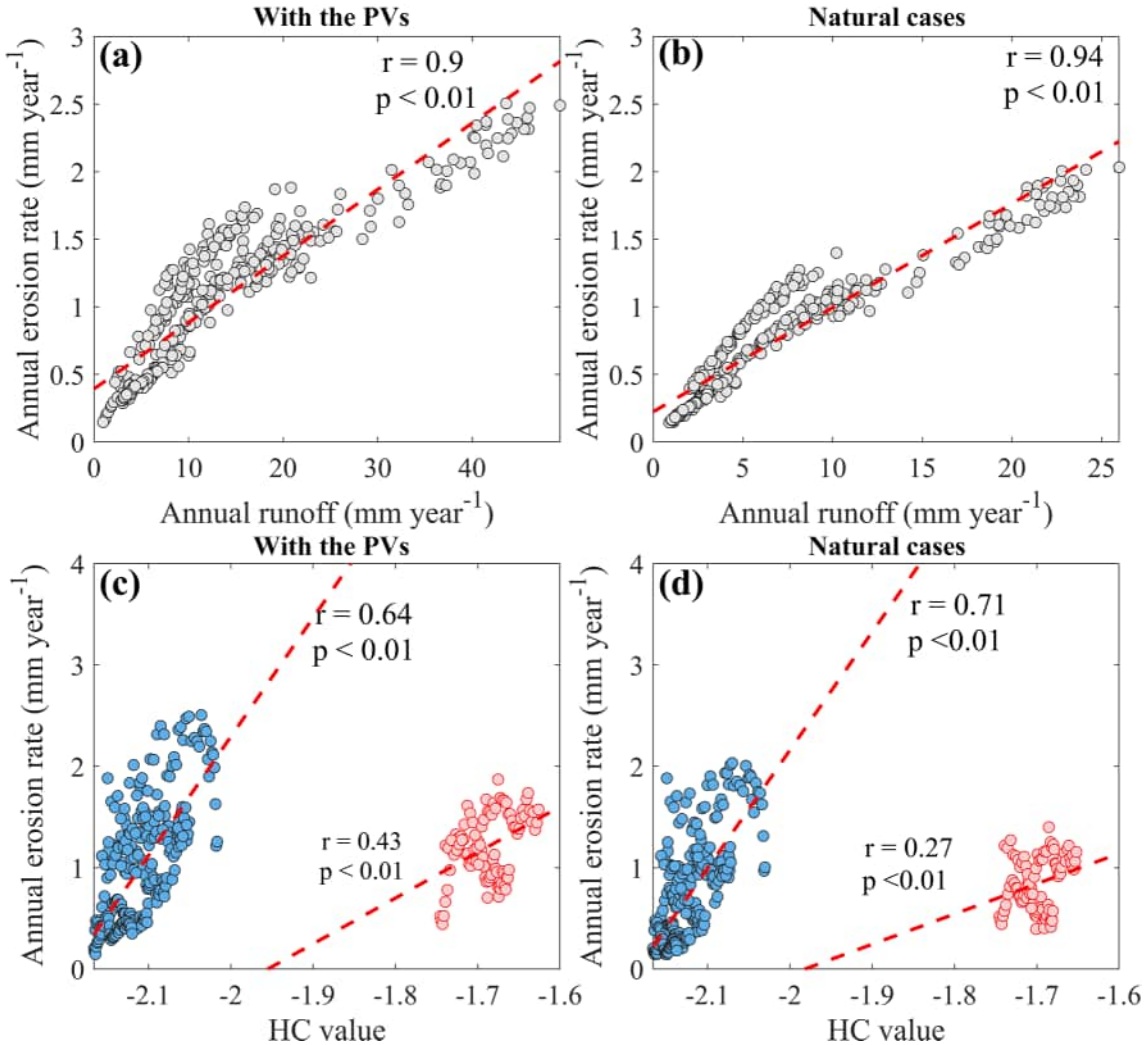

Figure 9. Relationships among soil erosion rate, annual runoff, and hydrologic connectivity. Relationship between soil erosion rate and annual runoff under scenarios with the installation of photovoltaic panels (PVs) (a) and the natural case (b); relationship between soil erosion rate and hydrological value (HC value) under scenarios with the installation of PVs (c) and the natural case (d). In panels (c and d), the blue and pink assembles represent the results of scenarios S1–S7, and scenarios S8 and S9, respectively. All data shown here are 5-year moving averages of the 50-year simulation results.

Based on results predicted in this study, we conceptualized the mechanism of a USF's effect on soil erosion as a runoff-erosion-HC positive feedback: that is, an increase in runoff incurs serious soil erosion and necessitates more developed river networks, and such development represents higher HC and stronger sediment transport capacity, as well as more concentrated runoff. As a result, higher HC can further increase soil erosion due to changes in junction paths. For example, PVs act as an imperious cover, and thus rainfall is concentrated along the downslope edge of the panels, incurring increased runoff, as well as rain splash erosion risks (Holland et al., 2021; Smith et al., 2011). Raindrop impacts are responsible for particle detachment and the creation of micro topography (Josserand & Zaleski, 2003), and this local erosion in turn might potentially create additional pathways for runoff and increase HC, thus furthering soil degradation processes at larger scales (Elamri et al., 2018). Furthermore, vegetation may reshape this positive feedback, because a change in HC could precipitate a feedback to vegetation dynamics by allowing more vegetation to grow along the flow paths, where water is more abundant and the sediment is rich in organic matter.

4.2. Does Higher Background HC Aggravate the Effects of USFs?

Besides causing local erosion along the edge of the panel via enhanced kinetic energy (L. M. Cook & McCuen, 2013), the significantly concentrated rainwater on the ground surface near PVs seems more likely to

generate Hortonian overland flow and floods on the slopes of hilly ground, and eroded soil under PVs is also more likely to reach a transport system in hilly environments, and subsequently result in considerable off-site sediment movement in USFs (Hernandez et al., 2014). For example, under the same precipitation conditions, we found that landscapes with higher HC were more likely to be exposed to the danger of soil erosion (Figure 8). Further, the more severe soil erosion in solar farms with higher relief amplitudes could be explained at least partly by the relatively higher HC in steeper terrain (Figure 7), and the separated patterns of HC in Figures 7 and 9 indicate that the precipitation amount has a more intensive influence on erosion rate than does terrain relief amplitude. Because the relief amplitudes of Scenarios S7 to S9 were all enhanced, however, Scenarios S8 and S9 had higher precipitation, which would significantly affect the production of runoff and erosion, as well as the landscape evolution process. From the modeling results of this work, it is also interesting to find that even USFs with similar relief amplitudes could result in very different effects on the soil erosion processes, as more dramatic changes and higher HC were usually detected in areas where a solar farm was sited (Figures S8 and S10 in Supporting Information S1). This phenomenon might be related to the fact that higher HC often leads to shorter runoff time and larger runoff kinetic energy (Poesen et al., 2003), and thus is more likely to build connections between PV-caused erosion at local scales and sediment transfers at larger scales, in USFs with higher background HC (Holland et al., 2021; Smith et al., 2011). Similarly, increasing vegetation cover could lower the HC in USFs (Crompton et al., 2023), and thus significantly reduce the risk of erosion (Figure 5). The basic logic behind these measures is that they protect the surface by restricting the movement of sediment and increase the hydraulic conductivity of the soil, resulting in greater throughflow and less overland flow, thereby reducing HC and erosion (Phalane, 2021).

4.3. Implications for Risk Control of USFs in Hilly Environments

USFs offer an opportunity to deliver ecosystem co-benefits, but their development and operation may also incur detrimental consequences to ecosystems (Randle-Boggis et al., 2020). Regarding the negative impact of USFs, some of the top concerns from governments and local communities are the risks of stormwater runoff and erosion (Brick, 2019; Chiabrando et al., 2009). Our results also confirmed that these risks are due to a 99.18%–154.26% increase in runoff after the installation of a USF (Figure 7). Further, our results showed that PVs could bring higher risks during the installation period than during the operational period, highlighting that vegetation protection is imperative for preventing erosion risk throughout the whole life span of a USF. Combining a USF planting process with allowing the naturally occurring vegetation to replenish itself with time can accomplish this goal (L. M. Cook & McCuen, 2013). Accordingly, where possible, herbaceous vegetation recruitment or re-establishment under the PVs is highly recommended, to protect soil stability and minimize soil erosion in a USF. When evaluating the potential to co-locate vegetation with solar-farm infrastructure, the redistribution of rainfall by PVs—which could potentially be used in concert with planting strategies to maximize plant growth or minimize soil erosion—should also be considered (Choi et al., 2020). It is noticeable that this research only focused on water erosion, but PVs could also significantly affect the wind field and thereby the wind erosion processes in a USF (Yadav et al., 2019). Although it is beyond the scope of this study, future works should consider accounting the contribution of wind erosion of soil in USFs, especially where wind hazards are a problem.

Based on our findings, from the perspective of hydrological connectivity, controlling the risks of stormwater erosion in USFs can also be achieved through measures that reduce the HC: for example, a gutter system can be installed to capture all the stormwater falling on the PVs and redirect it into a stormwater attenuation tank or infiltration soak-away (Phalane, 2021); on-site flood control structures (e.g., earthen berms, diversion ditches, and stormwater conveyance channels) can be constructed along the contour lines and across slopes for the purpose of intercepting surface runoff and diverting it to suitable outlets (Brick, 2019; Doorga et al., 2022; Murphy-Mariscal et al., 2018); buffer strips, detention basins or swales can even be built at the downgradient end of the application site to reduce the peak run-off rate or intercept extreme flows that may already be running offsite (Phalane, 2021). It is also recommended that erosion and silt management be considered carefully and monitored regularly in these hilly environments (Dhar et al., 2020; Phalane, 2021). This study provides a synthetic framework (i.e., SOFAR model) for the environmental impact (i.e., erosion risks) assessment of USFs, with the consideration of landscape ecohydrologic and geomorphic feedbacks over their life spans. The proposed method (i.e., combining the SOFAR model with an index of HC) also can serve as a decision support approach for the site selection and permitting process of a USF, based on the predicted spatial-temporal patterns of landform erosion and HC. Nevertheless, more studies should be carried out in order to further improve the assessment of the environmental impacts of USFs in a wide range of practical situations and PV-installation configurations.

5. Conclusions

The potential effects of USFs on soil erosion in hilly environments were investigated through modeling efforts in this work from the perspective of hydrological connectivity. Specifically, our results show that the selected USF considerably increased runoff (99.18%–154.26%), and incurred about 21.4%–74.84% and 25.35%–76.18% increases in soil erosion rate throughout the construction period and the operational period, respectively. Both the precipitation features (i.e., amount and variability) and the relief amplitude of the terrain were confirmed as important controlling factors for soil erosion; however, soil erosion processes are most sensitive to rainfall variability. Similarly, the USF incurred 0.08%–0.26% ($p < 0.05$) and 0.47%–0.91% increases ($p < 0.05$) in HC during the construction period and the operational period, respectively. In the USF, more serious erosion was also detected in the installation zones of the PVs, followed by the areas close to the river channel. The hypothesis that HC could be a critical indicator for sediment yield in a USF, and thus the long-term responses of soil erosion to USF installation and development could be explained and understood in terms of HC, was proved to be true. Our findings reveal the fundamental role of a USF in controlling the water and sediment yield of catchments and topography organization. We confirmed that USFs can increase soil erosion, mainly by increasing local HC and runoff, and higher background HC can in turn further aggravate the effects of USFs on soil erosion. Accordingly, through suitable USF designs and storm-water management that can potentially reduce the HC or at least prevent any increases in it, erosion-related risks caused by PVs within and around USFs can be considerably lowered. The outcomes from this study provide useful guidance for assessing the potential hydrologic effects of USF installation and operation in hilly environments—important information for those who plan, design, and deploy USF projects, especially in the context of climate change and increasing land scarcity.

Appendix A

The components of the solar irradiance incident on an inclined photovoltaic panel (PV) are: beam radiation coming directly from the sun, diffuse radiation from the entire illuminated hemisphere, and ground-reflected radiation. As reported in the literature, each of these components of solar irradiance incident on a PV is determined by calculating solar incidence angle (i), solar elevation angle (h_c) (Diez et al., 2021; Passias & Källbäck, 1984), solar declination (δ), and hour angle (ω). Aspect-controlled radiation has been recognized as a vital driver responsible for the co-evolution of vegetation, soil, and landscapes (Kumari et al., 2020; Yetemen et al., 2015; Zhou et al., 2013), which is also considered in this study, in order to avoid additional biases.

The daily extraterrestrial radiation (I_0, w m^{-2}) is estimated using the following equation:

$$I_0 = 1353\left[1 + 0.034\cos\left(\frac{2\pi n}{365}\right)\right]\frac{\sin(h_c)}{\sin(h_c) + \mathrm{C}} \tag{A1}$$

where parameter C, relating to atmospheric transparency, is an empirical coefficient, and solar elevation angle and solar incidence angle are estimated by Equations A2 and A3, respectively.

$$\sin(h_c) = \sin(\varphi)\sin(\delta) + \cos(\varphi)\cos(\delta)\cos(\omega) \tag{A2}$$

$$\begin{aligned}\cos(i) = {} & \sin(\delta)[\sin(\varphi)\cos(\beta) - \cos(\varphi)\sin(\beta)\cos(\gamma)] + \cos(\delta)\cos(\omega)[\cos(\varphi)\cos(\beta) \\ & + \sin(\varphi)\sin(\beta)\cos(\gamma)] + \cos(\delta)\sin(\beta)\sin(\gamma)\sin(\omega)\end{aligned} \tag{A3}$$

where parameters φ, β, and γ represent the latitude of the site, the inclination angle of the PV, and the azimuth angle of the PV (or aspect of each grid), respectively. The solar declination (δ) and the hour angle (ω) are given by

$$\delta = 23.45\sin\left(360\frac{284 + N}{365}\right) \tag{A4}$$

$$\omega = (\tau - 12)15^\circ \tag{A5}$$

where N is the day of the year, and the solar time τ is given by

$$\tau = T + \frac{E - 4\left(12 - L_{\log}\right)}{60} \tag{A6}$$

where T (h) is Beijing time, $L_{\log}$ is the local longitude, and E (min)—the corrected time difference attributable to the change in the speed of the earth's motion around the sun (Gualla, 2015)—is given by

$$E = 9.87\sin(2B) - 7.53\cos(B) - 1.5\sin(B) \tag{A7}$$

$$B = \frac{360(n-81)}{365} \tag{A8}$$

The total available solar radiation on an inclined PV is the sum of beam radiation, diffuse radiation, and ground-reflected radiation (Diez et al., 2021).

$$I_{\mathrm{PV}} = I_{b\beta} + I_{d\beta} + I_r \tag{A9}$$

Beam radiation (MJ m^{-2}) can be estimated based on extraterrestrial radiation (I_0, W m^{-2}). Beam radiation incident on a horizontal surface and on an inclined PV are given by Equations A10 and A11, respectively.

$$I_{bH} = I_0 P_1^m \sin(h_c) \tag{A10}$$

$$I_{b\beta} = I_0 P^m \cos(i) \tag{A11}$$

where P_1—atmospheric transparency—is a constant. The constant m—atmospheric quality—is a function of solar elevation angle ($m = 1/\sin(h_c)$).

Diffuse radiation from the entire illuminated hemisphere incident on a horizontal surface is estimated as

$$I_{dH} = \frac{1}{2} I_{bH} \frac{1 - P^m}{1 - 1.4\ln(P)} \tag{A12}$$

Diffuse radiation from the sky incident on an inclined PV ($I_{d\beta}$), estimated from I_{dH}, is given by the Klucher model of anisotropic distribution for all sky types (Klucher, 1979).

$$I_{d\beta} = I_{dH}(1 + \cos(\beta))\left[1 + F\sin^3\left(\frac{\beta}{2}\right)\right]\left[1 + F\cos^2(i)\cos^3(h_c)\right] \tag{A13}$$

$$F = 1 - \left(\frac{I_{dH}}{I_0}\right)^2 \tag{A14}$$

The radiation reflected by the ground surface, incident on an inclined PV under the anisotropic reflection assumption (Diez et al., 2021), is presented thus:

$$I_r = \frac{1}{2}\alpha(I_{bH} + I_{dH})[1 - \cos(\beta)]\left[1 + \sin^2\left(\frac{\pi}{4} - \frac{h_c}{2}\right)\right] \tag{A15}$$

where α is the ground albedo (i.e., the ratio of irradiation reflected from the ground to the irradiation incident on the ground).

Daily solar radiation values from 1980 to 2017 were not available; only daily sunshine duration (SSD) could be found. An alternative algorithm was therefore adopted to calculate the daily solar radiation. Daily solar radiation is equal to SSD multiplied by the daily average solar radiation, which is the average of all the per-hour solar radiation values projected by Equations A1–A8. The model assumes that every growing season has the same average solar radiation at the daily scale, and this is produced on the basis of 12 hr of SSD, so that daily solar radiation can be calculated from SSD records. The total available solar radiation on the horizontal ground surface and on a PV can be calculated by

$$I_G = \frac{\sum_j^{12}(I_{bH,j} + I_{dH,j})}{12} \tag{A16}$$

$$I_{\mathrm{PV}} = \frac{\sum_j^{12}(I_{b\beta,j} + I_{d\beta,j} + I_{r,j})}{12} \tag{A17}$$

In a large-scale solar farm where the PVs are mounted in rows, there is a masking effect: that is, the PVs in all the rows except the first one experience a partial blocking of the hemispheric radiation, and thus there is a reduction in the amount of diffuse radiation they receive (Passias & Källbäck, 1984). Therefore, the total available radiation for the sheltered area is estimated as

$$I_s = I_{\mathrm{PV}}(1 - \varepsilon - \alpha_{\mathrm{PV}})\eta + I_{ds} \tag{A18}$$

where ε is the efficiency with which a PV transfers the solar radiation to electricity, α_{PV} is the albedo of the PV's surface, and η is the PV's re-radiation coefficient. I_{dS} is the available diffuse radiation of the sheltered area.

$$I_{ds} = I_{dH}\frac{\xi}{\pi} \tag{A19}$$

where ξ is shading angle of the PV, which is given by

$$\xi = \pi - \arctan\left(\frac{h}{W}\right) - \arctan\left(\frac{H}{L\cos(\beta) - W}\right) \tag{A20}$$

where h (m) and H (m) are the height of the front and rear edges of the PV, respectively; L (m) is the length of the PV; and W (m) is the distance from a point in the sheltered zone to the front edge of the PV.

Appendix B

As introduced in Borselli et al. (2008), the sediment delivery ratio, one of the core contents of hydrologic connectivity, was determined by two aspects: (a) Upslope characteristics. For example, large basins have a lower sediment delivery ratio, because larger basins are characterized by lower average slope and tend to have more sediment storage capacity; (b) Downslope characteristics. For example, the path between source and sink of sediment is affected by topographic roughness and slope. Accordingly, a reasonable hydrological connectivity (HC) index should reflect both the above effects, and that fact is exactly the content of the HC index used in this study.

As described above, HC could be explained with the probability of sediment's reaching the source (defined as P_u), and the probability of the sediment's arriving at the sink from the source (defined as P_d). Accordingly, the probability of sediment in the source reaching the sink (P) can be expressed as:

$$P = P_u P_d \tag{B1}$$

Downslope components. First, it is assumed that there is a negative relationship between P_d and segment length d, because a longer flow path creates higher resistance and more loss of kinetic energy. However, other factors (e.g., vegetation cover, roughness, characteristics of the underlying surface, and slope) also influence P_d. For example, a rougher surface creates higher resistance for the transfer of sediment, but steeper topography generates a higher transfer capacity for sediment. Therefore, a weight factor (W), based on roughness, was introduced, to consider the effects of the underlying surface on sediment delivery, and the downslope component of HC can therefore be written as:

$$D_{\mathrm{dn}} = \sum_i \frac{d_i}{W_i S_i} \tag{B2}$$

where d_i (m) represents the length of the i_{th} grid along the downslope path; W_i is the weight of the i_{th} grid; and Si is the slope gradient of the i_{th} grid. In this study, the topographic method was used to calculate the weighting factor (Cavalli et al., 2013), that is,:

$$W = 1 - \left(\frac{\mathrm{RI}}{\mathrm{RI}_{\max}}\right) \tag{B3}$$

$$\mathrm{RI} = \sqrt{\frac{\sum_{i=1}^{25}(x_i - x_m)}{25}} \tag{B4}$$

where RI is residual topography; x_i is the value of one specific grid of the residual topography within the moving window; x_m is the mean elevation of 25 grids, and RI_{max} is the maximum value of RI in the 25 grids. Based on Equations B2–B4, we can find the negative relationship between roughness and weighting factor, and a rougher surface is associated with a lower weighting factor but higher D_{dn}. However, a rougher surface means a higher resistance of sediment delivery. Finally, the probability P_d is inversely proportional to D_{dn}, that is,:

$$P_d \propto D_{dn}^{-1} \tag{B5}$$

Upslope component. The upslope component (D_{up}) is the potential sediment quantity for the downslope sink, which is dependent on the area of upslope catchment and other factors such as D_{dn}. Based on Equation B3, a rougher surface means a lower weight factor, a lower slope is related to a lower probability of sediment reaching the source, and the potential sediment quantity is dependent on the area of the upslope catchment. Thus, D_{up} can be estimated as:

$$D_{up} = \overline{W} \cdot \overline{S}\sqrt{A} \tag{B6}$$

where $\overline{W}$ is the average weighting factor of the upslope contributing area; $\overline{S}$ is the average slope of the upslope contributing area; and A is the upslope contributing area. Here, the square root of A is used, to retain the same unit of D_{dn}. Accordingly, based on Equation B6, P_u is directly proportional to D_{up}:

$$P_d \propto D_{up} \tag{B7}$$

Thus, Equation B1 could be written as:

$$P = P_u P_d \propto \frac{D_{up}}{D_{dn}} = \frac{\overline{W} \cdot \overline{S}\sqrt{A}}{\sum_i \frac{d_i}{W_i S_i}} \tag{B8}$$

However, the rightmost term can easily vary over orders of magnitudes (making it especially sensitive to changes in denominator), and thus it was more convenient to adopt the logarithm of Equation B8, that is,:

$$HC_k = \log_{10}\left(\frac{D_{up,k}}{D_{dn,k}}\right) = \log_{10}\left(\frac{\overline{W_k} \cdot \overline{S_k}\sqrt{A_k}}{\sum_{i=k}^{k} d_i/(W_i \cdot S_i)}\right) \tag{B9}$$

Here, the value of term $\frac{\overline{W} \cdot \overline{S}\sqrt{A}}{\sum_i \frac{d_i}{W_i S_i}}$ is in the range of (0,+∞). Zero occurs when the terrain is absolutely flat, and +∞ occurs when upslope catchment is sufficiently large. Thus, the HC_k is in the range of (−∞,+∞). Meanwhile, due to logarithmic function was a monotone increasing function, the larger value of $\frac{\overline{W} \cdot \overline{S}\sqrt{A}}{\sum_i \frac{d_i}{W_i S_i}}$ meant a higher HC_k, and thus higher connectivity (or higher probability of sediment transported from source to sink).

Appendix C

The statistical index, Nash–Sutcliffe efficiency coefficient (NSE), was used for assessing the accuracy of the SOFAR model.

$$NSE = 1 - \frac{\sum_i^n \left(Q_0^i - Q_S^i\right)^2}{\sum_i^n \left(Q_0^i - \overline{Q_0}\right)^2} \tag{C1}$$

where Q_0^i and Q_S^i are observation and simulation results of daily VWC (v/v), respectively; i is the number of days in the calibration period; and $\overline{Q_0}$ is the average of the field observations of soil moisture content.

Conflict of Interest

The authors declare no conflicts of interest relevant to this study.

Data Availability Statement

Daily meteorological observations (1980–2016) are available from Ren et al. (2012), although these are not publicly available due to the copyright protection of the China Meteorological Data Service Center. However, they are available when registration is completed and the data request is approved. The MODIS products of LAI (MOD15A2, an 8-day composite data set at 500m resolution) used in this study are available in Myneni et al. (2021). The field observations of biomass, soil moisture contents and other microclimates are available in Liu et al. (2023a), and the code for the SOFAR model (solar farm model, SOFAR) used in this study is available in Liu et al. (2023b). Code for the SedInconnect model used in this study is available in Stefano et al. (2021).

Acknowledgments
This research was jointly supported by the National Natural Science Foundation of China (U23A2063/42177310), the Leading Talents Program of Gansu Province (E339040101), and the 2232 International Fellowship for Outstanding Researchers Program of the Scientific and Technological Research Council of Turkey (118C329). The authors thank the editors (Prof. Peter Troch, Prof. Erkan Istanbulluoglu) and the anonymous reviewers for their constructive and inspiring reviews.

References

Adeh, E. H., Selker, J. S., Higgins, C. W., & Villarini, M. (2018). Remarkable agrivoltaic influence on soil moisture, micrometeorology and water-use efficiency. *PLoS One*, *13*(11), e0203256. https://doi.org/10.1371/journal.pone.0203256

Armstrong, A., Ostle, N. J., & Whitaker, J. (2016). Solar park microclimate and vegetation management effects on grassland carbon cycling. *Environmental Research Letters*, *11*(7), 074016. https://doi.org/10.1088/1748-9326/11/7/074016

Baartman, J. E. M., Masselink, R., Keesstra, S. D., & Temme, A. J. A. M. (2013). Linking landscape morphological complexity and sediment connectivity. *Earth Surface Processes and Landforms*, *38*(12), 1457–1471. https://doi.org/10.1002/esp.3434

Baartman, J. E. M., Temme, A. J. A. M., & Saco, P. M. (2018). The effect of landform variation on vegetation patterning and related sediment dynamics. *Earth Surface Processes and Landforms*, *43*(10), 2121–2135. https://doi.org/10.1002/esp.4377

Barnard, T., Agnaou, M., & Barbis, J. (2017). Two dimensional modeling to simulate stormwater flows at photovoltaic solar energy sites. *Journal of Water Management Modeling*, 1–8. https://doi.org/10.14796/JWMM.C428

Barron-Gafford, G. A., Pavao-Zuckerman, M. A., Minor, R. L., Sutter, L. F., Barnett-Moreno, I., Blackett, D. T., et al. (2019). Agrivoltaics provide mutual benefits across the food–energy–water nexus in drylands. *Nature Sustainability*, *2*(9), 848–855. https://doi.org/10.1038/s41893-019-0364-5

Battany, M. C., & Grismer, M. E. (2000). Rainfall runoff and erosion in Napa Valley vineyards: Effects of slope, cover and surface roughness. *Hydrological Processes*, *14*(7), 1289–1304. https://doi.org/10.1002/(SICI)1099-1085(200005)14:7<1289::AID-HYP43>3.0.CO;2-R

Boix-Fayos, C., de Vente, J., Barberá, G., & Castillo, V. (2007). The impact of land use changes and hydrological control works on hydrological connectivity and sediment yield at the catchment scale. In *Paper presented at proceedings of the European geosciences union general assembly*.

Bolinger, M., & Seel, J. (2018). Utility-scale solar: Empirical trends in project technology, cost, performance, and PPA pricing in the United States.

Bórawski, P., Bełdycka-Bórawska, A., Szymańska, E. J., Jankowski, K. J., Dubis, B., & Dunn, J. W. (2019). Development of renewable energy sources market and biofuels in The European Union. *Journal of Cleaner Production*, *228*, 467–484. https://doi.org/10.1016/j.jclepro.2019.04.242

Borselli, L., Cassi, P., & Torri, D. (2008). Prolegomena to sediment and flow connectivity in the landscape: A GIS and field numerical assessment. *Catena*, *75*(3), 268–277. https://doi.org/10.1016/j.catena.2008.07.006

Bracken, L. J., & Croke, J. (2007). The concept of hydrological connectivity and its contribution to understanding runoff-dominated geomorphic systems. *Hydrological Processes: An International Journal*, *21*(13), 1749–1763. https://doi.org/10.1002/hyp.6313

Brick, R. (2019). Utility-scale solar construction: Best practices for reducing costs and ensuring environmental compliance. (Master's thesis). Johns Hopkins University. Retrieved from https://jscholarship.library.jhu.edu/server/api/core/bitstreams/9a06581d-57bb-4220-915f-771a5539dba1/content

Bryan, R., & Yair, A. (1982). *Badland geomorphology and piping*. Geo Books.

Buttle, J., Dillon, P., & Eerkes, G. (2004). Hydrologic coupling of slopes, riparian zones and streams: An example from the Canadian Shield. *Journal of Hydrology*, *287*(1–4), 161–177. https://doi.org/10.1016/j.jhydrol.2003.09.022

Cabal, C., De Deurwaerder, H. P. T., & Matesanz, S. (2021). Field methods to study the spatial root density distribution of individual plants. *Plant and Soil*, *462*(1–2), 25–43. https://doi.org/10.1007/s11104-021-04841-z

Carollo, F. G., Ferro, V., & Serio, M. A. (2018). Predicting rainfall erosivity by momentum and kinetic energy in Mediterranean environment. *Journal of Hydrology*, *560*, 173–183. https://doi.org/10.1016/j.jhydrol.2018.03.026

Cavalli, M., Trevisani, S., Comiti, F., & Marchi, L. (2013). Geomorphometric assessment of spatial sediment connectivity in small Alpine catchments. *Geomorphology*, *188*, 31–41. https://doi.org/10.1016/j.geomorph.2012.05.007

Chen, J., Brissette, F. P., Leconte, R., & Caron, A. (2012). A versatile weather generator for daily precipitation and temperature. *Transactions of the ASABE*, *55*(3), 895–906. https://doi.org/10.13031/2013.41522

Cheng, C.-T., Zhao, M.-Y., Chau, K. W., & Wu, X.-Y. (2006). Using genetic algorithm and TOPSIS for Xinanjiang model calibration with a single procedure. *Journal of Hydrology*, *316*(1–4), 129–140. https://doi.org/10.1016/j.jhydrol.2005.04.022

Chiabrando, R., Fabrizio, E., & Garnero, G. (2009). The territorial and landscape impacts of photovoltaic systems: Definition of impacts and assessment of the glare risk. *Renewable & Sustainable Energy Reviews*, *13*(9), 2441–2451. https://doi.org/10.1016/j.rser.2009.06.008

Choi, C. S., Cagle, A. E., Macknick, J., Bloom, D. E., Caplan, J. S., & Ravi, S. (2020). Effects of revegetation on soil physical and chemical properties in solar photovoltaic infrastructure. *Frontiers in Environmental Science*, *8*. https://doi.org/10.3389/fenvs.2020.00140

Cook, L. M., & McCuen, R. H. (2013). Hydrologic response of solar farms. *Journal of Hydrologic Engineering*, *18*(5), 536–541. https://doi.org/10.1061/(ASCE)HE.1943-5584.0000530

Cook, P. (2011). Infrastructure, rural electrification and development. *Energy for Sustainable Development*, *15*(3), 304–313. https://doi.org/10.1016/j.esd.2011.07.008

Crompton, O., Katul, G., Lapides, D., & Thompson, S. (2023). Hydrologic connectivity and patch-to-hillslope scale relations in dryland ecosystems. *Geophysical Research Letters*, *50*(10), e2022GL101801. https://doi.org/10.1029/2022GL101801

Dhar, A., Naeth, M. A., Jennings, P. D., & Gamal El-Din, M. (2020). Perspectives on environmental impacts and a land reclamation strategy for solar and wind energy systems. *Science of the Total Environment*, *718*, 134602. https://doi.org/10.1016/j.scitotenv.2019.134602

Dhonde, M., Sahu, K., & Murty, V. V. S. (2022). The application of solar-driven technologies for the sustainable development of agriculture farming: A comprehensive review. *Reviews in Environmental Science and Biotechnology*, *21*(1), 139–167. https://doi.org/10.1007/s11157-022-09611-6

Diez, F. J., Martínez-Rodríguez, A., Navas-Gracia, L. M., Chico-Santamarta, L., Correa-Guimaraes, A., & Andara, R. (2021). Estimation of the hourly global solar irradiation on the tilted and oriented plane of photovoltaic solar panels applied to greenhouse production. *Agronomy*, *11*(3), 495. https://doi.org/10.3390/agronomy11030495

Doorga, J., Rughooputh, S., & Boojhawon, R. (2022). Geolocating optimum sites for solar farms. In *Geospatial optimization of solar energy. Springer briefs in energy*. Springer. https://doi.org/10.1007/978-3-030-95213-6_4

Dunne, T., Zhang, W., & Aubry, B. F. (1991). Effects of rainfall, vegetation, and microtopography on infiltration and runoff. *Water Resources Research*, *27*(9), 2271–2285. https://doi.org/10.1029/91WR01585

Edalat, M. M. (2017). Remote sensing of the environmental impacts of utility-scale solar energy plants. (Doctoral dissertation). University of Nevada. Retrieved from https://api.semanticscholar.org/CorpusID:134878617

Edalat, M. M., & Stephen, H. (2017). Effects of two utility-scale solar energy plants on land-cover patterns using SMA of Thematic Mapper data. *Renewable and Sustainable Energy Reviews*, *67*, 1139–1152. https://doi.org/10.1016/j.rser.2016.09.079

Elamri, Y., Cheviron, B., Mange, A., Dejean, C., Liron, F., & Belaud, G. (2018). Rain concentration and sheltering effect of solar panels on cultivated plots. *Hydrology and Earth System Sciences*, *22*(2), 1285–1298. https://doi.org/10.5194/hess-22-1285-2018

Foerster, S., Wilczok, C., Brosinsky, A., & Segl, K. (2014). Assessment of sediment connectivity from vegetation cover and topography using remotely sensed data in a dryland catchment in the Spanish Pyrenees. *Journal of Soils and Sediments*, *14*(12), 1982–2000. https://doi.org/10.1007/s11368-014-0992-3

Freeman, M. C., Pringle, C. M., & Jackson, C. R. (2007). Hydrologic connectivity and the contribution of stream headwaters to ecological integrity at regional scales 1. *Journal of the American Water Resources Association*, *43*(1), 5–14. https://doi.org/10.1111/j.1752-1688.2007.00002.x

Gualla, F. (2015). Sun position and PV panels: A model to determine the best orientation. (Master's thesis). Lund University. Retrieved from https://lup.lub.lu.se/luur/download?func=downloadFile&recordOId=7994855&fileOId=7994856

Guan, J., Wang, Y., Sun, Y., & Wang, S. (2020). Suitable period and change of tourism climate in Ningxia in the past 39 years. *Arid Land Geography*, *43*, 339–348.

Hans Lambers, R. S. O. (2019). *Photosynthesis, respiration, and long-distance transport. Plant physiological ecology* (pp. 115–172). Springer Cham. https://doi.org/10.1007/978-3-030-29639-1_3

Hernandez, R. R., Easter, S. B., Murphy-Mariscal, M. L., Maestre, F. T., Tavassoli, M., Allen, E. B., et al. (2014). Environmental impacts of utility-scale solar energy. *Renewable & Sustainable Energy Reviews*, *29*, 766–779. https://doi.org/10.1016/j.rser.2013.08.041

Hernandez, R. R., Hoffacker, M. K., Murphy-Mariscal, M. L., Wu, G. C., & Allen, M. F. (2015). Solar energy development impacts on land cover change and protected areas. *Proceedings of the National Academy of Sciences of the United States of America*, *112*(44), 13579–13584. https://doi.org/10.1073/pnas.1517656112

Holland, R., Armstrong, A., & Carvalho, F. (2021). Development of a solar park carbon calculator (SPCC) to assist deployment decisions. In *Paper presented at EGU general assembly 2021*. https://doi.org/10.5194/egusphere-egu21-7677

Hooke, J. (2003). Coarse sediment connectivity in river channel systems: A conceptual framework and methodology. *Geomorphology*, *56*(1–2), 79–94. https://doi.org/10.1016/S0169-555X(03)00047-3

Hu, A., Levis, S., Hu, A., Levis, S., Meehl Gerald, A., Han, W., et al. (2016). Impact of solar panels on global climate. *Nature Climate Change*, *6*(3), 290–294. https://doi.org/10.1038/nclimate2843

Istanbulluoglu, E., Wang, T., & Wedin, D. A. (2012). Evaluation of ecohydrologic model parsimony at local and regional scales in a semiarid grassland ecosystem. *Ecohydrology*, *5*(1), 121–142. https://doi.org/10.1002/eco.211

Jahanfar, A., Drake, J., Gharabaghi, B., & Sleep, B. (2020). An experimental and modeling study of evapotranspiration from integrated green roof photovoltaic systems. *Ecological Engineering*, *152*, 105767. https://doi.org/10.1016/j.ecoleng.2020.105767

Jahanfar, A., Drake, J., Sleep, B., & Margolis, L. (2019). Evaluating the shading effect of photovoltaic panels on green roof discharge reduction and plant growth. *Journal of Hydrology*, *568*, 919–928. https://doi.org/10.1016/j.jhydrol.2018.11.019

Josserand, C., & Zaleski, S. (2003). Droplet splashing on a thin liquid film. *Physics of Fluids*, *15*(6), 1650–1657. https://doi.org/10.1063/1.1572815

Klucher, T. M. (1979). Evaluation of models to predict insolation on tilted surfaces. *Solar Energy*, *23*(2), 111–114. https://doi.org/10.1016/0038-092X(79)90110-5

Kompanizare, M., Petrone, R. M., Shafii, M., Robinson, D. T., & Rooney, R. C. (2018). Effect of climate change and mining on hydrological connectivity of surficial layers in the Athabasca Oil Sands Region. *Hydrological Processes*, *32*(25), 3698–3716. https://doi.org/10.1002/hyp.13292

Kruitwagen, L., Story, K. T., Friedrich, J., Byers, L., Skillman, S., & Hepburn, C. (2021). A global inventory of photovoltaic solar energy generating units. *Nature*, *598*(7882), 604–610. https://doi.org/10.1038/s41586-021-03957-7

Kumari, N., Saco, P. M., Rodriguez, J. F., Johnstone, S. A., Srivastava, A., Chun, K. P., & Yetemen, O. (2020). The grass is not always greener on the other side: Seasonal reversal of vegetation greenness in aspect-driven semiarid ecosystems. *Geophysical Research Letters*, *47*(15), e2020GL088918. https://doi.org/10.1029/2020gl088918

Laio, F., Porporato, A., Ridolfi, L., & Rodriguez-Iturbe, I. (2001). Plants in water-controlled ecosystems: Active role in hydrologic processes and response to water stress: II. Probabilistic soil moisture dynamics. *Advances in Water Resources*, *24*(7), 707–723. https://doi.org/10.1016/S0309-1708(01)00005-7

Lee, S. (2019). Erosion and storm water runoff: Power solar farm project. *Watershed Environmental Analysis*, 1–19.

Liu, H., Wu, C., Yu, Y., Zhao, W., Liu, J., Yu, H., et al. (2023a). Effect of solar farms on soil erosion in hilly environments: A modeling study from the perspective of hydrological connectivity [Dataset]. Zenodo. https://doi.org/10.5281/zenodo.8280888

Liu, H., Wu, C., Yu, Y., Zhao, W., Liu, J., Yu, H., et al. (2023b). Solar farm model [Software]. Zenodo. https://doi.org/10.5281/zenodo.8280905

Liu, Y., Zhang, R., Huang, Z., Cheng, Z., Lopezvicente, M., Ma, X., & Wu, G. (2019). Solar photovoltaic panels significantly promote vegetation recovery by modifying the soil surface microhabitats in an arid sandy ecosystem. *Land Degradation & Development*, *30*(18), 2177–2186. https://doi.org/10.1002/ldr.3408

Makaronidou, M. (2020). Assessment on the local climate effects of solar photovoltaic parks. (Doctoral dissertation). Lancaster University. Retrieved from https://api.semanticscholar.org/CorpusID:253495996

Marrou, H., Guilioni, L., Dufour, L., Dupraz, C., & Wery, J. (2013). Microclimate under agrivoltaic systems: Is crop growth rate affected in the partial shade of solar panels? *Agricultural and Forest Meteorology*, *177*, 117–132. https://doi.org/10.1016/j.agrformet.2013.04.012

Mermut, A. R., Luk, S. H., Römkens, M. J. M., & Poesen, J. W. A. (1997). Soil loss by splash and wash during rainfall from two loess soils. *Geoderma*, *75*(3–4), 203–214. https://doi.org/10.1016/S0016-7061(96)00091-2

Murphy-Mariscal, M., Grodsky, S. M., & Hernandez, R. R. (2018). *Solar energy development and the biosphere//LETCHER T M, FTHENAKIS V M. A comprehensive guide to solar energy systems* (pp. 391–405). Academic Press. https://doi.org/10.1016/B978-0-12-811479-7.00020-8

Myneni, R., Knyazikhin, Y., & Park, T. (2021). MODIS/Terra+Aqua leaf area index/FPAR 8-day L4 global 500m SIN grid V061 [Dataset]. NASA EOSDIS Land Processes Distributed Active Archive Center. https://doi.org/10.5067/MODIS/MCD15A2H.061

Nair, A. A., Rohith, A. N., Raj, C., & McPhillips, L. E. (2022). Evaluating the potential impacts of solar farms on hydrological responses. https://doi.org/10.13031/aim.202201262

Nawaz, M. F., Bourrie, G., & Trolard, F. (2013). Soil compaction impact and modelling. *A review. Agronomy for Sustainable Development*, *33*(2), 291–309. https://doi.org/10.1007/s13593-011-0071-8

Nouvellon, Y., Rambal, S., Seen, D. L., Moran, M. S., Lhomme, J. P., Begue, A., et al. (2000). Modelling of daily fluxes of water and carbon from shortgrass steppes. *Agricultural and Forest Meteorology*, *100*(2–3), 137–153. https://doi.org/10.1016/S0168-1923(99)00140-9

Oudes, D., & Stremke, S. (2021). Next generation solar power plants? A comparative analysis of frontrunner solar landscapes in Europe. *Renewable and Sustainable Energy Reviews*, *145*, 111101. https://doi.org/10.1016/j.rser.2021.111101

Passias, D., & Källbäck, B. (1984). Shading effects in rows of solar cell panels. *Solar Cells*, *11*(3), 281–291. https://doi.org/10.1016/0379-6787(84)90017-6

Phalane, I. (2021). Halfgewonnen solar PV Facility:hydrological impact assessment (pp. 1–39).

Poesen, J., Nachtergaele, J., Verstraeten, G., & Valentin, C. (2003). Gully erosion and environmental change: Importance and research needs. *Catena*, *50*(2–4), 91–133. https://doi.org/10.1016/S0341-8162(02)00143-1

Porporato, A., Laio, F., Ridolfi, L., & Rodriguez-Iturbe, I. (2001). Plants in water-controlled ecosystems: Active role in hydrologic processes and response to water stress: III. Vegetation water stress. *Advances in Water Resources*, *24*(7), 725–744. https://doi.org/10.1016/S0309-1708(01)00006-9

Pringle, C. M. (2001). Hydrologic connectivity and the management of biological reserves: A global perspective. *Ecological Applications*, *11*(4), 981–998. https://doi.org/10.1890/1051-0761(2001)011[0981:HCATMO]2.0.CO;2

Quijano-Baron, J., Saco, P. M., & Rodriguez, J. F. (2022). Modelling the effects of above and belowground biomass pools on erosion dynamics. *Catena*, *213*, 106123. https://doi.org/10.1016/j.catena.2022.106123

Rahman, A., Farrok, O., & Haque, M. M. (2022). Environmental impact of renewable energy source based electrical power plants: Solar, wind, hydroelectric, biomass, geothermal, tidal, ocean, and osmotic. *Renewable and Sustainable Energy Reviews*, *161*, 112279. https://doi.org/10.1016/j.rser.2022.112279

Randle-Boggis, R., White, P. C. L., Cruz, J., Parker, G., Montag, H., Scurlock, J., & Armstrong, A. (2020). Realising co-benefits for natural capital and ecosystem services from solar parks: A co-developed, evidence-based approach. *Renewable and Sustainable Energy Reviews*, *125*, 109775. https://doi.org/10.1016/j.rser.2020.109775

Ren, Z., Zou, F., Yu, Y., Wang, G., Zhang, Z., Fan, S., et al. (2012). Daily climatological database of China ground international exchange station (V3.0) [Dataset]. China Meteorological Data Service Center. https://data.cma.cn/data/cdcdetail/dataCode/A.0012.0001.S011.html

Rodriguez-Iturbe, I. (2000). Ecohydrology: A hydrologic perspective of climate-soil-vegetation dynamies. *Water Resources Research*, *36*(1), 3–9. https://doi.org/10.1029/1999WR900210

Saco, P. M., & Mariano, M. D. L. H. (2013). Ecogeomorphic coevolution of semiarid hillslopes: Emergence of banded and striped vegetation patterns through interaction of biotic and abiotic processes. *Water Resources Research*, *49*(1), 115–126. https://doi.org/10.1029/2012WR012001

Saco, P. M., Willgoose, G. R., & Hancock, G. R. (2007). Eco-geomorphology of banded vegetation patterns in arid and semi-arid regions. *Hydorlogy and Earth System Sciences*, *11*(6), 1717–1730. https://doi.org/10.5194/hess-11-1717-2007

Smith, J., Graves, P., Nayak, D., Smith, P., Perks, M., Gardiner, B., et al. (2011). Carbon implications of windfarms located on Peatlands–Update of the Scottish government carbon calculator tool. *Scottish Government, Scotland*. Retrieved from https://www.researchgate.net/publication/256473182

Souza, J., & Hooke, J. (2021). Influence of seasonal vegetation dynamics on hydrological connectivity in tropical drylands. *Hydrological Processes*, *35*(11), e14427. https://doi.org/10.1002/hyp.14427

Srivastava, A., Saco, P. M., Rodriguez, J. F., Kumari, N., Chun, K. P., & Yetemen, O. (2021). The role of landscape morphology on soil moisture variability in semi-arid ecosystems. *Hydrological Processes*, *35*(1), e13990. https://doi.org/10.1002/hyp.13990

Stefano, C., Alessandro, S., Giorgia, M., & Marco, C. (2021). HydrogeomorphologyTools/Sediment-Connectivity-and-Surface-Roughness-python-scripts: Sediment-Connectivity-and-Surface-Roughness-python-scripts (SedInConnect_scripts_Release1) [Software]. Zenodo. https://doi.org/10.5281/zenodo.5647422

Sun, L., Jiang, Y., Guo, Q., Ji, L., Xie, Y., Qiao, Q., et al. (2021). A GIS-based multi-criteria decision making method for the potential assessment and suitable sites selection of PV and CSP plants. *Resources, Conservation and Recycling*, *168*, 105306. https://doi.org/10.1016/j.resconrec.2020.105306

Sun, L., Zhang, G.-H., Liu, F., & Luan, L.-L. (2016). Effects of incorporated plant litter on soil resistance to flowing water erosion in the Loess Plateau of China. *Biosystems Engineering*, *147*, 238–247. https://doi.org/10.1016/j.biosystemseng.2016.04.017

Tang, L. C., & Low, J. M. (2020). Strategic intent of OBOR: Enhancing energy supply resilience. *Journal of Shipping and Trade*, *5*, 1–25. https://doi.org/10.1186/s41072-020-0058-1

Tanner, K. E., Moore-O'Leary, K. A., Parker, I. M., Pavlik, B. M., & Hernandez, R. R. (2020). Simulated solar panels create altered microhabitats in desert landforms. *Ecosphere*, *11*(4), e03089. https://doi.org/10.1002/ecs2.3089

Van Hateren, T. C., Jongen, H. J., Al-Zawaidah, H., Beemster, J. G. W., Boekee, J., Bogerd, L., et al. (2023). Where should hydrology go? An early-career perspective on the next IAHS scientific decade: 2023–2032. *Hydrological Sciences Journal*, *68*(4), 529–541. https://doi.org/10.1080/02626667.2023.2170754

Van Nieuwenhuyse, B. (2012). *Measuring and modelling hydrological surface connectivity*. Université catholique de Louvain.

Wacha, K. M., Papanicolaou, A., Giannopoulos, C. P., Abban, B. K., Wilson, C. G., Zhou, S., et al. (2018). The role of hydraulic connectivity and management on soil aggregate size and stability in the Clear Creek Watershed, Iowa. *Geosciences*, *8*(12), 470. https://doi.org/10.3390/geosciences8120470

Walston, L. J., Li, Y., Hartmann, H. M., Macknick, J., Hanson, A., Nootenboom, C., et al. (2021). Modeling the ecosystem services of native vegetation management practices at solar energy facilities in the Midwestern United States. *Ecosystem Services*, *47*, 101227. https://doi.org/10.1016/j.ecoser.2020.101227

Wischmeier, W. H., & Smith, D. D. (1978). *Predicting rainfall erosion losses—A guide to conservation planning* (pp. 62–67). USDA, Science and Education Administration.

Wu, C., Liu, H., Yu, Y., Zhao, W., Liu, J., Yu, H., & Yetemen, O. (2022). Ecohydrological effects of photovoltaic solar farms on soil microclimates and moisture regimes in arid Northwest China: A modeling study. *Science of the Total Environment*, *802*, 149946. https://doi.org/10.1016/j.scitotenv.2021.149946

Yadav, O., Rathore, V., & Singh, D. (2019). *Enhancing resilience of arid lands: The Indian experience*. In O. P. yadav, & N. R. Panwar (Eds.) https://doi.org/10.1016/j.solener.2023.02.018

Yang, Q., Huang, T., Wang, S., Li, J., Dai, S., Wright, S., et al. (2019). A GIS-based high spatial resolution assessment of large-scale PV generation potential in China. *Applied Energy*, *247*, 254–269. https://doi.org/10.1016/j.apenergy.2019.04.005

Yetemen, O., Istanbulluoglu, E., Flores-Cervantes, J. H., Vivoni, E. R., & Bras, R. L. (2015). Ecohydrologic role of solar radiation on landscape evolution. *Water Resources Research*, *51*(2), 1127–1157. https://doi.org/10.1002/2014WR016169

Yu, Y., Zhao, W., Martinez-Murillo, J. F., & Pereira, P. (2020). *Loess Plateau: From degradation to restoration*. (p. 140206). Elsevier.

Zhang, L., Xue, T., Gao, F., Wei, R., Wang, Z., Li, H., & Wang, H. (2021). Carbon storage distribution characteristics of vineyard ecosystems in Hongsibu, Ningxia. *Plants*, *10*(6), 1199. https://doi.org/10.3390/plants10061199

Zhang, L., Xue, T., Yuan, L., Gao, F., Hao, X., Yang, C., et al. (2022). The effect of vineyard reclamation on soil properties and microbial communities in desertified land in Hongsibu, Ningxia. *Catena*, *211*, 106002. https://doi.org/10.1016/j.catena.2021.106002

Zhang, W., Li, J., Wang, D., Bu, C., & Guo, W. (2004). Study on surface runoff forecast model in the sandstorm region of central Ningxia. *Yellow River*, *26*, 29–31.

Zhou, X., Istanbulluoglu, E., & Vivoni, E. R. (2013). Modeling the ecohydrological role of aspect-controlled radiation on tree-grass-shrub coexistence in a semiarid climate. *Water Resources Research*, *49*(5), 2872–2895. https://doi.org/10.1002/wrcr.20259

Zhu, Y., Jia, X., & Shao, M. (2018). Loess thickness variations across the Loess Plateau of China. *Surveys in Geophysics*, *39*(4), 715–727. https://doi.org/10.1007/s10712-018-9462-6

References From the Supporting Information

Chenlu, H. (2021). Temporal and spatial changes of soil erosion and its drive factors in the Loess Plateau in recent 40 years. (Master's thesis). Northwest University. Retrieved from https://www.cnki.net/

Guan, N., Yang, Z., Li, J., Xu, Z., Ren, Z., Wei, X., & Cheng, J. (2021). Dynamic changes and distribution characteristics of soil erosion in Ningxia from 2011 to 2019. *Soil and Water Conservation in China*, *05*, 38–41.

Liu, B., Xie, Y., Li, Z., Liang, Y., Zhang, W., Fu, S., et al. (2020). The assessment of soil loss by water erosion in China. *International Soil and Water Conservation Research*, *8*(4), 430–439. https://doi.org/10.1016/j.iswcr.2020.07.002

Qi, S., Sun, L., Zhang, Y., & Changshun, L. (2001). Impact of soil erosion on soil productivity of sloping field in hilly-gully region of Loess Plateau in south Ningxia. *Journal of Beijing Forestry University*, *23*, 34–37.

Zhang, X., Dong, P., Yu, Z., Liang, J., Liu, Y., & Gu, J. (2011). Monitoring and evaluation of soil erosion in Hongsibu Immigration Development Zone, Ningxia. *Soil and Water Conservation in China*, *12*, 51–53. https://doi.org/10.14123/j.cnki.swcc.2011.12.019

Zhang, X., Wang, D., Ma, K., Sun, D., Yang, F., & Lin, H. (2023). Spatiotemporal evolution of soil water erosion in Ningxia grassland based on the RUSLE-TLSD model. *Environmental Research*, *236*, 116744. https://doi.org/10.1016/j.envres.2023.116744

Impact of solar parks on runoff generation and associated land drainage/flood risk consequences.

BHS - 5th June 2014

[redacted] (EA retired)
[redacted]
[redacted]
[redacted])

JBA consulting

Large-scale solar PV deployment in the UK - 2011 to Feb 2014

Large-scale solar PV deployment in the UK - 2011 to Feb 2014*		
	No.	Capacity MWp
Operational	184	850
Under construction	48	538
Awaiting construction	194	1,656
TOTAL	**425**	**3,037**
In planning	98	1,149
GRAND TOTAL	**523**	**4,168**

Land use assuming 2ha/MWp
Land ha
425
269
828
1,518.5
574.5
2,084 ha

*Source: Dept of Energy & Climate Change - UK Solar PV Strategy Part 2 - April 2014

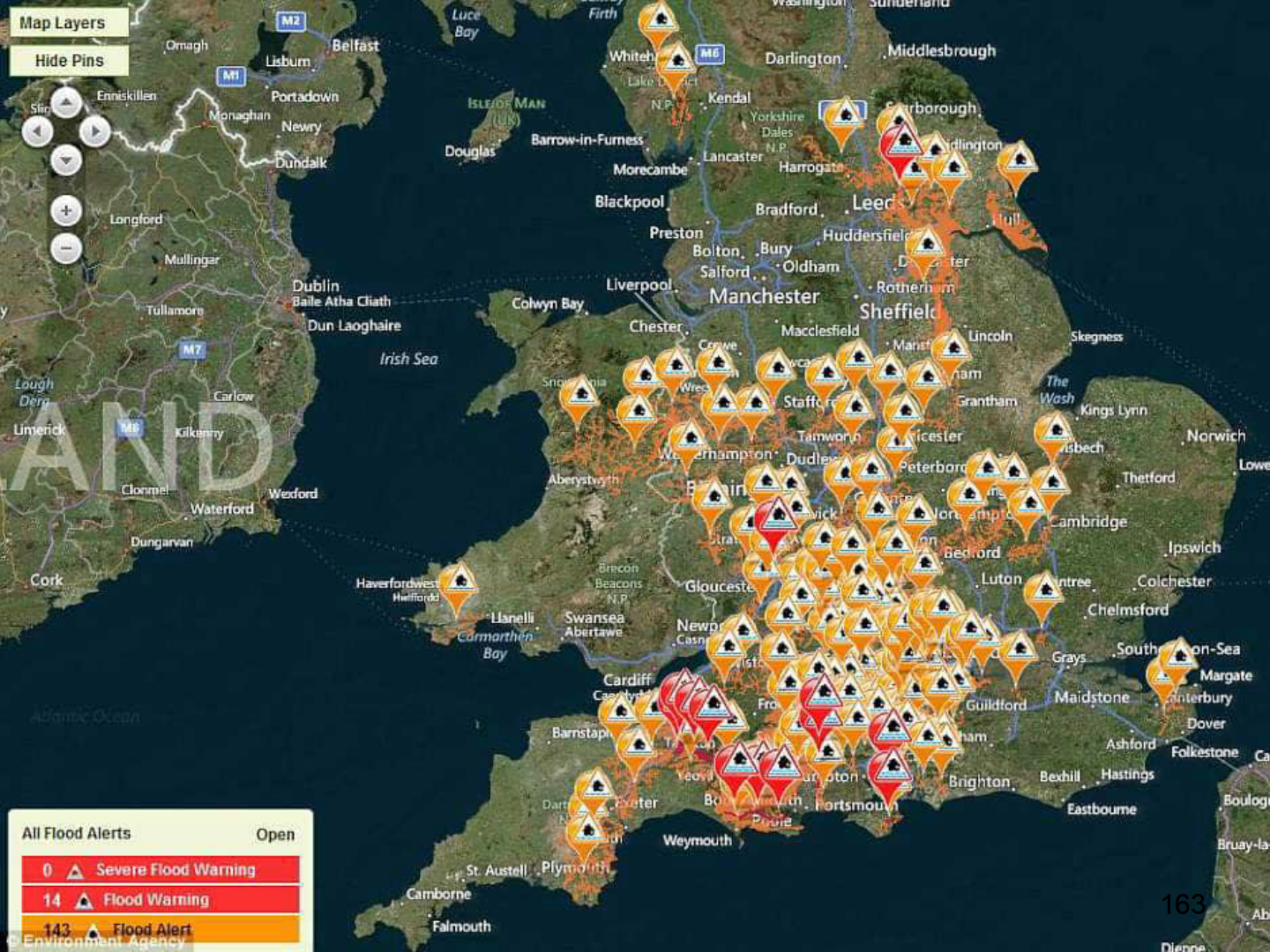
Map Layers
Hide Pins
Belfast
Omagh
Lisburn
Portadown
Enniskillen
Monaghan
Newry
Dundalk
Isle of Man (UK)
Douglas
Whitehaven
Kendal
Darlington
Middlesbrough
Barrow-in-Furness
Lancaster
Morecambe
Harrogate
Blackpool
Bradford
Preston
Bolton
Bury
Salford
Oldham
Liverpool
Manchester
Sheffield
Chester
Macclesfield
Lincoln
Skegness
Longford
Mullingar
Dublin
Baile Atha Cliath
Dun Laoghaire
Tullamore
Colwyn Bay
Irish Sea
Carlow
Kilkenny
Limerick
Clonmel
Waterford
Wexford
Dungarvan
Cork
Grantham
The Wash
Kings Lynn
Norwich
Thetford
Cambridge
Bedford
Luton
Ipswich
Colchester
Chelmsford
Haverfordwest
Llanelli
Swansea
Abertawe
Carmarthen Bay
Brecon Beacons N.P.
Gloucester
Cardiff
Barnstaple
Grays
Margate
Maidstone
Guildford
Dover
Ashford
Folkestone
Brighton
Bexhill
Hastings
Eastbourne
Weymouth
St. Austell
Camborne
Falmouth
All Flood Alerts
Open
0 Severe Flood Warning
14 Flood Warning
143 Flood Alert
© Environment Agency

The 2014 floods

The Somerset Moors

(a reminder)


GETTY IMAGES

The aftermath

What the 'experts' say about all that flooding in 2014

- "**Water management techniques** could have helped prevent the effect of flooding on villages, towns and over surrounding land seen recently."
- "We need to look at how forestry, **land management** and soft-engineered flood alleviation schemes can hold back water in the upper reaches of rivers….."

YES - quite right …. But it's all been said before……

…But its all been said before…..

DEFRA/EA R&D project FD2114 Review of impact of rural land use & management on flood generation

(E. O'Connell et al)

- *"There is substantial evidence that local flooding can be affected by changes in (*rural*) land management and management practices."*

Making Space for Water

- The Government will promote changes in rural land management to ameliorate runoff and reducing the incidence of flooding on a local scale

…But its all been said before…..

Catchment Flood Management Plans

- CFMPs apply the recommendations of FD2114
- They promote the use of rural land use and soil management to reduce rural runoff to reduce flooding at settlements in accordance with MSfW policy.
- They identify where it can be effective

Best Farming Practice & Environmental Stewardship

- *Encourage farmers to reduce runoff, soil erosion and pollution through good land and soil management*

…But its all been said before….

National Planning Policy Framework

- *"When determining planning applications LPA's should ensure flood risk is not increased elsewhere & is **reduced** wherever possible."*

What's been said before

- FD 2114 - rural land use & soil management affects local flooding
- M S for W - managing rural land & soil is part of government **policy** to manage flood risk
- CFMPs – **implement the policy** and say where it's **effective**.
- Best Farming Practice & Environmental stewardship **contribute to it's delivery**
- NPPF - provide an **opportunity to deliver the policy** … when considering applications for Solar Parks in rural areas

So what do FRAs for solar parks say ?

Flood Risk Assessments for Solar Parks some uncertainties for discussion

1. **Soil compaction or soil degradation due to construction and during operational lifetime**

2. **Assumption - Solar panels don't increase runoff significantly**

3. **Standard of mitigation - 100 year or what?**

The first uncertainty
Soil degradation

An example
Before
(Grade 2 agricultural Land! Carbon footprint? EIA?)

after

Soil condition – some numbers

Source: Richard Smith EA

Runoff volumes generated by 25mm of rain in 24 hours – plot size 10m x 4.5m

Runoff & soil condition

Runoff from maize stubble (IGER 2000)

Winter - Feb / April 2000, North Wyke Devon

Compacted stubble		Chisel ploughed stubble	
Runoff		Runoff	
m3/ha	% of rainfall	M3/ha	% of rainfall
433.5 m3/ha	20%	5.8 m3/ha	0.5%

Runoff from grassland (NSRI Cranfield 2007)

Grass – poor soil structure		Grass – good soil structure	
Runoff		Runoff	
m3/ha	% of rainfall	m3/ha	% of rainfall
	~60%		~2%

The problem soil condition

The solution - Deliver MSfW, Planning & CFMP policies and Best Farming Practice

1. **FRA's** need to take into account **soil condition**
2. **Pre-development runoff** calcs. should assume **soil is in good condition** in accordance with Best Farming Practice. (NPPF Reducing flood risk)
3. After construction the soil should be **chisel ploughed** to mitigate soil compaction during construction
4. **Planning applications** should include an enforceable **soil management plan** to keep soil in good condition & for **decommissioning**.

The second uncertainty
Do solar panels increase runoff?

- **Assumption - Solar panels don't increase runoff significantly** because…. rain falls off them and, regardless of ground slope, it flows evenly across the rain-shadow of the down slope row of panels… so most, if not all of the ground is mobilised for infiltration.

The assumption explained

In practice

Kinetic compaction & rivulets forming

Example to illustrate scale of issue

Area of rain-shadow not mobilised for infiltration				
8.25MW				
16ha site				
35,000 panels				
Solar panel footprint	5% not mobilised	10% not mobilised	20% not mobilised	30% not mobilised
50,000m2	2,500m2	5,000m2	10,000m2	15,000m2
%age of site area	1.6%	3.2%	6.2%	9.6%

- Area of rain-shadow not mobilised for infiltration is a function of **ground slope**
- **Research** is needed to guide practitioners
- Until then apply the **precautionary principle**

Appeal Decision
Appeal Ref: APP/D3315/A/13/2203242
Land at Glebe Farm, Tolland, Lydeard St Lawrence, Taunton TA4 3PR

17. The planning application was accompanied by a Flood Risk Assessment (FRA). A carefully considered and professionally well-informed letter of objection to the proposed development makes the important point that **it would be unsound to assume that rain falling on each row of solar panels would flow evenly into the rain-shadow of the row below, so as to mobilise the same percentage of the ground for infiltration as was available before the panels were installed.** Rather, because the panels would be set at a downward slope and aligned to follow the contours of the land, rain-water would be likely to fall in a column from the lowest corner of each panel, and could then form rivulets flowing down through the rain-shadows of the rows below without utilising their whole area for infiltration, thus increasing the amount of water run-off from the site.

18. **I find that argument persuasive.**

The third uncertainty
Standards of mitigation

- Flood risk to settlements - 100 year
- Flood risk to agricultural land - 10 to 20 year?
- Drowning of agricultural land drainage outfalls - 2 to 10 year ?

Thank-you Richard et al for reminding us poorly managed (or regulated) agricultural land and soil is the flood-risk elephant in the room, now and as agriculture responds to climate change and Govt. incentives for solar parks, bio-fuels etc

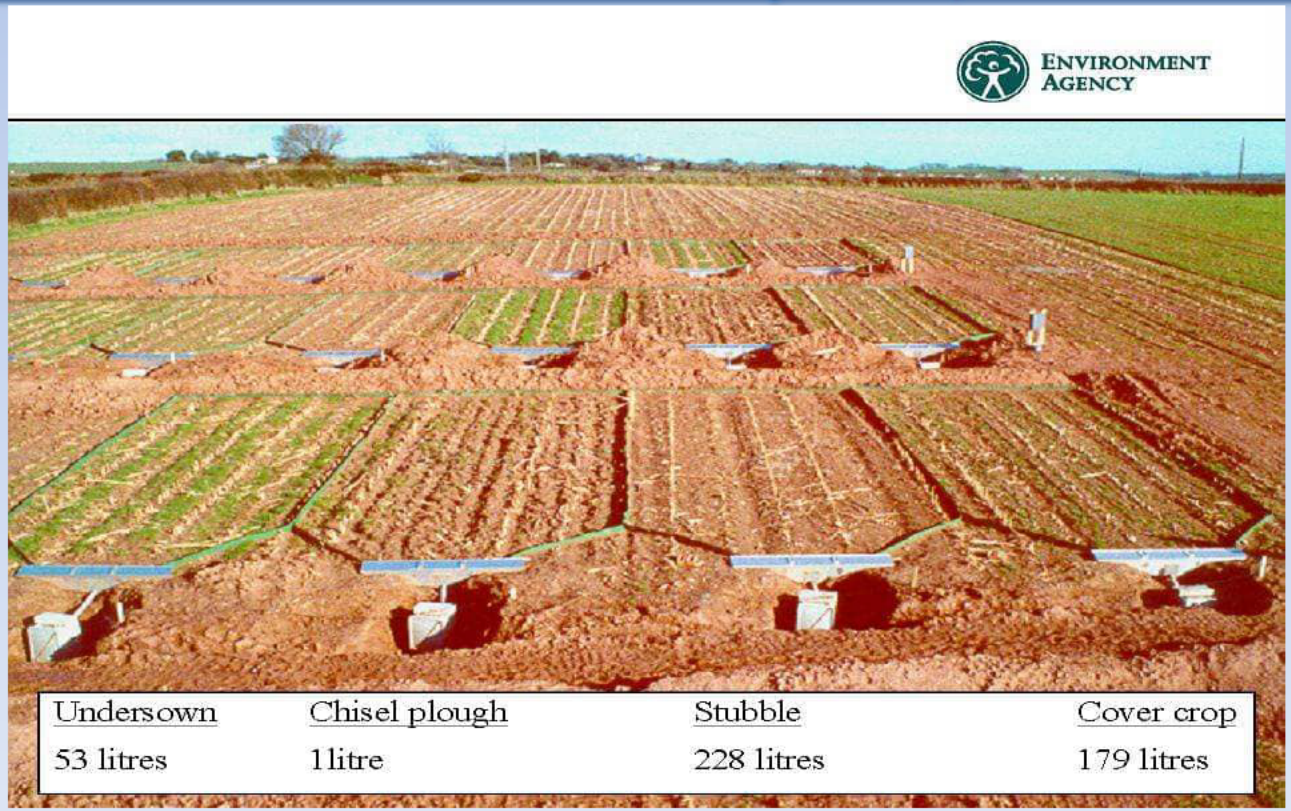

Source: Richard Smith EA

Runoff volumes generated by 25mm of rain in 24 hours – plot size 10m x 4.5m

Hydrol. Earth Syst. Sci., 22, 1285–1298, 2018
https://doi.org/10.5194/hess-22-1285-2018

Hydrology and Earth System Sciences
Open Access
EGU

Rain concentration and sheltering effect of solar panels on cultivated plots

Yassin Elamri[1,2], Bruno Cheviron[1], Annabelle Mange[1], Cyril Dejean[1], François Liron[1], and Gilles Belaud[3]

[1]UMR G-Eau, Irstea, Univ. Montpellier, 361 rue Jean-François Breton, 34136 Montpellier, France
[2]Sun'R SAS, 41 quai Fulchiron, 69005 Lyon, France
[3]UMR G-Eau, Montpellier SupAgro, Univ. Montpellier, 2 place Pierre Viala, 34060 Montpellier, France

Correspondence: Bruno Cheviron [redacted]@irstea.fr)

Received: 12 July 2017 – Discussion started: 27 July 2017
Revised: 18 October 2017 – Accepted: 12 December 2017 – Published: 20 February 2018

Abstract. Agrivoltaism is the association of agricultural and photovoltaic energy production on the same land area, coping with the increasing pressure on land use and water resources while delivering clean and renewable energy. However, the solar panels located above the cultivated plots also have a seemingly yes unexplored effect on rain redistribution, sheltering large parts of the plot but redirecting concentrated fluxes on a few locations. The spatial heterogeneity in water amounts observed on the ground is high in the general case; its dynamical patterns are directly attributable to the mobile panels through their geometrical characteristics (dimensions, height, coverage percentage) and the strategies selected to rotate them around their support tube. A coefficient of variation is used to measure this spatial heterogeneity and to compare it with the coefficient of uniformity that classically describes the efficiency of irrigation systems. A rain redistribution model (AVrain) was derived from literature elements and theoretical grounds and then validated from experiments in both field and controlled conditions. AVrain simulates the effective rain amounts on the plot from a few forcing data (rainfall, wind velocity and direction) and thus allows real-time strategies that consist in operating the panels so as to limit the rain interception mainly responsible for the spatial heterogeneities. Such avoidance strategies resulted in a sharp decrease in the coefficient of variation, e.g. 0.22 vs. 2.13 for panels held flat during one of the monitored rain events, which is a fairly good uniformity score for irrigation specialists. Finally, the water amounts predicted by AVrain were used as inputs to Hydrus-2D for a brief exploratory study on the impact of the presence of solar panels on rain redistribution at shallow depths within soils: similar, more diffuse patterns were simulated and were coherent with field measurements.

1 Introduction

The current climate change context induced by the production and consumption of highly polluting fossil fuels, responsible for the greenhouse effect, has in turn triggered the development of clean and renewable fuels, with a special focus on photovoltaic systems (IPCC, 2014). Recent times have seen a clear increase in land coverage by solar panels on roofs, used as parking shade houses or organized in solar farms (IPCC, 2011). In the last years, solar panels were installed above cultivated plots in France (Marrou, 2012), in Japan (Movellan, 2013), in India (Harinarayana and Vasavi, 2014), in the USA (Ravi et al., 2014) and in Germany (Osborne, 2016) so as to not create competition between different land uses (Dinesh and Pearce, 2016). These innovative devices termed "agrivoltaic" by Dupraz et al. (2011) allow maintaining the agricultural yield under certain conditions (Marrou et al., 2013b, c), together with water savings (Marrou et al., 2013a) which results in the expected higher values of the dedicated land use efficiency indicator (Marrou, 2012)

In addition to blocking and converting a part of the incoming solar radiation, the implementation of solar panels in natural settings has a series of direct or indirect effects on several terms of the hydrological budget in the equipped plots (Cook and McCuen, 2013; Barnard et al., 2017). Although far less studied, these on-site or off-site hydrological consequences should be addressed and modelled for site

preservation purposes in the general case and also because they are very likely to constrain the optimal irrigation and local site management strategies on the cultivated plots. For example, Diermanse (1999) showed that a correct simulation of runoff could often be achieved on the watershed scale from spatially averaged rainfall values, although clearly better results may be expected when explicitly accounting for the subscale spatial patterns of rain distribution (Faurès et al., 1995; Tang et al., 2007; Emmanuel et al., 2015). On the plot scale, rain interception and redistribution by the crops (Levia and Germer, 2015; Yuan et al., 2017) is already known to cause strong spatial heterogeneities (through stemflow, throughfall or improved water storage capabilities), thus raising multiple questions on soil microbiology, non-point source pollution and irrigation piloting (Lamm and Manges, 2000; Martello et al., 2015). The presence of solar panels will provide similar, additional issues close to those experienced in agroforestry when the vegetative cover is of various heights and nature, with a direct impact on the spatiotemporal patterns of rain redistribution (Jackson, 2000). In more detail and more specifically, the interception of rain by the impervious surface of the solar panels produces an "umbrella effect" that delineates a sheltered area. By contrast, its contour receives the collected fluxes, whose intensity or amounts may locally exceed those of the control conditions, depending on the dimensions, height and tilting angle of the panels as well as on wind velocity and direction. Cook and McCuen (2013) stated that one benefit of grass growing was to damp or even suppress any specific effect of solar panels on runoff on the plot scale. This also constitutes valuable preventive measures against erosion issues arising from concentrated flows in micro-gullies (Knapen et al., 2007; Gumiere et al., 2009) or attributable to the direct mechanical effects of droplet impacts, known as splash erosion (Nearing and Bradford, 1985; Josserand and Zaleski, 2003).

Agricultural soils should preferentially not be left bare under solar panel structures, because of increased risks of runoff and erosion but, these are only the most severe particular cases among the diverse rain redistribution effects investigated in the present paper. These are possibly described from geometrical arguments for an intuitive overview, suggesting three categories of zones on the ground in the agrivoltaic plots (AVs): (i) the non-impacted zones between panels that receive the same rain amounts as the control site, (ii) the sheltered zones located right under the panels that receive far less rainfall than in the control conditions and (iii) the border zones located where panels discharge the collected rain amounts.

In most cultivated plots, the spatial heterogeneity of rainfall is limited before that of the other determinants of the water budget and crop yield, typically the lateral and vertical variations of soil properties and the non-uniformity of irrigation. Conversely, the presence of solar panels may cause strong spatial heterogeneities possibly compared to that of the water abduction systems used for irrigation, whose efficiency is estimated from the values of a coefficient of uniformity (Burt et al., 1997; Playán and Mateos, 2006; Pereira et al., 2002). This paper therefore aims at characterizing the effective rain distribution in agrivoltaic plots from the calculation of discharge volumes at the outlet of the panels, depending on their tilting angle. Moreover, the procedure applies to mobile panels endowed with 1 degree of freedom, i.e. able to rotate around their support tube according to predefined strategies, which defines and introduces "dynamic agrivoltaism". Water redistribution in soils is also affected as briefly described here for coherence checks; it is not the main scope of the paper though it is crucial for crop growth and irrigation optimization.

Section 2 describes the experiments conducted on the agrivoltaic plot (Sect. 2.1) and in controlled conditions (Sect. 2.2), also presenting the AVrain model that predicts rain redistribution by the solar panels (Sect. 2.3). Section 3 shows the experimental and modelling results, discussed in Sect. 4. Section 5 gathers the conclusions and openings of this work.

2 Material and methods

2.1 Field experiments

2.1.1 Agrivoltaic plot

The agrivoltaic plot (AV) located on the experimental domain of Lavalette (Irstea Montpellier: 43.6466° N, 3.8715° E) covers an area of 490 m^2 equipped with four rows of quasi-joined agrivoltaic panels (PV) oriented north–south. The rectangular panels are 2 m long and 1 m wide for a total surface coverage of 152 m^2. They are elevated at 5 m and part of a metallic structure supported by pillars is separated by 6.4 m, forming square arrays, so as to allow agricultural machinery in the agrivoltaic plot. This coverage corresponds to a "half-density" in comparison with a classical free-standing plant. The tilting angle of the PV may vary between −50 and +50° with reference to the flat, horizontal case. This 1 degree of freedom rotation around the horizontal, transverse axis of the panels is ensured by jacks. These may be controlled for solar tracking during daytime or to obey other user-defined time-variable controls. The measurement campaign spreads from 18 October 2015 to 24 October 2016 and thus covers a full year. It encompasses 41 monitored rain events, 12 of which were recorded with a 1 min time step, among which 11 exhibit complete and reliable sets of data linked to the incoming and redistributed rain amount, as well as to the tilting angle of the panels.

2.1.2 Effective rain and soil water content measurements

The monitoring of rain amounts in the AV plot is ensured by a series of 21 collectors of 0.3 m diameter, aligned and

Figure 1. Effective rain and soil water content measurement under solar panels. Red arrows indicate the position of neutron probes, on a line parallel to that of the collectors, 1 m before it. Some of the P01 to P21 collectors have been identified on the picture for clarity.

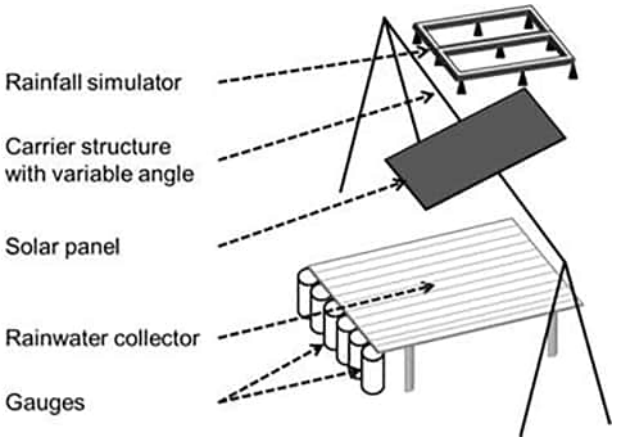

Figure 2. Experimental device used for indoor tests, focusing on lateral rain redistribution on the width of the panel, for various combinations of rain intensities and tilting angles of the panel.

joined so as to form a continuous line, centred under a PV row and transverse to it (Fig. 1). In the following, the collectors are termed P01 to P21 from west to east. In addition, P0 indicates the rain amount collected in control conditions, just beside the AV plot. All rain amounts collected are expressed as water depths (with $1\,\mathrm{mm} = 1\,\mathrm{L\,m^{-2}}$). The recordings were made for various angular positions of the PV, either held flat or inclined ($\pm 50°$) or during time-variable avoidance strategies that mainly consist in minimizing rain interception by the panels by deciding their titling angle based on wind direction. Rain amounts in the nearby control zone are measured with a tipping bucket rain gauge (Young 52203, Campbell Sci.). A wind-vane anemometer (Young 05103-L, Campbell Sci.) allows the recording of the wind direction and velocity.

Soil water content is measured with neutron probes (503DR Hydroprobe, CPN International) until 1 m depth. The soil is predominantly silty and deep. Seven neutron probes were installed at 0.0, 0.5, 1.0 and 3.2 m on both sides of the axis of rotation of the PV row (Fig. 1). Measurements are made once or twice a week on a regular basis but systematically before and after the events.

2.1.3 Experiments in controlled conditions

A reduced-size agrivoltaic device was built to characterize the influence of the tilting angle of the panels in indoor conditions, monitoring the collected rain amounts in the absence of wind with a focus on the lateral redistribution on the width of the panels (Fig. 2). The experimental device consisted of a $2\,\mathrm{m} \times 1\,\mathrm{m}$ panel on a supporting structure of reduced height, allowing tilting angles between 0 and 70°. A rainfall simulator composed of numerous fogging sprays was placed 1.8 m above the flat position of the panel, ensuring quasi-uniform rain conditions on the whole area of the panel, with tested intensities of 20, 35, 60 and $70\,\mathrm{mm\,h^{-1}}$ selected to be representative of the local rain intensities (corresponding to 1-, 3-, 16- and 32-year return periods, respectively). Water flowing out of the panel was collected on a tilted plane on which 10 half-cylinders were fixed, pouring water in the corresponding 10 joined collectors of 0.1 m diameter, covering the width of the panel. The collected amounts were weighted at the end of each test and converted into water depths.

2.2 Rain redistribution model (AVrain)

2.2.1 Model rationale

The modelling of rain redistribution by solar panels is a geometrical problem describing rain interception by an impervious surface of length L, tilting angle α_{PV} and height h above the ground, in which α_R is the angle of incidence of rainfall with respect to the vertical axis and θ_R denotes the plane in which the rain falls, with respect to the north in the present case (Fig. 3). The solution is studied in the vertical (x, z) plane so that the effects in the y direction will be discussed and evaluated but not explicitly described here. Finally, E is the spacing between the supporting pillars, allowing the estimation of an equivalent 1D surface coverage and thus the extension of local calculations to the whole agrivoltaic plot.

The angle of incidence (α_R in degree) of rainfall with respect to z may be estimated from the ratio between wind velocity (v_w in $\mathrm{m\,s^{-1}}$) and the velocity of the falling rain drops (v_d in $\mathrm{m\,s^{-1}}$), according to Van Hamme (1992).

$$\tan(\alpha_R) = \frac{v_w}{v_d} \tag{1}$$

In the above equation, v_d is drawn from the equation proposed by Gunn and Kinzer (1949) for the free-fall limit velocity of a rain drop in stagnant air, from measurements obtained with the electrical method, which is relevant for drop diameters between 0.1 and 5.7 mm:

$$v_d^2 = \frac{4}{3}\frac{g D (\rho_s - \rho)}{\rho c}, \tag{2}$$

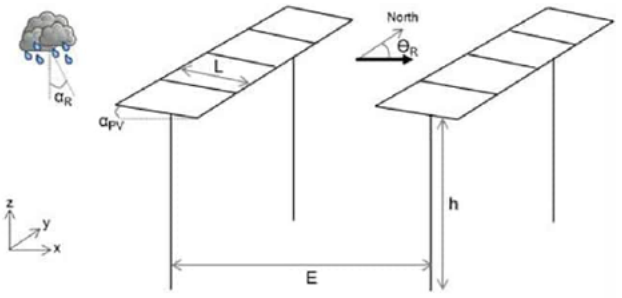

Figure 3. Scheme of the simulated scene, indicating the key parameters of the AVrain model that describes rain redistribution by the solar panels on agrivoltaic plots.

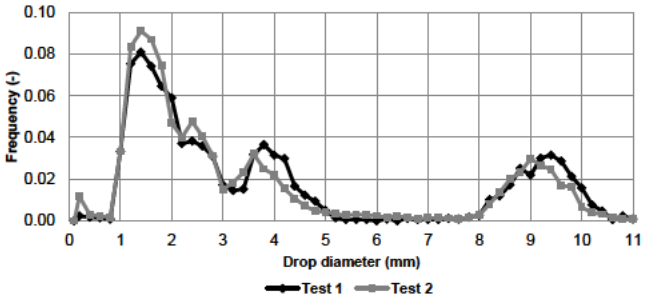

Figure 4. Drop-size distribution curve, obtained with a dual-beam spectro-pluviometer, for the drops falling from the edge of the solar panels. The frequency plotted on the y axis indicates the count of diameters D observed with respect to the total count (the step is about 0.2 mm for D).

where g is the acceleration of gravity ($\mathrm{m\,s^{-2}}$), ρ_s is water density ($\mathrm{kg\,m^{-3}}$), ρ is air density ($\mathrm{kg\,m^{-3}}$), D is the drop diameter (m) and c is the drag coefficient (–).

Drop size distribution has been linked to rain intensity (I in $\mathrm{mm\,h^{-1}}$) by Best (1950) from previous literature elements and measurements made by the author:

$$1 - F_{\mathrm{cum}} = \exp\left(-\left(\frac{D/1000}{1.3I^{0.232}}\right)^{2.25}\right), \quad (3)$$

where F_{cum} is the fraction of liquid water in the air comprised in drops with diameters less than D.

The determination of the angle of incidence of rainfall (α_R, °) from given rain intensity (I) and wind velocity (v_w) allows then

- the discrimination of the zones impacted by the presence of solar panels from those that will receive the same rain amounts as in the control zone and
- the calculation of the water amount intercepted by the solar panels (I_{PV}, $\mathrm{mm^{-1}}$) in function of I, α_{PV} (°), α_R (°), θ_{PV} (° N) and θ_R (° N), after Van Hamme (1992):

$$I_{\mathrm{PV}} = I\,(\cos\alpha_{\mathrm{PV}} - \tan\alpha_R \sin\alpha_{\mathrm{PV}} \cos(\theta_{\mathrm{PV}} - \theta_R)). \quad (4)$$

For simplicity, it is assumed that no significant lateral redistribution occurs on the width of the panels, resulting in no variation in the outlet flow in the transverse y direction. The relevance of this hypothesis is justified in the following: the tests in indoor conditions were designed to address this issue. It is also assumed that the wetting phase of the panels before runoff initiation (somehow the storage capacity of the panels) has no noticeable effects on the calculations. From observations, for low tilting angles, the I_{PV} value needed to trigger runoff is 0.2 mm at most, which is a small value compared to the other values involved in the analysis (and lower than the usual precision of rain gauges).

Runoff velocity (V, $\mathrm{m\,s^{-1}}$) is calculated with the Manning–Strickler formula, hypothesizing that flow width is much larger than flow depth, which makes flow depth approximately equal to the hydraulic radius. Manning's n coefficient is assumed to be $0.01\,\mathrm{s\,m^{-1/3}}$ after (Chow, 1959) because of the very smooth glass coating of solar panels.

The parabolic trajectory of the drops falling from the panels is calculated in similar ways for any drop size (i.e. diameter D) and characterized by the abscissa at which the free-falling drop touches ground (x^*, m) and the free-fall duration (t^*, s):

$$\begin{cases} x^* = a_x \dfrac{t^{*2}}{2} + V\cos\alpha_{\mathrm{PV}} t^* + x_0 \\ a_x = 2\cdot 10^{-4} \dfrac{v_w^2}{D/2} \\ t^* = \dfrac{V\sin\alpha_{\mathrm{PV}} + \sqrt{(V\sin\alpha_{\mathrm{PV}})^2 + 2gz_0}}{g}, \end{cases} \quad (5)$$

where a_x is the acceleration ($\mathrm{m\,s^{-2}}$) due to wind in the x direction, considering a drag coefficient of $c \approx 0.5$ for the drops in the air, V is the initial velocity of the fall ($\mathrm{m\,s^{-1}}$) and x_0 is the abscissa of the edge of the PV (m).

Drop diameter measurements (expressed further in mm for convenience) were conducted with a dual-beam spectro-pluviometer (Delahaye et al., 2006). A three-mode distribution of drop diameters was revealed with peaks at $D = 1.4$, 3.8 and 9.3 mm (Fig. 4). However, diameters $D > 7.5$ mm might be artifacts because rain drops this size would become unstable and split in two droplets during their fall (Niu et al., 2010). In the following numerical applications, a fixed diameter of $D = 1.5$ mm is selected as the reference case for simplicity. However, the sensitivity of the model to D is low and will be discussed later.

The AVrain model was developed with the R software to describe 2D (x, z) phenomena in the vertical plane, hypothesizing negligible effects in the transverse (y) direction (Fig. 1). The time step of AVrain is 1 min. The required climatic forcings are rain intensity (I), wind velocity (v_w) and direction (θ_R), which is assumed identical to rain direction.

The input parameters are the geometrical descriptors of the structure: the height of (the axis of rotation) of the panel (h), its length (L), tilting angle (α_{PV}) and orientation (θ_{PV}), plus the spacing between (pillars supporting the) solar panels (E). Only the tilting angle can be a function of time as it denotes the control exerted on the system. AVrain allows calculating rain redistribution (in x) in the form of effective cumulative rainfall amounts as a function of time. A known limitation of this simplified model is that the effects of the secondary slopes of the panels are not explicitly accounted for, although they are properly identified by the experiments in controlled conditions. These have shown that the combination of low tilting angles (i.e. primary slopes $\alpha_{PV} < 5°$) and low rain intensities lead to lateral dispersion on the edge of the panels. In these cases, this leads to concentrated water fluxes on the lower corner of the panel. However, the impact on the water balance (and its heterogeneity) is limited due to the low magnitude of the corresponding rainfall amounts, as discussed in Sect. 4.1.

2.2.2 Sensitivity analysis

The implementation of solar panels is very likely to affect crop management and irrigation strategies in the equipped plots, especially because of rain redistribution by the panels. The associated patterns of spatial heterogeneity may be described by the coefficient of variation (Cv) closely related to the coefficient that describes the uniformity of water distribution by the irrigation systems (ASAE, 1996; Burt et al., 1997), thus allowing easy comparisons. The choice of Cv as the target variable for sensitivity analysis acknowledges spatial heterogeneity is the key descriptor of the effects of solar panels on rain redistribution on the cultivated plots. In the following, Cv is calculated from the effective rain amounts (i.e. the cumulative water depths) simulated in the 21 joined collectors along the x axis. High Cv values indicate strong heterogeneities while values below 0.2 will be considered as acceptable, according to the standards of ASAE (1996) for irrigation uniformity. This threshold of 0.2 is also consistent with the reference values reported in Van der Gulik et al. (2014).

Using Cv as an indicator allows accounting for two sources of spatial heterogeneity: rain redistribution by the solar panels (with eventual local effective rain amounts that exceed the natural rain amounts measured in the control zone) and the sheltering effect of solar panels (with effective rain amounts far lower right under the panels than in the control zone). In more detail, Cv encompasses in a single indicator the spatial heterogeneity observed within the region located right under a solar panel, i.e. centred on the transverse y axis that connects two supporting pillars, as clearly seen in Fig. 1 where the P11 is the central collector. The width of the equipped region is E, selected as the parameter that describes the spacing between panels and further used to estimate the 1D spatial coverage of the plot by the panels, also taking place in the sensitivity analysis of the model.

The Morris (1991) method is used with Cv as the target variable to estimate the sensitivity of the AVrain model to assess the effect of its seven main parameters (see Table 1) on the spatial heterogeneity of rain redistribution by the solar panels. The combined one-at-a-time screenings of the parameter space introduced by Campolongo et al. (2007) have been used to cover a wide set of possible agrivoltaic installations, keeping all parameters within acceptable, realistic ranges of values. The "sensitivity" package of R (Pujol et al., 2017) was used to generate the associated 4000 parameter sets, obtained from $p = 7$ parameters with $d = 500$ draws each, dispatched within $r = 8$ levels. The control parameter (tilting angle θ_{PV} of the panels) was taken between -70 and $+70°$ but held fixed for the tested event ($P = 3.6$ mm, $v_w = 0.78\,\mathrm{m\,s^{-1}}$, $\theta_w = 285°$, described later).

2.3 Control simulations of soil moisture field by Hydrus-2D

Hydrus-2D (Simunek et al., 1999) may be used to simulate water redistribution in soils for different fixed tilting angles of the solar panel or strategies for operating the panels. The simulation domain finds itself in a vertical (x, z) plane; it is centred on the supporting pillar of a panel and covers a total width of 6.4 m, corresponding to the distance between two consecutive pillars. Hydrus-2D is instead used here for coherence checks and to gain an overview of water redistribution in soil than for detailed numerical simulations of the wetting front movements in space and time, thus allowing simplifying hypotheses on soil structure. The investigated soil depth is 1 m deep, well known from numerous local experiments, and predominantly silty. It is assumed homogeneous in the absence of significant contrast with depth and presented in Table 2.

The AVrain model provides the time-variable forcing data at the soil–atmosphere interface for Hydrus-2D, divided into five categories and accounting for time-variable tilting angles of the solar panel (Fig. 5):

- atmospheric conditions for zones not impacted by the presence of the solar panel,
- flux 1 (F1) conditions for zones impacted by the panel and located right under it,
- flux 2 (F2) conditions for zones impacted by the panel but not located under it,
- flux 3 (F3) conditions for zones located under the edge of the panel thus exposed to the largest effective rain amounts and
- flux 4 (F4) conditions for zones adjacent to those of the F3 conditions but on the sheltered side.

Table 1. Parameters and ranges of values used in the sensitivity analysis of the AVrain model.

Parameter	Description	Reference	Range	Unit
D	Size of the drops falling from the solar panels	1.5	0.1–7	mm
E	Spacing between solar panels	6.40	4–10	m
FactorP	Multiplying factor for precipitations	1	0.1–10	–
FactorV	Multiplying factor for wind velocity	1	0.1–10	–
H	Height of the solar panels	5.00	3–7	m
L	Length of the solar panels	2.00	1–3	m
θ_{PV}	Tilting angle of the solar panels	0	−70–70	°

Table 2. Soil parameters at the Lavalette experimental station used in Hydrus-2D. θ_r and θ_s denote, respectively, the residual and saturated volumetric soil water contents, α and n are empirical shape parameters of the Van Genuchten–Mualem model, K_s is the soil hydraulic conductivity at saturation and l is a pore connectivity parameter.

Depth (cm)	Clay (%)	Silt (%)	Sand (%)	θ_r ($cm^3\,cm^{-3}$)	θ_s ($cm^3\,cm^{-3}$)	α (cm^{-1})	n (–)	K_s ($cm\,hr^{-1}$)	l (–)
0–100	18	42	40	0.01	0.36	0.013	1.2	2.30	0.5

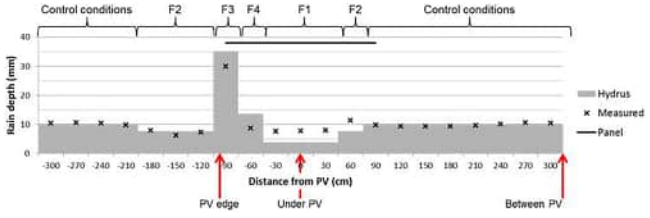

Figure 5. Time-variable upper boundary conditions used in Hydrus-2D for the tested rain event, during which the tilting angle of the panels was varied to minimize rain interception (avoidance strategy).

Hydrus-2D currently allows five types of time-variable upper boundary conditions, which suggests using F2 on both sides of the panel, as indicated in Fig. 5 where only the leftmost position of F2 corresponds to the choices listed above. However, the rightmost position of F2 seems the most suitable default choice given the known soil filling dynamics and the expected effective rain amounts. Zero-flux boundary conditions apply on the vertical limits of the domain and free drainage is relevant for a bottom boundary condition because the water table is several metres under the limit of the domain. For simplicity, the initial soil water content will be assumed homogeneous, selecting a value close to the available observations ($\theta = 0.15$).

3 Results

3.1 Rain redistribution measurements on the dynamic agrivoltaic plot

The influence of variable-tilting-angle solar panels on rain redistribution was measured thanks to a wide series of rain events covering a full year. For each event, we put a focus on the spatial heterogeneity, which is assumed to be a crucial issue for the hydrological balance of solar panels on crops. This heterogeneity is characterized with the coefficient of variation Cv of rain depths. Table 3 gathers Cv values obtained for the most documented rain events in the available records. It enables comparisons between Cv and the tilting angle (or operating strategy) of the solar panels for various rain intensities. The least heterogeneous rain redistributions were observed for panels in abutment (Fig. 6a and b) mainly due to decreased surface coverage, from 30 % for flat panels to 20 % for panels in abutment, resulting in a lesser rain interception. However, the relevancy of this strategy depends on the angle of the wind with respect to the panels (α_R vs. θ_R) identifying these as second-order but non-negligible factors, according to which Cv may become twice as large for panels "facing the wind" or "back to the wind". By contrast, the most heterogeneous rain redistribution was observed for a flat panel ($\alpha_{PV} = 0$) maximizing rain interception and concentration by the panel (Fig. 6c), collecting 11 times more rain than in the control zone, in the F4 domain of Fig. 5, with Cv = 2.13.

Strategies involving time-variable tilting angles α_{PV} offer multiple possibilities, among which the previously mentioned avoidance strategy is relevant to decreasing the spatial heterogeneity (Fig. 6d) and results in Cv = 0.22, which is a fairly good homogeneity. For all the events listed in Table 3,

only the avoidance strategy was able to provide an acceptable level of uniformity in the agrivoltaic plot, i.e. a spatial heterogeneity then would not need to be corrected on purpose, with a dedicated precision irrigation device to ensure equivalent water availability conditions during crop growth. In all cases, the effective rain depth was more important on the sides of the panel (collectors 9 and 13 in Figs. 1 and 6). There are non-impacted zones in the free space between panels, where the effective rain is the same as in the control zone. On the contrary, the sheltering effect is strong right under the panels and the effective rain is always far lower than in natural conditions.

3.2 Evaluation and sensitivity analysis of the AVrain model

The rain redistribution model AVrain was tested for 11 rain events involving flat panels, panels in abutment (either back to the wind or facing the wind) and avoidance strategies, as presented in Table 4. AVrain describes rain redistribution with a satisfying mean determination coefficient of $R^2 = 0.88$. The values of MAPE (mean absolute percentage error) mostly were between 0.1 and 0.3, and regression coefficients greater than 1 indicate that the model tends to overestimate the real effective rain amounts. However, Fig. 7 shows that the overestimations occur near the drip line (i.e. the aplomb, which is used in its technical sense to designate the point on the ground located exactly under the edge of the panel) of the panels, totalizing about 25 % of the committed errors.

The sensitivity analysis of AVrain was conducted with the Morris (1991) method modified and improved by Campolong et al. (2007), selecting Cv as the target variable. Figure 8 shows its results, where μ^* on the x axis is the mean of the individual elementary effects (thus the sensitivity of the parameter tested alone) and σ on the y axis represents the SD of the elementary effects (thus the sensitivity of the parameter tested in interaction with other parameters). The Morris plot allows identifying the parameters that have (i) a negligible overall effect, denoted by low values of both μ^* and σ; (ii) a linear effect, denoted by high values of μ^*; or (iii) nonlinear or interactive effects, denoted by high values of σ. The sensitivity measures (μ^*, σ) reported in Fig. 8 for each parameter have been normalized by the value of the highest sensitivity measure (σ) for the most sensitive parameter (FactorV).

The position of the parameters above the 1 : 1 line in Fig. 8 signals that AVrain is more sensitive to the interactions between parameters than to individual variations in the parameter values, which reinforces the fact that strong heterogeneities in effective rain amounts most likely occur when several conditions are met at once in the forcings (wind direction, drop size), the controls (tilting angle) and the structure (fixed characteristics of the panels). In particular, the high sensitivity score of FactorV compared to the low score of FactorP indicates that wind velocity tends to influence rain redistribution patterns far more than rain amounts, likely because wind velocity intervenes in the calculation of the angle of incidence of rainfall and in that of the trajectory of the drops falling from the panels. The drop size itself was found to have a non-negligible but rather weak influence, although a wide range (0.1 to 7.0 mm) of values was tested. The fact that AVrain is more sensitive to the tilting angle (control exerted on the system) than to the structure parameters (fixed once selected during the installation) is a crucial result of the analysis, indicating there is room for optimization. Conversely, the higher sensitivity of AVrain to wind velocity than to the tilting angle confirms that the optimization strategies should be decided from wind characteristics that dictate the angle of incidence of rainfall.

In an overview of Fig. 8, the Morris method unveils the hierarchy of effects. This proves especially useful when investigating the interactions between the structure parameters. For example, the combinations between panel length and spacing (defining surface coverage) are expected to have more effect on the target variable than the combinations involving panel height, making height a second-order parameter, at least for the tested (realistic) ranges of values and the chosen target variable. This conclusion would have been impossible to reach when separately testing the effects of variations in length, spacing and height of the panels, as proven by Fig. 9, which only acknowledges adverse effects (on Cv) of length and spacing on one side and of height on the other side.

From Fig. 8, the influence of the tilting angle may be expected to be larger than that of the structure parameters, anticipating thus that the avoidance strategy (i.e. operating the panels so as to minimize rain interception) will be likely to significantly reduce Cv whatever the structure parameters. This point is further investigated by Fig. 10, comparing a flat panel with a piloting of the panel according to the avoidance strategy, for various combinations of panels length and spacing (previously proven to have more influence on Cv than the height of the panels). Small-sized panels with a low spacing between them is advocated as the best configuration to reduce Cv in avoidance strategies, which is simulated to be far more efficient than panel held flat. However, this analysis indicates the direction to follow when only rain redistribution issues are tackled but external constraints will surely exist when deciding the in situ implementation of such agrivoltaic installations, for example in the form of limit values for the spacing between panels (to allow agricultural activities).

3.3 Rain redistribution in soils

Water content profiles were measured in the agrivoltaic plot immediately before one of the rain events, and then 6 to 12 h after it, to identify the dynamics and magnitude of rain redistribution in soils, as a consequence of rain redistribution on the soil surface. As expected, the spatial heterogeneity observed on the soil surface is transferred but becomes a bit

Table 3. Rain events with their identification (ID), date, rain amounts on the control zone (P0), tilting angle of the solar panels (α_{PV}) and the associated measured coefficient of variation (Cv) whose highest values indicate the strongest spatial heterogeneities in rain redistribution by the solar panels. In the "Comments" column, avoidance strategy indicates a time-variable α_{PV} angle to minimize rain interception by the panels in real time.

ID	Date	P0 (mm)	α_{PV}	Cv (–)	Comments
#01	18 October 2015	4.8	−50 to 0°	1.14	Solar tracking
#02	07 December 2015	5.1	−50 to −30°	0.98	Solar tracking
#03	12 February 2016	14.6	−50°	0.97	Transverse wind (south)
#04	09 March 2016	5.1	−50°	0.96	Facing the wind
#05	17 March 2016	4.1	+50°	0.40	Back to the wind
#06	21 April 2016	3.6	0°	2.13	Flat panel
#07	30 April 2016	3.0	0°	1.15	Flat panel
#08	22 May 2016	8.4	0°	0.72	Flat panel
#09	28 May 2016	13.5	0°	1.28	Flat panel
#10	31 May 2016	4.5	0°	1.63	Flat panel
#11	14 September 2016	14.8	−50 to +50°	0.22	Avoidance strategy
#12	12 October 2016	203.6	0°	0.51	Flat panel

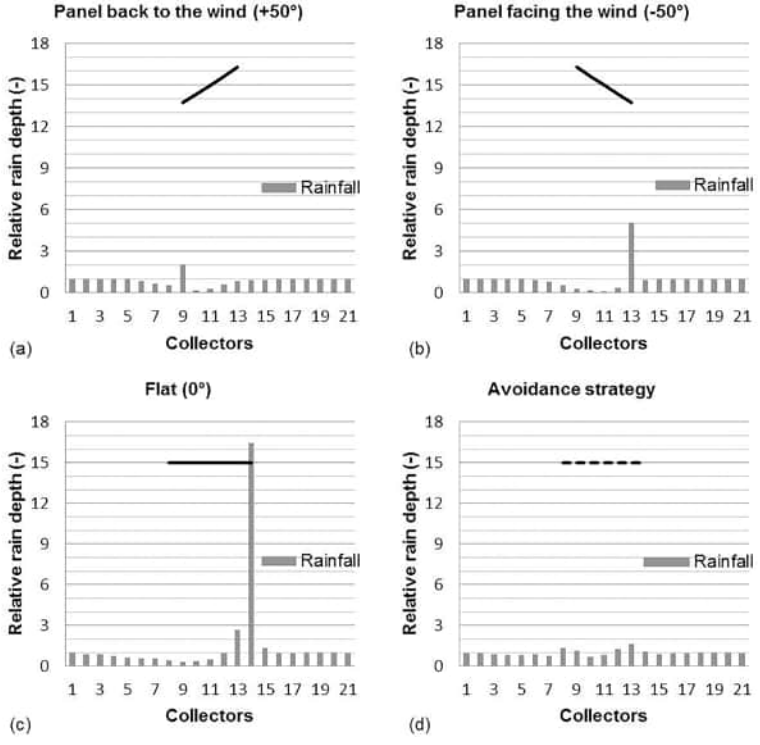

Figure 6. Examples of rain redistribution for various rain events, tilting angle and operating strategies of the solar panels, measured in the collectors displayed in Fig. 1. Relative rain depths are given with respect to the control zone where rain amounts are collected in the pluviometer.

fuzzy in the first 30 cm of soil, due to lateral homogenization (ponding with significant surface runoff, lateral diffusion associated with soil dispersivity). Nevertheless, the spatial patterns are clearly visible within soils, especially for the flat panels case (Fig. 11a) for which three distinct zones may be identified: (i) between panels, with similar behaviour as in the control zone; (ii) under panels, with a noticeable sheltering effect and thus drier soils; and (iii) under the edge of the panels, where the increased soil water content is attributable to the large effective amounts poured on the soil surface. In Fig. 11a, the maximal soil water storage variation was observed under the edge of the panels, estimated at 6.7 mm in accordance with the location of the effective rain amount poured on the soil surface (24.0 mm). Between pan-

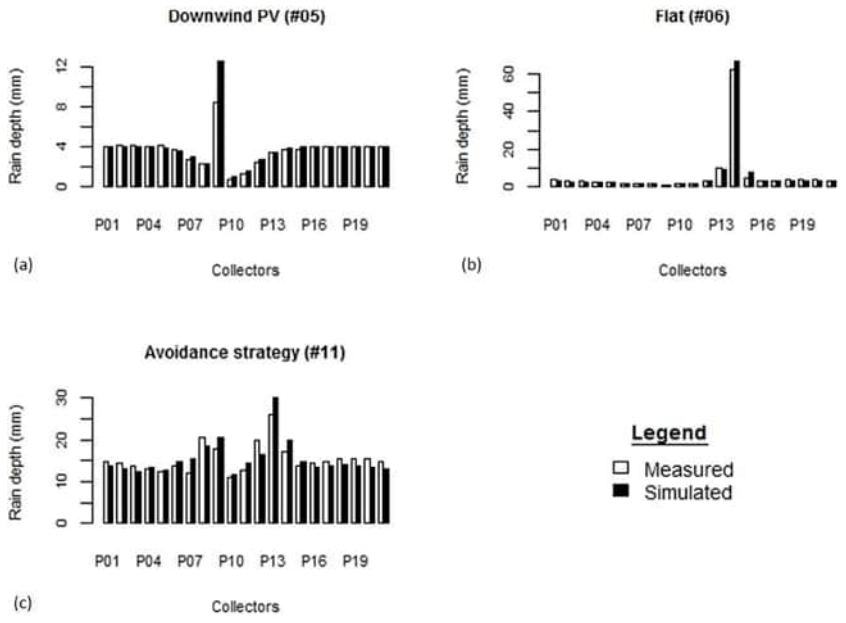

Figure 7. Examples of rain redistribution by the solar panels simulated by the AVrain model and compared to field measurements for three very different events and managements of the solar panels (see Tables 3 and 4 for details).

Table 4. Performances of the AVrain model that describes rain redistribution by the solar panels, identifying each event (ID), indicating the mean absolute percentage error (MAPE), normalized root mean square error (NRMSE), linear correlation coefficient and coefficient of determination (R^2) next to the simulated coefficients of variation (Cv). The highest Cv values signal the strongest spatial heterogeneities in rain redistribution by the solar panels.

ID	MAPE	NRMSE	Slope of regression line	R^2	Cv
#01	0.29	0.22	1.21	0.89	1.15
#02	0.25	0.22	1.45	0.86	1.21
#03	0.41	0.10	0.82	0.83	0.75
#05	0.07	0.13	1.10	0.86	0.46
#06	0.14	0.13	1.06	1.00	2.28
#07	0.21	0.20	0.89	0.98	1.25
#08	0.13	0.11	0.88	0.99	0.72
#09	0.23	0.12	1.38	0.97	1.50
#10	0.22	0.17	1.04	0.96	2.34
#11	0.11	0.08	1.00	0.75	0.19
#12	0.17	0.03	1.13	0.56	0.78

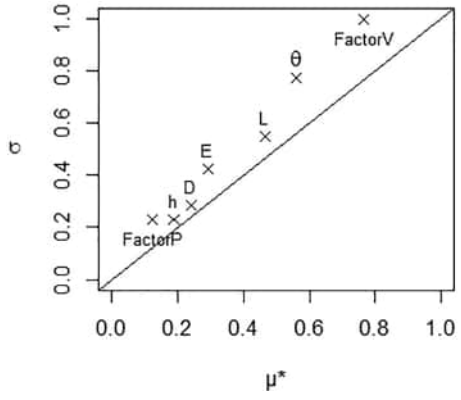

Figure 8. Sensitivity analysis of the AVrain model by the Morris (1991) method improved by Campolongo et al. (2007), where μ* indicates the linear part of the total sensitivity score for each parameter while σ indicates the non-linear or interactive part. In the Morris plot, D is the drop diameter, E the spacing between solar panels, FactorP is the multiplying factor for precipitations with respect to the reference case, FactorV is the multiplying factor for wind velocity with respect to the reference case, h is the height of the solar panels, L is their length and θ_{PV} is their tilting angle (see Table 1 for the reference values and ranges of the parameters). The target variable of the analysis was the coefficient of variation that measures the spatial heterogeneity of rain redistribution by the solar panels. The tested rain event was #06 in Tables 3 and 4.

els, the storage variation was 2.0 mm for 3.0 mm of effective rain. Under panels, the storage variation was 4.7 mm for only 1.3 mm of effective rain, which reinforces the hypothesis of lateral redistribution, either within the soil or at its surface, from the nearby zones. In Fig. 11b, the avoidance strategy tested for a rain event of 60 mm in the control zone resulted in a maximal storage variation of 91 mm between panels due to a drier initial soil water content, 76 mm under panels and 43 mm near the aplomb of the edge of the panels, while significant ponding was observed.

The simulation of rain redistribution in soils was made by Hydrus-2D for a single rain event (#11) to compare the soil

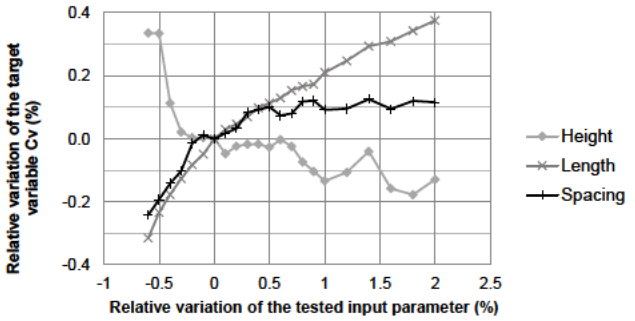

Figure 9. Graph showing the influence of the structure parameters (spacing E, height h, length L) of the agrivoltaic installation on the spatial heterogeneity of rain redistribution by the solar panels, from the simulated values of the coefficient of variation (Cv).

water content fields obtained in the flat panel case (Fig. 12a) or when using the avoidance strategy (Fig. 12b). The time-variable atmospheric conditions required by Hydrus-2D were provided by the outputs of AVrain at the minute time step, with the five-zone discretization discussed in Sect. 2.4 and shown in Fig. 5. Starting from a rather dry, realistic and approximately homogeneous soil water content of $\theta = 0.15\,\mathrm{cm^3\,cm^{-3}}$, the objectives of these exploratory simulations were not to capture the finest spatial patterns of the wetting front, but instead to assess whether the observed noticeable differences in rain redistribution trends could easily be reproduced and quantified by Hydrus-2D. As expected, the flat panel case leads to the creation of a sharp contrast in soil water content, near the aplomb of the edge of the panel, in the form of a wet bulb that propagates downward by gravity and sideward by diffusion. This result in the vertical plane is in coherence with a well-known 3D effect of drip irrigation – that the vertical and horizontal deformations of the ellipsoidal bulb will depend on soil properties: coarse soils will produce very elongated bulbs in the vertical direction while silty soils are likely to produce more significant lateral redistribution. However, the simulated spatial heterogeneities in soil water content remain very pronounced for the flat panel case in comparison with the avoidance strategy (Fig. 12b). In this paper, the choice of the coefficient of variation (Cv) to qualify the spatial heterogeneities allowed the reconnection to the coefficient of uniformity classically used in irrigation science, addressing water delivery on the soil surface, typically by sprinkler irrigation. Here, Fig. 12a resembles the 2D or 3D patterns characteristic of surface or subsurface drip irrigation while Fig. 12b recalls the quasi-1D patterns of (high-performance) sprinkler irrigation.

3.4 Effects of the transverse slope of the panels

The underlying hypotheses made in the construction of the AVrain model led to the formulation of a 2D (x, z) model, thus discarding all phenomena arising from variations in the transverse (y) direction or, at least, not representing them in an explicit manner. If relevant, indirect assessments of their effects should still be made, outside AVrain but to investigate if the model stays valid or in which conditions significant uncertainties may exist in its predictions. Among transverse effects likely to exist in real conditions, only the effects of transverse slopes of the panels were anticipated, observed and deemed significant, though limited to particular contexts. These contexts are summed up in the cases when the tilting angle (i.e. the prevalent slope) of the panels is very low, so that the transverse, secondary slope becomes of the same order.

Tests in controlled conditions were conducted with a duration of 15 min, under a rain intensity of $20\,\mathrm{mm\,h^{-1}}$. Rain redistribution on the width of the panel appears for tilting angles lower than 20° and the width of the outlet becomes very narrow for tilting angles lower than 5° (Fig. 13). In the latter case, about 90 % of the collected water drops from the panel through a 20 cm wide outlet. In the general case, such effects may be explicitly calculated from the slopes (prevalent, secondary) and water depth on the panel. Such effects are likely to increase the effective rain amounts observed in the field at the aplomb of the edge of the flat panels (Fig. 6c).

4 Discussion

4.1 Rain redistribution by the solar panels

The 2D AVrain model was developed to describe rain interception and redistribution by the solar panels and fulfills its objectives well: it allows the identification of the sheltered zones and of the zones in which the effective rain amounts exceed the natural rain amounts of the control zone, with a correct quantification of the associated fluxes. The angle of incidence of rainfall was found to be a key variable in the determination of the spatial patterns of heterogeneity in the effective rain amounts falling on the ground. This angle is difficult to measure but the equations derived by Gunn and Kinzer (1949) and Best (1950) allow estimating it in indirect ways.

If relevant, the AVrain model may be adapted to account for additional geometrical characteristics of the solar panels, for example to better describe the effects of the secondary (transverse) slope when it becomes of the same order as the tilting angle of the panels (i.e. their prevalent slope). This is the typical case in which the secondary slope is likely to increase the heterogeneity of rain redistribution by redistributing the collected water along the width of the panels. The presence and effect of a ridge on the length and/or width of the panels could be explicitly modelled with the techniques used in hydrology for thin flows over a weir. Even if the presence of a small ridge may affect the threshold of (approximately) 2 mm water depth thought to trigger runoff on the panels (in controlled conditions and without a ridge), it

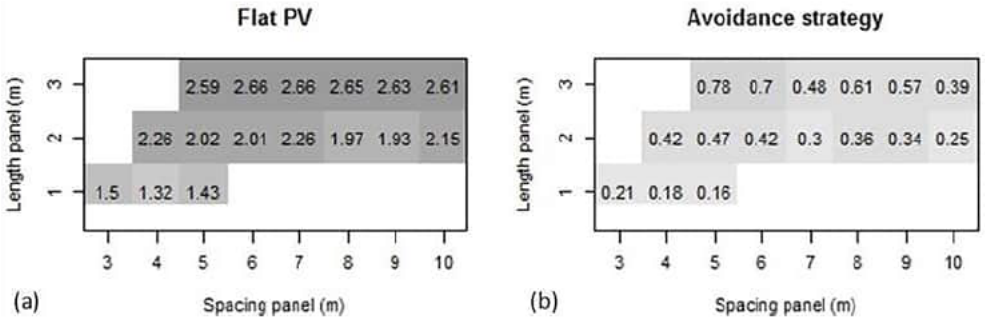

Figure 10. Influence of the structure parameters (spacing E, length L) of the panels on the spatial heterogeneity of rain redistribution from the simulated values of the coefficient of variation (Cv) for panels held flat (**a**) or operated according to the avoidance strategy (**b**). The combinations of E and L values may be assimilated to equivalent 1D surface coverage between 20 and 60 % by dividing L by E. Only the realistic combinations have been simulated here: blank cells indicate those that are not.

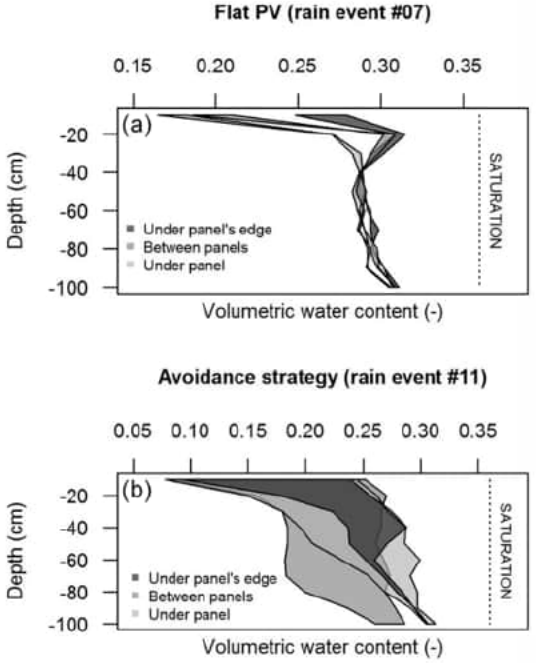

Figure 11. Variations of soil water storage in soil regions located near the aplomb of the panel's edge (dark grey), between panels (medium grey) and under panels (light grey) for different strategies for operating the panels, holding panels flat during rain event #07 (**a**) or operating them according to the avoidance strategy that minimizes rain interception during rain event #11 (**b**). For each case, the leftmost and rightmost line indicate the water content profile before and after the event, respectively. Event #11 was considered as the sum of two successive events for a total rainfall of 60 mm in the control zone.

is hypothesized here that any explicit modelling would not provide a significant added value, for two reasons: the stored volumetric amounts are small when the panels are held nearly flat in the absence of rain and the avoidance strategy is recommended when rain occurs.

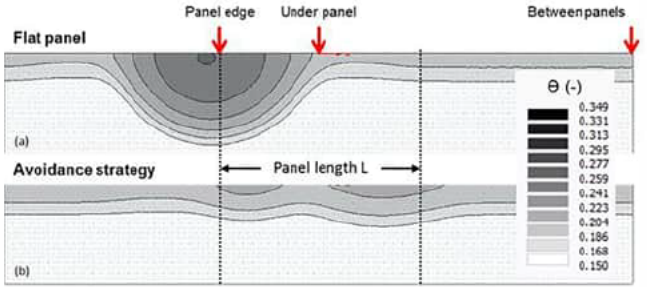

Figure 12. Simulation of soil water patterns with Hydrus-2D, in regions located near the aplomb of the panel's edge, under panels or between panels, when holding the panels flat (**a**) or operating them according to the avoidance strategy (**b**) to reduce the heterogeneity of rain redistribution by the panels during event #11 (see Tables 3 and 4). The vertical arrows recall the positions of the neutron probes used to collect water content data plotted in Fig. 11.

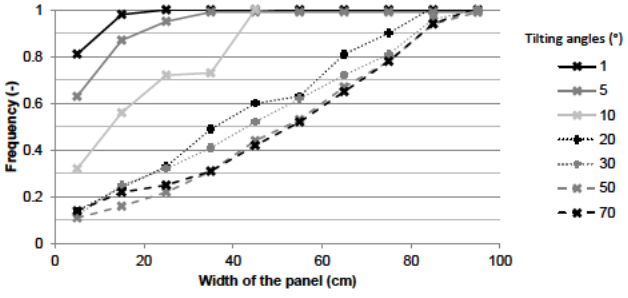

Figure 13. Influence of the transverse slope of the solar panels on the lateral rain redistribution along the width of the panel, tested for a 20 mm h^{-1} rain intensity and "prevalent" tilting angles of the panels between 1 and 70°. The results are expressed in a cumulative distribution of the collected amounts at the outlets placed along the width of the panel.

4.2 Rain redistribution in soils

Hydrus-2D was used to simulate rain redistribution in soils, using the spatially distributed output variables of the AVrain model to provide the required time-variable atmospheric conditions. Five such conditions at most can be used as climatic forcings for Hydrus-2D, which seemed to be a limitation for the present purpose but could be handled, thus, with the a posteriori indication that the chosen trick has the value of a good practice. In coherence with the field observations, the simulated fields of soil water content emphasized the interest in using the avoidance strategy to decrease the spatial heterogeneities of soil water content in the agrivoltaic plots, thus confirming that the tilting angle of the panels is a strong control parameter.

Even if the spatial heterogeneity of rain redistribution is less drastic in soils than on the soil surface, due to lateral diffusion, it remains strong enough to necessitate a dedicated remediation in the form of precision irrigation, unless the avoidance strategy is used. In other words the avoidance strategy (that consists in minimizing rain interception and redistribution by commanding the appropriate time-variable tilting angle of the panels) has implications in the relevant irrigation strategy, making it less complex. This is an opening to a more global optimization problem in dealing with the various sources of heterogeneity, which will certainly be compared with the observed heterogeneities in crop yield on the agrivoltaic plots. In addition to the heterogeneities in the forcings (irrigation and rain redistribution) the modeller will surely have to also address these in soils, for example by means of geophysical methods that offer the possibility of similar spatial resolutions (e.g. electrical resistivity tomography, refraction seismology)

4.3 Rain and crop-induced operation of solar panels

Some aspects specific to cultivated plots need to be mentioned here, although the primary scope of this paper is to focus on the hydrological side. The panels left with a low tilting angle (high surface coverage and rain interception) are likely to have unwanted direct effects on the soil and plants underneath. For example, leafy vegetables might be damaged by the repeated drop impacts or even more so by the occasional curtains of water falling from the panels a few metres above, even if their storage capacity is limited. Such problems will typically occur in the morning, when panels are first operated, given that they are generally left flat during nighttime. They could also occur during heavy rains, even when using the avoidance strategy, which results in a damped but non-zero flux concentration near the aplomb of the edges of the solar panels. In the bare soil periods, it is rather the erosion risk that should be handled, especially the splash erosion (Nearing and Bradford, 1985; Josserand and Zaleski, 2003; Planchon and Mouche, 2010) where drop impacts are responsible for particle detachment and for the creation of microtopography. This, in turn, creates pathways for runoff and further soil degradation processes. Nevertheless, avoidance strategies fed by real-time wind and precipitation data (collected at a 30 s time step) are powerful means to handle these issues, which will certainly be included in the more general optimization strategies suitable for the cultivated agrivoltaic plots. In some contexts, randomized positions of the solar could be another option to reduce the consequence on soil of rain concentration and maximize homogeneity in the long term.

5 Conclusions

Agrivoltaism represents a modern, relevant solution to the growing food and energy demands associated with a global population increase, especially in the current climate change context. Nevertheless, there are unresolved issues specific to the implementation of solar panels on the cultivated plots, for example regarding the adaptation of the plants to the forced intermittent shading conditions or the impact of the panels on the hydrological budget and behaviour of the plot. This paper has tackled the pending question of rain redistribution by dynamic solar panels, i.e. panels endowed with 1 degree of freedom in rotating around their supporting axis, so that their tilting angle may vary in time and be controlled on purpose for a very short term of a few minutes.

A dramatic difference was observed and simulated, in terms of spatial patterns of rain redistribution on the ground, between the case of panels held flat and panels moved according to so-called avoidance strategies that consist in minimizing rain interception by the panels during the course of rain events (and eventually adapting the command of the panels to short-term changes in wind and rain conditions within a single event). The avoidance strategies resulted in far lower coefficients of variation (i.e. heterogeneity measures) used to describe the spatial variations in the effective rain amounts falling on the ground, under the panels, between panels or near the aplomb of the edges of the panels. The measures of heterogeneity obtained for avoidance strategies had low enough values to be compared with the fairly good uniformity scores used to quantify the ability of irrigation systems to deliver similar water amounts in the different zones of a given plot. Hence, it is likely that the most relevant irrigation strategies will suppress or attenuate the need for precision irrigation within the equipped plots. On the contrary, basic strategies that consist in holding the panels flat induce very strong spatial heterogeneities, with local effective rain amounts that exceed those of the control zone and may be responsible for increased runoff and erosion risks on bare soils, not to mention the risks associated with direct, repeated impacts on the soil aggregates (possibly leading to soil compaction and crust formation) and on the plants that find themselves near the aplomb of the edge of the panels. The flat panel case has one additional disadvantage: the panels are

never strictly flat, so any transverse slope of comparable order will have the consequence of redirecting all the collected water towards a narrow outlet on the width of the panels.

However, the mechanistic AVrain model derived in this paper shows that the control exerted on the tilting angle of the panels is strong enough for the user to cope with most meteorological conditions (rain intensity, wind direction and velocity) and realistic structure characteristics (height, length and spacing of the panels) to achieve the targeted short-term event-based optimization of rain redistribution. It is very likely that more general and complex methods should be used when considering at the same time the hydrological budget, crop growth and energy production, as well as seasonal objectives. To prepare ground, the soil part of the problem has also been investigated here, showing with Hydrus-2D simulations that rain redistribution patterns in soils resembled those observed on the soil surface, though less contrasted due to lateral diffusion processes on the soil surface (ponding) or within soils (at least where significant lateral dispersion coexists with gravity). Future research leads include a finer parameterization of Hydrus-2D for a stronger coupling with the results of the AVrain model, as a verification tool for the adaptation of simpler 1D approaches to model water budget, irrigation strategies and crop growth in agrivoltaic conditions (Khaledian et al., 2009; Mailhol et al., 2011; Cheviron et al., 2016) within global optimization strategies.

Code and data availability. Data collection and model development were performed in the frame of the Sun'Agri2B project that links the Sun'R SAS society with Irstea and other academic or non-academic partners.

Author contributions. YE performed most of the experiments and developed the model, under the supervision of BC and GB. AM contributed to the first stages of the experiments and model development while CD and FL helped in handling the metrological and technical parts of the work.

Competing interests. There are no known competing interests based on scientific grounds. However, there may be conflicts of interest on commercial grounds with societies other than Sun'R SAS also engaged in agrivoltaic activities.

Acknowledgements. This study was conducted within the frame of the SunAgri2b project, supported by the Provence–Alpes–Côte d'Azur and Rhône-Alpes regions, CAPI, BPI France, Communauté de Communes Pays d'Aix, Grand Lyon, and the Agence Nationale pour la Recherche et la Technologie. The experimental platform was co-funded by Irstea, Région Île-de-France and Paris Entreprises. The first author is a PhD student and a member of both the Sun'R SAS society and the OPTIMISTE research team of Irstea Montpellier, France, to which all co-authors also belong. OPTIMISTE stands for Optimization of the Piloting and Technologies of Irrigation, Minimization of InputS, and Transfers in the Environment and is one of the research teams in the "G-Eau" joint research unit that addresses water management, actors and uses.

Edited by: Lixin Wang
Reviewed by: two anonymous referees

References

ASAE: Field evaluation of microirrigation systems, no. EP405.1, ASAE Standards, Amer. Soc. Agric. Engr., St. Joseph, MI., 756–759, 1996.

Barnard, T., Agnaou, M., and Barbis., J.: Two dimensional modeling to simulate stormwater flows at photovoltaic solar energy sites, J. Water Manage. Model., 25, https://doi.org/10.14796/JWMM.C428, 2017.

Best, A. C: The size distribution of raindrops, Q. J. Roy. Meteor. Soc., 76, 16–36, 1950.

Burt, C. M., Clemmens, A. J., Strelkoff, T. S., Solomon, K. H., Bliesner, R. D., Hardy, L. A., Howell, T. A., and Eisenhauer., D. E.: Irrigation performance measures: efficiency and uniformity, J. Irrig. Drain. E.-ASCE, 123, 423–442, https://doi.org/10.1061/(ASCE)0733-9437(1997)123:6(423), 1997.

Campolongo, F., Cariboni, J., and Saltelli., A.: An effective screening design for sensitivity analysis of large models, Environ. Modell. Softw., 22, 1509–1518, 2007.

Cheviron, B., Vervoort, R. W., Albasha, R., Dairon, R., Le Priol, C., and Mailhol, J. C.: A framework to use crop models for multiobjective constrained optimization of irrigation strategies, Environ. Modell. Softw., 86, 145–157, 2016.

Chow, V. T.: Open Channel Hydraulics, McGraw-Hill Book Company, 1959.

Cook, L. M. and McCuen, R. H.: Hydrologic response of solar farms, J. Hydrol. Eng., 18, 536–541, 2013.

Delahaye, J.-Y., Barthès, L., Golé, P., Lavergnat, J., and Vinson., J. P.: A dual-beam spectropluviometer concept, J. Hydrol., 328, 110–120, 2006.

Diermanse, F. L. M.: Representation of natural heterogeneity in rainfall–runoff models, Phys. Chem. Earth Pt. B, 24, 787–792, 1999.

Dinesh, H. and Pearce, J. M.: The potential of agrivoltaic systems, Renew. Sust. Energ. Rev., 54, 299–308, 2016.

Dupraz, C., Marrou, H., Talbot, G., Dufour, L., Nogier, A., and Ferard., Y.: Combining solar photovoltaic panels and food crops for optimising land use: towards new agrivoltaic schemes, Renew. Energ., 36, 2725–2732, 2011.

Emmanuel, I., Andrieu, H., Leblois, E., Janey, N., and Payrastre., O.: Influence of rainfall spatial variability on rainfall? Runoff modelling: benefit of a simulation approach?, J. Hydrol., 531, 337–348, 2015.

Faurès, J.-M., Goodrich, D. C., Woolhiser, D. A., and Sorooshian., S.: Impact of small-scale spatial rainfall variability on runoff modeling, J. Hydrol., 173, 309–326, 1995.

Gumiere, S. J., Le Bissonnais, Y., and Raclot, D.: Soil resistance to interrill erosion: model parameterization and sensitivity, Catena, 77, 274–284, 2009.

Gunn, R. and Kinzer, G. D.: The terminal velocity of fall for water droplets in stagnant air, J. Meteorol., 6, 243–248, 1949.

Harinarayana, T. and Sri Venkata Vasavi, K.: Solar energy generation using agriculture cultivated lands, Smart Grid Renewable Eng., 5, 31–42, 2014.

IPCC: Renewable Energy Sources and Climate Change Mitigation: Summary for Policymakers and Technical Summary: Special Report of the Intergovernmental Panel on Climate Change, Cambridge University Press, New York, 2011.

IPCC: Climate Change: Impacts, Adaptation and Vulnerability, Contribution of Working Group II to the Fifth Assessment Report of the Intergovernmental Panel on Climate Change, Cambridge University Press, New York, 2014.

Jackson, N. A.: Measured and Modelled Rainfall Interception Loss from an Agroforestry System in Kenya, Agr. Forest Meteorol., 100, 323–336, 2000.

Josserand, C. and Zaleski, S.: Droplet splashing on a thin liquid film, Phys. Fluids, 15, 1650, https://doi.org/10.1063/1.1572815, 2003.

Khaledian, M. R., Mailhol, J. C., Ruelle, P., and Rosique., P.: Adapting PILOTE model for water and yield management under direct seeding system: the case of corn and durum wheat in a Mediterranean context, Agr. Water Manage., 96, 757–770, 2009.

Knapen, A., Poesen, J., Govers, G., Gyssels, G., and Nachtergaele., J.: Resistance of soils to concentrated flow erosion: a review, Earth-Sci. Rev., 80, 75–109, 2007.

Lamm, F. R. and Manges, H. L.: Partitioning of sprinkler irrigation water by a corn canopy, T. ASAE, 43, 909–918, 2000.

Levia, D. F. and Germer, S.: A review of stemflow generation dynamics and stemflow-environment interactions in forests and shrublands: stemflow review, Rev. Geophys., 53, 673–714, 2015.

Mailhol, J. C., Ruelle, P., Walser, S., Schütze, N., and Dejean., C.: Analysis of AET and yield predictions under surface and buried drip irrigation systems using the crop model PILOTE and Hydrus-2-D, Agr. Water Manage., 98, 1033–1044, 2011.

Marrou, H.: Produire des aliments ou de l'énergie: faut-il vraiment choisir? – Evaluation agronomique du concept d'"agrivoltaïsme", Montpellier Sup'Agro, Montpellier, 2012.

Marrou, H., Dufour, L., and Wery., J.: How does a shelter of solar panels influence water flows in a soil–crop system?, Eur. J. Agron., 50, 38–51, 2013a.

Marrou, H., Guilioni, L., Dufour, L., Dupraz, C., and Wery., J.: Microclimate under agrivoltaic systems: is crop growth rate affected in the partial shade of solar panels?, Agr. Forest Meteorol., 177, 117–132, 2013b.

Marrou, H., Wery, J., Dufour, L., and Dupraz., C.: Productivity and radiation use efficiency of lettuces grown in the partial shade of photovoltaic panels, Eur. J. Agron., 44, 54–66, 2013c.

Martello, M., Ferro, N., Bortolini, L., and Morari., F.: Effect of incident rainfall redistribution by maize canopy on soil moisture at the crop row scale, Water, 7, 2254–2271, 2015.

Morris, M. D.: Factorial sampling plans for preliminary computational experiments, Technometrics, 33, 161–174, 1991.

Movellan, J.: Japan next-generation farmers cultivate crops and solar energy, Renewable Energy World, available at: http://buyersguide.renewableenergyworld.com/ (last access: 14 February 2018), 2013.

Nearing, M. A. and Bradford, J. M.: Single waterdrop splash detachment and mechanical properties of soils1, Soil Sci. Soc. Am. J., 49, 547–552, 1985.

Niu, S., Jia, X., Sang, J., Liu, X., Lu, C., and Liu., Y.: Distributions of raindrop sizes and fall velocities in a semiarid plateau climate: convective versus stratiform rains, J. Appl. Meteorol. Clim., 49, 632–645, 2010.

Osborne, M.: Fraunhofer ISE resurrects agrophotovoltaics, PVTECH, available at: https://www.pv-tech.org/news/fraunhofer-ise-resurrects-agrophotovoltaics (last access: 14 February 2018), 2016.

Pereira, L. S., Oweis, T., and Zairi., A.: Irrigation management under water scarcity, Agr. Water Manage., 57, 175–206, 2002.

Planchon, O. and Mouche, E.: A physical model for the action of raindrop erosion on soil microtopography, Soil Sci. Soc. Am. J., 74, 1092–1103, 2010.

Playán, E. and Mateos, L.: Modernization and optimization of irrigation systems to increase water productivity, Agr. Water Manage., 80, 100–116, 2006.

Pujol, G., Iooss, B., and Janon., A.: Global Sensitivity Analysis of Model Outputs (Version, 1.14.0), Package "sensitivity", 2017.

Ravi, S., Lobell, D. B., and Field., C. B.: Tradeoffs and synergies between biofuel production and large solar infrastructure in deserts, Environ. Sci. Technol., 48, 3021–3030, 2014.

Simunek, J., Sejna, M., and van Genuchten, M. T.: The HYDRUS-2-D Software Package for Simulating the Two-Dimensional Movement of Water, Heat, and Multiple Solutes in Variably-Saturated Media (Version, 2.0), US Salinity Laboratory, Agricultural Research Service, US Department of Agriculture, Riverside, California, 1999.

Tang, Q., Oki, T., Kanae, S., and Hu., H.: The influence of precipitation variability and partial irrigation within grid cells on a hydrological simulation, J. Hydrometeorol., 8, 499–512, 2007.

Van Hamme, T.: La pluie et le topoclimat, Hydrologie Continentale, 7, 51–73, 1992.

Van der Gulik, T., Tam, S., and Petersen, A.: B. C. Sprinkler Irrigation Manual, edited by: the B. C. Ministry of Agriculture and Fisheries, Irrigation Industry Association, B. C., Canada, 2014.

Yuan, C., Gao, G., and Fu, B.: Comparisons of stemflow and its bio-/abiotic influential factors between two xerophytic shrub species, Hydrol. Earth Syst. Sci., 21, 1421–1438, https://doi.org/10.5194/hess-21-1421-2017, 2017.

Journal of Hydrology 557 (2018) 631–642

Contents lists available at ScienceDirect

Journal of Hydrology

journal homepage: www.elsevier.com/locate/jhydrol

Review papers

Does soil compaction increase floods? A review

Abdallah Alaoui [a,*], Magdalena Rogger [b], Stephan Peth [c], Günter Blöschl [b]

[a] University of Bern, Bern, Switzerland
[b] Institute of Hydraulic Engineering and Water Resources Management, Vienna University of Technology, Vienna, Austria
[c] Department of Soil Science, University of Kassel, Kassel, Germany

ARTICLE INFO

Article history:
Received 8 August 2017
Received in revised form 19 December 2017
Accepted 20 December 2017
Available online 26 December 2017
This manuscript was handled by Marco Borga, Editor-in-Chief, with the assistance of Daniele Penna, Associate Editor

Keywords:
Soil compaction
Floods
Land use changes
Soil hydrology
Upscaling flow processes

ABSTRACT

Europe has experienced a series of major floods in the past years which suggests that flood magnitudes may have increased. Land degradation due to soil compaction from crop farming or grazing intensification is one of the potential drivers of this increase. A literature review suggests that most of the experimental evidence was generated at plot and hillslope scales. At larger scales, most studies are based on models. There are three ways in which soil compaction affects floods at the catchment scale: (i) through an increase in the area affected by soil compaction; (ii) by exacerbating the effects of changes in rainfall, especially for highly degraded soils; and (iii) when soil compaction coincides with soils characterized by a fine texture and a low infiltration capacity. We suggest that future research should focus on better synthesising past research on soil compaction and runoff, tailored field experiments to obtain a mechanistic understanding of the coupled mechanical and hydraulic processes, new mapping methods of soil compaction that combine mechanical and remote sensing approaches, and an effort to bridge all disciplines relevant to soil compaction effects on floods.

Contents

1. Introduction . . . 632
2. Soil compaction processes . . . 632
   2.1. Types and causes of soil compaction . . . 632
   2.2. Soil properties . . . 633
      2.2.1. Soil structure . . . 633
      2.2.2. Soil texture . . . 633
      2.2.3. Organic matter . . . 633
      2.2.4. Water content . . . 633
   2.3. Time scales of soil compaction . . . 633
   2.4. Macropore flow – surface runoff relationship . . . 634
   2.5. Mapping soil compaction . . . 634
3. Experimental evidence of soil compaction effects on floods . . . 634
   3.1. Plot scale . . . 634
   3.2. Hillslope scale . . . 634
   3.3. Catchment scale . . . 635
4. Modelling evidence of soil compaction on floods . . . 636
   4.1. Area of compaction . . . 637
   4.2. Rainfall and compaction . . . 637
   4.3. Soil texture exacerbating compaction effects . . . 637
5. Research gaps . . . 637
   5.1. Areal coverage . . . 637
   5.2. Patchiness/Connectivity . . . 638

* Corresponding author.
E-mail [redacted]cde.unibe.ch (A. Alaoui).

https://doi.org/10.1016/j.jhydrol.2017.12.052
0022-1694/

5.3. Temporal variability . . . 638
5.4. Feedbacks . . . 638
5.5. Masking . . . 638
5.6. Model parameterization . . . 638
6. Ways forward . . . 638
6.1. Meta analyses . . . 638
6.2. Additional field experiments . . . 638
6.3. Mapping soil compaction . . . 638
6.4. Bridging gap between different disciplines . . . 638
7. Conclusions . . . 639
Acknowledgements . . . 639
References . . . 639

1. Introduction

Europe has experienced a series of major floods in the past years which may suggest that flooding is becoming more frequent and severe (e.g., Hall et al., 2014). Destructive floods occurred in several European countries like Germany and Poland in August 2002, in western Austria in 2005, in Italy in November 1994, October 2000, and autumn 2011; the UK in October 2000, summer 2007, and the winters of 2013/14 and 2015/16; in Central Europe in July 1997, summer 2010, and June 2013; the Balkan region in May 2014; and, most recently, in Germany, France and Belgium in June 2016 (Kundzewicz et al., 2017). In order to project any changes into the future it is important to understand the drivers that have triggered flood changes in the past. There are three potential drivers, climate change, hydraulic structures and land use change (Viglione et al., 2016; Hall et al., 2014; Blöschl et al., 2017). Among these, land use change effects are probably the least well understood (e.g., Peña et al., 2016; Rogger et al., 2017).

Humans have interfered with landscapes over millennia, at an ever increasing rate. In the last centuries, global rain-fed cropland and pastureland have increased by 460% and 560%, respectively (Scanlon et al., 2007). Land use change tends to follow a set pattern: from the restoration of natural vegetation to boundary clearing, then to subsistence agriculture and small-scale farms and, as a final point, to intensive agriculture, urban areas and protected recreational lands (Foley et al., 2005). These land use changes are often associated with soil degradation, particularly if heavy machinery is used, but grazing intensification may also lead to major modifications of the soils (Carroll et al., 2004; O'Connell et al., 2004). Some 33 million hectares are affected by soil compaction in Europe (Oldeman et al., 1991, cited by Birkas, 2008). Of these, 20 million hectares are in Eastern Europe, which amounts to 37.5% of the agricultural land (Birkas, 2008; Batey, 2009).

Soil compaction can cause a number of environmental and agronomic problems, including increased leaching of agrochemicals to the recipient waters, emission of greenhouse gases, crop yield losses, erosion and flooding (Holman et al., 2003; Doerner and Horn, 2006; Singh and Hadda, 2014). While soil compaction effects on surface runoff are relatively well understood at the local scale (Rogger et al., 2017), the larger-scale effects are rather elusive and the literature is rather fragmented. To the best of the authors' knowledge, no literature review has been published on the impacts of soil compaction on flood processes at the catchment scale. The main aim of this review is to summarise current knowledge on the subject in an organised way, identify gaps and propose new avenues to better understanding soil compaction effects on floods. While the focus is on soil compaction effects on floods, we refer to land use instead of soil compaction in cases where the degree of compaction is not specifically quantified in the literature.

2. Soil compaction processes

2.1. Types and causes of soil compaction

Compaction is defined as an increase in soil bulk density and reduction in soil porosity (Boone, 1988; da Silva et al., 1994). In contrast, soil shearing does not necessarily reduce soil porosity, but does destroy the continuity of macropores (e.g., Horn et al., 1995; Alaoui et al., 2011a). Together they are referred to as soil deformation (e.g., Alaoui et al., 2011a).

The ability of a soil to resist non-recoverable deformation during loading (the soil strength) is influenced by several factors such as texture, structure, organic matter content and in particular the soil water content (Gill and Vanden Berg, 1967; Horn, 1988). The behaviour of a soil during loading is therefore usually examined as a function of soil water content (Young and Warkentin, 1966). Soil strength can be estimated from stress-strain relationships obtained from laboratory experiments (Casagrande, 1936) or from pedo-transfer functions (Van den Akker, 2004; Horn and Fleige, 2003). The vulnerability to compaction may be assessed by comparing soil strength with the vertical loading. Soil compaction may affect the surface and the subsurface.

Surface (topsoil) compaction: Compaction at the soil surface (down to the depth reached by tillage) may result from stock grazing (trampling) and traffic loading (Table 1). Trampling effects depend on stock density, animal weight, hoof size, soil moisture, soil type, plant type and field slope (e.g., Zhao et al., 2010; Krümmelbein et al., 2006). It mainly affects the pore geometry at the soil surface (Nie et al., 2001; Vzzotto et al., 2000) and the topsoil matrix (Alaoui and Helbling, 2006). It may reduce the number of earthworms, resulting in an additional reduction in infiltration (e.g., Hills, 1971). The compaction depth does not usually exceed 10 cm (Greenwood and McKenzie 2001). Surface compaction may result from traffic loading, especially from tractors with mounted or trailed implements. Below the contact surface between soil and tire, the soil deforms under normal and shear stresses (e.g. Horn and Rostek, 2000). The shear stress rises sharply with an increase in traction force and wheel slip, which may lead to the detachment of a weak topsoil layer vulnerable to erosion and surface runoff (Battiato et al., 2013). Tractor passes can form an anisotropic soil pore system due to the simultaneous movement of particles forward and downwards and to wheel slippage (Pagliai et al., 2003; Peng and Horn, 2008). The changes can form a platy structure in the upper few centimetres with elongated pores that are oriented parallel to the soil surface. These pores are not vertically continuous and induce mainly horizontal water fluxes (Horn et al., 2003; Pagliai et al., 2003).

Subsurface (subsoil) compaction: The mechanical strength of structured (characterized by the matrix and macropore domains) soils mainly depends on aggregation, actual and maximum predrying, and the composition and arrangement of the pore system

Table 1
Types and causes of soil compaction.

Type of compaction	Description/causes	Example references
Traffic loads	The principal causes of compaction are compressive forces applied to compressible soil from wheels under tractors, trailers and harvesters, during the passage of tillage implements on the soil (particularly powered rotary equipment)	Hamza and Anderson (2005), Arvidsson et al. (2002), Milne and Haynes (2004)
Cattle grazing/stock trampling	Trampling-induced soil compaction in a pasture characterized by its spatially heterogeneous distribution. It mainly affects pore geometry (or structure) at the soil surface (surface compaction)	Alaoui et al. (2011a), Krümmelbein et al. (2006), Vzzotto et al. (2000)
Puddling	Tillage induced compaction of the subsoil in paddy rice fields leading to hardpans during cultivation in water saturated conditions	Samson et al. (2002)
Urbanization	Caused by the use of heavy machinery, the relocation of building materials, and trampling by humans, especially near sidewalks or driveways, at construction sites, and in public green spaces	Edmonson et al. (2011), Jim (1998), Pouyat et al. (2007)
Industrial activities	Caused during extraction of minerals, installation of underground pipelines or remodelled landscapes using heavy machinery	Batey (2009), Batey and McKenzie (2006)

(Horn and Rostek, 2000). The more negative the pore water pressure, the more pronounced is the strength increase. Thus, under humid climatic conditions soils usually get weaker with depth. Subsoil compaction risks increase with farm size, machine weight (e.g., harvester) and the drive for greater productivity. Once subsoil damage occurs, it can be extremely difficult and expensive to alleviate (Jones et al., 2003). Usually, the first pass of a wheel causes a major portion of the total topsoil compaction (Bakker and Davis, 1995; Botta et al., 2006; Silva et al., 2008), whereas repeated traffic with low axle loads can affect the subsoil (Balbuena et al., 2000; Hamza and Anderson, 2005).

2.2. Soil properties

2.2.1. Soil structure

Laboratory experiments have shown that the inter-aggregate structure of soils is more susceptible to compaction than the soil aggregates themselves (Li and Zhang, 2009). Macroporosity is therefore more sensitive to compaction than total porosity (Alakukku, 1996). Jégou et al. (2002) showed that soil compaction decreases the continuity of burrow systems. Soils with mainly horizontal pores are more susceptible to compaction than those with vertical pores (Hartge and Bohne, 1983; Schäffer et al., 2008).

2.2.2. Soil texture

The degree of compaction (actual bulk density expressed as a percentage of the reference-compaction state of a given soil, Håkansson and Lipiec, 2000) also depends on soil texture. For example, silt loam soils with low colloid contents are more susceptible than medium or fine textured loamy and clayey soils at low water contents, while sandy soils are only slightly susceptible to soil compaction (Horn et al., 1995). Smith et al. (1997) showed that a loamy soil subjected to varied pressures and moisture contents was resistant to compaction when dried and susceptible to compaction when wet, while a loamy sand soil showed smaller increases in compaction with increasing load and moisture content.

2.2.3. Organic matter

Increases in soil organic matter may reduce compactibility by increasing resistance to deformation and/or by increasing elasticity (rebound effects; Soane, 1990). High organic carbon contents can even reduce soil compaction at high moisture levels in clay and silty clay soils (Smith et al.,1997; Nawaz et al., 2013; Hamza and Anderson, 2005; Smith et al., 1997).

2.2.4. Water content

Soil water content is usually the most important factor influencing soil compaction (Soane and Van Ouwerkerk, 1994; Hamza and Anderson, 2005). Traffic experiments on arable land with heavy excavators (weighing up to 47 tons) showed a decrease in the frequency and volume of macropores down to depths of 0.65 m and 1.0 m for dry and wet soils, respectively (Dumbeck, 1984). Wet conditions in autumn, winter and spring exacerbate the effect of heavy machinery on compaction. Arvidsson et al. (2001) showed that the risk of soil compaction with commonly used machinery in southern Sweden is 100% for spring slurry application and more than 60% after October in sugar beet harvesting. Yung et al. (2010) found that high compaction was due to the footslope staying wetter for a longer period during the spring and early summer because of cover crop residues.

2.3. Time scales of soil compaction

Environmental and management related factors tend to interact on different time scales in driving the temporal dynamics of the structure related soil hydraulic properties (Mapa et al., 1986; Kay, 1990; Bodner et al., 2013). For example, Kohl and Markart (2002) showed that compaction effects are usually largest in autumn after the grazing period, but soils may recover during winter and spring due to freezing/thawing processes, plant root activity and microbial activity. Soils which are wet during critical times of land management operations, such as ploughing and harvesting, can be prone to compaction and structural damage (Earl, 1997; Holman et al., 2003) and can result in long term effects that are mainly observed where a plough pan (a compacted layer that tends to form just below the ploughing depth) develops. A stable, natural soil structure may only be achieved after several years when changing practices from regular soil loosening to no-tillage (Wright et al., 1999). Soils under long term no-tillage with low "self-mulching potential" (low clay and organic matter content) may tend towards high bulk density and low water permeability (Munkholm et al., 2003).

Persistent compaction effects are often observed for the subsoil of agriculturally used fields. Even after their abandonment, soil compaction may be persistent over decades (Kellner and Hubbart, 2016), indicating a long memory effect. Potential factors controlling this memory are land-use, soil type, topography and climate (Cambi et al., 2015; Rogger et al., 2017). For some soils, the compaction may be measurable even after 14 years (Berisso et al., 2012; Etana et al., 2013), and may persist over 30 years if underground pipelines have been installed or the landscape remodelled using heavy machinery (Batey, 2009). The impact of 13 years of cattle grazing was still measurable in a secondary teak forest after 10 years of growth (Zimmermann et al., 2006), and former agricultural plots showed increased runoff 30 years after afforestation (Hümann et al., 2011). While some forest soils tend to recover in a few years (Mace, 1971; Shoulders and Terry,

1978), others take 10–20 years to recover from shallow compaction (Dickerson, 1976; Froehlich, 1979; Jakobsen, 1983). Compaction of deep layers can persist over 100 years (Greacen and Sands, 1980).

2.4. Macropore flow – surface runoff relationship

Macropores (i.e., biopores) represent only 0.23–2.00% of the total soil volume, but may account for about 74–100% of the total water flux (Alaoui and Helbling, 2006). They are the most sensitive pores to compaction. Their volume reduction may significantly reduce vertical infiltration and thus increase surface runoff (e.g., Gerke, 2006; Hendrickx and Flury, 2001; Alaoui, 2015). Severing their connectivity between the top-few centimetres and the underlying macropores additionally reduces infiltration (Alaoui et al., 2011b; Jégou et al., 2002; Alaoui, 2015).

The flow through macropores depends on the initial and boundary conditions and the exchange between the matrix and macropore domains which in turn depends on soil moisture, texture, degree of compaction and organic matter (Kluitenberg and Horton, 1990; Zehe and Blöschl, 2004; McGrath et al., 2009; Larsbo, 2011). Since these variables are rarely known at the field scale (Jarvis et al., 2012), one usually resorts to quantifying their spatially integrated effects as effective hydraulic properties (Blöschl and Sivapalan, 1995). One possibility is to classify these properties into pedons or spatial units (Addiscott and Mirza, 1998; Seyfried and Wilcox, 1995). An interesting observation is that of structural hierarchy (Brewer, 1964; Hadas, 1987; Dexter, 1988; Dexter et al., 2008). The mean sizes of the pores separating the soil aggregates at progressively higher levels are themselves progressively bigger (e.g., Dexter et al., 2008). This structural hierarchy can be extended to the hillslope scale. In humid climates, lateral preferential flow can dominate stream response in catchments with steep slopes and permeable soils on low permeability rocks (Weiler and McDonnell, 2007; Anderson et al., 2009; Cammeraat and Kooijman, 2009). Compaction can affect this hierarchy, possibly resulting in a more heterogeneous spatial distribution of flow processes.

2.5. Mapping soil compaction

When assessing the effects of soil compaction on floods one would ideally like to know the spatial distribution and extent of soil compaction, or at least the soil compaction risk. A number of approaches have been developed for assessing the soil compaction risk although, invariably, they have focused on agricultural applications rather than floods. Van den Akker, (1988, 1994) computed soil stresses due to tractor wheels based on the relationships of Söhne (1958) by dividing the contact area into small units and aggregating the stresses from point loads of all units. Lebert (2010) estimated the soil compaction risk for the arable land in Germany using results of Houšková (2008), while Troldborg et al. (2013) used Bayesian belief networks by combining data from standard soil surveys, land use and expert judgement. D'Or and Destain (2014) computed the preconsolidation stress (determined based on the stress-strain relationship of soil obtained during laboratory compression according to Casagrande (1936)) from pedotransfer functions (Horn and Fleige, 2003), based on pedological, mechanical and hydraulic characteristics within a geostatistical framework. Recently, geophysical techniques for investigating subsurface compaction in agricultural soils have been advanced, such as ground penetrating radar (Lane et al., 2016, Wang et al., 2016, André et al., 2012), although these are usually limited to rather small scales. Mapping methods can be assisted by GPS based modelling of spatial patterns of field traffic intensity (Duttmann et al., 2013).

3. Experimental evidence of soil compaction effects on floods

3.1. Plot scale

Compaction of the topsoil due to tillage practices results in a reduced infiltration capacity and increases the probability of surface runoff formation during heavy precipitation (e.g., Byrd et al., 2002). Furthermore, the spatial variability of compaction due to the trafficked rows and non-trafficked interrows tends to enhance the spatial variability of surface and subsurface flow paths (Liebig et al., 1993; Mohanty et al., 1996). Kim et al. (2010) conducted field experiments on Mexico silt loam with field treatments of uniformly compacted and non-compacted plots. They found an increase in the bulk density of the compacted plot of 8%, and a decrease in saturated hydraulic conductivity of 69%, respectively, which would translate into increased surface runoff. Battiato et al. (2015) studied the effect of slipping driving wheels of agricultural equipment on surface runoff generation during sprinkling experiments. They found that the runoff coefficient increased from 0.79 with a minimum slip of 1% to 1.00 with a maximum slip of 27%, indicating that all the rainwater would be transformed into surface runoff at high slip.

The formation of a plough pan in the subsoil changes the direction of water percolation by impeding vertical infiltration and enhancing interflow. Bertolino et al. (2010), for instance, found that soils in South-eastern Brasilia with a plough pan at about 20 cm depth stay longer saturated after rainfall events and favour surface runoff during intense rainy periods. Singh and Hadda (2014) reported a decrease in the infiltration rate with increasing subsoil compaction. They observed a decrease in infiltration rate by a factor of 2.0–2.3 under two different treatments of their sandy loam soil. The decrease in infiltration rate and cumulative infiltration was due to a decrease in total porosity under higher subsoil compaction.

Using infiltration and dye tracer experiments, supplemented by soil textural and structural data, Alaoui et al. (2012) investigated flow pathways on grassland and forest hillslopes in order to identify the controls of surface runoff generation. They showed that the two types of land use lead to different flow processes, mainly vertical infiltration for the forest soil and mainly surface runoff for the grassland soil (Fig. 1). This is due to the larger root water uptake by trees, and thus lower soil moisture, and the larger unsaturated hydraulic conductivity of forest soils as compared to compacted grassland soils. The low efficiency of grassland soil macropores in transporting water vertically downward can be explained by (i) the fine and dense topsoil layers caused by the land use that limits water fluxes into the underlying macropores and (ii) their restricted number, their tortuosity, and the restricted interaction between macropores and the matrix below the topsoil layer. The larger root water uptake of forest soil as compared to grassland soil can be viewed as an additional factor enhancing its storage capacity (difference between total porosity and maximal soil moisture measured during infiltration) and, consequently, may reduce the generation of surface runoff. Storage capacity may provide key information on the strength of macropore flow and the interaction between macropores and the soil matrix that are highly sensitive to the degree of soil compaction (e.g., Alaoui, 2015).

3.2. Hillslope scale

At the hillslope scale, changes in the soil structure due to mechanical stresses resulting from tillage practices or cattle trampling can increase lateral fluxes in the topsoil (interflow) and surface runoff (Doerner and Horn, 2006). At the soil surface, structure-degraded or crusty soils caused by a lack of soil cover or by heavy

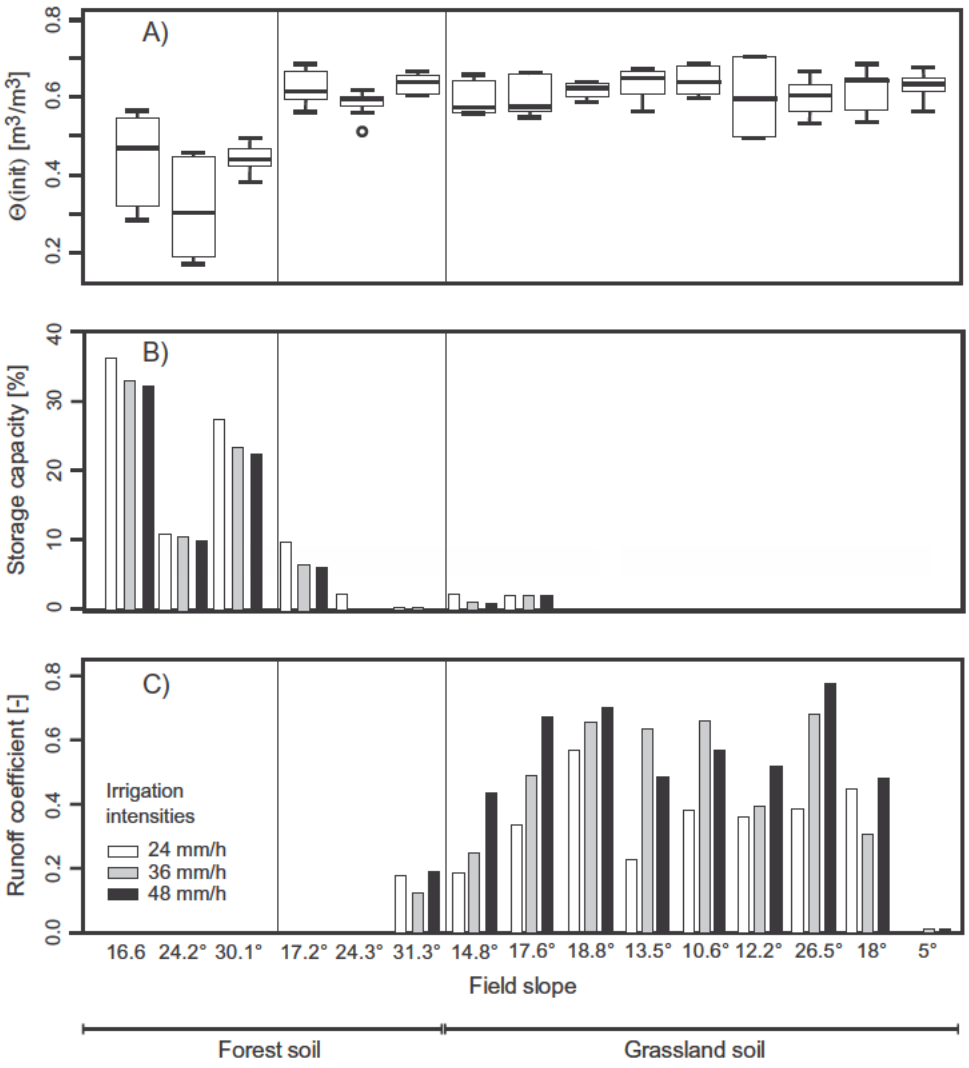

Fig. 1. Measured soil moisture variation before irrigation with median, upper and lower quartiles, outer fences, and outliers, confidence interval of 95% (A); storage capacity (B); and runoff coefficient specific to an individual irrigation (defined as surface runoff divided by the corresponding rainfall, both measured during one hour and expressed as depth over plot area in mm (C) for forest and grassland soils at plots in the Bernese Oberland, Switzerland. In A, each box contains 9 measurements at the topsoil during three irrigation intensities (Alaoui et al., 2012, modified).

agricultural machines, may lead to ponding of water or overland flow in sloping landscapes and potentially to increased erosion (Battiato et al., 2015). At the hillslope scale, the conditions that affect surface runoff generation have often been investigated using sprinkling experiments. Scherrer et al. (2007) conducted sprinkling experiments on 60 m^2 hillslope sites at 18, mainly grassland, locations in Switzerland with rates of 50–100 mm/h during 3–6 h. They found that infiltration inhibitors, such as compacted topsoils in combination with surface sealing, and permanently hydrophobic humus in combination with poor macropore development were linked to surface runoff excess in some locations. Attributes such as vegetation, slope, soil clay content and antecedent soil moisture were not directly linked to surface runoff excess. Other studies showed that compaction of water repellent, dry soils in forested catchments may lead to a 'temporary' Hortonian overland flow (e.g., Badoux et al., 2006; Schwarz, 1986; Kohl et al., 1997; Markart et al., 2004).

3.3. Catchment scale

The catchment evidence reported in the literature is mostly related to stock trampling effects (e.g., Holman et al., 2003; Pattison and Lane, 2011). Stocking densities have recently increased in a number of countries and this has been correlated with increasing floods. For example, in Wales, 72% of the agricultural land was under grassland production to support sheep farming in 2005. Sheep numbers in the UK increased from 19.7 million in 1950 to 40.2 million in 1990 (Fuller and Gough, 1999). Stock tends to reduce the vegetation cover, which may lead to soil surface crusting and reduced overland flow resistance (Ferrero, 1991). It may also lead to a decrease in evapotranspiration (Owens et al., 1997). Heathwaite et al. (1990) found that infiltration capacity was reduced by 80% on grazed areas compared to fields with no stock. Overall, stock trampling may impact on runoff generation and, possibly, downstream flood risk (Pattison and Lane, 2011). For example, in the Derwent catchment sheep stocking rates doubled between 1944 and 1975 which coincided with a runoff increase of 25% (Evans, 1996). Similarly, increasing flow peaks in the upper catchment of the River Lune was qualitatively related to increased stock densities (Orr and Carling, 2006). Within the Yorkshire Ouse catchment, over 40% of the sites investigated after the autumn 2000 floods had high soil degradation, and this was estimated to have caused a runoff increase of between 0.8% and 9.4% (Holman et al., 2003). Heathwaite et al. (1989) found that

7% of the rainfall was converted to runoff in ungrazed fields, while this increased to 53% in grazed fields.

Although urban soils are often thought to be of poor quality and highly compacted (Lorenz and Lal, 2009; Pickett and Cadenasso, 2009), little attention has been paid to its impact on floods (Edmondson et al., 2011). Arnold and Gibbons (1996) and White and Greer (2006) concluded that storm runoff and peak flow increase with urban development as the proportion of impervious land increases. For example, Mercer Creek, an urban stream in western Washington, had an earlier and higher peak discharge, and a larger volume, during a one-day storm on February 1, 2000 than Newaukum Creek, a nearly rural stream (Konrad, 2016). In general, runoff increases with the fraction of built-up area in a catchment, but the relationship is not necessarily linear (Chen et al., 2015). Importantly, the location of built-up area within the catchment matters because of spatial flow connectivity (Warburton et al., 2012; Sanyal et al., 2014).

4. Modelling evidence of soil compaction on floods

Numerous studies have attempted to relate land use changes and flood changes based on hydrological modelling (Table 2). In this review we have included studies that are not strictly on soil compaction but more generally on land use to put soil compaction into a broader context. The studies fall into three groups: (i) increasing areas of compacted soils (Grayson et al., 2010; Schilling et al., 2014a,b; Peña et al., 2016; Fohrer et al. 2001); (ii) changes in rainfall exacerbated by highly degraded and compacted soils (e.g., Viglione et al., 2016; Holman et al., 2003), and (iii) soil

Table 2
Modelling evidence of land use change and soil compaction effects on peak discharge at the catchment scale.

References	Model/ Approach	Catchment/area	Land use distribution	Data used and analysis	Main outcomes
Grayson et al. (2010)	Storm hydrograph data	Trou Beck (UK) (11.4 km^2)	Blanket peat: 75%	Weather station Gauging stations Hourly measurements of surface runoff at plot scale Soil properties obtained from a combination of data collected from previous study and visual soil examination	Peak flows are significantly higher and lag times shorter when blanket peat cover is reduced.
Schilling et al. (2014a, b)	SWAT model	Raccoon River watershed (USA) (9400 km^2)	Agricultural area with row crop of corn and soybean: 76%; agricultural grassland: 17%; forest: 4%; urban areas; water: 1%.	No direct measurements of soil properties were performed Soil layer data obtained from the Soil Survey Geographic database to characterize soil properties	Converting all cropland to perennial vegetation drastically reduced peak discharge. Converting half of the land to perennial vegetation or extended rotations reduced flooding potential.
Peña et al. (2016)	TETICS, conceptual distributed hydrological model	Combeima River catchment (Columbia) (217 km^2)	1) Grassland (increase by 37.5%): forest (decrease by 32.1%); crops decrease by 6.2%) from 1991 to 20002) Forest (increase by 7.0%); crops (increase by 55.9%); grassland (decrease by 30.5%)	No direct measurements of soil properties were performed (obtained using pedo-transfer function) Existing land use historical evolution Hydrometric station Weather stations	1) First changes in land use produced an increase of 2.1% of mean annual maximum flow. 2) secondary changes produced a 7.0% decrease in the maximum annual flows.
Fohrer et al. (2001)	SWAT model	Dietzhölze watershed (Germany) (82 km^2)	Forest: 55.4%; fallow area: 27.6%; grassland: 10.1%; field crop: 0.5%.	No direct measurements of soil properties were performed (crop, soil and tillage parameters were obtained from regional data sets and literature) Daily weather data Calibration and validation were performed using streamflow measurements	The decrease of forest due to an increase of grassland amplifies the peak flows and thus risk of flooding.
Viglione et al. (2016)	Finger printing attribution	97 catchments (Austria) (areas ranging from 10 to 79,500 km^2)	Intensification of agriculture with heavy machines (area not specified)	Hourly and daily precipitation data of 900 rainfall stations	Precipitation change is the main driver of increasing flood trends in Upper Austria. For small catchments, land use change plays an important role.
Holman et al. (2003)	SCS Runoff Curve Number (CN) method	4 catchments (UK): Ouse (4829 km^2); Severn (9753 km^2); Bourne 853 km^2); Uck (103 km^2)	Agricultural area (%): Ouse (71); Severn (73); Bourne (47); Uck (53). Related structural degradation mainly due to compaction may have occurred over 45% of the Severn, 30–35% of the Ouse and Uck, and 20% of the Bourne.	No direct measurements of soil properties were performed (detailed observations of soil horizon properties at the pedon scale) Soil structural degradation was qualitatively linked to the type of management system to illustrate the potential magnitude of the hydrological impact of the extrapolated soil structural degradation	Excess rapid response runoff during autumn floods of 2000 was related to the highly degraded and compacted soils in fodder maize fields (due to harvesting under wet soil conditions).
Roy and Mistri (2013)	Kinematic wave, SCS Curve Number Method	Kunur River Basin (India) (922.40 km^2)	Low infiltration rate with fine sandy loam, dense forest, and degraded wood: 55%; Fine clay to silt soil with agricultural land (35%); moderate infiltration rate with coarse texture land, pasture, and open scrap area (7%); urban area (3%)	No direct measurements of soil properties were performed Curve number of the watershed was obtained from Soil Conservation Service to link land use, soil characteristics and peak discharge	Peak flood discharge was mainly due to the low infiltration capacity of the fine material covering 55% of the basin (e.g., degraded wood land) and agricultural land (35%).

type effects, i.e. fine texture and low infiltration capacity of degraded forest and wood land soils (Roy and Mistri, 2013).

4.1. Area of compaction

Most studies reviewed found a direct relationship between increased area of compacted soil and peak discharge. Grayson et al. (2010) reported that the storm hydrograph in their 11.4 km^2 catchment was significantly affected by the area of bare peat, so revegetation of eroded blanket peatland could be beneficial in reducing flood peaks. Schilling et al. (2014a,b) suggest that land afforestation in the Raccoon River watershed could reduce both the number of flood events and the frequency of severe floods. Peña et al. (2016) analysed the relationship between changes in topsoil hydraulic properties (static storage capacity and saturated hydraulic conductivity) due to changes in land use and peak flows using a conceptual distributed hydrological model (Table 2). In their study, grassland area increased by 37.5% while forests and crops decreased by 32.1 and 6.2%, respectively, between the 1991 and 2000 scenarios. These changes produced an increase of 2.1% in the mean annual floods. In the 2007 scenario, forest and crop areas were increased by 7.0% and 55.9%, while grassland was decreased by 30.5% compared to the 2000 scenario which translated in a 7.0% decrease of the mean annual floods. Fohrer et al. (2001) used the SWAT (Soil and Water Assessment Tool) model to quantify the hydrologic response of several catchments to land use change and noted that a decrease in forest cover may amplify flood peaks for the Dietzhölze catchment in Germany.

The outcomes cited above are supported by other studies. Hess et al. (2010) modelled the impacts of improved soil conditions on peak discharges across England and Wales. They showed that changes in land management can reduce small floods while the effect on large flood peaks (100 year floods) is less than 5%. McIntyre and Marshall (2010) proposed that agriculturally improved grassland (which at some point had been drained, ploughed and fertilized) produces a flashier response than grassland in a more natural condition in the UK. Naef et al. (2002) modelled the effect of converting pasture to forest showing that fast-response dominant runoff processes may become slower. However, subsurface flow processes, occurring mainly in the deep soil layers or in the bedrock, are often outside the sphere of influence of land use change. Yan et al. (2013) attributed changes in streamflow to changes in the extent of farmland, forest and urban areas in a Chinese catchment while Chen et al. (2015) reported a direct relationship between rapid urbanisation and peak discharge.

4.2. Rainfall and compaction

While the studies mentioned above have focused on a single driver, a number of multidriver studies have been published recently. For example, Villarini and Strong (2014) and Prosdocimi et al. (2015) considered precipitation and a land use indicator as covariates in US and UK contexts, respectively. While Villarini and Strong (2014) attributed flood changes to rainfall variability changes, Prosdocimi et al. (2015) focused on the dominant role of urbanisation. Viglione et al. (2016) reported precipitation change to be the main driver of increasing flood trends in Upper Austria, while they identified land use change as an important driver in small catchments (Fig. 2). They reasoned that the effect of land use change on floods decreases with catchment area due to a shift in runoff generation mechanisms. In small catchments with short response times, floods are mostly generated by high intensity, short duration storms, so the infiltration excess mechanism is dominant. In large catchments with long response times, floods are mostly generated by low intensity, long duration storms, so the saturation excess mechanism is dominant. Since land use change affects the infiltration excess mechanism more strongly (through reduced infiltration capacity associated with soil compaction) than the saturation excess mechanism, the land use change effect on floods decreases with catchment area (Fig. 2). In their four UK catchments, Holman et al. (2003) showed that rapid response runoff during the autumn floods of 2000 was related to the widespread highly degraded and compacted soils in fodder maize fields due to harvesting under wet soil conditions. At larger catchment scales, agricultural land management does not seem to have affected flooding in the UK (O'Connell et al., 2007) which suggests that the effect of compaction does decrease with catchment area.

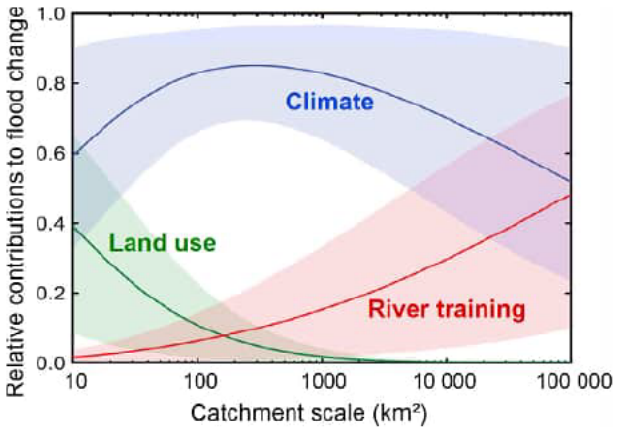

Fig. 2. Attribution of observed trends of mean annual floods in Upper Austria (1950–2012, 97 catchments) to land use change (intensification of agriculture with heavy machines), climate and river training, y axis is dimensionless (from Viglione et al., 2016).

4.3. Soil texture exacerbating compaction effects

The effect of compaction on increasing peak discharges may be enhanced if topsoils are fine textured with low infiltration capacities. Roy and Mistri (2013) showed a direct relationship between the extent of area covered by fine material and peak discharge in their Kunur watershed (India). Based on the hydrological soil groups, the areas with particularly large peak discharges were characterized by fine sandy loam, dense forest and degraded wood land (55%), followed by areas characterized by fine clay to silt soils and agricultural land use (35%). Similarly, Alaoui et al. (2011b) found that, compared to forest hillslopes, grassland hillslopes had higher micropore volumes in the topsoil down to 0.35 m. The topsoils of the hillslopes that generated surface runoff had higher clay contents than the hillslopes without surface runoff. As clay content was closely correlated with micropore volume, the authors concluded that the high clay content enhances matrix flow, delays water routing into the macropores, and thus increases surface runoff.

5. Research gaps

Research gaps on soil compaction effects on floods mainly remain at the medium and large catchment scales, and in particular regarding the question whether the effects really decrease with area and why. We consider the following to be key research gaps.

5.1. Areal coverage

A first order control of the effect on floods is the total area of soil compaction within a catchment which, however, can vary tremendously in space and time depending on agricultural practices (Fiener et al., 2011; Green et al., 2003). Methods are needed to

reliably map soil compaction in the landscape. These may be based on a combination of field surveys, spatial soil data and, possibly, remote sensing.

5.2. Patchiness/Connectivity

The spatial arrangement of compacted soils may be equally important as their area per se. This is because of the role of spatial connectivity and patchiness on runoff generation and routing from the hillslope to the catchment scales (Western et al., 1998). A better understanding of the effects of connectivity and location would be useful for deriving scaling relationships for upscaling land-use change effects to the catchment scale.

5.3. Temporal variability

The seasonal variability in topsoil compaction due to regular agricultural practices such as harvesting and subsequent field traffic is important for flood generation, if maximum rainfall coincides with maximum compaction during the year. Current models do not account for this variability. More research is needed on understanding these links across scales.

5.4. Feedbacks

Many of the processes involved in compaction effects on floods are interlinked (Rogger et al., 2017). For example, the mechanical and hydraulic processes during soil deformation are coupled, which exacerbates soil compaction since more compact soils generally remain wet for a longer time of the year. Identifying the most important feedbacks related to soil compaction processes is therefore of key interest for upscaling their impacts to the catchments scale.

5.5. Masking

In most instances, changes in floods at the catchment scale are related to more than one control, including climate and river training. Quantitative knowledge of these components is necessary to isolate the impact of soil compaction on floods. Blöschl et al. (2007) and Viglione et al. (2016), among others, suggested that the impact of land use on floods decreases with catchment scale, but more quantitative analyses in different climates are needed to attribute flood changes to their drivers including soil compaction.

5.6. Model parameterization

Studies on land-use change impacts at the catchment scale currently are mostly modelling studies that are based on assumptions of how model parameters change with changing land-use (e.g. Salazar et al., 2012). An important task is to improve soil compaction parameterization at the hillslope and catchment scales. The parameterizations should account for flow connectivity and patchiness.

6. Ways forward

We believe that the research gaps summarised above can be addressed by focusing on four research strands: (i) synthesizing past research related to soil compaction and runoff by meta analyses, (ii) complementing this knowledge by additional field experiments, (iii) developing novel methods for mapping soil compaction, and (iv) learning from disciplines such as agricultural sciences and soil physics where extensive knowledge on soil compaction exists.

6.1. Meta analyses

As suggested by Rogger et al. (2017) comparative meta analyses of existing studies related to soil compaction and runoff processes would be a first step towards generalising the findings from individual case studies (see, e.g., Koricheva and Gurevitch, 2014; Mutema et al., 2015). Soil compaction studies have often been performed in agricultural contexts, but do address very relevant information related to flood processes such as changes in pore structure, hydraulic conductivity and bulk density. To facilitate future meta-analyses it would be important for publications to fully report the relevant information, ideally in a consistent way (Koutsoyiannis et al., 2016). Data on soil physical properties measured in the field, compaction assessments and maps of compaction susceptibility of soils should be made publically available in a similar way as the European Hydropedological Data Inventory (EU-HYDI, Tóth et al., 2013) and the HYPRES-database (Wösten et al., 1999).

6.2. Additional field experiments

Existing long-term experimental sites should be upgraded to better address the question of soil compaction effects on floods. Specifically, the evolution of hydraulic soil characteristics and its dynamics during the year, including changes in the macropore volume, connectivity and functionality, should be monitored over long periods of time in addition to runoff. Of particular interest is the memory effect of soils, i.e. how fast a change in soil conditions translates into a corresponding change in flood characteristics. In order to obtain a mechanistic description of the coupled mechanical and hydraulic processes, tailored field experiments should be conducted. These would consist of treatment and wheeling experiments on plots under different crop management practices and soils, where soil deformation and stress-strain processes are measured as well as the stress induced changes in hydraulic conductivity and their time dependency during loading and soil deformation. This research should build on the findings of the meta-analyses mentioned above.

6.3. Mapping soil compaction

There is a lot of potential in developing new mapping methods that may assist in understanding the spatial compaction patterns and thus upscaling compaction effects to the catchment scale (Blöschl, 2006). Data from geophysical techniques such as ground penetrating radar (Lane et al., 2016), GPS based modelling of field traffic (Duttmann et al., 2013) and perhaps remote sensing data (e.g., Ryan et al., 2014; Joshi et al., 2016) could be combined. Since soil compaction may persist over decades, knowledge of the land use history would be a benefit.

6.4. Bridging gap between different disciplines

Collaborations between hydrology and sister disciplines has dramatically increased in the recent decade, but there is room for improvement in particular regarding soils. Bringing soil science, pedology, agricultural sciences and hydrology closer together through joint projects, conferences and publications would assist in a more permanent contribution to advancing science. Batey (2009) noted that "*several authors recommend that monitoring of soil physical conditions, including compaction should be part of routine soil management*". We suggest that monitoring compaction

processes would also be of enormous benefit for water management.

7. Conclusions

Based on the literature review, we can distinguish three ways in which soil compaction impacts peak discharge at the catchment scale: (i) by an increase in the area affected by soil compaction; (ii) by changes in rainfall events, exacerbated by highly degraded soils; and (iii) by coincidence of soil compaction with fine topsoils in degraded lands. More specifically, the following conclusions can be drawn on the effects of soil compaction on floods:

1. Experimental studies at the plot and hillslope scales suggest consistent evidence of the impact of soil compaction on increasing surface runoff. Locally, compaction tends to reduce infiltration and increase surface runoff. With increasing scale, the tendency of reduced infiltration and increased surface runoff persists, but is modulated by numerous other factors such as surface sealing, permanently hydrophobic humus, and poor macropore development. At the catchment scale, studies tend to be more speculative as most of the evidence comes from non quantitative reasoning. Increasing floods in some regions were attributed to increased stocking densities, as suggested by marked differences of surface runoff between grazed and ungrazed fields. The literature suggests that storm runoff increases with urban development as the proportion of impervious land increases, but this relationship is not necessarily linear. The location of built-up area within the mosaic of land uses may affect the spatial flow connectivity and consequently surface runoff in many ways.
2. Modelling studies suggest that soil compaction may affect peak discharges at the catchment scale, but the magnitude of this effect varies between studies. In small catchments with short response times, floods are mostly generated by the infiltration excess mechanism from high intensity, short duration storms. In this case, the reduction of infiltration capacity by soil compaction can have a major effect on flood peaks. In large catchments, where floods are often produced by the saturation excess mechanism from lower intensity, longer duration storms, the effect of soil compaction of flood peaks is less obvious. Overall, soil compaction effects on floods tend to increase with the size of the compacted area, but its spatial arrangement in the landscape does matter.
3. Research gaps include the reliable mapping of soil compaction in the landscape, understanding the patchiness of compacted soils and the spatial connectivity of flow paths. They also include a better understanding of the temporal variability of compacted soil characteristics, feedbacks between floods and soil compaction at different time scales, and unravelling the multitude of factors that may mask the relationship between soil compaction and floods. Future research and funding should give high priority to understanding the links between soil compaction and floods at the catchment scale, as it will provide key information on one of the important drivers of floods.

Acknowledgements

The present work was developed within the framework of the Panta Rhei Research Initiative of the International Association of Hydrological Sciences (IAHS) as a contribution of the Working Groups "Understanding Flood Changes" and "Changes in Flood Risk." Funding was partly provided by the Austrian Science Foundation (FWF projects I 3174-N29 and P 23723-N21), the SYSTEM-RISK project (EU grant 676027) and the European Research Council, Flood Change project (ERC advanced grant 291152). We also would like to thank the handling editor as well as the three reviewers for their constructive comments which considerably improved this paper.

References

Addiscott, T.M., Mirza, N.A., 1998. Modelling contaminant transport at catchment or regional scale. Environ. Manage. 27 (1), 211–221.
Alakukku, L., 1996. Persistence of soil compaction due to high axle load traffic: I. Short-term effects on the properties of clay and organic soils. Soil Till. Res. 37, 211–222.
Alaoui, A., 2015. Modelling susceptibility of grassland soil to macropore flow. J. Hydrol. 525, 536–546. https://doi.org/10.1016/j.jhydrol.2015.04.016.
Alaoui, A., Helbling, A., 2006. Evaluation of soil compaction using hydrodynamic water content variation: comparison between compacted and non-compacted soil. Geoderma 134, 97–108.
Alaoui, A., Lipiec, J., Gerke, H.H., 2011a. A review of the changes in the soil pore system due to soil deformation: A hydrodynamic perspective. Soil Tillage Res. 115–116, 1–15.
Alaoui, A., Caduff, U., Gerke, H.H., Weingartner, R., 2011b. Preferential flow effects on infiltration and runoff in grassland and forest soils. Vadose Zone J. 10, 367–377.
Alaoui, A., Spiess, P., Beyeler, M., Weingartner, R., 2012. Up-scaling surface runoff from plot to catchment scale. Hydrol. Res. 43 (4). https://doi.org/10.2166/nh.2012.057.
Anderson, S.H., Udawatta, R.P., Seobi, T., Garrett, H.E., 2009. Soil water content and infiltration in agroforestry buffer strips. Agrofor. Syst. 75, 5–16.
André, F., van Leeuwen, C., Saussez, S., Van Durmen, R., Bogaert, P., Moghadas, D., de Rességuier, L., Delvaux, B., Vereecken, H., Lambot, S., 2012. High-resolution imaging of a vineyard in south of France using ground-penetrating radar, electromagnetic induction and electrical resistivity tomography. J. Appl. Geophys. 78, 113–122.
Arnold Jr., C.L., Gibbons, C.J., 1996. Impervious surface coverage: the emergence of a key environmental indicator. J. Am. Plann. Assoc. 62 (2), 243–258.
Arvidsson, J., Trautner, A., van den Akker, J.J.H., Schjønning, Per, 2001. Subsoil compaction caused by heavy sugarbeet harvesters in southern Sweden: II. Soil displacement during wheeling and model computations of compaction. Soil and Tillage Res. 60 (1–2), 79–89. https://doi.org/10.1016/S0167-1987(01)00168-4. ISSN 0167-1987.
Arvidsson, J., Trautner, A., Keller, T., 2002. Influence of Tyre Inflation Pressure on Stress and Displacement in the Subsoil. In: Pagliai, M., Jones, R. (Eds.), Sustainable Land Management – Environmental Protection. A Soil Physical Approach, Advances in Geoecology, 35. Catena Verlag, GeoEcology, Reiskirchen, Germany, pp. 331–338.
Badoux, A., Witzig, J., Germann, P.F., Kienholz, H., Lüscher, P., Weingatner, R., Hegg, Ch., 2006. Investigations on the runoff generation at the profile and plot scales, Swiss Emmental. Hydrol. Process. 20, 377–394.
Bakker, D.M., Davis, R.J., 1995. Soil deformation observations in a Vertisol under field traffic. Aust. J. Soil Res. 33, 817–832.
Balbuena, R.H., Terminiello, A.M., Claverie, J.A., Casado, J.P., Marlats, R., 2000. Soil compaction by forestry harvester operation. Evolution of physical properties. Revista Brasileira de Engenharia Agricola e Ambiental 4, 453–459 (in Spanish).
Batey, T., 2009. Soil compaction and soil management – a review. Soil Use Manag. 25, 335–345.
Batey, T., McKenzie, M., 2006. Soil compaction: identification directly in the field. Soil Use Manage. 22, 123–131.
Battiato, A., Alaoui, A., Diserens, E., 2015. Impact of normal and shear stresses due to wheel slip on hydrological properties of an agricultural clay loam: experimental and new computerized approach. J. Agricul. Sci. 7 (4), 1–15.
Battiato, A., Diserens, E., Laloui, L., Sartori, L., 2013. A mechanistic approach to topsoil damage due to slip of tractor tyres. J. Agric. Sci. Appl. 2 (3), 160–168.
Berisso, F.E., Schjønning, P., Keller, T., Lamandé, M., Etana, A., de Jonge, L.W., Iversen, B.V., Arvidsson, J., Forkman, J., 2012. Persistent effects of subsoil compaction on pore size distribution and gas transport in a loamy soil. Soil Tillage Res. 122, 42–51. https://doi.org/10.1016/j.still.2012.02.005. ISSN 0167-1987.
Bertolino, A.V.F.A., Fernandes, N.F., Miranda, J.P.L., Souza, A.P., Lopes, M.R.S., Palmieri, F., 2010. Effects of plough pan development on surface hydrology and on soil physical properties in Southeastern Brazilian plateau. J. Hydrol. 393, 94–104. https://doi.org/10.1016/j.jhydrol.2010.07.038. ISSN 0022-1694.
Birkas, M., 2008. Environmentally sound adaptable tillage. Akademia Kiado, Budapest, Hungary.
Blöschl, G., Ardoin-Bardin, S., Bonell, M., Dorninger, M., Goodrich, D., Gutknecht, D., Matamoros, D., Merz, B., Shand, P., Szolgay, J., 2007. Atwhat scales do climate variability and land cover change impact on flooding and low flows? Hydrol. Processes 21, 1241–1247. https://doi.org/10.1002/hyp.6669.
Blöschl, G., 2006. Hydrologic synthesis - across processes, places and scales. Special section on the vision of the CUAHSI National Center for Hydrologic Synthesis (NCHS). Water Resour. Res. 42. article number W03S02.
Blöschl, G., Hall, J. Parajka, R. A. P. Perdigão, B. Merz, B. Arheimer, G. T. Aronica, A. Bilibashi, O. Bonacci, M. Borga, I. Canjevac, A. Castellarin, G. B. Chirico, P. Claps, K. Fiala, N. Frolova, L. Gorbachova, A. Gül, J. Hannaford, S. Harrigan, M. Kireeva, A. Kiss, T. R. Kjeldsen, S. Kohnová, J. J. Koskela, O. Ledvinka, N. Macdonald, M.

Mavrova-Guirguinova, L. Mediero, R. Merz, P. Molnar, A. Montanari, C. Murphy, M. Osuch, V. Ovcharuk, I. Radevski, M. Rogger, J. L. Salinas, E. Sauquet, M. Šraj, J. Szolgay, A. Viglione, E. Volpi, D. Wilson, K. Zaimi and N. Živkovic, 2017. Changing climate shifts timing of European floods. Science, 357 (6351) 588–590, doi: 10.1126/science.aan2506.

Blöschl, G., Sivapalan, M., 1995. Scale issues in hydrological modelling – a review. Hydrol. Process. 9, 251–290.

Bodner, G., Scholl, P., Loiskandl, W., Kaul, H.-P., 2013. Environmental and management influences on temporal variability of near saturated soil hydraulic properties. Geoderma 204–205, 120–129.

Botta, G., Jorajuria, D., Rosatto, H., Ferrero, C., 2006. Light tractor traffic frequency on soil compaction in the Rolling Pampa region of Argentina. Soil Till. Res. 86, 9–14.

Boone, F.R., 1988. Weather and other environmental factors influencing crop responses to tillage and traffic. Soil Till. Res. 11, 283–324.

Brewer, R., 1964. Fabric and Mineral Analysis of Soils. John Wiley and Sons (Eds), New York. 482 pp.

Byrd, E.J., Kolka, R.K., Warner, R.C., Ringe, J.M. 2002. Soil Water Percolation and Erosion on Uncompacted Surface Mine Soil in Eastern Kentucky. In: National Meeting of the American Society of Mining and Reclamation, Lexington, KY, June 9-13, 2002. Published by ASMR, 3134 Montavesta Rd., Lexington, KY, 40502.

Cambi, M., Certini, G., Neri, F., Marchi, E., 2015. The impact of heavy traffic on forest soils: A review. Forest Ecology Manage. 338, 124–138.

Cammeraat, E.L.H., Kooijman, A.M., 2009. Biological control of pedological and hydrogeomorphological processes in a deciduous forest ecosystem. Biologia 64, 428–432.

Carroll, Z.L., Reynolds, B. Emmett, B.A., Sinclair, F.L., Ruiz de Ona, C., Williams, P. 2004. The effect of stocking density on soil in upland Wales. Report to Country Council for Wales Report FC 73-02-280. No 630, Centre for Ecology and Hydrology.

Casagrande, A., 1936. The determination of the pre-consolidation load and its practical significance. In: Proceedings of the international conference on soil mechanics and foundation engineering. Harvard University Cambridge, pp. 60–64.

Chen, X., Tian, C., Xu, X., Meng Q, Cui, G., Zhang, Q. Xiang, L., 2015. Analyzing the effect of urbanization on flood characteristics at catchment levels Proc. IAHS 370 2015 33 38 10.5194/piahs-370-33-2015.

da Silva, A.P., Kay, B.D., Perfect, E., 1994. Characterization of the least limiting water range of soils. Soil Sci. Soc. Am. J. 58, 1775–1781.

Dexter, A.R., 1988. Advances in characterization of soil structure. Soil Till. Res. 11, 199–238.

Dexter, A.R., Czyz, E.A., Richard, G., Reszkowska, A., 2008. A user-friendly water retention function that takes account of the textural and structural pores spaces in soil. Geoderma 143, 243–253.

Dickerson, B.P., 1976. Soil compaction after tree-length skidding in northern Mississippi. Soil Sci. Soc. Am. J. 40, 965–966.

Doerner, J., Horn, R., 2006. Anisotropy of pore functions in structured Stagnic Luvisols in the Weichselian moraine region in N Germany. J. Plant Nutr. Soil Sci. 169, 213–220. https://doi.org/10.1002/jpln.200521844.

D'Or, D., Destain, M.F., 2014. Toward a tool aimed to quantify soil compaction risks at a regional scale: Application to Wallonia (Belgium). Soil Till. Res. 144, 53–71.

Dumbeck, G., 1984. Einfluss aussergewöhnlicher Druckbelastung auf das Bodengefüge und die Durchwurzelung. Mitteilungen der Deutschen Bodenkundlichen Gesellschaft 40, 61–62.

Duttmann, R., Brunotte, J., Bach, M., 2013. Spatial analyses of field traffic intensity and modeling of changes in wheel load and ground contact pressure in individual fields during a silage maize harvest. Soil Tillage Res. 126, 100–111.

Earl, R., 1997. Prediction of trafficability and workability from soil moisture deficit. Soil Till. Res. 40, 155–168.

Edmondson, J.L., Davies, Z.G., McCormack, S.A., Gaston, K.J., Leake, J.R., 2011. Are soils in urban ecosystems compacted? A citywide analysis. Biol. Lett. 7, 771–774.

Etana, A. et al., 2013. Persistent subsoil compaction and its effects on preferential flow patterns in a loamy till soil. Geoderma 192, 430–436.

Evans, R., 1996. Soil Erosion and its Impacts in England and Wales. Friends of the Earth, London, p. 121.

Ferrero, A.F., 1991. Effect of compaction simulating cattle trampling on soil physical characteristics in woodland. Soil Till. Res. 19, 319–329.

Fiener, P., Auerswald, K., Van Oost, K., 2011. Spatio-temporal patterns in land use and management affecting surface runoff response of agricultural catchments – a review. Earth-Sci. Rev. 106, 92–104.

Foley, J.A., DeFries, R., Asner, G.P., Barford, C., Bonan, G., Carpenter, S.R., Chapin, F.S., Coe, M.T., Daily, G.C., Gibbs, H.K., Helkowski, J.H., Holloway, T., Howard, E.A., Kucharik, C.J., Monfreda, C., Patz, J.A., Prentice, C., Ramankutty, N., Snyder, P.K., 2005. Global consequences of land use. Science 309, 570. https://doi.org/10.1126/ science.1111772.

Fohrer, N., Haverkamp, S., Eckhardt, K., Frede, H.G., 2001. Hydrologic response to land use changes on the catchment scale. Phys. Chem. Earth. 26, 577–582.

Froehlich, H.A., 1979. Soil compaction from logging equipment: effects on growth of young ponderosa pine. J. Soil Water Conserv. 34, 276–278.

Fuller, R.J., Gough, S.J., 1999. Changes in sheep numbers in Britain: implications for bird populations. Biol. Conserv. 91, 73–89.

Gerke, H.H., 2006. Preferential flow description for structured soils. J. Plant Nutr. Soil Sci. 169, 382–400.

Gill, W.R., Vanden Berg, G.E., 1967. Soil Dynamics in Tillage and Traction, 316. Agricultural Research Service, U.S.D.A., p. 511.

Grayson, R., Holden, J., Rose, R., 2010. Long-term change in storm hydrographs in response to peatland vegetation change. J. Hydrol. 389, 336–343.

Greacen, E.L., Sands, R., 1980. A review of compaction of forest soils. Aust. J. Soil Res. 18, 163–189.

Green, T.R., Ahuja, L.R., Benjamin, J.G., 2003. Advances and challenges in predicting agricultural management effects on soil hydraulic properties. Geoderam 116, 3–27.

Greenwood, K.L., McKenzie, B.M., 2001. Grazing effects on soil physical properties and the consequences for pastures: a review. Aust. J. Exp. Agric. 41, 1231–1250.

Hadas, A., 1987. Long-term tillage practice effects on soil aggregation modes and strength. Soil Sci. Soc. Am. J. 51, 191–197.

Håkansson, I., Lipiec, J., 2000. A review of the usefulness of relative bulk density values in studies of soil structure and compaction. Soil Till. Res. 53, 71–85.

Hall, J., Arheimer, B., Borga, M., Brázdil, R., Claps, P., Kiss, A., Kjeldsen, T.R., Kriaučiūnienė, J., Kundzewicz, Z.W., Lang, M., Llasat, M.C., Macdonald, N., McIntyre, N., Mediero, L., Merz, B., Merz, R., Molnar, P., Montanari, A., Neuhold, C., Parajka, J., Perdigão, R.A.P., Plavcová, L., Rogger, M., Salinas, J.L., Sauquet, E., Schär, C., Szolgay, J., Viglione, A., Blöschl, G., 2014. Understanding flood regime changes in europe: a state of the art assessment. Hydrol. Earth Syst. Sci. 18, 2735–2772. https://doi.org/10.5194/hess-18-2735-2014.

Hamza, M.A., Anderson, W.K., 2005. Soil compaction in cropping systems. A review of the nature, causes and possible solutions. Soil Tillage Res. 82, 121–145.

Hartge, K.H., Bohne, H., 1983. Effect of pore geometry on compressibility of soil and development of rye seedings. Z.f. Kulturtechnik und Flurbereinigung 24, 5–10.

Heathwaite, A.L., Burt, T.P., Trudgill, S.T., 1989. Runoff, sediment, and solute delivery in agricultural drainage basins - a scale dependent approach. In: Ragone, S. (Ed.), Regional characterization of water *quality*. IAHS Publ., pp. 175–191.

Heathwaite, A.L., Burt, T.P., Trudgill, S.T., 1990. Land-use controls on sediment production in a lowland catchment, south-west England. In: Boardman, J., Foster, I.D.L., Dearing, J.A. (Eds.), Soil Erosion on Agricultural Land. John Wiley and Sons, Ltd., Chichester, UK, pp. 70–86.

Hendrickx, J.M.H., Flury, M., 2001. Uniform and preferential flow mechanisms in the vadose zone. In: Conceptual models of flow and transport in the fractured vadose zone. National Academy Press, Washington D.C, pp. 149–187.

Hess, T.M., Holman, I.P., Rose, S.C., Rosolova, Z., Parrott, A., 2010. Estimating the impact of rural land management changes on catchment runoff generation in England and Wales. Hydrol. Process. 24, 1357–1368.

Hills, R.C., 1971. Lateral flow under cylinder infiltrometers–a graphical correction procedure. J. Hydrol. 13, 153–162.

Holman, I.P., Hollis, J.M., Bramley, M.E., Thompson, T.R.E., 2003. The contribution of soil structural degradation to catchment flooding: a preliminary investigation of the 2000 floods in England and Wales. Hydrol. and Earth Syst. Sci. 7 (5), 754–765.

Horn, R., 1988. Compressibility of arable land. Catena Supp 11, 53–71.

Horn, R., Domzał, H., Slowińska-jurkiewicz, A., van Ouwerkerk, C., 1995. Soil compaction processes and their effects on the structure of arable soils and the environment. Soil Tillage Res. 35, 23–36.

Horn, R., Fleige, H., 2003. A method for assessing the impact of load on mechanical stability and on physical properties of soils. Soil Tillage Res. 73, 89–99.

Horn, R., Rostek, J., 2000. Subsoil compaction processes-state of knowledge. Adv. Geoecol. 32, 4–54.

Horn, R., Way, T., Rostek, J., 2003. Effect of repeated tractor wheeling on stress/strain properties and consequences on physical properties in structured arable soils. Soil Till. Res. 73, 101–106.

Houšková, B., 2008. The Natural Susceptibility of Soils to Compaction. Office for the Official Publications of the European Communities, Luxembourg.

Hümann, M., Schüler, G., Müller, C., Schneider, R., Johst, M., Caspari, T., 2011. Identification of runoff processes – The impact of different forest types and soil properties on runoff formation and floods. J. Hydrol. 409, 637–649. https://doi.org/10.1016/j.jhydrol.2011.08.067.

Jakobsen, B.F., 1983. Persistence of compaction effects in a forest Kraznozem. Aust. For. Res. 13, 305–308.

Jarvis, N.J., Moeys, J., Koestel, J., Hollis, J.M., 2012. Preferential flow in a pedological perspective. In: Lin, H. (Ed.), Hydropedology: Synergistic integration of soil science and hydrology. Academic Press, Waltham, MA, pp. 75–120. https://doi.org/10.1016/B978-0-12-386941-8.00003-4.

Jégou, D., Brunotte, J., Rogasik, H., Capowiez, Y., Diestel, H., Schrader, S., Cluzeau, D., 2002. Impact of soil compaction on earthworm burrow systems using X-ray computed tomography: preliminary study. Eur. J. Soil Biol. 38, 329–336.

Jim, C.Y., 1998. Urban soil characteristics and limitations for landscape planting in Hong Kong. Landsc Urban Plan 40 (4), 235–249.

Jones, R.J.A., Spoor, G., Thomasson, A.J., 2003. Vulnerability of subsoils in Europe to compaction: a preliminary analysis. Special Issue of Soil & Tillage Res. on Subsoil Compaction. Soil Till. Res. 73, 131–143.

Joshi, N., Baumann, M., Ehammer, A., Fensholt, R., Grogan, K., Hostert, P., Jepsen, M., Kuemmerle, T., Meyfroidt, P., Mitchard, E., Reiche, J., Ryan, C., Waske, B., 2016. A review of the application of optical and radar remote sensing data fusion to land use mapping and monitoring. Remote Sens. 8, 70. https://doi.org/10.3390/rs8010070.

Kay, B.D., 1990. Rates of change of soil structure under different cropping systems. Adv. Soil Sci. 12, 1–52.

Kellner, E., Hubbart, J., 2016. Agricultural and forested land use impacts on floodplain shallow groundwater temperature regime. Hydrol. Process. 30, 625–636. https://doi.org/10.1002/hyp.10645.
Kim, H., Anderson, S.H., Motavalli, P.P., Gantzer, C.J., 2010. Compaction effects on soil macropore geometry and related parameters for an arable field. Geoderma 160, 244–251.
Kluitenberg, G.J., Horton, R., 1990. Effect of solute application method on preferential transport of solutes in soils. Geoderma 46, 283–297.
Kohl, B., Markart G., 2002. Dependence of surface runoff on rain intensity. In: Proceedings of the International Conference on Flood Estimation, March 6-8, Berne, Switzerland, 139–146
Kohl, B., Markart, G., Stary, U., Proske, H., Trinkaus, P., 1997. Abfluss-und Infiltrationsverhalten von Böden unter Fichtenalbeständen in der Gleinalm (Stmk.) [Drainage and infiltration characteristics of spruce forest soils in the 'Gleinalm' alp (Steiermark)]. Berichte der Forstlichen Bundesversuchsanstalt Wien 96, 27–32.
Konrad, C.P., 2016. Effects of Urban Development on Floods. U.S. Geological Survey (USGS) Fact Sheet 076-03. https://pubs.usgs.gov/fs/fs07603/
Koricheva, J., Gurevitch, J., 2014. Uses and misuses of meta-analysis in plant ecology. J. Ecol. 102 (4), 828–844.
Koutsoyiannis, D., Blöschl, G., Bárdossy, A., Cudennec, C., Hughes, D., Montanari, A., Neuweiler, I., Savenije, H., 2016. Joint editorial: Fostering innovation and improving impact assessment for journal publications in hydrology. J. Hydrol. 537, A1–A4.
Krümmelbein, J., Wang, Z., Zhao, Y., Peth, S., Horn, R., 2006. Influence of various grazing intensities on soil stability, soil structure and water balance of grassland soils in Inner Mongolia, P.R. China. In: Horn, R., Fleige, H., Peth, S., Peng, X. (Eds.), Soil management for sustainability, Advances in GeoEcology, vol. 38. Catena Verlag, Reiskirchen, pp. 93–101.
Kundzewicz, Z., Pinskwar, I., Brakenridge, G.R., 2017. Changes in river flood hazard in Europe: a review. Hydrol. Res. https://doi.org/10.2166/nh.2017.016.
Lane, A.L., Peterson, P.G., Hedley, C.B., McColl, S.T., Fuller, I.C., 2016. Using ground penetrating radar to map soil drainage patterns to improve irrigation efficiency. In: Currie, L.D., Singh, R. (Eds.), Integrated nutrient and water management for sustainable farming. http://flrc.massey.ac.nz/publications.html. Occasional Report No. 29. Fertilizer and Lime Research Centre, Massey University, Palmerston North, New Zealand. 10p.
Larsbo, M., 2011. An episodic transit time model for quantification of preferential solute transport. Vadose Zone J. 10, 378–385.
Lebert, M., 2010. Entwicklung eines Prüfkonzeptes zur Erfassung der tatsächlichen Verdichtungsgefährdung landwirtschaftlich genutzter Böden. Report, Umweltbundesamt, Germany, http://www.uba.de/uba-info-medien/4027.html.
Li, X., Zhang, L.M., 2009. Characterization of dual-structure pore-size distribution of soil. Can. Geotech. J. 46, 129–141.
Liebig, M.A. et al., 1993. Controlled wheel traffic effects on soil properties in ridge tillage. Soil Sci. Soc. Am. J. 57 (4), 1061–1066.
Lorenz, K., Lal, R., 2009. Biochemical C and N cycles in urban soils. Environ. Int. 35, 1–8. https://doi.org/10.1016/j.envint.2008.05.006.
Mace Jr., A.C., 1971. Recovery of forest soils from compaction by rubber-tired skidders. Minnesota Forestry Research Notes No. 266. University of Minnesota, St. Paul.
Mapa, R.B., Green, R.E., Santo, L., 1986. Temporal variability of soil hydraulic properties with wetting and drying subsequent to tillage. Soil Sci. Soc. Am. J. 50, 1133–1138.
Markart, G., Kohl, B., Sotier, B., Schauer, T., Bunza, G. Stern, R., 2004. Provisorische Geländeanleitung zur Abschätzung des Oberflächenabflussbeiwertes auf alpinen Boden-/ Vegetationseinheiten bei konvektiven Starkregen [A simple Code of Practice for Assessment of Surface Runoff Coefficients for Alpine Soil-/ Vegetation Units in Torrential Rain] (Version 1.0). BFW Dokumentationen. Bundesamt und Forschungszentrum für Wald, Wien.
McGrath, G.S., Hinz, C., Sivapalan, M., 2009. A preferential flow leaching index. Water Resour. Res. 45, W11405. https://doi.org/10.1029/2008WR007265.
McIntyre, N., Marshall, M., 2010. Identification of rural land management signals in runoff response. Hydrol. Proc. 24, 3521–3534.
Milne, R.M., Haynes, R.J., 2004. Comparative effects of annual and permanent dairy pastures on soil physical properties in the Tsitsikamma region of South Africa. Soil Use Manage. 20, 81–88.
Mohanty, B.P., Horton, R., Ankeny, M.D., 1996. Infiltration and macroporosity under a row crop agricultural field in a glacial till soil 1. Soil science 161 (4), 205–213.
Munkholm, L.J., Schjønning, P., Rasmussen, K.J., Tanderup, K., 2003. Spatial and temporal effects of direct drilling on soil structure in the seedling environment. Soil Tillage Res. 71, 163–173.
Mutema, M., Chaplot, V., Jewitt, G., Chivenge, P., Blöschl, G., 2015. Annual water, sediment, nutrient, and organic carbon fluxes in river basins: A global meta-analysis as a function of scale. Water Resour. Res. 51, 8949–8972. https://doi.org/10.1002/2014WR016668.
Nawaz, M.F., Bourrié, G., Trolard, F., 2013. Soil compaction impact and modelling. A review. Agron. Sustain. Dev. 33, 291–309.
Naef, F., Scherrer, S., Weiler, M., 2002. A process based assessment of the potential to reduce flood runoff by land use change. J. Hydrol. 267, 74–79.
Nie, Z.N., Ward, G.N., Michael, A.T., 2001. Impact of pugging by dairy cows on pastures and indicators of pugging damage to pasture soil in south-western Victoria. Aust. J. Agricul. Res. 52 (1), 37–43.
O'Connell, P.E.O., Beven, K., Carney, J.N., Clements, R.O., Ewen, J., Fowler, H., Harris, G., Hollis, J., Morris, J., O'Donnell, G.M.O., Packman, J.C., Parkin, A., Quinn, P.F., Rose, S.C., Shepher, M., Tellier., S. 2004. Review of Impacts of Rural Land Use and Management on Flood Generation. Report A: Impact Study Report. R&D Technical Report FD2114/TR, Defra, London, UK 152 pp
O'Connell, E., Ewen, J., O'Donnell, G., Quinn, P., 2007. Is there a link between agricultural land-use management and flooding? Hydrol. Earth Syst. Sci. 11, 96–107.
Oldeman, R., Hakkeling, R.T.A., Sombroek, W., 1991. World Map on the Status of Human-Induced Soil Degradation. An Explanatory Note. Global Assessment of Soil Degradation. GLASOD. ISRIC - Winand Centre - ISSS - FAO - ITC, Wageningen.
Orr, H.G., Carling, P.A., 2006. Hydro-climatic and land use changes in the River Lune catchment, NW England: Implications for catchment amangement. River Res. and Appl. 22, 239–325.
Owens, L.B., Edwards, W.M., Van Keuren, R.W., 1997. Runoff and sediment losses resulting from winter feeding on pastures. J. Soil Water Conserv. 52, 194–197.
Pagliai, M., Marsili, A., Servadio, P., Vignzzi, N., Pellegrini, S., 2003. Changes in some physical properties of a clay soil in Central Italy following the passage of rubber tracked and wheeled tractors of medium power. Soil Till. Res. 73, 119–129.
Pattison, I., Lane, S.N., 2011. The link between land-use management and fluvial flood risk: a chaotic conception. Prog. Phys. Geogr. 36 (1), 72–92.
Peña, L.E., Barrios, M., Francés, F., 2016. Flood quantiles scaling with upper soil hydraulic properties for different land uses at catchment scale. J. Hydrol. 541, 1258–1272.
Peng, X.H., Horn, R., 2008. Time-dependent, anisotropic pore structure and soil strength in a 10-year period after intensive tractor wheeling under conservation and conventional tillage. J. Plant Nutr. Soil Sci. 171, 936–944.
Pickett, S.T.A., Cadenasso, M.L., 2009. Altered resources, disturbance, and heterogeneity: a framework for comparing urban and non-urban soils. Urban Ecosyst. 12, 23–44. https://doi.org/10.1007/s11252-008-0047-x.
Pouyat, R.V., Yesilonis, I.D., Russell-Anelli, J., Neerchal, N.K., 2007. Soil chemical and physical properties that differentiate urban land-use type and cover types. Soil Sci. Soc. Am. J. 71 (3), 1010–1019.
Prosdocimi, M., Calligaro, S., Sofia, G., Dalla Fontana, G., Tarolli, P., 2015. Bank rosion in agricultural drainage networks: new challenges from structure-from-motion photogrammetry for post-event analysis. Earth Surf. Processes Landform 40 (14), 1891–1906. https://doi.org/10.1002/esp.3767.
Rogger, M., Alaoui, A., Bloeschl, G., et al., 2017. Land-use change impacts on floods – Challenges and opportunities for future research. Water Resour. Res. 53. https://doi.org/10.1002/ 2017WR020723.
Roy, S., Mistri, B., 2013. Estimation of peak flood discharge for an ungauged river: a case study of the Kunur River, West Bengal. Geography J., 11 https://doi.org/10.1155/2013/214140.
Ryan, C.M., Berry, N.J., Joshi, N., 2014. Quantifying the causes of deforestation and degradation and creating transparent REDD+ baselines: A method and case study from central Mozambique. Appl. Geogr. 53, 45–54.
Salazar, S., Francés, F., Komma, J., Blume, T., Francke, T., Bronstert, A., Blöschl, G., 2012. A comparative analysis of the effectiveness of flood management measures based on the concept of "retaining water in the landscape" in different European hydro-climatic regions. Nat. Hazards Earth Syst. Sci. 12, 3287–3306. https://doi.org/10.5194/nhess-12-3287-2012.
Samson, B.K., Hasan, M., Wade, L.J., 2002. Penetration of hardpans by rice lines in the rainfed lowlands. Field Crops Res 76, 175–188.
Sanyal, J., Densmore, A.L., Carbonneau, P., 2014. Analysing the effect of land-use/cover changes a sub-catchment levels on downstream flood peaks: a semi-distributed modelling approach with sparse data. Catena 118, 28–40.
Scanlon, Bridget R. et al., 2007. Global impacts of conversions from natural to agricultural ecosystems on water resources: Quantity versus quality. Water Resour. Res. 43, 3.
Scherrer, S., Naef, F., Fach, A.O., Cordery, I., 2007. Formation of runoff at the hillslope scale during intense precipitation. Hydrol. Earth Syst. Sci. 11, 907–922.
Schilling, K.E., Gassman, P.W., Kling, C.L., Campbell, T., Jha, M.K., Wolter, C.F., Arnold, J.G., 2014a. The potential for agricultural land use change to reduce flood risk in a large watershed. Hydrol. Process. 28, 3314–3325. https://doi.org/10.1002/hyp.9865.
Schwarz, O., 1986. Zum Abflussverhalten von Waldböden bei künstlicher Beregnung [Runoff characteristics of forest soils as affected by artificial irrigation]. In: Einsele, G. (Ed.), DFG–Research Report on the landscape ecological project 'Schönuch'. VCH Publisher, Weinheim, pp. 161–179.
Schäffer, B., Schulin, R., Boivin, P., 2008. Changes in shrinkage of restored soil caused by compaction beneath heavy agricultural machinery. Eur J Soil Sci 59, 771–783.
Schilling, O.S., Doherty, J., Kinzelbach, W., Wang, H., Yang, P.N., Brunner, P., 2014b. . Using tree ring data as a proxy for transpiration to reduce predictive uncertainty of a model simulating groundwater–surface water–vegetation interactions,. J. Hydrol. 519 (Part B), 2258–2271. https://doi.org/10.1016/j.jhydrol.2014.08.063.
Shoulders, E., Terry, T.A., 1978. Dealing with site disturbances from harvesting and site preparation in the lower coastal plain. In: Proceedings of the Symposium on Principles of Maintaining Productivity on Prepared Sites. Mississippi State University, USA, pp. 85–97.
Seyfried, M.S., Wilcox, B.P., 1995. Scale and the nature of spatial variability: field examples having implications for hydrologic modeling. Water Resour. Res. 31 (1), 173–184. https://doi.org/10.1029/94WR02025.
Silva, S., Barros, N., Costa, L., Leite, F., 2008. Soil compaction and eucalyptus growth in response to forwarder traffic intensity and load. Rev Bras Cienc Solo 32, 921–932.

Singh, J., Hadda, M.S., 2014. Soil and plant response to subsoil compaction and slope steepness under semi-arid irrigated condition. Int. J. Food, Agric. Veter. Sci. 4 (3), 95–104. ISSN 2277-209X.
Smith, C., Johnston, M., Lorentz, S., 1997. Assessing the compaction susceptibility of South African forestry soils. I. The effect of soil type, water content and applied pressure on uni-axial compaction. Soil Till Res 41, 53–73.
Soane, B.D., 1990. The role of organic matter in soil compactibility: A review of some practical aspects. Soil Tillage Res. 16, 179–201.
Soane, B.D., Van Ouwerkerk, C., 1994. Soil compaciton problems in world agriculture. In: Soane, B.D., Van Ouwerkerk, C. (Eds.), Soil compaction in crop production. Elsevier Science & Technology, Amsterdam, pp. 1–21.
Söhne, W., 1958. Fundamentals of pressure distribution and soil compaction under tractor tires. Agricultural engineering, May.
Tóth, B., Makó, A., Tóth, G., Farkas, C., Rajkai, K., 2013. Comparison of pedotransfer functions to estimate the van Genuchten parameters from soil survey information. Agrokémia és Talajtan 62, 5–22.
Troldborg, M., Aalders, I., Towers, W., Hallett, P.D., McKenzie, B.M., Bengough, A.G., Lilly, A., Ball, B.C., Hough, R.L., 2013. Application of Bayesian Belief Networks to quantify and map areas at risk to soil threats: Using soil compaction as an example. Soil Tillage Res. 132, 56–68.
Van den Akker, J.J.H., 2004. SOCOMO: a soil compaction model to calculate soil stresses and the subsoil carrying capacity. Soil Tillage Res. 79, 113–1227.
Van den Akker, J.J.H., 1988. Model computations of subsoil stress distribution and compaction due to field traffic. In: Proceedings of the 11th International Conference of ISTRO, Edinburth, UK, pp. 403–408.
Van den Akker, J.J.H., 1994. Prevention of subsoil compaction by tuning the wheel load tot he bearing capacity of the subsoil. In: Proceedings of the 13th International Conference of ISTRO, Aalborg, Denmark, pp. 537–542.
Villarini, G., Strong, A., 2014. Roles of climate and agricultural practices in discharge changes in an agricultural watershed in Iowa. Agric. Ecosyst. Environ. 188, 204–211. https://doi.org/10.1016/j.agee.2014.02.036.
Viglione, A., Merz, B., Viet Dung, N., Parajka, J., Nester, T., Blöschl, G., 2016. Attribution of regional flood changes based on scaling fingerprints. Water Resour. Res. 52, 5322–5340. https://doi.org/10.1002/2016WR019036.
Vzzotto, V.R., Marchezan, E., Segabinazzi, T., 2000. Effects of cattle trampling on lowland soil physical properties. Ciencia Rural. 30, 965–969.
Warburton, M.L., Schulze, R.E., Jewitt, G.P.W., 2012. Hydrological impacts of land use change in three diverse South African catchments. J. Hydrol. 414–415, 118–135.
Wang, P., Hu, Z., Zhao, Y., Li, X., 2016. Experimental study of soil compaction effects on GPR signals. J. Appl. Geophys. 126, 128–137.
Weiler, M., McDonnell, J.J., 2007. Conceptualizing lateral preferential flow and flow networks and simulating the effects on gauged and ungauged hillslopes. Water Resour. Res. 43, W03403. https://doi.org/10.1029/2006WR004867.
Western, A.W., Blöschl, G., Grayson, R.B., 1998. How well do indicator variograms capture the spatial connectivity of soil moisture? Hydrol. Process. 12, 1851–1868.
White, M.D., Greer, K.A., 2006. The effects of watershed urbanization on the stream hydrology and riparian vegetation of Los Penasquitos Creek. California Landsc. Urban Plann. 74, 125–138.
Wösten, J.H.M., Lilly, A., Nemes, A., Le Bas, C., 1999. Development and use of a database of hydraulic properties of European soils. Geoderma 90, 169–185.
Wright, S.F., Starr, J.L., Paltineanu, I.C., 1999. Changes in aggregate stability and concentration of glomalin during tillage management transition. Soil Sci. Soc. Am. J. 63, 1825–1829.
Yan, D., Schneider, U.A., Schmid, E., Huang, H., Pan, L., Dilly, O., 2013. Interactions between land use change, regional development, and climate change in the Poyang Lake district from 1985 to 2035. Agric. Syst. 119, 10–21.
Young, R.N., Warkentin, B.P., 1966. Introduction to Soil Behavior. The Macmillan Co., New York, p. 451.
Yung, K.Y., Kitchen, N.R., Sudduth, K.A., Lee, K.S., Chung, S.O., 2010. Soil compaction varies by crop management system over a claypan soil landscape. Soil Tillage Res. 107, 1–10.
Zehe, E., Blöschl, G., 2004. Predictability of hydrologic response at the plot and catchment scales: role of initial conditions. Water Resour. Res. 40, W10202. 10·1029/2003WR002869.
Zhao, Y., Peth, S., Horn, R., Krümmelbein, J., Ketzer, B., Gao, Y., Doerner, J., Bernhofer, C., Peng, X., 2010. Modeling grazing effects on coupled water and heat fluxes in Inner Mongolia grassland. Soil Till. Res. 109, 75–86.
Zimmermann, B., Elsenbeer, H., De Moraes, J.M., 2006. The influence of land-use changes on soil hydraulic properties: Implications for runoff generation. Forest Ecol. Manage. 222 (1–3), 29–38. https://doi.org/10.1016/j.foreco.2005.10.070.

ENVIRONMENTAL RESEARCH
LETTERS

PURPOSE-LED PUBLISHING™

LETTER • OPEN ACCESS

Plant and soil responses to ground-mounted solar panels in temperate agricultural systems

To cite this article: Fabio Carvalho *et al* 2025 *Environ. Res. Lett.* **20** 024003

IOP Publishing Environ. Res. Lett. 20 (2025) 024003 https://doi.org/10.1088/1748-9326/ada45b

ENVIRONMENTAL RESEARCH
LETTERS

LETTER

Plant and soil responses to ground-mounted solar panels in temperate agricultural systems

Fabio Carvalho[1,*], Hannah Montag[2], Laura Bentley[3], Radim Šarlej[1,6], Rosanne C Broyd[1,7], Hollie Blaydes[1], Marta Cattin[1,8], Miranda Burke[1], Abby Wallwork[1], Sammani Ramanayaka[1], Piran C L White[4], Stuart P Sharp[1], Tom Clarkson[2] and Alona Armstrong[1,5]

[1] Lancaster Environment Centre, Lancaster University, Lancaster LA1 4YQ, United Kingdom
[2] Clarkson & Woods Ecological Consultants, Blackford BS28 4PA, United Kingdom
[3] UK Centre for Ecology and Hydrology, Bangor LL57 2UW, United Kingdom
[4] Department of Environment and Geography, University of York, York YO10 5NG, United Kingdom
[5] Energy Lancaster, Lancaster University, Lancaster LA1 4FY, United Kingdom
[6] Currently at Institute of Botany, Ulm University, Ulm 89081, Germany.
[7] Currently at UK Centre for Ecology and Hydrology, Lancaster LA1 4AP, United Kingdom.
[8] Currently at the Environment Agency, Lutra House, Dodd Way, Walton Summit, Bamber Bridge, Preston PR5 8BX.
* Author to whom any correspondence should be addressed.

E-mail: [redacted]@lancaster.ac.uk

OPEN ACCESS

RECEIVED
8 October 2024

REVISED
6 December 2024

ACCEPTED FOR PUBLICATION
31 December 2024

PUBLISHED
10 January 2025

Keywords: ecosystem services, energy transition, land use change, photovoltaic panels, soil carbon storage, soil health, solar energy

Supplementary material for this article is available online

Abstract

In the move to decarbonise energy supplies to meet Net Zero targets, ground-mounted solar farms have proliferated around the world, with uncertain implications for hosting ecosystems. We provide some of the first evidence on the effects of ground-mounted solar panels on plant and soil properties in temperate agricultural systems. We sampled 32 solar farms in England and Wales in summer 2021. Plant cover and aboveground biomass, as well as soil nutrients and physiochemical properties, were quantified on land underneath solar panels, in the gaps between rows of solar arrays, and in control land (pasture) adjacent to three solar farms. Plant cover and aboveground biomass were significantly lower under solar panels than in the gaps between solar arrays and in pastures. Soil compaction was 14.4% and 15.5% higher underneath solar panels than in gaps and pastures, respectively. Soil organic carbon was 9% lower under solar panels than in gaps, while particulate organic matter was 29.1% and 23.6% lower under solar panels than in gaps and pastures, respectively. Soil mineral nitrogen was 30.5% higher under solar panels than in gaps, while soil (plant-available) phosphorus was approximately 60% higher in solar farm soils than in pasture soils. Reductions in solar radiation and changes to microclimate caused by solar panels may be driving lower plant productivity and growth, with consequences for nutrient cycling and soil properties. However, impacts must be considered in light of the previous land use and the total land area under solar panels, in the gaps between solar arrays, and around the margins of the solar farm. Our findings can inform solar farm design and management options (e.g. increase the proportion of land unaffected by solar panels, enhance plant cover under solar panels) to ensure the long-term provision of ecosystem services (e.g. soil carbon storage) within this fast-growing land use.

1. Introduction

The global deployment of renewable energy technologies has accelerated in the last decade in response to expanding policy support, growing energy security concerns, and the need to meet Net Zero targets to mitigate climate change (IEA 2024). Solar photovoltaic (PV) technologies are currently leading this growth in renewable energy (Ember 2024), mostly in the form of ground-mounted solar farms due to policy incentives for large-scale developments and declining module prices (IEA 2023). The increase in

solar farm development is expected to continue in the coming decades (Nijsse *et al* 2023) and is likely to intensify competition for land to produce food, generate energy, and conserve nature (Capellán-Pérez *et al* 2017). It is thus becoming increasingly important to quantify and understand solar farm impact on ecosystems, especially considering the potential to manage solar farms for positive environmental outcomes (Randle-Boggis *et al* 2020).

Solar farms are commonly built on agricultural land (Tinsley *et al* 2024) and managed as grasslands in temperate regions (Carvalho *et al* 2023, 2024a), offering both risks and opportunities for ecosystem health (Randle-Boggis *et al* 2020). Existing data indicate effects on microclimate and ecosystem processes (Armstrong *et al* 2016) and on plant and soil properties (Lambert *et al* 2021). For instance, the installation of PV arrays may have negative environmental impacts by disrupting soil aggregate stability and the native vegetation, resulting in topsoil erosion (Hernandez *et al* 2014). The removal of topsoil during construction can also reduce soil carbon (Choi *et al* 2020), nitrogen, and phosphorus (Geissen *et al* 2013), as well as increase soil bulk density and affect the soil's structural and hydraulic properties (Geissen *et al* 2013, Udom *et al* 2018). However, solar farms can also have positive environmental impacts, and have the potential to deliver several co-benefits beyond low-carbon electricity when compared to conventional fossil fuel sources (Turney and Fthenakis 2011). For instance, construction and land management techniques conducive to providing local biodiversity benefits (e.g. allocating space for semi-natural habitats) can help restore degraded habitats (Gazdag and Parker 2019, Semeraro *et al* 2020) and result in enhanced ecosystem services (Randle-Boggis *et al* 2020). Despite this recent evidence, relatively little is known of the effects of solar farms on plant and soil properties in temperate agricultural systems. This is an important knowledge gap since solar farms are expected to become increasingly common features of agricultural landscapes in coming decades as part of the low-carbon energy transition (IEA 2023).

The aim of this study was to investigate the effects of ground-mounted solar panels on plant and soil properties across solar farms in England and Wales. We compared plant (cover and aboveground biomass) and soil (organic carbon, mineral-associated organic matter (MAOM), particulate organic matter (POM), total nitrogen, C/N ratio, mineral nitrogen, nitrate, plant-available phosphorus, bulk density, and pH) properties from areas underneath solar panels to areas between rows of solar arrays and to control land adjacent to solar farms (permanent pasture) representing the previous land use. These properties are thought to broadly capture complex plant-soil interactions that drive the functioning of terrestrial ecosystems and the delivery of numerous ecosystem services (Bardgett and Wardle 2010) and are commonly used as primary indicators of soil quality in national monitoring programmes (e.g. Emmett *et al* 2010).

2. Methods

2.1. Plant, soil, and climate data

We sampled 32 operational solar farms in England and Wales (figure 1) between June and September 2021 following standard protocols (Carvalho *et al* 2023). At each site, four replicate plots were randomly placed on land underneath solar panels ('under') and in between the rows of solar arrays ('gaps'; figure 1). In three sites (where permission was granted by landowners; figure 1), four additional plots were sampled in permanent pastures adjacent to these solar farms ('control'). Total plant cover (visual percentage estimation of vegetation cover within a quadrat as seen from above) and plant aboveground biomass (AGB) harvested at the soil surface with a pair of shears were sampled within 30 × 30 cm quadrats at each plot. Soils were sampled within the same quadrats to 10 cm depth and 5 cm diameter with a cylindrical metal corer. Four replicate soil samples were collected from each quadrat; three samples were homogenised in the laboratory for soil analyses and one sample was kept separate for bulk density measurements. Plant and soil properties directly linked to the delivery of multiple ecosystem services (e.g. biomass production, soil carbon storage, nutrient cycling) were estimated following standard published methods (table 1).

We adopted the soil classification system derived by Feeney *et al* (2023), based on the NATMAP vector dataset by Cranfield University (National Soil Resources Institute 2001), to characterise our sites by soil class. This soil classification captures key structural properties of soils, including texture, drainage, organic carbon/matter content, depth, flood risk, and the degree of modification from human activity (see supplementary material in Feeney *et al* 2023). Site-specific air temperature and rainfall data (annual averages for the 1991–2020 period provided on a 12 km British National Grid) were sourced from the UK's Met Office Climate Data Portal (https://climatedataportal.metoffice.gov.uk/).

2.2. Data analyses

All numerical analyses were performed in R 4.4.1 (R Core Team 2024). Plant and soil properties were either arcsine- (percentage variables converted to proportions; table 1) or $\log_{10}$- (continuous variables; table 1) transformed to reduce skewness and the effect of outliers prior to analyses, which largely followed the ten-step protocol outlined in Zuur *et al* (2009) to implement model selection in linear mixed modelling

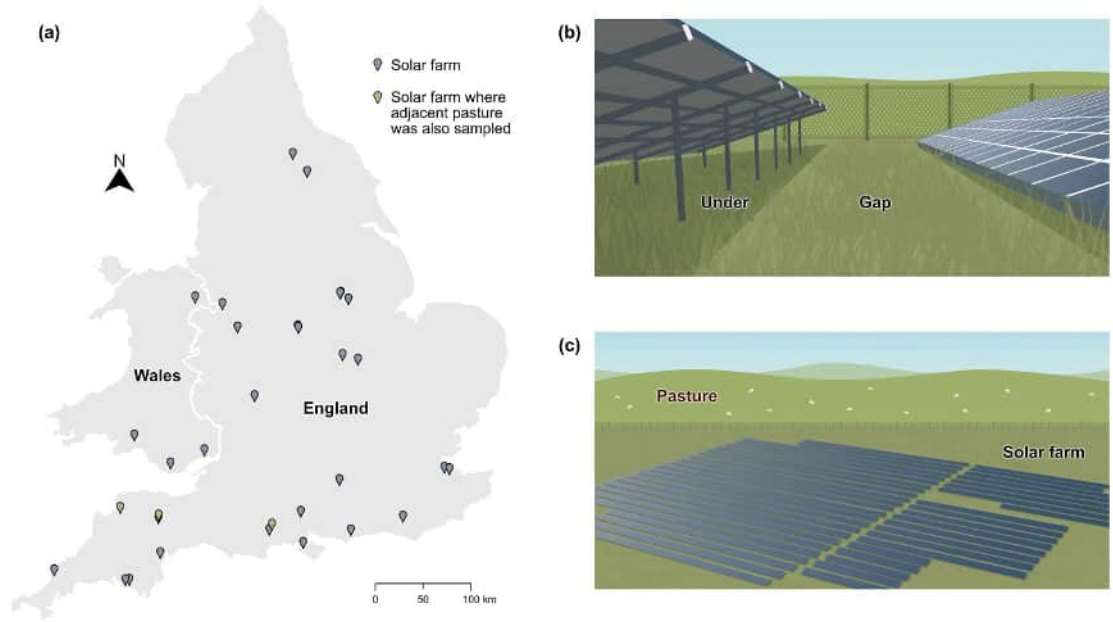

Figure 1. Location of the 32 solar farms sampled in England and Wales in summer 2021 (a) alongside visual representations of the treatments where plant and soil data were collected (b) and (c). Sites coloured in green denote the three solar farms where the adjacent pasture was sampled as a control treatment.

Table 1. Plant and soil properties measured on 32 solar farms in England and Wales in summer 2021. AGB = plant aboveground biomass, SOC = soil organic carbon, MAOM = mineral-associated organic matter, POM = particulate organic matter, N = nitrogen, P = phosphorus, BD = bulk density.

Property	Unit	Method	References
Plant cover	% cover	Visual plot-level estimation	Damgaard (2014)
AGB	Tonnes ha^{-1}	Destructive harvesting & oven-drying (60°C to constant mass)	Sala and Austin (2000)
SOC	% dry soil	Dry combustion (Vario EL Cube Elemental Analyser, Elementary, Stockport, UK) after acid (HCl) treatment	Harris *et al* (2001) Nayak *et al* (2019)
MAOM	% dry soil	Organic matter fractionation by size	Cotrufo *et al* (2019)
POM	% dry soil	Organic matter fractionation by size	Cotrufo *et al* (2019)
Total soil N	% dry soil	Dry combustion (Vario EL Cube Elemental Analyser, Elementary, Stockport, UK)	Emmett *et al* (2008)
Soil C/N ratio	NA	Soil organic carbon divided by total soil nitrogen	Emmett *et al* (2008)
Soil mineral N	mg N kg^{-1} dry soil	2 M KCl-extraction (NH_4 + NO_3 estimation in an Auto Analyser, Seal-Analytics©, Southampton, UK)	Emmett *et al* (2008)
Soil nitrate	Proportion of mineral N	2 M KCl-extraction (NO_3 estimation in an Auto Analyser, Seal-Analytics©, Southampton, UK)	Emmett *et al* (2008)
Soil Olsen P	mg P kg^{-1} dry soil	$NaHCO_3$-extraction (Auto Analyser, Seal-Analytics©, Southampton, UK)	Emmett *et al* (2008)
Soil BD	g dry soil cm^{-3}	Dried sample mass (110 °C for 24 h) over volume	Emmett *et al* (2008)
Soil pH	NA	Fresh soil pH in water (soil-water suspension)	Emmett *et al* (2008)

and address heterogeneity of variance and spatial correlation by testing different combinations of variance and auto-correlation structures.

We determined the effects of solar panels on plant and soil properties by testing the differences between the under and gap treatments (n = 256 per property; 32 sites × 4 replicates × 2 treatments) with linear mixed effects models fitted with the *nlme* package (Pinheiro and Bates 2023). Furthermore, we compared the two solar farm treatments (under and gap) to a control treatment (pasture outside the boundaries of the solar farm) for three sites where data were available (n = 36 per property; 3 sites × 4 replicates × 3 treatments).

In addition to *treatment*, the fixed effects included variables to account for local conditions (*soil class*), differences in climate between sites (*mean annual air temperature* and *rainfall*), and time since land use conversion (*age* of solar farms). The variable *site* was fitted as a random effect. The models that used data

from the three sites with adjacent pasture (control) only included *treatment, mean annual rainfall* and the *age* of solar farms, since *site* and *soil class* were colinear and *air temperature* showed low variability (coefficient of variation = 2.1%). Marginal means and pairwise differences between treatments were then estimated with the *emmeans* package (Lenth 2023) after back-transforming plant and soil properties to their original units.

Finally, for the three sites with data available for the adjacent pasture, we weighted the marginal means of the under and gap treatments to provide a solar farm weighted mean of plant and soil properties by accounting for the proportion of land within the under and gap treatments. Weighted means were calculated by summing the product of the weights (i.e. the proportions of the under and gap areas to the total solar farm area) times the marginal mean value of each variable and divided by the sum of the weights. The under and gap treatments accounted, on average, for 33% ± 0.06% (±1 SD) and 37% ± 0.09% (±1 SD) of the land between the three sites, respectively.

3. Results

3.1. Effects of solar panels on plant and soil properties

Areas under solar panels showed lower plant cover and AGB, lower soil carbon—when measured as soil organic carbon (SOC) and POM—and lower soil C/N ratio than areas in the gaps between solar arrays (figure 2). Soils under solar panels were more compacted and lower in total nitrogen than in gap areas, while (plant-available) mineral nitrogen and nitrate were higher under solar panels than in the gaps (figure 2). There were no statistical differences in MAOM, soil (plant-available) phosphorus (Olsen P), and soil pH between the two treatments (figure 2).

Older solar farms (ages ranged between 0.3 and 10.1 years old) tended to show higher plant cover, MAOM, POM, and soil nitrate than younger sites, though most differences were only marginally significant (table A1). Wetter sites showed higher plant AGB and higher soil carbon and nitrogen (measured in their different forms) than drier sites, while wetter soils were less compacted and lower in pH than drier soils (table A1). Measures of soil carbon and nitrogen varied among soil classes, but differences in air temperature between the sampled sites had no influence on the measured plant and soil properties (table A1).

3.2. Solar farms vs pasture

In the three sites where data for the adjacent pasture were available (figure 1), there were few statistical differences in plant and soil properties between gap areas and pastures (figure 3(b)), but areas under solar panels revealed higher soil compaction and lower plant cover, AGB, and POM than pastures (figure 3(a)). Solar farms generally showed higher soil (plant-available) nutrients than pastures, particularly Olsen P (figures 3(a) and (b)), though differences in mineral nitrogen and nitrate were only marginally significant (table A2). Rainfall had no influence on the results, but older sites showed marginally higher soil carbon and nitrogen (and marginally lower soil compaction) than younger sites (table A2).

When comparing solar farm weighted means (i.e. by accounting for the proportion of land under solar panels and in gap areas) to pasture means (table 2), SOC was slightly higher in solar farms than in pastures. In addition, the differences between the solar farm weighted means and the pastures were lower for plant cover, AGB, POM, and soil bulk density compared to the differences between the under areas and pasture (figure 3(a) and table 2).

4. Discussion

Our analyses are the first to demonstrate solar farm impacts on a suite of plant and soil properties across a range of sites and offer important insights into the effects of ground-mounted solar panels on plants and soils. Below, we discuss our results by grouping them into measures of plant (plant cover and AGB) and soil properties, including soil carbon and nitrogen (SOC, MAOM, POM, total nitrogen, and C/N ratio), soil (plant-available) nutrients (mineral nitrogen, nitrate, and Olsen P), and soil physiochemical properties (bulk density and pH).

4.1. Plant properties

Our findings, covering a range of solar farms with different design and site characteristics, indicate that plant cover and AGB are lower underneath solar panels than in gaps and pasture. However, effects may be context-dependent as plant cover has also been found to be unaltered by solar panels in some cases (Lambert *et al* 2021). Solar panels have been found to reduce plant photosynthetic rates and biomass by altering soil temperature and lowering receipts of photosynthetically active radiation (Vervloesem *et al* 2022) in temperate (Armstrong *et al* 2016) and Mediterranean (Lambert *et al* 2021, 2023) systems. Lambert *et al* (2023) found reduced plant biomass under solar panels to be due to higher allocation of resources to chlorophyll production to offset shading conditions, which in turn compromised resource allocation for biomass production of aboveground parts. However, the relationship between chlorophyll and biomass production is likely complex and highly variable between species (Paliwal *et al* 1986).

Management practices adopted by some operators may also have an impact on plant cover and biomass, including herbicide spraying to control weeds (often prominent under solar panels in summer; personal observation) and the sowing of low-statured

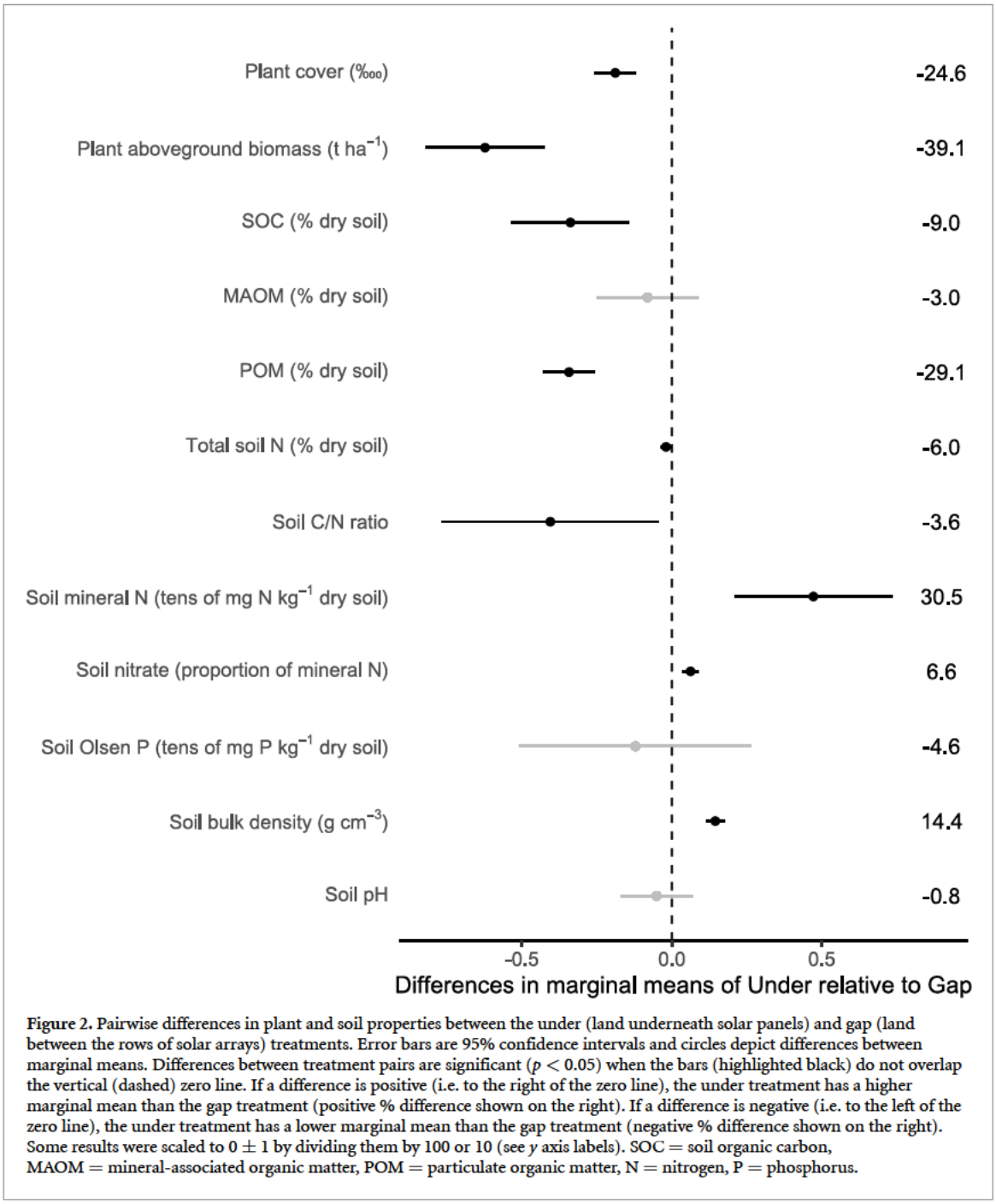

Figure 2. Pairwise differences in plant and soil properties between the under (land underneath solar panels) and gap (land between the rows of solar arrays) treatments. Error bars are 95% confidence intervals and circles depict differences between marginal means. Differences between treatment pairs are significant ($p < 0.05$) when the bars (highlighted black) do not overlap the vertical (dashed) zero line. If a difference is positive (i.e. to the right of the zero line), the under treatment has a higher marginal mean than the gap treatment (positive % difference shown on the right). If a difference is negative (i.e. to the left of the zero line), the under treatment has a lower marginal mean than the gap treatment (negative % difference shown on the right). Some results were scaled to 0 ± 1 by dividing them by 100 or 10 (see *y* axis labels). SOC = soil organic carbon, MAOM = mineral-associated organic matter, POM = particulate organic matter, N = nitrogen, P = phosphorus.

species to avoid shading of solar panels. The regular use of areas under solar panels for shelter by grazing sheep (personal observation on several sites) may also impact plant establishment and growth through heavy trampling.

The effect of solar panels on microclimate, coupled with land management decisions, also seem to influence plant community composition, diversity, and abundance, as well as the presence of indicator species (Armstrong *et al* 2016, Schindler *et al* 2018, Uldrijan *et al* 2021, 2022, Lambert *et al* 2022), by recruiting species tolerant to specific microclimatic, soil, and management conditions (Uldrijan *et al* 2021). This filtering may have implications for plant cover and AGB and affect ecosystem functioning (Hernandez *et al* 2014), trophic interactions (Uldrijan *et al* 2022), and the development of fire prone vegetation (Vaverková *et al* 2022).

4.2. Soil carbon and nitrogen

The lower soil carbon found for areas underneath solar panels compared to gap areas and pastures may be directly linked to the effects of solar panels on microclimate, solar radiation, and photosynthetic rates mentioned above. These effects can negatively impact plant establishment and growth, and reduce plant-derived carbon input to soils through altered plant tissue chemistry and litter quality and

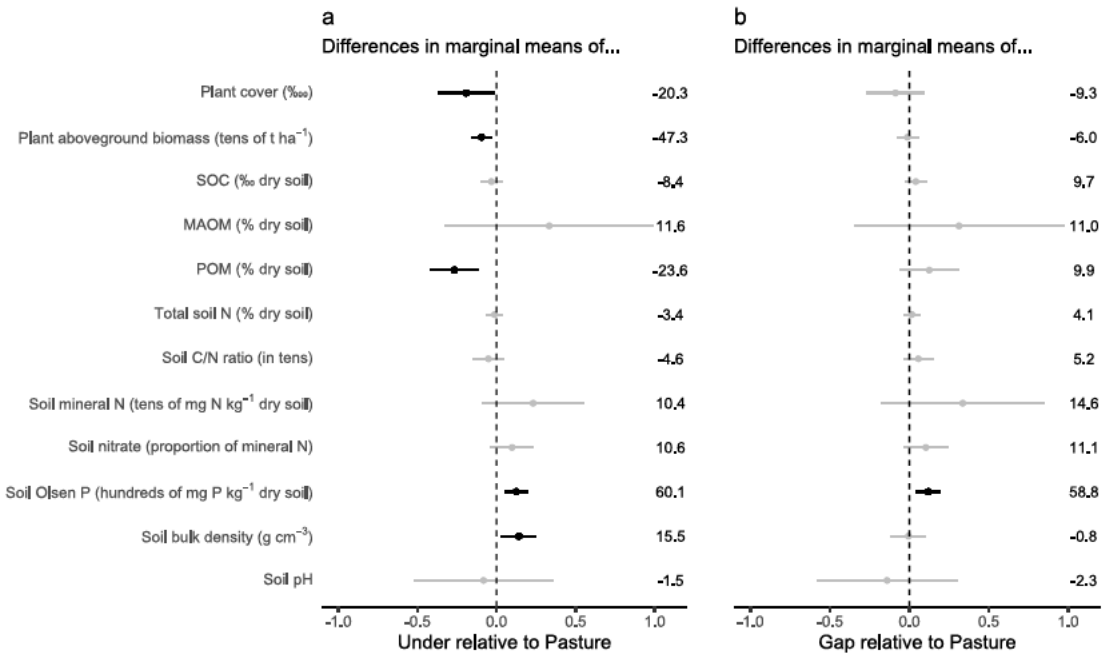

Figure 3. Pairwise differences in plant and soil properties between pasture (control treatment) and (a) the under treatment (land underneath solar panels) and (b) the gap treatment (land between the rows of solar arrays). Tukey adjustment was used to correct the *p* values for comparing three estimates (under, gap, and control), but only comparisons between under and pasture (a) and gap and pasture (b) are shown. Error bars are 95% confidence intervals and circles depict differences between marginal means. Differences between treatment pairs are significant ($p < 0.05$) when the bars (highlighted black) do not overlap the vertical (dashed) zero line. If a difference is positive (i.e. to the right of the zero line), the under (a) and gap (b) treatments showed a higher marginal mean than the pasture treatment (positive % difference shown on the right). If a difference is negative (i.e. to the left of the zero line), the under (a) and gap (b) treatments showed a lower marginal mean than the pasture treatment (negative % difference shown on the right). Some results were scaled to 0 ± 1 by dividing them by 100 or 10 (see *y* axis labels). SOC = soil organic carbon, MAOM = mineral-associated organic matter, POM = particulate organic matter, N = nitrogen, P = phosphorus.

Table 2. Mean differences in plant and soil properties between solar farms and pastures. Means are the marginal means of pairwise tests following mixed linear models fitted to the three sites where data were available for the adjacent pasture, but solar farm means were weighted by the proportion of land taken by the under and gap treatments. If a difference is negative in the final column, solar farms showed a lower mean than pastures.

Variable	Solar farm weighted mean	Pasture marginal mean	% Difference
Plant cover (%)	80.94	94.58	−14.4
Plant aboveground biomass (AGB) (t ha^{-1})	1.50	2.01	−25.2
Soil organic carbon (SOC) (%)	3.88	3.81	1.8
Mineral-associated organic matter (MAOM) (%)	2.84	2.52	11.3
Particulate organic matter (POM) (%)	1.07	1.13	−5.2
Total soil nitrogen (%)	0.38	0.38	0.6
Soil C/N ratio	10.97	10.90	0.6
Soil mineral nitrogen (mg kg^{-1})	22.78	19.91	12.6
Soil nitrate (proportion of mineral nitrogen)	0.92	0.82	10.9
Soil (plant-available) phosphorus (Olsen P) (mg kg^{-1})	20.54	8.34	59.4
Soil bulk density (g cm^{-3})	0.83	0.77	7.7
Soil pH	5.94	6.06	−1.9

quantity (Gill *et al* 2002). Similarly, the lower total soil nitrogen recorded underneath solar panels compared to gap areas may be due to relatively low levels of plant-soil feedbacks (e.g. nitrogen fixation through N-fixing bacteria; van der Putten *et al* 2013) and nutrient cycling under reduced levels of plant-derived organic matter input and microbial activity (Lambert *et al* 2023), as recorded in soils under solar panels elsewhere (Choi *et al* 2020, Lambert *et al* 2021, Moscatelli *et al* 2022). In addition, vegetation removal and soil disturbance due to tillage, levelling, trenching works, machinery compaction, and/or topsoil removal before or during solar farm construction may increase erosion and mineralisation rates of organic

matter and also result in reduced SOC (Quinton *et al* 2010, Gregory *et al* 2015) and nitrogen (Lambert *et al* 2021, Moscatelli *et al* 2022) content.

The lower POM observed underneath solar panels compared to gaps and pasture could be a direct result of lower plant biomass, since POM is mostly plant-derived, fast-cycling, and relatively vulnerable to disturbance (Cotrufo *et al* 2019). Reductions in POM may have important implications for long-term changes in SOC considering temperate grasslands can store significant fractions of organic carbon in POM pools (Denef *et al* 2013), making construction and management practices that reduce soil disturbance and maximise carbon input to soils particularly important. Lower POM can also have consequences for soil aggregate stability (Zech *et al* 2022) and negatively impact soil infiltration and erosion rates (Abu-Hamdeh *et al* 2006). In addition, despite being predominantly of microbial origin and relatively slow-cycling, MAOM can receive substantial carbon contributions from plant-derived organic matter and be closely related to short-term SOC cycling (Yu *et al* 2022). Therefore, despite no differences in MAOM between treatments found here, MAOM could be negatively affected over time under solar panels if plant-derived carbon inputs remain low. Moreover, MAOM tends to rapidly saturate under organic fertilisation (Stewart *et al* 2007, Just *et al* 2023), after which the continuous sequestration and storage of soil carbon is only possible through additional POM accrual (Cotrufo *et al* 2019). This could have consequences for long-term soil carbon storage under solar panels, since MAOM is a more persistent form of carbon than POM. Reductions in POM and MAOM could also have consequences for microbial growth and the soil food web by affecting supply of labile carbon and nutrients to plants and microbiota (Lavallee *et al* 2020), as evidenced elsewhere by lower microbiological activity and nutrient cycling under solar panels due to low soil organic matter (Lambert *et al* 2021, 2023, Moscatelli *et al* 2022). Given the potential for temperate grasslands to uptake carbon (Ostle *et al* 2009), there is ample evidence of the importance of land management on soil carbon (Carvalho and Armstrong 2021), and these should be carefully considered in relation to local conditions.

4.3. Soil (plant-available) nutrients

Given solar farms are rarely fertilised, the persistence of plant-available nutrients (nitrogen and phosphorus) in solar farm soils after construction, particularly underneath solar panels, may be a legacy of previous land fertilisation regimes under agricultural production since declines in inorganic nutrients may take several years to occur after cessation of agricultural activities (Parkhurst *et al* 2022a, 2022b), especially if they are not continually removed through harvesting (McLauchlan 2006). Vervloesem *et al* (2022) attributed higher nutrient content in soils underneath solar panels to their relatively low exposure to sun and rain compared to gap areas that could result in nutrient accumulation over time due to reduced leaching. In addition, the microbial carbon deficiency commonly found under solar panels (Lambert *et al* 2021, 2023) triggered by relatively low plant carbon inputs (rhizodeposition) may be driving microbial targeting of MAOM carbon pools with relatively low C/N ratio to result in excess nitrogen release into the soil via nitrogen mineralisation (Mooshammer *et al* 2014). These effects could lead to negative outcomes for biodiversity and ecosystem functioning long after land use change given the well-documented relationships between soil nutrients and plant species richness and abundance (Isbell *et al* 2019).

Despite the differences in soil nutrients among treatments described above, comparisons between sites under varying conditions and of different ages are difficult since the legacy of agricultural effects on soil properties can be highly variable and dependent on several factors, including time since land use change, post-agricultural management, climate, and mineralogy (McLauchlan 2006).

4.4. Soil physiochemical properties

Compaction of agricultural soils is typically associated with regular trafficking of agricultural machinery or the presence of grazing livestock, and its effects have been well documented (Gregory *et al* 2015), including increased risk of flooding and soil erosion (Batey 2009) and reduced biodiversity (Roovers *et al* 2004). The higher soil compaction under solar panels compared to gap areas and pastures is likely the result of a mixed legacy of previous (and current) agricultural practices (notably livestock grazing) and the use of heavy machinery during construction. Soils in the gaps showed similar levels of compaction to pasture, possibly due to largely successful revegetation efforts after solar farm construction and relatively low levels of disturbance during solar farm operation. In contrast, low levels of vegetation establishment and growth under solar panels may be directly related to high soil compaction due to reduced plant root penetration and water cycling that would help increase soil porosity and aeration, and reduce compaction (Correa *et al* 2019).

There were no statistical differences in soil pH between treatments, but soils under solar panels were slightly more acidic than in gap areas and pastures. Previous research found lower soil pH under solar panels compared to other land use types (Vervloesem *et al* 2022), which was attributed to low soil carbon and nitrogen (Aciego Pietri and Brookes, 2008, Chen *et al* 2016) and high (plant-available) nutrient concentrations (Chen *et al* 2015) under solar panels affecting soil fauna and the concentration of mineral cations. Soil pH will vary considerably from site

to site though depending on several factors, including soil type and texture, climate, topography, mineralogy, and water availability (Slessarev *et al* 2016).

5. Implications

The results presented here showed that, across a range of solar farms within temperate agricultural systems, the most marked impact of ground-mounted solar panels is on vegetation, with cascading effects on soil properties. This indicates that solar farms in temperate systems with a past agricultural legacy should be actively managed (e.g. by seeding diverse native species mixtures and maintaining structured habitats) to maximise delivery of plant- and soil-related ecosystem services. This is particularly true for biomass production and long-term soil carbon storage and sequestration, given the observed effects of solar panels on vegetation and their consequences for soil properties (e.g. soils being deprived of plant carbon inputs due to relatively low plant biomass under solar panels). However, our results suggest that past biotic and abiotic agricultural legacies can be overcome to allow solar farms to deliver environmental benefits other than low carbon electricity, given plant and soil properties in the gaps between solar arrays were generally similar to control conditions, suggesting no deterioration of ecosystem functioning in solar farms if converted from agricultural land. In fact, plant cover and soil carbon showed signs of improvement as solar farms aged (tables A1 and A2), meaning plant- and soil-related ecosystem services could improve over time if solar farms were managed accordingly (Randle-Boggis *et al* 2020) and offered the right policy incentives (Carvalho *et al* 2024b).

Solar farms can be designed and managed to deliver positive plant and soil outcomes. Regarding design, increasing the height of solar panels over the ground to offset the negative effects of shading and changes to microclimate on plant productivity, or increasing the proportion of gap areas (and other areas within solar farms such as margins) to favour plant development and consequently benefit soils through enhanced carbon inputs would be beneficial. Areas under solar panels account for approximately 39% of land in an average solar farm in the UK (but it could be as high as 70% in some cases; Blaydes, unpublished digitised solar farm data), offering scope to manage the remainder to deliver net positive outcomes for nature. In fact, differences in plant and soil properties between solar farms and pastures were lower than differences between under and pasture when accounting for the proportion of land in the different treatments (under and gap), while soil carbon was slightly higher in solar farms than in pastures on average (table 2), even if margins were not considered in this study. These results suggest solar farms can deliver net environmental gains across the site if enough area is set-aside for conservation away from solar arrays. However, increasing the proportion of land not over sailed by solar panels may result in higher land take for solar farms, meaning overall outcomes will depend on the type of land use being converted.

Finding management solutions to enhance vegetative cover under solar panels in temperate systems will be challenging, given the relative novelty of this type of land use and the fact plant and soil responses to active land management are highly dependent on local conditions. Management options may include the use of low impact machinery during construction to reduce soil compaction, the reduction in soil (plant-available) nutrients to promote species diversity (Isbell *et al* 2013, Midolo *et al* 2019), the regular monitoring of soil pH to formulate soil remediation measures if needed (Neina 2019), the sowing of generic all-purpose seed mixes that can establish on a range of soils and contain shade-tolerate species, and the use of conservation cutting and grazing to promote structured and diverse habitats to benefit wildlife. Frequent monitoring using standardised approaches (Carvalho *et al* 2023) will ensure the delivery of land management objectives and the collection of data that are comparable across sites. This will be key in guaranteeing the long-term provision of ecosystem services and in offering a broad picture of the ecosystem effects of this rapidly expanding novel land use.

6. Conclusions

Solar energy, especially in the form of ground-mounted solar farms, is set to play an important role in decarbonising electricity supplies worldwide. To address both the climate and biodiversity crises, the effects of ground-mounted solar panels on plants and soils must be considered before, during, and after solar farm development and contextualised to local conditions. In addition, the overall impact of a solar farm must be appropriately scaled to account for net environmental change across the site after land development given contrasting effects experienced by areas under solar panels to those in the gaps between solar arrays.

Given the relative youth of solar farms and their anticipated growth, it is critical that ecosystem responses to solar farm development and management are continually monitored to maximise positive biodiversity outcomes. The development of solar farms on agricultural land may lead to benefits for some ecosystem services over time (considering time lags in soil response to land use change), but developing ways to address the legacy of previous agricultural land use and enhancing plant cover under solar panels should be the focus of future research.

Other explanatory variables not included here (e.g. previous land use, land management, gap width, solar panel height and angle) should be considered

in upcoming studies as they may also drive plant and soil responses to solar farm development and can be altered to maximise positive biodiversity outcomes. In addition, the expected growth in solar farms may be accompanied by integrated battery storage facilities, introducing other environmental impacts (Simpa *et al* 2024). Consequently, the effects of battery storage facilities on soils should be considered in future research as they become increasingly more common.

Plant and soil properties may offer foundational indicators to investigate the impacts of solar farms on ecosystem services, but better understanding of the potential effects of solar farms on wider biodiversity (e.g. invertebrates, birds, mammals) is also needed to develop ways to manage solar farms that can benefit nature recovery in the fullest sense.

Data availability statement

The data cannot be made publicly available upon publication because they are owned by a third party and the terms of use prevent public distribution. The data that support the findings of this study are available upon reasonable request from the authors.

Acknowledgments

This research was undertaken as part of the UK Energy Research Centre (UKERC) Research Programme, funded by the UK Research and Innovation Energy Programme under Grant Numbers EP/S029575/1, and within the Knowledge Transfer Partnership (KTP) between Lancaster University and Clarkson & Woods Ecological Consultants under Grant Number KTP12947. KTPs aim to help businesses improve their competitiveness and productivity through the better use of knowledge, technology, and skills held within the UK knowledge base. KTPs are funded by UKRI through Innovate UK with the support of co-funders, including the Scottish Funding Council, Welsh Government, Invest Northern Ireland, Defra, and BEIS. Innovate UK manages the KTP Programme and facilitates its delivery through a range of partners, including the Knowledge Transfer Network (KTN), Knowledge Bases, and Businesses. Additional support was provided by a NERC Industrial Innovation Fellowship (NE/R013489/1) awarded to Alona Armstrong. We also thank Cameron Blaydes and Freya Olsson for help with laboratory work and Clare Benskin from Lancaster University for advice on laboratory methodologies.

Author contributions

Fabio Carvalho, Alona Armstrong, Hannah Montag, Tom Clarkson, Stuart P Sharp, and Piran C L White conceived the ideas and designed the methodology. Fabio Carvalho conducted field work and Rosanne C Broyd, Miranda Burke, Fabio Carvalho, Marta Cattin, Sammani Ramanayaka, Radim Sarlej, and Abby Wallwork performed laboratory work. Hollie Blaydes produced the map and graphics in figure 1. Laura Bentley advised on the use of soil classes and performed data selection. Fabio Carvalho analysed the data and led the writing of the manuscript. All authors contributed critically to the drafts and gave final approval for submission.

Conflict of interest

Fabio Carvalho was co-funded by Clarkson & Woods Ltd, Hannah Montag is employed by Clarkson & Woods Ltd, Hollie Blaydes was co-funded by Low Carbon Investment Management Ltd, and Tom Clarkson is Managing Director of Clarkson & Woods Ltd. Marta Cattin is currently employed by the Environment Agency; the views expressed are hers and those of the authors and are not formal positions of the Environment Agency.

ORCID iDs

Fabio Carvalho https://orcid.org/0000-0002-6305-5602
Laura Bentley https://orcid.org/0000-0001-5055-7673
Rosanne C Broyd https://orcid.org/0000-0002-0532-0674
Hollie Blaydes https://orcid.org/0000-0002-7753-4938
Marta Cattin https://orcid.org/0000-0002-3659-5179
Miranda Burke https://orcid.org/0000-0002-6891-3725
Abby Wallwork https://orcid.org/0000-0003-2189-4341
Sammani Ramanayaka https://orcid.org/0000-0002-8774-009X
Piran C L White https://orcid.org/0000-0002-7496-5775
Stuart P Sharp https://orcid.org/0000-0002-3059-2532
Alona Armstrong https://orcid.org/0000-0001-8963-4621

References

Abu-Hamdeh N H, Abo-Qudais S A and Othman A M 2006 Effect of soil aggregate size on infiltration and erosion characteristics *Eur. J. Soil Sci.* **57** 609–16
Aciego Pietri J C and Brookes P C 2008 Relationships between soil pH and microbial properties in a UK arable soil *Soil Biol. Biochem.* **40** 1856–61
Armstrong A, Ostle N J and Whitaker J 2016 Solar park microclimate and vegetation management effects on grassland carbon cycling *Environ. Res. Lett.* **11** 074016
Bardgett R D and Wardle D A 2010 *Aboveground-belowground Linkages: Biotic Interactions, Ecosystem Processes, and Global Change* (Oxford University Press)

Batey T 2009 Soil compaction and soil management—a review *Soil Use Manage.* **25** 335–45
Capellán-Pérez I, de Castro C and Arto I 2017 Assessing vulnerabilities and limits in the transition to renewable energies: land requirements under 100% solar energy scenarios *Renew. Sustain. Energy Rev.* **77** 760–82
Carvalho F *et al* 2023 Towards a standardized protocol to assess natural capital and ecosystem services in solar parks *Ecol. Solut. Evid.* **4** e12210
Carvalho F *et al* 2024b Integrated policymaking is needed to deliver climate and ecological benefits from solar farms *J. Appl. Ecol.* (https://doi.org/10.1111/1365-2664.14745)
Carvalho F and Armstrong A 2021 Solar parks could become significant carbon stores: active grassland management with organic fertiliser, sheep grazing and seeding could increase the amount of carbon stored in grassland soils *N8 AgriFood Food Systems Policy Hub* N8 AgriFood p 3 (available at: https://zenodo.org/records/5578084) (Accessed 13 May 2024)
Carvalho F, Healing S and Armstrong A 2024a Enhancing soil carbon in solar farms through active land management: a systematic review of the available evidence *Environ. Res. Ecol.* **3** 042001
Chen D, Lan Z, Hu S and Bai Y 2015 Effects of nitrogen enrichment on belowground communities in grassland: relative role of soil nitrogen availability vs. soil acidification *Soil Biol. Biochem.* **89** 99–108
Chen D, Li J, Lan Z, Hu S, Bai Y and Niu S 2016 Soil acidification exerts a greater control on soil respiration than soil nitrogen availability in grasslands subjected to long-term nitrogen enrichment *Funct. Ecol.* **30** 658–69
Choi C S, Cagle A E, Macknick J, Bloom D E, Caplan J S and Ravi S 2020 Effects of revegetation on soil physical and chemical properties in solar photovoltaic infrastructure *Front. Environ. Sci.* **8** 140
Correa J, Postma J A, Watt M, Wojciechowski T and Zhang J 2019 Soil compaction and the architectural plasticity of root systems *J. Exp. Bot.* **70** 6019–34
Cotrufo M F, Ranalli M G, Haddix M L, Six J and Lugato E 2019 Soil carbon storage informed by particulate and mineral-associated organic matter *Nat. Geosci.* **12** 989–94
Damgaard C 2014 Estimating mean plant cover from different types of cover data: a coherent statistical framework *Ecosphere* **5** art20
Denef K, Galdo I D, Venturi A and Cotrufo M F 2013 Assessment of soil C and N stocks and fractions across 11 European soils under varying land uses *Open J. Soil Sci.* **3** 297–313
Ember 2024 Global electricity review 2024 Ember (available at: https://ember-climate.org/insights/research/global-electricity-review-2024/) (Accessed 10 May 2024)
Emmett B A *et al* 2008 Countryside survey technical report No.03/07—soils manual v1.0 (available at: https://nora.nerc.ac.uk/id/eprint/5201/) (Accessed 9 November 2023)
Emmett B A *et al* 2010 Countryside Survey: soils Report from 2007 *CS Technical Report No. 9/07* UKCEH Project No. C03259 (NERC/Centre for Ecology and Hydrology) (available at: https://countrysidesurvey.org.uk/science/soils (Accessed 18 November 2023)
Feeney C J *et al* 2023 Development of soil health benchmarks for managed and semi-natural landscapes *Sci. Total Environ.* **886** 163973
Gazdag D and Parker G 2019 *Handbook of Climate Change and Biodiversity* ed W Leal Filho *et al* (Springer) pp 391–402
Geissen V, Wang S, Oostindie K, Huerta E, Zwart K B, Smit A, Ritsema C J and Moore D 2013 Effects of topsoil removal as a nature management technique on soil functions *CATENA* **101** 50–55
Gill R A, Polley H W, Johnson H B, Anderson L J, Maherali H and Jackson R B 2002 Nonlinear grassland responses to past and future atmospheric CO_2 *Nature* **417** 279–82
Gregory A S *et al* 2015 A review of the impacts of degradation threats on soil properties in the UK *Soil Use Manage.* **31** 1–15
Harris D, Horwáth W R and van Kessel C 2001 Acid fumigation of soils to remove carbonates prior to total organic carbon or CARBON-13 isotopic analysis *Soil Sci. Soc. Am. J.* **65** 1853–6
Hernandez R R *et al* 2014 Environmental impacts of utility-scale solar energy *Renew. Sustain. Energy Rev.* **29** 766–79
IEA 2023 Renewable energy market update—June 2023 (International Energy Agency) (available at: www.iea.org/reports/renewable-energy-market-update-june-2023 (Accessed 1 December 2023)
IEA 2024 Clean energy market monitor—March 2024 (International Energy Agency) (available at: www.iea.org/reports/clean-energy-market-monitor-march-2024 (Accessed 24 June 2024)
Isbell F, Reich P B, Tilman D, Hobbie S E, Polasky S and Binder S 2013 Nutrient enrichment, biodiversity loss, and consequent declines in ecosystem productivity *Proc. Natl Acad. Sci.* **110** 11911–6
Isbell F, Tilman D, Reich P B and Clark A T 2019 Deficits of biodiversity and productivity linger a century after agricultural abandonment *Nat. Ecol. Evol.* **3** 1533–8
Just C *et al* 2023 Soil organic carbon sequestration in agricultural long-term field experiments as derived from particulate and mineral-associated organic matter *Geoderma* **434** 116472
Lambert Q, Bischoff A, Cueff S, Cluchier A and Gros R 2021 Effects of solar park construction and solar panels on soil quality, microclimate, CO_2 effluxes, and vegetation under a Mediterranean climate *Land Degrad. Dev.* **32** 5190–202
Lambert Q, Bischoff A, Enea M and Gros R 2023 Photovoltaic power stations: an opportunity to promote European semi-natural grasslands? *Front. Environ. Sci.* **11** 1137845
Lambert Q, Gros R and Bischoff A 2022 Ecological restoration of solar park plant communities and the effect of solar panels *Ecol. Eng.* **182** 106722
Lavallee J M, Soong J L and Cotrufo M F 2020 Conceptualizing soil organic matter into particulate and mineral-associated forms to address global change in the 21st century *Glob. Change Biol.* **26** 261–73
Lenth R V 2023 emmeans: estimated marginal means, aka least-squares means R package version 1.8.9 (available at: https://CRAN.R-project.org/package=emmeans)
McLauchlan K 2006 The nature and longevity of agricultural impacts on soil carbon and nutrients: a review *Ecosystems* **9** 1364–82
Midolo G, Alkemade R, Schipper A M, Benítez-López A, Perring M P and De Vries W 2019 Impacts of nitrogen addition on plant species richness and abundance: a global meta-analysis *Glob. Ecol. Biogeogr.* **28** 398–413
Mooshammer M *et al* 2014 Adjustment of microbial nitrogen use efficiency to carbon: nitrogen imbalances regulates soil nitrogen cycling *Nat. Commun.* **5** 3694
Moscatelli M C, Marabottini R, Massaccesi L and Marinari S 2022 Soil properties changes after seven years of ground mounted photovoltaic panels in Central Italy coastal area *Geoderma Reg.* **29** e00500
National Soil Resources Institute 2001 NATMAP vector. LandIS land information system (Cranfield University) (available at: www.landis.org.uk/data/nmvector.cfm)
Nayak A K, Rahman M M, Naidu R, Dhal B, Swain C K, Nayak A D, Tripathi R, Shahid M, Islam M R and Pathak H 2019 Current and emerging methodologies for estimating carbon sequestration in agricultural soils: a review *Sci. Total Environ.* **665** 890–912
Neina D 2019 The role of soil pH in plant nutrition and soil remediation *Appl. Environ. Soil Sci.* **2019** 5794869
Nijsse F J M M, Mercure J-F, Ameli N, Larosa F, Kothari S, Rickman J, Vercoulen P and Pollitt H 2023 The momentum of the solar energy transition *Nat. Commun.* **14** 6542
Ostle N J, Levy P E, Evans C D and Smith P 2009 UK land use and soil carbon sequestration *Land Use Policy* **26** S274–S83
Paliwal K, Sivaraj T K, Natarajan K and Peter Marian M 1986 Chlorophyll content in different plant species of Nagamalai hills and its significance on biomass production *Proc. Indian Natl Sci.* **96** 471–4

Parkhurst T, Prober S M, Hobbs R J and Standish R J 2022a Global meta-analysis reveals incomplete recovery of soil conditions and invertebrate assemblages after ecological restoration in agricultural landscapes *J. Appl. Ecol.* **59** 358–72
Parkhurst T, Standish R J and Prober S M 2022b P is for persistence: soil phosphorus remains elevated for more than a decade after old field restoration *Ecol. Appl.* **32** e2547
Pinheiro J and Bates D (R Core Team) 2023 nlme: linear and nonlinear mixed effects models R package version 3.1–163 (available at: https://CRAN.R-project.org/package=nlme)
Quinton J N, Govers G, Van Oost K and Bardgett R D 2010 The impact of agricultural soil erosion on biogeochemical cycling *Nat. Geosci.* **3** 311–4
R Core Team 2024 *R: A Language and Environment for Statistical Computing* (R Foundation for Statistical Computing)
Randle-Boggis R J, White P C L, Cruz J, Parker G, Montag H, Scurlock J M O and Armstrong A 2020 Realising co-benefits for natural capital and ecosystem services from solar parks: a co-developed, evidence-based approach *Renew. Sustain. Energy Rev.* **125** 109775
Roovers P, Baeten S and Hermy M 2004 Plant species variation across path ecotones in a variety of common vegetation types *Plant Ecol.* **170** 107–19
Sala O E and Austin A T 2000 *Methods in Ecosystem Science* ed O E Sala *et al* (Springer New York) pp 31–43
Schindler B Y, Blaustein L, Lotan R, Shalom H, Kadas G J and Seifan M 2018 Green roof and photovoltaic panel integration: effects on plant and arthropod diversity and electricity production *J. Environ. Manage.* **225** 288–99
Semeraro T *et al* 2020 A conceptual framework to design green infrastructure: ecosystem services as an opportunity for creating shared value in ground photovoltaic systems *Land* **9** 238
Simpa P, Solomon N O, Adenekan O A and Obasi S C 2024 The safety and environmental impacts of battery storage systems in renewable energy *World J. Adv. Res. Rev.* **22** 564–80
Slessarev E W, Lin Y, Bingham N L, Johnson J E, Dai Y, Schimel J P and Chadwick O A 2016 Water balance creates a threshold in soil pH at the global scale *Nature* **540** 567–9
Stewart C E, Paustian K, Conant R T, Plante A F and Six J 2007 Soil carbon saturation: concept, evidence and evaluation *Biogeochemistry* **86** 19–31
Tinsley E, Froidevaux J S P and Jones G 2024 The location of solar farms within England's ecological landscape: implications for biodiversity conservation *J. Environ. Manage.* **372** 123372
Turney D and Fthenakis V 2011 Environmental impacts from the installation and operation of large-scale solar power plants *Renew. Sustain. Energy Rev.* **15** 3261–70
Udom B E, Omovbude S and Abam P O 2018 Topsoil removal and cultivation effects on structural and hydraulic properties *CATENA* **165** 100–5
Uldrijan D, Černý M and Winkler J 2022 Solar park: opportunity or threat for vegetation and ecosystem *J. Ecol. Eng.* **23** 1–10
Uldrijan D, Kováčiková M, Jakimiuk A, Vaverková M D and Winkler J 2021 Ecological effects of preferential vegetation composition developed on sites with photovoltaic power plants *Ecol. Eng.* **168** 106274
van der Putten W H *et al* 2013 Plant–soil feedbacks: the past, the present and future challenges *J. Ecol.* **101** 265–76
Vaverková M D, Winkler J, Uldrijan D, Ogrodnik P, Vespalcová T, Aleksiejuk-Gawron J, Adamcová D and Koda E 2022 Fire hazard associated with different types of photovoltaic power plants: effect of vegetation management *Renew. Sustain. Energy Rev.* **162** 112491
Vervloesem J, Marcheggiani E, Choudhury M D A M and Muys B 2022 Effects of photovoltaic solar farms on microclimate and vegetation diversity *Sustainability* **14** 7493
Yu W, Huang W, Weintraub-Leff S R and Hall S J 2022 Where and why do particulate organic matter (POM) and mineral-associated organic matter (MAOM) differ among diverse soils? *Soil Biol. Biochem.* **172** 108756
Zech S, Schweizer S A, Bucka F B, Ray N, Kögel-Knabner I and Prechtel A 2022 Explicit spatial modeling at the pore scale unravels the interplay of soil organic carbon storage and structure dynamics *Glob. Change Biol.* **28** 4589–604
Zuur A, Ieno E N, Walker N, Saveliev A A and Smith G M 2009 *Mixed Effects Models and Extensions in Ecology with R* (Springer)